THIS DOCUMENT PROVIDED BY THE ABBOTT AEROSPACE
TECHNICAL LIBRARY
ABBOTTAEROSPACE.COM

METRIC

MIL-HDBK-785(AR)

30 MARCH 1990

MILITARY HANDBOOK

DESIGN OF TOWED ARTILLERY WEAPON SYSTEMS

AMSC N/A

FSG 10GP

DISTRIBUTION STATEMENT A. Approved for public release; distribution is unlimited.

THIS DOCUMENT PROVIDED BY THE ABBOTT AEROSPACE
TECHNICAL LIBRARY
ABBOTTAEROSPACE.COM

FOREWORD

1. This military handbook is approved for use by all Activities and Agencies of the Department of the Army and is available for use by all Departments and Agencies of the Department of Defense.

2. Beneficial comments (recommendations, additions, deletions) and any pertinent data that may be of use in improving this document should be addressed to: Commander, US Army Armament Research, Development, and Engineering Center, ATTN: SMCAR-BAC-S, Picatinny Arsenal, NJ 07806-5001, by using the self-addressed Standardization Document Improvement Proposal (DD Form 1426) appearing at the end of this document or by letter.

3. This handbook was developed under the auspices of the US Army Materiel Command's Engineering Design Handbook Program, which is under the direction of the US Army Management Engineering College.

THIS DOCUMENT PROVIDED BY THE ABBOTT AEROSPACE
TECHNICAL LIBRARY
ABBOTTAEROSPACE.COM

CONTENTS

Paragraph *Page*
FOREWORD ii
LIST OF ILLUSTRATIONS x
LIST OF TABLES xv
LIST OF ABBREVIATIONS AND ACRONYMS xvii

CHAPTER 1
INTRODUCTION

1-0 LIST OF SYMBOLS 1-1
1-1 PURPOSE 1-1
1-2 ELEMENTS OF TOWED ARTILLERY SYSTEMS 1-2
1-2.1 SUBSYSTEMS COMPRISING A TOWED ARTILLERY SYSTEM 1-3
1-2.1.1 Ammunition 1-3
1-2.1.2 Tube and Breech 1-4
1-2.1.3 Recoil System 1-6
1-2.1.4 Cradle 1-7
1-2.1.5 Top Carriage 1-7
1-2.1.6 Bottom Carriage 1-8
1-2.1.7 Equilibrator 1-9
1-2.1.8 Elevating Mechanism 1-9
1-2.1.9 Traversing Mechanism 1-10
1-2.1.10 Fire Control Equipment 1-10
1-2.1.11 Travel Gear 1-10
1-2.2 VARIATION IN SUBSYSTEM CONFIGURATIONS 1-10
1-3 SYSTEM DYNAMICS 1-14
1-3.1 RECOIL DYNAMICS 1-14
1-3.2 DYNAMIC LOAD ANALYSIS 1-20
1-3.3 DYNAMIC EFFECTS ON WEAPON STABILITY AND PRECISION 1-20
REFERENCES 1-21

CHAPTER 2
PRELIMINARY DESIGN AND TRADEOFF ANALYSIS OF TOWED ARTILLERY SYSTEMS

2-0 LIST OF SYMBOLS 2-1
2-1 SYSTEM DESIGN AND ENGINEERING 2-4
2-2 SYSTEM REQUIREMENTS AND CONSTRAINTS 2-6
2-3 PRELIMINARY BALLISTIC AND CANNON DEFINITION 2-8
2-4 PRELIMINARY RECOIL MECHANISM DESIGN 2-13
2-5 COMPONENT PRELIMINARY SIZING 2-23
2-6 DESIGN FOR TOWING 2-29
2-7 SYSTEM TRADEOFFS AND PARAMETER SELECTION 2-32
2-7.1 SELECTION OF BASIC WEAPON CONFIGURATIONS 2-32
2-7.2 BALLISTIC SOLUTIONS 2-32
2-7.3 WEAPON ALTERNATIVES 2-36
2-7.4 WEIGHT ESTIMATIONS 2-36

THIS DOCUMENT PROVIDED BY THE ABBOTT AEROSPACE
TECHNICAL LIBRARY
ABBOTTAEROSPACE.COM

CONTENTS (cont'd)

Paragraph *Page*

2-7.5 WEAPON STABILITY 2-37
2-7.6 PARAMETER VARIATIONS 2-37
2-7.7 DECISION RULE FOR OPTIMAL SYSTEM SECTION 2-37
REFERENCES 2-48

CHAPTER 3
ARTILLERY SYSTEM KINEMATIC AND DYNAMIC ANALYSIS

3-0 LIST OF SYMBOLS 3-1
3-1 STATIC AND QUASI-STATIC ANALYSIS 3-5
3-1.1 INPUT FORCE DETERMINATION 3-5
3-1.2 STATIC AND QUASI-STATIC FORCE ANALYSIS 3-6
3-1.3 KINEMATIC ANALYSIS 3-13
3-2 CONVENTIONAL METHODS OF DYNAMIC ANALYSIS OF ARTILLERY 3-18
3-2.1 1-DEGREE-OF-FREEDOM RECOIL MODEL 3-18
3-2.2 2-DEGREE-OF-FREEDOM RECOIL MODEL 3-22
3-2.3 DYNAMIC MODELS OF INTERMEDIATE LEVEL OF COMPLEXITY 3-28
3-2.4 FORCE ANALYSIS 3-29
3-2.5 ANALYSIS AND CONTROL OF WEAPON STABILITY 3-33
3-2.6 TESTING FOR MODEL REFINEMENT AND VALIDATION 3-33
3-3 NUMERICAL INTEGRATION OF EQUATIONS OF MOTION 3-34
3-4 ADVANCED METHODS OF ARTILLERY DYNAMIC ANALYSIS 3-39
3-4.1 APPLICATION OF EQUATION MANIPULATION LANGUAGES TO LAGRANGE'S EQUATIONS 3-39
3-4.2 DYNAMIC ANALYSIS OF LARGE-SCALE SYSTEMS 3-41
REFERENCES 3-47

CHAPTER 4
MECHANISM DESIGN

4-0 LIST OF SYMBOLS 4-1
4-1 ELEVATING MECHANISMS 4-2
4-1.1 TYPES OF ELEVATING MECHANISMS 4-2
4-1.1.1 Ball-Screw Type 4-2
4-1.1.2 Pinion and Arc Type 4-3
4-1.2 ELEVATING MECHANISM COMPONENTS 4-3
4-1.2.1 Gear Trains 4-4
4-1.2.2 Clutches and No-Back Devices 4-7
4-1.2.3 Handwheels 4-9
4-1.2.4 Cushioning of Peak Firing Loads 4-9
4-1.2.5 Travel Locks 4-9
4-2 TRAVERSING MECHANISMS 4-12
4-2.1 TYPES OF TRAVERSING MECHANISMS 4-12
4-2.1.1 Pintle Traverse 4-13
4-2.1.2 Base Ring and Race Traverse 4-15
4-2.1.3 Off-Carriage Traverse 4-18
4-2.2 TRAVERSING MECHANISM COMPONENTS 4-19
4-2.2.1 Gear Trains 4-19
4-2.2.2 Antibacklash Devices 4-22

THIS DOCUMENT PROVIDED BY THE ABBOTT AEROSPACE
TECHNICAL LIBRARY
ABBOTTAEROSPACE.COM

CONTENTS (cont'd)

Paragraph *Page*

4-2.2.3 Clutches and No-Back Devices 4-23
4-2.2.4 Handwheels 4-24
4-2.2.5 Travel Locks 4-24
4-3 WEAPON-LOWERING AND -RAISING MECHANISMS 4-25
4-4 SUSPENSION SYSTEM 4-25
4-5 LINKAGE FOR VARIABLE RECOIL 4-27
REFERENCES 4-28

CHAPTER 5
EQUILIBRATOR DESIGN

5-0 LIST OF SYMBOLS 5-1
5-1 INTRODUCTION 5-5
5-1.1 TYPES OF EQUILIBRATORS 5-5
5-1.2 FACTORS INFLUENCING EQUILIBRATOR DESIGN 5-9
5-1.2.1 Weight Moment of Tipping Parts 5-9
5-1.2.2 Friction 5-11
5-1.2.3 Packing Friction 5-11
5-1.2.4 Geometric Considerations 5-12
5-1.3 SELECTING AN EQUILIBRATOR TYPE 5-12
5-2 MECHANICS OF EQUILIBRATORS 5-12
5-2.1 GEOMETRY AND FORCE ANALYSIS 5-12
5-2.2 MECHANICS AND KINEMATICS OF PERFECT EQUILIBRATION 5-18
5-2.3 MECHANICS AND KINEMATICS OF APPROXIMATE EQUILIBRATION 5-20
5-2.4 FRICTION EFFECTS ON EQUILIBRATION 5-22
5-3 SPRING EQUILIBRATOR DESIGN 5-25
5-3.1 A PERFECT BALANCE EQUILIBRATOR 5-25
5-3.2 AN APPROXIMATE BALANCE EQUILIBRATOR 5-26
5-3.3 COMPONENT DESIGN AND MANUFACTURING PROCESS 5-28
5-3.3.1 Spring Design 5-28
5-3.3.2 Manufacturing Processes 5-31
5-4 PNEUMATIC EQUILIBRATOR DESIGN 5-32
5-4.1 APPROXIMATE BALANCE EQUILIBRATOR 5-32
5-4.1.1 Force Versus Gas Volume Relation 5-32
5-4.1.2 Performance of the Equilibrator Including Friction 5-39
5-4.2 COMPONENT DESIGN AND MANUFACTURING PROCESSES 5-40
5-4.2.1 Cylinder Design 5-41
5-4.2.2 Piston Rod 5-42
5-4.2.3 Terminals 5-42
5-4.2.4 Packing Design 5-43
5-4.2.5 Equilibrator Adjustment 5-45
5-5 OPTIMIZATION OF APPROXIMATE EQUILIBRATOR IMBALANCE 5-48
5-5.1 MINIMIZATION OF APPROXIMATE EQUILIBRATOR IMBALANCE 5-48
5-5.2 LEAST SQUARE IMBALANCE MINIMIZATION 5-48
5-5.3 NONLINEAR PROGRAMMING METHODS FOR IMBALANCE MINIMIZATION 5-50
5-5.3.1 Design Formulation 5-50
5-5.3.2 Optimization Methods 5-51
5-5.3.3 Example of Nonlinear Programming Method 5-51
REFERENCES 5-54

THIS DOCUMENT PROVIDED BY THE ABBOTT AEROSPACE
TECHNICAL LIBRARY
ABBOTTAEROSPACE.COM

CONTENTS (cont'd)

Paragraph *Page*

CHAPTER 6
BEARING DESIGN

6-0 LIST OF SYMBOLS 6-1
6-1 INTRODUCTION 6-1
6-1.1 BEARING FUNCTIONS AND LOADS 6-1
6-1.2 ANTIFRICTION BEARING TYPES AND AVAILABILITY 6-4
6-2 TRUNNION BEARINGS 6-6
6-2.1 JOURNAL BEARINGS 6-6
6-2.1.1 Friction in Journal Bearings 6-6
6-2.1.2 Bearing Loads 6-7
6-2.1.3 Strength and Stiffness of Journal Bearings 6-7
6-2.1.4 Materials 6-8
6-2.1.5 Bearing Design 6-8
6-2.2 STRESS DISTRIBUTION IN JOURNAL BEARINGS 6-9
6-2.2.1 Force Distribution 6-9
6-2.2.2 Contact Stress Analysis 6-9
6-2.3 ANTIFRICTION ROLLER BEARINGS 6-10
6-2.3.1 Bearing Capacity 6-10
6-2.3.2 Self-Aligning Bearings 6-11
6-2.3.3 Bearing Shields and Seals 6-11
6-2.3.4 Lubrication 6-11
6-3 TRAVERSE BEARINGS 6-12
6-3.1 PINTLE BEARINGS 6-12
6-3.2 LARGE DIAMETER TRAVERSE BEARINGS 6-13
6-3.3 BALL JOINT AND FOLLOWER BEARINGS FOR 360-DEG TRAVERSE 6-13
REFERENCES 6-14

CHAPTER 7
CRADLE DESIGN

7-0 LIST OF SYMBOLS 7-1
7-1 INTRODUCTION 7-5
7-2 EQUIPMENT ASSOCIATED WITH CRADLES 7-6
7-2.1 RECOIL MECHANISM 7-6
7-2.2 TRUNNIONS 7-6
7-2.3 ELEVATING MECHANISM 7-7
7-2.4 EQUILIBRATOR 7-7
7-3 TYPES OF CRADLES 7-7
7-3.1 U-TYPE CRADLE 7-7
7-3.2 O-TYPE CRADLE 7-8
7-3.3 EFFECT OF FRICTION ON SLIDING SURFACES 7-9
7-3.4 EFFECT OF TEMPERATURE VARIATION ON SLIDING SURFACES 7-9
7-3.5 SUGGESTED MATERIALS FOR CRADLE 7-10
7-3.6 MANUFACTURING PROCEDURES 7-10
7-4 PRELIMINARY DESIGN OF CRADLES 7-10
7-4.1 LOAD ANALYSIS FOR CRADLE STRUCTURE 7-11
7-4.1.1 Firing Loads 7-11
7-4.1.2 Loads on Various Components of Cradle Structure 7-12
7-4.1.2.1 Recoil Attachment to Cradle 7-12

THIS DOCUMENT PROVIDED BY THE ABBOTT AEROSPACE
TECHNICAL LIBRARY
ABBOTTAEROSPACE.COM

CONTENTS (cont'd)

Paragraph *Page*

7-4.1.2.2 Equilibrator Attachment 7-14
7-4.1.2.3 Elevating Arc 7-15
7-4.1.2.4 Attachment for Transmitting Rifling Torque 7-15
7-4.2 STRENGTH REQUIREMENTS 7-20
7-4.2.1 Location and Design of Trunnions 7-20
7-4.2.2 Sliding Surfaces of U-Type Cradle 7-25
7-4.2.3 Design of Cradle Body 7-28
7-4.3 REFINED LOAD ANALYSIS AND STRESS CALCULATIONS 7-30
7-5 SAMPLE CRADLE DESIGN PROBLEM 7-33
7-5.1 PRELIMINARY DESIGN CALCULATIONS 7-34
7-5.1.1 Load Analysis 7-34
7-5.1.2 Rails and Slides 7-35
7-5.1.3 Equilibrator Load 7-37
7-5.1.4 Elevating Gear Load 7-40
7-5.1.5 Trunnion Loads 7-42
7-5.1.6 Stress and Deflection 7-45
7-5.2 REFINED DESIGN CALCULATIONS AT SEVEN SELECTED CROSS SECTIONS 7-49
7-5.2.1 Stress Calculations for Section 1 7-56
7-5.2.2 Stress Calculations for Section 2 7-57
7-5.2.3 Stress Calculations for Section 3 7-57
7-5.2.4 Stress Calculations for Section 4 7-57
7-5.2.5 Stress Calculations for Section 5 7-57
7-5.2.6 Stress Calculations for Section 6 7-58
7-5.2.7 Stress Calculations for Section 7 7-58
7-6 DESIGN FOR RIFLING TORQUE 7-58
7-6.1 STRESSES AT SECTION 0.127 m 7-60
7-6.2 STRESSES AT SECTION 0.254 m 7-60
7-6.3 STRESSES AT SECTION 1.016 m 7-61
7-7 ADVANCED DESIGN TECHNIQUES 7-61
7-7.1 FINITE ELEMENT MODEL 7-62
7-7.2 NASTRAN STRESS ANALYSIS 7-65
REFERENCES 7-66

CHAPTER 8
TOP CARRIAGE DESIGN

8-0 LIST OF SYMBOLS 8-1
8-1 INTRODUCTION 8-3
8-2 EQUIPMENT ASSOCIATED WITH TOP CARRIAGE 8-3
8-2.1 EQUILIBRATORS 8-3
8-2.2 ELEVATING MECHANISMS 8-3
8-2.3 TRAVERSING MECHANISMS 8-3
8-2.4 TRUNNION BEARINGS 8-4
8-2.5 TRAVERSE BEARINGS 8-4
8-3 DESCRIPTION OF TOP CARRIAGE 8-4
8-3.1 TYPES OF TOP CARRIAGES 8-4
8-3.2 CONSTRUCTION AND MANUFACTURING PROCEDURES 8-4
8-3.3 MATERIALS FOR TOP CARRIAGES 8-6
8-4 PRELIMINARY DESIGN OF TOP CARRIAGE 8-6
8-4.1 LOAD ANALYSIS 8-7

THIS DOCUMENT PROVIDED BY THE ABBOTT AEROSPACE
TECHNICAL LIBRARY
ABBOTTAEROSPACE.COM

CONTENTS (cont'd)

Paragraph *Page*

8-4.2 STRESS ANALYSIS 8-8
8-5 SAMPLE TOP CARRIAGE DESIGN PROBLEM 8-8
8-5.1 LOAD ANALYSIS 8-11
8-5.1.1 Lifting Load 8-11
8-5.1.2 Equilibrator Load 8-14
8-5.1.3 Trunnion Load 8-15
8-5.2 STRESS ANALYSIS 8-16
8-5.2.1 Case 1. Lifting Force Only 8-16
8-5.2.2 Case 2. Equilibrator Force Only 8-22
8-5.2.3 Case 3. Lifting and Equilibrator Forces Combined 8-25
8-5.2.4 Case 4. Equilibrator and Trunnion Forces Combined 8-25
8-5.2.5 Transverse Shear Stress Calculations 8-28
8-6 ADVANCED DESIGN TECHNIQUES FOR TOP CARRIAGE STRUCTURES 8-30
8-6.1 FINITE ELEMENT MODEL 8-30
8-6.2 NASTRAN STRESS ANALYSIS 8-33
REFERENCES 8-36

CHAPTER 9
BOTTOM CARRIAGE DESIGN

9-0 LIST OF SYMBOLS 9-1
9-1 INTRODUCTION 9-3
9-2 TYPES OF BOTTOM CARRIAGES 9-6
9-2.1 STRUCTURES FOR BOTTOM CARRIAGES 9-6
9-2.1.1 Bottom Carriage for On-Carriage Traverse Weapons 9-6
9-2.1.2 Bottom Carriage for Off-Carriage Traverse Weapons 9-10
9-2.2 MATERIALS 9-10
9-2.3 MANUFACTURING ASPECTS 9-11
9-3 PRELIMINARY DESIGN OF BOTTOM CARRIAGE 9-11
9-3.1 LOAD ANALYSIS 9-12
9-3.2 STRESS ANALYSIS 9-12
9-4 SAMPLE BOTTOM CARRIAGE DESIGN PROBLEM 9-13
9-4.1 LOAD ANALYSIS 9-13
9-4.2 STRESS ANALYSIS 9-13
9-4.2.1 Trails 9-15
9-4.2.2 Bottom Carriage Main Body 9-20
9-4.2.3 Buckling of Vertical Plates 9-34
9-4.2.4 Bottom Carriage Trail Lugs 9-35
9-5 ADVANCED DESIGN FOR BOTTOM CARRIAGE STRUCTURES 9-40
9-5.1 FINITE ELEMENT MODEL 9-40
9-5.1.1 General 9-40
9-5.1.2 Computation of Equivalent Loads 9-45
9-5.2 NASTRAN STRESS ANALYSIS 9-53
9-6 BOTTOM CARRIAGE-SOIL INTERACTION 9-55
9-6.1 TRAIL SPADE/GROUND INTERACTION 9-56
9-6.2 FIRING BASE (WITH AND WITHOUT STAKES)—GROUND INTERACTION 9-56
9-6.3 EFFECTS OF SOIL VARIABILITY 9-57
REFERENCES 9-57

THIS DOCUMENT PROVIDED BY THE ABBOTT AEROSPACE
TECHNICAL LIBRARY
ABBOTTAEROSPACE.COM

CONTENTS (cont'd)

Paragraph *Page*

CHAPTER 10
DESIGN FOR MAINTAINABILITY

10-1 INTRODUCTION 10-1
10-2 CATEGORIES OF MAINTENANCE 10-1
10-2.1 UNIT MAINTENANCE 10-1
10-2.2 DIRECT SUPPORT MAINTENANCE 10-2
10-2.3 GENERAL SUPPORT MAINTENANCE 10-2
10-2.4 DEPOT MAINTENANCE 10-2
10-3 ACCESSIBILITY 10-2
10-4 IDENTIFICATION AND LABELING 10-3
10-5 INTERCHANGEABILITY 10-3
10-6 STANDARDIZATION 10-3
10-7 SAFETY 10-4
10-8 SERVICING AND LUBRICATION 10-4
10-9 SIMPLIFICATION 10-4
REFERENCES 10-5

CHAPTER 11
HUMAN FACTORS

11-1 INTRODUCTION 11-1
11-2 HUMAN BODY MEASUREMENTS (ANTHROPOMETRY) 11-1
11-3 THE HUMAN BEING AS A SYSTEM COMPONENT 11-5
11-3.1 VISUAL PRESENTATION OF INFORMATION 11-6
11-3.2 SKIN SENSES 11-6
11-3.3 NOISE 11-8
11-4 DESIGN OF CONTROLS 11-8
11-5 DESIGN OF DISPLAYS 11-11
REFERENCES 11-12

APPENDIX A A-1
APPENDIX B B-1
APPENDIX C C-1
GLOSSARY G-1
INDEX I-1

THIS DOCUMENT PROVIDED BY THE ABBOTT AEROSPACE
TECHNICAL LIBRARY
ABBOTTAEROSPACE.COM

LIST OF ILLUSTRATIONS

Figure No	*Title*	*Page*
1-1	M198 Towed Artillery System	1-3
1-2	Family of Separate Loading 155-mm Ammunition	1-4
1-3	Semifixed 105-mm Ammunition	1-5
1-4	M199 Gun Tube and Breech for M198 Howitzer	1-5
1-5	Schematic Diagram of M198 Recoil Mechanism	1-6
1-6	U-Type Cradles	1-7
1-7	O-Type Cradles	1-8
1-8	Top Carriage Structure for M198 Howitzer	1-9
1-9	Tension-Type Pneumatic Equilibrator for M198 Howitzer	1-10
1-10	Elevating Mechanism Schematic for M198 Howitzer	1-11
1-11	Traversing Mechanism With Gear on Top Carriage	1-12
1-12	Panoramic Telescope M1 and Telescope Mount M3	1-12
1-13	M102 Box-Trail 105-mm Howitzer	1-13
1-14	M204 Soft Recoil 105-mm Howitzer	1-14
1-15	Double Recoil Mechanism	1-15
1-16	Elevating Gears	1-15
1-17	Recoil and Reaction Forces	1-16
1-18	Typical Breech Force vs Time Curve	1-17
1-19	Recoil Force System	1-18
2-1	Model of Towed Artillery Preliminary System Design	2-4
2-2	Pressure vs Travel and Tube Design Pressure	2-9
2-3	Breech Force vs Time, 155-mm Howitzer	2-12
2-4	Overpressure vs Muzzle Brake Factor	2-13
2-5	Trapezoidal Recoil Force	2-14
2-6	Schematic of Puteaux Recoil Mechanism	2-15
2-7	Recuperator	2-20
2-8	Cradle Weight vs Recoil Force	2-24
2-9	Elevating and Equilibrator Weight vs Tipping Parts Weight	2-25
2-10	Spade-Float Geometry and Ground Reactions	2-27
2-11	Pressure Distribution on Spades	2-29
2-12	Angles of Approach and Departure	2-30
2-13	Turning Geometry	2-30
2-14	Forces Acting on Weapon During Turning	2-31
2-15	Conventional Recoil Systems	2-33
2-16	Soft Recoil Systems	2-34
2-17	Bottom Carriage Weight vs Recoil Force	2-38
2-18	Top Carriage Weight vs Recoil Force	2-39
2-19	Support Assembly Weight vs Recoil Force	2-40
2-20	Trail Weight vs Recoil Force	2-41
2-21	Suspension System Weight vs Total System Weight	2-42
2-22	Weight of Traversing Mechanism vs Traversing Parts Weight	2-43
3-1	Free-Body Diagram of Recoiling Mass	3-7
3-2	Free-Body Diagram of Cradle	3-9
3-3	Free-Body Diagram of Top Carriage	3-10
3-4	Free-Body Diagram of Nonelevating Mass M_D	3-12
3-5	Equilibrator Demand Curve for M198 Howitzer	3-14
3-6	Schematic Representation of M198 Howitzer	3-15
3-7	Geometry of Elevating Mechanism for M198 Howitzer	3-17

THIS DOCUMENT PROVIDED BY THE ABBOTT AEROSPACE
TECHNICAL LIBRARY
ABBOTTAEROSPACE.COM

LIST OF ILLUSTRATIONS (cont'd)

Figure No	*Title*	*Page*
3-8	In-Battery Position of Recoiling Parts	3-19
3-9	Forces on Recoiling Parts	3-19
3-10	Out-of-Battery Position of Recoiling Parts	3-21
3-11	Breech Force as a Function of Time	3-21
3-12	Breech Force as a Function of Time, Starting From Instant Recoiling Parts Begin to Move	3-21
3-13	2-Degree-of-Freedom Model	3-23
3-14	3-Degree-of-Freedom Artillery Model	3-29
3-15	Free-Body Diagram of Recoiling Parts	3-30
3-16	Free-Body Diagram of Cradle and Recoiling Parts	3-32
3-17	Function y_t vs Time	3-37
3-18	Self-Propelled M110A1 Howitzer	3-40
3-19	Rigid Bodies Connected by a Vector r_p and Rotational Joints	3-42
3-20	Rigid Bodies Connected by a Spring-Damper-Actuator Combination	3-44
4-1	Screw- and Nut-Type Elevating Mechanisms	4-2
4-2	Ball-Screw Device	4-3
4-3	Pinion- and Arc-Type Elevating Mechanisms	4-4
4-4	Elevation Firing Couple Diagram	4-5
4-5	Smith No-Back Device	4-8
4-6	Travel Lock for Elevating Parts	4-10
4-7	Gun Tube Travel Lock	4-11
4-8	Off-Carriage Traverse for M102 Howitzer	4-12
4-9	Pintle Traverse	4-13
4-10	Split Trail Mount Showing Traversing Range	4-14
4-11	Traversing Mechanism With Gear on Top Carriage	4-14
4-12	Manually Operated Traversing Mechanism	4-15
4-13	Powered Traversing Mechanism	4-16
4-14	Screw and Nut Traversing Mechanism	4-16
4-15	Traversing Mechanism for M198 Howitzer	4-17
4-16	Handwheel Force vs Roller Load	4-18
4-17	Traverse Force vs Roller Load	4-19
4-18	Weight Moment Diagram	4-20
4-19	Traverse Firing Couple Diagram	4-21
4-20	Schematic Diagram for Harmonic Drive	4-22
4-21	Antibacklash Device, Tangential Spring Type	4-23
4-22	Antibacklash Device, Axial Spring Type	4-24
4-23	Road Arm Pivot for Firing Base Emplacement	4-25
4-24	Lowering Firing Base	4-26
4-25	Suspension Loads at 6-g Vertical Acceleration	4-26
4-26	Suspension Loads at 3-g Lateral Acceleration	4-26
4-27	Front View of Variable Recoil Assembly	4-27
5-1	Pull-Type Equilibrator	5-5
5-2	Push-Type Equilibrator	5-5
5-3	Chain-Type Equilibrator	5-6
5-4	Spring Equilibrator	5-7
5-5	Torsion-Bar Equilibrator	5-7
5-6	Pneumatic Equilibrator	5-8
5-7	Hydropneumatic Equilibrator	5-8
5-8	Spring-Loaded Hydraulic Reservoir	5-9
5-9	Types of Equilibrators	5-9
5-10	Geometry of Weight Moment of Tipping Parts	5-10
5-11	Equilibrator Geometry Showing Components	5-10

THIS DOCUMENT PROVIDED BY THE ABBOTT AEROSPACE
TECHNICAL LIBRARY
ABBOTTAEROSPACE.COM

LIST OF ILLUSTRATIONS (cont'd)

Figure No	*Title*	*Page*
5-12	Piston Seal Assembly Showing Pressure Distribution and Applied Loads	5-11
5-13	Geometry of Equilibrator Shown Below Trunnions	5-13
5-14	Geometry of Equilibrator Shown Above Trunnions	5-14
5-15	Force-Deflection Curve of a Spring	5-18
5-16	Trend Curve of Total Spring Energy	5-21
5-17	Equilibrator Force Curve	5-21
5-18	Kinematics of Equilibrator; Point B = B(θ) at Elevation θ	5-22
5-19	Free-Body Diagrams	5-23
5-20	Geometry of Spring Equilibrator	5-26
5-21	Geometry of a Typical Pneumatic Equilibrator	5-35
5-22	Geometry for Weight Moment	5-36
5-23	Equilibrator Performance Curves for a Frictionless System	5-39
5-24	Equilibrator Performance Curves Including Friction	5-40
5-25	Two Methods of Applying Pressure in a Cylinder	5-41
5-26	Cylinder Head, Rod End	5-42
5-27	Piston Rod Showing Applied Loads and Moments	5-42
5-28	Cylinder Terminal	5-43
5-29	Loading Diagram of Pin and Bearing	5-43
5-30	Typical Packing Assembly	5-44
5-31	Variable Moment-Arm Adjustment	5-46
5-32	Equilibrator Geometry for Adjustment	5-47
5-33	Approximate Fitting of a Straight Line to a Set of Points	5-49
5-34	Equilibrator Configuration	5-52
6-1	Trunnion Bearing (Antifriction Type)	6-2
6-2	Ball Bushing	6-3
6-3	Contact Area in Ball and Roller Bearings	6-3
6-4	Nomenclature of a Ball Bearing	6-4
6-5	Types of Ball Bearings	6-4
6-6	Types of Roller Bearings	6-5
6-7	Journal-Bearing Friction as a Function of $Z\omega/p$	6-7
6-8	Effect of a Shaft Deflection on Bearing Alignment	6-8
6-9	Pressure Distribution Across Contact Surfaces of Two Cylinders	6-10
6-10	Self-Aligning Roller Bearings	6-11
6-11	Flat-Race Thrust Bearing	6-12
6-12	Self-Aligning Roller Thrust Bearing	6-13
6-13	Large Diameter Traverse Bearing Force Distribution	6-13
6-14	Ball Joint and Follower Traverse Bearing	6-14
7-1	Perspective View of Cradle Structure	7-6
7-2	U-Type Cradle With Attached Recoil Mechanism	7-7
7-3	U-Type Cradle With Integral Recoil Mechanism	7-8
7-4	O-Type Cradles	7-9
7-5	Loads Transmitted to Cradle	7-12
7-6	Equilibrator Attachments, Cantilever Type	7-14
7-7	Equilibrator Attachment, Simple Beam Type	7-15
7-8	External Loads on Cradle for Single Recoil System	7-16
7-9	Elevating Arc	7-18
7-10	Forces Due to Rifling Torque	7-19
7-11	Trunnion Location With Respect to Recoil Forces	7-21
7-12	Load Distribution on Trunnion Structure	7-23
7-13	Load Distribution on Rails, U-Type Cradle	7-26
7-14	End View of Sliding Structure Showing Bearing Liner	7-27

THIS DOCUMENT PROVIDED BY THE ABBOTT AEROSPACE
TECHNICAL LIBRARY
ABBOTTAEROSPACE.COM

LIST OF ILLUSTRATIONS (cont'd)

Figure No	*Title*	*Page*
7-15	Tube Assembly Showing Rails	7-27
7-16	Sleigh With Attached Recoil Cylinders, Gun Tube Secured With Yokes	7-27
7-17	Sleigh With Integral Recoil Cylinders	7-28
7-18	Slide and Guide Showing Assumed Deflections	7-29
7-19	Free-Body Diagram of Cradle Structure (M198)	7-31
7-20	Free-Body Diagram of Cradle Structure and Top Carriage Due to Lifting Loads	7-33
7-21	Trunnion Housing and Cross Section of Cradle	7-38
7-22	Longitudinal Section and Applied Loads on Cradle	7-39
7-23	Loads on Elevating Arc	7-41
7-24	Trunnion Loads and Reactions	7-44
7-25	*M/I* Diagram	7-48
7-26	Free-Body Diagrams of M198 Howitzer Cradle Structure	7-51
7-27	Torque Reaction on Guide Assembly	7-59
7-28	NASTRAN Model 1 for Cradle of M198	7-63
7-29	NASTRAN Model 2 for Cradle of M198	7-64
7-30	NASTRAN Model 3	7-65
8-1	Typical Top Carriage Structure	8-5
8-2	Top Carriage Structure for M198 Towed Howitzer	8-5
8-3	Free-Body Diagram of Top Carriage	8-9
8-4	Segments and Sections for Load Analysis	8-10
8-5	Moment Arms	8-11
8-6	Components of Lifting Force *F* in Lifting Lug Parallel and Perpendicular to Sections	8-12
8-7	Cross Section of Side Frame of Top Carriage for M198	8-19
8-8	Beam Cross Sections	8-29
8-9	Finite Element Model for Beam Elements	8-31
8-10	Finite Element Model for Plate Elements	8-32
9-1	Split Trail Gun Showing Primary Loads	9-4
9-2	Four-Point Contact Ball Bearing	9-5
9-3	Schematic Representation of Soft Recoil XM204 Towed Howitzer	9-5
9-4	Supporting Bracket Installation	9-6
9-5	Equalizing Support	9-7
9-6	Firing Platform	9-7
9-7	M198 Towed Howitzer Bottom Carriage	9-8
9-8	Pedestal	9-8
9-9	Leveling Socket Assembly	9-9
9-10	Leveling Mechanism	9-9
9-11	Bottom Carriage (Main Body) Free-Body Diagram 22.5 deg Traverse	9-14
9-12	Free-Body Diagram for Right Trail	9-15
9-13	Section Properties (Trail) at Section 1	9-18
9-14	Section Properties (Trail) at Sections 2 Through 24	9-19
9-15	Division of Bearing Radius Into 10 Equal Parts	9-20
9-16	Bearing Reaction, Moment	9-22
9-17	Bottom Carriage Maximum Bending Moments (Axis Through One Trail Pin and Firing Pedestal)	9-29
9-18	Bottom Carriage Section Properties at Section 1	9-31
9-19	Bottom Carriage Section Properties at Section 2	9-31
9-20	Bottom Carriage Section Properties at Section 3	9-32
9-21	Bottom Carriage Section Properties at Section 4	9-32
9-22	Bearing Arc Length AB	9-34
9-23	Trail Lugs	9-36
9-24	Lower Lug	9-37

THIS DOCUMENT PROVIDED BY THE ABBOTT AEROSPACE
TECHNICAL LIBRARY
ABBOTTAEROSPACE.COM

LIST OF ILLUSTRATIONS (cont'd)

Figure No	*Title*	*Page*
9-25	Upper Lug	9-38
9-26	Bottom Carriage Trail Lugs	9-39
9-27	Lower Lug as a Curved Beam Fixed at A and B	9-39
9-28	Finite Element Model of Trails (Nodes and Elements)	9-41
9-29	Element Coordinate System for Bar Element	9-41
9-30	Element Coordinate System for QUAD2 Element (Quadrilateral Plate Element)	9-42
9-31	Element Coordinate System for TRIA2 Element (Triangular Plate Element)	9-42
9-32	Top View of Main Body — Finite Element Model (Nodes and Elements)	9-44
9-33	Bottom View of Main Body — Finite Element Model (Nodes and Elements)	9-45
9-34	Top View of Main Body — Finite Element Model (Vertical Plate Elements)	9-46
9-35	Modeling of Connection Between Trails and Main Body	9-46
9-36	Representative Angles Associated With Load-Carrying Grid Points	9-47
9-37	Angles for Calculation of Projected Radii on OA	9-49
9-38	Influence of Relative Density of Sand and Effective Yield Y on Coefficient of Earth Pressure K_φ	9-56
11-1	Maximum Lifting Strengths for Varying Load Locations of Center of Gravity (CG)	11-3
11-2	Maximum Linear Grip Strengths for Various Handle Openings	11-4
11-3	Maximum Mass Lifting Capacity	11-5
11-4	The Human Information Processing System	11-6
11-5	Approximate Limits of Normal Color Differentiation	11-7
11-6	Easily Recognizable Knob Shapes	11-8
11-7	Acceptable Controls for Various Types of System Responses	11-10
A-1	Position Vector of Mass Element	A-4
A-2	Location of Point A in Global System	A-5
A-3	Simplified 2-Degree-of-Freedom Artillery Model	A-8
C-1	Elastic Solid of Arbitrary Shape	C-4
C-2	Some Finite Elements	C-6
C-3	Hollow Rectangular Cantilever Beam	C-7
C-4	Finite Element Models for Hollow Rectangular Beam	C-7
C-5	One-Degree-of-Freedom System (Basic Oscillator)	C-14
C-6	Two-Degree-of-Freedom Model	C-21

THIS DOCUMENT PROVIDED BY THE ABBOTT AEROSPACE
TECHNICAL LIBRARY
ABBOTTAEROSPACE.COM

LIST OF TABLES

Table No.	Title	Page
2-1	Ballistics Data, M198 Howitzer	2-6
2-2	Ballistic Solutions	2-35
2-3	Weapon System Alternatives	2-36
2-4	Weight Tabulation	2-44
2-5	Element Performance Ratings $(PR)_i$	2-46
2-6	Computation of Total Performance Ratings	2-47
4-1	Firing Torque T_f with Maximum Displacement of Trunnion Axis ($a = 15d$, $b = 16d$)	4-6
4-2	Firing Torque T_f with Intermediate Displacement of Trunnion Axis ($a = 7d$, $b = 8d$)	4-6
5-1	Comparative Evaluation of Equilibrators	5-12
5-2	Moment Arm Calculations—Spring Equilibrator Design	5-28
5-3	Weight Moment Calculations—Spring Equilibrator Design	5-28
5-4	Spring Performance Calculations—Pneumatic Equilibrator Design	5-31
5-5	Moment Arm Calculations—Pneumatic Equilibrator Design	5-35
5-6	Weight Moment Calculations	5-36
5-7	Torque Required to Elevate (Friction Not Considered)	5-37
5-8	Data for Least Square Optimization	5-50
5-9	Comparison of Nonlinear Programming Design to Convention Design	5-53
6-1	Composition and Characteristics of Bearing Alloys	6-9
7-1	Summary of F_V, ΣF_V, M_x, M_y, and M^e	7-46
7-2	Data for Computing I_c^e	7-46
7-3	Moments of Areas About Station—0.381 m	7-49
7-4	Cross-Sectional Properties of Cradle Body for M198 Towed Howitzer	7-50
7-5	Forces Acting on Cradle for M198 Towed Howitzer	7-50
7-6	Forces Acting on the Cradle Body for M198 Towed Howitzer	7-52
7-7	Values of M_{ci} and P_i for Case 1	7-54
7-8	Values of M_{ci} and P_i for Case 2	7-55
7-9	Values of M_{ci} and P_i for Case 3	7-55
7-10	Values of M_{ci} and P_i for Case 4	7-56
7-11	Values of M_{ci} and P_i for Case 5	7-56
7-12	Maximum Bending Moments and Maximum Axial Forces	7-56
8-1	Analysis of Equilibrator and Trunnion Loads for Selected Firing Angles	8-15
8-2	Moment Arms to All Sections	8-17
8-3	Moments and Normal Forces Created on All Sections By Lifting Force F For Loading Conditions A and B	8-18
8-4	Maximum Tensile (+) and Compressive (−) Stresses in all Sections of Trunnion Arms Created by Lifting Force Alone	8-20
8-5	Torsional Shearing Stresses for Sections 1, 2, 4, and 10	8-21
8-6	Moments Created by Equilibrator Force on All Sections for Selected Angles of Elevation	8-23
8-7	Maximum Tensile (+) and Compressive (−) Stresses in all Sections Created by Equilibrator Force Alone	8-24
8-8	Sample Tensile Stress Calculations	8-24
8-9	Maximum Tensile (+) and Compressive (−) Stresses in all Sections Created by Lifting and Equilibrator Forces Combined	8-25
8-10	Moments Created by Trunnion Forces on Sections 10-20 For Selected Angles of Elevation	8-26
8-11	Sum of Moments M_E and M_T from Equilibrator and Trunnion Forces on Section 10-20 for Selected Angles of Elevation	8-27
8-12	Maximum Tensile (+) and Compressive (−) Stresses in Trunnion Arms Created by Equilibrator and Trunnion Forces at Selected Angles of Elevation	8-28

THIS DOCUMENT PROVIDED BY THE ABBOTT AEROSPACE
TECHNICAL LIBRARY
ABBOTTAEROSPACE.COM

LIST OF TABLES (cont'd)

Table No	Title	Page
8-13	Maximum Tensile (+) and Compressive (−) Stresses in Sections 10-20 of Trunnion Arms Created by Equilibrator and Trunnion Forces Combined	8-29
8-14	Comparison of Finite Element and Hand Calculations of Stresses Created by the Equilibrator Force Alone	8-34
8-15	Comparison of Finite Element and Hand Calculations of Stresses Created by Lifting and Equilibrator Forces Combined	8-35
8-16	Comparison of Finite Element and Hand Calculations of Stresses Created by Equilibrator and Trunnion Forces Combined	8-36
9-1	Forces on Bottom Carriage for Four Loading Conditions (From dynamic force analysis (traverse = 22.5 deg))	9-15
9-2	Trail Section Properties	9-16
9-3	Maximum Stresses in Trail	9-17
9-4	Portion of B_{RR} or B_{RT} Transmitted to Each Segment	9-21
9-5	Normal Force Distribution Due to B_{RM}	9-24
9-6	Equations for Bending Moment	9-25
9-7	Values of Constants Shown in Bending Moment Equations	9-28
9-8	Bending Moments M_b in Main Body of Bottom Carriage	9-30
9-9	Total Bending Moments (M_b) in Main Body of Bottom Carriage for Sections Beyond $x' = 0.9387$ m	9-30
9-10	Section Properties for Main Body of Bottom Carriage	9-33
9-11	Stresses in Main Body of Bottom Carriage	9-33
9-12	Grid Point Coordinates in Basic Coordinate System	9-43
9-13	Equivalent Distribution of B_{RR} at Grid Points	9-48
9-14	Equivalent Vertical Load Distribution of B_{RT} at Load-Carrying Grid Points	9-49
9-15	Proportion p' of p at Grid Points	9-50
9-16	Representative Arc Lengths for Load-Carrying Grid Points	9-51
9-17	Moment Contributions M' Due to Equivalent Loads at Grid Points	9-51
9-18	Equivalent Grid Point Forces F' due to B_{RM}	9-52
9-19	Total Vertical Load F_V Due to B_{RM} and B_{RT}	9-53
9-20	Nodal Forces for Elevation of 35 Deg	9-53
9-21	Nodal Forces for Elevation of 55 Deg	9-54
9-22	Nodal Forces for Elevation of 75 Deg	9-54
9-23	Comparison of the Results from FEM (Finite Element Method) and Conventional Stress Analysis	9-55
11-1	Maximum Masses Acceptable to Various Percentages of Male and Female Populations While Lifting a 0.48 × 0.34 × 0.14 m Tote Box	11-2
11-2	Maximum Masses Acceptable to Various Percentages of Male and Female Populations While Lowering a 0.48 × 0.34 × 0.14 m Tote Box	11-2
11-3	Human Senses and Energies that Stimulate Them	11-7
11-4	Sound Intensity Levels	11-9
11-5	Conventional Control Movements	11-10
11-6	Recommended Manual Controls Where Force and Range Settings Are Important	11-11
B-1	General Material Properties	B-6

THIS DOCUMENT PROVIDED BY THE ABBOTT AEROSPACE
TECHNICAL LIBRARY
ABBOTTAEROSPACE.COM

LIST OF ABBREVIATIONS AND ACRONYMS

ANSI = American National Standards Institute
CL = centerline
DADS = dynamic analysis and design system
DMAP = direct matrix abstract program
DRAM = Dynamic Response of Articulated Machinery
EFC = effective full-charge
FEM = finite element method
HE = high explosive
IMP = Integrated Mechanism Program
IMSL = International Mathematical and the Statistical Library
MIL-STD = military standard
NASTRAN = NASA Structural Analysis
QE = quadrant elevation
R&D = research and development
rms = root mean square

THIS DOCUMENT PROVIDED BY THE ABBOTT AEROSPACE
TECHNICAL LIBRARY
ABBOTTAEROSPACE.COM

CHAPTER 1
INTRODUCTION

This chapter defines the purpose and scope of the handbook. The elements of a towed artillery system are defined; their functions and the interfaces between subsystems are discussed. Variations in configuration of a towed artillery system employing the soft recoil principle of operation and full 360-deg off-carriage traverse are discussed. Methods used to analyze the dynamics of towed systems and the role of dynamic models in system design are introduced. The use of dynamic models for load analysis, recoil mechanism design, and weapon stability analysis is discussed and illustrated.

1-0 LIST OF SYMBOLS

$B(t)$ = breech force, N
F_g = propellant gas force, N
g = acceleration due to gravity, m/s^2
I = impulse of breech force, N·s
J = polar moment of inertia of weapon about spade, kg·m^2
K_0 = constant recoil force, N
$K(t)$ = recoil force, N
k_G = spring rate of soil at firing base, N/m
L = length of recoil, m
M_r = mass of recoiling parts, kg
t = time, s
t_1 = time over which breech force acts, s
t_r = recoil stroke time, s
W = weapon weight, N
W_r = weight of recoiling parts, N
x = position of recoiling parts. m
$\dot{x}$ = recoil velocity, m/s
y_{CG} = horizontal distance from spade to weapon center of gravity, m
y_G = horizontal distance from spade to firing base, m
y_T = horizontal distance from spade to trunnion, m
z_T = trunnion height, m
θ = angle of elevation, rad
ϕ = pitch angle of weapon, rad

1-1 PURPOSE

The purpose of this handbook is to present and illustrate design methods for towed artillery systems and their components. Towed systems are artillery weapons transported by prime movers that are separate from the artillery weapon. Towed artillery systems are capable of emplacement, delivery of fire, and displacement by a field artillery crew. The towed artillery weapon system consists of

1. Ammunition
2. Tube and breech
3. Recoil mechanism
4. Carriage structures
5. Mechanisms allowing for elevation, traverse, and emplacement
6. Fire control equipment

THIS DOCUMENT PROVIDED BY THE ABBOTT AEROSPACE
TECHNICAL LIBRARY
ABBOTTAEROSPACE.COM

7. Travel gear
8. Prime mover.

Design of ammunition, tube and breech, recoil mechanism, fire control equipment, and prime mover are treated in related handbooks. The component designs of the remaining weapon subsystems are discussed in this handbook. Also system design, including tradeoffs among the various subsystems comprising the towed artillery system, is treated in this handbook together with tradeoff considerations involving components and subsystems that are treated in the related design handbooks.

Towed artillery system design and integration are defined as the process of meeting the requirements for towed artillery weapon systems within both user-imposed and technological constraints. Inputs to system design are provided by user requirements on range, payload, precision, rate of fire, weapon versatility, level of invulnerability, allowed weight, airdrop, transportability, durability, reliability, maintainability, and other pertinent demands placed on the weapon system. Human factors considerations, technological constraints, weapon-soil interaction, and other related constraints play an important role in creating a suitable design. Although a great deal of effort during development of a towed artillery weapon system is devoted to component design and development, it is important that the system designer pay careful attention to system level tradeoffs and interfaces among the components of the artillery system.

One of the basic functions of system design is selection of a principle of operation of the towed artillery weapon. In this principle such alternatives as conventional hydropneumatic versus soft recoil mechanisms, on-carriage versus off-carriage traverse, use of muzzle brake, and use of ground-anchoring techniques are considered. In conjunction with component design specialists, the artillery system engineer must

1. Select candidate components and subsystems that offer the potential for meeting system requirements and constraints.
2. Create a system model that reflects component performance and limitations.
3. Use system models to define component and subsystem performance requirements and carry out tradeoff analysis that guides design of components.

These system design activities dominate the preliminary design phase of an artillery system and must continue throughout development of the entire weapon system.

Examples of system level considerations that influence component design are user requirements on emplacement time, traversing capability, and soil conditions on which the weapon must be capable of operating. These requirements may determine the acceptability of using stakes and spades as ground anchors and lead to the selection of a conventional hydropneumatic or a soft recoil mechanism, and—after considering the inherent advantages of each—the loads that must be transmitted to ground and the system weight. Basic tradeoffs must often be developed for competing design approaches and negotiations entered into with the user community in order to arrive at decisions leading to subsystem selection and specific design requirements.

The scope of this handbook includes both system level design and detailed design of mechanisms, equilibrators, bearings, cradles, and carriages. Preliminary design and tradeoff analysis is presented and includes considerations of ammunition, tube and breech, recoil mechanism, fire control equipment, human factors, and other components comprising the artillery weapon. System kinematic and dynamic modeling methods are presented and used in system level tradeoff determination and in the definition of component load-carrying requirements. The results of preliminary system design and tradeoff analysis provide the basis for the discussion of the detailed design of mechanisms, equilibrators, bearings, cradles, and carriages. Design for strength is a major consideration in virtually all component designs presented in this handbook. Classical mechanics of material approaches to stress analysis and the more modern finite element method of stress analysis are used in design of components. The designer is also required to satisfy all military specifications and standards applicable to the component designed. A wide range of mechanical design techniques and technologies are involved in system and component design.

1-2 ELEMENTS OF TOWED ARTILLERY SYSTEMS

The M198, 155-mm towed artillery system shown in Fig. 1-1 is typical of modern towed artillery systems. This air transportable system is the most modern towed artillery system developed through the 1970s and uses conventional artillery design technology and lightweight construction techniques. It is used in this paragraph to illustrate the major components that comprise the towed artillery system.

THIS DOCUMENT PROVIDED BY THE ABBOTT AEROSPACE
TECHNICAL LIBRARY
ABBOTTAEROSPACE.COM

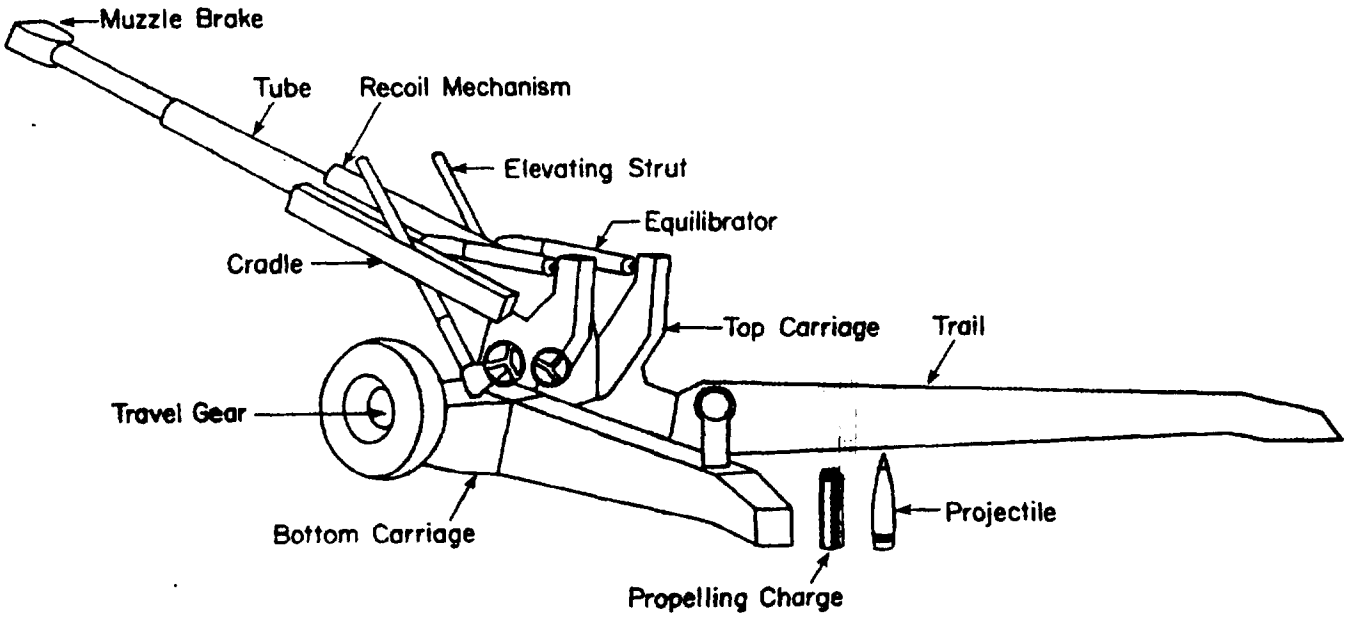

Figure 1-1. M198 Towed Artillery System

1-2.1 SUBSYSTEMS COMPRISING A TOWED ARTILLERY SYSTEM

The principal subsystems of a towed artillery system, such as that shown in Fig. 1-1, are

1. Ammunition
2. Tube and breech
3. Recoil system
4. Cradle
5. Top carriage
6. Bottom carriage
7. Equilibrator
8. Elevating mechanism
9. Traversing mechanism
10. Fire control equipment
11. Travel gear
12. Prime mover.

Except for variations in towed artillery system design employing soft recoil and some designs employing off-carriage traverse, these subsystems are universally employed in towed artillery systems. Some variations in system design that involve slightly different subsystem composition are discussed in par. 1-2.2. In order to be precise in subsequent detailed design discussions, definitions of the subsystems are presented in the paragraphs that follow.

1-2.1.1 Ammunition

Ammunition for a towed artillery system consists of a family of rounds of varying zone charge and projectile type. Fig. 1-2 shows propelling charges and a variety of projectiles employed in a 155-mm towed artillery weapon system. Propelling charges vary from Zone 1 through Zone 8, with progressive increases in propelling charge and muzzle velocity. Projectiles fired from the 155-mm towed system include conventional high explosive (HE), a family of submunition cargo rounds, a guided projectile, and nuclear projectiles. This family of ammunition is separate loading, which means that the projectile is first inserted into the tube and rammed into the forcing cone and the propelling charge is loaded separately into the chamber. A primer that ignites the propelling charge is inserted separately into the breechblock.

This variety of charges and projectile types must be considered in artillery system design because of (1) the variability of the breech force associated with each and (2) the requirement for the weapon to fire each of the

THIS DOCUMENT PROVIDED BY THE ABBOTT AEROSPACE
TECHNICAL LIBRARY
ABBOTTAEROSPACE.COM

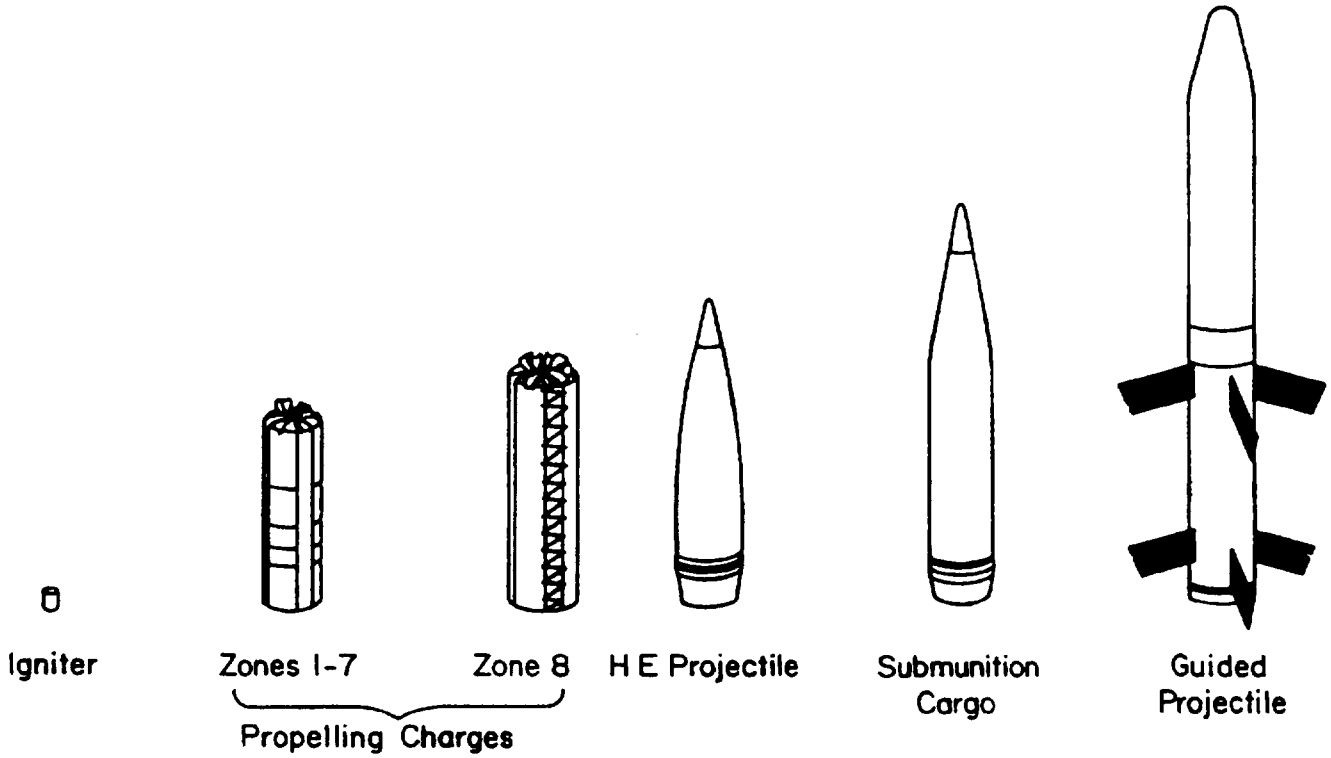

Figure 1-2. Family of Separate Loading 155-mm Ammunition

rounds of ammunition in the family with acceptable performance of the recoil mechanism and stress levels in all components of the system. In addition to force input considerations, ammunition handling considerations play a key role in the design of a towed artillery system because the weapon must be served by a field artillery crew. The weight of projectiles and the desired rate of fire of the system play an important role in determining the kind of ammunition handling equipment that must be designed as part of the towed system. For example, for 155-mm systems with projectiles weighing about 445 N, manual insertion and ramming of the projectile in the chamber is not generally practical. Therefore, a loading tray and auxiliary ramming equipment must be considered. Thus human factors considerations play a crucial role in determining a rate of fire that can be achieved with a large caliber weapon, and these factors dictate the design of ammunition handling equipment that is part of the towed artillery system.

In contrast to the separate loading ammunition generally employed in large caliber systems, semifixed ammunition is employed in 105-mm systems. Fig. 1-3 shows the semifixed ammunition employed in the current versions of US Army 105-mm artillery. Since the 105-mm projectile weighs about 140 N, the entire projectile and propelling charge can be incorporated in a single package that can be handled, loaded, and rammed into the weapon chamber. This feature leads to substantially higher rates of fire than can be achieved with large caliber weapons. As intermediate calibers are considered, the human factors aspect of the ability of a crew to handle a semifixed round must receive careful consideration. Semifixed ammunition generally is packaged with the highest zone charge. Charge increments are removed prior to loading to achieve a round of ammunition with a lower charge. The primer for semifixed ammunition is contained in the cartridge case; accordingly, no separate provision needs to be made for primer insertion into the breechblock.

For details concerning ammunition characteristics and design, refer to Refs. 1-4.

1-2.1.2 Tube and Breech

The tube and breech assembly consists of the tube, the breech ring, the breechblock, and, in many cases, the muzzle brake, which is attached to the tube. The breech ring contains interrupted threads or a wedge guide to allow locking of the breechblock to provide a seal for the chamber during firing. Also a breech closing and locking mechanism is required to allow the crew to open and close the breech and to accomplish the locking

THIS DOCUMENT PROVIDED BY THE ABBOTT AEROSPACE
TECHNICAL LIBRARY
ABBOTTAEROSPACE.COM

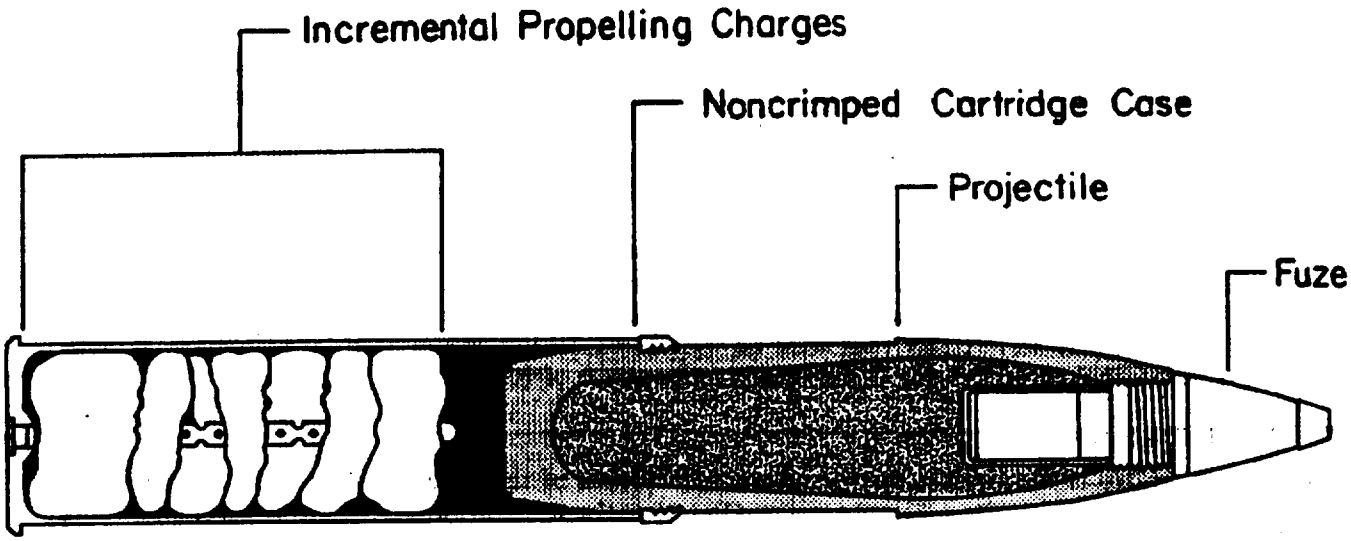

Figure 1-3. Semifixed 105-mm Ammunition

function. The space required for carrying out these functions must be carefully considered in design of the towed system. Human factors considerations are required concerning the ability of the crew to exert forces of the required level to carry out the functions of breech closure, locking, and unlocking. Fig. 1-4 shows the tube and breech for the M198 weapon system, which employs an interrupted thread screw breechblock with a thermal warning device.

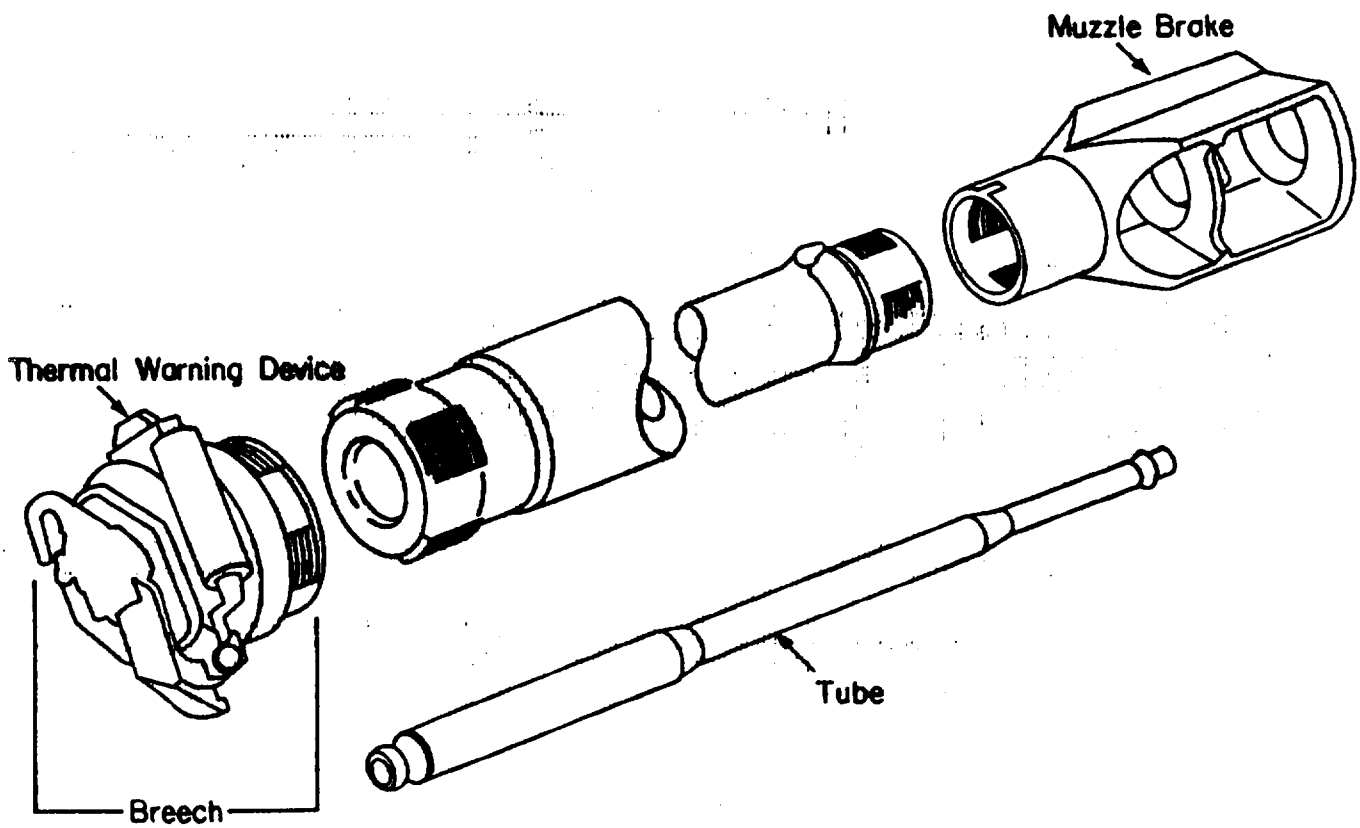

Figure 1-4. M199 Gun Tube and Breech for M198 Howitzer

THIS DOCUMENT PROVIDED BY THE ABBOTT AEROSPACE
TECHNICAL LIBRARY
ABBOTTAEROSPACE.COM

The muzzle brake, if used, is attached to the muzzle of the tube to provide a reduction—by deflecting propellant gases as they exit the tube—in the impulse delivered to the recoiling parts during firing. The efficiency of a muzzle brake must be determined during system design, considering the blast overpressure levels that can be tolerated by the artillery crew and also meet the requirements as specified in Military Standard (MIL-STD) 1474 (Ref. 5). Muzzle brake efficiency and its effect on recoil mechanism design and dynamics are considered in Ref. 6, details of muzzle brake design may be found in Ref. 7, and details on tube and breech design are found in Refs. 8 and 9, respectively.

Although selection of tube rifling twist is dictated by ammunition design, the twist selected plays a role in the design of the sliding bearings required to allow recoil motion between the recoiling parts and the cradle of the weapon, and in design of trunnion bearings. The torque exerted on the projectile by the tube must be resisted by these bearings to provide an interface that must be considered during design of a towed artillery system. Design of the translational recoil bearing is discussed in Chapter 6 of Ref. 6.

1-2.1.3 Recoil System

The recoil mechanism is the subsystem that allows for motion of the recoiling parts and generates the retarding force required to bring these parts to rest and to return them to the battery position during the firing cycle. A schematic of the M198 hydropneumatic recoil mechanism is shown in Fig. 1-5. Fluid throttling through a variable area orifice is employed to generate the retarding force required to bring the recoiling parts to rest after the round is fired. A nitrogen gas recuperator stores energy during the recoil cycle and provides the needed thrust to propel the recoiling parts forward to the in-battery position during the counterrecoil cycle.

The recoil system is the most critical of the towed artillery subsystems with regard to system integration. Selection of the recoil length, recoil force level, and the type of recoil and counterrecoil system dictates force levels that are encountered by other subsystems and the layout of the weapon system to provide free space for recoil and stability of the weapon system. Detailed design considerations for recoil systems may be found in Ref. 6, which presents both preliminary design techniques of importance in towed artillery system design and detailed recoil mechanism design data and techniques.

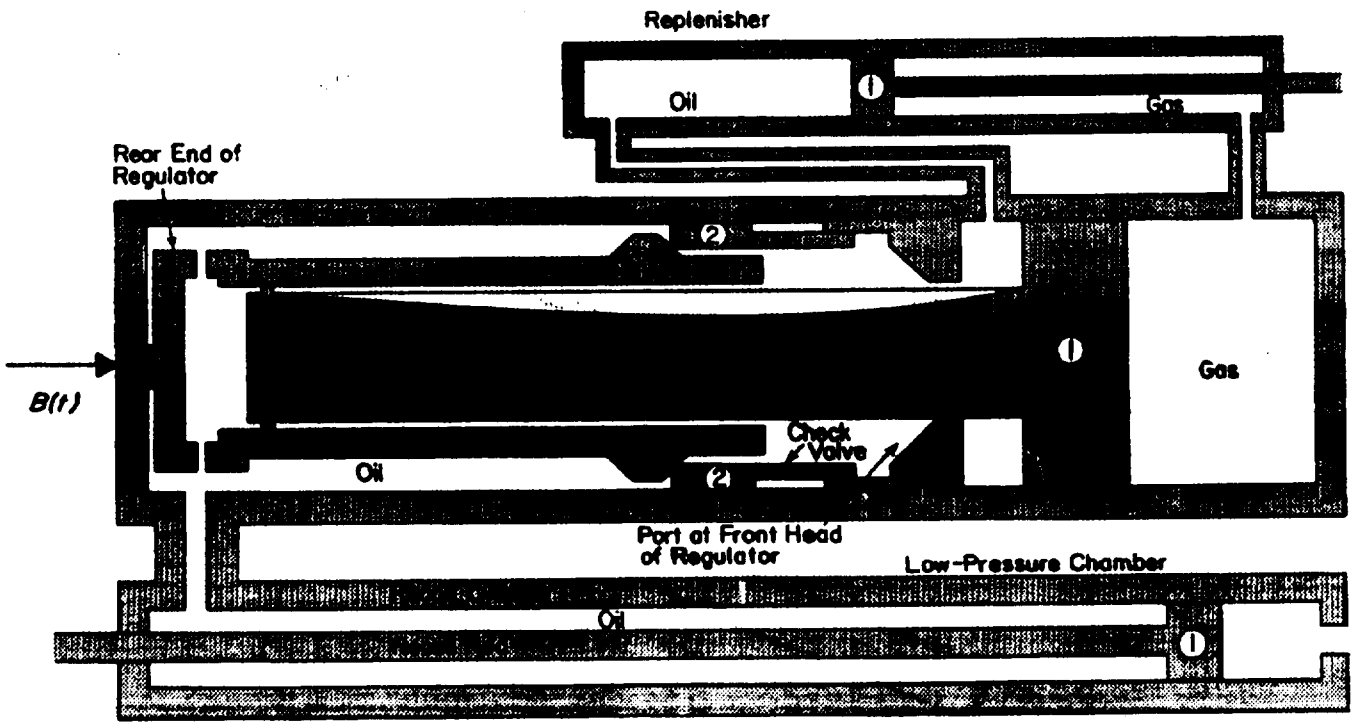

Figure 1-5. Schematic Diagram of M198 Recoil Mechanism

THIS DOCUMENT PROVIDED BY THE ABBOTT AEROSPACE
TECHNICAL LIBRARY
ABBOTTAEROSPACE.COM

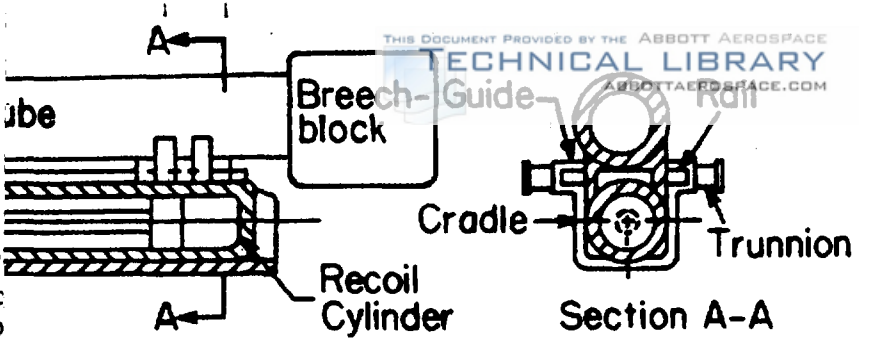

1-2.1.4 The c
gun tub
of the v
Ther
Details
steel or
lightwe
Othe
equilibr
attache
whethe
mechar
The
membe
at the f
The
airdrop
the wea

le With Attached Recoil Mechanism

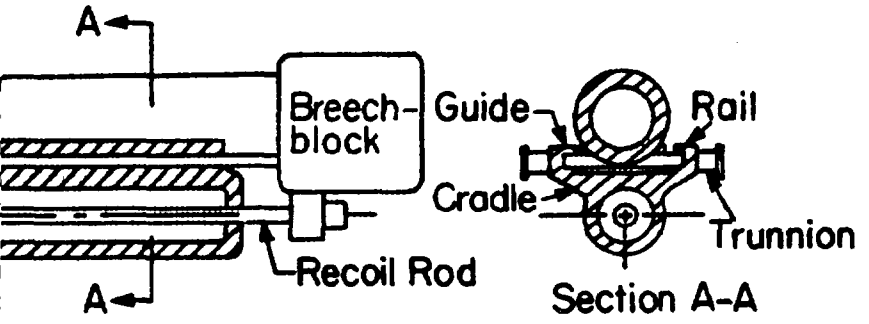

le With Integral Recoil Mechanism

1-2.1.5 The t
trunnio
structu
the top

Figure 1-6. U-Type Cradles

Crad

ire of the tipping parts that pivots about the trunnion and supports the
il. The angle between the cradle and top carriage controls the elevation
the top carriage to orient the gun tube in azimuth.
uction for the cradle, the U-type (Fig. 1-6) and the O-type (Fig. 1-7).
is and design are presented in Chapter 7. Cradles are fabricated of alloy
gs, forgings, or weldments are used to form the basic structure. For
alloy or a composite material may be preferable.
cradle are the recoil mechanism, trunnions, elevating mechanism, and
il mechanism are attached to the cradle, and the movable portions are
nnions are considered to be components of the cradle, regardless of
ed on the side frames of the top carriage or on the cradle. The elevating
arriage and cradle to control the elevation of the weapon.

Rail m is a U-shaped aluminum weldment with box sections as structural
ed at the rear of the cradle arms. The gun tube slides through a bearing
rails slide through guides attached to each side of the cradle.
thstand firing load, transit loads, and shock loads generated during
sible to reduce deflection of the structure, which affects the precision of

rting structure for the cradle. It supports the tipping parts through the
ing loads from the cradle to the bottom carriage or other supporting
ators and houses the elevating and traversing mechanisms. In traverse

e

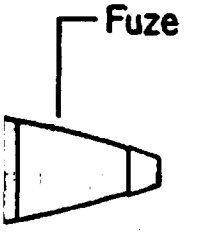

n design of the
exert forces of
shows the tube
chblock with a

roke

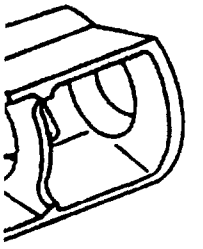

THIS DOCUMENT PROVIDED BY THE ABBOTT AEROSPACE
TECHNICAL LIBRARY
ABBOTTAEROSPACE.COM

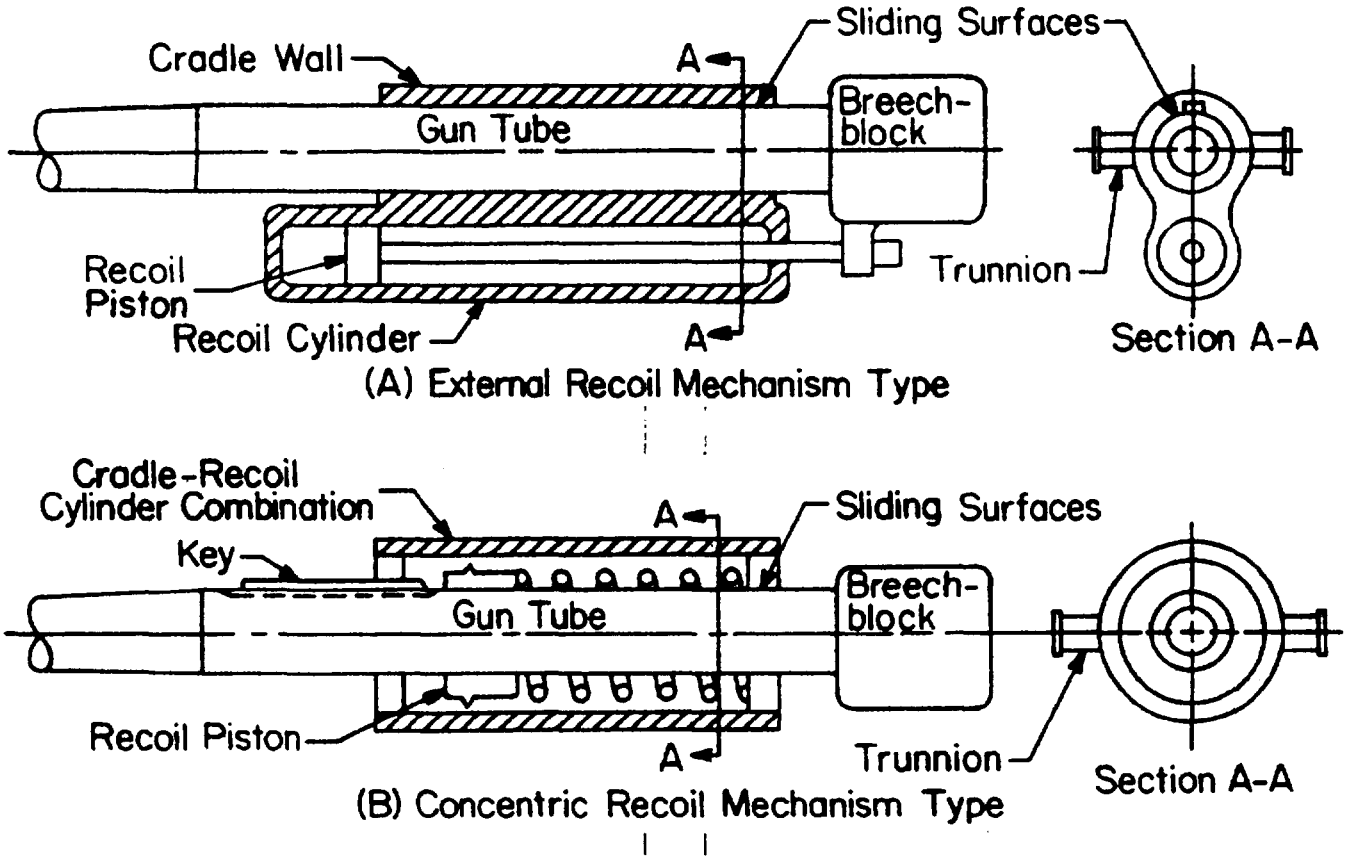

Figure 1-7. O-Type Cradles

Fig. 1-8 shows a typical top carriage structure. Variations in the geometry of the top carriage structure should be expected for different weapon systems. These are necessary to accommodate other equipment associated with the top carriage. The equipment associated with the top carriage are equilibrators, elevating mechanisms, and traversing mechanisms. Design of top carriage structure is discussed in Chapter 8.

The top carriage generally is made of steel, although aluminum alloys have been used in modern weapons to achieve a light weight. The structure may be fabricated by forging, casting, or welding. Weldments are generally cheaper and can be fabricated in a relatively shorter time because commercially available stock may be used. The top carriage of the M198 system, for example, is made by welding aluminum box sections.

1-2.1.6 Bottom Carriage

The bottom carriage is the part of the weapon which supports the top carriage, provides the pivot for the traversing parts, and contains the ground anchors. The bottom carriage and its components—including wheels, trails, and outriggers—provide the structural foundation for the weapon. When emplaced and during firing, the bottom carriage transmits carriage loads to the ground. During transit it may become the chassis for the vehicle.

The bottom carriage for a weapon system can have one of several different types of construction. For example, for the 155-mm M198 Howitzer, shown in Fig. 1-1, the bottom carriage consists of a main body with a firing base and hinges, which provide connections with the split trails. Each trail is made of a box section. The firing base is lowered to the ground for emplacement and firing of the weapon. Some bottom carriages consist of only a firing base or firing platform. This arrangement for the bottom carriage allows for 360-deg off-carriage traverse of the weapon.

The bottom carriage could be a casting, forging, or a weldment made of steel or an aluminum alloy. The main body carriage for the M198 system is a KO-1 aluminum alloy casting. The KO-1 aluminum alloy contains silver, manganese, magnesium, titanium, and copper. This aluminum alloy is as strong as steel but is more desirable due to its light weight. For appropriate strength specifications, see Ref. 10.

THIS DOCUMENT PROVIDED BY THE ABBOTT AEROSPACE
TECHNICAL LIBRARY
ABBOTTAEROSPACE.COM

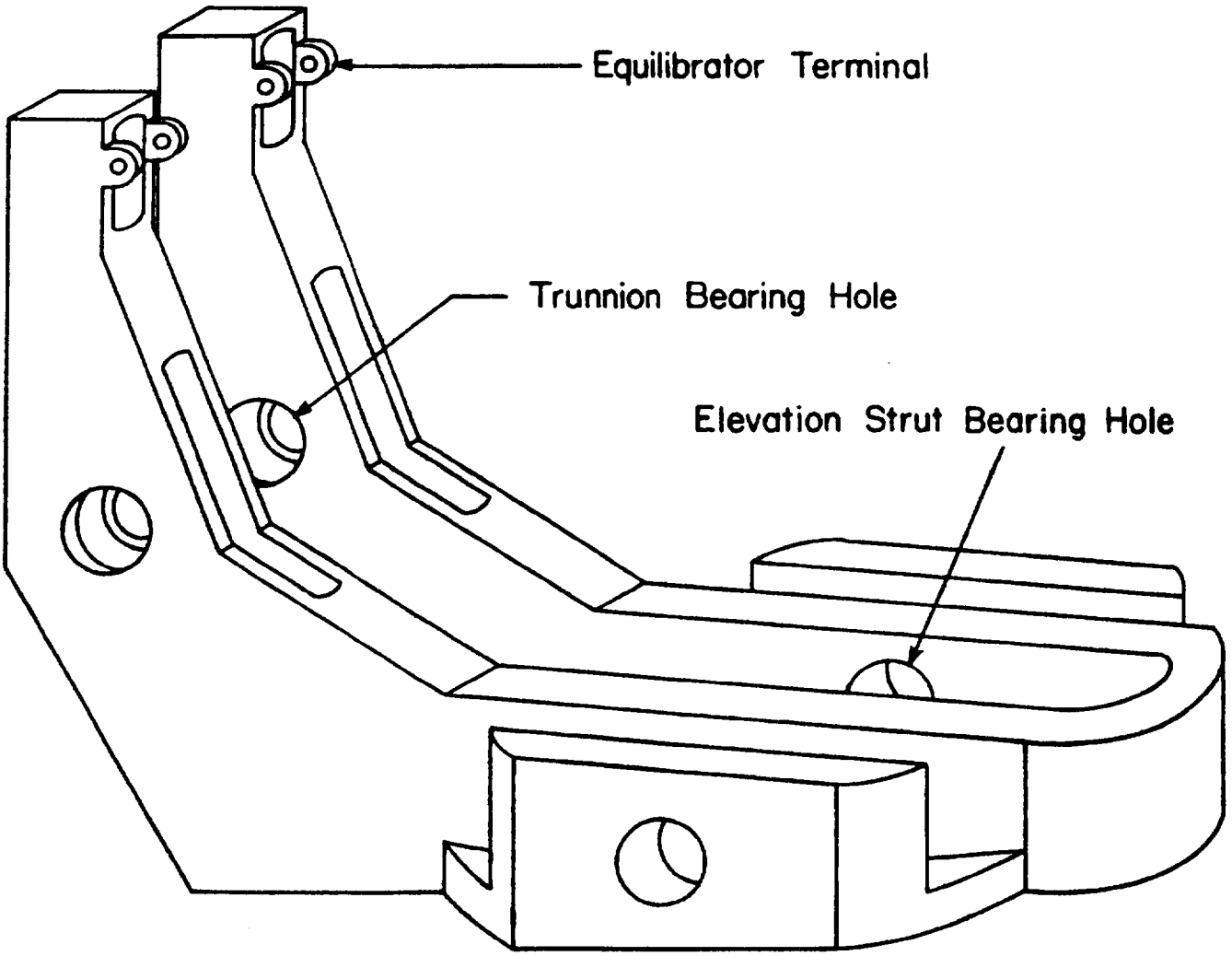

Figure 1-8. Top Carriage Structure for M198 Howitzer

1-2.1.7 Equilibrator

The equilibrator is a force-producing mechanism that provides the moment needed to counterbalance the moment generated by the muzzle preponderance of the tipping parts about the weapon trunnion. The equilibrator acts between the cradle and top carriage, and it generates a force that places the tipping parts approximately in equilibrium throughout the extremes of elevation of the tipping parts. With a properly designed equilibrator, the torque input requirements at the elevating handwheel are such that the crew can elevate and depress the weapon with moderate effort.

A schematic diagram of the M198 equilibrator is shown in Fig. 1-9. This equilibrator is of the pneumatic type, i.e., the force is generated by compressed nitrogen gas. For small caliber weapons, a mechanical spring equilibrator is often adequate; however, for large caliber weapons with a large moment imbalance about the trunnion, pneumatic equilibrators are generally more effective. The equilibrator attachment points on the cradle and top carriage play an important role in determining the effectiveness of the equilibrator and play a key role in system design.

1-2.1.8 Elevating Mechanism

The elevating mechanism is composed of a handwheel, gearing, and structural components that precisely control the elevation angle between the cradle and top carriage. Modern towed artillery elevating mechanisms

THIS DOCUMENT PROVIDED BY THE ABBOTT AEROSPACE
TECHNICAL LIBRARY
ABBOTTAEROSPACE.COM

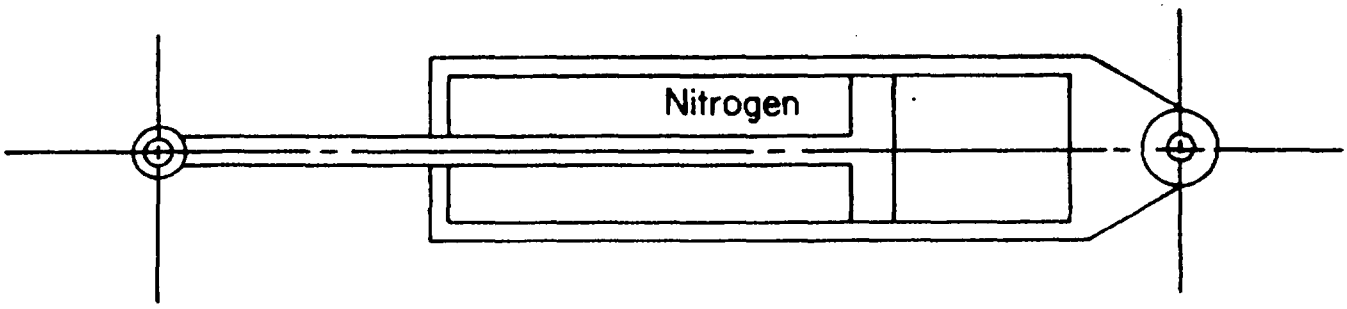

Figure 1-9. Tension-Type Pneumatic Equilibrator for M198 Howitzer

employ an elevating strut that operates between the top carriage and cradle to control the rotation of the cradle about the trunnion.

The elevating mechanism employed in the M198 Howitzer is shown in Fig. 1-10. It includes a no-back device, a mechanical clutch in the case of the M198, that precludes torque feedback to the handwheel during firing. Gearing design must be carried out to provide a high degree of precision in location of the tipping parts and often requires the incorporation of springs within the gearing system to prevent extreme loads on precision gears during firing and the associated high loads that are transmitted through the weapon support structure. Consideration must also be given to eliminating backlash or to providing for a preloading on the gear system in a direction that precludes free motion of the tipping parts during the in-bore period, which would degrade precision.

1-2.1.9 Traversing Mechanism

The traversing mechanism consists of a handwheel and gearing which precisely controls azimuth of the top carriage with respect to the bottom carriage, hence orienting the gun tube in azimuth.

A schematic traversing mechanism is shown in Fig. 1-11. Gearing, with the incorporation of a no-back device to prevent feedback of torque through the traversing handwheel, is required to carry out the traversing function. Torque requirements on the no-back device for the traversing mechanism are generally less severe than in the case of elevation in which moments may occur during firing.

1-2.1.10 Fire Control Equipment

Fire control for a towed artillery system includes a telescope, a ground-based reference, and azimuth and elevation readouts located on the weapon. This equipment provides a reference for the crew as to the actual elevation and azimuth of the tube. Elements of the fire control subsystem for the M198 towed artillery system are shown in Fig. 1-12; design of this equipment is discussed in Ref. 11. Its location on the towed artillery system and its attachment to the top carriage and cradle are important considerations in system design. The location of the equipment, to allow ready access by the crew in order to assure accurate positioning of the top carriage and cradle, is a human factor that must be given careful consideration.

1-2.1.11 Travel Gear

Travel gear for a towed artillery system includes wheels, tires, wheel bearings, and a mechanism for raising the wheels to lower the firing base of the bottom carriage to the ground in preparation for a fire mission and to elevate the bottom carriage off the ground when displacing the weapon and preparing for travel. The wheels and travel gear for the M198 Howitzer are shown in Fig. 1-1. Principal design considerations for the travel gear concern selection of tires and wheel bearings suitable for loads encountered during travel and in the design of lowering and raising mechanisms that allow the crew to emplace and displace the weapon.

1-2.2 VARIATION IN SUBSYSTEM CONFIGURATIONS

The subsystems discussed in par. 1-2.1 are those normally employed in a towed artillery weapon system. There are towed system configurations, however, that involve substantial differences in design approach for some subsystems. The most substantial variation involves off-carriage traverse, as used in the M102 and M204

THIS DOCUMENT PROVIDED BY THE ABBOTT AEROSPACE
TECHNICAL LIBRARY
ABBOTTAEROSPACE.COM

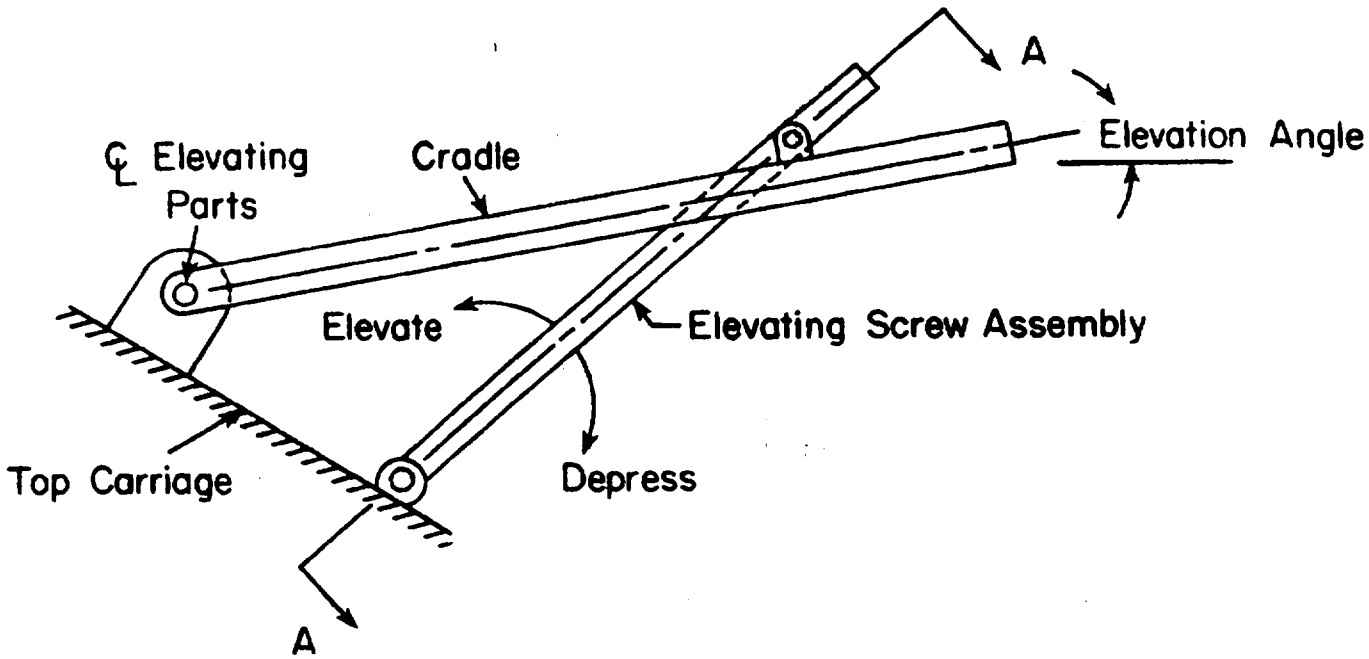

(A) Side View

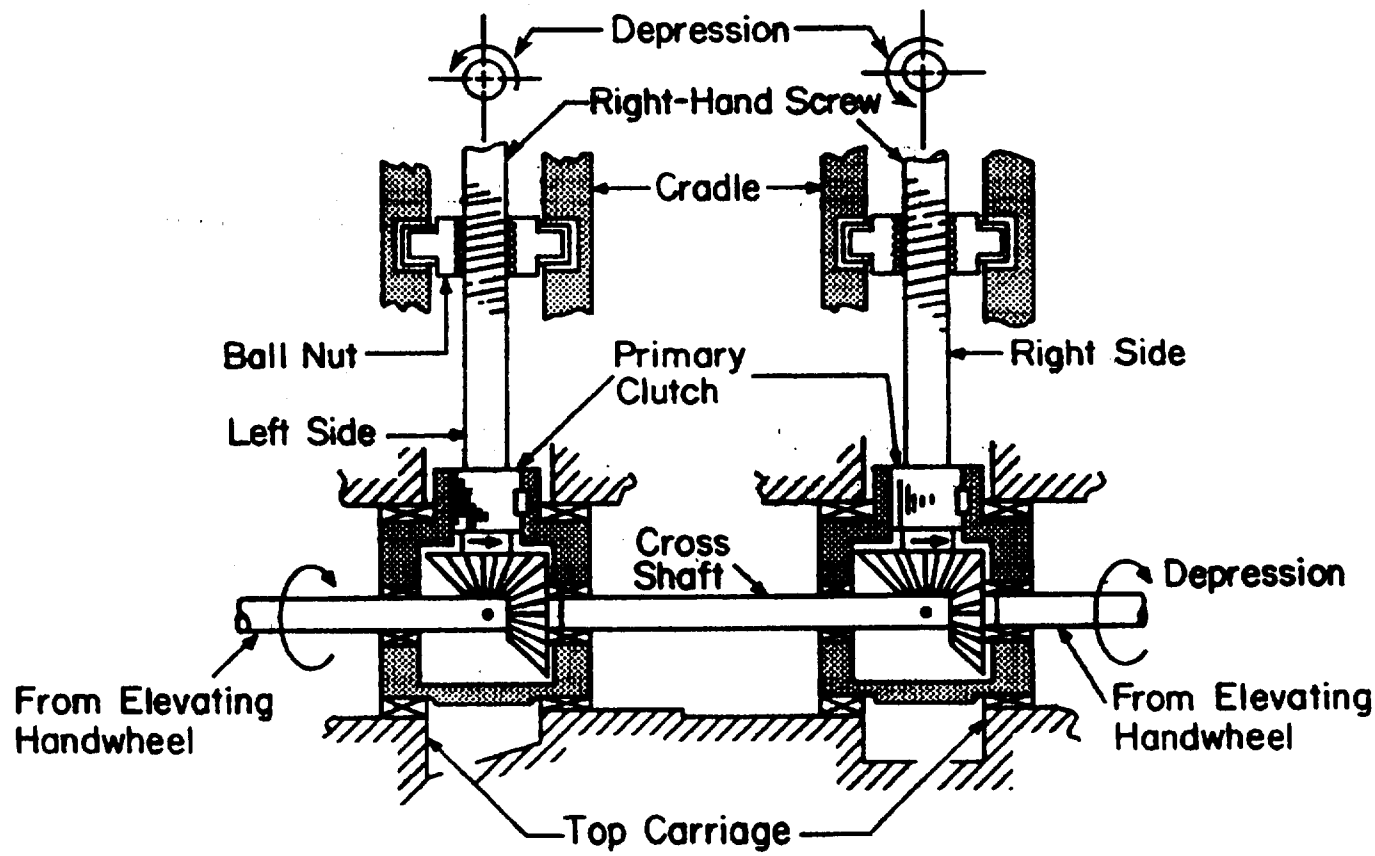

(B) Section A-A

Figure 1-10. Elevating Mechanism Schematic for M198 Howitzer

THIS DOCUMENT PROVIDED BY THE ABBOTT AEROSPACE
TECHNICAL LIBRARY
ABBOTTAEROSPACE.COM

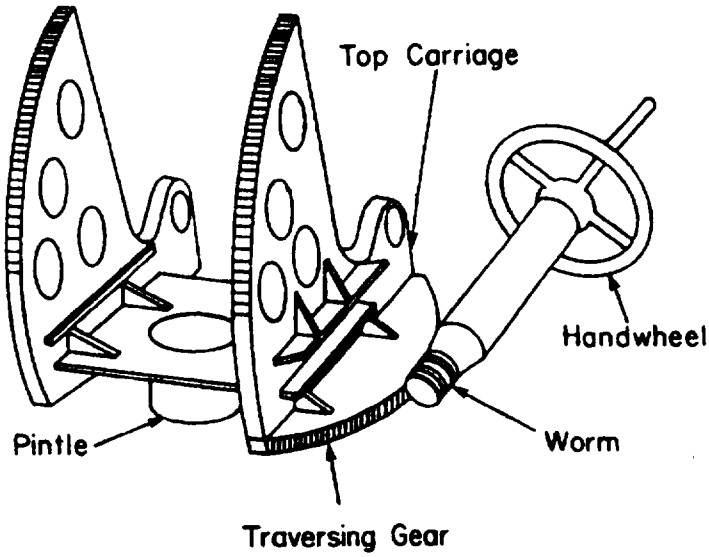

Figure 1-11. Traversing Mechanism With Gear on Top Carriage

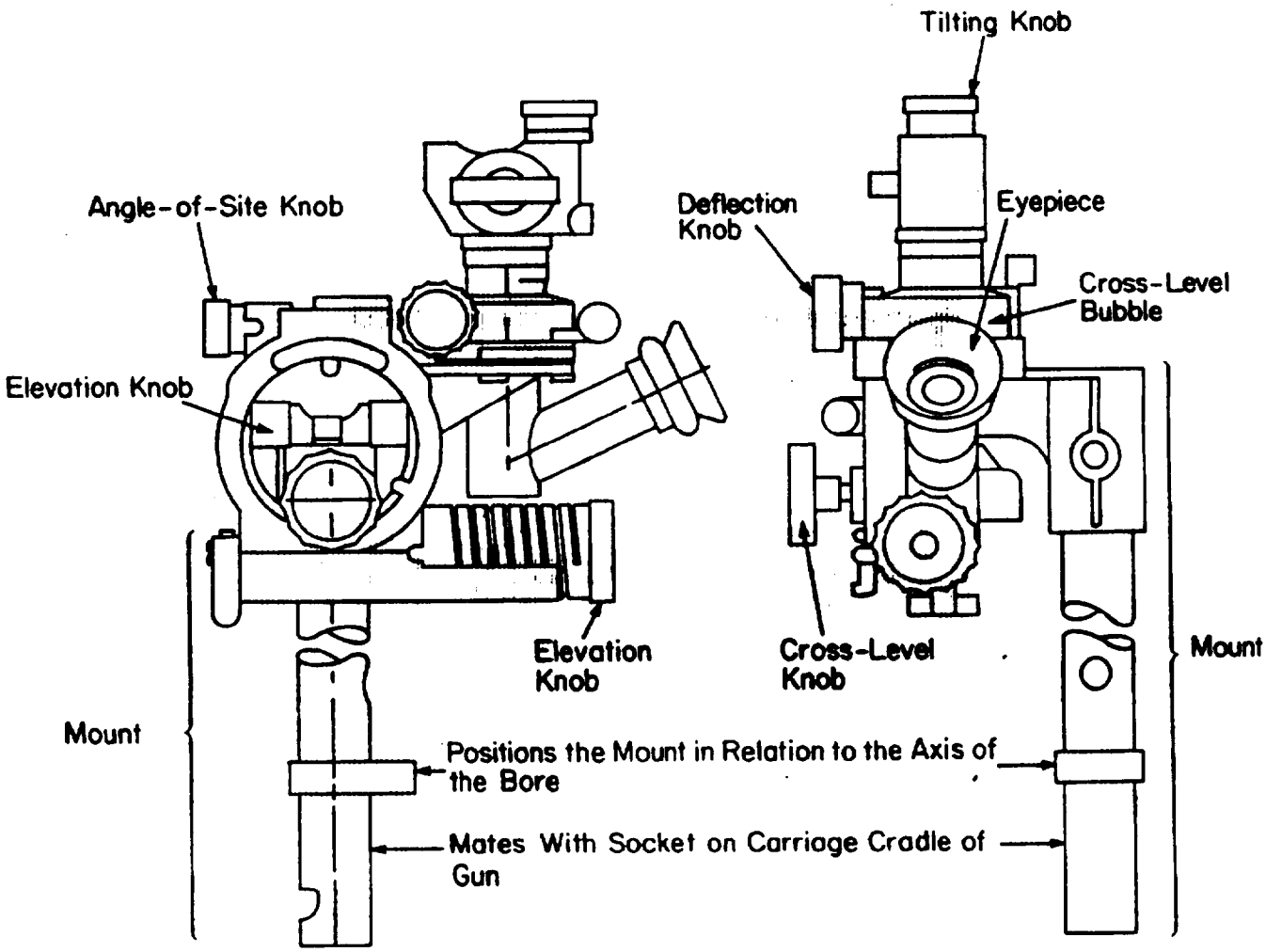

Figure 1-12. Panoramic Telescope M1 and Telescope Mount M3

THIS DOCUMENT PROVIDED BY THE ABBOTT AEROSPACE
TECHNICAL LIBRARY
ABBOTTAEROSPACE.COM

Howitzers, which are shown in Figs. 1-13 and 1-14, respectively. These systems are designed to provide for 360-deg traverse capability by making ground contact directly with the top carriage, which has large, ground-bearing rollers to provide weapon stability. In such a configuration, only the firing base makes contact with the ground and performs the function of the bottom carriage.

The M102 uses a wishbone box-trail configuration, shown in Fig. 1-13, in which a single roller makes contact with the ground and provides pitch stability for the weapon. Lateral stability is provided by a ball joint and follower bearing between the top carriage and firing base. This mechanism is discussed in par. 6-3.3.

The M204 soft recoil howitzer shown in Fig. 1-14 also provides a full 360-deg traverse capability, but it has trails with two ground-bearing rollers forward of the firing base. The basically different principle of recoil mechanism operation also implies substantial differences in the approach used to design the subsystem. The soft recoil mode of operation accelerates the recoiling parts forward prior to firing. The firing impulse drives the recoiling parts rearward, and the firing cycle ends in the full rear position. As will be explained in par. 1-3, this principle of operation is capable of an approximate factor of 4 reduction in peak recoil load and a substantially faster firing cycle than that of conventional recoil mechanisms. Thus structural components are required to carry much lower recoil loads, and ground anchoring is readily accomplished. The soft recoil mechanism, however, creates unique new design requirements—misfire buffers at the forward end of the recoil travel stroke and overshoot buffers at the rear of the stroke—to prevent damage in the case of cookoff or zone setting errors.

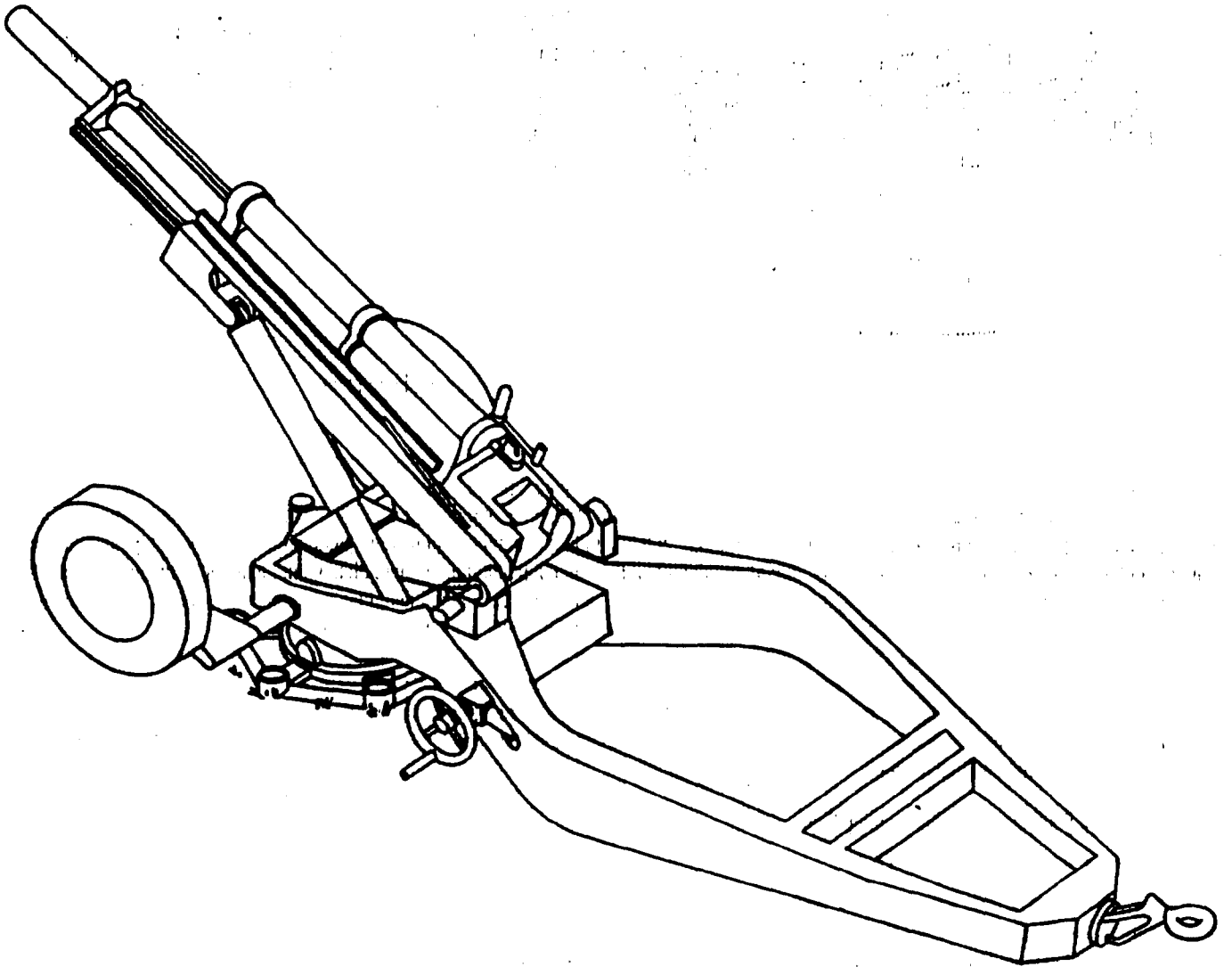

Figure 1-13. M102 Box-Trail 105-mm Howitzer

THIS DOCUMENT PROVIDED BY THE ABBOTT AEROSPACE
TECHNICAL LIBRARY
ABBOTTAEROSPACE.COM

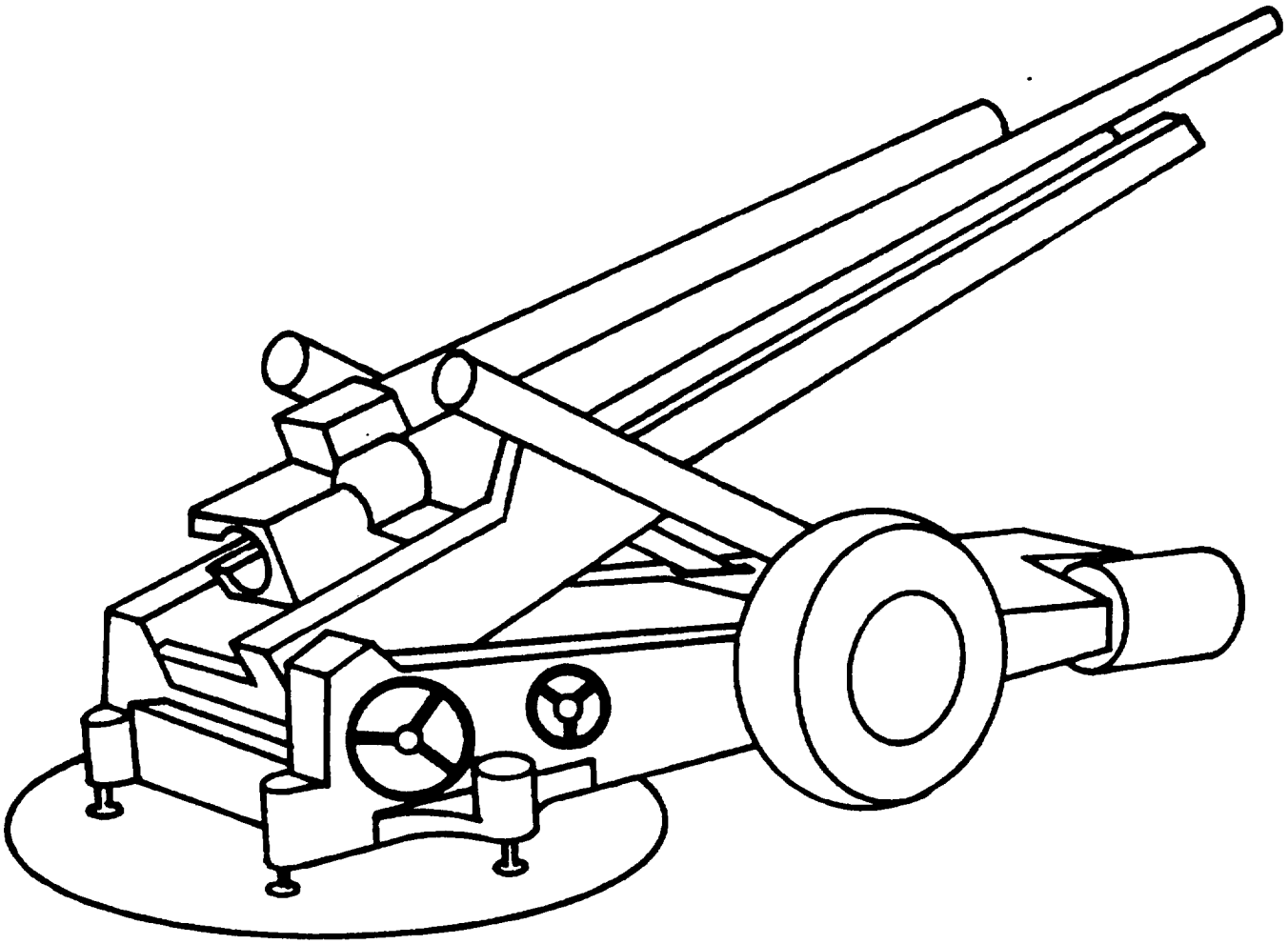

Figure 1-14. M204 Soft Recoil 105-mm Howitzer

Double recoil mechanisms employed in older style weapons, but not employed in modern artillery design, also imply a variation in functions from those described in par. 1-2.1. The double recoil mechanism shown in Fig. 1-15, allows translational motion of some parts of the top carriage, with a second recoil mechanism incorporated to resist this translational motion. Although it is theoretically possible to reduce peak recoil loads with this technique, doing so creates substantial complexity in mechanism and structural design. Further, with modern variable length recoil mechanisms, adequate recoil control can be obtained with a single recoil mechanism. Therefore, this concept is not discussed further in this handbook.

Elevating mechanisms employing large radius elevating gears and a screwdriving gear, as shown in Fig. 1-16, were used in older style weapons. The bulky nature of these gears and the difficulty in maintaining tight gearing tolerances have lead primarily to the use of elevating struts in modern artillery weapons. Since large radius elevating gears are not foreseen as a viable alternative in towed artillery system designs of the future, they are not discussed in this handbook.

1-3 SYSTEM DYNAMICS

1-3.1 RECOIL DYNAMICS

The basic function of an artillery weapon is to launch a high-velocity projectile with high precision by using the force of high-pressure burning propellant to accelerate the projectile down the bore and into flight. Since this process occurs in a very short time, on the order of 15 ms, interior ballistics play a crucial role in weapon performance. The sequence of events in conventional weapon artillery is initiated by igniting the propelling

THIS DOCUMENT PROVIDED BY THE ABBOTT AEROSPACE
TECHNICAL LIBRARY
ABBOTTAEROSPACE.COM

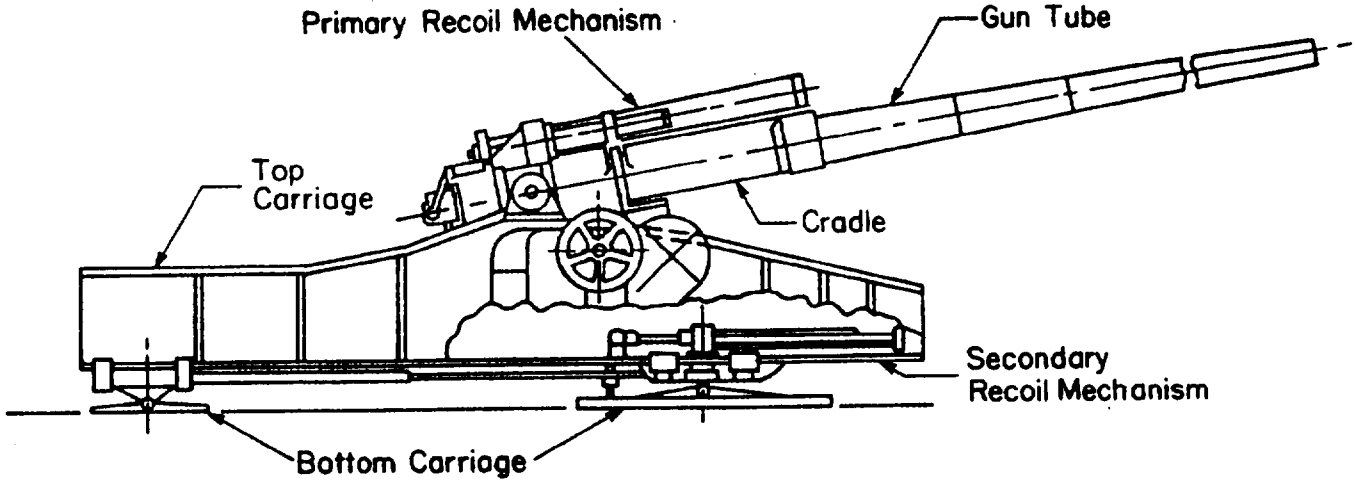

Figure 1-15. Double Recoil Mechanism

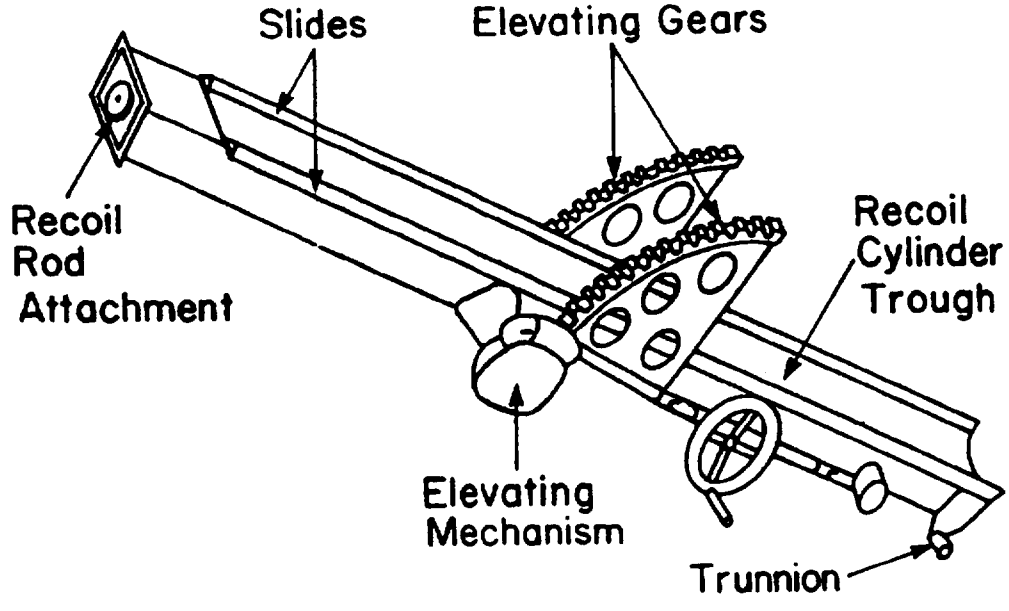

Figure 1-16. Elevating Gears

charge, generating a high pressure that acts on the recoiling parts of the weapon with a total force $B(t)$, as shown in Fig. 1-17, and called the breech force. (See Ref. 6 for further discussion of breech force.) The breech force peaks rapidly, as shown in Fig. 1-18, and accelerates the recoiling parts rearward.

Since the recoiling parts are initially at rest in a conventional artillery weapon, the rearward momentum after the projectile and gases leave the tube must be equal to the total impulse of the applied breech force, which is the integral of $B(t)$ over the in-bore period,

$$I = \int_0^{t_1} B(t)dt, \text{ N·s} \tag{1-1}$$

where

I = impulse of breech force, N·s
$B(t)$ = breech force, N
t = time, s
t_1 = time over which breech force acts, s.

THIS DOCUMENT PROVIDED BY THE ABBOTT AEROSPACE
TECHNICAL LIBRARY
ABBOTTAEROSPACE.COM

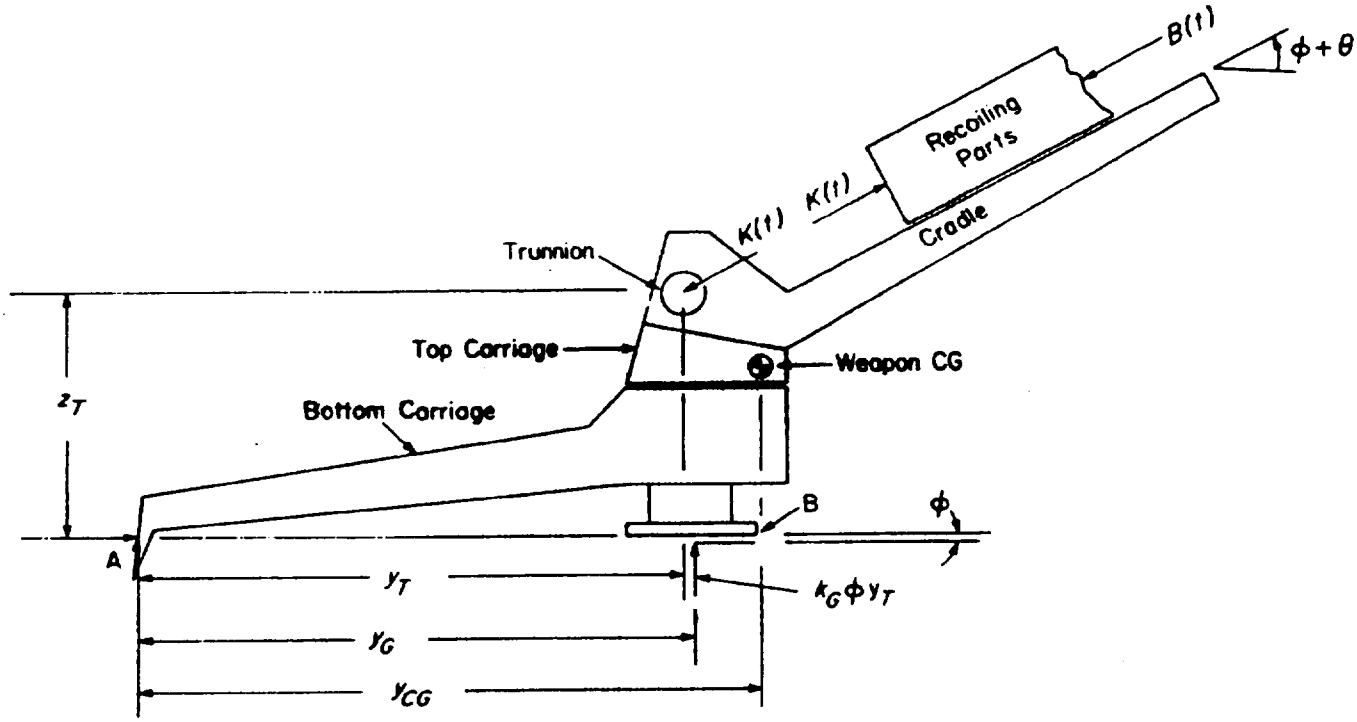

Figure 1-17. Recoil and Reaction Forces

A detailed method of calculating the breech force is presented in Chapter 2, Ref. 6. It is presumed here that the impulse I is known from interior ballistics. For example, for a 155-mm artillery round, the maximum impulse may be $I = 29{,}700$ N·s. Equate the momentum of the recoiling parts, with mass 3600 kg, to this impulse to determine recoil velocity $\dot{x}$, i.e.,

$$3600\,\dot{x} = -29{,}700 \text{ N·s} \tag{1-2}$$

where

$\dot{x}$ = recoil velocity, m/s.

Thus the free recoil velocity of the recoiling parts is

$$\dot{x} = -8.25 \text{ m/s.} \tag{1-3}$$

The muzzle velocity of the projectile is 660 m/s, but since the mass of the recoiling parts is much larger than the mass of the projectile, the free recoil velocity of the recoiling parts is much lower (about 1/80) than the muzzle velocity of the projectile.

It now becomes the function of the recoil mechanism to bring the recoiling parts to rest within the allowed length of recoil L by using a recoil force $K(t)$ generated by a hydropneumatic recoil mechanism, as shown in Fig. 1-17. The design objective of the recoil mechanism is to make the recoil force as nearly constant as possible, denoted here as K_0. A recoil force free-body diagram is shown in Fig. 1-19, where the pitch angle ϕ of the weapon is taken as zero (no weapon hop) and motion after $B(t)$ is zero is of interest. Newton's equation of motion for the recoiling parts may be written as

$$(W_r/g)\ddot{x} = -W_r\sin\theta + K_0 - F_g, \text{ N} \tag{1-4}$$

THIS DOCUMENT PROVIDED BY THE ABBOTT AEROSPACE
TECHNICAL LIBRARY
ABBOTTAEROSPACE.COM

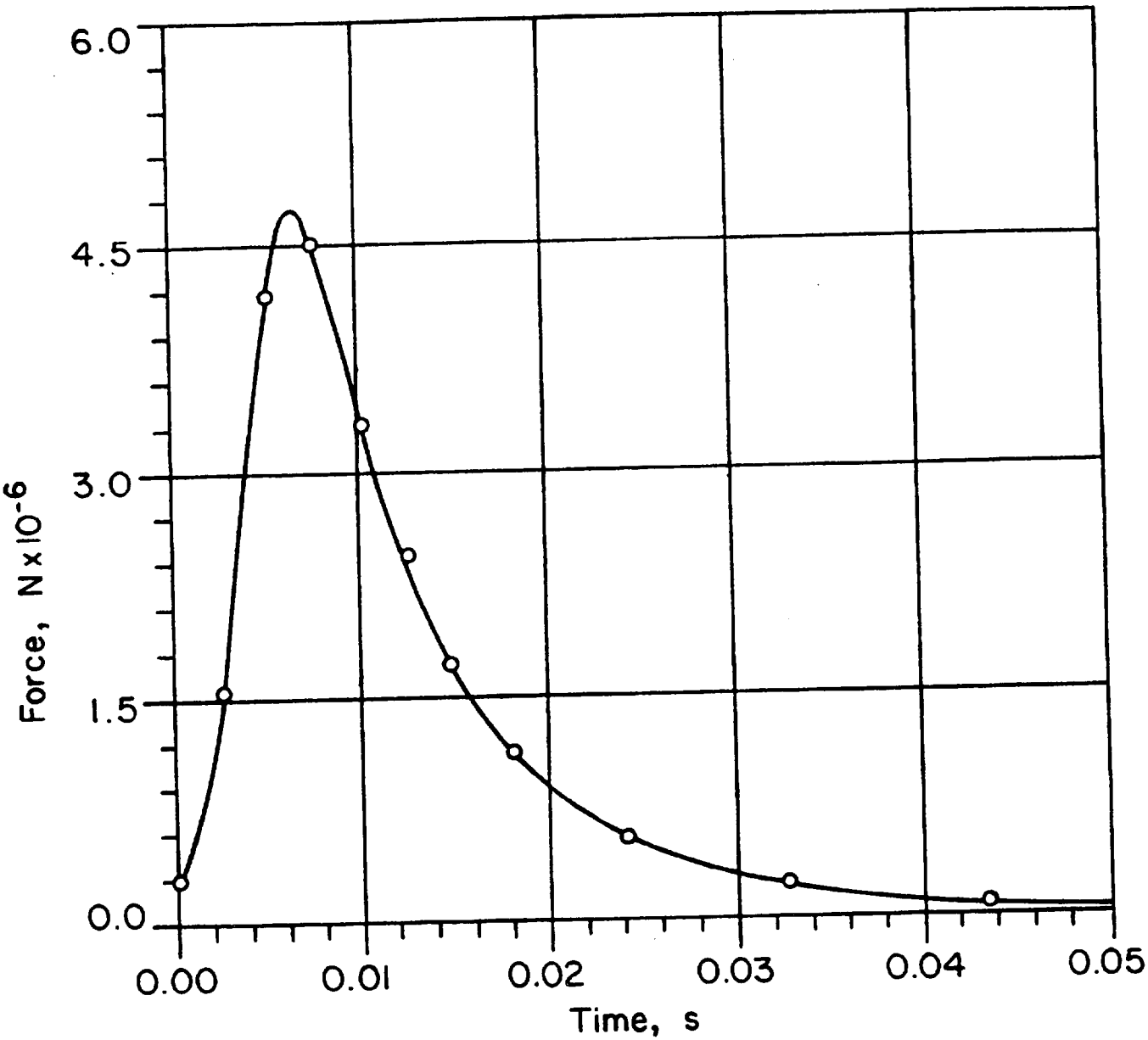

Figure 1-18. Typical Breech Force vs Time Curve

where

W_r = weight of recoiling parts, N
g = acceleration due to gravity, m/s^2
θ = angle of elevation, rad
F_g = propellant gas force, N
K_0 = constant recoil force, N.

After a few milliseconds the value of F_g reaches zero and, for approximations, may be neglected.

Equating the impulse of the breech force to the initial momentum of the recoiling part, as in Eq. 1-2, the initial conditions of free recoil are

THIS DOCUMENT PROVIDED BY THE ABBOTT AEROSPACE
TECHNICAL LIBRARY
ABBOTTAEROSPACE.COM

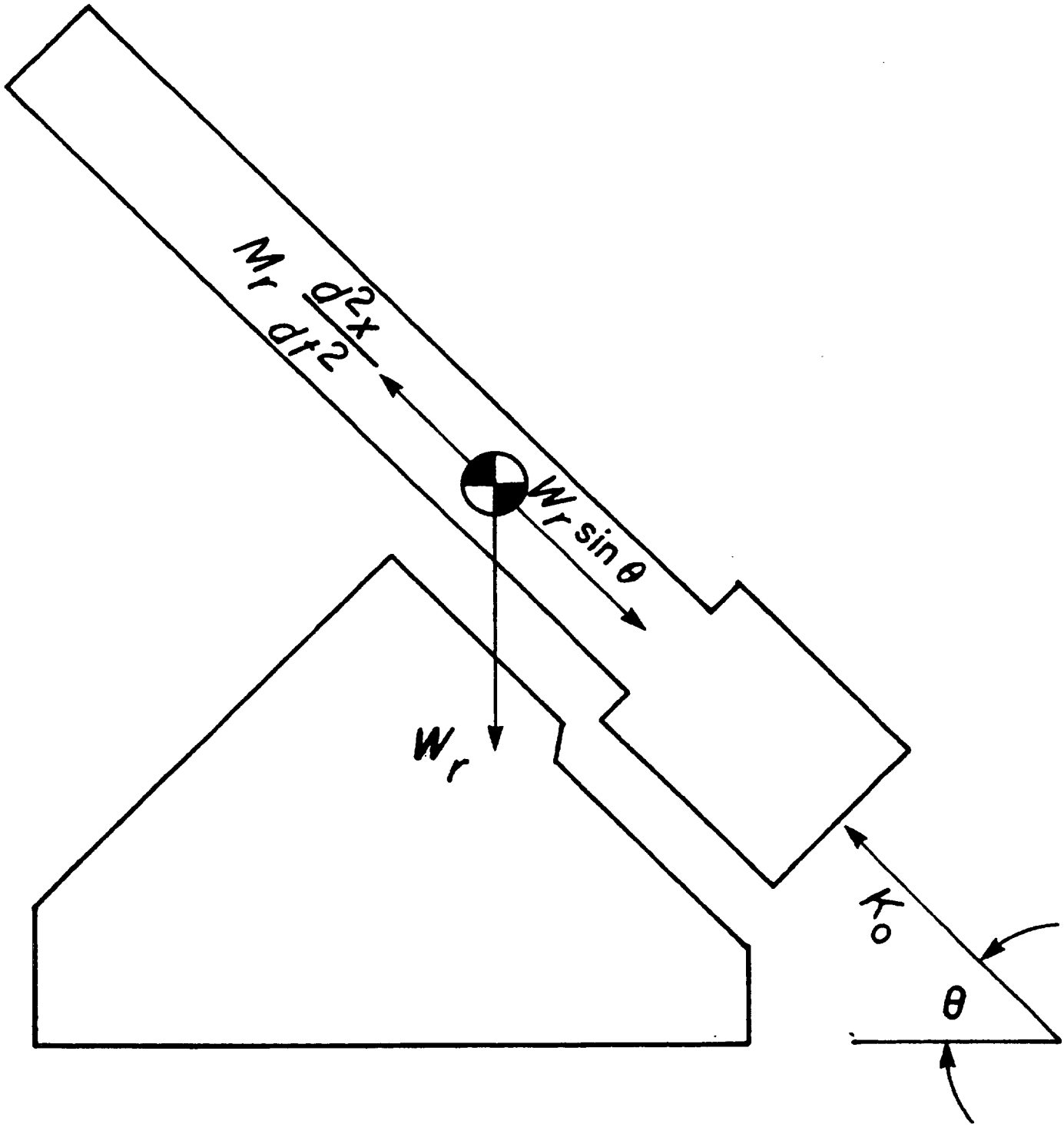

Figure 1-19. Recoil Force System

THIS DOCUMENT PROVIDED BY THE ABBOTT AEROSPACE
TECHNICAL LIBRARY
ABBOTTAEROSPACE.COM

$$x(0) = 0, \text{ m}$$
$$\dot{x}(0) = -\frac{Ig}{W_r}, \text{ m/s} \tag{1-5}$$

where

x = position of recoiling parts, m

and where the free recoil velocity is determined as in Eq. 1-2.

The initial value problem of Eqs. 1-4 and 1-5 can be integrated to obtain

$$\dot{x}(t) = [(K_0 - W_r\sin\theta)\frac{g}{W_r}]t - \frac{Ig}{W_r}, \text{ m/s}$$
$$x(t) = \frac{1}{2}[(K_0 - W_r\sin\theta)\frac{g}{W_r}]t^2 - \frac{Igt}{W_r}, \text{ m.} \tag{1-6}$$

Since the recoiling parts come to rest with recoil length $L>0$, the condition $\dot{x}(t_r) = 0$ can be used in Eq. 1-6 to find the recoil stroke time t_r, and that time can be substituted into the second part of Eq. 1-6, where $x(t_r) = -L$, since recoil travel is negative,

$$t_r = \frac{I}{K_0 - W_r\sin\theta}, \text{ s} \tag{1-7}$$

$$L = \frac{I^2 g}{2W_r(K_0 - W_r\sin\theta)}, \text{ m} \tag{1-8}$$

where

t_r = recoil stroke time, s
L = length of recoil, m.

These equations relate design parameters of the artillery weapon. Eq. 1-8 can be used to define the constant recoil force K_0 required to bring the recoiling parts to rest in a given recoil length L as

$$K_0 = W_r\sin\theta + \frac{I^2 g}{2W_r L}, \text{ N.} \tag{1-9}$$

Since the second term in Eq. 1-9 is the largest, its variation with design parameters is important. It indicates that for a given impulse I, the recoil force varies inversely with both the recoil length L and the weight of recoiling parts W_r. Thus if low recoil forces are desired, it is important to increase both the weight of recoiling parts and the recoil length. This design consideration is particularly important for towed artillery systems and has led to the adoption of approaches to the design of recoil mechanisms that place as much equipment as possible on the recoiling parts, which minimizes the recoil force for a fixed recoil length L.

A similar analysis of the soft recoil method of operation, presented in detail in Ref. 6, yields the following recoil force relation for soft recoil artillery

$$K_0 = W_r\sin\theta + \frac{I^2 g}{8W_r L}, \text{ N.} \tag{1-10}$$

THIS DOCUMENT PROVIDED BY THE ABBOTT AEROSPACE
TECHNICAL LIBRARY
ABBOTTAEROSPACE.COM

By comparing Eqs. 1-9 and 1-10, it is apparent that the recoiling force level required for soft recoil is only slightly greater than one-fourth the recoil force level required for conventional artillery. This basic property of soft recoil makes it very attractive for applications in which a low recoil force is important.

1-3.2 DYNAMIC LOAD ANALYSIS

Since the recoil force calculated in the preceding paragraph is applied to the carriage of the towed artillery system during a short period of time, dynamic response of the weapon to these recoil loads must be carefully analyzed and determined during the design. A dynamic model of the entire artillery piece is generally constructed during the early phase of preliminary design, and refinements are incorporated during the progress of weapon development. Models of the dynamic response of towed artillery generally involved motion of the recoiling parts, pitch motion of the tipping parts, and pitch motion of the bottom carriage. Flexibility of elements of the structure and of the ground contact are included in these models to determine load distribution throughout the system for the purposes of stress analysis and design for adequate strength.

In addition to dynamic load analysis due to recoil forces, dynamic analysis must be carried out under airdrop and transport loading. This type of dynamic analysis generally is done with a quasistatic model. Deceleration of the entire system due to impact with the ground is employed, with experimental data, to obtain impact accelerations measured in number of g's. This deceleration is then used to calculate effective inertial loads that are placed at the center of mass of the parts of the system (D'Alembert's principle). These loads are then analyzed, and reactions at joints are determined. Once the joint reactions are known, a stress analysis of each of the major components of the system can be conducted.

Dynamic analysis of the entire weapon system is presented in Chapter 2, along with load determination at joints of the artillery weapon. These force data are then used in subsequent chapters for stress analysis and design for adequate weapon strength.

1-3.3 DYNAMIC EFFECTS ON WEAPON STABILITY AND PRECISION

Dynamic models of weapon pitch motion presented in Chapter 3 include the effect of translational motion of the recoiling parts, pitch motion of the tipping parts about the trunnion, elastic deflection of structural elements, and pitch motion of the bottom carriage.

To illustrate the method used for weapon stability analysis, consider the weapon structure (bottom carriage, top carriage, and cradle) as rigid bodies and ignore the motion of the recoiling parts. The center of mass of the entire weapon is located at the point CG in Fig. 1-17. Summing moments about the spade at point A in Fig. 1-17, the equation of pitch motion of the system is

$$J\ddot{\phi} = k_G y_G^2 \phi - W y_{CG} + K(t)\cos(\theta + \phi) y_T - K(t)\sin(\theta + \phi) z_T, \text{ N·m} \qquad (1\text{-}11)$$

where

J = polar moment of inertia of weapon about spade, kg·m^2
ϕ = pitch angle of weapon, rad
k_G = spring rate of soil at firing base, N/m
y_G = horizontal distance from spade to firing base, m
W = weapon weight, N
y_{CG} = horizontal distance from spade to weapon center of gravity, m
$K(t)$ = recoil force, N
y_T = horizontal distance from spade to trunnion, m
z_T = trunnion height, m.

Eq. 1-11, with initial conditions

$$\left.\begin{aligned} \phi(0) &= 0 \\ \dot{\phi}(0) &= 0 \end{aligned}\right\} \qquad (1\text{-}12)$$

is integrated to obtain the pitch motion $\phi(t)$. The maximum pitch moment generated by the recoiling forces occurs when the angle of elevation $\theta = 0$.

THIS DOCUMENT PROVIDED BY THE ABBOTT AEROSPACE
TECHNICAL LIBRARY
ABBOTTAEROSPACE.COM

In design of the weapon, one objective is to select the trail length so that the second term on the right of Eq. 1-11 is large enough to cause the pitch moment always to be negative and hence assure maintenance of ground contact during firing. If this is not possible, then at high zones, where the recoil force is largest, some hop of the weapon will occur. Another design alternative that is presented in Ref. 6 is to employ a recoil mechanism with variable recoil length in which the recoil length at low elevations is substantially larger than is possible at high elevations. By use of this technique, Eq. 1-9 shows that lower recoil forces can be achieved at low elevations and hence enhance weapon stability.

Eq. 1-11 for pitch motion and the basic tradeoff relations for recoil force level defined in Eq. 1-9 show that the system designer has several parameters at his disposal by which to obtain good weapon stability during firing. It is important that these stability analyses be performed during the preliminary design phase and as the weapon design is refined in order to guarantee that when a prototype weapon is tested, it will have acceptable firing stability.

A similar stability analysis is required for the determination of overturning moments and assessment of stability of a conventional artillery piece in counterrecoil, and the stability of a soft recoil weapon in case of a misfire. In both these cases forward motion of the recoiling parts is arrested by a buffer that creates moments that tend to tip the weapon forward, which may cause loss of contact at the spades and even result in the tipping over of a soft recoil weapon. Analysis of these overturning moments requires that moments be summed about point B in Fig. 1-17. Analysis of overturning moments is presented in Chapter 3.

A final note of some importance in pitch dynamics of the weapon concerns the maintenance of precise orientation of the recoiling parts during the in-bore period of the projectile. Once Eq. 1-11 is integrated, forces in the elevating mechanism and forces between the cradle and recoiling parts can be calculated. It is important that these forces act to maintain positive contact between surfaces that are in contact prior to firing of the round. If this contact is lost, free pitch motion of the tube can occur and degrade the precision of projectile launch. This is a subtle point that requires the attention of the design team to assure that the weapon system has the required degree of precision.

REFERENCES

1. AMCP 706-244, Engineering Design Handbook, *Ammunition Series, Section 1, Artillery Ammunition—General, With Table of Contents, Glossary, and Index for Series*, September 1963.
2. AMCP 706-245, Engineering Design Handbook, *Ammunition Series, Section 2, Design for Terminal Effects*, July 1964.
3. AMCP 706-242, Engineering Design Handbook, *Design for Control of Projectile Flight Characteristics*, September 1966.
4. AMCP 706-247, Engineering Design Handbook, *Ammunition Series, Section 4, Design for Projection*, July 1964.
5. MIL-STD 1474 , *Noise Limits for Army Materiel*, 20 April 1984.
6. MIL-HDBK-778(AR), *Recoil Systems*, July 1988.
7. AMCP 706-251, Engineering Design Handbook, *Muzzle Devices*, May 1968.
8. AMCP 706-252, Engineering Design Handbook, *Gun Tubes*, February 1964.
9. DARCOM-P 706-253, Engineering Design Handbook, *Breech Mechanism Design*, February 1979.
10. *Annual Book of ASTM Standards*, Vol. 1, Part 4, American Society for Testing and Materials, Philadelphia, PA, 1986.
11. AMCP 706-327, Engineering Design Handbook, *Fire Control Series, Section 1, Fire Control Systems—General*, January 1968.
12. L. J. Pavagadhi, *Optimum Control Fluidic Recoil Mechanism*, Technical Report ARLCD-TR-82024, US Army Armament Research and Development Command, Dover, NJ, 1982.

THIS DOCUMENT PROVIDED BY THE ABBOTT AEROSPACE
TECHNICAL LIBRARY
ABBOTTAEROSPACE.COM

CHAPTER 2
PRELIMINARY DESIGN AND TRADEOFF ANALYSIS OF TOWED ARTILLERY SYSTEMS

This chapter presents methods and examples for preliminary design of towed artillery systems. Considerations that are important early in the design process, such as definition of requirements and constraints, are identified and discussed. Analytical and empirical relationships for estimating weights, ballistic and cannon parameters, recoil mechanism sizing, and design of other components of the system are presented and illustrated. Use of these relationships to estimate characteristics of subsystems and tradeoffs is discussed and illustrated. Considerations in design for towing are discussed. Finally, a method of considering system level tradeoffs and optimum parameter selection for component design is presented.

2-0 LIST OF SYMBOLS

A = bore area, m^2
A_{CR} = cross-sectional area of control rod, m^2
A_{ff} = surface area of front float or firing base, m^2
A_{fr} = surface area of rear float, m^2
A_N = diaphragm area, m^2
A_p = area of recoil piston minus area of recoil rod, m^2
a = LeDuc parameter, m/s
a_L = lateral acceleration, m/s^2
a_t = thread root area of recoil rod, m^2
B = breech force as a function of projectile travel in bore, N
$B_M = P_M A$ = maximum breech force, N
B_0 = breech force at projectile exit, N
b = LeDuc parameter, m
b_c = bearing capacity of soil, Pa
b_s = width of float or spade, m
C = in-battery sustaining factor > 1, dimensionless
c = apparent cohesion of soil, Pa
D_I = inner diameter of recoil cylinder, m
D_i = inner diameter of tube, m
D_N = diameter of recuperator cylinder, m
D_o = outer tube diameter, m
D_1 = outside diameter of recoil cylinder, m
D_2 = outer diameter of gas portion of recuperator cylinder, m
D_3 = outside diameter of oil portion of recuperator cylinder, m
d = maximum recoil rod diameter, m
d_c = centroid of breech force vs time curve, s
d' = minimum diameter of recoil rod threads, m
E_1 = Young's modulus for recoil cylinder material, Pa
E_2 = Young's modulus of recuperator cylinder material, Pa
F = force on top carriage, N
f_g = frictional force between recoiling parts and cradle guide, N
f_p = frictional force between recoil cylinder and recoil piston, N

THIS DOCUMENT PROVIDED BY THE ABBOTT AEROSPACE
TECHNICAL LIBRARY
ABBOTTAEROSPACE.COM

f_R = frictional force between recoil rod and recoil cylinder, N
G = impulse of force during gas ejection period, for a tube without a muzzle brake, kg·m/s
G_0 = momentum of projectile and gas at projectile exit, kg·m/s
G_1 = momentum imparted to breech by gas during gas ejection period, with a muzzle brake, kg·m/s
g = acceleration due to gravity, m/s^2
h = height of spade, m
I = total impulse of breech force, (including muzzle brake effect), N·s
I_1 = impulse during gas ejection period, with muzzle brake, N·s
I_2 = impulse during gas ejection period, without muzzle brake, N·s
I_3 = impulse during in-bore period, N·s
$(IF)_i$ = importance factor for ith factor, dimensionless
K_{max} = maximum force acting on recoiling parts, N
$K(t)$ = total recoil force, N
K_0 = constant recoil force, N
k_1 = stress concentration factor due to threads, dimensionless
L = length of short recoil, m
L_s = length of float, m
L_1 = total length of recoil cylinder, m
L' = length of long recoil, m
ℓ = length of recuperator cylinder containing gas, m
ℓ_p = distance of pintle to weapon wheels, m
M_r = mass of recoiling parts, kg
$N_\phi = \tan^2(\pi/4 + \phi_s/2)$ = flow value, dimensionless
P = recoil design pressure, Pa
= pressure in bore, Pa
P_e = mean chamber pressure, Pa
P_M = maximum chamber pressure, Pa
P_N = initial gas pressure in recuperator, Pa
$(P_N)_{max}$ = maximum gas pressure in recuperator, Pa
$(PR)_i$ = performance rating in ith factor, dimensionless
$(PR)_{total}$ = total performance rating, dimensionless
p = design pressure, Pa
p_ℓ = lateral pressure on spade, Pa
p_v = pressure on soil due to vertical force component from trails, Pa
Q = dimensionless quantity (see Eq. 2-4)
R = force acting on recoil rod, N
R_f = vertical reaction force at rear float, N
R_{H1} = horizontal ground reaction at Point 1, N
R_{H2} = horizontal ground reaction at Point 2, N
R_{V1} = vertical ground reaction at Point 1, N
R_{V2} = vertical ground reaction at Point 2, N
R_{V3} = vertical ground reaction at front float or firing base, N
RT_b = specific impetus of propellant, J/kg
r_{ff} = radius of front float, m
Δr_1 = limit of radial expansion, m
Δr_2 = acceptable expansion limit based on seal design, m
Δr_3 = allowable radial expansion limit, m

THIS DOCUMENT PROVIDED BY THE ABBOTT AEROSPACE
TECHNICAL LIBRARY
ABBOTTAEROSPACE.COM

S_f = safety factor, dimensionless
SI = stability index, dimensionless
t = time, s
t_r = time of recoil, s
t_0 = time to projectile exit, s
t_1 = rise time of $K(t)$ = fall time of $K(t)$, s
U_0 = tube length, m
u = travel of projectile in bore, m
V_i = initial gas volume, m^3
v = absolute velocity of projectile as a function of position in bore, m/s
v_p = muzzle velocity of projectile, m/s
v_0 = velocity of recoiling parts at projectile exit, m/s
W = tube diameter ratio, dimensionless
W_c = weight of propelling charge, N
W_{CR} = weight of control rod, N
W_{CT} = total weight of recuperator cylinder, N
W_P = weight of projectile, N
W_r = total weight of recoiling parts, N
W_{rec} = total recuperator weight, N
W_{reg} = weight of regulator assembly, N
W_T = total weapon weight, N
W_1 = weight of recoil cylinder, N
W_2 = weight of recoil cylinder assembly, N
w = wheelbase, m
x = absolute displacement of recoiling parts, m
Y = stroke of control rod, m
y = absolute displacement of control rod, m
y_{CG} = height of weapon center of gravity, m
α_a = angle of approach, rad
β = muzzle brake factor, dimensionless
β_d = angle of departure, rad
γ = ratio of specific heats, dimensionless
γ_s = side slope, rad
δ = wall thickness of recoil cylinder, m
δ_2 = wall thickness in gas portion of cylinder, m
δ_3 = wall thickness in oil portion of cylinder, m
Θ = angle of elevation, rad
μ_1 = Poisson's ratio of recoil cylinder materials, dimensionless
μ_2 = Poisson's ratio of recuperator cylinder material, dimensionless
ρ_1 = weight density of recoil cylinder material, N/m^3
ρ_2 = weight density of recuperator cylinder material, N/m^3
ρ_3 = weight density of control rod material, N/m^3
σ = normal stress on sheared surface of soil, Pa
σ_c = circumferential stress in recoil cylinder, Pa
σ_l = longitudinal stress in recoil cylinder, Pa
σ_n = normal stress in recoil cylinder, Pa
σ_y = yield strength of tube material, Pa

THIS DOCUMENT PROVIDED BY THE ABBOTT AEROSPACE
TECHNICAL LIBRARY
ABBOTTAEROSPACE.COM

σ_1 = allowable stress in recoil rod, Pa
σ_2 = recoil cylinder material yield strength, Pa
σ_3 = gas cylinder material yield strength, Pa
σ_4 = oil cylinder material yield strength, Pa
τ = shear strength of soil, Pa
ϕ = duration of gas ejection period, s
ϕ_s = angle of internal shearing resistance of soil, rad

2-1 SYSTEM DESIGN AND ENGINEERING

The design of a towed artillery system begins with a set of user requirements and a concept of system operation. As outlined in Chapter 1, the process of transforming this set of specifications and associated technological and human constraints into an optimized artillery system is a long and demanding task. The purpose of this paragraph is to outline a system design procedure that has functioned informally in the past and can assist both the system and component designers in relating their tasks and objectives for interaction during conceptual, preliminary, and detailed design.

The process of system design is illustrated schematically in Fig. 2-1. Initially, the operational requirements are formulated by the field artillery user. These requirements are then analyzed by the artillery design team relative to technological and human factor constraints, which provide quantitative input to an initial phase of system design. During this initial phase, the artillery system design team should expect to interact with the user to assure that the quantitative requirements and constraints defined for system performance are in fact consistent with user needs. These requirements and constraints include definition of an acceptable blast overpressure in the crew area; definition of ground-anchoring techniques that are acceptable to the user; definition of crew functions in emplacement, fire control, azimuth control, elevation control, and ammunition handling; and other pertinent aspects of concept definition as they affect user requirements.

This initial phase of concept definition may lead to consideration of alternate modes of system operation such as conventional versus soft recoil, adoption of split trails with the associated limitation in on-carriage traverse, and consideration of off-carriage traverse with perhaps a full 360-deg traverse capability. During the early stages of system definition, several system concepts may appear acceptable and attractive and may be carried through preliminary design.

For each of the concepts considered, data are available to obtain a preliminary definition of the ballistic cycle and the tube required to launch the family of projectiles associated with the system (indicated as the next step in Fig. 2-1). Par. 2-3 summarizes preliminary ballistic and tube parameter selection. Chapter 2 of Ref. 1 presents a more detailed derivation and illustration of techniques for ballistic and tube definition. These techniques provide the system designer with an initial estimate of tube weight and breech force acting as an input to the system, and they permit engineers to proceed with preliminary design of the remaining components of the system.

As illustrated next in Fig. 2-1, the various recoil mechanism types being considered are defined. The principal variables that must be selected during preliminary design are the recoil length and recoil force level, which are consistent with system requirements. Calculations leading to these parameters and to an estimate of

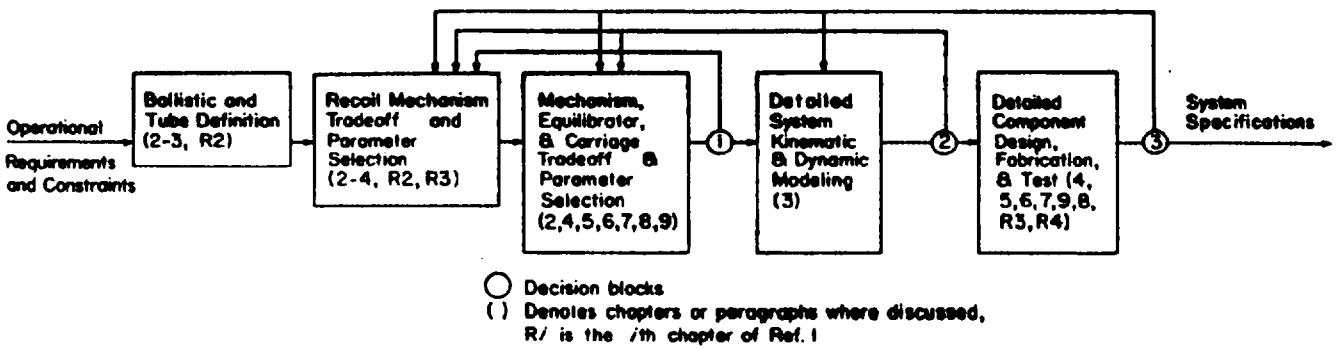

Figure 2-1. Model of Towed Artillery Preliminary System Design

THIS DOCUMENT PROVIDED BY THE ABBOTT AEROSPACE
TECHNICAL LIBRARY
ABBOTTAEROSPACE.COM

recoil mechanism weight are outlined in par. 2-4 and in more detail in Chapters 2 and 3 of Ref. 1. Of equal importance to the selection of nominal values for recoil mechanism parameters are parametric relationships established among recoil length, recoil force, and muzzle brake efficiency—all of which are the basis for tradeoff analysis and optimization of the system.

With recoil force levels defined and the weight of recoiling parts and recoil mechanism estimated, preliminary design of mechanisms, bearings, equilibrator, and carriage components is initiated, as indicated in Fig. 2-1. Trunnion height is determined to insure adequate ground clearance at high-elevation firing. Weapon stability criteria for low-elevation firing then determine trail length and ground-anchoring parameters for spades or stakes in the firing base. Loads that must be supported by carriage components and bearings during firing and weapon transport are determined through dynamic analysis. Stress calculations then lead to the sizing of structural members and bearings and hence define the weight of structural and bearing components. With these weights established, gearing ratios, handwheel sizes, equilibrator force, and emplacement lever force are determined by human factors considerations. Specifically, the handwheel torque required to elevate and traverse the weapon must remain within acceptable levels for effective operation by the crew. Once these parameters are selected, the sizes and weights of the mechanisms and equilibrator are established. In addition to selecting nominal values for the design parameters considered, parametric relationships are defined that are the basis for tradeoff considerations at the system level.

With completion of preliminary sizing of all components of the system, the first major decision, block ① in Fig. 2-1, is encountered. Total system weight is now compared with weight requirements specified by the user. For example, air transportability may dictate severe weight constraints that may not be satisfied by the preliminary designs selected. A feedback loop is then required to consider tradeoffs that allow for a reduction in system weight. If, after completion of this loop, system weight constraints are not met, the design team must consider tradeoffs among user-imposed requirements to determine the impact on system design of the relaxation of requirements. At this point the design team has data to present to the user to define the impact on system weight of the various constraints imposed by the user and to initiate a discussion to define acceptable modifications of user requirements to meet overall system constraints.

The remaining feasible concepts are now subjected to detailed system kinematic and dynamic modeling, as shown in Fig. 2-1, which support the design of the recoil mechanism and define dynamic loads acting on all components of the system. Dynamic modeling techniques are presented in Chapter 3 and support design of all system components. The importance of system dynamic analysis cannot be overstressed since the basic function of the recoil mechanism and the supporting structure of the artillery weapon is to transmit to the ground the extremely high ballistic forces generated during the short in-bore period of the projectile. Dynamic loads on components, weapon stability, and ground reaction forces can be substantially higher than estimates arrived at through a static load analysis or a simplified dynamic analysis.

Evaluation of dynamic loads and comparison with simplified load analysis used in preliminary design lead to the second major decision block ② in Fig. 2-1. If dynamic loads exceed those used in preliminary design of the recoil mechanism and other components, the design process must branch back to recoil mechanism tradeoff and parameter selection and to tradeoff and parameter selection of other components of the system. Tradeoff relations developed during preliminary design and refined during dynamic analysis then are the basis for modification of the design of all components to meet strength and stability constraints under the refined loads.

Once acceptable levels of performance are achieved, through reanalysis and design iteration, detailed component design and fabrication of a prototype weapon system proceed as shown in Fig. 2-1. Design techniques involved in this phase of development are presented in Chapters 4 through 9 of this handbook and Chapters 3 and 4 of Ref. 1.

Completion of detailed component design and system prototype fabrication leads to prototype testing and evaluation. If the foregoing preliminary design and dynamic analysis have been done carefully, the prototype should perform very nearly at acceptable levels. Due, however, to numerous uncertainties involved in field use of the weapon system, technical problems are likely to occur during the first prototype testing and evaluation. These problems lead to the third major decision block ③ in Fig. 2-1. Test results from prototype testing are compared with system dynamic model predictions and performance predictions for the recoil mechanism and other components of the system. These comparisons are the basis for identification of the source of technical difficulties. If careful tradeoff analyses have been developed during the early phases of design, the source of the difficulties can be pinpointed and fixes can be defined. These modifications are defined and then subjected to a detailed system dynamic analysis to assure that they are acceptable in a system context. Following detailed

THIS DOCUMENT PROVIDED BY THE ABBOTT AEROSPACE
TECHNICAL LIBRARY
ABBOTTAEROSPACE.COM

evaluation of modifications and system performance, which is done by using data obtained during prototype testing, the detailed component design phase can be reentered and an advanced or engineering development prototype can be fabricated.

As this discussion illustrates, the system design team—consisting of component engineers and system dynamic analysts—must interact continuously. Careful tradeoff analysis and dynamic simulation during design iterations can substantially increase the confidence of the design team—prior to the very expensive phase of prototype fabrication and test—in pinpointing technical difficulties and carrying out tradeoff analyses to define fixes. The iterative procedure outlined in this paragraph has been carried out in the past with varying levels of formality. It has been an effective tool in the design of towed artillery systems in the past and offers the potential for substantial gains in system performance and the effectiveness of system design in the future.

2-2 SYSTEM REQUIREMENTS AND CONSTRAINTS

Artillery system requirements and associated operational constraints are defined by the field artillery user and are based on an operational scenario and a concept of weapon system operation. Quantitative requirements and constraints on a towed artillery system, however, generally are defined jointly by the user and developer as outlined in par. 2-1. The first technical step in definition of a towed artillery system involves range and terminal effect requirements to defeat the spectrum of targets the system is expected to engage. Many times the system being developed will be constrained to use existing ammunition, particularly projectiles that are already in the inventory. For example, in developing a new 155-mm system, several projectiles will be common to the towed system and to existing or developmental self-propelled systems. Thus the principal issue resolves to the range required and the associated exterior ballistic calculations leading to definition of the muzzle velocity that must be delivered by the towed artillery system.

An extensive literature exists on terminal and exterior ballistic analysis. Basic references of interest to the artillery designer are Refs. 2, 3, 4, 5, and 6. Although it is valuable for the artillery system designer to have basic information concerning terminal and exterior ballistics, these specialized fields are generally well covered by ammunition and ballistic engineers. For the purposes of towed artillery design, therefore, it should be expected that ammunition designers and ballisticians will provide the principal interface with the user in defining the projectile types, projectile shapes, projectile weights, and muzzle velocities required to achieve the desired range. This will involve the definition of several rounds of ammunition that must be fired by the artillery weapon. For example, Table 2-1 provides projectile weight and muzzle velocity required to deliver projectiles to the desired range for a family of ammunition to be fired by the M198 Howitzer. Of particular concern to the

TABLE 2-1
BALLISTICS DATA, M198 HOWITZER

Basic Design	M107 Zone 5	XM549 Zone 8
Projectile weight W_p, N	432	427
Charge weight W_c, N	24.3	125
Maximum chamber pressure P_M, Pa	1.06×10^8	3.17×10^8
Muzzle velocity v_p, m/s	375	826
Tube length U_0, m	5.08	5.08
Bore area A, m^2	0.0192	0.0192
Propellant specific impetus RT_b, J/kg	0.941	1.09
Muzzle brake factor β, dimensionless	0.7	0.7
Calculated Data		
Maximum breech force B_M, N	2.04×10^6	6.09×10^6
Breech force at projectile exit B_0, N	1.21×10^5	1.37×10^6
Time to projectile exit t_0, s	0.0271	0.0123
Impulse during in-bore period I_3, N·s	16,620	41,240
Impulse during gas ejection period, without muzzle brake I_2, N·s	2531	14,780
Impulse during gas ejection period, with muzzle brake I_1, N·s	761	4435

THIS DOCUMENT PROVIDED BY THE ABBOTT AEROSPACE
TECHNICAL LIBRARY
ABBOTTAEROSPACE.COM

must be given in design to the number of rounds at a lower zone that are equivalent to one round at the highest zone. A fatigue failure criterion, based on the EFC life required, must be brought into weapon component design.

8. *Reaction Times for Weapon Emplacement and Displacement.* The user will generally specify times of emplacement and displacement of the weapon system by the artillery crew. These times play an important role in defining basic weapon configuration and mechanism design for firing base emplacement and displacement and may dictate the ground-anchoring technique employed.

9. *Reliability and Maintainability Requirements.* User-stated requirements on mean rounds between failure must receive careful consideration in design of all mechanisms within the artillery system. Maintainability requirements specified by the user can also play an important role in the design of numerous components of the towed system. Maintenance functions to be carried out by the artillery crew, by direct support maintenance, and by higher levels of maintenance must be clearly understood in order that selected maintainability design approaches allow for maintenance and replacement of components at the required echelon.

9. *Reliability and Maintainability Requirements.* User-stated requirements on mean rounds between failure must receive careful consideration in design of all mechanisms within the artillery system. Maintainability requirements specified by the user can also play an important role in the design of numerous components of the towed system. Maintenance functions to be carried out by the artillery crew, by direct support maintenance, and by higher levels of maintenance must be clearly understood in order that selected maintainability design approaches allow for maintenance and replacement of components at the required echelon.

The foregoing requirement considerations should be considered typical and not exhaustive. It is imperative that the system design team carefully consider user requirements and analyze their impact on the design of all components of the artillery systems. Since there is considerable interaction between system level requirements and component design, members of the design team should be involved in analysis of user requirements and in negotiation with the user to ensure that the requirements are practically achievable. Further, as indicated in par. 2-1, tradeoffs must be established to show the user the penalties associated with severe requirements. This process will be of a continuing nature, as indicated in Fig. 2-1.

2-3 PRELIMINARY BALLISTIC AND CANNON DEFINITION

As noted in par. 2-2, terminal ballistics considerations and range requirements specified by the user generally determine the weapon caliber, projectile weight, and projectile muzzle velocity that are required to achieve range and terminal effects. Ammunition and tube designers then begin to determine charge weight and characteristics to propel the projectile to the required muzzle velocity. Tube length is selected jointly by the tube and charge design teams. The weapon designer, however, needs estimates of charge and tube characteristics to allow him to begin preliminary design of the numerous components of the towed artillery weapon system. He cannot simply wait until detail charge and tube design are complete before he begins the process of weapon design.

Ballistic modeling techniques suitable for preliminary selection of charge and tube characteristics are presented in Chapter 2 of Ref. 1. Simplified ballistic models are based on the LeDuc equation relating projectile velocity v to projectile travel u as follows:

$$v = \left(\frac{au}{b+u}\right), \text{ m/s} \tag{2-1}$$

where

v = absolute velocity of projectile as a function of position in bore, m/s
u = travel of projectile in bore, m
a = LeDuc parameter, m/s
b = LeDuc parameter, m.

The LeDuc parameters are determined in Chapter 2 of Ref. 1 and lead to the expression for breech force B as a function of projectile travel:

$$B = B_M\left[\frac{27Q^2U_0^2u}{4(QU_0+u)^3}\right], \text{ N} \tag{2-2}$$

THIS DOCUMENT PROVIDED BY THE ABBOTT AEROSPACE
TECHNICAL LIBRARY
ABBOTTAEROSPACE.COM

where

$$B_M = P_M A = \text{maximum breech force, N} \tag{2-3}$$

$$Q = \frac{27}{16}\left(\frac{P_M}{P_e}\right) - 1 - \sqrt{\left[\frac{27}{16}\left(\frac{P_M}{P_e}\right) - 1\right]^2 - 1}, \quad \text{dimensionless} \tag{2-4}$$

$$\frac{P_M}{P_e} = \frac{2gU_0P_MA}{v_p^2\left(W_p + \frac{W_c}{2}\right)}, \text{ dimensionless} \tag{2-5}$$

U_0 = tube length, m
A = bore area, m^2
P_M = maximum chamber pressure, Pa
P_e = mean chamber pressure, Pa
g = acceleration due to gravity = 9.81 m/s^2
W_p = weight of projectile, N
W_c = weight of propelling charge, N
v_p = muzzle velocity of projectile, m/s.

With an estimate of maximum chamber pressure P_M known as a bound on performance of tube material, bore area A known, tube length U_0 known, weight of projectile W_p known, and weight of charge W_c known, Eqs. 2-2 through 2-5 determine the breech force as a function of travel u, for $u \leq U_0$. The pressure P in the bore is then

$$P = B/A, \text{ Pa.} \tag{2-6}$$

The form of the pressure versus travel relationship predicted by Eq. 2-6 is shown in Fig. 2-2.

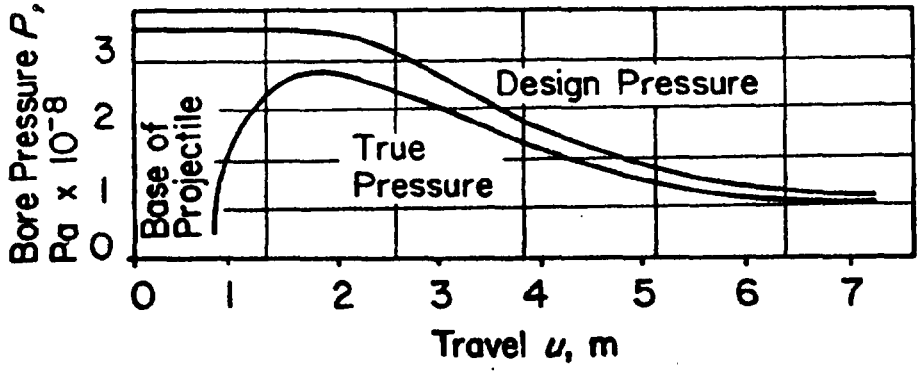

Figure 2-2. Pressure vs Travel and Tube Design Pressure

To obtain an estimate of tube wall thickness, it is necessary to define the greatest pressure to which each section of the bore is subjected during projectile travel. This is done as explained in Ref. 8, i.e., by using a factor of at least 1.05 times the greatest in-bore pressure forward of the given section of the tube, as indicated by the design pressure curve shown in Fig. 2-2. This design pressure can now be used to estimate wall thickness of the tube by using the Lamé equation for stress in a thick-walled cylinder as given in Eq. 55c, Ref. 8, as

THIS DOCUMENT PROVIDED BY THE ABBOTT AEROSPACE
TECHNICAL LIBRARY
ABBOTTAEROSPACE.COM

$$W = \left[\frac{1 + \frac{2p}{\sigma_y}\sqrt{1 - \frac{3}{4}\left(\frac{p}{\sigma_y}\right)^2}}{1 - 3\left(\frac{p}{\sigma_y}\right)^2} \right]^{1/2}, \text{ dimensionless} \qquad (2\text{-}7)$$

where

$W = D_o / D_i$ = tube diameter ratio, dimensionless
D_o = outer tube diameter, m
D_i = inner tube diameter, m
p = design pressure, Pa
σ_y = yield strength of tube material, Pa.

A typical value of yield strength σ_y for tube material is 10.34×10^8 Pa (150,000 psi). With the design pressure p known as a function of tube length and D_i as the inner tube diameter, the outer tube diameter D_o can now be determined along the tube and the weight of the tube can be calculated. The weight of the breechblock and breech locking assembly may be estimated based on historical data for the ratio of breech weight to tube weight for the type of breech locking assembly selected. A reasonable value is 25% of the weight of the tube, which is true for modern weapons such as the M204, 105-mm Howitzer, and the M198, 155-mm Howitzer.

The foregoing sequence of calculations leads to an estimate of tube and breech weight, the major component of the weight of the recoiling parts. This estimate will not be precisely the weight arrived at during detailed design of the tube and breech, but it does provide an estimate of adequate accuracy to allow the weapon designer to initiate calculations and preliminary design of the remainder of the system.

Two parameters in the foregoing analysis that may not be known during the preliminary design process are the tube length U_0 and the weight of the propelling charge W_c. To estimate these parameters, a computational algorithm given in par. 2-3.3, Ref. 1, for approximation of ballistic parameters may be employed. For details of this algorithm, refer to Ref. 1.

With the foregoing interior ballistic knowledge during the in-bore period of the projectile, the equation of motion for the projectile can be integrated and the time t_0 to projectile exit can be calculated from Eq. 2-61, Ref. 1, as

$$t_0 = \frac{8\left(W_p + \frac{W_c}{2}\right)v_p(Q+1)^2}{27 g P_M A Q}, \quad \text{s} \qquad (2\text{-}8)$$

where Q is given by Eq. 2-4 and
t_0 = time to projectile exit, s.

Knowledge of the breech force up to the time of projectile exit is not adequate for input to system design. At projectile exit, high-pressure gas remains in the tube and is free to exit the bore and pass through a muzzle brake, if one is employed. The dynamics of this gas ejection period thus play an important role in the determination of the breech force acting on the recoiling parts after the time t_0 of projectile exit. The breech force B during the gas ejection period is derived in par. 2-3.2.3, Ref. 1, as

$$B = (1 - \beta)B_0\left(1 + \frac{t - t_0}{\phi}\right)^{-9.69}, \quad \text{N} \qquad (2\text{-}9)$$

where

β = muzzle brake factor, dimensionless

THIS DOCUMENT PROVIDED BY THE ABBOTT AEROSPACE
TECHNICAL LIBRARY
ABBOTTAEROSPACE.COM

$$B_0 = B_M \left[\frac{27Q^2}{4(Q+1)^3} \right], \quad \text{N} \tag{2-10}$$

= breech force at projectile exit, N

$t \geq t_0$ = time, s

ϕ = duration of gas ejection period, s

$= 8.7G/B_0$, s (2-11)

$$G = 1.342 \left(\frac{W_c}{g} \right) \left[1 + \frac{W_c}{12W} \right] \sqrt{RT_b - \left(0.0433 + 0.1486 \frac{W_p}{W_c} \right) v_p^2}, \text{ kg·m/s} \tag{2-12}$$

= impulse of breech force during gas ejection period for a tube without a muzzle brake, kg·m/s

RT_b = specific impetus of propellant, J/kg.

To illustrate the use of these equations to calculate breech force, consider the design data for the M198, 155-mm Howitzer (Ref. 9) given in Table 2-1. To illustrate graphically the variation in breech force as a function of time and to show the effect of the muzzle brake on breech force, breech force B is plotted as a function of time in Fig. 2-3. It is important to note that the effect of the muzzle brake is greatest at the high zone charge. This effect is seen by noting the breech force reduction in Fig. 2-3 and the impulse reduction in Table 2-1.

The breech force versus time history of Eq. 2-9 may now be used as a forcing function acting on the recoiling parts after the time t_0 of projectile exit. Because the in-bore period t_0 of the projectile is very small, the equations of motion for the recoiling parts may be approximated by equating the momentum of the projectile and gases exiting the tube to the momentum of the recoiling parts. First,

$$G_0 = \frac{1}{g} \left(W_p + \frac{W_c}{2} \right) v_p, \quad \text{kg·m/s} \tag{2-13}$$

where

G_0 = momentum of projectile and gas at projectile exit, kg·m/s.

Now it is possible to obtain the velocity of the recoiling parts at projectile exit as

$$v_0 = \left(\frac{W_p + \frac{W_c}{2}}{W_r} \right) v_p, \quad \text{m/s} \tag{2-14}$$

where

v_0 = velocity of recoiling parts at projectile exit, m/s

W_r = weight of recoiling parts, N.

At this point in preliminary design, the weight of recoiling parts is not known. When it is known, the motion of the recoiling parts can be calculated by integrating Newton's equations of motion for the recoiling parts with the initial condition established by Eq. 2-14 and the breech force of Eq. 2-9.

Note, finally, that since the breech force acting during the gas ejection period of Eq. 2-9 is reduced by the effect of the muzzle brake factor β, the actual momentum imparted by the gases during the gas ejection period is

$$G_1 = (1 - \beta)G, \quad \text{kg·m/s} \tag{2-15}$$

THIS DOCUMENT PROVIDED BY THE ABBOTT AEROSPACE
TECHNICAL LIBRARY
ABBOTTAEROSPACE.COM

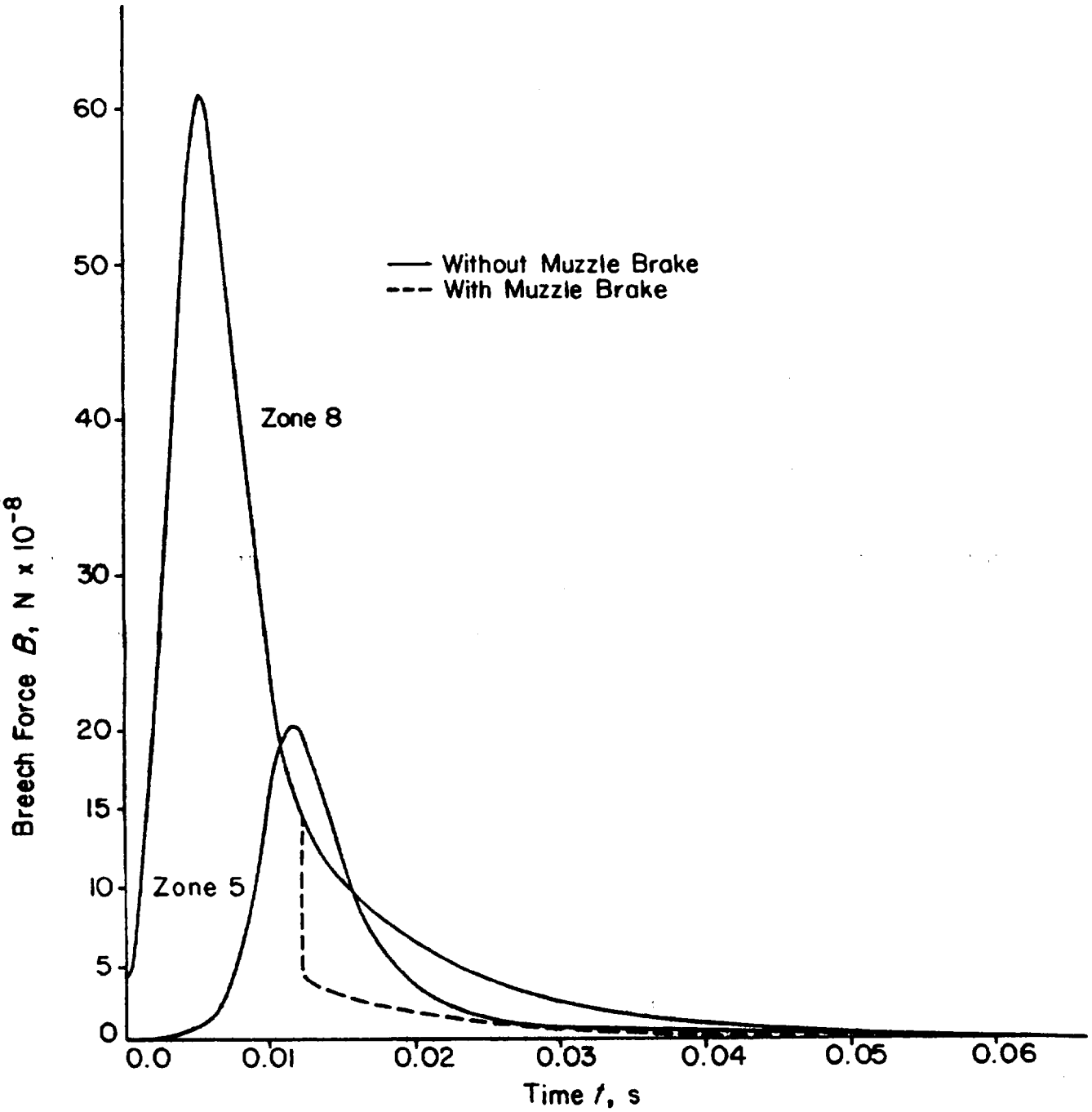

Figure 2-3. Breech Force vs Time, 155-mm Howitzer

where

G_1 = momentum imparted to the breech by gas force during the gas ejection period, with a muzzle brake, kg·m/s.

The role of the muzzle brake in system design is illustrated by Eq. 2-15, i.e., reducing the impulse applied to the recoiling parts during the gas ejection period. If a high-efficiency muzzle brake with a factor β greater than 1 is employed, the momentum imparted to the recoiling parts is actually negative and compensates for some of the

THIS DOCUMENT PROVIDED BY THE ABBOTT AEROSPACE
TECHNICAL LIBRARY
ABBOTTAEROSPACE.COM

momentum imparted to the recoiling parts during the in-bore period. Practical limits on efficiency of the muzzle brake are dictated, however, by the blast overpressure that results in the crew area.

Blast overpressure in the crew area is a complex function of the design geometry of the muzzle brake, the geometry of the weapon, and the elevation of the weapon (Ref. 10). Therefore, experimental methods (Ref. 11) are required to determine blast overpressures in the crew area for candidate muzzle brakes. Because the largest overpressures in the crew area occur approximately 130% of the tube length to the rear of the muzzle, data on blast overpressure are measured at that location for brakes with varying muzzle brake efficiencies. The result is a graphical representation of the form shown in Fig. 2-4. This curve can now be used to select the maximum muzzle brake factor β that is consistent with blast overpressure constraints. With an overpressure limit of 20.7×10^3 Pa, the muzzle brake factor of $\beta = 0.7$ is suggested by the data of Fig. 2-4.

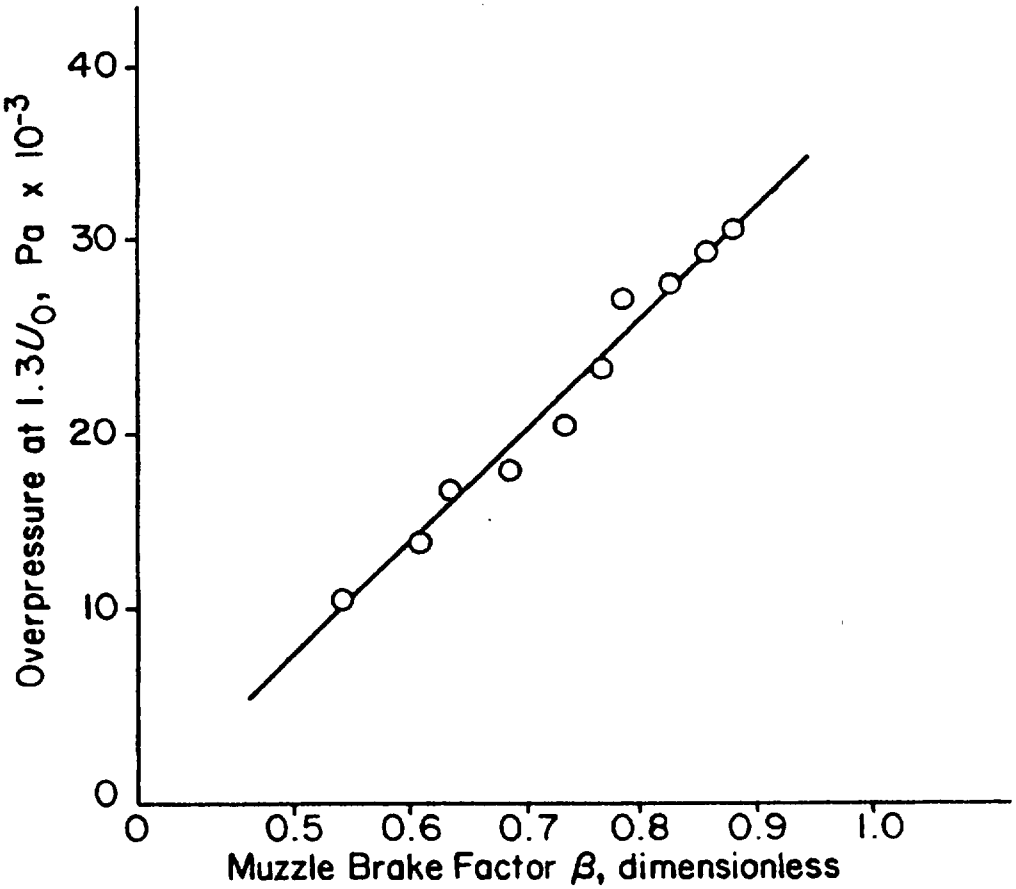

Figure 2-4. Overpressure vs Muzzle Brake Factor

By the use of the predictive methods in Refs. 12 and 13, blast overpressure in the crew area for a weapon without a muzzle brake can be predicted. Empirical evidence (Refs. 12 and 13) then leads to a rule of thumb that for a well designed muzzle brake with $\beta = 1$, i.e., the overpressure is approximately three times as high as would occur if no muzzle brake were employed. For 155-mm artillery, such as the M198, this rule of thumb (Refs. 12 and 13) can be sharpened to predict that an increase of 0.1 in β will lead to an increase in blast overpressure of 1.72×10^3 Pa.

2-4 PRELIMINARY RECOIL MECHANISM DESIGN

Since the recoil mechanism plays a dominant role in determining the levels of force applied to all components of the towed system, its preliminary design must be carried out carefully. Detailed design

THIS DOCUMENT PROVIDED BY THE ABBOTT AEROSPACE
TECHNICAL LIBRARY
ABBOTTAEROSPACE.COM

techniques and examples for recoil mechanisms are presented in Ref. 1. Consideration here is focused on the preliminary sizing and weight estimation for the recoil mechanism.

The design equations for a recoil mechanism are, from Eq. 2-139 of Ref. 1,

$$I + M_r g t_r \sin\Theta = \int_0^{t_r} K(t)dt, \text{ N·s} \tag{2-16}$$

and from Eqs. 2-140 and 2-138 of Ref. 1,

$$M_r L + d_c I + \frac{1}{2}(M_r g t_r^2 \sin\Theta) = \int_0^{t_r} tK(t)dt, \text{ N·s}^2 \tag{2-17}$$

where

I = total impulse of breech force (including muzzle brake effect), N·s
M_r = mass of recoiling parts, kg
t = time, s
t_r = time of recoil, s
Θ = angle of elevation, rad
$K(t)$ = total recoil force, N
L = length of short recoil, m
d_c = centroid of breech force versus time curve, s.

Assume a trapezoidal shape for $K(t)$ versus t shown in Fig. 2-5; Eqs. 2-16 and 2-17 are, respectively,

$$I + M_r g t_r \sin\Theta = K_{max}(t_r - t_1), \text{ N·s} \tag{2-18}$$

$$M_r L + d_c I + \frac{1}{2}(M_r g t_r^2 \sin\Theta) = \frac{1}{2} K_{max} t_r (t_r - t_1), \text{ N·s}^2 \tag{2-19}$$

where

K_{max} = maximum force acting on recoiling parts, N
t_1 = rise and fall time of $K(t)$, s.

Thus, with I, d_c, g, t_1, and the maximum elevation Θ known and M_r estimated, Eqs. 2-18 and 2-19 may be solved for K_{max} and t_r. It remains, however, to obtain an accurate estimate of the mass of recoiling parts, which depends on the recoil mechanism design.

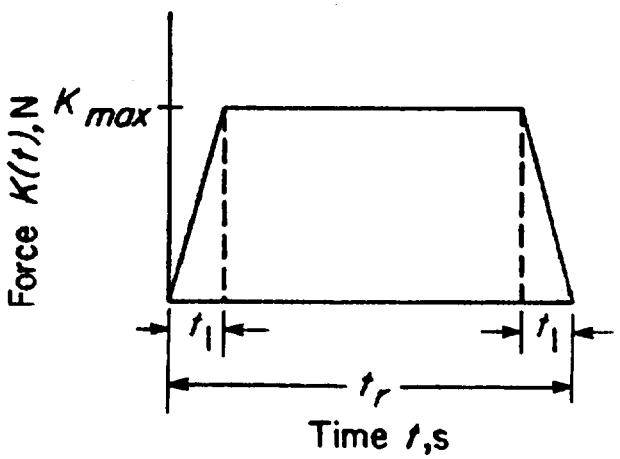

Figure 2-5. Trapezoidal Recoil Force

THIS DOCUMENT PROVIDED BY THE ABBOTT AEROSPACE
TECHNICAL LIBRARY
ABBOTTAEROSPACE.COM

Consider the physical geometry of the recoil cylinder of the Puteaux recoil mechanism shown in Fig. 2-6. Select a recoil cylinder design pressure P (defined by choice of seal design). Then the force R on the recoil rod is

$$R = A_p P + f_p + f_R, \text{ N} \tag{2-20}$$

where

R = force acting on recoil rod, N
A_p = area of recoil piston minus area of recoil rod, m^2
P = recoil design pressure, Pa
f_p = frictional force between recoil cylinder and recoil piston, N
f_R = frictional force between recoil rod and recoil cylinder, N.

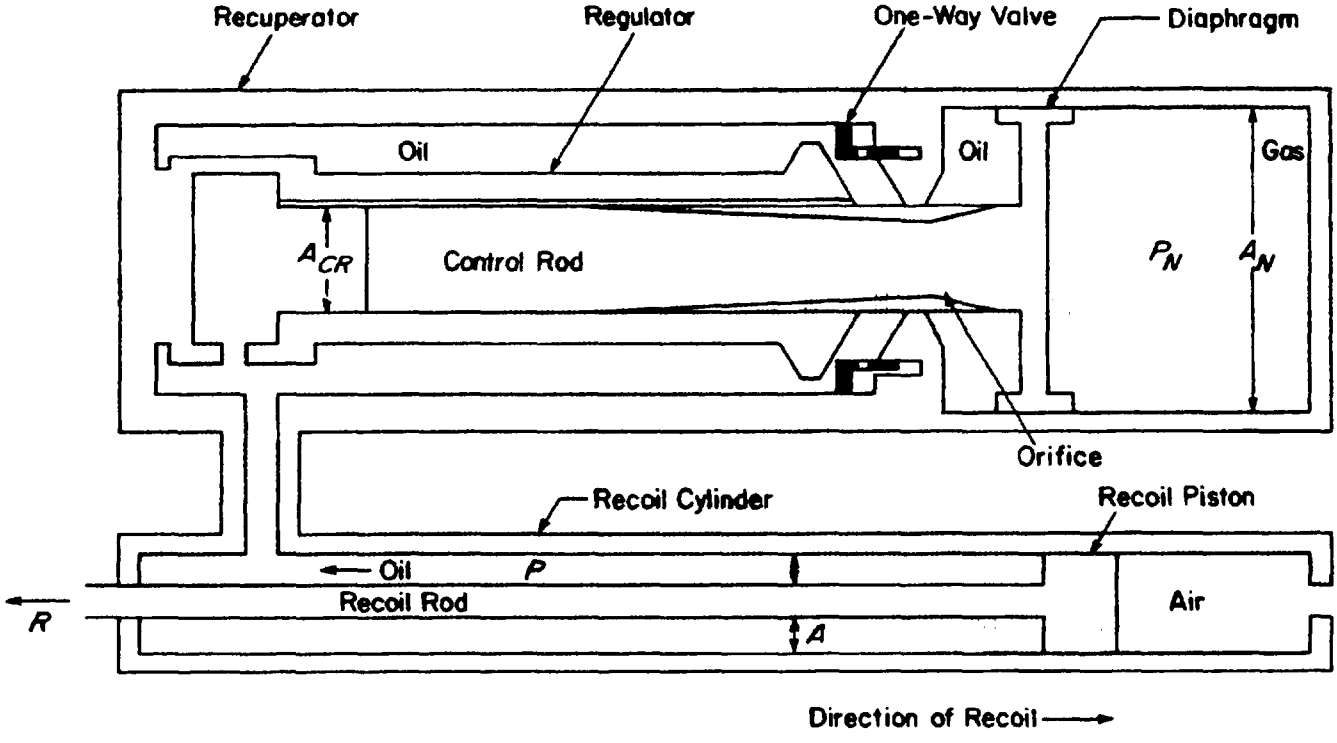

Figure 2-6. Schematic of Puteaux Recoil Mechanism

Finally, the maximum force K_{max} acting on the recoiling parts is

$$K_{max} = R + f_g = A_p P + f_p + f_R + f_g, \text{ N} \tag{2-21}$$

where

f_g = frictional force between the recoiling parts and cradle guide, N.

With estimates for K_{max}, P, f_p, f_R, and f_g, Eq. 2-21 gives

$$A_p = \frac{K_{max} - f_g - f_p - f_R}{P}, \text{ m}^2. \tag{2-22}$$

The thread root area of the recoil rod may now be determined as

THIS DOCUMENT PROVIDED BY THE ABBOTT AEROSPACE
TECHNICAL LIBRARY
ABBOTTAEROSPACE.COM

$$a_1 = \frac{k_1 R}{\sigma_1}, \text{ m}^2 \tag{2-23}$$

where

a_1 = thread root area of recoil rod, m^2
k_1 = stress concentration factor due to threads, dimensionless
σ_1 = allowable stress in recoil rod, Pa.

The minimum diameter d' of the recoil rod threads is

$$d' = \sqrt{\frac{4a_1}{\pi}}, \text{ m} \tag{2-24}$$

where

d' = minimum diameter of recoil rod threads, m.

The maximum recoil rod diameter d (dependent upon the thread root area) can be chosen from a table of standard screw threads.

The inside diameter of the cylinder is now computed from Eq. 2-21

$$A_p = R/P = \frac{\pi}{4}(D_I^2 - d^2) = \frac{K_{max} - f_p - f_R - f_g}{P}, \text{ m}^2 \tag{2-25}$$

so

$$D_I = \left[\frac{4(K_{max} - f_p - f_R - f_g)}{\pi P} + d^2\right]^{1/2}, \text{ m} \tag{2-26}$$

where

D_I = inner diameter of recoil cylinder, m
d = recoil rod diameter, m.

The wall thickness of the recoil cylinder is now determined and is based on strength and stiffness considerations. From the mechanics of thin-walled pressure vessels (Ref. 14), the stress components are

$$\sigma_\ell = \frac{P(D_I^2 - d^2)}{4D_I\delta}, \text{ Pa} \tag{2-27}$$

$$\sigma_c = \frac{D_I P}{2\delta}, \text{ Pa} \tag{2-28}$$

$$\sigma_n = P, \text{ Pa} \tag{2-29}$$

where

σ_ℓ = longitudinal stress in recoil cylinder, Pa
σ_c = circumferential stress in recoil cylinder, Pa
σ_n = normal stress in recoil cylinder, Pa
δ = wall thickness of recoil cylinder, m.

THIS DOCUMENT PROVIDED BY THE ABBOTT AEROSPACE
TECHNICAL LIBRARY
ABBOTTAEROSPACE.COM

The von Mises yield criterion is used as a material failure criterion (Refs. 9 and 14), which is

$$\sigma_2 \geq \left[\frac{1}{2} (\sigma_\ell - \sigma_c)^2 + \frac{1}{2} (\sigma_c - \sigma_n)^2 + \frac{1}{2} (\sigma_n - \sigma_\ell)^2 \right]^{1/2}, \text{Pa} \tag{2-30}$$

where

σ_2 = recoil cylinder material yield strength, Pa.

Square Eq. 2-30, and substitute from Eqs. 2-27, 2-28, and 2-29 to give

$$2\sigma_2^2 \geq \left(\frac{P}{4\delta D_I} \right)^2 \left[(D_I^2 + d^2)^2 + 4D_I^2(D_I - 2\delta)^2 + (4D_I\delta - D_I^2 + d^2)^2 \right], \text{Pa}^2. \tag{2-31}$$

Solve this inequality (Eq. 2-31) for δ. The stress constraint requires that

$$\delta \geq \left\{ \left[\frac{4\sigma_2^2}{P^2} (3D_I^4 + d^4) - 3(D_I^2 + d^2)^2 \right]^{1/2} - (3D_I^2 - d^2) \right\} \left[8D_I \left(\frac{\sigma_2^2}{P^2} - 1 \right) \right]^{-1}, \text{m}. \tag{2-32}$$

The wall thickness of the cylinder must also be large enough so that the radial expansion of the cylinder is small and leakage does not occur around the seals. With the limit Δr_1 on radial expansion known from seal considerations, the equation for radial expansion is (Refs. 15 and 16)

$$\Delta r_1 \geq \frac{D_I P}{2E_1} \left[\frac{(D_I + 2\delta)^2 + D_I^2}{(D_I + 2\delta)^2 - D_I^2} + \mu_1 \right], \quad \text{m} \tag{2-33}$$

where

Δr_1 = limit of radial expansion, m
E_1 = Young's modulus for recoil cylinder material, Pa
μ_1 = Poisson's ratio for recoil cylinder material, dimensionless.

The solution of this inequality (Eq. 2-33) for δ gives

$$\delta \geq \frac{D_I}{2} \left\{ \left[\frac{2E_1\Delta r_1 + PD_I(1 - \mu_1)}{2E_1\Delta r_1 - PD_I(1 + \mu_1)} \right]^{1/2} - 1 \right\}, \text{m} \tag{2-34}$$

which is a limit on the wall thickness required if radial expansion is to be properly limited. The radial expansion limit Δr_1 will be assumed to be 0.0004 times the cylinder bore diameter, i.e., $\Delta r_1 = 0.0004 D_I$.

The outside diameter D_1 of the recoil cylinder is

$$D_1 = D_I + 2\delta, \text{ m} \tag{2-35}$$

and δ is the larger of the two limits obtained in Eqs. 2-32 and 2-34.

The total length L_1 of the recoil cylinder is

$$L_1 = L' + 5D_I, \text{ m} \tag{2-36}$$

where

L' = length of long recoil, m

THIS DOCUMENT PROVIDED BY THE ABBOTT AEROSPACE
TECHNICAL LIBRARY
ABBOTTAEROSPACE.COM

and $5D_I$ represents an approximation of the additional length needed for stuffing box and end assemblies (Ref. 15).

The weight W_1 of the recoil cylinder is now calculated as

$$W_1 = \frac{\pi}{4}\,(L' + 5D_I)\,(D_1^2 - D_I^2)\,\rho_1, \quad \text{N} \tag{2-37}$$

where

ρ_1 = weight density of recoil cylinder material, N/m^3.

Finally, the weight W_2 of the recoil cylinder assembly that is attached to the recoiling parts is

$$W_2 = W_1 + \frac{\pi}{2}\,D_I(D_I^2 - d^2)\,\rho_1, \quad \text{N} \tag{2-38}$$

and $\pi D_I(D_I^2 - d^2)\rho_1/2$ represents an approximation (Ref. 15) of the additional weight needed for miscellaneous components such as bearing assembly, insert assembly, spring assemblies, spacers, packings, and nuts. (See Ref. 15.)

The task of defining the weight of the remaining parts of the recoil mechanism is somewhat more complicated. Refer to Fig. 2-6; in order to assure that the recuperator forces the recoiling parts into battery prior to firing, it is necessary that (See Ref. 15.)

$$P_N = \frac{C}{A_N}\,(W_r \sin\theta + f_g + f_p + f_R), \quad \text{Pa} \tag{2-39}$$

where

C = in-battery sustaining factor > 1, dimensionless
A_N = diaphragm area, m^2
P_N = initial gas pressure in recuperator, Pa.

The in-battery sustaining factor C is selected to provide an acceptably high force to hold the recoiling parts in-battery.

Because the volume of oil displaced in long recoil must equal the gas volume reduction in the recuperator,

$$A_N Y = A_p L', \quad \text{m}^3 \tag{2-40}$$

where

Y = stroke of control rod, m.

By the gas law for isotropic expansion,

$$(P_N)_{max} = P_N \left(\frac{V_i}{V_i - A_N Y} \right)^{\gamma}, \quad \text{Pa} \tag{2-41}$$

where

$(P_N)_{max}$ = maximum gas pressure in recuperator, Pa
V_i = initial gas volume, m^3
γ = ratio of specific heats, dimensionless.

$(P_N)_{max}$ must be low enough to prevent leakage between the gas and oil; therefore, it is determined by the choice of seals. If $(P_N)_{max}$ is known, Eqs. 2-40 and 2-41 may be solved for V_i as

THIS DOCUMENT PROVIDED BY THE ABBOTT AEROSPACE
TECHNICAL LIBRARY
ABBOTTAEROSPACE.COM

$$V_i = \frac{A_p L' \left[\frac{(P_N)_{max}}{P_N} \right]^{1/\gamma}}{\left[\frac{(P_N)_{max}}{P_N} \right]^{1/\gamma} - 1}, \quad \text{m}^3. \tag{2-42}$$

Then the length ℓ of the recuperator cylinder initially containing gas is

$$\ell = \frac{V_i}{A_N}, \quad \text{m}. \tag{2-43}$$

Thus

$$D_N = \sqrt{4A_N/\pi}, \quad \text{m} \tag{2-44}$$

where

D_N = diameter of recuperator cylinder, m.

The overall length of the recoil cylinder (L_1 in Eq. 2-36) having been determined, it is assumed that the recuperator cylinder must have the same length and is of the form ($\ell + Y + 3D_N$), where $3D_N$ is an approximation of the length needed for the diaphragm, head assembly, and clearance (Ref. 15). That is,

$$L_1 = \ell + Y + 3D_N, \quad \text{m}. \tag{2-45}$$

From Eqs. 2-40 and 2-43 and by adding V_i to both sides of Eq. 2-40,

$$A_N(\ell + Y) = A_p L' + V_i, \quad \text{m}^3. \tag{2-46}$$

Substitution of ($\ell + Y$) from Eq. 2-45 into Eq. 2-46 yields

$$A_N(L_1 - 3D_N) = A_p L' + V_i, \quad \text{m}^3 \tag{2-47}$$

or since $A_N = \pi D_N^2/4$,

$$\frac{\pi D_N^2}{4}(L_1 - 3D_N) = A_p L' + V_i, \quad \text{m}^3. \tag{2-48}$$

The result is a cubic equation in D_N, i.e.,

$$D_N^3 - \frac{L_1 D_N^2}{3} + \frac{4(A_p L' + V_i)}{3\pi} = 0, \quad \text{m}^3. \tag{2-49}$$

Eq. 2-49 can easily be solved on a digital computer for D_N. Then A_N, ℓ, and Y can be determined. The immediate problem is to know which root for D_N is the most practical from an engineering design standpoint. Descarte's rule of signs states that an expression of the form $ax^3 - bx^2 + c = 0$ will always have zero or two positive roots. From a physical standpoint, there must be at least one positive root. Therefore, the solution of the cubic will give two positive roots and one negative root. The negative root is eliminated, and the most realistic positive root is chosen. To do this, the assumption is made that the ratio of the control rod stroke Y to the maximum recoil length L' will never be less than 0.65 and never greater than 1. From Eq. 2-40,

THIS DOCUMENT PROVIDED BY THE ABBOTT AEROSPACE
TECHNICAL LIBRARY
ABBOTTAEROSPACE.COM

$$\frac{Y}{L'} = \frac{A_p}{A_N}, \quad \text{dimensionless.} \tag{2-50}$$

Each positive root of D_N is computed, and since $A_N = \pi D_N^2/4$, the condition $0.65 \leq A/A_N \leq 1$ is checked. The root D_N that satisfies this condition will be the desired root. From previous experience, there should be only one root that satisfies this condition.

By using the basic inside diameter D_N, there are two cylinder sections with which to be concerned—one under only gas pressure and the other under oil pressure as shown in Fig. 2-7. The proper cylinder wall thickness is determined by choosing the larger δ computed from radial expansion and cylinder stress relationships. In the gas portion the thickness based on radial expansion constraints must satisfy (See Eq. 2-34.)

$$\delta_2 \geq \frac{D_N}{2}\left\{\left[\frac{2E_2\Delta r_2 + (P_N)_{max}D_N(1-\mu_2)}{2E_2\Delta r_2 - (P_N)_{max}D_N(1+\mu_2)}\right]^{1/2} - 1\right\}, \quad \text{m} \tag{2-51}$$

where

δ_2 = wall thickness in gas portion of cylinder, m
Δr_2 = an acceptable expansion limit based on seal design = $0.0004D_N$, m
E_2 = Young's modulus of recuperator cylinder material, Pa
μ_2 = Poisson's ratio of recuperator cylinder material, dimensionless.

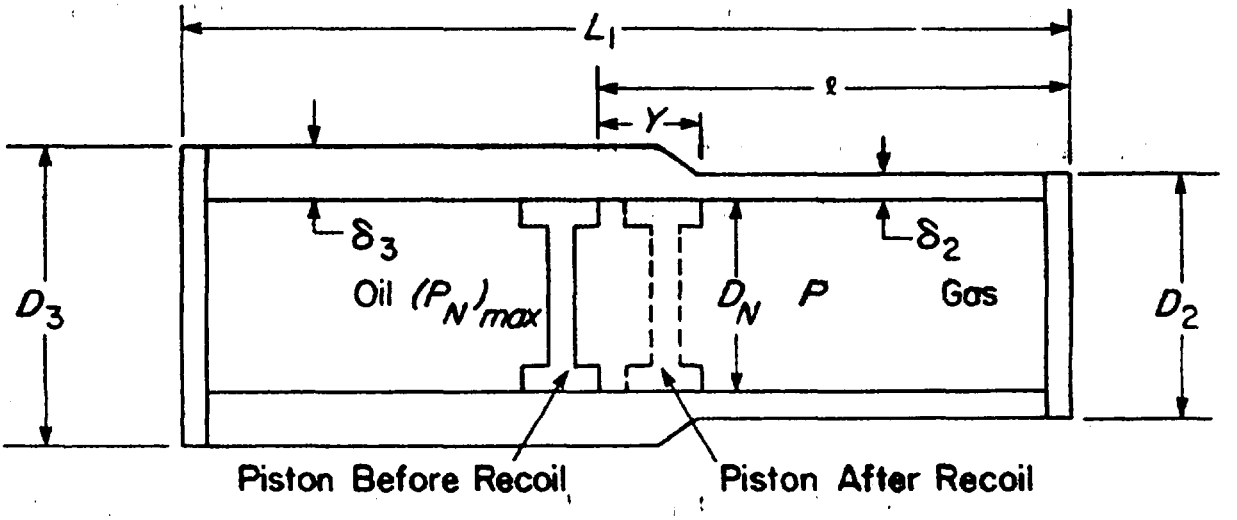

Figure 2-7. Recuperator

Based on stress constraints, the thickness must also satisfy

$$\delta_2 \geq \left\{\left[\frac{4\sigma_3^2}{(P_N)_{max}^2}(3D_N^4) - 3D_N^4\right]^{1/2} - 3D_N^2\right\}\left[8D_N\left(\frac{\sigma_3^2}{(P_N)_{max}^2} - 1\right)\right]^{-1}, \text{m} \tag{2-52}$$

where

σ_3 = gas cylinder material yield strength, Pa

which is obtained from Eq. 2-32 with $d = 0$ because there is no rod in this cylinder.

THIS DOCUMENT PROVIDED BY THE ABBOTT AEROSPACE
TECHNICAL LIBRARY
ABBOTTAEROSPACE.COM

Then the outside diameter D_2 of the gas portion is

$$D_2 = D_N + 2\delta_2, \text{ m.} \tag{2-53}$$

Similarly, in the oil portion of the recuperator cylinder, the thickness based on expansion conditions must satisfy

$$\delta_3 \geq \frac{D_N}{2}\left\{\left[\frac{2E_2\Delta r_3 + PD_N(1-\mu_2)}{2E_2\Delta r_3 - PD_N(1+\mu_2)}\right]^{1/2} - 1\right\}, \quad \text{m} \tag{2-54}$$

where the inside diameters of the oil and gas cylinders must be the same (See Fig. 2-6.) and

δ_3 = wall thickness in oil portion of cylinder, m
Δr_3 = allowable radial expansion limit = $0.0008D_N$, m.

Thickness based on stress conditions must satisfy

$$\delta_3 \geq \left\{\left[\frac{4\sigma_4^2}{P^2}(3D_N^4) - 3D_N^4\right]^{1/2} - 3D_N^2\right\}\left[8D_N\left(\frac{\sigma_4}{P^2} - 1\right)\right]^{-1}, \text{ m} \tag{2-55}$$

where
σ_4 = oil cylinder material yield strength, Pa.

Then the outside diameter D_3 of the oil portion of the recuperator is

$$D_3 = D_N + 2\delta_3, \text{ m.} \tag{2-56}$$

The total weight W_{CY} of the recuperator cylinder, as shown in Fig. 2-7, is

$$W_{CY} = \frac{\pi}{4}(D_2^2 - D_N^2)(\ell - Y)\rho_2 + \frac{\pi}{4}(D_3^2 - D_N^2)(L_1 - \ell + Y)\rho_2, \text{ N} \tag{2-57}$$

where
ρ_2 = weight density of recuperator cylinder material, N/m^3.

The weight W_{CR} of the control rod shown in Fig. 2-6 is

$$W_{CR} = A_{CR}(Y + D_N)\rho_3, \quad \text{N} \tag{2-58}$$

where
A_{CR} = cross-sectional area of control rod, m^2
ρ_3 = weight density of control rod material, N/m^3

and a length of control rod of D_N after travel Y should be retained in its bearings for stability.

The control rod area can be derived from the following equations of motion if it is assumed that the breech force is expended and that oil pressure on the diaphragm is zero:

$$\frac{W_r\ddot{x}}{g} = -A_pP, \quad \text{N} \tag{2-59}$$

THIS DOCUMENT PROVIDED BY THE ABBOTT AEROSPACE
TECHNICAL LIBRARY
ABBOTTAEROSPACE.COM

$$\frac{W_{CR}\ddot{y}}{g} = A_{CR}P - A_N P_N\,, \quad \text{N} \tag{2-60}$$

where

P = recoil design pressure, Pa
x = absolute displacement of recoiling parts, m
y = absolute displacement of control rod, m.

The volume of oil entering the recuperator is $A_p x$, which must equal the reduction in gas volume $A_N(y - x)$, so

$$y = \left(\frac{A_p + A_N}{A_N}\right) x\,, \quad \text{m} \tag{2-61}$$

and

$$\ddot{y} = \left(\frac{A_p + A_N}{A_N}\right) \ddot{x}\,, \quad \text{m/s}^2. \tag{2-62}$$

From Eqs. 2-59 and 2-60,

$$\frac{W_r \ddot{x}}{W_{CR}\ddot{y}} = \frac{-A_p P}{A_{CR}P - A_N P_N}\,, \text{ dimensionless.} \tag{2-63}$$

The substitution of the expression for $\ddot{y}$ from Eq. 2-62 into Eq. 2-63 yields

$$\frac{W_r \ddot{x}}{W_{CR}\left(\frac{A_p + A_N}{A_N}\right)\ddot{x}} = \frac{-A_p P}{A_{CR}P - A_N P_N}\,, \text{ dimensionless.} \tag{2-64}$$

Substitution of the expression for W_{CR} from Eq. 2-58 into Eq. 2-64 yields

$$\frac{W_r}{\left(\frac{A_p + A_N}{A_N}\right) A_{CR}(Y + D_N)\rho_3} = \frac{-A_p P}{A_{CR}P - A_N P_N}\,, \text{ dimensionless.} \tag{2-65}$$

Therefore,

$$A_{CR} = \frac{W_r A_N P_N}{W_r P + \left(\frac{A_p + A_N}{A_N}\right)(Y + D_N)A_p P \rho_3}\,, \quad \text{m}^2. \tag{2-66}$$

The weight of the control rod is now determined from Eq. 2-58.

The weight W_{reg} of the regulator assembly shown in Fig. 2-6, excluding the control rod, is approximated (Ref. 15) by

THIS DOCUMENT PROVIDED BY THE ABBOTT AEROSPACE
TECHNICAL LIBRARY
ABBOTTAEROSPACE.COM

$$W_{reg} = \left(\frac{5}{8}\right) A_N(Y + 1.5D_N)\rho_2, \quad \text{N.} \tag{2-67}$$

The 5/8 factor represents a reduction in the sectional density because of the proportion of oil to steel in this portion of the system. (See Ref. 15.)

The total recuperator weight W_{rec} is

$$W_{rec} = W_{CY} + W_{CR} + W_{reg}, \quad \text{N.} \tag{2-68}$$

With these equations the designer can now calculate the total weight of recoil mechanism components that move in recoil. A refined estimate of the total weight W_r of recoiling parts can now be calculated using the tube and breech weights calculated in par. 2-3 and the weight of the recoil mechanism calculated in this paragraph. Because W_r plays an important role in recoil force determination and is a substantial part of the total weight of a towed system, the design team now has the weight and force data needed to proceed to preliminary design of the other components of the system.

Although the analysis presented here has been for Puteaux-type recoil mechanisms that are commonly used in towed artillery systems, the same type of analysis can be used for preliminary design of other types of recoil mechanisms. For soft recoil mechanism applications, refer to Ref. 16.

Some basic tradeoffs exist that may assist the designer in distributing weight within the recoil mechanism and the towed system. For $\Theta = 0$ the expression for $K_{max}(t_r - t_1)$ from Eq. 2-18 can be substituted into Eq. 2-19 to obtain

$$t_r = \frac{2(M_r L + d_c I)}{I}, \quad \text{s.} \tag{2-69}$$

Eq. 2-18, with Eq. 2-69, yields

$$K_{max} = \frac{I^2}{2(M_r L + d_c I) - t_1 I}, \quad \text{N.} \tag{2-70}$$

Thus, if M_r can be increased, K_{max} can be decreased. This is the reason the designer should attach as many of the recoil mechanism components as possible to the recoiling parts, i.e., to increase M_r. This simple tradeoff provides the primary reason Puteaux-type recoil mechanisms that move with the recoiling parts are used in towed artillery systems. Heavier tubes generally have longer life, so this tradeoff lends even greater support for a relatively heavy tube, provided system weight constraints can be met.

A final note concerns friction of packings, seals, and guides in the recoil mechanism. There is no counterrecoil buffer in the Puteaux-type recoil mechanism; therefore, friction plays an important role in counterrecoil dynamics. A substantial amount of friction is desirable to minimize problems associated with slamming the recoiling parts into battery.

2-5 COMPONENT PRELIMINARY SIZING

As noted in par. 2-4, the recoil mechanism plays a dominant role in determining the level of force applied to all components of the weapon system during firing. Consequently, considerable effort has been spent to develop methods for accurately estimating preliminary sizes of recoil mechanism parts (Refs. 1, 17, and 18) and the weight of recoiling parts. Mathematical models for estimating preliminary sizes of other components of the weapon system have not, however, been developed. Therefore, historical data should be used to estimate the preliminary sizes and weights of these components for the near future. Mathematical models for these components need to be developed for use in preliminary design.

The components whose weights and preliminary sizes need to be estimated are the cradle, elevating mechanism, equilibrator, top carriage, bottom carriage, suspension system, traverse system, trails, and support assembly. To estimate weights of these components at the preliminary design stage, historical data

THIS DOCUMENT PROVIDED BY THE ABBOTT AEROSPACE
TECHNICAL LIBRARY
ABBOTTAEROSPACE.COM

from older or existing weapon systems may be used. Historical data—indicating that the weight of components varies linearly with the peak recoil force—are extrapolated to estimate the weight of the system under development (Ref. 18). Once the weights of components have been estimated, the total weight of the weapon can be determined.

In Ref. 18 data for existing 105-mm towed howitzers have been summarized. Weight of various components or subsystems has been plotted against the peak recoil force the weapon experiences. A typical graph of this type for the cradle is shown in Fig. 2-8. Such graphs of historical data for systems similar to the one being

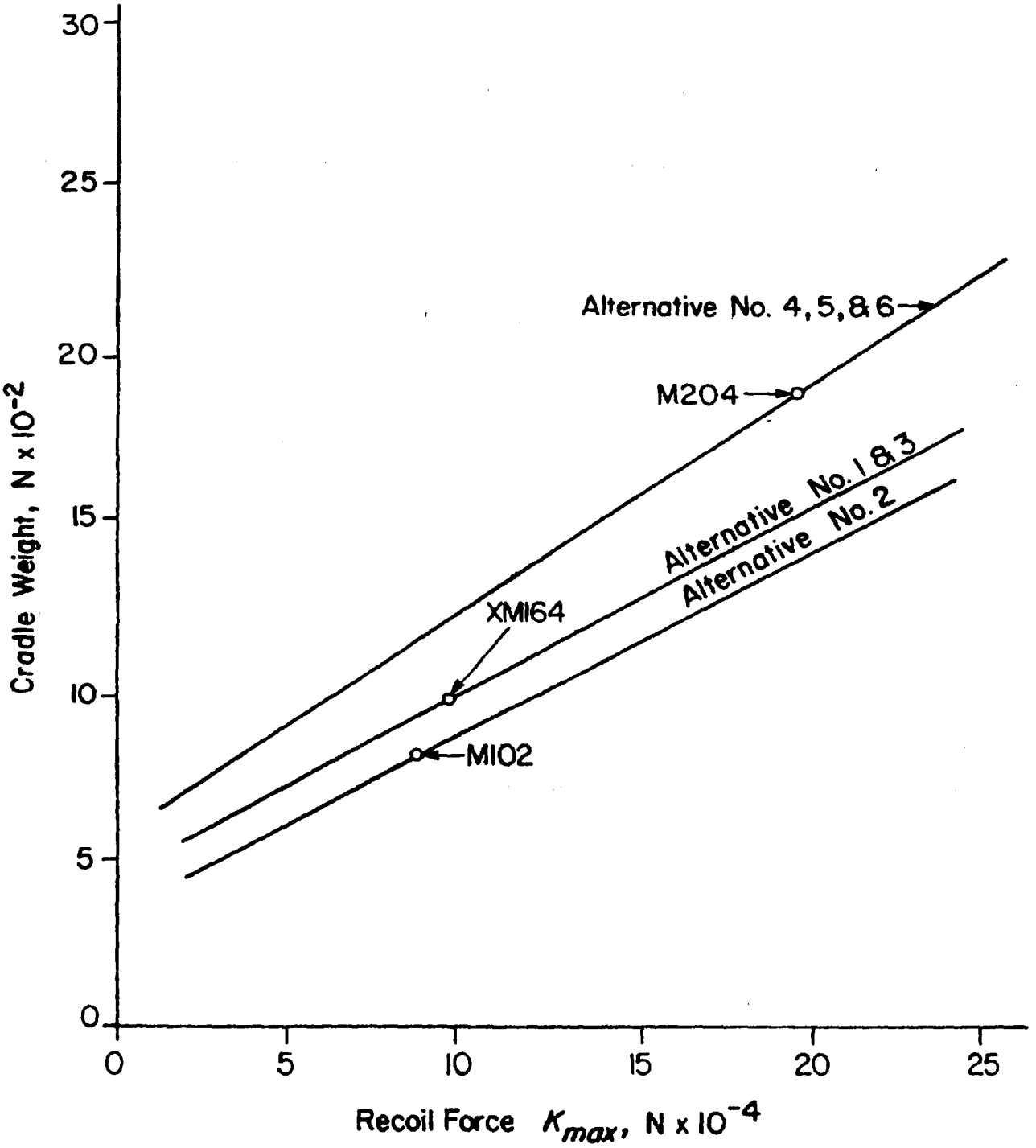

Figure 2-8. Cradle Weight vs Recoil Force

THIS DOCUMENT PROVIDED BY THE ABBOTT AEROSPACE
TECHNICAL LIBRARY
ABBOTTAEROSPACE.COM

designed are then used to estimate weights of the components. Note from Fig. 2-8 that cradle weight for the soft recoil system (M204) is greater than it is for conventional systems. This difference is due to the requirement for greater structural stiffness of the soft recoil weapon and the additional travel required by misfire and overshoot buffers.

With peak recoil force and recoiling parts weight determined by the method of pars. 2-3 and 2-4, the weight of the cradle is determined from Fig. 2-8. Now the total weight of the tipping parts is known, and preliminary sizing of the elevating and equilibrator mechanisms can proceed. From historical data (Ref. 18) the weight of these mechanisms is found to vary linearly with the weight of tipping parts, as shown in Fig. 2-9. From this graph a preliminary estimate of elevating and equilibrator mechanism weights is obtained.

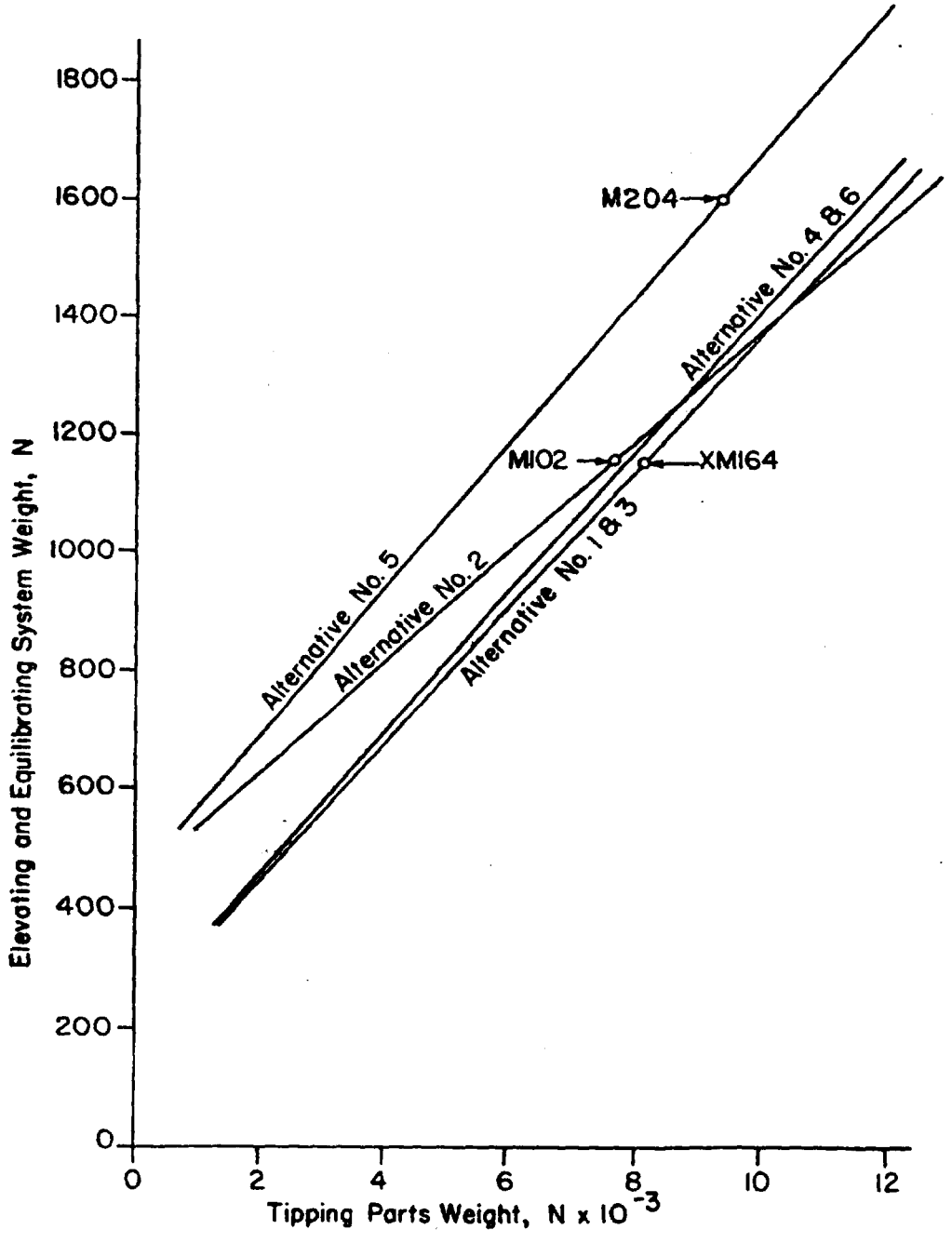

Figure 2-9. Elevating and Equilibrator Weight vs Tipping Parts Weight

THIS DOCUMENT PROVIDED BY THE ABBOTT AEROSPACE
TECHNICAL LIBRARY
ABBOTTAEROSPACE.COM

Similar historical data graphs are employed to estimate weights of top and bottom carriage, traversing mechanism, trails, firing base, and suspension system. Refs. 17 and 18 present data and analysis of weights for 105-mm towed systems. A similar set of curves can be developed for 155-mm systems by using data on related US and foreign designs. Data for intermediate caliber weapons will require interpolation between historical data curves for standard calibers; accordingly, greater error may be expected.

Design of each of the components of the system is iterative, beginning with estimates of size and weight obtained in pars. 2-3, 2-4, and in this paragraph. Component design is continually improved as more refined data become available. The preliminary design of components can begin once the recoil force level is known from calculations of Ref. 1 and par. 2-4. For this purpose, simplified, determinate structural models may be used to check for the strength of these components. Detailed design of elevating system, equilibrators, traversing system, cradle, top carriage, and bottom carriage is presented in the subsequent chapters of this handbook.

An important consideration at the preliminary design stage is the interaction of the bottom carriage with the ground. The weapon is supported on the ground through the bottom carriage during firing, and all forces during firing are transmitted to the ground through the bottom carriage. It is therefore necessary that the ground offer a stable reaction without allowing appreciable displacement of the bottom carriage.

The parts of the bottom carriage which come in contact with the ground are the spades and floats at the rear end of the trails and the firing base (firing platform or front float) that is lowered to the ground in preparation for firing. Spades are vertical plates embedded in the ground, whereas floats are horizontal plates (sometimes ribbed or in the form of a box) resting on the ground. Spades resist horizontal reactions from the ground in the form of passive ground pressure, and floats resist vertical ground reactions. Design for strength of the plates making up the spades and floats is based on simplifying assumptions that the ground reactions are uniformly distributed over the contact surface.

To determine sizes of spades, floats, and firing platforms, ground reaction forces must be calculated. The top carriage, through the traverse bearing, transmits recoil force F to the bottom carriage during firing (Fig. 2-10). This force is generally largest at high firing elevation angles, although design should also be checked for all elevation angles. The magnitude of the force F depends on the recoil force, firing elevation angle, and equilibrator force. The reaction forces R_{V1}, R_{H1}, R_{V2}, R_{H2}, and R_{V3} (Refer to Fig. 2-10.)

where

R_{V1} = vertical ground reaction at Point 1, N
R_{H1} = horizontal ground reaction at Point 1, N
R_{V2} = vertical ground reaction at Point 2, N
R_{H2} = horizontal ground reaction at Point 2, N
R_{V3} = vertical ground reaction at front float or firing base, N

are calculated based on simplifying assumptions during preliminary design. Statically determinate models, such as those presented in Chapter 3, are generally used in calculating these forces. Simplified models for calculating ground reaction are presented in Chapter 9. The reaction forces are presumed known for the discussion that follows.

The sizes of the firing base (or front float) and the rear float are determined first. The surface area A_{fr} of the rear float must be

$$A_{fr} = \frac{R_f S_f}{b_c}, \text{ m}^2 \tag{2-71}$$

where

R_f = vertical reaction force at the rear float (maximum of R_{V1} and R_{V2}), N
b_c = bearing capacity of soil, Pa
S_f = safety factor (three to six), dimensionless.

The bearing capacity of various soils may be found in Ref. 19.

THIS DOCUMENT PROVIDED BY THE ABBOTT AEROSPACE
TECHNICAL LIBRARY
ABBOTTAEROSPACE.COM

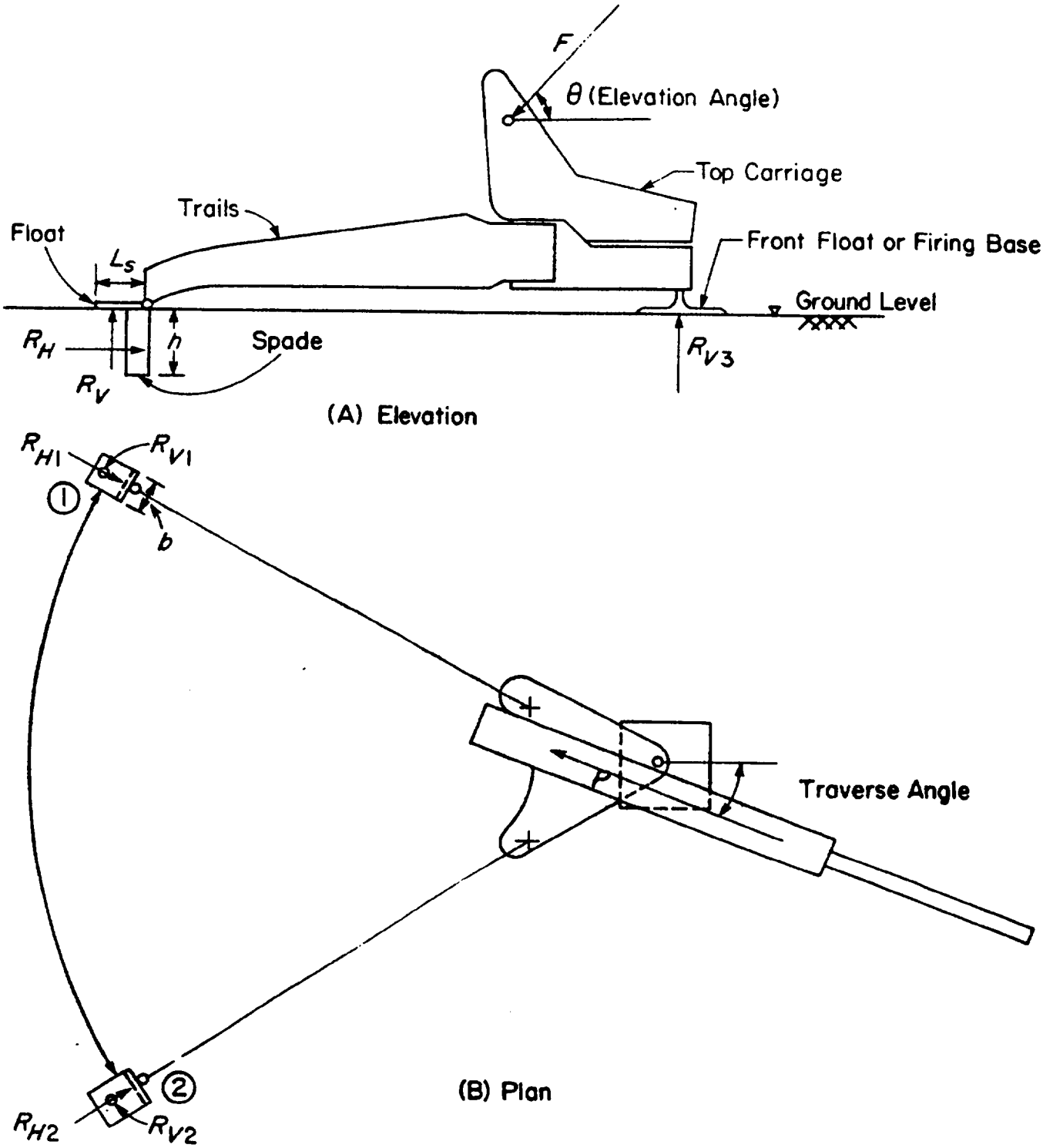

Figure 2-10. Spade-Float Geometry and Ground Reactions

The rear float is generally a flat rectangular plate. Thus the surface area A_{fr} that comes in contact with the soil is

$$A_{fr} = b_s L_s, \quad \text{m}^2 \tag{2-72}$$

THIS DOCUMENT PROVIDED BY THE ABBOTT AEROSPACE
TECHNICAL LIBRARY
ABBOTTAEROSPACE.COM

where

b_s = width of float, m
L_s = length of float, m.

The dimensions b_s and L_s can be determined based on fabrication and practical considerations.

Similarly, the surface area A_{ff} of the front float or firing base is

$$A_{ff} = \frac{R_{V3} S_f}{b_c}, \ \text{m}^2. \tag{2-73}$$

The radius r_{ff} of a circular front float is then given as

$$r_{ff} = \sqrt{\frac{A_{ff}}{\pi}}, \ \text{m}. \tag{2-74}$$

The determination of the size of the spade is more involved. Here, shear strength of the soil and its cohesiveness determine the size of the spade. The width of the spade is usually the same as the width b_s of the rear float. Therefore, it is necessary to determine only the height h of the spade.

In estimating the size of the spade, the determination of the lateral passive pressure of the soil on the spade is required. Prediction of lateral earth pressure depends on the type of soil and its loading history. This prediction usually requires the solution of a continuum mechanics problem. The process is further complicated by the lack of knowledge of the initial stress conditions, the constitutive law for the soil, and realistic boundary conditions. Constitutive relations for sands and lightly consolidated clays prepared in a laboratory are well established. However, for natural soils encountered in field conditions, these relations are not well understood. The conflict between real and ideal conditions has led to approximations in predicting lateral soil pressures. Theories based on the state of plastic equilibrium (or limited equilibrium, which implies impending failure of the soil mass) are used to determine lateral pressure when such pressures are the dominant unknowns. The transition from the state of plastic equilibrium to that of plastic flow represents failure of the soil mass.

There are a number of criteria proposed for the failure of soils and other similar materials. One of the widely used and the simplest criterion is that due to Mohr-Coulomb, Refs. 18 and 19. It postulates that the material at a point will fail if the shear stress at that point in the medium satisfies the condition

$$\tau = c + \sigma \tan\phi_s, \quad \text{Pa} \tag{2-75}$$

where

τ = shear strength of soil, Pa
c = apparent cohesion of soil, Pa
σ = normal stress on sheared surface of soil, Pa
ϕ_s = angle of internal shearing resistance of soil, rad.

The parameters c and ϕ_s are properties of a soil and can be determined by experiment. More discussion on these experiments and the Mohr-Coulomb law may be found in Refs. 18 and 19. Once the normal pressure on the soil and the type of soil have been determined, the shear strength of the soil can be determined from Eq. 2-75.

To determine the height of the spade, the lateral pressure on the spade must be found. The lateral pressure at the bottom of the spade is determined once c and ϕ_s for the soil and the vertical pressure on the soil have been determined. The vertical pressure p_v on the soil, resulting from the vertical force component of the spade, is known from the reaction force R_{V1} or R_{V2} at the float and is given as

$$p_v = \frac{R_{V1}(\text{or } R_{V2})}{b_s L_s}, \quad \text{Pa}. \tag{2-76}$$

THIS DOCUMENT PROVIDED BY THE ABBOTT AEROSPACE
TECHNICAL LIBRARY
ABBOTTAEROSPACE.COM

The lateral pressure p_ℓ at the base of the spade can be computed using the Mohr-Coulomb law and the Mohr's circle (Refs. 18 and 19) as

$$p_\ell = \frac{p_v}{N_\phi} - \frac{2c}{\sqrt{N_\phi}}, \quad \text{Pa} \tag{2-77}$$

where

$N_\phi = \tan^2(\pi/4 + \phi_s/2)$ = flow value, dimensionless.

Distribution of the lateral pressure on the spade is as shown in Fig. 2-11. This pressure distribution on the spade is assumed to be uniform because the passive pressure due to soil mass is negligible. From equilibrium considerations for the spade, its height h is given as

$$h = \frac{R_{H1}(\text{or } R_{H2})\, S_f}{p_\ell\, b_s}, \quad \text{m.} \tag{2-78}$$

This height should be adjusted for fabrication and other practical considerations.

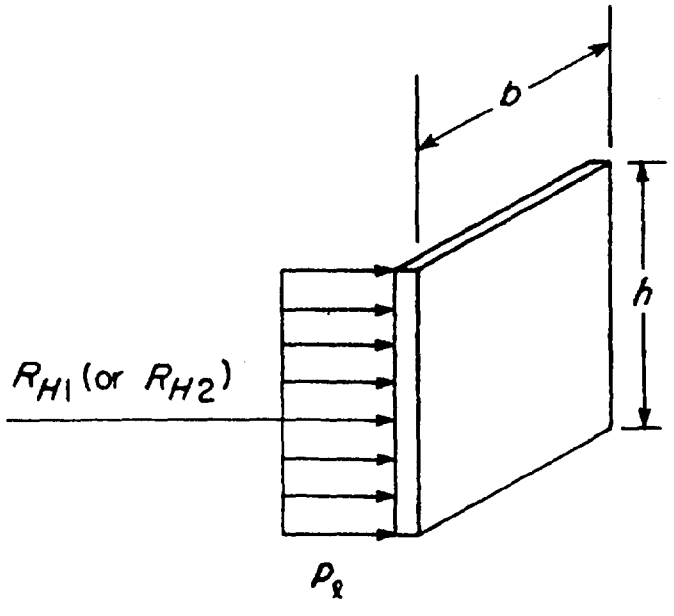

Figure 2-11. Pressure Distribution on Spades

2-6 DESIGN FOR TOWING

Because the towed artillery weapon must be towed by one or more prime movers, towing considerations must be introduced early in the design process. Weapon geometry is often substantially influenced by the requirements that the weapon be towed over rough terrain and that turning radii for the vehicle and weapon can be achieved. Further, tires must be selected to achieve allowable ground pressures, and brakes must be designed to provide stable stopping of the weapon and prime mover. Also wheelbase and tire elasticity play a role in assuring stability of the weapon during towing.

As shown in Fig. 2-12, adequate clearance must be allowed between the bottom carriage and other parts of the weapon to allow towing over irregular terrain. An angle α_a of approach and an angle β_d of departure generally will be established based on terrain considerations. These angles define reference lines above which all components of the weapon must be located. Initial weapon layout and subsequent design must not be

THIS DOCUMENT PROVIDED BY THE ABBOTT AEROSPACE
TECHNICAL LIBRARY
ABBOTTAEROSPACE.COM

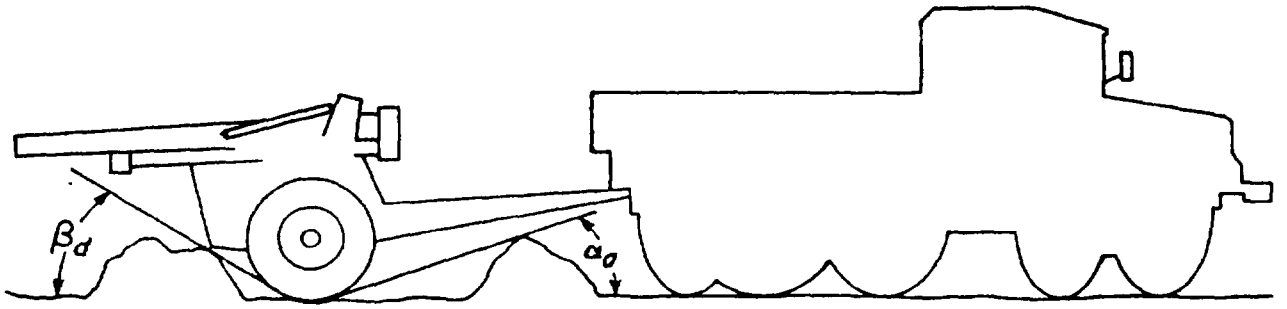

Figure 2-12. Angles of Approach and Departure

allowed to violate these clearance conditions. Similarly, as indicated in Fig. 2-13, the distance ℓ_p from the pintle to the weapon wheels and the geometry of the weapon structure near the pintle must be selected to allow the weapon and prime mover to negotiate turns of a given radius of curvature specified by the user. Tires for the road gear must be selected to support the weight of the vehicle on soft soils (without exceeding specified ground pressure levels), to provide sufficient traction during braking, and to provide adequate weapon stability. Pneumatic tires are almost exclusively used in modern towed artillery design. For an introduction to the mechanics of pneumatic tires, refer to Chapter 1 of Ref. 20. Also detailed performance data on tires are available from commercial tire manufacturers.

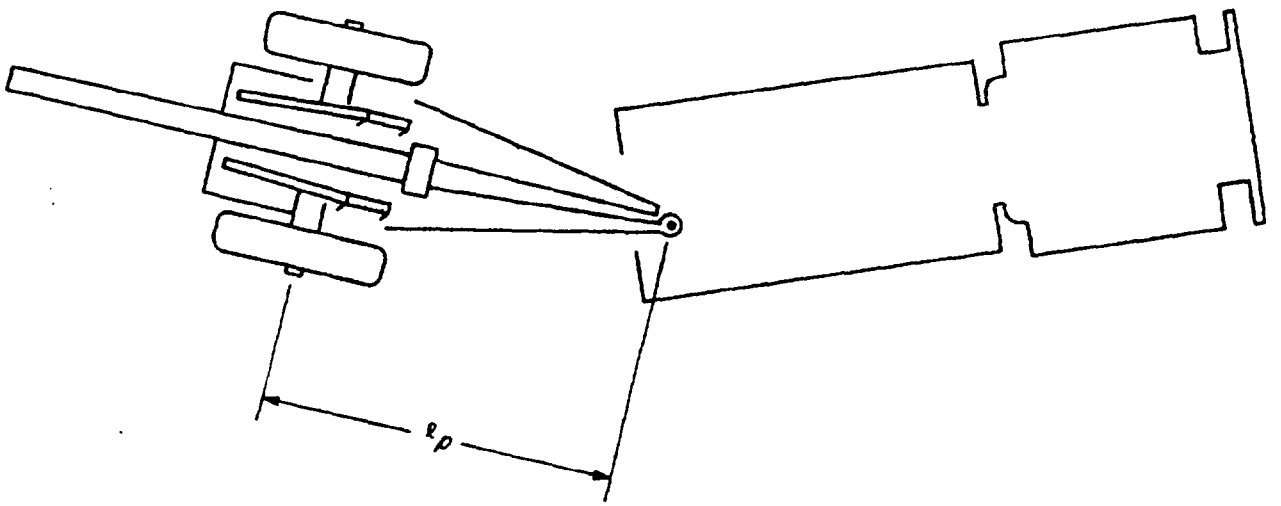

Figure 2-13. Turning Geometry

Braking requirements and the design of brake systems suitable for towed artillery weapons are discussed in considerable detail in Ref. 21. The optimum braking force for the weapon brake system is defined in par. 9-2, Ref. 21, and depends on the characteristics of the prime mover and surface conditions that may be encountered. The braking force and pintle force are determined to provide adequate weapon stability during braking; this determination also depends upon the prime mover. For detailed analysis of brake and pintle forces, refer to Chapter 3 of Ref. 20 and Chapters 5 and 9 of Ref. 21.

The stability of the towed weapon on extreme side slopes may be analyzed to determine the wheelbase w shown in Fig. 2-14. The summation of moments about the contact point between the left tire and ground in Fig. 2-14, presuming the right tire is just leaving the ground, yields the criterion for weapon stability as

$$\frac{W_T a_L y_{CG} \cos\gamma_s}{g} + \frac{W_T a_L \frac{w}{2} \sin\gamma_s}{g} + W_T y_{CG} \sin\gamma - W_T \frac{w}{2} \cos\gamma_s = 0 \qquad (2\text{-}79)$$

THIS DOCUMENT PROVIDED BY THE ABBOTT AEROSPACE
TECHNICAL LIBRARY
ABBOTTAEROSPACE.COM

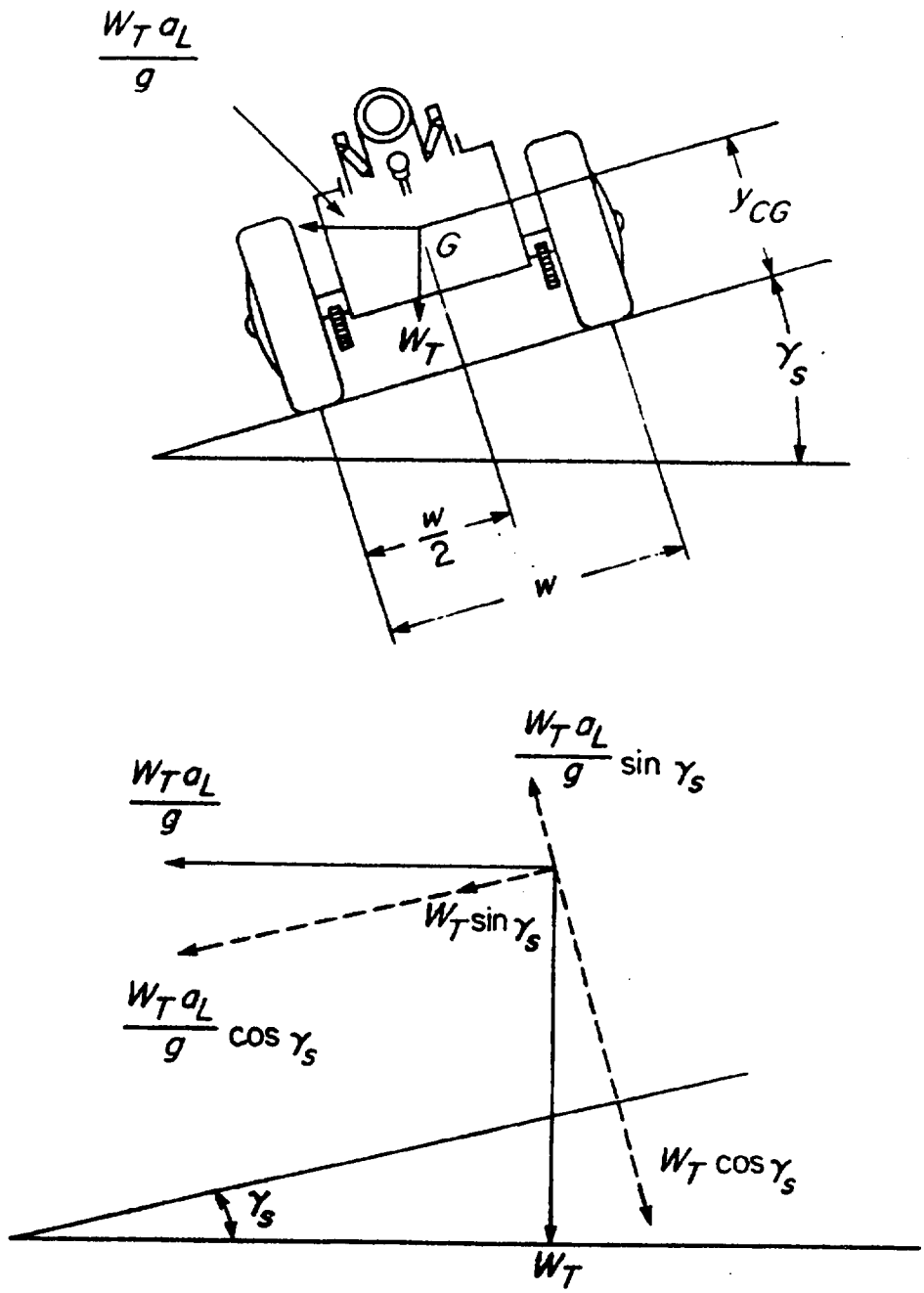

Figure 2-14. Forces Acting on Weapon During Turning

where

W_T = total weapon weight, N
a_L = lateral acceleration, m/s^2
y_{CG} = height of weapon center of gravity, m
γ_s = side slope, rad
w = wheelbase, m.

For example, if the weapon weighs 7000 N and the height and center of gravity are 1.0 m, then in order for the weapon to be stable on a flat surface (i.e., $\gamma_s = 0$) with 0.75g lateral acceleration, Eq. 2-79 requires

THIS DOCUMENT PROVIDED BY THE ABBOTT AEROSPACE
TECHNICAL LIBRARY
ABBOTTAEROSPACE.COM

$$7000\left(\frac{3}{4}\right)(1) - 7000\left(\frac{w}{2}\right) = 0$$

or

$$w = 1.5 \text{ m.}$$

In addition to the quasistatic analysis presented, the dynamic stability of the weapon must also be carefully analyzed during towing over rough terrain and on smooth roads. Typical ground contours may be employed and weapon dynamics analyzed as the weapon is towed over these terrains. More complex, and as discussed in Refs. 20 and 21, roll stability of the weapon during high-speed towing on even regular roads also must be carefully analyzed. The basic theory of stability of dynamical systems may be employed for such analysis but is beyond the scope of this discussion. For details and further references, refer to Refs. 20 and 21.

2-7 SYSTEM TRADEOFFS AND PARAMETER SELECTION

Pars. 2-1 and 2-2 provide a qualitative guide to factors that must be considered in design of a towed artillery system. Pars. 2-3 through 2-6 provide methods for the preliminary design of subsystems comprising the towed artillery system. It remains to (1) select each of the subsystems making up a candidate weapon system and (2) make tradeoffs and comparisons between competing alternatives. An example of considerations leading to parameter selection of a family of 105-mm candidate weapons and the selection of the best candidate is presented in this paragraph. The example, drawn from Refs. 17 and 18, illustrates tradeoffs and system level considerations that typically are encountered in the design of a new towed artillery weapon system.

A systematic method is needed for evaluating all possible solutions to a stated user need. This method requires that all feasible solutions be considered and that the best approaches from a technical standpoint be recommended. Therefore, a simple and uniform method of evaluating all possible solutions is needed. One such method is presented here with application to a user requirement for a 105-mm system.

2-7.1 SELECTION OF BASIC WEAPON CONFIGURATIONS

An effort is initially made to generate all the possible basic weapon configurations a 105-mm towed system could assume. Two basic types of recoil systems were identified that could be employed on a 105-mm weapon—the conventional Puteaux hydropneumatic, dependent system and a soft recoil system. There are three different carriage configurations that can be used with either of these recoil systems—box-trail, split trail, or pedestal base (four trail).

The combination of two recoil systems with three carriage configurations yields a series of six different basic weapon configurations. These six alternative system configurations are listed as follows and are depicted in Figs. 2-15 and 2-16:

1. *Alternative No. 1.* Split trail, conventional recoil mechanism, as typified by the XM164 Howitzer
2. *Alternative No. 2.* Box-trail, conventional recoil mechanism as typified by the M102 Howitzer
3. *Alternative No. 3.* Pedestal base (4-5 trails), conventional recoil mechanism, typified by a Swedish 105-mm Howitzer
4. *Alternative No. 4.* Pedestal base, soft recoil (fire-out-of-battery recoil mechanism)
5. *Alternative No. 5.* Box-trail, soft recoil, typified by the XM204 Howitzer
6. *Alternative No. 6.* Split trail (forward), soft recoil.

2-7.2 BALLISTIC SOLUTIONS

Two ballistic solutions that would meet user requirements were obtained. Solution No. 1 has a lengthened M137-type cannon with a shot travel of 3.56 m, whereas Solution No. 2 has a 2.64-m shot travel and an increased chamber volume. Table 2-2 gives the pertinent data used.

Each of these solutions was considered with and without a muzzle brake. For those options employing a muzzle brake, the following data were used:

Brake Efficiency	=	0.8
Brake Weight	=	333 N
Muzzle Blast in Crew Area	≤	13,800 Pa.

THIS DOCUMENT PROVIDED BY THE ABBOTT AEROSPACE
TECHNICAL LIBRARY
ABBOTTAEROSPACE.COM

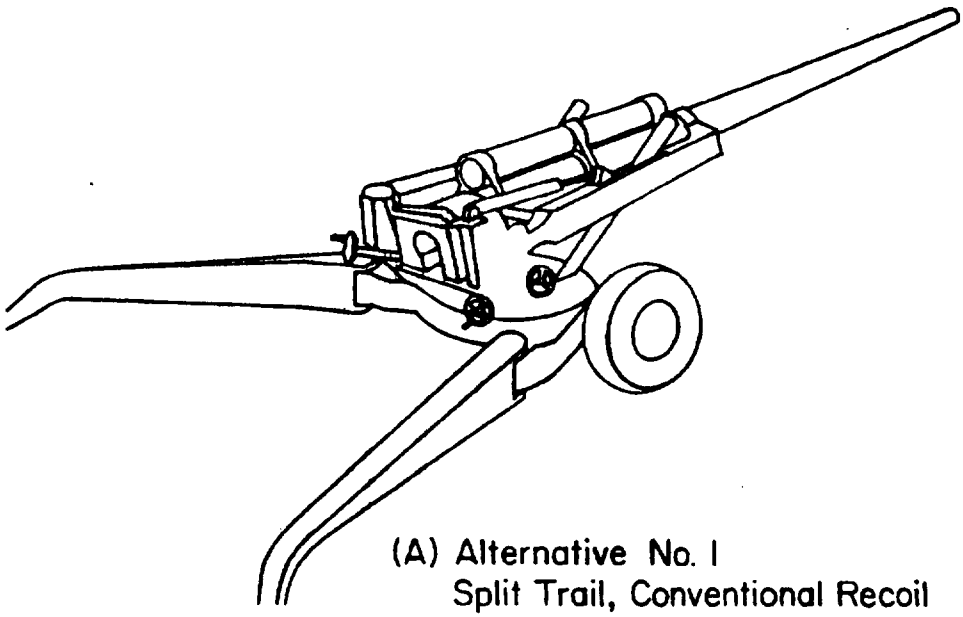

(A) Alternative No. 1
Split Trail, Conventional Recoil

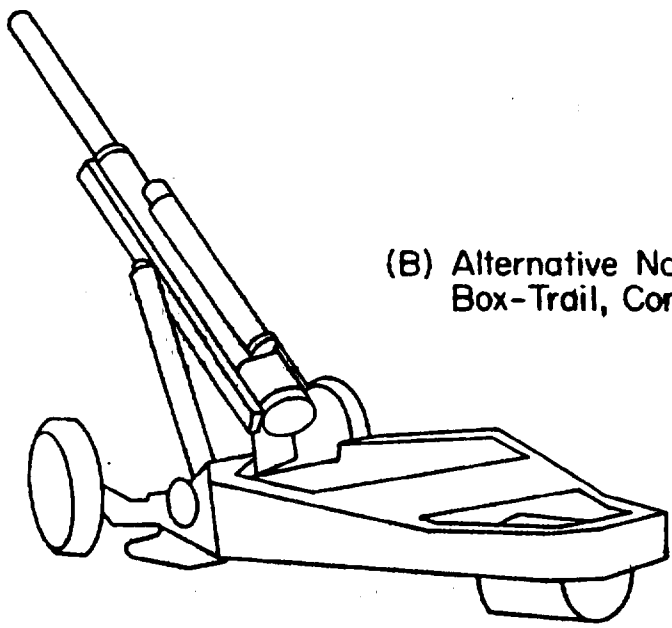

(B) Alternative No. 2
Box-Trail, Conventional Recoil

Figure 2-15. Conventional Recoil Systems

(cont'd on next page)

THIS DOCUMENT PROVIDED BY THE ABBOTT AEROSPACE
TECHNICAL LIBRARY
ABBOTTAEROSPACE.COM

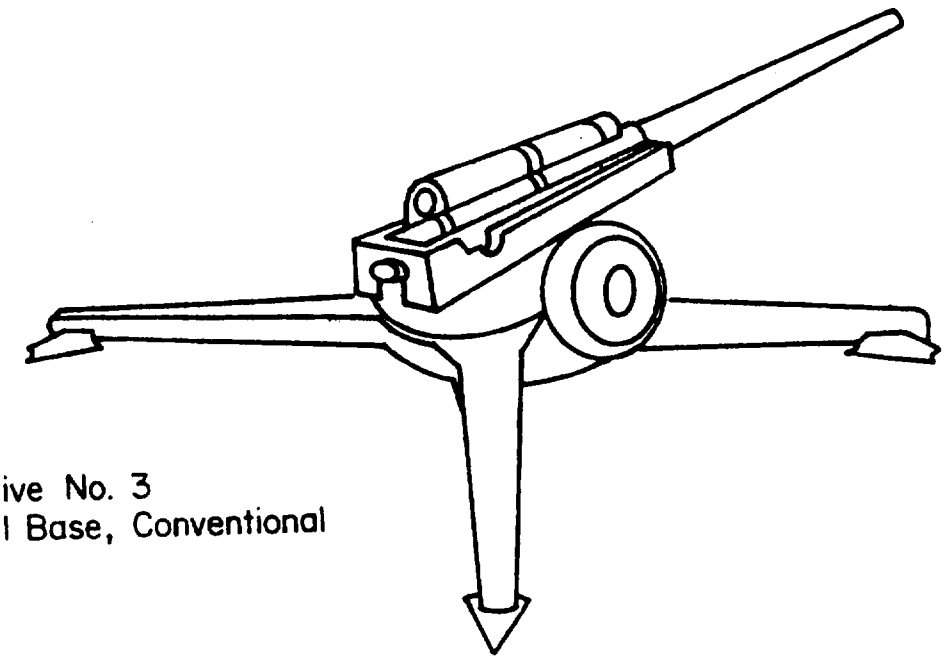

(C) Alternative No. 3
Pedestal Base, Conventional
Recoil

Figure 2-15. (cont'd)

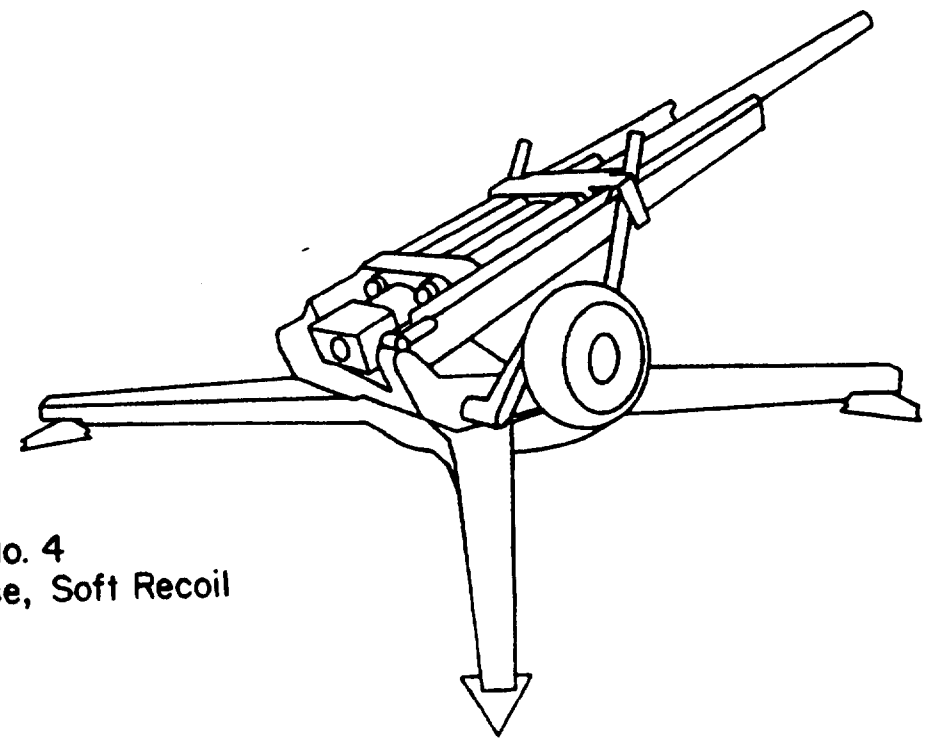

(A) Alternative No. 4
Pedestal Base, Soft Recoil

Figure 2-16. Soft Recoil Systems

(cont'd on next page)

THIS DOCUMENT PROVIDED BY THE ABBOTT AEROSPACE
TECHNICAL LIBRARY
ABBOTTAEROSPACE.COM

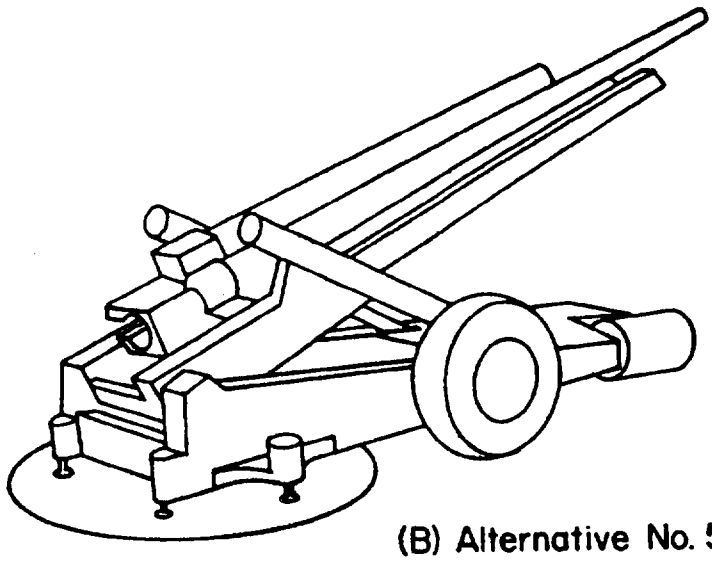

(B) Alternative No. 5
Box-Trail, Soft Recoil

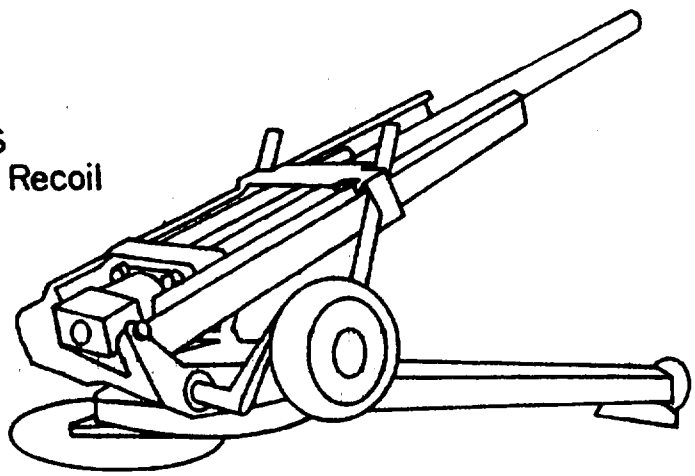

(C) Alternative No. 6
Split Trail, Soft Recoil

Figure 2-16. (cont'd)

TABLE 2-2
BALLISTIC SOLUTIONS

Ballistic Solution Number 1:	
Chamber Volume	2.34×10^{-3} m^3
Maximum Chamber Pressure	3.10×10^{8} Pa
Projectile Weight	127 N
Propellant Charge Weight	18.2 N
Muzzle Velocity	683 m/s
Ballistic Solution Number 2:	
Chamber Volume	3.34×10^{-3} m^3
Maximum Chamber Pressure	2.41×10^{8} Pa
Projectile Weight	127 N
Propellant Charge Weight	23.1 N
Muzzle Velocity	693 m/s

THIS DOCUMENT PROVIDED BY THE ABBOTT AEROSPACE
TECHNICAL LIBRARY
ABBOTTAEROSPACE.COM

These combinations of charges and brakes yield four possible ballistic solutions with the following characteristics:

1. Ballistic Solution No. 2, without a muzzle brake, gives a total cannon weight of 5446 N for an Effective Full Charges (EFC) life of 7500.
2. Ballistic Solution No. 2, with a muzzle brake, gives a total cannon weight of 5779 N for a 7500-EFC life.
3. Ballistic Solution No. 1, without a muzzle brake, gives a total cannon weight of 5695 N for a 7500-EFC life.
4. Ballistic Solution No. 1, with a muzzle brake, gives a total cannon weight of 6028 N for a 7500-EFC life.

2-7.3 WEAPON ALTERNATIVES

Since each of the six basic weapon configurations can use any one of the four ballistic solutions of par. 2-7.2, the weapon systems shown in Table 2-3 are possible.

TABLE 2-3
WEAPON SYSTEM ALTERNATIVES

Alternative No.	Configuration
1a	Split trail, conventional recoil, Ballistic Solution No.2
1b	Same as 1a, with muzzle brake
1c	Split trail, conventional recoil, Ballistic Solution No. 1
1d	Same as 1c, with muzzle brake
2a	Box-trail, conventional recoil, Ballistic Solution No. 2
2b	Same as 2a, with muzzle brake
2c	Box-trail, conventional recoil, Ballistic Solution No. 1
2d	Same as 2c, with muzzle brake
3a	Pedestal base, conventional recoil, Ballistic Solution No. 2
3b	Same as 3a, with muzzle brake
3c	Pedestal base, conventional recoil, Ballistic Solution No. 1
3d	Same as 3c, with muzzle brake
4a	Pedestal base, soft recoil, Ballistic Solution No. 2
4b	Same as 4a, with muzzle brake
4c	Pedestal base, soft recoil, Ballistic Solution No. 2
4d	Same as 4c, with muzzle brake
5a	Box-trail, soft recoil, Ballistic Solution No. 2
5b	Same as 5a, with muzzle brake
5c	Box-trail, soft recoil, Ballistic Solution No. 1
5d	Same as 5c, with muzzle brake
6a	Split trail, soft recoil, Ballistic Solution No. 2
6b	Same as 6a, with muzzle brake
6c	Split trail, soft recoil, Ballistic Solution No. 1
6d	Same as 6c, with muzzle brake

2-7.4 WEIGHT ESTIMATIONS

At this point, a method of calculating the total system weight for each of the 24 alternative systems is needed. A computer program based on the method presented in par. 2-4 was used in estimating the weight of the recoiling parts for each of the alternatives. This program also yielded values for peak rod pull and weapon impulse. See Ref. 18 for a description of the program.

To estimate the weight of the nonrecoiling parts, weapon weights are broken down into component parts. Because all of the alternatives are larger than any existing 105-mm system, some form of extrapolation is necessary. To minimize errors, the procedure that follows was used. Three existing 105-mm weapons were broken down into component weights. The component weights were then generated for three nonexisting 105-mm systems with the concept configuration. These three nonexisting systems are of the same size and range capability as the existing systems from which the component weights were taken; therefore, no extrapolation (only interpolation) was required.

Thus component weights were estimated without the necessity of error-producing extrapolation. To facilitate uniform extrapolation of component weights, other than recoiling parts, a series of extrapolation

THIS DOCUMENT PROVIDED BY THE ABBOTT AEROSPACE
TECHNICAL LIBRARY
ABBOTTAEROSPACE.COM

graphs were developed in Ref. 18. These extrapolations are based on fixed weights and weights that scale with the size of the subsystem and the loads it must support. The component weight estimation methods discussed in par. 2-5 are used in constructing the extrapolation, and the weight estimates obtained are plotted in Figs. 2-8, 2-9, and 2-17 through 2-22. It is emphasized that state-of-the-art materials and construction methods are considered in this analysis. Artillery systems developed in the future can anticipate some evolution in these areas that will favorably influence total system performance.

The graphs of Figs. 2-8, 2-9, and 2-17 through 2-22 may be used in the extrapolation of subsystem weights of the 24 alternative systems. Most of the plots are self-explanatory. All graphs are constructed using the basic premise that components can be mathematically described by both a fixed and a variable component. Fixed weights are represented by portions of structure governed by geometric considerations or other operational characteristics that are not functionally related to weapon weight, recoil force, etc. Some explanation of the suspension system weight versus system weight of Fig. 2-21 is necessary. The steps in the plots are due to the necessity of using wheels and tires in the inventory.

Information needed to calculate estimated system weight is now available in Figs. 2-8, 2-9, and 2-17 through 2-22. Weapon impulse is calculated using data for the ballistic solution and the method of par. 2-3. Values for each alternative are given in Table 2-4. Cannon weight, recoil mechanism weight, and recoil force are calculated by using the methods presented in pars. 2-3 and 2-4. These parameters are presented in Table 2-4. With these data the extrapolation curves of Figs. 2-8, 2-9, and 2-17 through 2-22 are used to obtain the remaining component weights, with results given in Table 2-4, along with total system weight.

2-7.5 WEAPON STABILITY

Weapon hop stability is assessed using the stability index introduced and illustrated in par. 2-5.2, Ref. 1,

$$SI = K_0 / W_T, \quad \text{dimensionless} \tag{2-80}$$

where

SI = stability index, dimensionless
K_0 = constant recoil force, N.

Values of the stability index for each of the system alternatives are calculated and given in Table 2-4. For weapons with spades the SI can be as large as 4.0, but with stakes only an SI of 2.5 can be tolerated.

2-7.6 PARAMETER VARIATIONS

With the equations and extrapolation graphs developed in this chapter, the design team can carry out tradeoff analyses and investigate the effect of parameter variations. If a change in tube weight is considered, for example, the recoil force will change as predicted analytically in par. 2-5.3, Ref. 1, and the component weights appearing in Table 2-4 will be recalculated using Figs. 2-8, 2-9, and 2-17 through 2-22. A new system weight is then obtained, and the sensitivity of system weight to tube weight is determined. Similar parameter variation calculations can be made with respect to any of the design parameters the system design team may wish to consider.

2-7.7 DECISION RULE FOR OPTIMAL SYSTEM SECTION

A tradeoff analysis may be used to select the most cost-effective solution to the system requirement. The salient points are as follows:

1. All parameters relevant to the mission profile are itemized. The "priority of characteristics" as stated by the user will be augmented by other parameters thought to be relevant by the design team.

2. The performance rating PR of each alternative solution with respect to a given characteristic is assigned. This is accomplished on a 0 to 10 scale—zero indicates a complete failure to satisfy performance requirements, and 10 indicates a completely satisfactory rating.

3. An importance factor IF is assigned to each parameter being evaluated. This will reflect guidance from the user, in the form of requirement statements, as well as experience represented by the artillery system design team. The IF reflects the thought that some parameters are more critical to mission performance than others.

THIS DOCUMENT PROVIDED BY THE ABBOTT AEROSPACE
TECHNICAL LIBRARY
ABBOTTAEROSPACE.COM

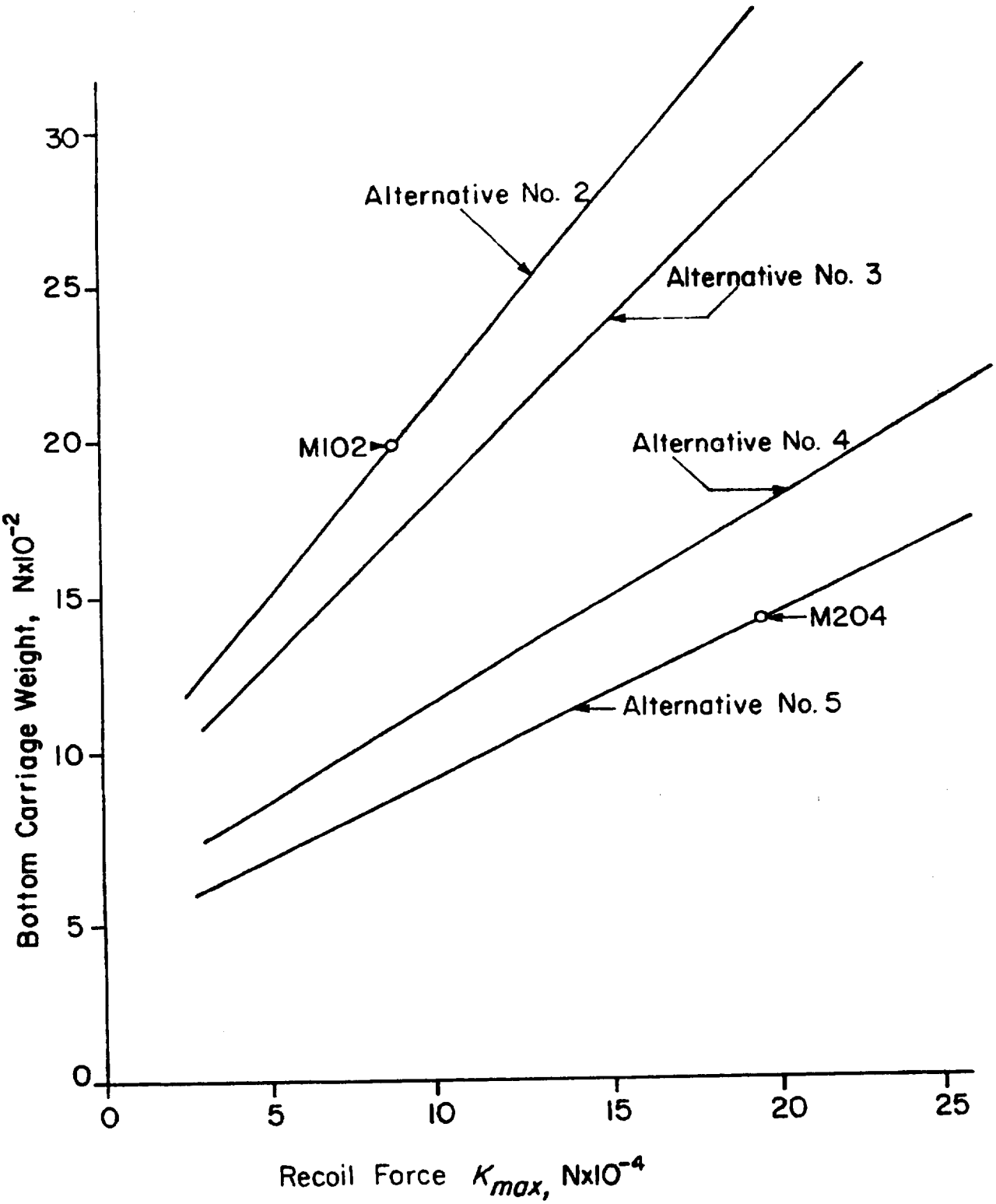

Figure 2-17. Bottom Carriage Weight vs Recoil Force

THIS DOCUMENT PROVIDED BY THE ABBOTT AEROSPACE
TECHNICAL LIBRARY
ABBOTTAEROSPACE.COM

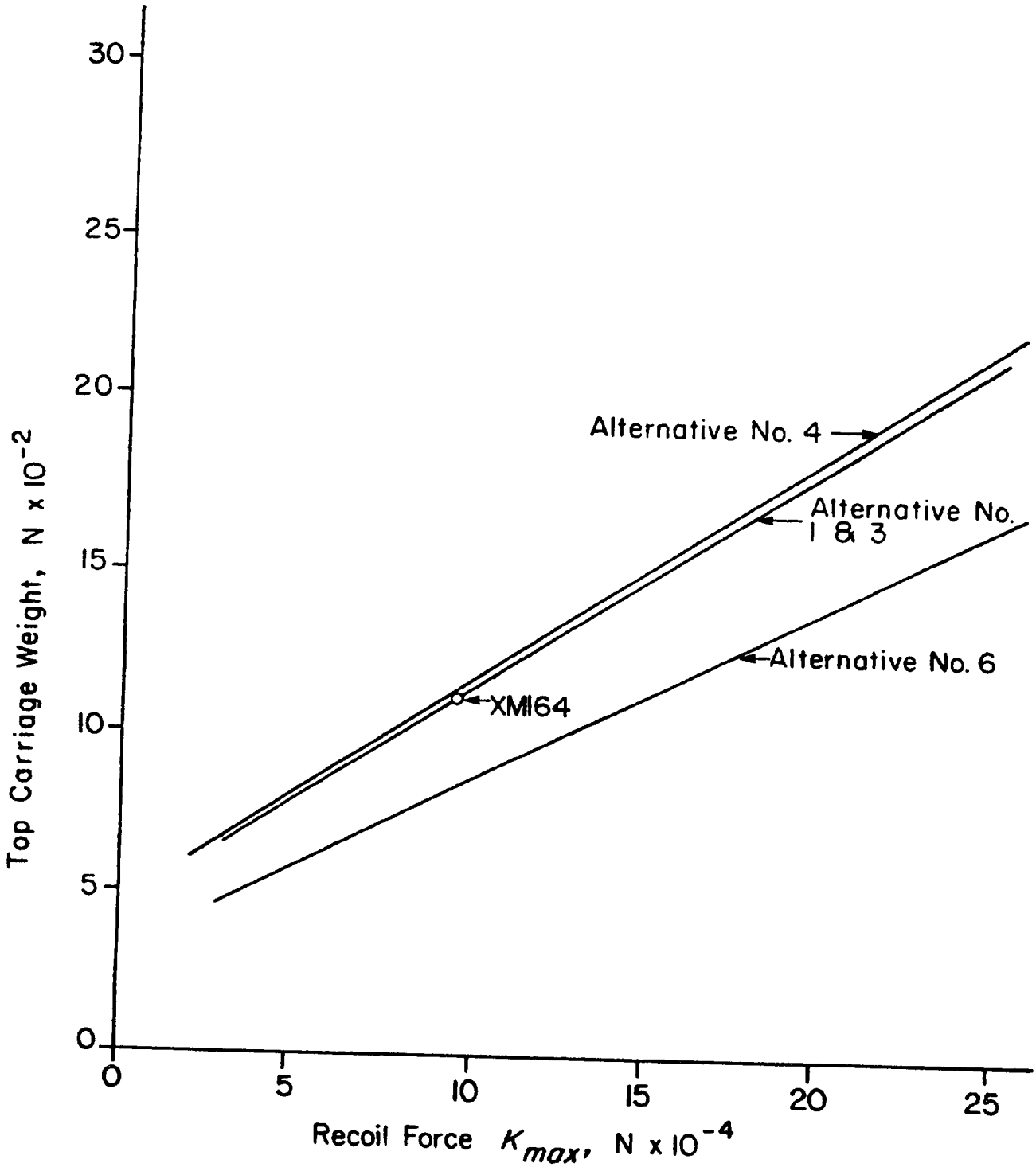

Figure 2-18. Top Carriage Weight vs Recoil Force

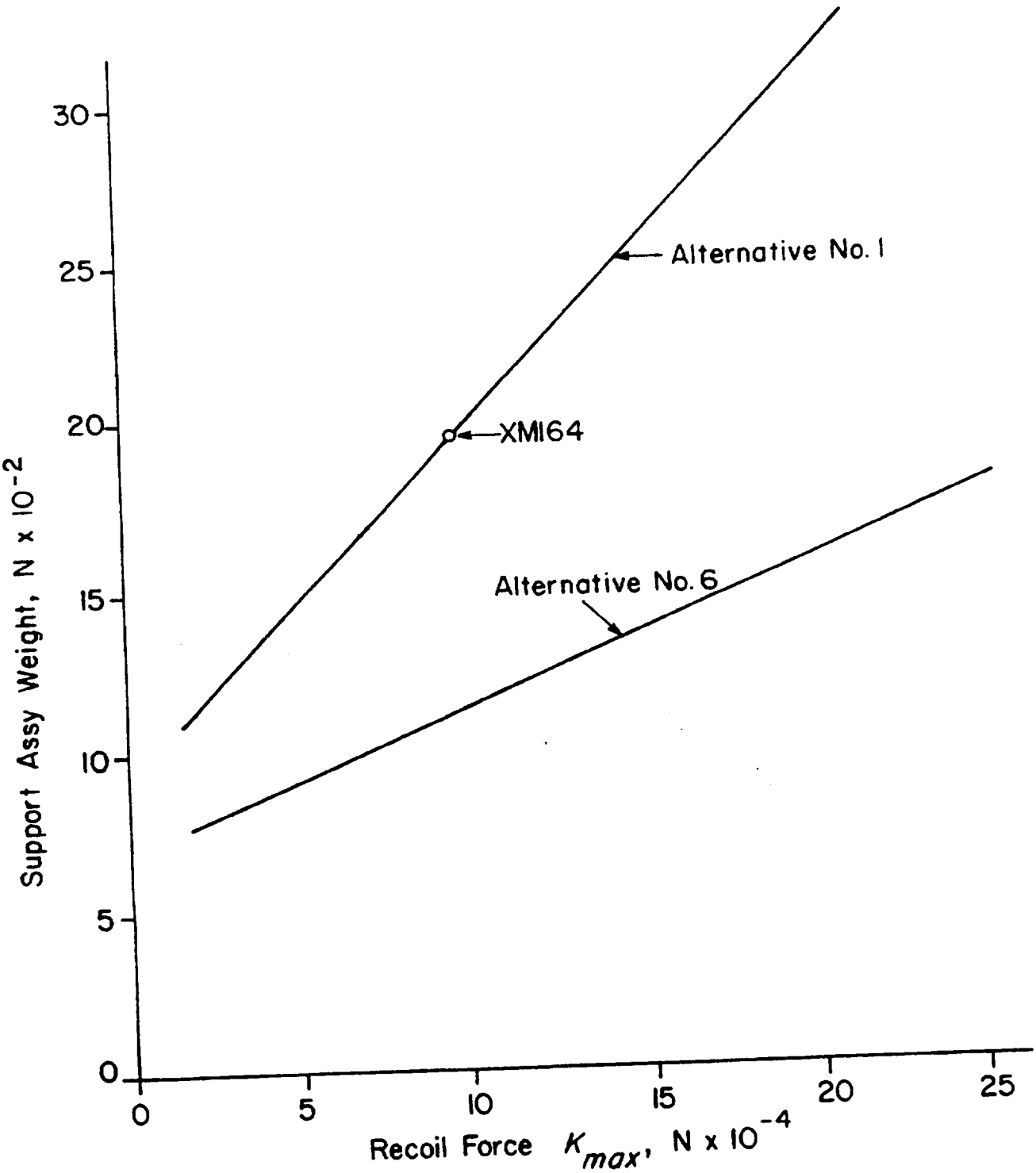

Figure 2-19. Support Assembly Weight vs Recoil Force

THIS DOCUMENT PROVIDED BY THE ABBOTT AEROSPACE TECHNICAL LIBRARY ABBOTTAEROSPACE.COM

THIS DOCUMENT PROVIDED BY THE ABBOTT AEROSPACE
TECHNICAL LIBRARY
ABBOTTAEROSPACE.COM

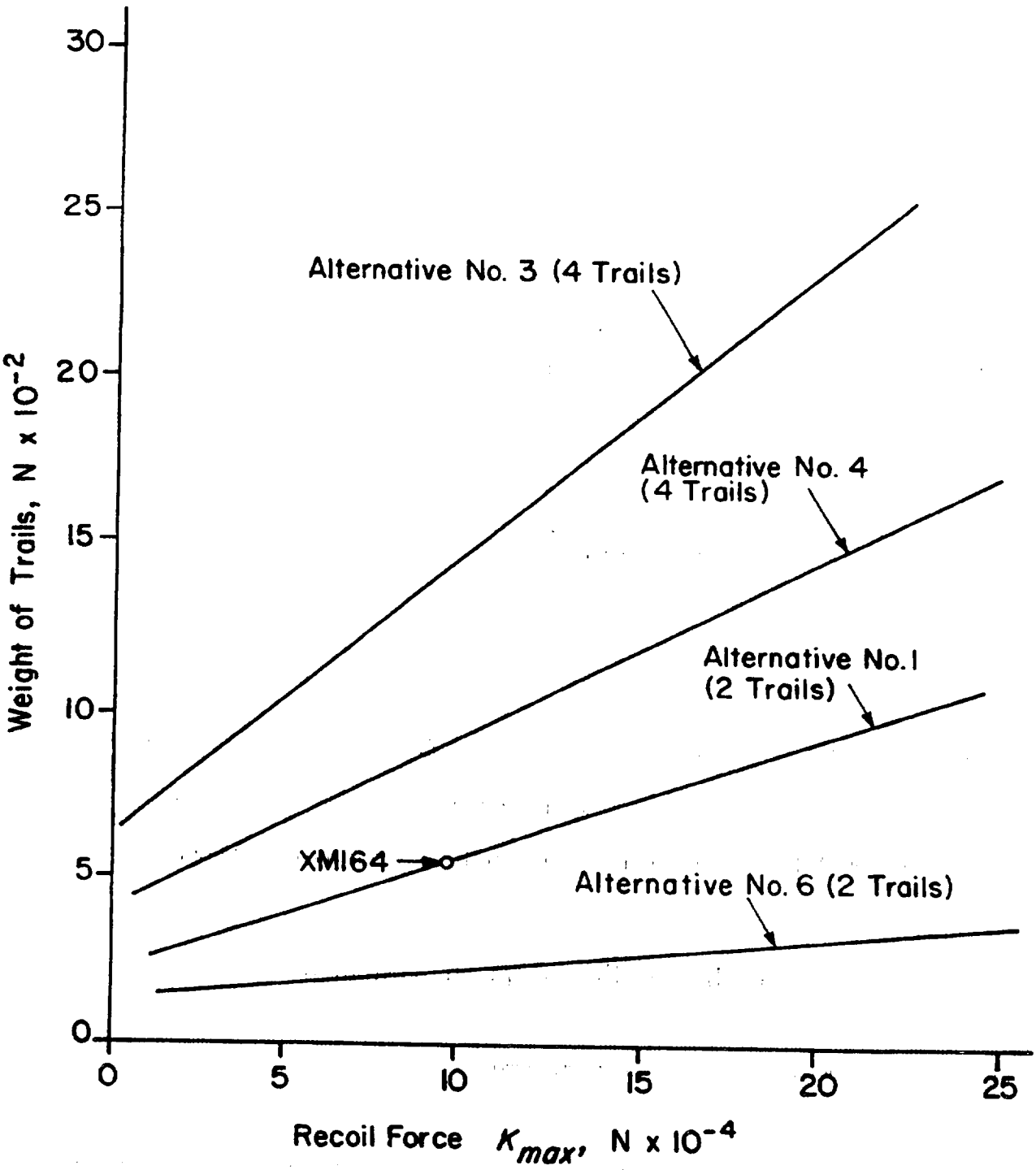

Figure 2-20. Trail Weight vs Recoil Force

THIS DOCUMENT PROVIDED BY THE ABBOTT AEROSPACE
TECHNICAL LIBRARY
ABBOTTAEROSPACE.COM

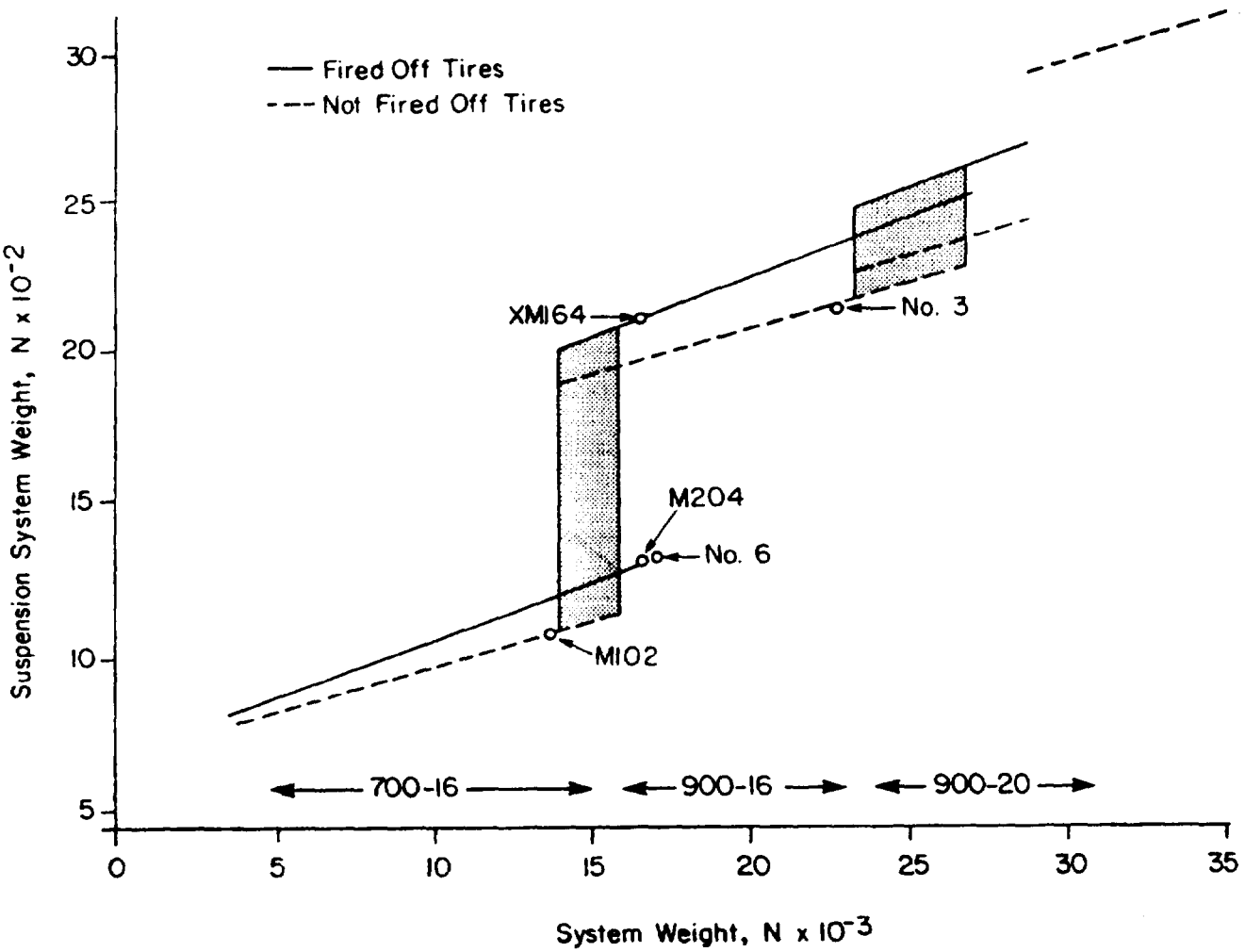

Figure 2-21. Suspension System Weight vs Total System Weight

4. The total measure of performance for each alternative solution is calculated by the equation

$$(PR)_{total} = \sum_{i=1}^{20}(PR)_i(IF)_i, \text{ dimensionless} \qquad (2\text{-}81)$$

where

$(PR)_{total}$ = total performance rating, dimensionless
$(PR)_i$ = performance rating in ith factor, dimensionless
$(IF)_i$ = importance factor for ith factor, dimensionless.

5. The decision technique is then completed by selecting the alternative with the maximum total performance rating.

The assigned performance ratings and importance factors are tabulated in Table 2-5. Table 2-6 gives tabular values of the terms in Eq. 2-81. Therefore, the last column in Table 2-6 contains the total performance ratings of all 20 alternatives.

The rationale used in assigning element performance ratings is explained as follows:

1. $i = 1$ Reliability/Availability. Soft recoil systems rank slightly lower in this regard because

a. Misfires will occur at a predicted rate of about one per 1000 rounds. This event will cause a mission interruption of short duration because a special technique will be required to reestablish normal functioning.

THIS DOCUMENT PROVIDED BY THE ABBOTT AEROSPACE
TECHNICAL LIBRARY
ABBOTTAEROSPACE.COM

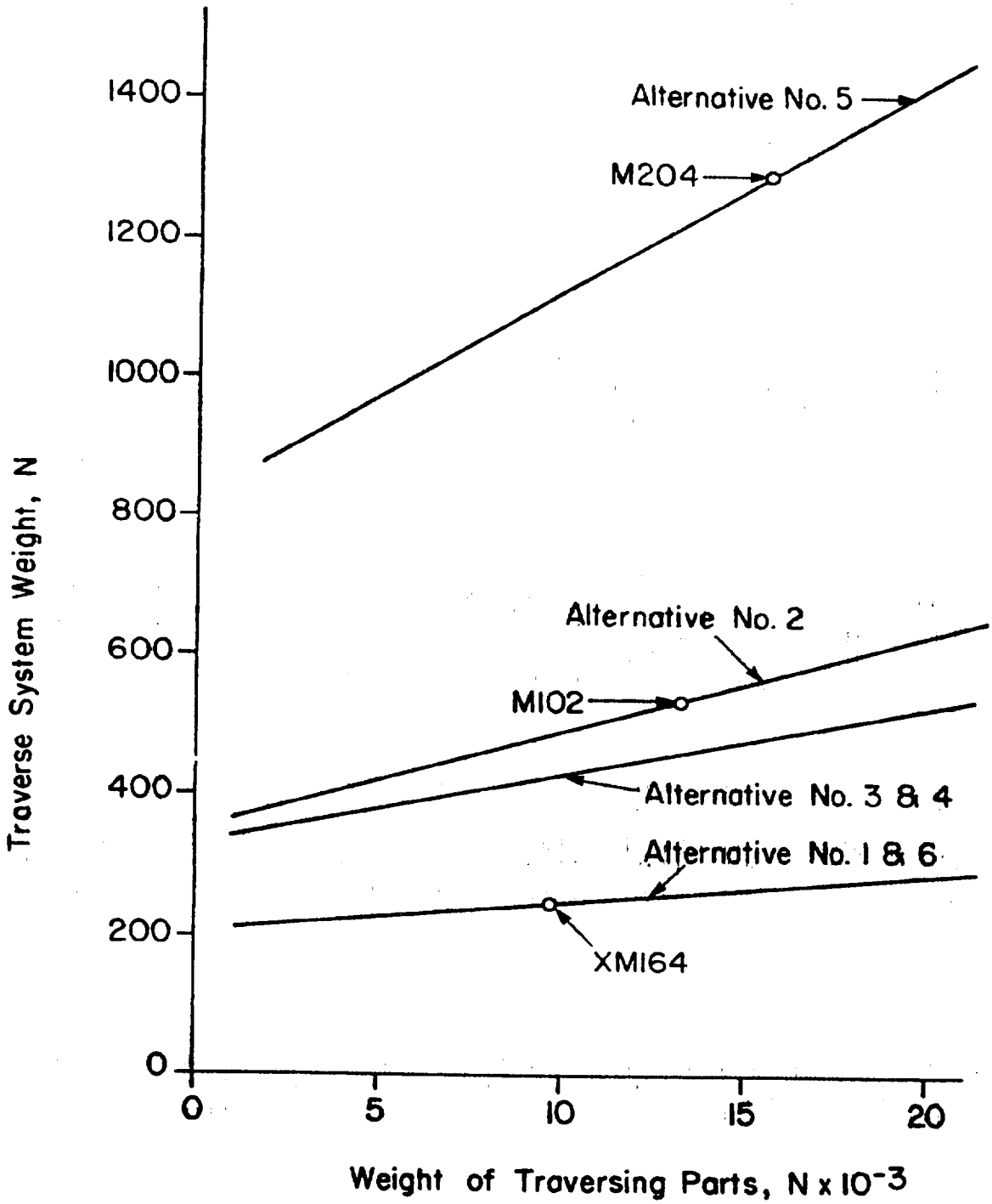

Figure 2-22. Weight of Traversing Mechanism vs Traversing Parts Weight

THIS DOCUMENT PROVIDED BY THE ABBOTT AEROSPACE
TECHNICAL LIBRARY
ABBOTTAEROSPACE.COM

TABLE 2-4
WEIGHT TABULATION

		a	b	c		d	e	f	g	h	i
Alternative	Weapon Impulse I, N·s	Cannon Weight, N	Recoil Mechanism Weight, N	Recoil Force Long Recoil, N	Recoil Force Short Recoil or Overload, N	Cradle Weight, N	Tipping Parts Weight, N ①	Elevating Mechanism Weight, N	Bottom Carriage Weight, N	Sight Mount Weight, N	Top Carriage Weight, N
1a	12,363	5446	2879	73,109	125,494	1133	9569	1311	—	289	635
1b	10,289	5780	2266	52,460	92,251	951	9108	1266	—	289	524
1c	11,461	5713	2670	62,092	107,586	1035	9529	1297	—	289	582
1d	9,969	6028	2266	47,547	84,393	906	9311	1279	—	289	502
2a	12,363	5446	2879	73,109	125,494	1013	9449	1319	2399	275	—
2b	10,289	5780	2266	52,460	92,251	826	8983	1270	2035	275	—
2c	11,461	5713	2670	62,092	107,586	910	9404	1311	2470	275	—
2d	9,969	6028	2266	47,547	84,393	782	9187	1288	1924	275	—
3a	12,363	5446	2879	73,109	125,494	1133	9569	1311	2043	289	635
3b	10,289	5780	2266	52,460	92,251	951	9108	1266	1746	289	524
3c	11,461	5713	2670	62,092	107,586	1035	9529	1297	2106	289	582
3d	9,969	6028	2266	47,547	84,393	906	9311	1279	1670	289	502
4a	12,363	5446	2559	24,371	173,605	1732	9848	1653	1639	275	813
4b	10,289	5780	1985	17,485	127,728	1422	9298	1581	1359	275	657
4c	11,461	5713	2464	20,697	148,807	1288	9576	1350	1488	275	746
4d	9,969	6028	1959	15,850	118,110	1137	9235	1310	1302	275	626
5a	12,363	5446	2559	24,371	173,605	1732	9848	1653	1315	275	—
5b	10,289	5780	1985	17,485	127,728	1422	9298	1581	1088	275	—
5c	11,461	5713	2464	20,697	148,807	1288	9576	1617	1186	275	—
5d	9,969	6028	1959	15,850	118,110	1137	9235	1573	1040	275	—
6a	12,363	5446	2559	24,371	173,605	1732	9848	1653	—	275	609
6b	10,289	5780	1985	17,485	127,728	1422	9298	1581	—	275	489
6c	11,461	5713	2464	20,697	148,807	1288	9576	1350	—	275	542
6d	9,969	6028	1959	15,850	118,110	1137	9235	1310	—	275	462

① Col. e = Col. a + Col. b + Col. d + 111 N

(cont'd on next page)

b. If the lanyard is pulled on a soft recoil weapon, the cannon will accelerate forward whether or not the weapon is loaded and ready to fire. This increases the possibility of an accident.

2. $i = 2$ Stability in Firing Position. Soft recoil systems demonstrate their greatest asset here. Systems with muzzle brakes are more stable than those without due to reduced recoil forces. The stability index presented in Table 2-5 gives a good indication of the relative positions of competing alternatives. Conventional recoil systems that require staking are totally inadequate based on experience with the M102 system and the fact that higher muzzle velocities are being considered.

3. $i = 3$ Precision. All systems are equal based on both analytical and empirical results.

4. $i = 4$ Range, Maximum. All competitive systems are new and will be designed to fire to the essential maximum range stated by the combat developer. Any changes in this parameter would not be expected to change the relative ranking of competing alternatives.

5. $i = 5$ Weight. This performance measure is highly relevant to artillery systems that will be used in the air mobile role. The M102 developmental program placed a very high priority on obtaining a lightweight system. Soft recoil systems offer the potential of slight weight savings and, therefore, rank higher in this measure.

THIS DOCUMENT PROVIDED BY THE ABBOTT AEROSPACE
TECHNICAL LIBRARY
ABBOTTAEROSPACE.COM

TABLE 2-4 (cont'd)

	j	k	ℓ	m	n	o	p	q	r	s		
Alternative	Support Assistant Weight, N	Trail Weight, N	Suspension Weight, N	Traverse System Weight, N	Baseplate Weight, N	Misc. Carriage Equip. Weight, N	Weight Below Trunnions, N ①	Weight of Misc. Equipment, N	Total System Weight (Emplaced), N	Stability Index ②	Traverse Capability	Ground-Anchoring Method
1a	1128	3243	2221	253	——	426	9,506	444	19,076	3.83	Limited On-Carriage Speed Shift	Spades
1b	946	2710	2155	249	——	426	8,565	444	17,672	2.97		
1c	1031	2976	2186	253	——	426	9,040	444	18,569	3.34		
1d	902	2532	2155	249	——	426	8,334	444	17,645	2.69		
2a	——	——	1999	578	422	564	7,556	844	17,006	4.30	Full On-Carriage	Spades
2b	——	——	1972	569	422	564	7,107	844	16,090	3.26		
3c	——	——	1999	578	422	564	7,618	844	16,601	3.74		
3d	——	——	1979	564	422	564	7,014	844	16,197	2.94		
3a	——	8352	2346	444	444	666	16,530	444	26,099	2.80	Full On-Carriage	Stakes
3b	——	6975	2275	435	444	666	14,619	444	23,727	2.21		
3c	——	7663	2319	453	444	666	15,819	444	25,348	2.45		
3d	——	6486	2266	449	444	666	14,051	444	23,363	2.04		
4a	——	6575	2301	453	444	666	14,819	444	24,669	0.99	Full On-Carriage	None ④
4b	——	5375	2141	444	444	666	12,942	444	22,243	0.79		
4c	——	5908	2252	453	444	666	13,582	444	23,163	0.89		
4d	——	5109	2119	444	444	666	12,295	444	21,532	0.74		
5a	——	——	2017	1311	578	280	7,429	555	17,259	1.41	Full On-Carriage	None ④
5b	——	——	1986	1284	578	280	7,072	555	16,357	1.07		
5c	——	——	1986	1311	578	280	7,233	555	16,810	1.23		
5d	——	——	1964	1297	578	280	7,007	555	16,246	0.98		
6a	720	1510	2017	258	578	426	8,046	444	17,894	1.36	Limited On-Carriage Speed Shift	None ④
6b	613	1333	1986	253	578	426	7,534	444	16,832	1.04		
6c	657	1377	1986	253	578	426	7,444	444	17,023	1.22		
6d	591	1199	1964	249	578	426	7,054	444	16,290	0.97		

① Col. p = Col. f + g + h + i + j + k + ℓ + m + n + o
② Col. s = Col. c (long recoil)/Col. r
④ Small stakes required only in extreme conditions.

6. $i = 6$ Mobility. The mobility of the various competitive systems is directly related to system weight. This dependence is reflected in the ratings given.

7. $i = 7$ Traverse. The traverse ratings are related to the time and difficulty involved in making gross shifts in azimuth. Therefore, those systems having a 6400-mils on-carriage traverse system rank higher than those having a limited on-carriage system plus a speed shift capability.

8. $i = 8$ Maintainability. All competitive systems will be designed to meet the requirements stated by the combat developer.

9. $i = 9$ Reaction Time. The reaction time is closely related to the type of ground anchoring that must be deployed prior to weapon firing. Thus those systems requiring no staking or spreading of trails rank highest.

10. $i = 10$ Rate of Fire. The soft-recoil-type systems rank slightly higher in this area because the recoil cycle time is less for weapons that are fired in the out-of-battery mode.

11. $i = 11$ Survivability. All alternative systems were considered to have the same survivability.

12. $i = 12$ Overall Size. Because their overall length is only about two-thirds that of conventional systems, soft recoil systems employing forward trails rank very high on this point.

13. $i = 13$ Transportability. Transportability is related to the overall size and weight of the systems. Therefore, shorter weapons have higher ratings.

THIS DOCUMENT PROVIDED BY THE ABBOTT AEROSPACE
TECHNICAL LIBRARY
ABBOTTAEROSPACE.COM

TABLE 2-5
ELEMENT PERFORMANCE RATINGS $(PR)_i$

	*Reliability & Availability	*Stability in Firing Position	*Precision	*Range (max)	*Weight	*Mobility	*Traverse	*Maintainability	*Reaction Time	*Rate of Fire	*Survivability	*Overall Size	*Transportability	*Growth Potential	*Access to Crew Area	*Storage Life	*Blast Pressure (Crew Area)	*Training Required	*Payoff to Related R&D	*Development Time Cost
IF_i =	1	1	1	1	1	0.9	0.9	0.9	0.8	0.8	0.8	0.7	0.7	0.7	0.6	0.5	0.4	0.4	0.3	0.2
i =	1	2	3	4	5	6	7	8	9	10	11	12	13	14	15	16	17	18	19	20
Alt. No.																				
1a	9	4	10	10	7	7	3	10	4	9	9	5	8	3	5	9	5	9	3	9
1b	9	6	10	10	9	9	3	10	6	9	9	5	8	3	5	9	3	9	3	9
1c	9	6	10	10	8	8	3	10	5	9	9	5	8	3	5	9	5	9	3	9
1d	9	7	10	10	8	8	3	10	6	9	9	5	8	3	5	9	3	9	3	9
2a	9	0	10	10	9	9	10	10	0	9	9	5	8	1	3	9	5	9	3	9
2b	9	2	10	10	10	10	10	10	1	9	9	5	8	1	3	9	3	9	3	9
2c	9	1	10	10	9	9	10	10	1	9	9	5	8	1	3	9	5	9	3	9
2d	9	3	10	10	10	10	10	10	2	9	9	5	8	1	3	9	3	9	3	9
3a	9	3	10	10	1	1	9	10	2	9	9	4	8	5	4	9	5	9	4	9
3b	9	4	10	10	3	3	9	10	3	9	9	4	8	5	4	9	3	9	4	9
3c	9	3	10	10	2	2	9	10	3	9	9	4	8	5	4	9	5	9	4	9
3d	9	4	10	10	3	3	9	10	4	9	9	4	8	5	4	9	3	9	4	9
4a	8	8	10	10	2	2	10	10	9	10	9	4	9	9	7	9	9	7	9	9
4b	8	9	10	10	5	5	10	10	9	10	9	4	9	9	7	9	7	7	9	9
4c	8	9	10	10	3	3	10	10	9	10	9	4	9	9	7	9	9	7	9	9
4d	8	10	10	10	4	4	10	10	10	10	9	4	9	9	7	9	7	7	9	9
5a	8	6	10	10	9	9	10	10	7	10	9	10	10	9	9	9	9	7	9	9
5b	8	7	10	10	10	10	10	10	8	10	9	10	10	9	9	9	7	7	9	9
5c	8	7	10	10	9	9	10	10	8	10	9	10	10	9	9	9	9	7	9	9
5d	8	9	10	10	10	10	10	10	9	10	9	10	10	9	9	9	7	7	9	9
6a	8	6	10	10	8	8	5	10	7	10	9	10	10	9	9	9	9	7	9	9
6b	8	7	10	10	10	10	5	10	8	10	9	10	10	9	9	9	7	7	9	9
6c	8	7	10	10	9	9	5	10	8	10	9	10	10	9	9	9	9	7	9	9
6d	8	9	10	10	10	10	5	10	9	10	9	10	10	9	9	9	7	7	9	9

$(PR)_i$

*User Requirements

14. i = 14 Growth Potential. The growth potential of a weapon system is related to the possibility of increasing its range or projectile payload. The M102-type system ranks very low in this area because it is overextended in the alternative system.

15. i = 15 Access to Crew Area. Forward trail, soft recoil weapons rank very high; there are no trails to step over or stand inside when working near the breech.

16. i = 16 Storage Life. All alternative systems were considered to have the same storage life.

17. i = 17 Blast Pressure in Crew Area. Weapons equipped with muzzle brakes rank lower than the corresponding systems without brakes. Soft recoil systems rank higher than conventional recoil systems because the tube is displaced forward during the time the muzzle blast occurs.

18. i = 18 Training Required. Soft recoil weapons rank slightly lower in this area because they are new and slightly more sophisticated than weapons with a conventional recoil system.

THIS DOCUMENT PROVIDED BY THE ABBOTT AEROSPACE
TECHNICAL LIBRARY
ABBOTTAEROSPACE.COM

TABLE 2-6
COMPUTATION OF TOTAL PERFORMANCE RATINGS

	*Reliability & Availability	Stability in Firing Position	*Precision	*Range (max)	Weight	*Mobility	*Traverse	*Maintainability	*Reaction Time	*Rate of Fire	*Survivability	Overall Size	*Transportability	Growth Potential	Access to Crew Area	*Storage Life	Blast Pressure (Crew Area)	Training Required	*Payoff to Related R&D	Development Time Cost	$(PR)_{max}$ for Each Alternative
IF_i =	1	1	1	1	1	0.9	0.9	0.9	0.8	0.8	0.8	0.7	0.7	0.7	0.6	0.5	0.4	0.4	0.3	0.2	
i =	1	2	3	4	5	6	7	8	9	10	11	12	13	14	15	16	17	18	19	20	
Alt. No.																					
1a	9	4	10	10	7	6.3	2.7	9.0	3.2	7.2	7.2	3.5	5.6	2.1	3.0	4.5	2.0	3.6	0.9	1.8	102.6
1b	9	6	10	10	9	8.1	2.7	9.0	4.8	7.2	7.2	3.5	5.6	2.1	3.0	4.5	1.2	3.6	0.9	1.8	109.2
1c	9	6	10	10	8	7.2	2.7	9.0	4.0	7.2	7.2	3.5	5.6	2.1	3.0	4.5	2.0	3.6	0.9	1.8	107.3
1d	9	7	10	10	8	7.2	2.7	9.0	4.8	7.2	7.2	3.5	5.6	2.1	3.0	4.5	1.2	3.6	0.9	1.8	108.3
2a	9	0	10	10	9	8.1	9.0	9.0	0	7.2	7.2	3.5	5.6	0.7	1.8	4.5	2.0	3.6	0.9	1.8	102.9
2b	9	2	10	10	10	9.0	9.0	9.0	.8	7.2	7.2	3.5	5.6	0.7	1.8	4.5	1.2	3.6	0.9	1.8	106.8
2c	9	1	10	10	9	8.1	9.0	9.0	.8	7.2	7.2	3.5	5.6	0.7	1.8	4.5	2.0	3.6	0.9	1.8	104.7
2d	9	3	10	10	10	9.0	9.0	9.0	1.6	7.2	7.2	3.5	5.6	0.7	1.8	4.5	1.2	3.6	0.9	1.8	108.6
3a	9	3	10	10	1	0.9	8.1	9.0	1.6	7.2	7.2	2.8	5.6	3.5	2.4	4.5	2.0	3.6	1.2	1.8	94.4
3b	9	4	10	10	3	2.7	8.1	9.0	2.4	7.2	7.2	2.8	5.6	3.5	2.4	4.5	1.2	3.6	1.2	1.8	99.2
3c	9	3	10	10	2	1.8	8.1	9.0	2.4	7.2	7.2	2.8	5.6	3.5	2.4	4.5	2.0	3.6	1.2	1.8	97.5
3d	9	4	10	10	3	2.7	8.1	9.0	3.2	7.2	7.2	2.8	5.6	3.5	2.4	4.5	1.2	3.6	1.2	1.8	100.0
4a	8	8	10	10	2	1.8	9.0	9.0	7.2	8.0	7.2	2.8	6.3	6.3	4.2	4.5	3.6	2.8	2.7	1.8	115.2
4b	8	9	10	10	5	4.5	9.0	9.0	7.2	8.0	7.2	2.8	6.3	6.3	4.2	4.5	2.8	2.8	2.7	1.8	121.1
4c	8	9	10	10	3	2.7	9.0	9.0	7.2	8.0	7.2	2.8	6.3	6.3	4.2	4.5	3.6	2.8	2.7	1.8	118.1
4d	8	10	10	10	4	3.6	9.0	9.0	8.0	8.0	7.2	2.8	6.3	6.3	4.2	4.5	3.6	2.8	2.7	1.8	121.0
5a	8	6	10	10	9	8.1	9.0	9.0	5.6	8.0	7.2	7.0	7.0	6.3	5.4	4.5	3.6	2.8	2.7	1.8	131.0
5b	8	7	10	10	10	9.0	9.0	9.0	6.4	8.0	7.2	7.0	7.0	6.3	5.4	4.5	2.8	2.8	2.7	1.8	133.9
5c	8	7	10	10	9	8.1	9.0	9.0	6.4	8.0	7.2	7.0	7.0	6.3	5.4	4.5	3.6	2.8	2.7	1.8	133.2
5d	8	9	10	10	10	9.0	9.0	9.0	7.2	8.0	7.2	7.0	7.0	6.3	5.4	4.5	2.8	2.8	2.7	1.8	137.1
6a	8	6	10	10	8	7.2	4.5	9.0	5.6	8.0	7.2	7.0	7.0	6.3	5.4	4.5	3.6	2.8	2.7	1.8	124.6
6b	8	7	10	10	10	9.0	4.5	9.0	6.4	8.0	7.2	7.0	7.0	6.3	5.4	4.5	2.8	2.8	2.7	1.8	129.4
6c	8	7	10	10	9	8.1	4.5	9.0	6.4	8.0	7.2	7.0	7.0	6.3	5.4	4.5	3.6	2.8	2.7	1.8	128.3
6d	8	9	10	10	10	9.0	4.5	9.0	7.2	8.0	7.2	7.0	7.0	6.3	5.4	4.5	2.8	2.8	2.7	1.8	132.2

$(PR)_i(IF)_i$

*User Requirements

19. i = 19 Payoff to Related R&D. Soft recoil weapons rank much higher here; they provide the possibility of lighter, more stable 155-mm and larger towed systems in addition to lighter, more stable self-propelled systems.

20. i = 20 Development Time, Cost. All systems were considered to rank about the same in this area.

The system performance evaluation method used here should not be taken as the only way to compare alternative systems. Rather, it provides a balance between quantitative tradeoffs and qualitative considerations, which must receive the attention of the design team and the user. For more refined methods of design tradeoff analysis and optimization, refer to Refs. 22 and 23.

THIS DOCUMENT PROVIDED BY THE ABBOTT AEROSPACE
TECHNICAL LIBRARY
ABBOTTAEROSPACE.COM

REFERENCES

1. MIL-HDBK-778(AR), *Recoil Systems*, 18 July 1988.
2. AMCP 706-140, Engineering Design Handbook, *Trajectories, Differential Effects, and Data for Projectiles*, August 1963.
3. M. E. Backman, *Terminal Ballistics*, NWC TP 5780, Naval Weapons Center, China Lake, CA, 1976.
4. AMCP 706-160, Engineering Design Handbook, *Elements of Terminal Ballistics, Part One, Introduction, Kill Mechanisms and Vulnerability*, November 1962.
5. AMCP 706-161, Engineering Design Handbook, *Elements of Terminal Ballistics, Part Two, Collection and Analysis of Data Concerning Targets*, November 1962.
6. AMCP 706-247, Engineering Design Handbook, *Ammunition Series, Section 4, Design for Projection*, July 1964.
7. MIL-STD 1474· , *Noise Limits for Army Materiel*, 20 April 1984.
8. AMCP 706-252, Engineering Design Handbook, *Gun Tubes*, February 1964.
9. M. C. Nerdahl and H. O. Sand, *Design Data for Towed Artillery Weapon Systems*, Technical Note N-RRA-N-3-10-73, Artillery Weapon Systems Directorate, Weapons Laboratory, Rock Island Arsenal, Rock Island, IL, February 1973.
10. AMCP 706-251, Engineering Design Handbook, *Muzzle Devices*, May 1968.
11. M. J. Salsbury and C. R. Shaffer, *Experimental Investigation of Muzzle Brakes for the XM198 Howitzer*, Technical Report RE-70-3442, Artillery Systems Laboratory, Research and Engineering Directorate, US Army Weapons Command, Rock Island Arsenal, Rock Island, IL, 1970.
12. M. J. Salsbury, *Polar Blast Field of 105-mm Howitzers, Measured and Predicted*, Report RE TR 71-11, Artillery Systems Laboratory, US Army Weapons Command, Rock Island Arsenal, Rock Island, IL, 1971.
13. P. S. Westine and J. C. Hokanson, *Prediction of Standoff Distances to Prevent Loss of Hearing From Muzzle Blast*, Report R-CR-75-003, Artillery and Armored Weapon Systems Directorate, Rock Island Arsenal, Rock Island, IL, 1975.
14. A. P. Boresi, O. M. Sidebottom, F. B. Seely, and J. O. Smith, *Advanced Mechanics of Materials*, John Wiley and Sons, Inc., New York, NY, 1978.
15. R. H. Coberly and J. W. Frantz, *Mathematical Design of a Puteaux Recoil Mechanism*, Technical Note 69-0694, Science and Technology Laboratory, Research and Engineering Directorate, US Army Weapons Command, Rock Island Arsenal, Rock Island, IL, 1969.
16. F. B. Seely and J. O. Smith, *Advanced Mechanics of Materials*, John Wiley and Sons, Inc., New York, NY, 1957.
17. R. J. Toering, *Mathematical Design of a "Soft Recoil" Recoil Mechanism*, Technical Note, Artillery/ Air Defense Weapon Systems Laboratory, Research and Engineering Directorate, US Army Weapons Command, Rock Island Arsenal, Rock Island, IL, 1971.
18. R. E. Seamands and R. J. Toering, *Selecting Best Recoiling Parts in an Artillery System*, Technical Report No. RE-TR-71-19, Artillery/ Air Defense Weapon Systems Laboratory, Research and Engineering Directorate, US Army Weapons Command, Rock Island Arsenal, Rock Island, IL, April 1971.
19. R. J. Toering and R. E. Seamands, *Configuration Optimization Study of the 105-mm Weapon Systems*, Technical Report No. RE-70-0517, Artillery Systems Laboratory, Research and Engineering Directorate, US Army Weapons Command, Rock Island Arsenal, Rock Island, IL, March 1970.
20. K. Terzaghi and R. B. Peck, *Soil Mechanics in Engineering Practice*, John Wiley and Sons, Inc., New York, NY, 1967.
21. J. Y. Wong, *Theory of Ground Vehicles*, Wiley-Interscience, John Wiley and Sons, Inc., New York, NY, 1978.
22. AMCP 706-358, Engineering Design Handbook, *Analysis and Design of Automotive Brake Systems*, December 1976.
23. AMCP 706-192, Engineering Design Handbook, *Computer-Aided Design of Mechanical Systems*, July 1973.
24. DARCOM-P 706-193, Engineering Design Handbook, *Computer-Aided Design of Mechanical Systems, Part Two*, September 1977.

THIS DOCUMENT PROVIDED BY THE ABBOTT AEROSPACE
TECHNICAL LIBRARY
ABBOTTAEROSPACE.COM

CHAPTER 3
ARTILLERY SYSTEM KINEMATIC AND DYNAMIC ANALYSIS

Kinematic analysis is first carried out to define quantitatively relative motion that may occur in the towed artillery system. Forces acting between components of the system are then determined under the influence of gravitational force and those due to impact loading that occurs during transport of the weapon. The equilibrator force-elevation demand curve is defined as input to subsequent equilibrator design. Dynamic models that predict motion of the weapon system during firing are derived, and their use in the analysis of weapon stability is illustrated. Testing for validation and refinement of model parameters is discussed. Numerical integration methods for calculating numerical solutions of equations of motion are reviewed, and advanced methods for computer generating and integrating system equations of motion are presented.

3-0 LIST OF SYMBOLS

$[A^T]$ = transformation matrix from (y,z) to (η,ζ) frame, dimensionless
A_{EQ} = effective area in each equilibrator, m^2
a_j,b_j = constants of numerical integration algorithm, dimensionless
a_η = acceleration of recoiling parts along η-axis, m/s^2
$B(t)$ = breech force, N
b_B = distance of point B along X_B-axis, m
b_T = distance of trunnion along X_B-axis, m
c_B = distance of point B along Y_B-axis, m
c_{ij} = damping coefficient that may depend on generalized coordinates and time, N·m/m
c_T = distance of trunnion along Y_B-axis, m
E = interface load between recoiling parts and cradle, N
F = inertial load due to an acceleration of ng, N
$F(\ )$ = vector of functions
$F_{0_{ij}}$ = actuator force applied along element that may depend upon generalized coordinates and time, N
$(FEL)_\theta$ = total force in elevation struts, N
$(FEQ)_\theta$ = force in equilibrator at elevation ϕ, N
F_i = vector of applied forces on body i, N
F_{ij} = resultant force vector, N
$F_{i\eta}$ = η-component of ith breech force acting on recoiling parts, N
F_{x_i} = x-component of ith dynamic force on body, N
F_{y_i} = y-component of ith dynamic force on body, N
F'_i = vector of constraint forces on body i, N
$f(t,y,\dot{y})$ = function of time, displacement, and velocity, respectively, m/s^2
$G(\eta)$ = function of η, N
g = acceleration due to gravity = 9.81 m/s^2
H = horizontal reaction at the spades, N
$H(\eta)$ = function of η, $N\cdot s^2/m^2$
h = time interval between successive grid points, s
h_i = time step, s
I = polar moment of inertia of body, $kg\cdot m^2$
I_B = polar moment of inertia of mass M_B about center of mass, $kg\cdot m^2$
I_r = polar moment of inertia of recoiling parts about center of mass, $kg\cdot m^2$
i = unit vector along X-axis, dimensionless

THIS DOCUMENT PROVIDED BY THE ABBOTT AEROSPACE
TECHNICAL LIBRARY
ABBOTTAEROSPACE.COM

i_A = unit vector along X_A-axis, dimensionless
i_B = unit vector along X_B-axis, dimensionless
i_H = unit vector along global X_H-axis, dimensionless
J_i = centroidal polar moment of inertia of body i, kg·m^2
j = unit vector along Y-axis, dimensionless
j_A = unit vector along Y_A-axis, dimensionless
j_B = unit vector along Y_B-axis, dimensionless
j_H = unit vector along global Y_H-axis, dimensionless
j' = unit vector along the η-axis, dimensionless
$K(t)$ = recoil force, N
K_1 = spring constant of spring in front supports, N·m/rad
$K(0)$ = value of $K(t)$ under static conditions, N
K_{max} = peak recoil force, N
k = total number of moments on body, dimensionless
k = unit vector along the Z-axis, dimensionless
k_{ij} = elastic spring coefficient that may depend on generalized coordinates and time, N/m
k' = unit vector along the ζ-axis, dimensionless
L = Y-coordinate of ground spring, m
L_{EL} = length of elevating strut, m
ℓ_{ij} = deformed spring length, m
$\ell_{0_{ij}}$ = undeformed spring length, m
M_B = mass of nonrecoiling parts, kg
M_e = mass of nonrecoiling elevating parts, kg
M_T = moment on traverse bearing in the YZ-plane, N·m
m_s = mass of spade assembly, kg
M_t = mass of traversing parts, kg
M_r = mass of recoiling parts, kg
M_v = mass of vehicle, kg
m = mass of component, kg
m_H = moment about O, N·m
m_i = mass of body i, kg
N = normal reaction of cradle on recoiling parts, N
= number of rounds fired, dimensionless
n = multiplying factor, i.e., number of g's experienced by component, dimensionless
n_f = total number of forces acting on the body, dimensionless
P_0 = pressure of gas in each equilibrator at $\theta = 0$, Pa
p = integer characterizing the algorithm, dimensionless
$\dot{p}_i$ = rate of change with respect to time of linear momentum vector of body i, kg·m/s^2
Q_η = generalized force corresponding to generalized coordinate η, N
Q_ϕ = generalized force corresponding to generalized coordinate ϕ, N·m
Q^i = vector of generalized forces acting on body i, N
Q_x^i, Q_y^i, Q_ϕ^i = generalized forces on body i in the x-, y-, and ϕ-directions, N, N, N·m, respectively
q = composite vector of all system generalized coordinates, m
q^i = vector of generalized coordinates, m
q^0 = specified initial values of generalized coordinates, m
δq = virtual displacement of generalized coordinates, m
$\dot{q}$ = generalized velocities, m/s

THIS DOCUMENT PROVIDED BY THE ABBOTT AEROSPACE
TECHNICAL LIBRARY
ABBOTTAEROSPACE.COM

$\dot{q}^{0}$ = specified initial values of generalized velocities, m/s
r_A = position vector of center of mass of M_r in global coordinate system, m
$r_{A/O}$ = position vector of point A relative to O, m
$r_{A/T}$ = position vector of point A relative to T, m
r_B = position vector of mass M_B, m
$r_{B/O}$ = position vector of center of mass of the cradle relative to O, m
$r_{B/T}$ = position vector of center of mass of the cradle with respect to trunnion, m
$r_{D/O}$ = position vector of center of mass of bottom carriage and trails relative to O, m
r_i = position vector of O_i, m
r_{ij} = position vector of p_{ij} relative to O_i, m
r_j = position vector of O_j, m
r_{ji} = position vector of p_{ji} relative to O_j, m
r_p = position vector of point p_{ji} relative to point p_{ij}, m
$r_{s_{ij}}$ = vector $[(\ell_{ij}\cos\alpha)i + (\ell_{ij}\sin\alpha)j]$ between points s_{ij} and s_{ji}, m
$r_{T/O}$ = position vector of trunnion relative to O, m
$r_{TC/O}$ = position vector of center of mass of top carriage relative to O, m
S_1 = clip reaction in side rail bearings, N
S_2 = clip reaction in barrel bearings, N
T = kinetic energy of system, J
T_B = kinetic energy of mass M_B, J
T_H = horizontal reaction at trunnion, N
T_i = kinetic energy of body i, J
T_η = force in the η-direction on cradle due to trunnion, N
T_j = jth dynamic moment on body, N·m
T_r = kinetic energy of mass M_r, J
T_V = vertical reaction at trunnion, N
T_ζ = force in the ζ-direction on the cradle due to trunnion reaction, N
T_ϕ = reaction moment at trunnion, N·m
TCY = force due to bottom carriage on top carriage in the Y-direction, N
TCZ = force on top carriage due to bottom carriage, N
t = time, s
t_0 = instant at which $E = 0$, s
= time at initial grid point, s
t_i = ith grid point, s
t_n = nth time grid point, s
V = potential energy of system, J
V_{pivot} = vertical reaction at spades, N
V_{spring} = vertical reaction of ground on firing base, N
V_0 = volume of gas in each equilibrator at $\theta = 0$, m^3
v_B = velocity vector of B, m/s
v_r = velocity vector of A, m/s
W_B = weight of cradle, N
W_D = weight of bottom carriage and trails, N
W_r = weight of the recoiling parts, N
W_{TC} = weight of top carriage, N
δW = virtual work of $K(t)$ and $B(t)$, J
δW_i = virtual work of forces acting on body i, J

THIS DOCUMENT PROVIDED BY THE ABBOTT AEROSPACE
TECHNICAL LIBRARY
ABBOTTAEROSPACE.COM

x_i = x-coordinate of O_i, m
$\ddot{X}_A$ = acceleration of recoiling parts in global X-direction, m/s^2
$\ddot{x}$ = acceleration of body along x-direction, m/s^2
Y_D = Y-coordinate of center of mass of bottom carriage and trails, m
Y_{EL} = distance along Y-axis of attachment point of elevating strut on top carriage from the spade, m
Y_{EQ} = horizontal distance between spade and attachment point of equilibrator on top carriage, m
Y_T = horizontal distance between spade and trunnion, m
Y_{TB} = Y-coordinate of traverse bearing from spade, m
Y_{TC} = Y-coordinate of top carriage relative to O, m
$\ddot{Y}_A$ = acceleration of recoiling parts in global Y-direction, m/s^2
y = displacement, m
y_i = y-coordinate of O_i, m
y_n = value of y at nth time grid point, units same as units of y
y_0 = initial value of y, m
y_1 = displacement, m
y_2 = velocity, m/s
$\dot{y}$ = first time derivative of $y(t)$, m/s
$\dot{y}(0)$ = initial value of $\dot{y}(t)$, m/s
$\ddot{y}$ = acceleration in y-direction, m/s^2
Z_{EL} = distance along Z-axis of attachment point of elevating strut on top carriage from spade, m
Z_{EQ} = vertical distance of attachment points of equilibrator on top carriage from firing base, m
Z_T = vertical distance of trunnion from firing base, m
Z_{TB} = Z-coordinate of traverse bearing from spade, m
Z_{TC} = Z-coordinate of top carriage relative to O, m
θ = cannon angle of elevation, rad
α = angle between direction of force $(FEQ)_\theta$ and negative η-axis, rad
β = angle shown in Fig. 3-7, rad
Δ = angle shown in Fig. 3-7, rad
ζ_A = distance along ζ-axis of center of mass of recoiling parts from trunnion, m
ζ_{EL} = distance along ζ-axis of attachment point of elevating strut on cradle from trunnion, m
ζ_{EQ} = distance along ζ-axis of attachment point of equilibrator on cradle from trunnion, m
ζ_0 = initial displacement of recoiling parts, m
ζ_1 = displacement of recoiling parts, m
ζ_2 = velocity of recoiling parts, m/s
ζ = distance along ζ-axis of point of application of rod pull from trunnion, m
η = displacement of recoiling parts, m
= distance of A along X_A-axis, m
= translation of recoiling parts relative to cradle, m
η_A = distance along η-axis of center of mass of recoiling parts from trunnion, m
η_B = distance along X_B-axis of center of mass of M_B from trunnion, m
η_{EL} = distance along η-axis of attachment point of elevating strut on cradle from trunnion, m
η_{EQ} = distance along η-axis of attachment point of equilibrator on cradle from trunnion, m
η_F = distance along η-axis of front rail bearing from trunnion, m
η_{ij} = coordinate of point p_{ij} along η_r-axis, m
η_{ji} = coordinate of point p_{ji} along η_r-axis, m
η_L = out-of-battery position of W_r along Y-axis, m
η_N = distance along X_A-axis of point of application of normal reaction, m

THIS DOCUMENT PROVIDED BY THE ABBOTT AEROSPACE
TECHNICAL LIBRARY
ABBOTTAEROSPACE.COM

η_p = multiplying factor corresponding to peak recoil force, dimensionless
η_R = distance along η-axis of rear rail bearing from trunnion, m
η_0 = in-battery position of W_r along Y-axis, m
$\dot{\eta}$ = velocity of recoiling parts, m/s
λ = Lagrange multiplier vector with m-components
μ = coefficient of friction between recoiling parts and cradle, dimensionless
ξ_{ij} = coordinate of point p_{ij} along ξ_i-axis, m
ξ_{jk} = coordinate of point p_{jk} along ξ_j-axis, m
(ξ_i,η_i) = body-fixed coordinate system relative to global system, m
ξ_0 = distance along y_A-axis of contact surface between recoiling parts and cradle, m
ξ_1 = distance along Y_A-axis of contact surface between recoiling parts and cradle, m
= distance of A along Y_A-axis, m
= distance along Y_A-axis of point of application of $B(t)$, m
τ = angle between direction of force $(FEL)_\theta$ and negative η-axis, rad
= time period over which differential equation is integrated, s
$\Phi(q,t)$ = vector of constraint functions
ϕ = pitch angle of undercarriage, rad
ϕ_i = angular orientation (ξ_i,η_i) body-fixed coordinate system relative to global system, rad
ϕ_{st} = angle ϕ under static conditions, rad
ϕ_1 = pitch angle of top carriage relative to ground, rad
ϕ_2 = pitch angle of cradle rotation relative to top carriage, rad
$\ddot{\phi}$ = angular acceleration of body, rad/s^2
= angular acceleration of recoiling parts, rad/s^2

3-1 STATIC AND QUASI-STATIC ANALYSIS

3-1.1 INPUT FORCE DETERMINATION

Forces acting on components of a towed artillery system are of two types: static loads and dynamic loads. Static loads on components usually are due to the weight of the bodies in the system or to pretensioned springs in the system. Dynamic loads occur due to motion of the system and can only be determined exactly by solving the equations of motion for the system. There are some dynamic loads, however, that can be approximated without having to solve the equations of motion. Such loads are called "quasi-static". Quasi-static loads can be determined by applying d'Alembert's principle, which can be written as (Ref. 1)

$$\boldsymbol{F}_i + \boldsymbol{F}'_i - \dot{\boldsymbol{p}}_i = 0, \text{ N} \tag{3-1}$$

where*

$\boldsymbol{F}_i$ = vector of applied forces on body i, N
$\boldsymbol{F}'_i$ = vector of constraint forces on body i, N
$\dot{\boldsymbol{p}}_i$ = rate of change with respect to time of linear momentum vector of body i, kg·m/s^2.

The negative of the momentum rate of change, $-\dot{\boldsymbol{p}}_i$, can be looked upon as an inertial force. Thus by knowing the acceleration of the body from experiment or analysis, it is possible to predict the inertial load.

The concept of determining inertial loads can be illustrated by considering a component of mass m of the weapon which experiences a worst case g-loading of ng meters/second. The inertial load F in the direction of this acceleration is

$$F = -mng, \text{ N} \tag{3-2}$$

where

F = inertial load due to an acceleration of ng, N
m = mass of component, kg
n = multiplying factor, i.e., number of g's experienced by component, dimensionless
g = acceleration due to gravity = 9.81 m/s^2.

*A bold italic symbol will be used to represent a vector.

THIS DOCUMENT PROVIDED BY THE ABBOTT AEROSPACE
TECHNICAL LIBRARY
ABBOTTAEROSPACE.COM

Inertial forces on a body always act through the center of mass of the body. This makes it important to locate the centers of mass of all bodies in the system in some suitable coordinate system. Location of the center of mass is also important when writing the kinetic energy of the body for the derivation of its equations of motion.

Inertial forces experienced by a weapon during transportation seldom exceed the loads produced during firing. However, local structural members to which the conveying components are attached may be subjected to large forces. Accordingly, the total structure should be investigated to detect any critical loads that may appear during transportation. The determination of these forces is thus required for stress analysis of components of the system.

The travel load that usually produces the greatest stress in a carriage structure is due to a 6-g acceleration that may occur over very rough terrain. For a system such as the M204 Howitzer, the carriage has a mass of 2160 kg (Ref. 2). The force F on the carriage under travel conditions can be written from Eq. 3-2 as

$$F = -2160\ (6 \times 9.81) = 127{,}138\ \text{N}\ (28{,}582\ \text{lb}).$$

This force acts through the center of mass of the carriage.

A quasi-static treatment of peak recoil force can also be performed to determine the g-load due to this force. Let the peak recoil force be K_{max} and mass of recoiling parts M_r. From Eq. 3-2

$$\left.\begin{aligned} K_{max} &= M_r \eta_p g,\ \text{N} \\ \text{or} \\ \eta_p g &= \frac{K_{max}}{M_r},\ \text{m/s}^2 \end{aligned}\right\} \qquad (3\text{-}3)$$

where

K_{max} = peak recoil force, N
M_r = mass of recoiling parts, kg
η_p = multiplying factor corresponding to peak recoil forces, i.e., number of g's experienced by recoiling parts, dimensionless.

From Eq. 3-3 it is evident that η_p defines the g-loading corresponding to the peak recoil force. The quasi-static allowable limits of the materials must be determined prior to the application of Eq. 3-3.

3-1.2 STATIC AND QUASI-STATIC FORCE ANALYSIS

A rigid body in a plane has 3 degrees of freedom—2 in translation and 1 in rotation. A body in 3 dimensions, on the other hand, has 6 degrees of freedom—3 in translation and 3 in rotation. In either case, for a body to be in static equilibrium requires that the vector sum of the forces and moments acting on the body be zero. In the planar case this leads to three scalar equations. To write the three equations of equilibrium, a free-body diagram of each body in the system should first be drawn. Summation of the forces acting on the body along each of two coordinate directions gives two scalar equations. The third scalar equation can be written by taking moments about any point on the body.

As an illustration of the technique for static force analysis, the M198, 155-mm towed Howitzer (Ref. 3) is considered. This system consists of a cannon and recoiling parts, which are supported by the cradle at three points—the bearing at the front cradle support and the rail bearings at the rear on each side of the cradle. The tipping parts are pinned to the top carriage at the trunnion and are balanced by equilibrators and positioned in elevation by two elevating struts. The trails, bottom carriage, and firing base support the traversing parts on a traverse bearing. The spades at the end of each trail and the firing base provide the bearing surface required to anchor the weapon in the ground.

The clip reactions S_1 and S_2 due to the weight of the recoiling parts on the cradle are shown in Fig. 3-1. Summation of forces in the η-direction gives

$$K - W_r \sin\theta = 0 \qquad (3\text{-}4)$$

or

$$K = W_r \sin\theta,\ \text{N} \qquad (3\text{-}5)$$

THIS DOCUMENT PROVIDED BY THE ABBOTT AEROSPACE
TECHNICAL LIBRARY
ABBOTTAEROSPACE.COM

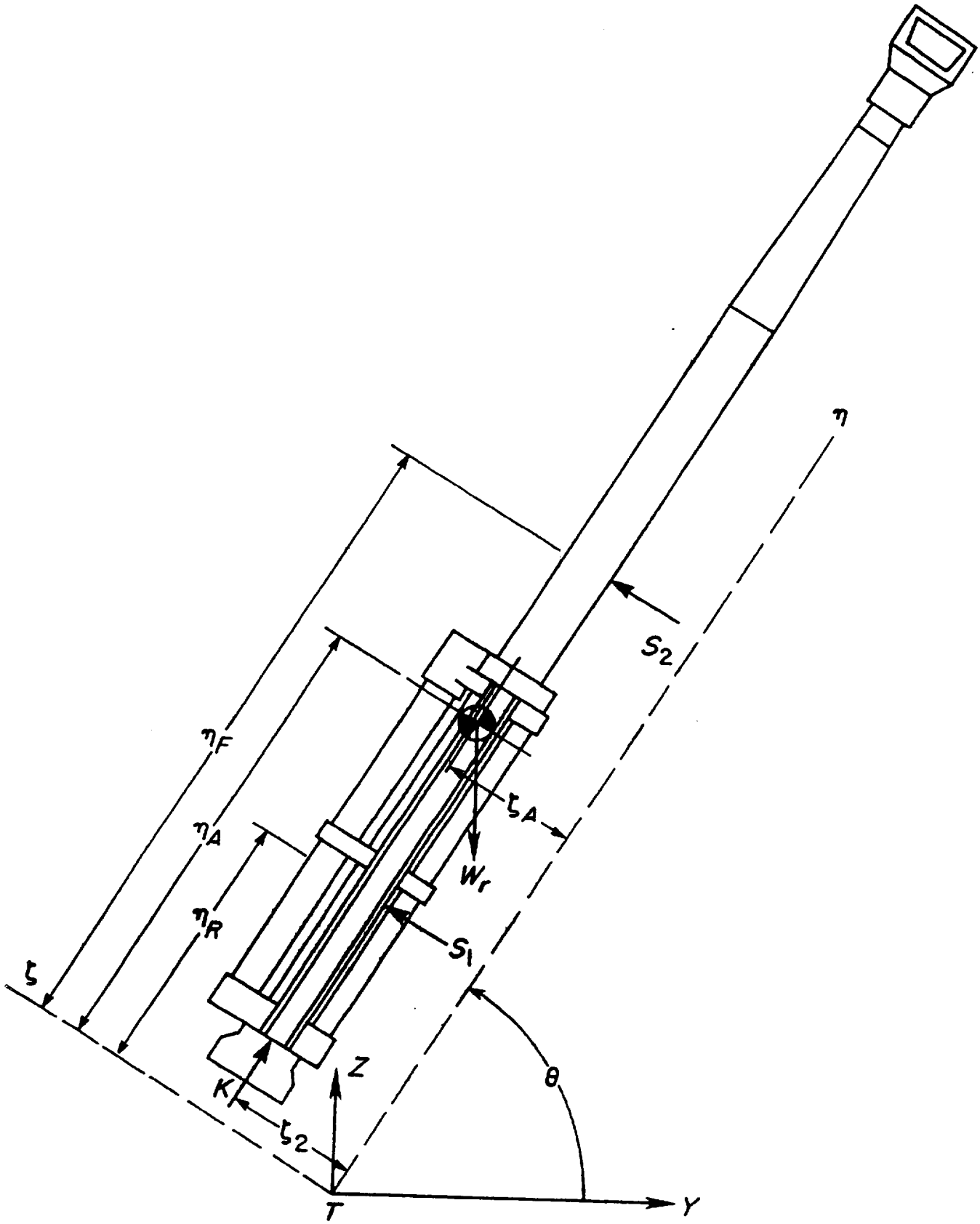

Figure 3-1. Free-Body Diagram of Recoiling Mass

THIS DOCUMENT PROVIDED BY THE ABBOTT AEROSPACE
TECHNICAL LIBRARY
ABBOTTAEROSPACE.COM

where

W_r = weight of the recoiling parts, N
K = recoil force, N
θ = cannon angle of elevation, rad.

In this special case of static equilibrium, the recoil force K is just the counterrecoil force that holds the recoiling parts in battery.

Summation of forces in the ζ-direction gives

$$S_1 + S_2 - W_r\cos\theta = 0 \tag{3-6}$$

or

$$S_1 + S_2 = W_r\cos\theta, \text{ N} \tag{3-7}$$

where

S_1 = clip reaction in side rail bearings, N
S_2 = clip reaction in barrel bearings, N.

Summation of moments about the center of mass of the recoiling parts gives

$$S_1(\eta_A - \eta_R) - S_2(\eta_F - \eta_A) - K(\zeta_A - \zeta_2) = 0$$

and substitution of the expression for K from Eq. 3-5 gives

$$S_1(\eta_A - \eta_R) - S_2(\eta_F - \eta_A) = W_r(\zeta_A - \zeta_2)\sin\theta, \text{ N·m.} \tag{3-8}$$

The solution of Eqs. 3-7 and 3-8 for S_1 and S_2 is

$$S_1 = \frac{W_r[(\eta_F - \eta_A)\cos\theta + (\zeta_A - \zeta_2)\sin\theta]}{\eta_F - \eta_R}, \text{ N} \tag{3-9}$$

$$S_2 = W_r\cos\theta - S_1, \text{ N} \tag{3-10}$$

where

η_F = distance along η-axis of front rail bearing from trunnion, m
η_A = distance along η-axis of center of mass of recoiling parts from trunnion, m
ζ_A = distance along ζ-axis of center of mass of recoiling parts from trunnion, m
ζ_2 = distance along ζ-axis of point of application of rod pull from trunnion, m
η_R = distance along η-axis of rear rail bearing from trunnion, m.

The static force developed by the equilibrators is independent of the mass of recoiling parts. Also this force depends on the type of equilibrator used. For the M198 Howitzer, two pneumatic equilibrators are employed. The force in the equilibrators can be determined as a function of the gun position by applying the isothermal gas law. The forces in these equilibrators can be written as (Ref. 4)

$$(FEQ)_\theta = \frac{2A_{EQ}P_0V_0}{V_0 - A_{EQ}\{[(EQ1) + 2(EQ2)\cos\theta - 2(EQ3)\sin\theta]^{1/2} - [(EQ1) + 2(EQ2)]^{1/2}\}}, \text{ N} \tag{3-11}$$

with

$EQ1 = (Y_T - Y_{EQ})^2 + (Z_T - Z_{EQ})^2 + \eta_{EQ}^2 + \zeta_{EQ}^2$, m^2
$EQ2 = (Y_T - Y_{EQ})\eta_{EQ} + (Z_T - Z_{EQ})\zeta_{EQ}$, m^2
$EQ3 = (Y_T - Y_{EQ})\eta_{EQ} - (Z_T - Z_{EQ})\eta_{EQ}$, m^2

THIS DOCUMENT PROVIDED BY THE ABBOTT AEROSPACE
TECHNICAL LIBRARY
ABBOTTAEROSPACE.COM

where

$(FEQ)_\theta$ = force in equilibrator at elevation θ, N
A_{EQ} = effective area in each equilibrator, m^2
P_0 = pressure of gas in each equilibrator at $\theta = 0$, Pa
V_0 = volume of gas in each equilibrator at $\theta = 0$, m^3
Y_T = horizontal distance between spade and trunnion, m
Y_{EQ} = horizontal distance between spade and attachment point of equilibrator on top carriage, m
Z_T = vertical distance of trunnion from firing base, m
Z_{EQ} = vertical distance of attachment points of equilibrator on top carriage from firing base, m
η_{EQ} = distance along η-axis of attachment point of equilibrator on cradle from trunnion, m
ζ_{EQ} = distance along ζ-axis of attachment point of equilibrator on cradle from trunnion, m.

A free-body diagram of the cradle is shown in Fig. 3-2. The unknown forces on the cradle are T_V, T_H, and $(FEL)_\theta$. Summation of forces in the η-direction gives

$$T_\eta - (FEQ)_\theta \cos\theta - (FEL)_\theta \cos\tau - K - W_B \sin\theta = 0 \qquad (3\text{-}12)$$

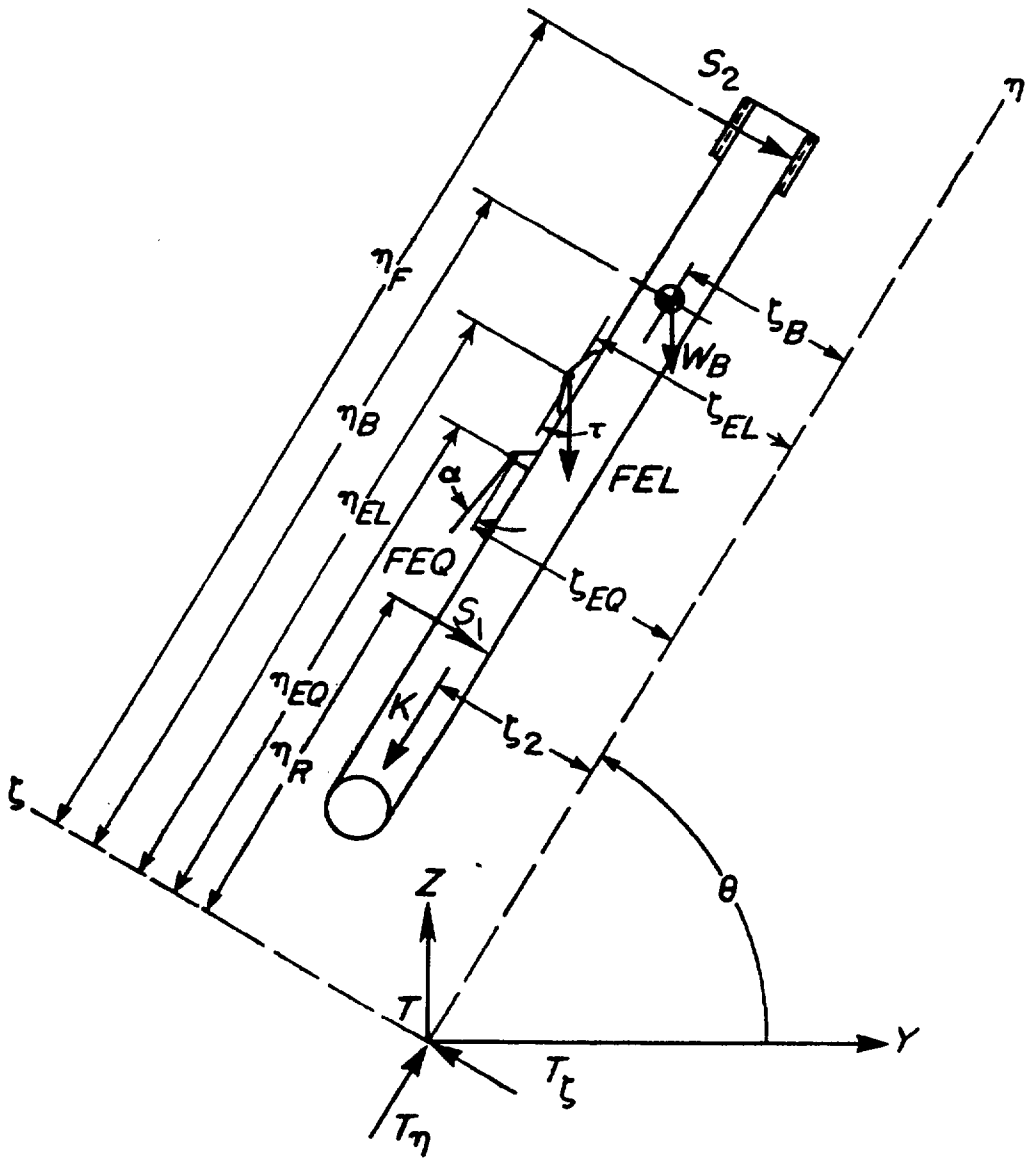

Figure 3-2. Free-Body Diagram of Cradle

THIS DOCUMENT PROVIDED BY THE ABBOTT AEROSPACE
TECHNICAL LIBRARY
ABBOTTAEROSPACE.COM

where

T_η = force in the η-direction on cradle due to trunnion, N
W_B = weight of cradle, N
α = angle between direction of force $(FEQ)_\theta$ and negative η-axis, rad
τ = angle between direction of force $(FEL)_\theta$ and negative η-axis, rad
$(FEL)_\theta$ = total force in elevating struts, N.

Summation of forces in the ζ-direction gives

$$T_\zeta + (FEQ)_\theta \sin\alpha - (FEL)_\theta \sin\tau - (S_1 + S_2) - W_B \cos\theta = 0 \tag{3-13}$$

where

T_ζ = force in the ζ-direction on the cradle due to the trunnion reaction, N.

Summation of moments about the trunnion T gives

$$\begin{aligned} &-S_1\eta_R - S_2\eta_F + K\zeta_2 - W_B(\eta_B\cos\theta - \zeta_B\sin\theta) \\ &+ [(FEQ)_\theta\cos\alpha]\zeta_{EQ} + [(FEQ)_\theta\sin\alpha]\eta_{EQ} \\ &- [(FEL)_\theta\sin\tau]\eta_{EL} + [(FEL)_\theta\cos\tau]\zeta_{EL} = 0. \end{aligned} \tag{3-14}$$

From the geometry of the system (see Figs. 3-2 and 3-3), the following expressions for α and τ may be written:

$$\alpha = \theta + \mathrm{Tan}^{-1}\left(\frac{Z_{EQ} - Z_T - \eta_{EQ}\sin\theta - \zeta_{EQ}\cos\theta}{Y_T + \eta_{EQ}\cos\theta - \zeta_{EQ}\sin\theta - Y_{EQ}}\right), \text{ rad} \tag{3-15}$$

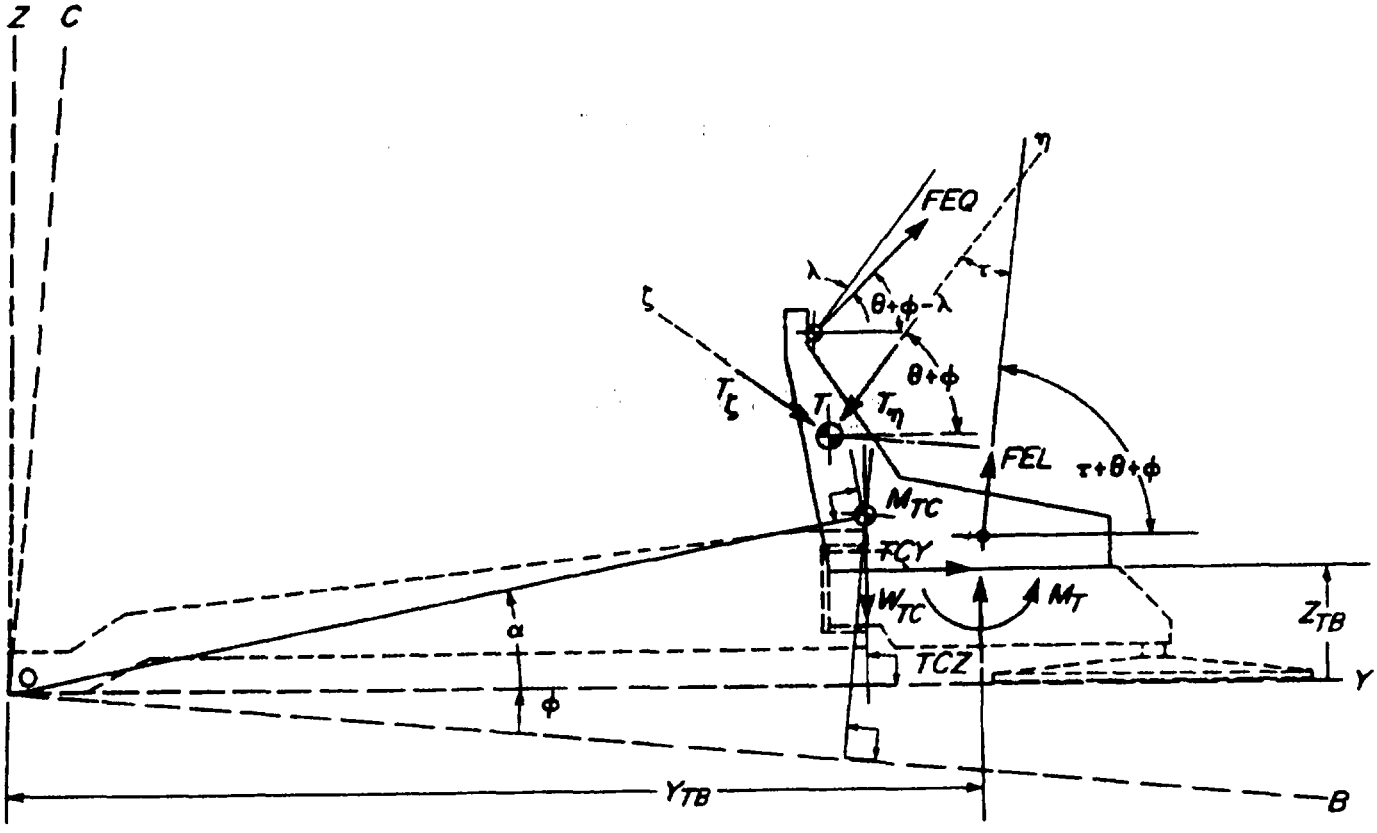

Figure 3-3. Free-Body Diagram of Top Carriage

THIS DOCUMENT PROVIDED BY THE ABBOTT AEROSPACE
TECHNICAL LIBRARY
ABBOTTAEROSPACE.COM

$$\tau = \mathrm{Tan}^{-1}\left(\frac{Z_T + \eta_{EL}\sin\theta + \zeta_{EL}\cos\theta - Z_{EL}}{Y_T + \eta_{EL}\cos\theta - \zeta_{EL}\sin\theta - Y_{EL}}\right) - \theta, \text{ rad} \tag{3-16}$$

where

η_{EL} = distance along η-axis of attachment point of elevating strut on cradle from trunnion, m
ζ_{EL} = distance along ζ-axis of attachment point of elevating strut on cradle from trunnion, m
Y_{EL} = distance along Y-axis of attachment point of elevating strut on top carriage from spade, m
Z_{EL} = distance along Z-axis of attachment point of elevating strut on top carriage from spade, m.

Solve Eqs. 3-12, 3-13, and 3-14 and use Eqs. 3-5, 3-9, 3-10, and 3-13 to eliminate K, S_1, and S_2, respectively,

$$(FEL)_\theta = \frac{(FEQ)_\theta(\eta_{EQ}\sin\alpha + \zeta_{EQ}\cos\alpha) - W_r(\eta_A\cos\theta - \zeta_A\sin\theta) - W_B(\eta_B\cos\theta - \zeta_B\sin\theta)}{\eta_{EL}\sin\tau - \zeta_{EL}\cos\tau}, \text{ N} \tag{3-17}$$

$$T_\eta = (FEQ)_\theta\cos\alpha + (FEL)_\theta\cos\tau + (W_r + W_B)\sin\theta, \text{ N} \tag{3-18}$$

$$T_\zeta = (W_r + W_B)\cos\theta + (FEL)_\theta\sin\tau - (FEQ)_\theta\sin\alpha, \text{ N}. \tag{3-19}$$

Consider the free-body diagram of the top carriage shown in Fig. 3-3. For pitch angle $\phi = 0$, the equations of static equilibrium can be written as

$$TCY + (FEL)_\theta\cos(\tau + \theta) - T_\eta\cos\theta + T_\zeta\sin\theta + (FEQ)_\theta\cos(\theta - \alpha) = 0 \tag{3-20}$$

where

TCY = force due to bottom carriage on top carriage in the Y-direction, N.

$$TCZ + (FEL)_\theta\sin(\tau + \theta) - T_\eta\sin\theta - T_\zeta\cos\theta + (FEQ)_\theta\sin(\theta - \alpha) - W_{TC} = 0 \tag{3-21}$$

where

TCZ = force on top carriage due to bottom carriage, N
W_{TC} = weight of top carriage, N.

Summation of moments about the center of the traverse bearing gives

$$\begin{aligned} &M_T - (FEL)_\theta[\cos(\tau + \theta)(Z_{EL} - Z_{TB}) + \sin(\tau + \theta)(Y_{TB} - Y_{EL})] \\ &\quad + T_\eta[(Z_T - Z_{TB})\cos\theta + (Y_{TB} - Y_T)\sin\theta] \\ &\quad - T_\zeta[(Z_T - Z_{TB})\sin\theta - (Y_{TB} - Y_T)\cos\theta] \\ &\quad -(FEQ)_\theta[(Z_{EQ} - Z_{TB})\cos(\theta - \alpha) + (Y_{TB} - Y_{EQ})\sin(\theta - \alpha)] \\ &\quad + W_{TC}(Y_{TB} - Y_{TC}) = 0 \end{aligned} \tag{3-22}$$

where

M_T = moment on traverse bearing in the YZ-plane, N·m
Z_{TB} = Z-coordinate of traverse bearing from spade, m
Y_{TB} = Y-coordinate of traverse bearing from spade, m.

Solve Eqs. 3-20 and 3-21 and use Eqs. 3-18 and 3-19—together with trigonometric identities—to eliminate $(FEQ)_\theta$, T_η, and T_ζ, respectively, to get

$$TCY = 0, \text{ N} \tag{3-23}$$

$$TCZ = W_r + W_B + W_{TC}, \text{ N}. \tag{3-24}$$

THIS DOCUMENT PROVIDED BY THE ABBOTT AEROSPACE
TECHNICAL LIBRARY
ABBOTTAEROSPACE.COM

By substituting Eqs. 3-18 and 3-19 into Eq. 3-22, expanding terms with trigonometric identities, using Eqs. 3-15 and 3-16, and applying Eq. 3-17,

$$M_T = W_r(Y_T + \eta_A\cos\theta - \zeta_A\sin\theta - Y_{TB}) + W_B(Y_T + \eta_B\cos\theta - \zeta_B\sin\theta - Y_{TB}) - W_{TC}(Y_{TB} - Y_{TC}),\ \text{N·m.} \tag{3-25}$$

Finally, consider the free-body diagram of the bottom carriage and the trails in Fig. 3-4. For $\phi = 0$,

$$H - TCY = 0 \tag{3-26}$$

where

H = horizontal reaction at the spades, N

and

$$V_{pivot} - TCZ + V_{spring} - W_D = 0 \tag{3-27}$$

where

W_D = weight of bottom carriage and trails, N
V_{pivot} = vertical reaction at the spades, N
V_{spring} = vertical reaction of ground on firing base, N.

Moments about the point O give

$$V_{spring}L - (TCZ)Y_{TB} + (TCY)Z_{TB} - W_DY_D - M_T = 0 \tag{3-28}$$

where

L = Y-coordinate of ground spring, m
Y_D = Y-coordinate of center of mass of bottom carriage and trails, m.

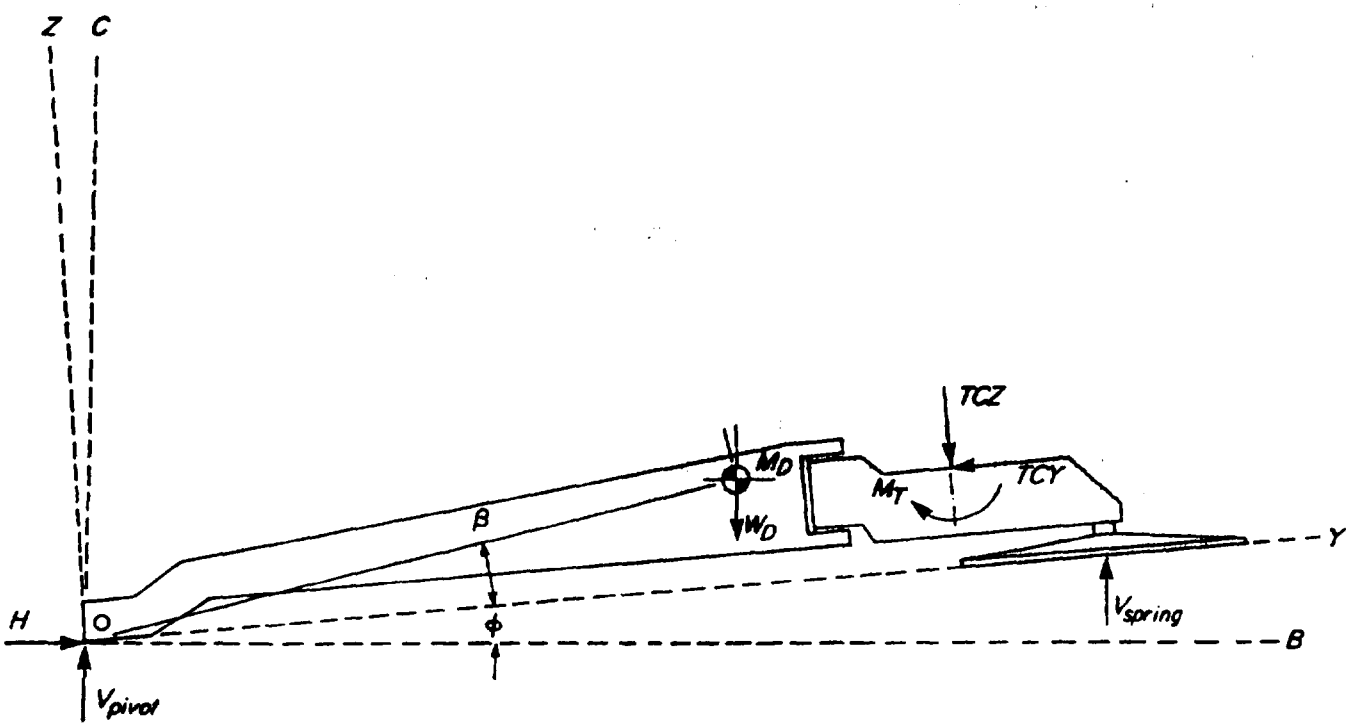

Figure 3-4. Free-Body Diagram of Nonelevating Mass M_D

THIS DOCUMENT PROVIDED BY THE ABBOTT AEROSPACE
TECHNICAL LIBRARY
ABBOTTAEROSPACE.COM

The simultaneous solution of Eqs. 3-26, 3-27, and 3-28 and use of Eqs. 3-23, 3-24, and 3-25 to eliminate TCY, TCZ, and M_T, respectively, give

$$H = 0 \tag{3-29}$$

$$V_{spring} = \frac{W_r(Y_T + \eta_A\cos\theta - \zeta_A\sin\theta) + W_B(Y_T + \eta_B\cos\theta - \zeta_B\sin\theta) + W_{TC}Y_{TC} + W_DY_D}{L}, \text{ N} \tag{3-30}$$

$$V_{pivot} = W_r + W_B + W_{TC} + W_D - V_{spring}, \text{ N}. \tag{3-31}$$

The equilibrators in artillery systems usually are designed to minimize the force on the elevating strut. This in turn translates into minimizing the force on the elevating handwheel. The force that the equilibrator is required to produce at specified angles of elevation is given in the form of a demand curve. To generate this curve, consider Eq. 3-17 and set the left-hand side equal to zero (ideal case of $FEL = 0$) to obtain

$$(FEQ)_\theta = \frac{W_r(\eta_A\cos\theta - \zeta_A\sin\theta) + W_B(\eta_B\cos\theta - \zeta_B\sin\theta)}{\eta_{EQ}\sin\alpha + \zeta_{EQ}\cos\alpha}, \text{ N}.$$

Angle α is given by Eq. 3-15 as

$$\alpha = \theta + \text{Tan}^{-1}\left(\frac{Z_{EQ} - Z_T - \eta_{EQ}\sin\theta - \zeta_{EQ}\cos\theta}{Y_T + \eta_{EQ}\cos\theta - \zeta_{EQ}\sin\theta - Y_{EQ}}\right), \text{ rad}.$$

Consider the following data for the M198 Howitzer (Ref. 12):

W_r = 31,620.0 N
W_B = 5115.0 N
η_A = 2.246 m
ζ_A = 0.0004 m
η_B = 1.648 m
ζ_B = −0.034 m
η_{EQ} = 1.403 m
ζ_{EQ} = 0.191 m
Z_T = 1.422 m
Y_T = 4.059 m
Z_{EQ} = 1.911 m
Y_{EQ} = 3.993 m.

The demand curve of $(FEQ)_\theta$ as a function of θ is calculated and plotted for the M198 Howitzer as shown in Fig. 3-5. Achieving this function of force versus elevation is the design goal for the equilibrator.

In summary, a general procedure for static analysis of any body in a system should first involve drawing a free-body diagram for that body. The force and moment equilibrium equations are then written to determine the unknown forces on the body. This procedure can be carried out for all the bodies in the system.

3-1.3 KINEMATIC ANALYSIS

A planar kinematic model of the M198 Howitzer is shown in Fig. 3-6. The recoiling parts are supported on the cradle in a bearing at the front and two rail bearings at each side, just forward of the trunnion. The recoiling parts can thus only translate relative to the cradle. The cradle in turn is pivoted in the top carriage at the trunnion. This location allows the cradle to rotate in elevation about the trunnion bearing, relative to the top carriage. The equilibrator and elevating strut are pinned at one end to the top carriage and to the cradle at the other end. The equilibrator does not constitute a geometric constraint between the cradle and the top

THIS DOCUMENT PROVIDED BY THE ABBOTT AEROSPACE
TECHNICAL LIBRARY
ABBOTTAEROSPACE.COM

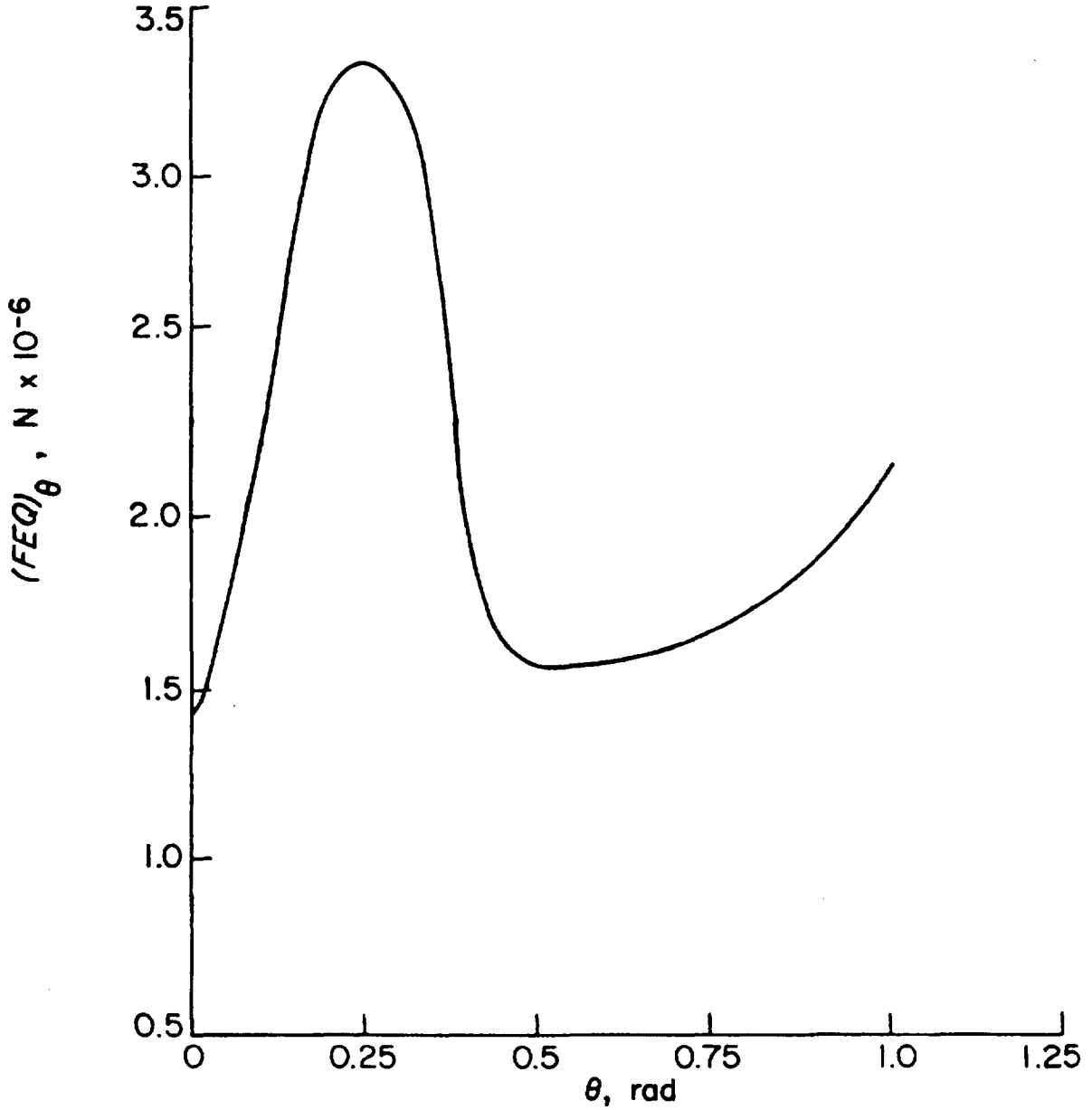

Figure 3-5. Equilibrator Demand Curve for M198 Howitzer

carriage. This statement is true because the length of the equilibrator does not determine the elevation of the cradle. The length of the elevating strut, on the other hand, constitutes a geometric constraint on the position of the elevating parts. Specification of the length of the elevating strut fixes the angle of elevation of the elevating parts. The top and bottom carriages are constrained to relative rotation in azimuth at the traverse bearing. The axis of this bearing is perpendicular to the firing base of the weapon. This joint allows rotation of the traversing parts—i.e., top carriage, cradle, and recoiling parts—relative to the bottom carriage. Spades at the end of each trail provide the bearing surfaces required to anchor the weapon in the ground, and the spades resist horizontal translation during firing.

To locate the position of the center of mass of the recoiling parts relative to fixed point O, locate point A shown in Fig. 3-6 in a coordinate system embedded in the cradle, i.e., in the (η,ζ)-coordinate system with origin at the trunnion T. Then,

$$r_{A/T} = \eta_A j' + \zeta_A k', \text{ m} \tag{3-32}$$

THIS DOCUMENT PROVIDED BY THE ABBOTT AEROSPACE
TECHNICAL LIBRARY
ABBOTTAEROSPACE.COM

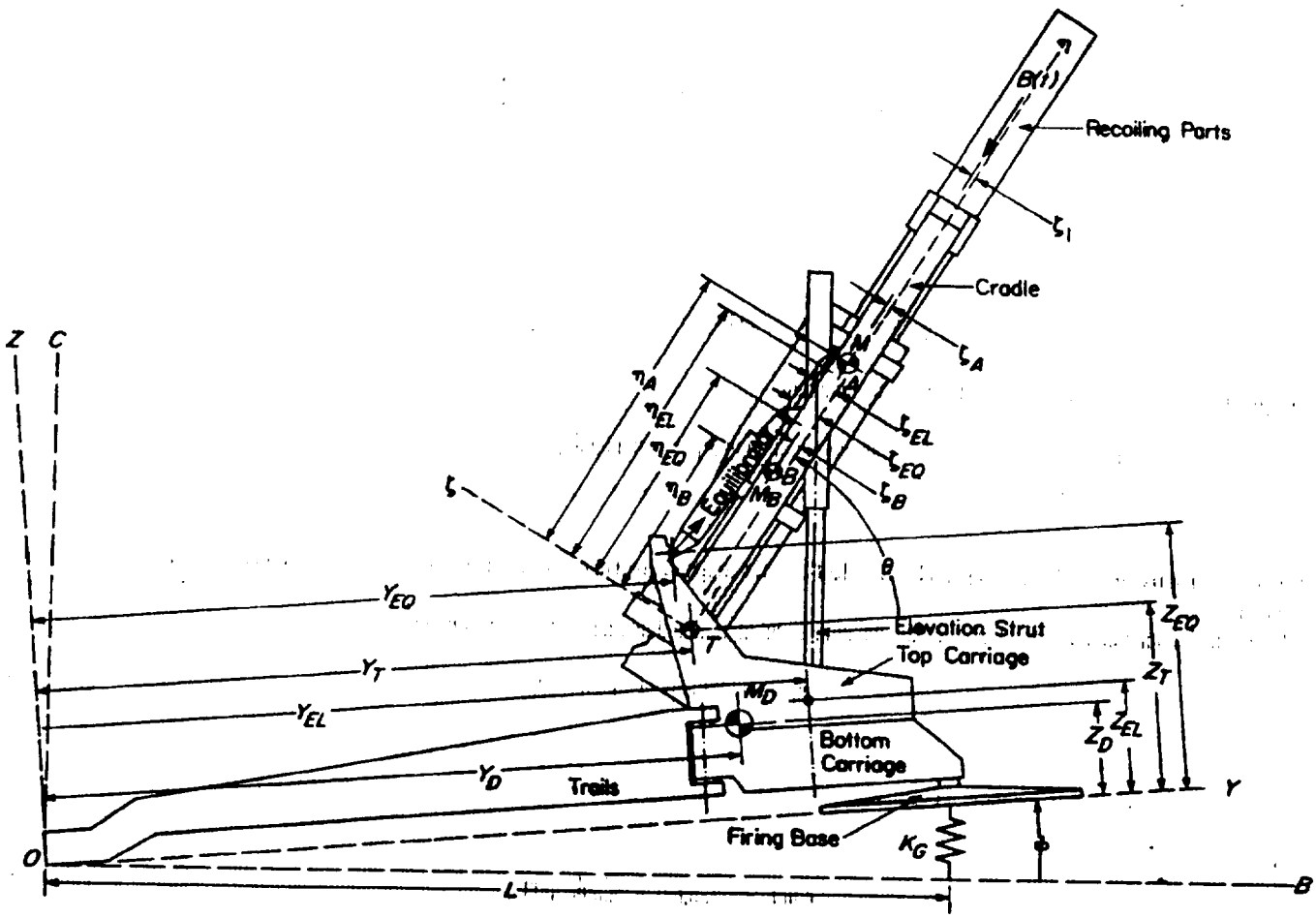

Figure 3-6. Schematic Representation of M198 Howitzer

where

$r_{A/T}$ = position vector of point A relative to T, m
j' = unit vector along the η-axis, dimensionless
k' = unit vector along the ζ-axis, dimensionless.

The position vector of the trunnion T with respect to O can be written as

$$r_{T/O} = Y_T j + Z_T k, \text{ m} \tag{3-33}$$

where

$r_{T/O}$ = position vector of trunnion relative to O, m
j = unit vector along Y-axis, dimensionless
k = unit vector along Z-axis, dimensionless.

By use of the vector identity

$$r_{A/O} = r_{T/O} + r_{A/T} \tag{3-34}$$

where

$r_{A/O}$ = position vector of point A relative to O, m.

By Eqs. 3-32 and 3-33

$$r_{A/O} = Y_T j + Z_T k + \eta_A j' + \zeta_A k'. \tag{3-35}$$

THIS DOCUMENT PROVIDED BY THE ABBOTT AEROSPACE
TECHNICAL LIBRARY
ABBOTTAEROSPACE.COM

Note that the (η,ζ)-coordinate system makes an angle of θ with the (Y,Z)-system. A transformation matrix $[A^T]$ that converts (y,z)-components of vectors in the (Y,Z)-coordinate system to corresponding components in the (η,ζ)-coordinate system is (Ref. 3)

$$[A^T] = \begin{bmatrix} \cos\theta & \sin\theta \\ -\sin\theta & \cos\theta \end{bmatrix}. \tag{3-36}$$

Therefore, the (η,ζ)-coordinates of a point that has (Y,Z)-coordinates (y,z) are

$$\begin{bmatrix} \eta \\ \zeta \end{bmatrix} = \begin{bmatrix} \cos\theta & \sin\theta \\ -\sin\theta & \cos\theta \end{bmatrix} \begin{bmatrix} y \\ z \end{bmatrix}. \tag{3-37}$$

The position vector of point A thus becomes

$$\begin{aligned} r_{A/O} &= Y_T j + Z_T k + \eta_A(\cos\theta j + \sin\theta k) + \zeta_A(-\sin\theta j + \cos\theta k) \\ &= (Y_T + \eta_A\cos\theta - \zeta_A\sin\theta)j + (Z_T + \eta_A\sin\theta + \zeta_A\cos\theta)k. \end{aligned} \tag{3-38}$$

The only unknown in Eq. 3-38 is the angle θ. This angle can be determined once the length of the elevating strut is specified.

The position vector of the center of mass of the cradle can now be written as

$$r_{B/O} = r_{B/T} + r_{T/O}, \text{ m} \tag{3-39}$$

where

$r_{B/O}$ = position vector of center of mass of the cradle relative to O, m
$r_{B/T}$ = position vector of center of mass of the cradle with respect to trunnion, m.

Also

$$r_{B/T} = \eta_B j' + \zeta_B k', \text{ m} \tag{3-40}$$

and $r_{T/O}$ is given in Eq. 3-33. By use of the transformation matrix A in Eq. 3-37, $r_{B/O}$ can be written as

$$r_{B/O} = (Y_T + \eta_B\cos\theta - \zeta_B\sin\theta)j + (Z_T + \eta_B\sin\theta + \zeta_B\cos\theta)k, \text{ m}. \tag{3-41}$$

Refer to Fig. 3-3; the position vector for the location of the center of mass of the top carriage can be written as

$$r_{TC/O} = Y_{TC} j + Z_{TC} k, \text{ m} \tag{3-42}$$

where

Y_{TC} = Y-coordinate of top carriage relative to O, m
Z_{TC} = Z-coordinate of top carriage relative to O, m
$r_{TC/O}$ = position vector of center of mass of top carriage relative to O, m.

Similarly, for the bottom carriage and trails,

$$r_{D/O} = Y_D j + Z_D k, \text{ m} \tag{3-43}$$

where

$r_{D/O}$ = position vector of center of mass of bottom carriage and trails relative to O, m.

Under static conditions, the recoil mechanism exerts sufficient force to keep the recoiling parts pressed against stops in the cradle. This removes the translational degree of freedom of the recoiling parts relative to

THIS DOCUMENT PROVIDED BY THE ABBOTT AEROSPACE
TECHNICAL LIBRARY
ABBOTTAEROSPACE.COM

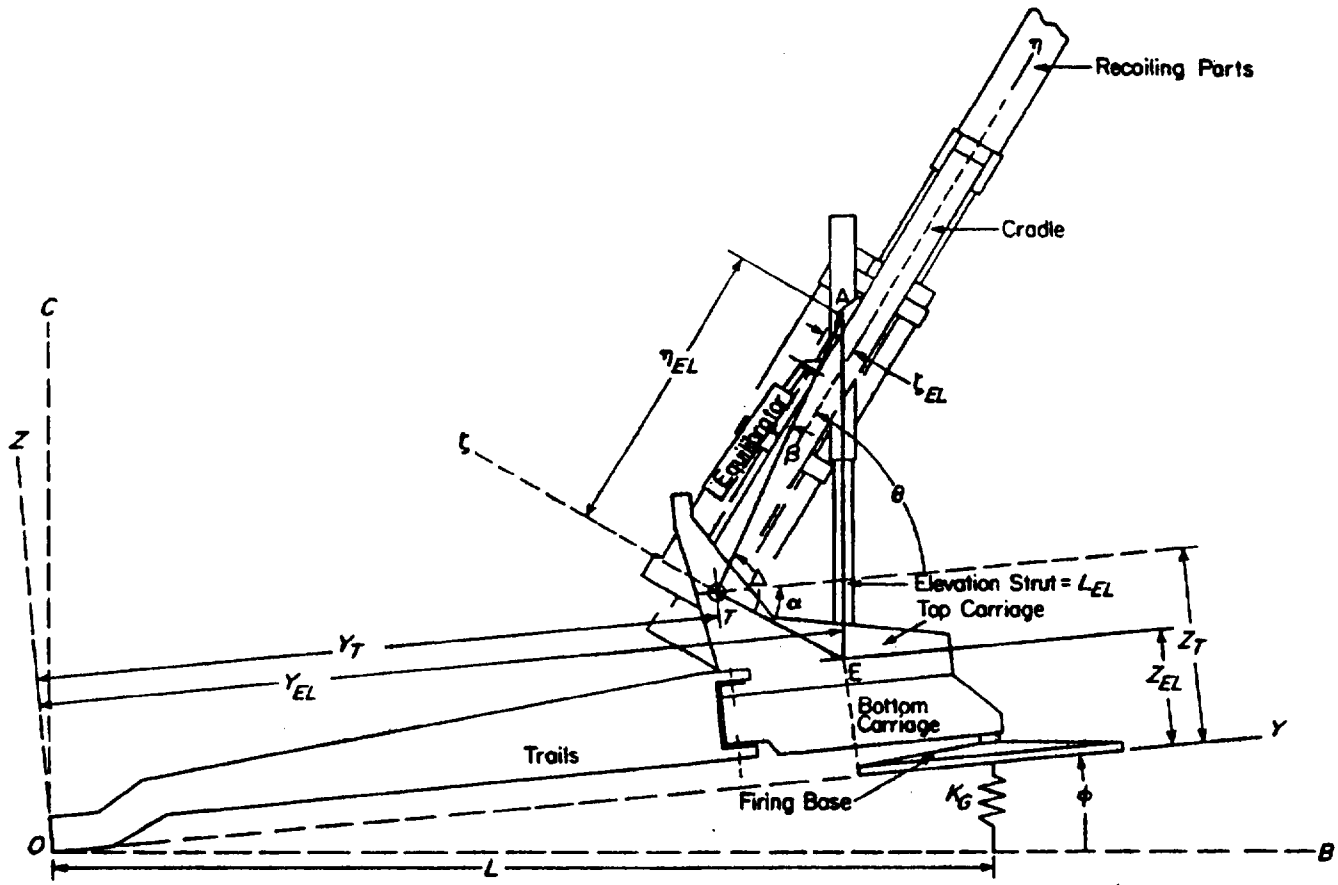

Figure 3-7. Geometry of Elevating Mechanism for M198 Howitzer

the cradle. This only holds for kinematic analysis of the weapon. The rotational degree of freedom of the tipping parts is controlled by the length of the elevating strut. Consider the triangle formed by points A, T, and E in Fig. 3-7. The cosine law (Ref. 6) can be applied to determine angle ATE = Δ, in terms of the sides of the triangle ATE, as

$$\cos\Delta = \frac{\overline{AT}^2 + \overline{TE}^2 - \overline{AE}^2}{2(\overline{AT})(\overline{TE})}$$

where

$\overline{AT}^2 = \eta_{EL}^2 + \zeta_{EL}^2$, m^2
$\overline{TE}^2 = (Z_T - Z_{EL})^2 + (Y_T - Y_{EL})^2$, m^2
$\overline{AE}^2 = L_{EL}^2$, m^2
L_{EL} = length of elevating strut, m
Δ = angle shown in Fig. 3-7, rad.

Thus

$$\Delta = \text{Cos}^{-1}\left[\frac{(\eta_{EL}^2 + \zeta_{EL}^2) + (Z_T - Z_{EL})^2 + (Y_T - Y_{EL})^2 - L_{EL}^2}{2(\eta_{EL}^2 + \zeta_{EL}^2)[(Z_T - Z_{EL})^2 + (Y_T - Y_{EL})^2]}\right], \text{rad.} \qquad (3\text{-}45)$$

Also angles α and β shown in Fig. 3-7 can be written as

$$\beta = \text{Tan}^{-1}\left(\frac{\zeta_{EL}}{\eta_{EL}}\right), \text{rad} \qquad (3\text{-}46)$$

THIS DOCUMENT PROVIDED BY THE ABBOTT AEROSPACE
TECHNICAL LIBRARY
ABBOTTAEROSPACE.COM

$$\alpha = \text{Tan}^{-1}\left(\frac{Z_T - Z_{EL}}{Y_{EL} - Y_T}\right), \text{ rad.} \tag{3-47}$$

Therefore, the angle of elevation θ can be written as

$$\theta = \Delta - \alpha - \beta, \text{ rad} \tag{3-48}$$

where angles Δ, α, β are given by Eqs. 3-45, 3-46, and 3-47, respectively. The angle of elevation can thus be controlled by changing the length of the elevating strut.

For simple models, such as the model of the M198 Howitzer considered here, it is usually possible to solve for the position of the centers of mass of each component of the system in closed form. This method is not applicable to more complex models or to positions in three dimensions. For such models, numerical techniques must be employed.

Performing kinematic analysis of a system is an essential step before a dynamic model can be developed. The procedure for kinematic analysis illustrated in this paragraph makes it relatively easy to develop a dynamic model of the system. Because expressions for the position vectors of the centers of mass of the bodies in the system have already been developed, they can be differentiated with respect to time to obtain velocities of the centers of mass. Once the velocities have been determined, the kinetic energy of each body is easy to compute. Lagrange's equations of motion can then be applied to write the equations of motion for the system. (See Appendix A.)

3-2 CONVENTIONAL METHODS OF DYNAMIC ANALYSIS OF ARTILLERY

3-2.1 1-DEGREE-OF-FREEDOM RECOIL MODEL

The elementary equation of recoil motion for a conventional artillery weapon in which no hop occurs, i.e., $\phi = 0$, is discussed first. Define that portion of an artillery weapon that translates under the action of firing as the "recoiling parts". The equation of motion that defines the translation of recoiling parts is called the "recoil equation".

In Fig. 3-8 the mass M_r of the recoiling parts translates due primarily to the forces $K(t)$ and $B(t)$, where $B(t)$ is the breech force due to the burning propellant and $K(t)$ is the recoil force. The force $K(t)$ consists of two components —i.e., (1) a dissipative force that resists motion and (2) the force of an energy-storing device that returns the gun to the firing position after recoil translation has stopped. It is tacitly assumed that the recoil force is a function of time only, whereas it is actually a function of velocity and displacement, which are, in turn, functions of time. The exact form of $K(t)$ is dependent upon the particular type of recoil mechanism and associated geometry chosen but is generally of the form

$$K(t) = H(\eta)\dot{\eta}^2 + G(\eta), \text{ N} \tag{3-49}$$

where

$K(t)$ = recoil force, N
$H(\eta)$ = function of η, N·s^2/m^2
$G(\eta)$ = function of η, N.

Consider the free-body diagram of recoiling parts shown in Fig. 3-9. Under static conditions, the equation of equilibrium may be written as

$$K(0) - E + \mu W_r \cos\theta - W_r \sin\theta = 0 \tag{3-50}$$

where

$K(0)$ = value of $K(t)$ under static conditions, N
E = interface load between recoiling parts and cradle, N
μ = coefficient of friction, dimensionless
W_r = weight of recoiling parts, N
θ = cannon angle of elevation, rad.

THIS DOCUMENT PROVIDED BY THE ABBOTT AEROSPACE
TECHNICAL LIBRARY
ABBOTTAEROSPACE.COM

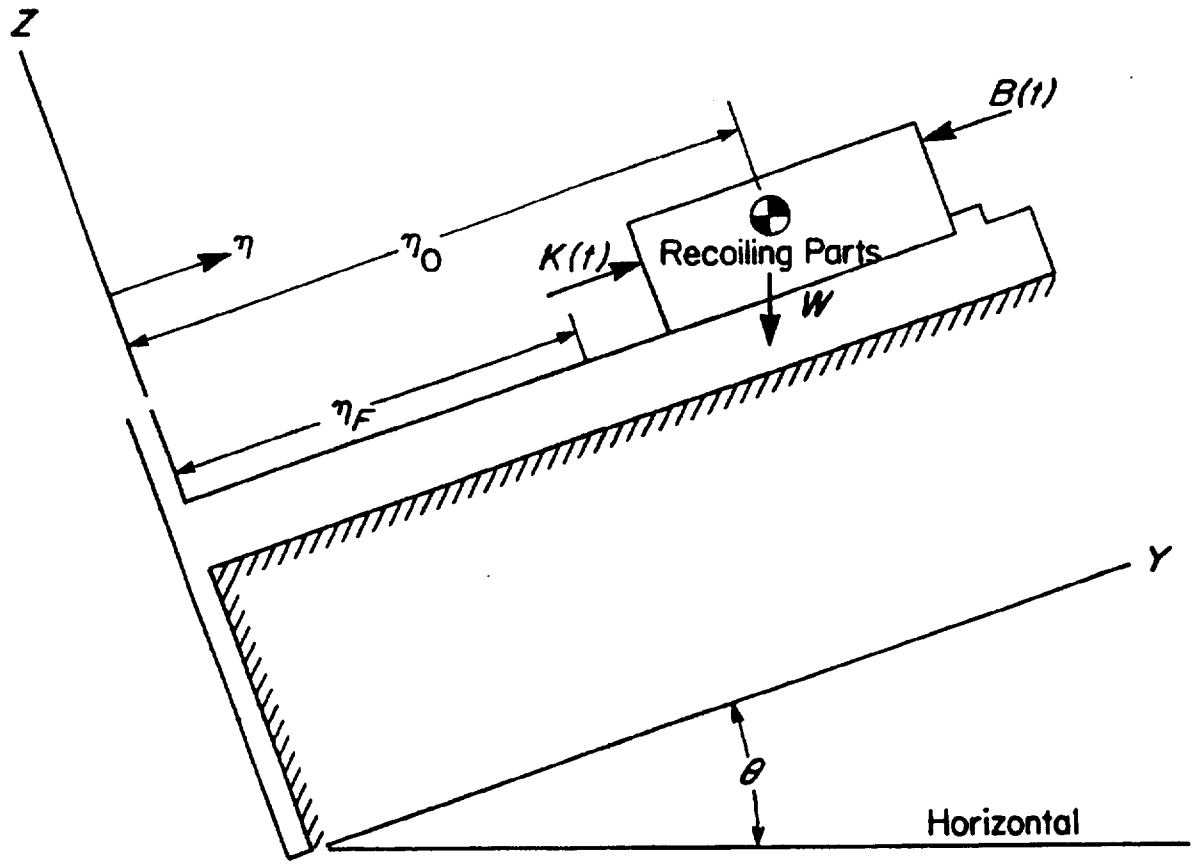

Figure 3-8. In-Battery Position of Recoiling Parts

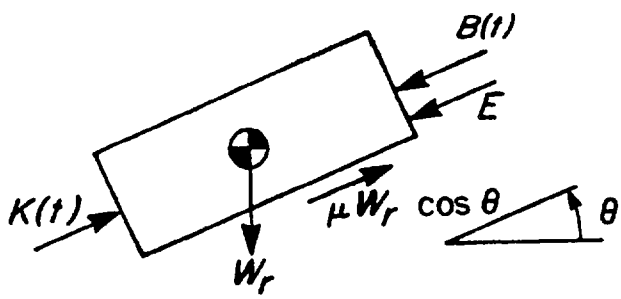

Figure 3-9. Forces on Recoiling Parts

Since $K(t)$ has a value $K(0)$ under static conditions, when the breech force $B(t)$ is initiated, there will be no motion of the recoiling parts until the interface load E, which holds the recoiling parts in battery prior to firing, disappears. The equation for this period is

$$K(0) - E + \mu W_r \cos\theta - W_r \sin\theta - B(t) = 0 \tag{3-51}$$

where

$B(t)$ = breech force, N.

Thus E goes to zero when

$$B(t) = B(t_0) = K(t_0) + \mu W_r \cos\theta - W_r \sin\theta, \text{ N} \tag{3-52}$$

where

t_0 = instant at which $E = 0$, s.

THIS DOCUMENT PROVIDED BY THE ABBOTT AEROSPACE
TECHNICAL LIBRARY
ABBOTTAEROSPACE.COM

Note that in Eq. 3-52 the recoil force is $K(t_0) = K(0)$. This is because at $t = t_0$ the velocity of the recoiling parts is zero.

The equation of motion for the recoiling parts for $t > t_0$, using Newton's equations of motion (See Appendix A.), can be written as

$$\sum_i F_{i\eta} = M_r a_\eta \tag{3-53}$$

where

$F_{i\eta}$ = η-component of ith breech force acting on recoiling parts, N
M_r = mass of recoiling parts, kg
a_η = acceleration of recoiling parts along η-axis, m/s^2.

From Fig. 3-9 the equation of motion can now be written as

$$M_r\ddot{\eta} = K(t) - B(t) - W_r\sin\theta - W_r\mu(\text{sgn }\dot{\eta})\cos\theta, \text{ N} \tag{3-54}$$

where

$$\text{sgn }\dot{\eta} = \begin{cases} +1, \text{ for } \dot{\eta} > 0 \\ 0, \text{ for } \dot{\eta} = 0 \\ -1, \text{ for } \dot{\eta} < 0. \end{cases}$$

The initial conditions are $\eta = \eta_0$ and $\dot{\eta} = 0$.

The Lagrangian approach (See Appendix A.) can also be used to arrive at the same equation of motion as Eq. 3-54. The kinetic energy T of the recoiling parts can be written as

$$T = \frac{1}{2} M_r(\dot{\eta})^2, \text{ J.} \tag{3-55}$$

The generalized forces Q_η can be written as

$$Q_\eta = K(t) - B(t) - W_r\sin\theta - W_r\mu(\text{sgn }\dot{\eta})\cos\theta, \text{ N} \tag{3-56}$$

where

Q_η = generalized force along η-axis, N.

The substitution of T and Q_η from Eqs. 3-55 and 3-56, respectively, into Eq. A-57 gives

$$M_r\ddot{\eta} = K(t) - B(t) - W_r\sin\theta - W_r\mu(\text{sgn }\dot{\eta})\cos\theta, \text{ N} \tag{3-57}$$

which is the same equation of motion as Eq. 3-54.

The preceding analysis considered the recoiling parts to be in battery when firing the weapon. Out-of-battery firing can be analyzed in a similar way. The initial position for out-of-battery firing of a soft recoil system is depicted in Fig. 3-10. (Compare it with the conventional in-battery position shown in Fig. 3-8.) The recoiling parts are held in the out-of-battery position by a latch mechanism. When the latch is released, the recoiling parts are accelerated in the positive η-direction. When the recoiling parts reach the position denoted by η_F, the weapon is fired. The resulting breech force stops the recoiling parts and accelerates them in the negative η-direction, i.e., past the η_L position. The recoil force eventually stops this motion and starts the recoiling parts moving again in the positive η-direction until they reach the latch position, where they are caught by the latch and held.

As with the conventional recoil cycle, an interface load E exists between the recoiling parts and the latch. When the latch is released, the interface load immediately disappears, and hence no criterion, such as Eq. 3-52, is needed. The equation of motion for this firing position will be the same as that for in-battery firing, i.e., with initial conditions $\eta = \eta_L$ and $\dot{\eta} = 0$. The breech force $B(t)$ is initiated when $\eta = \eta_F$ and $\dot{\eta}$ is positive. Note that a variability Δt in ignition delay will affect the position of the recoiling parts when the breech force is initiated. Thus $B(t)$ will be initiated when $\eta = \eta_F + \Delta\eta$, where $\Delta\eta$ is the change in travel associated with a Δt.

THIS DOCUMENT PROVIDED BY THE ABBOTT AEROSPACE
TECHNICAL LIBRARY
ABBOTTAEROSPACE.COM

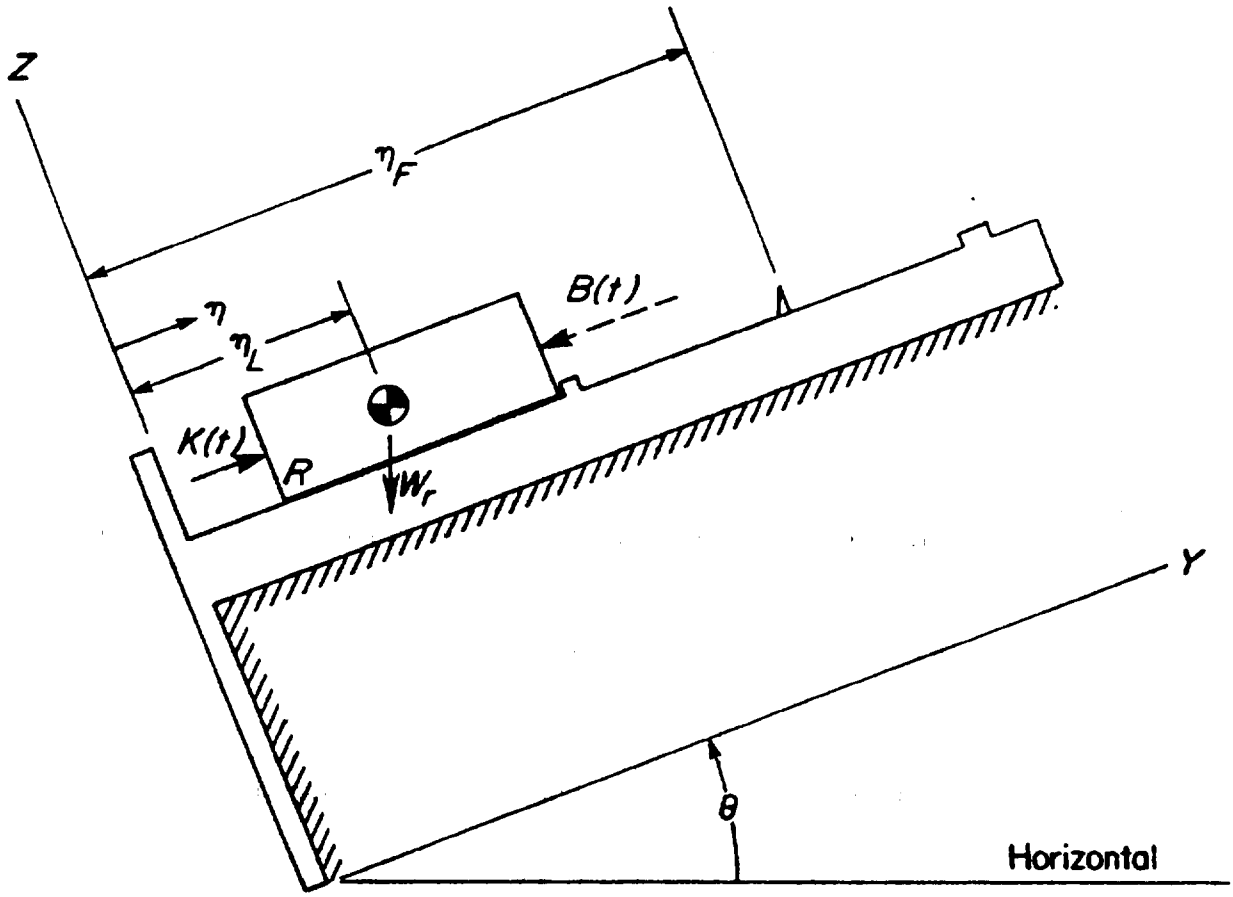

Figure 3-10. Out-of-Battery Position of Recoiling Parts

The first shot from a high-rate-of-fire weapon may be fired from the in-battery position, and all succeeding shots may be fired from some fixed travel position. Thus, in Fig. 3-8, when the weapon is fired, the breech force (Fig. 3-11) drives the recoiling parts in the negative η-direction until they are stopped by the recoil force. The recoil force then drives the recoiling parts in the positive η-direction. When the recoiling parts reach the position η_F ($\dot{\eta}$ positive), the automatic cycle starts. The breech force (Fig. 3-12) is initiated again, which stops the recoiling parts and drives them in the negative η-direction until they are stopped by the recoil force, which

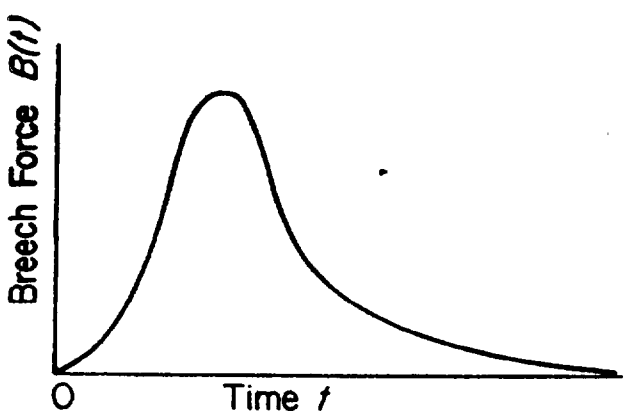

Figure 3-11. Breech Force as a Function of Time

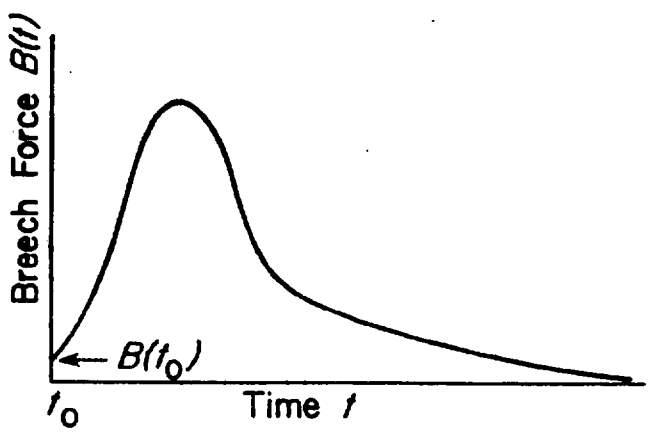

Figure 3-12. Breech Force as a Function of Time, Starting From Instant Recoiling Parts Begin to Move

THIS DOCUMENT PROVIDED BY THE ABBOTT AEROSPACE
TECHNICAL LIBRARY
ABBOTTAEROSPACE.COM

then drives the recoiling parts forward to the position η_F, where the cycle is repeated. This cycling continues until the last shot is fired, and when the last shot is fired, the breech force again stops the moving recoiling parts and reverses their direction of motion until they are stopped by the recoil force. The recoil force then drives the recoiling parts back to the in-battery position. The equation of motion is thus

$$M_r\ddot{\eta} = K(t) - B(t) - W_r\sin\theta - W_r\mu(\text{sgn}\ \dot{\eta})\cos\theta \tag{3-58}$$

where initial conditions are $\eta = \eta_0$ and $\dot{\eta} = 0$. Note that $B(t)$ is initiated when $t = t_0$ and thereafter each time at which $\eta = \eta_F$ (with $\dot{\eta}$ positive) for $(N - 1)$ times, where N is the number of rounds fired.

The 1-degree-of-freedom model developed in this paragraph has limited applicability. For example, it does not take into account the effect of weapon firing on the motion of other parts of the weapon, such as the top and bottom carriages. In this respect, the model is unable to account for secondary recoil effects or hop. Weapon models with a larger number of degrees of freedom can be developed in a manner similar to that for the single degree-of-freedom model. Either of the two approaches, Newtonian or Lagrangian, could be used to develop higher degree-of-freedom models. The Newtonian approach typically requires the free-body diagram of each body to be considered separately, and all the forces acting on the body must be known before the equation of motion can be written. The Lagrangian approach, on the other hand, requires only that the kinetic energy of the entire system and externally applied forces be known. This makes the Lagrangian approach better suited for large-scale systems because the reaction forces do not appear in the equations.

3-2.2 2-DEGREE-OF-FREEDOM RECOIL MODEL

A generalization of the single degree-of-freedom model developed in par. 3-2.1 is now considered. A pitching degree of freedom is added to the single degree-of-freedom recoil model. The weapon now consists of two masses M_r and M_B, where M_r is the mass of the recoiling parts and M_B is the remaining mass of the weapon, which does not recoil but rotates about point O, as shown in Fig. 3-13. The rotational motion of the system represents the pitching degree of freedom of the weapon.

Three coordinate systems are defined for this model. The X_HOY_H-coordinate system (global) is fixed in the ground with point O at the rear floats of the weapon. The X_ATY_A-coordinate system is fixed in mass M_B at the trunnion and rotates with the elevating parts. Also fixed in mass M_B is the X_BOY_B-coordinate system. The forward support of the weapon is represented by a spring. The external forces acting on the system are the breech force $B(t)$ and the recoil force $K(t)$.

To write the equations of motion for this system, the kinetic energy of the system must first be written. The position vector r_A for the center of mass of M_r in the global coordinate system can be written as

$$r_A = r_{A/T} + r_{T/O},\ \text{m} \tag{3-59}$$

where

r_A = position vector of center of mass of M_r in global coordinate system, m
$r_{A/T}$ = position vector of A relative to trunnion, located at T, m
$r_{T/O}$ = position vector of trunnion relative to O, m.

In vector notation,

$$r_{A/T} = \eta i_A + \xi_1 j_A,\ \text{m} \tag{3-60}$$

where

i_A = unit vector along X_A-axis, dimensionless
j_A = unit vector along Y_A-axis, dimensionless
η = distance of A along X_A-axis, m
ξ_1 = distance of A along Y_A-axis, m.

Similarly,

$$r_{T/O} = b_T i_B + c_T j_B,\ \text{m} \tag{3-61}$$

where

i_B = unit vector along X_B-axis, dimensionless

THIS DOCUMENT PROVIDED BY THE ABBOTT AEROSPACE
TECHNICAL LIBRARY
ABBOTTAEROSPACE.COM

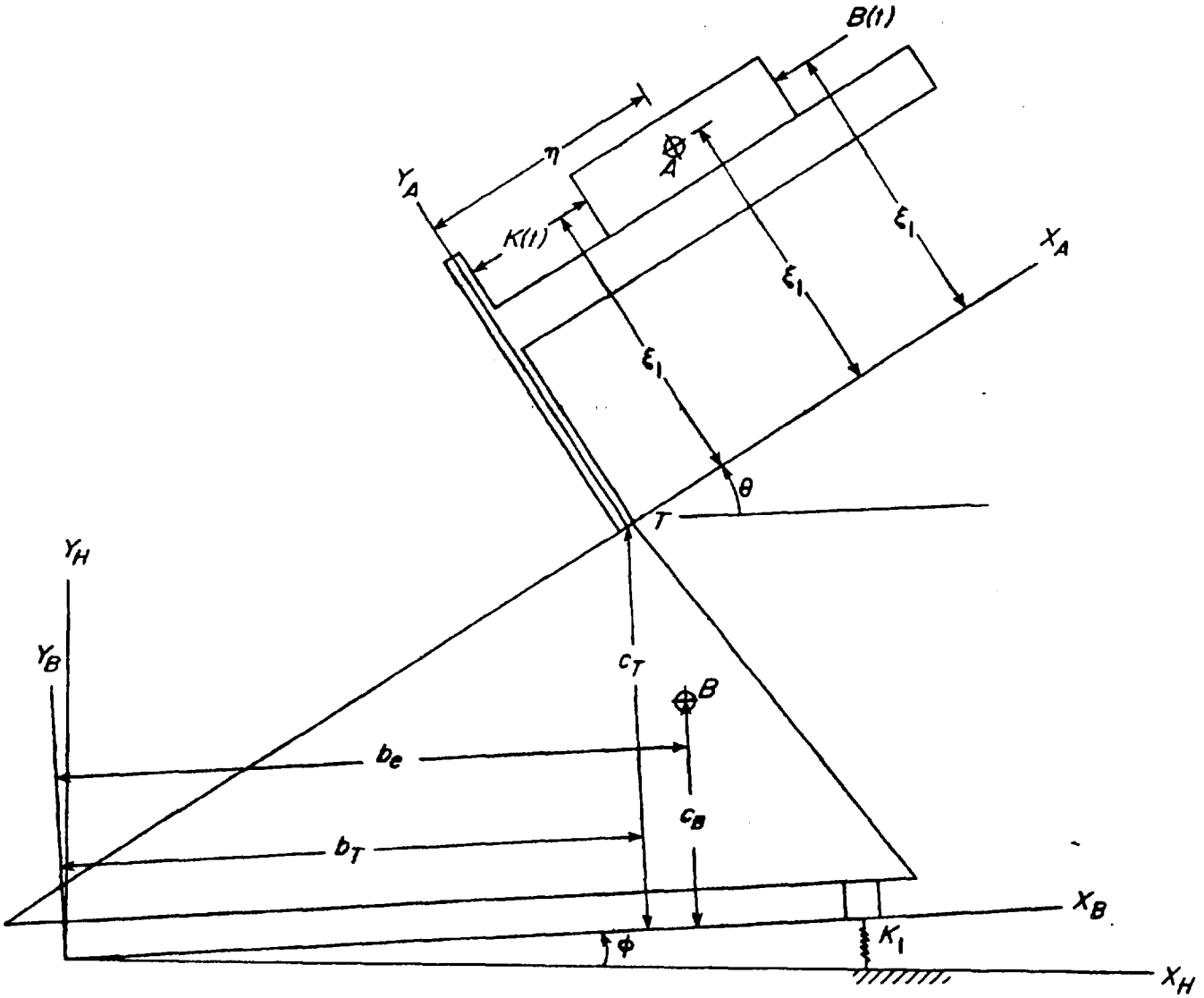

Figure 3-13. 2-Degree-of-Freedom Model

j_B = unit vector along Y_B-axis, dimensionless
b_T = distance of trunnion along X_B-axis, m
c_T = distance of trunnion along Y_B-axis, m.

Substitution of the right-hand sides of Eqs. 3-60 and 3-61 into Eq. 3-59 gives

$$r_A = \eta i_A + \xi_1 j_A + b_T i_B + c_T j_B, \text{ m.} \tag{3-62}$$

Before differentiating Eq. 3-62 to obtain the velocity of A, it is desirable to write the unit vectors—i.e., i_A, j_A, i_B, and j_B—in the rotating coordinate system in terms of those in the global reference frame. Use the transformation matrix of Eq. 3-36:

$$i_B = \cos\phi i_H + \sin\phi j_H, \text{ dimensionless} \tag{3-63}$$

$$j_B = -\sin\phi i_H + \cos\phi j_H, \text{ dimensionless} \tag{3-64}$$

where

i_H = unit vector along global X_H-axis, dimensionless

THIS DOCUMENT PROVIDED BY THE ABBOTT AEROSPACE
TECHNICAL LIBRARY
ABBOTTAEROSPACE.COM

j_H = unit vector along global Y_H-axis, dimensionless
ϕ = angle between global X_H-axis and body-fixed X_B-axis, rad (This is the pitch angle of the weapon.).

Similarly,

$$i_A = \cos(\phi + \theta) i_H + \sin(\phi + \theta) j_H, \text{ dimensionless} \tag{3-65}$$

$$j_A = -\sin(\phi + \theta) i_H + \cos(\phi + \theta) j_H, \text{ dimensionless.} \tag{3-66}$$

By substituting the expressions for i_B, j_B, i_A, and j_A from Eqs. 3-63, 3-64, 3-65, and 3-66, respectively, Eq. 3-62 becomes

$$r_A = [\eta\cos(\phi + \theta) - \xi_1\sin(\phi + \theta) + b_T\cos\phi - c_T\sin\phi] i_H + [\eta\sin(\phi + \theta) + \xi_1\cos(\phi + \theta) + b_T\sin\phi + c_T\cos\phi] j_H, \text{ m.} \tag{3-67}$$

The position vector of the center of mass M_B can be written as

$$r_B = b_B i_B + c_B j_B, \text{ m} \tag{3-68}$$

where
r_B = position vector of mass M_B, m
b_B = distance of point B along X_B-axis, m
c_B = distance of point B along Y_B-axis, m.

Eq. 3-68 can be written in terms of unit vectors in the global coordinate system as

$$r_B = (b_B\cos\phi - c_B\sin\phi) i_H + (b_B\sin\phi + c_B\cos\phi) j_H, \text{ m.} \tag{3-69}$$

Eqs. 3-67 and 3-68 can now be differentiated with respect to time to get velocities of masses M_r and M_B as—remembering that θ, ξ_1, b_B, and c_B are constants—

$$v_r = \frac{dr_A}{dt} = \left\{\dot\eta\cos(\phi + \theta) + \dot\phi[-\eta\sin(\phi + \theta) - \xi_1\cos(\phi + \theta) - b_T\sin\phi - c_T\cos\phi]\right\} i_H + \left\{\dot\eta\sin(\phi + \theta) + \dot\phi\cos(\phi + \theta) - \xi_1\sin(\phi + \theta) + b_T\cos\phi - c_T\sin\phi]\right\} j_H, \text{ m/s} \tag{3-70}$$

$$v_B = \frac{dr_B}{dt} = \dot\phi(-b_B\sin\phi - c_B\cos\phi) i_H + \dot\phi(b_B\cos\phi - c_B\sin\phi) j_H, \text{ m/s} \tag{3-71}$$

where
v_r = velocity vector of A, m/s
v_B = velocity vector of B, m/s.

Eqs. 3-70 and 3-71 can be further simplified by the observation that angle ϕ is small and stays small during motion of the weapon. The following small angle approximations can thus be applied (Ref. 1):

$$\sin\phi \approx \phi$$

THIS DOCUMENT PROVIDED BY THE ABBOTT AEROSPACE
TECHNICAL LIBRARY
ABBOTTAEROSPACE.COM

$$\cos\phi \approx 1 - \frac{1}{2}\phi^2 \text{ (from series expansion of } \cos\phi)$$

$$\sin(\theta + \phi) \approx (1 - \frac{1}{2}\phi^2)\sin\theta + \phi\cos\theta$$

$$\cos(\theta + \phi) \approx (1 - \frac{1}{2}\phi^2)\cos\theta - \phi\sin\theta$$

where θ and ϕ are expressed in radians. Eqs. 3-70 and 3-71 can thus be rewritten as

$$v_r = \Big\langle \dot{\eta}[(1 - \frac{1}{2}\phi^2)\cos\theta - \phi\sin\theta] + \dot{\phi}\{-\eta[(1 - \frac{1}{2}\phi^2)\sin\theta + \phi\cos\theta]$$

$$- \xi_1[(1 - \frac{1}{2}\phi^2)\cos\theta - \phi\sin\theta] - b_T\phi - c_T(1 - \frac{1}{2}\phi^2)\}\Big\rangle i_H$$

$$+ \Big\langle \dot{\eta}[(1 - \frac{1}{2}\phi^2)\sin\theta + \phi\cos\theta] + \dot{\phi}\{\eta[(1 - \frac{1}{2}\phi^2)\cos\theta - \phi\sin\theta]$$

$$- \xi_1[(1 - \frac{1}{2}\phi^2)\sin\theta + \phi\cos\theta] + b_T(1 - \frac{1}{2}\phi^2) - c_T\phi\}\Big\rangle j_H, \text{ m/s} \qquad (3\text{-}72)$$

$$v_B = \dot{\phi}[-b_B\phi - c_B(1 - \frac{1}{2}\phi^2)]i_A + \dot{\phi}[(b_B(1 - \frac{1}{2}\phi^2) - c_B\phi]j_H, \text{ m/s.} \qquad (3\text{-}73)$$

The kinetic energy of mass M_r can now be written as

$$T_r = \frac{1}{2}M_r(v_r \cdot v_r) + \frac{1}{2}I_r\dot{\phi}^2, \text{ J} \qquad (3\text{-}74)$$

where

T_r = kinetic energy of mass M_r, J
M_r = mass of recoiling parts, kg
I_r = polar moment of inertia of recoiling parts about center of mass, kg·m^2.

By performing the dot product indicated in Eq. 3-74 and by neglecting higher order terms greater than ϕ^2; the result is

$$T_r = \frac{1}{2}M_r\{\dot{\eta}^2 + \dot{\phi}^2[\xi_1^2 + \eta^2 + b_T^2 + 2b_T(\eta\cos\theta - \xi_1\sin\theta) + c_T^2$$

$$+ 2c_T(\eta\sin\theta + \xi_1\cos\theta)] - 2\dot{\eta}\dot{\phi}[\xi_1 - b_T\sin\theta + c_T\cos\theta]\} + \frac{1}{2}I_r\dot{\phi}^2, \text{ J.} \qquad (3\text{-}75)$$

Similarly, kinetic energy T_B for mass M_B is given as

$$T_B = \frac{1}{2}M_B(b_B^2 + c_B^2)\dot{\phi}^2 + \frac{1}{2}I_B\dot{\phi}^2, \text{ J} \qquad (3\text{-}76)$$

THIS DOCUMENT PROVIDED BY THE ABBOTT AEROSPACE
TECHNICAL LIBRARY
ABBOTTAEROSPACE.COM

where

M_B = mass of nonrecoiling parts, kg
I_B = polar moment of inertia of nonrecoiling parts about center of mass, kg·m^2.

The total kinetic energy T of the system is the sum of the kinetic energies of the two masses, i.e.,

$$T = T_r + T_B = \frac{1}{2} M_r\{\dot{\eta}^2 + \dot{\phi}^2[\xi_1^2 + \eta^2 + b_T^2 + b_T(\eta\cos\theta - \xi_1\sin\theta) + c_T^2 + c_T(\eta\sin\theta + \xi_1\cos\theta)] - 2\dot{\eta}\dot{\phi}(\xi_1 - b_T\sin\theta + c_T\cos\theta)\} + \frac{1}{2} M_B(b_B^2 + c_B^2)\dot{\phi}^2 + \frac{1}{2}(I_r + I_B)\dot{\phi}^2, \text{ J.} \quad (3\text{-}77)$$

Computation of potential energy can be done as explained in Appendix A. The potential energy of conservative forces acting on the system is the sum of potential energy of mass systems M_r and M_B and train energy in the spring. The heights of the masses M_r and M_B above the reference plane are simply the j_H-components of r_A and r_B, respectively, from Eqs. 3-67 and 3-69. Thus

$$V = V_A + V_B + V_{spring}$$

or

$$V = M_r g[\eta\sin(\phi + \theta) + \xi_1\cos(\phi + \theta) + b_T\sin\phi + c_T\cos\phi] + M_B g(b_B\sin\phi + c_B\cos\phi) + \frac{1}{2} K_1[(\phi + \phi_{st})]^2, \text{ J} \quad (3\text{-}78)$$

where

V = potential energy of system, J
K_1 = spring constant of spring at front support, N·m/rad
g = acceleration due to gravity, m/s^2
ϕ_{st} = angle ϕ under static conditions, rad.

The generalized force determination for $K(t)$ and $B(t)$ follows from the procedure explained in Appendix A. The virtual work δW of $K(t)$ and $B(t)$ is

$$\delta W = K(t)\delta\eta - \delta r_A \cdot [B(t)i_A], \text{ J.}$$

Taking the total differential of Eq. 3-67, with η and ϕ as variables, gives

$$\delta r_A = \{[\cos(\phi + \theta)]\delta\eta + [-\eta\sin(\phi + \theta) - \xi_1\cos(\phi + \theta) - b_T\sin\phi - c_T\cos\phi]\delta\phi\}i_H + \{[\sin(\phi + \theta)\delta\eta] + [\eta\cos(\phi + \theta) - \xi_1\sin(\phi + \theta) + b_T\cos\phi - c_T\sin\phi]\delta\phi\}j_H, \text{ m.}$$

THIS DOCUMENT PROVIDED BY THE ABBOTT AEROSPACE
TECHNICAL LIBRARY
ABBOTTAEROSPACE.COM

By use of this result and Eq. 3-65, the virtual work δW is

$$\delta W = [K(t) - B(t)]\delta\eta$$

$$+ B(t)[\xi_1 + b_T\sin\phi\cos(\phi + \theta) + c_T\sin\phi\sin(\phi + \theta)]\delta\phi$$

$$+ c_T\cos\phi\cos(\phi + \theta) - b_T\cos\phi\sin(\phi + \theta)$$

$$= [K(t) - B(t)]\delta\eta + B(t)[\xi_1 - b_T\sin\theta + c_T\cos\theta]\delta\phi, \text{ J.}$$

Thus

$$Q_\phi = B(t)(\xi_1 + c_T\cos\theta - b_T\sin\theta), \text{ N·m} \tag{3-79}$$

$$Q_\eta = K(t) - B(t), \text{ N} \tag{3-80}$$

where

Q_ϕ = generalized force corresponding to generalized coordinate ϕ, N·m
Q_η = generalized force corresponding to generalized coordinate η, N
$B(t)$ = breech force, N
$K(t)$ = recoil force, N.

The equations of motion for this 2-degree-of-freedom system can now be written. As previously stated, the two degrees of freedom are the distance η and the pitching angle ϕ. The Lagrange equations of motion (Appendix A) for this system, with Lagrangian $L = T - V$, are

$$\frac{d}{dt}\left(\frac{\partial L}{\partial \dot\eta}\right) - \frac{\partial L}{\partial \eta} = Q_\eta \tag{3-81}$$

$$\frac{d}{dt}\left(\frac{\partial L}{\partial \dot\phi}\right) - \frac{\partial L}{\partial \phi} = Q_\phi. \tag{3-82}$$

By using Eqs. 3-77 and 3-78 for T and V, respectively, and Eqs. 3-79 and 3-80 for Q_ϕ and Q_η, respectively, Eqs. 3-81 and 3-82 yield

$$M_r\ddot\eta - M_r[\xi_1 - b_T\sin\theta + c_T\cos\theta]\ddot\phi - \frac{1}{2}M_r[2\eta\dot\phi^2 + b_T\dot\phi^2\cos\theta +$$

$$c_T\dot\phi^2\sin\theta + M_r g\sin(\phi + \theta)] = K(t) - B(t), \text{ N.} \tag{3-83}$$

$$\{M_r[\xi_1^2 + \eta^2 + b_T^2 + b_T(\eta\cos\theta - \xi_1\sin\theta) + c_T^2 + c_T(\eta\sin\theta + \xi_1\cos\theta)] + M_B(b_B^2 + c_B^2)$$

$$+ I_r + I_B\}\ddot\phi + M_r[2\eta + b_T\cos\theta + c_T\sin\theta]\dot\phi\dot\eta - M_r(\xi_1 - b_T\sin\theta + c_T\cos\theta)\ddot\eta$$

$$+ M_r g[\eta\cos(\phi + \theta) - \xi_1\sin(\phi + \theta) + b_T\cos\phi - c_T\sin\phi] + M_B g(b_B\cos\phi - c_B\sin\phi)$$

$$+ K_1(\phi + \phi_{s1}) = B(t)(\xi_1 + c_T\cos\theta - b_T\sin\theta), \text{ J.} \tag{3-84}$$

THIS DOCUMENT PROVIDED BY THE ABBOTT AEROSPACE
TECHNICAL LIBRARY
ABBOTTAEROSPACE.COM

Since ϕ and $\dot{\phi}$ are expected to be small, terms of higher order in these variables may be neglected and the small angle approximations $\sin\phi \approx \phi$ and $\cos\phi \approx 1$ may be used to simplify Eqs. 3-83 and 3-84 to yield

$$M_r\ddot{\eta} - M_r(\xi_1 - b_T\sin\theta + c_T\cos\theta)\ddot{\phi} = K(t) - B(t) - M_r g(\phi\cos\theta + \sin\theta), \text{ N} \tag{3-85}$$

$$\{M_r[\xi_1^2 + \eta^2 + b_T^2 + b_T(\eta\cos\theta - \xi_1\sin\theta) + c_T^2 + c_T(\eta\sin\theta + \xi_1\cos\theta)]$$

$$+ M_B(b_B^2 + c_B^2) + I_r + I_B\}\ddot{\phi} + M_r(2\eta + b_T\cos\theta + c_T\sin\theta)\dot{\phi}\dot{\eta}$$

$$- M_r(\xi_1 - b_T\sin\theta + c_T\cos\theta)\ddot{\eta} = B(t)(\xi_1 + c_T\cos\theta - b_T\sin\theta)$$

$$- K_1(\phi + \phi_{st}) - M_r g(\eta\cos\theta - \eta\phi\sin\theta - \xi_1\phi\cos\theta - \xi_1\sin\theta$$

$$+ b_T - c_T\phi) - M_B g(b_B - c_B\phi), \text{ J.} \tag{3-86}$$

Eqs. 3-85 and 3-86 give two Lagrangian equations of motion for the 2-degree-of-freedom model considered here. It should be pointed out that Eqs. 3-85 and 3-86 are applicable only for time $t > t_0$, where t_0 can be computed from Eq. 3-52. As noted earlier, there is no motion of the system for $t \leq t_0$.

Solution of Eqs. 3-85 and 3-86 (or Eqs. 3-83 and 3-84 if ϕ or $\dot{\phi}$ is large) can be obtained by using techniques of numerical integration of differential equations. Par. 3-3 outlines these techniques.

The solution of Lagrange's equations of motion only gives values of the generalized coordinates. To analyze reactions, for example, between mass M_B and ground, requires the use of Newton's laws. Analysis of ground reaction is important in the study of the stability of the weapon.

Because the front support of the weapon is being modeled as a torsional spring, the reaction moment about point O can be obtained as

$$m_H = K_1(\phi + \phi_{st}), \text{ N·m} \tag{3-87}$$

where

m_H = moment about O, N·m.

For the weapon to be stable, it is necessary that

$$m_H \leq 0. \tag{3-88}$$

If Eq. 3-88 is not satisfied at any instant during the recoil or counterrecoil cycles, the weapon will exhibit hop.

The front support of the weapon could have been modeled as a linear spring. In this case, however, weapon stability is assured by making certain that the force in this spring is always compressive.

3-2.3 DYNAMIC MODELS OF INTERMEDIATE LEVEL OF COMPLEXITY

Models with one and two degrees of freedom have been developed in the previous paragraphs. These models are of great value in design, but because they ignore rotation of the cradle about the trunnion, they cannot be used to account for elevation pitch due to this rotation. Although of little importance in design for weapon stability, this pitch motion can influence accuracy.

Fig. 3-14 shows a schematic of a 3-degree-of-freedom artillery model, which includes the pitch angle ϕ_2 of rotation of the cradle relative to the top carriage. The generalized coordinates for such a model are pitch angle ϕ_1 of top carriage relative to ground, pitch angle ϕ_2 of cradle relative to top carriage, and translation η of recoiling parts relative to cradle. Definition of this model is elementary, but the calculations involved in deriving the equations of motion (using Lagrange's equations) are extremely complicated. The reader is referred to Ref. 7 for details of such a derivation for the 3-degree-of-freedom model and for higher degree-of-freedom models. Once derived, these equations can be programmed and solved on a digital computer to predict pitch motion of the system to include accuracy loss due to oscillation of the cradle relative to the top carriage.

THIS DOCUMENT PROVIDED BY THE ABBOTT AEROSPACE
TECHNICAL LIBRARY
ABBOTTAEROSPACE.COM

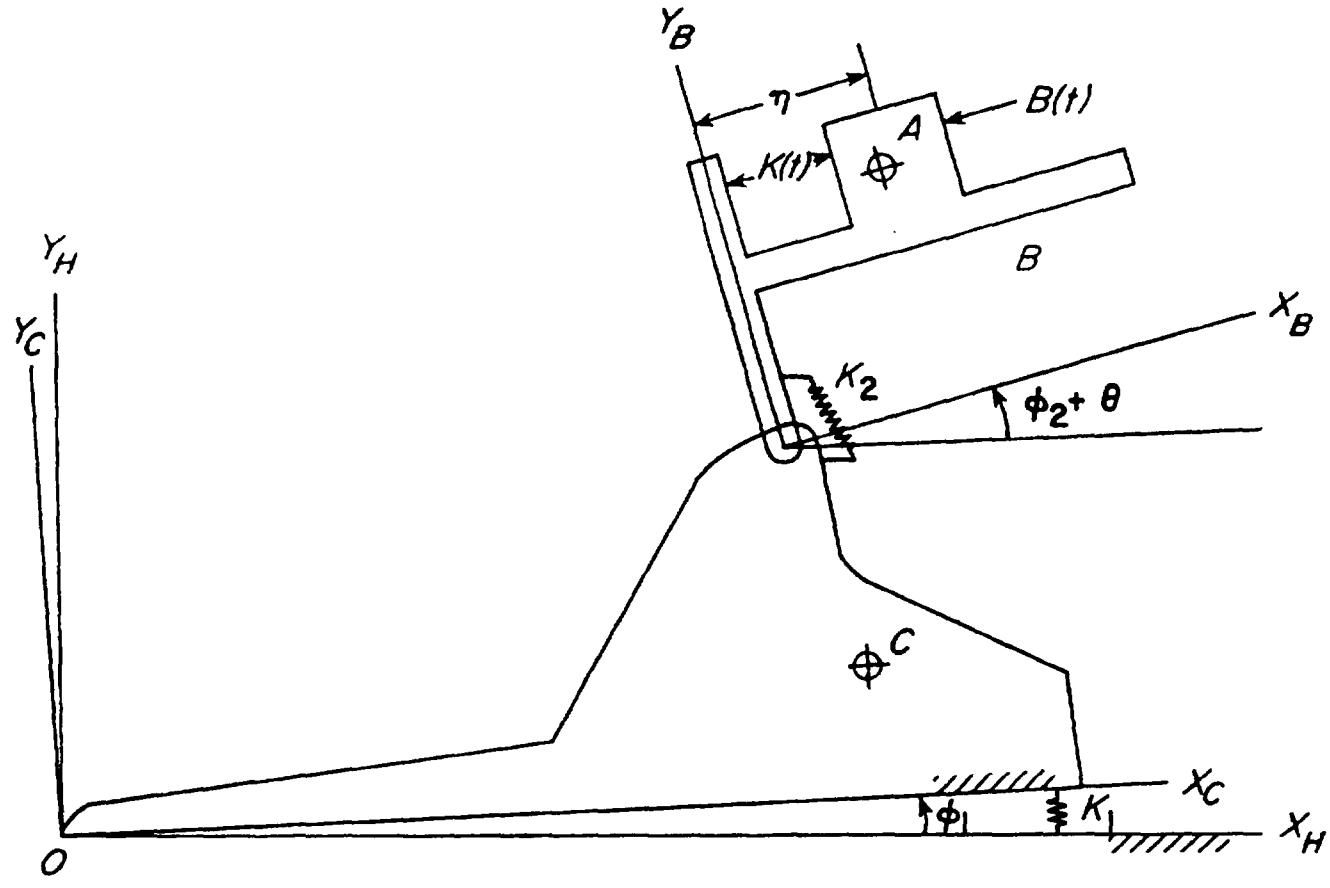

Figure 3-14. 3-Degree-of-Freedom Artillery Model

Modern mobility requirements have led to the design and development of new generations of lightweight towed artillery, such as the M198 towed Howitzer, with a high impulse cannon that leads to an extreme dynamic response. It is no longer acceptable to perform only pitch plane dynamic analysis because fully three-dimensional dynamic response can be important in performance of lightweight towed systems. Extension of manual methods of deriving equations of motion for complex three-dimensional dynamics is virtually hopeless. Therefore, attention has turned in recent years to automated methods for computer formulation and solution of the equations of motion of mechanical systems by use of commercial quality computer programs, such as those outlined in par. 3-4.2. Such established computer analysis tools permit the engineer to concentrate on accounting for important effects, rather than on tedious and error-prone manual derivation of equations and construction of *ad hoc* numerical integration computer programs. Use of such tools in modern design is strongly encouraged.

3-2.4 FORCE ANALYSIS

Solution of equations of motion only gives the time histories of generalized coordinates. Computation of reaction forces and forces at interfaces between bodies must be done separately. This requirement contrasts the Newtonian approach in which the solution for reaction forces is obtained along with that for other variables.

The dynamic reaction forces in a system can be solved by using d'Alembert's principle (Ref. 1). This method is also known as the kinetostatic approach. In this approach the analyst first draws a free-body diagram of each body in the system. Since the acceleration of each body has already been solved for, d'Alembert's equations of equilibrium for the body can be written in terms of unknown reaction forces. For a body in the plane, the reaction forces

$$\sum_{i}^{nf} F_{x_i} - M\ddot{x} = 0 \tag{3-89}$$

THIS DOCUMENT PROVIDED BY THE ABBOTT AEROSPACE
TECHNICAL LIBRARY
ABBOTTAEROSPACE.COM

$$\sum_{i}^{nf} F_{y_i} - M\ddot{y} = 0 \tag{3-90}$$

$$\sum_{j}^{k} T_j - I\ddot{\phi} = 0 \tag{3-91}$$

where

F_{x_i} = x-component of ith dynamic force on body, N
F_{y_i} = y-component of ith dynamic force on body, N
$\ddot{x}$ = acceleration of body along x-direction, m/s^2
$\ddot{y}$ = acceleration of body along y-direction, m/s^2
n_f = total number of forces acting on body, dimensionless
T_j = jth dynamic moment on body, N·m
k = total number of moments on body, dimensionless
I = polar moment of inertia of body, g·m^2
$\ddot{\phi}$ = angular acceleration of body, rad/s^2.

It should be noted that only reactions due to dynamic forces are being considered here. Reactions due to static forces, such as weight, can be determined by the analysis given in par. 3-1.2.

Consider the example of determining forces between recoiling parts and the cradle. Fig. 3-15 shows the free-body diagram of the recoiling parts. The externally applied forces are the breech and recoil forces. The interfacial forces are the normal reaction and frictional forces. Note that while computing the reaction forces,

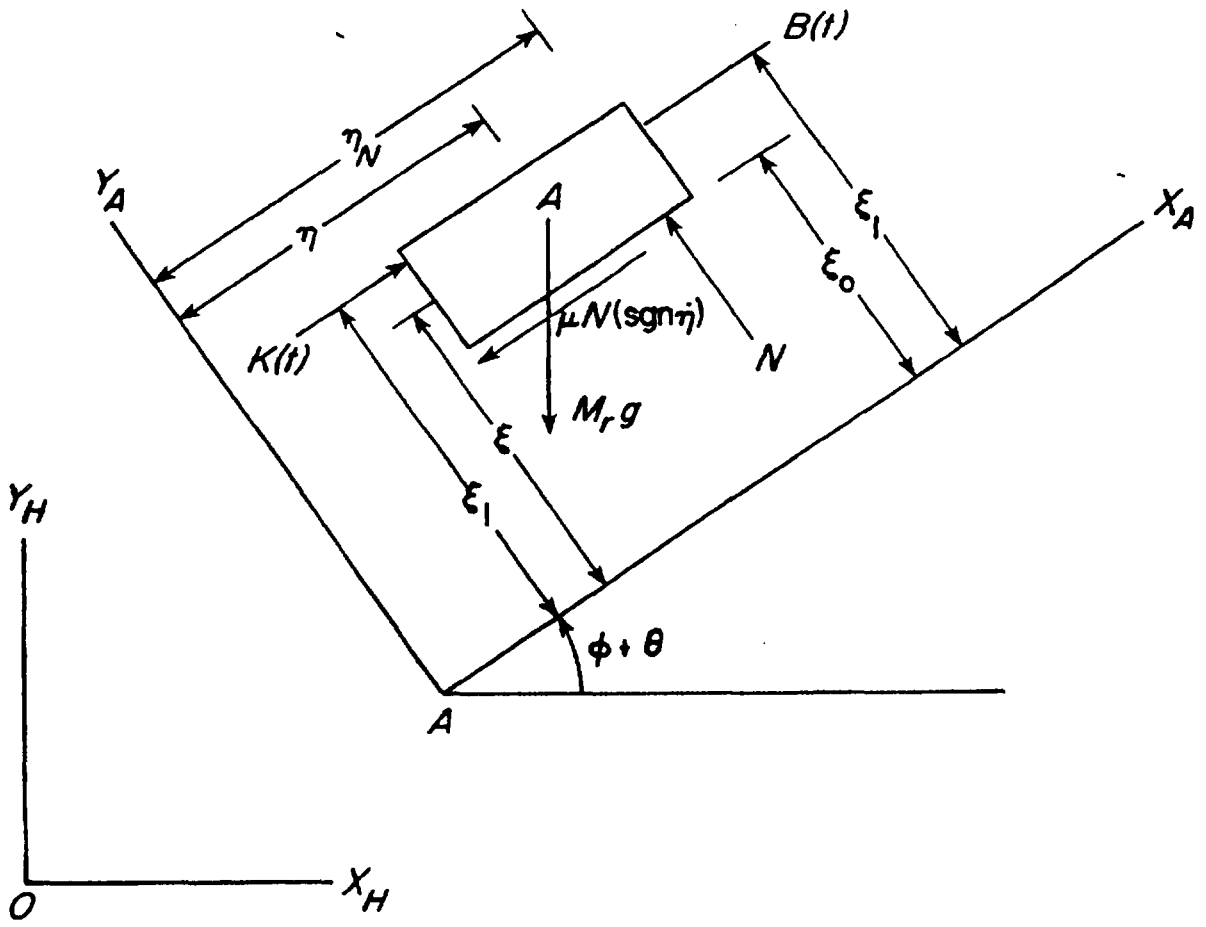

Figure 3-15. Free-Body Diagram of Recoiling Parts

THIS DOCUMENT PROVIDED BY THE ABBOTT AEROSPACE
TECHNICAL LIBRARY
ABBOTTAEROSPACE.COM

the frictional forces are being included. This is valid only if these forces were also considered in the equations of motion of the system. Write d'Alembert's equations of equilibrium for the recoiling parts, i.e., from Eqs. 3-89 through 3-91,

$$-B(t)\cos(\phi+\theta)+K(t)\cos(\phi+\theta)-N\sin(\phi+\theta)$$

$$-\mu N(\operatorname{sgn}\dot{\eta})\cos(\phi+\theta)-M_r\ddot{x}_A=0 \tag{3-92}$$

$$-B(t)\sin(\phi+\theta)+K(t)\sin(\phi+\theta)-N\cos(\phi+\theta)$$

$$-\mu N(\operatorname{sgn}\dot{\eta})\sin(\phi+\theta)-M_r\ddot{y}_A=0 \tag{3-93}$$

$$(\xi_1-\xi)B(t)-(\xi_1-\xi)K(t)-\mu N(\operatorname{sgn}\dot{\eta})(\xi-\xi_0)$$

$$+(\eta_N-\eta)N-I_r\ddot{\phi}=0 \tag{3-94}$$

where

μ = coefficient of friction between recoiling parts and cradle, dimensionless
N = normal reaction of cradle on recoiling parts, N

$$\operatorname{sgn}\dot{\eta}=\begin{cases}-1, \text{ for } \dot{\eta}<0\\ 0, \text{ for } \dot{\eta}=0\\ +1, \text{ for } \dot{\eta}>0\end{cases}$$

M_r = mass of recoiling parts, kg
$\ddot{x}_A$ = acceleration of recoiling parts in global X-direction, m/s^2
$\ddot{y}_A$ = acceleration of recoiling parts in global Y-direction, m/s^2
ξ_1 = distance along Y_A-axis of point of application of $B(t)$, m
ξ_0 = distance along Y_A-axis of contact surface between recoiling parts and cradle, m
η_N = distance along X_A-axis of point of application of normal reaction N, m
$\ddot{\phi}_A$ = angular acceleration of recoiling parts, rad/s^2.

From Eqs. 3-92 to 3-94 it can be seen that there are two unknowns—N and η_N. Eqs. 3-92 and 3-93 have only one unknown N. Hence either equation could be used to determine this quantity. Therefore, from Eq. 3-92

$$N=\frac{M_r\ddot{x}_A+\cos(\phi+\theta)[B(t)-K(t)]}{-\mu(\operatorname{sgn}\dot{\eta})\cos(\phi+\theta)-\sin(\phi+\theta)}, \text{ N.} \tag{3-95}$$

From Eq. 3-94

$$\eta_N=\frac{1}{N}\{I_r\ddot{\phi}+(\xi_1-\xi)[K(t)-B(t)]\}+\mu(\operatorname{sgn}\dot{\eta})(\xi-\xi_0)+\eta, \text{ m.} \tag{3-96}$$

To find the reaction forces acting on the cradle, consider a free-body diagram of the cradle, as in Fig. 3-16. The externally applied forces on this body are the normal and frictional force due to the recoiling parts and the recoil force. The reactions on this body are the two components of trunnion reactions and a moment at the trunnion. The equations of equilibrium for this body can be written as, using Eqs. 3-89 through 3-91,

$$-K(t)\cos(\phi+\theta)-N\sin(\phi+\theta)+\mu N(\operatorname{sgn}\dot{\eta})\cos(\phi+\theta)+T_H-M_B\ddot{x}_B=0 \tag{3-97}$$

$$-K(t)\sin(\phi+\theta)-N\cos(\phi+\theta)+\mu N(\operatorname{sgn}\dot{\eta})\sin(\phi+\theta)+T_V-M_B\ddot{y}_B=0 \tag{3-98}$$

THIS DOCUMENT PROVIDED BY THE ABBOTT AEROSPACE
TECHNICAL LIBRARY
ABBOTTAEROSPACE.COM

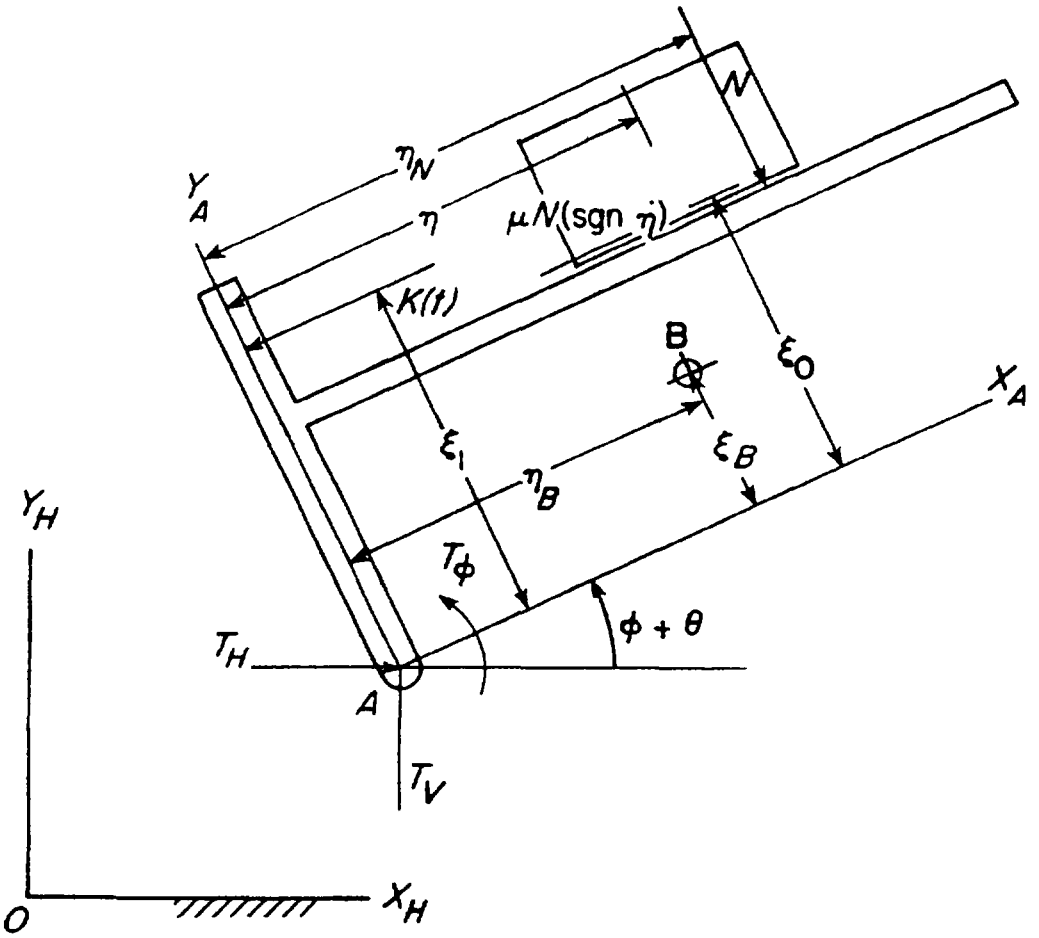

Figure 3-16. Free-Body Diagram of Cradle and Recoiling Parts

$$K(t)\xi_1 - N\eta_N - \mu N(\text{sgn } \ddot{\eta})\xi_0 + T_\phi - I_B\ddot{\phi} = 0 \tag{3-99}$$

where

$K(t)$ = recoil force, N
T_H = horizontal reaction at trunnion, N
T_V = vertical reaction at trunnion, N
T_ϕ = reaction moment at trunnion, N·m.

The reactions can be determined from Eqs. 3-97 to 3-99, as

$$T_H = K(t)\cos(\phi + \theta) + N[\sin(\phi + \theta) - \mu(\text{sgn } \dot{\eta})\cos(\phi + \theta)] + M_B\ddot{x}_B, \text{ N} \tag{3-100}$$

$$T_V = K(t)\sin(\phi + \theta) + N[\cos(\phi + \theta) - \mu(\text{sgn } \dot{\eta})\sin(\phi + \theta)] + M_B\ddot{y}_B, \text{ N} \tag{3-101}$$

$$T_\phi = -K(t)\xi_1 + N[\eta_N + \mu(\text{sgn } \dot{\eta})\xi_0] + I_B\ddot{\phi}, \text{ N·m.} \tag{3-102}$$

As noted earlier, reactions given by Eqs. 3-95, 3-100, 3-101, and 3-102 are due to dynamic effects only. To arrive at the total reactions, the static and dynamic reactions must be added.

The process of computing reaction forces as described requires that each body be considered separately. This procedure, though not involved, does not lend itself to adaptation in a general-purpose computer code for

THIS DOCUMENT PROVIDED BY THE ABBOTT AEROSPACE
TECHNICAL LIBRARY
ABBOTTAEROSPACE.COM

numerical integration of Lagrange's equations. As will be explained in par. 3-4.2, an alternative method of writing Lagrange's equations makes it possible to compute reaction as a part of the numerical integration procedure.

3-2.5 ANALYSIS AND CONTROL OF WEAPON STABILITY

A lightweight artillery weapon or a weapon fired while resting on its tires is subject to a large pitching motion that requires unacceptably large azimuth correction by the crew. Unlike a hard mount (weapon rests on a baseplate), the flexible mount can withstand substantial pitch motion.

During the recoil stroke, when the weapon is fired at a high angle of elevation, tires under a large load will compress, and when counterrecoil begins, the tires act like springs and unload, which sends the tires off the ground. At low-elevation firing, instability is the result of the recoiling force lifting the weapon upward in rotation about the pivot point of the trail spades. In either case, when the weapon comes to rest, the likelihood of its being zeroed in for the next round has been reduced considerably.

With respect to hop weapon stability can be characterized in terms of the reaction force between the weapon base and ground. For heavy weapons resting on hard mounts, it is possible to eliminate weapon hop completely. However, for weapons firing from flexible mounts, it is not possible to eliminate weapon hop completely; therefore, these weapons must be designed to minimize hop.

By use of the models developed in pars. 3-2.2 and 3-2.3, it is possible to draw some conclusions about weapon stability. The interface between the weapon base and ground in each of these models is characterized by a pivot at the rear of the trails, with a spring acting around the end of the spade.

Modeling of the front support by a torsional spring is equivalent to having a linear spring acting at the front support. The reaction between the front support and ground thus generates a moment in the torsional spring. The stability analysis performed for the 2-degree-of-freedom model in par. 3-2.2 is also valid for higher degree-of-freedom models.

The moment about the rear pivot is an explicit function of one generalized coordinate only. From the equations of motion developed for the weapon, however, it is evident that weapon hop also depends on geometric variables defining the weapon design. Therefore, the stability characteristics of the weapon can be altered by modifying the design of the weapon. Some of the geometric variables affecting stability are trail length, support location, and location of centers of gravity. Characteristics of the recoil mechanism, such as shape of the recoil force curve and recoil travel, also influence weapon stability.

Modern techniques of computer-aided design have been used successfully to improve weapon stability characteristics. A parametric study of weapon hop by using an analog computer is described in Ref. 8. The parameters that were varied for this study were recoil force curve shape, weapon spring rate, trail length, and recoil travel. (The weapon spring rate in this study was related to the stiffness of tires.) The conclusion reached was that by varying these parameters it is possible to reduce weapon hop considerably.

An optimization approach to weapon stability is described in Refs. 9 and 10. The problem is set up as one of minimizing weapon hop subject to constraints on velocities of recoil and counterrecoil. The design variables are recoil force variation with time and recoil length. A design sensitivity analysis, i.e., sensitivity of cost and constraint functions to changes in design, is developed using the state space optimal design (Ref. 11) approach. The optimization problem is solved using the steepest descent method (Ref. 10).

3-2.6 TESTING FOR MODEL REFINEMENT AND VALIDATION

The equations of motion are a set of differential equations based on the laws of mechanics and the geometry of the physical system. The use of a computer is usually necessary to solve this set of equations, especially if the system under study is complex and a sufficient amount of detail is required to characterize it. If the use of a computer becomes necessary, mathematical expressions, physical constraints, and logic must be transformed into a computer program. The equations and their solution techniques comprise a mathematical or computer model. If such a model is to be of value, it must be amenable to analysis and its output must represent the behavior of the physical system with sufficient accuracy so that useful information can be obtained concerning the actual system.

Real world conditions cannot be modeled exactly; therefore, inherent inaccuracies will exist in the model because the modeler must resort to simplifications and abstractions of the actual, physical system. The important point is that an acceptable level of confidence must be established so that inferences drawn from the output of the model are correct and the model generates the same behavior characteristics as the actual system. Confidence in the output of the model is gained through model validation, which is a check on the agreement

THIS DOCUMENT PROVIDED BY THE ABBOTT AEROSPACE
TECHNICAL LIBRARY
ABBOTTAEROSPACE.COM

between the behavior of the model and that of the actual system. Correctness of the model can only be measured relative to the physical system; however, models may be validated according to various criteria.

To compare the simulated response of the model with field test data, it is necessary to define what data are to be collected from field tests. It is generally the designer's responsibility to specify what data he would like to have measured in field tests. The output from a computer model is generally a time history of the generalized coordinates. It may not always be possible to measure all of these quantities in a field test; however, enough data should be collected from field tests to permit drawing of conclusions about the validity of the computer model. Accordingly, the designer should interact with testing and instrumentation specialists to assure that the measurements he wants can practicably be made.

Model validation requires kinematic data such as position, velocity, and acceleration. Position and velocity data may be measured by displacement and velocity transducers, respectively. Because these data must be collected during firing of the weapon, some electronic device is required to record these data. A commonly used recorder is the strip chart recorder in which the signal from the transducer is plotted against time on a continuous chart.

Acceleration measurements can be taken by an accelerometer and also be plotted on a strip chart. Force measurements can be obtained from a load cell. There is no universally used technique for stress measurement. Stress, however, can be determined by strain measurements. Strain is usually measured by strain gages, and because strain is a multidimensional quantity, several strain gages are required to determine the state of strain at a point.

3-3 NUMERICAL INTEGRATION OF EQUATIONS OF MOTION

Par. 3-2 presented techniques for deriving the equations of motion of artillery systems. Closed form solutions of these equations are impossible to obtain, so numerical techniques must be employed to obtain solutions. Virtually all numerical integration techniques in the literature have been developed for integrating systems of first-order differential equations. Equations of motion for mechanical systems, on the other hand, are systems of second-order differential equations. To reduce these second-order differential equations to a standard first-order form for numerical integration requires that additional variables be defined. The procedure is illustrated for a single second-order differential equation

$$\ddot{y} = f(t,y,\dot{y}) \tag{3-103}$$

with initial conditions

$$y(0) = Y_0 \tag{3-104}$$

$$\dot{y}(0) = \dot{Y}_0 \tag{3-105}$$

where

$\ddot{y}$ = acceleration in y-direction, m/s^2
$f(t,y,\dot{y})$ = function of time, displacement, and velocity, respectively, m/s^2
t = time, s
y = displacement, m
$\dot{y}$ = first time derivative of $y(t)$, m/s
y_0 = initial value of $y(t)$, m
$\dot{y}_0$ = initial value of $\dot{y}(t)$, m/s.

Define functions $y_1(t)$ and $y_2(t)$ as

$$y_1(t) \equiv y(t) \tag{3-106}$$

$$y_2(t) \equiv \dot{y}(t) \tag{3-107}$$

where

y_1 = displacement, m
y_2 = velocity, m/s.

THIS DOCUMENT PROVIDED BY THE ABBOTT AEROSPACE
TECHNICAL LIBRARY
ABBOTTAEROSPACE.COM

Differentiate both sides of Eq. 3-107 with respect to time to give

$$\dot{y}_2(t) = \ddot{y}(t). \tag{3-108}$$

By comparing Eq. 3-103 and 3-108, the following equation can be written

$$\dot{y}_2 = f(t,y_1,y_2). \tag{3-109}$$

Differentiate both sides of Eq. 3-106 with respect to time, and compare it with Eq. 3-107 to give

$$\dot{y}_1(t) = y_2(t). \tag{3-110}$$

The initial conditions of Eqs. 3-104 and 3-105 can now be written as

$$y_1(0) = Y_0 \tag{3-111}$$

$$y_2(0) = \dot{Y}_0. \tag{3-112}$$

Eqs. 3-109 and 3-110, with initial conditions of Eqs. 3-111 and 3-112, form a system of first-order differential equations. This system of equations is equivalent to the second-order differential equation of Eq. 3-103 with initial conditions of Eqs. 3-104 and 3-105. This procedure can also be used to reduce a system of n second-order differential equations to a system of $2n$ first-order differential equations.

It is convenient to write systems of differential equations in vector form. A system of n first-order differential equations could be symbolically written as

$$\dot{y} = G(t,y) \tag{3-113}$$

where

$$y = \begin{bmatrix} y_1(t) \\ y_2(t) \\ \cdot \\ \cdot \\ \cdot \\ y_n(t) \end{bmatrix} = \text{vector of } y_i\text{'s}$$

and

$$G(t,y) = \begin{bmatrix} f_1(t,y_1,y_2,\ldots,y_n) \\ \cdot \\ \cdot \\ \cdot \\ f_n(t,y_1,y_2,\ldots,y_n) \end{bmatrix} = \text{vector of functions of time } t \text{ and } y_i.$$

The initial condition can be written as

$$y(0) = Y_0 \tag{3-114}$$

THIS DOCUMENT PROVIDED BY THE ABBOTT AEROSPACE
TECHNICAL LIBRARY
ABBOTTAEROSPACE.COM

where

$$y_0 = \begin{bmatrix} y_{1,0} \\ y_{2,0} \\ \cdot \\ \cdot \\ \cdot \\ y_{n,0} \end{bmatrix} = \text{vector of specified initial values.}$$

The reduction technique previously developed is now used to reduce the equation of motion for the 1-degree-of-freedom model of Eq. 3-58 to the standard first-order form. Define two functions $\zeta_1(t)$ and $\zeta_2(t)$ such that

$$\zeta_1 \equiv \eta, \text{ m} \tag{3-115}$$

$$\zeta_2 \equiv \dot{\eta}, \text{ m/s} \tag{3-116}$$

where

η = displacement of recoiling parts, m
$\dot{\eta}$ = velocity of recoiling parts, m/s
ζ_1 = displacement of recoiling parts, m
ζ_2 = velocity of recoiling parts, m/s.

Substitution for $\ddot{\eta}$ in Eq. 3-58, the equation of motion for the 1-degree-of-freedom model, gives

$$\dot{\zeta}_2 = \frac{1}{M_r}\left[K(t) - B(t) - W_r \sin\theta - W_r \mu (\text{sgn } \zeta_2)\cos\theta\right], \text{ m/s}^2. \tag{3-117}$$

From Eqs. 3-115 and 3-116

$$\dot{\zeta}_1 = \zeta_2. \tag{3-118}$$

The initial conditions for the system that is initially at rest now become

$$\zeta_1(0) = \zeta_0, \text{ m} \tag{3-119}$$

$$\zeta_2(0) = 0, \text{ m/s} \tag{3-120}$$

where

ζ_0 = initial displacement of recoiling parts, m.

Eqs. 3-117 and 3-118 together with the initial conditions, Eqs. 3-119 and and 3-120, are in the standard form for numerical integration.

Solutions of differential equations such as Eq. 3-103 are, in general, functions of time. Closed form solutions for these differential equations are impossible; therefore, numerical methods are used to construct approximate solutions at discrete points in the total simulation interval. Fig. 3-17 shows the graph of solution $y_1(t)$ of a differential equation. The time period over which the differential equation is being integrated runs from t_0 to τ. Given the necessary initial conditions on y_1 and its derivatives at t_0, the numerical integration algorithm predicts the value of y_1 at time t_1. The function value at t_1 having been predicted, the algorithm predicts the function value at time t_2, and so on. Numerical integration algorithms thus effectively progress from the initial time t_0 to the terminal time τ by stepping through a time grid. The interval between two successive time grid points is called the time step, i.e.,

$$h_i = t_{i+1} - t_i, \; i \geq 0, \text{ s} \tag{3-121}$$

THIS DOCUMENT PROVIDED BY THE ABBOTT AEROSPACE
TECHNICAL LIBRARY
ABBOTTAEROSPACE.COM

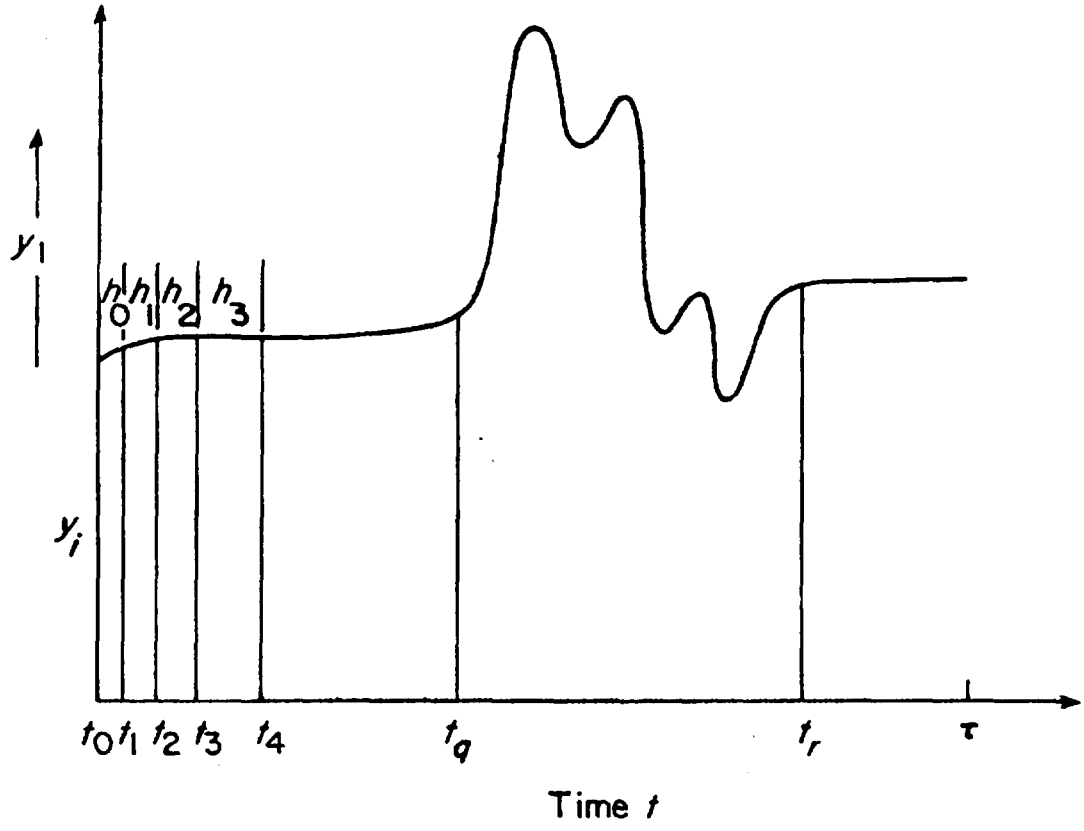

Figure 3-17. Function y_1 vs Time

where

h_i = time step, s
t_{i+1} = $(i + 1)$st time grid point, s
t_i = ith time grid point, s.

Many numerical integration algorithms keep time step h_i constant from time t_0 to τ,

$$h_0 = h_1 = h_2 = \cdots = h_N = h_{N+1}, \text{ s} \tag{3-122}$$

where

$N + 1$ = last grid point.

Numerical integration methods are broadly classified as single-step methods and multistep methods. Single-step methods use the information available only at one point in time to predict the solution at the next point in time. The most commonly used single-step method is the Runge-Kutta method. The general form of this method is given as (Ref. 12)

$$y_{n+1} = y_n + hF(t_n, y_n, h; G), \; n \geq 0 \tag{3-123}$$

where

y_{n+1} = value of y at $(n + 1)$st time grid point, units same as units of y
y_n = value of y at nth time grid point, units same as units of y
t_n = nth time grid point, s
t_{n+1} = $(n + 1)$st time grid point, s
$h = t_{n+1} - t_n$ = time step, s
$F( )$ = vector of functions.

The choice of the function F in Eq. 3-123 is made to minimize the estimated truncation error in the numerical solution. Since the numerical solution is approximate, there is always some error—the truncation error—

THIS DOCUMENT PROVIDED BY THE ABBOTT AEROSPACE
TECHNICAL LIBRARY
ABBOTTAEROSPACE.COM

between the numerical solution and the true solution. True solutions are rarely known; hence, only estimates for the truncation error can be found.

Runge-Kutta methods (Ref. 12) have been used extensively in the past. They are simple to program and use. The number of evaluations of the functions F required by this family of methods is, however, greater than for multistep methods.

One of the simplest Runge-Kutta methods, also known as the trapezoidal method, is given as (Ref. 12)

$$y_{n+1} = y_n + \frac{h}{2}\{G(t_n, y_n) + G[t_{n+1}, y_n + hG(t_n, y_n)]\}. \tag{3-124}$$

The terms in braces in Eq. 3-124, multiplied by 2, represent the function F of Eq. 3-123.

Consider the first-order form of the equations of motion given by Eqs. 3-117 and 3-118. These equations can be written as

$$\dot{\zeta}_1 = f_1(\zeta_2) = \zeta_2, \text{ m/s} \tag{3-125}$$

$$\dot{\zeta}_2 = f_2(t, \zeta_2), \text{ m/s}^2. \tag{3-126}$$

By use of Eq. 3-124, the numerical integration rule for this system can be written as

$$(\zeta_1)_{n+1} = (\zeta_1)_n + \frac{h}{2}\left\langle f_1[(\zeta_2)_n] + f_1\{(\zeta_2)_n + hf_2[t_n, (\zeta_2)_n]\}\right\rangle, \quad \text{m}$$

which simplifies to

$$(\zeta_1)_{n+1} = (\zeta_1)_n + h(\zeta_2)_n + \frac{h^2}{2} f_2[t_n, (\zeta_2)n], \text{ m} \tag{3-127}$$

$$(\zeta_2)_{n+1} = (\zeta_2)_n + \frac{h}{2}\left\langle f_2[t_n, (\zeta_2)_n] + f_2\{t_{n+1}, (\zeta_2)_n + hf[t_n, (\zeta_2)_n]\}\right\rangle, \text{ m/s}. \tag{3-128}$$

By recognizing the right-hand side of Eq. 3-117 to be $f_2(t, \zeta_2)$, Eq. 3-128 can be simplified to

$$\begin{aligned}(\zeta_2)_{n+1} = (\zeta_2)_n + \frac{h}{2M_r}\Bigg\langle & K(t_n) - B(t_n) - 2W_r\sin\theta - W_r\mu\,\text{sgn}[(\zeta_2)_n]\cos\theta \\ & + K(t_{n+1}) - B(t_{n+1}) - W_r\mu\,\text{sgn}\Bigg\{(\zeta_2)_n + \frac{h}{M_r}\Bigg[K(t_n) - B(t_n) \\ & - W_r\sin\theta - W_r\mu\,\text{sgn}[(\zeta_2)_n]\cos\theta\Bigg]\Bigg\}\Bigg\rangle\cos\theta, \text{ m/s}.\end{aligned} \tag{3-129}$$

Eqs. 3-127 and 3-129 are the two equations for the numerical integration of Eqs. 3-117 and 3-118.

Multistep methods used to predict the value of the solution at the following time grid point use information available at a number of time grid points preceding the current time. Consider the time grid points to be defined as

$$t_n = t_0 + nh, \text{ s} \tag{3-130}$$

where

t_n = time at nth grid point, s
t_0 = time at initial grid point, s
h = time interval between successive grid points, i.e., time step, s.

The general form of a multistep numerical integration algorithm is (Ref. 12)

$$y_{n+1} = \sum_{j=0}^{p} a_j y_{n-j} + h\sum_{j=-1}^{p} b_j G(t_{n-j}, y_{n-j}), \; n = p, p+1, \ldots \tag{3-131}$$

where

a_j and b_j = constants of numerical integration algorithm, dimensionless
p = integer characterizing the algorithm, dimensionless.

THIS DOCUMENT PROVIDED BY THE ABBOTT AEROSPACE
TECHNICAL LIBRARY
ABBOTTAEROSPACE.COM

If either $a_p \neq 0$ or $b_p \neq 0$, the method is called a $(p + 1)$ step method because $(p + 1)$ previous solution values are being used to compute y_{n+1}. To start the algorithm, the values of $y_1, \ldots, y_p$ must be obtained by other means, usually from a single-step method.

If $b_{-1} = 0$ in Eq. 3-131, then y_{n+1} occurs on only the left side of Eq. 3-131. Such equations characterize explicit methods of numerical integration. If $b_{-1} \neq 0$, then y_{n+1} occurs on both sides of Eq. 3-131 and the equation is called an implicit method. Implicit methods are usually solved by the iterative Newton-Raphson method (Ref. 12).

The choice of coefficients a_j and b_j in any of these algorithms is based on satisfying theorems related to stability and convergence of multistep methods. The most commonly used explicit methods are the Adams-Bashforth equations. The most commonly used implicit equations are the Adams-Moulton equations. These equations, up to order 3, are given in Ref. 12.

As noted, implicit equations have y_{n+1} appearing on both sides of Eq. 3-131. Therefore, some means is required to predict the value of y_{n+1}. This can be done by using an explicit equation as a predictor for y_{n+1}. The implicit equation is then used to give a better value of y_{n+1} by solving the nonlinear algebraic equation, Eq. 3-131, for y_{n+1}. This technique is called a predictor-corrector algorithm.

Multistep methods are of various orders. The choice of order of method to be used should be based on the truncation error of the method. The choice of step size is also related to truncation error. Setting a tolerance level for truncation error dictates the integration step size. Ref. 12 gives truncation error estimates for the numerous integration methods.

The most commonly used numerical integration methods for differential equations are available as standard computer codes. Two such packages of computer codes are the International Mathematical and the Statistical Library (IMSL) (Ref. 13) and HARWELL subroutine library (Ref. 14). Either one of these subroutine libraries is available on most computer installations. Some of the subroutines in these libraries, though based on ideas similar to those given in this paragraph, are considerably more sophisticated in terms of error control. These codes automatically change order and step size of integration to keep the error within tolerances specified by the user. One of the reasons for having variable order and step size can be seen from Fig. 3-17. In the region bounded by t_0 and t_q, the change in function value is small. The algorithm is generally able to take large steps in this region and still satisfy error tolerance requirements. In the region bounded by t_q and t_r, the function changes rapidly. For the integration algorithm to satisfy the error tolerance, it is necessary that it take a smaller step size than in the preceding region. Ref. 12 discusses in detail the rationale behind variable step size and order methods.

3-4 ADVANCED METHODS OF ARTILLERY DYNAMIC ANALYSIS

3-4.1 APPLICATION OF EQUATION MANIPULATION LANGUAGES TO LAGRANGE'S EQUATIONS

The equations of motion for models of varying complexity were developed in par. 3-2. These equations, as is evident, are complex, nonlinear differential equations. Experience has demonstrated that manual modeling of multidegree-of-freedom systems requires many hours of tedious manipulation of expressions, and there is the risk of generating numerous errors. These shortcomings can be overcome by using automated computer procedures (Ref. 15) that employ equation manipulation languages, such as FORMAC (Ref. 15) or MACSMYA. (See article by Hussain and Noble in Ref. 16.)

FORMAC, as developed by IBM, provides for the symbolic manipulation of mathematical expressions, e.g., expressions such as SIN(X) can be differentiated, evaluated, replaced, and compared. After differentiation, expressions that occur repeatedly can be replaced by new variable names, and thus a number of arithmetical operations can be eliminated. Since PL/I is a subset of FORMAC, all of the facilities of PL/I are available. The FORMAC output consists of coded differential expressions that are automatically punched on cards (error-free) in FORTRAN format and ready for numerical integration. The end product is a computer program written in FORTRAN. Care must be exercised when writing expressions for differentiation by FORMAC because this manipulation language only computes partial derivatives.

A semiautomated technique for simulating a self-propelled M110A1, Howitzer (Fig. 3-18), using FORMAC, is developed in Ref. 15. This weapon is modeled as an 11-degree-of-freedom mechanical system. The model has five distinct masses, i.e., the vehicle M_v, the spade assembly M_s, those parts that traverse but do not elevate M_t, those parts that elevate but do not recoil M_e, and the recoiling parts M_r.

The generalized coordinates are defined based on the following logic: The entire system can translate

THIS DOCUMENT PROVIDED BY THE ABBOTT AEROSPACE
TECHNICAL LIBRARY
ABBOTTAEROSPACE.COM

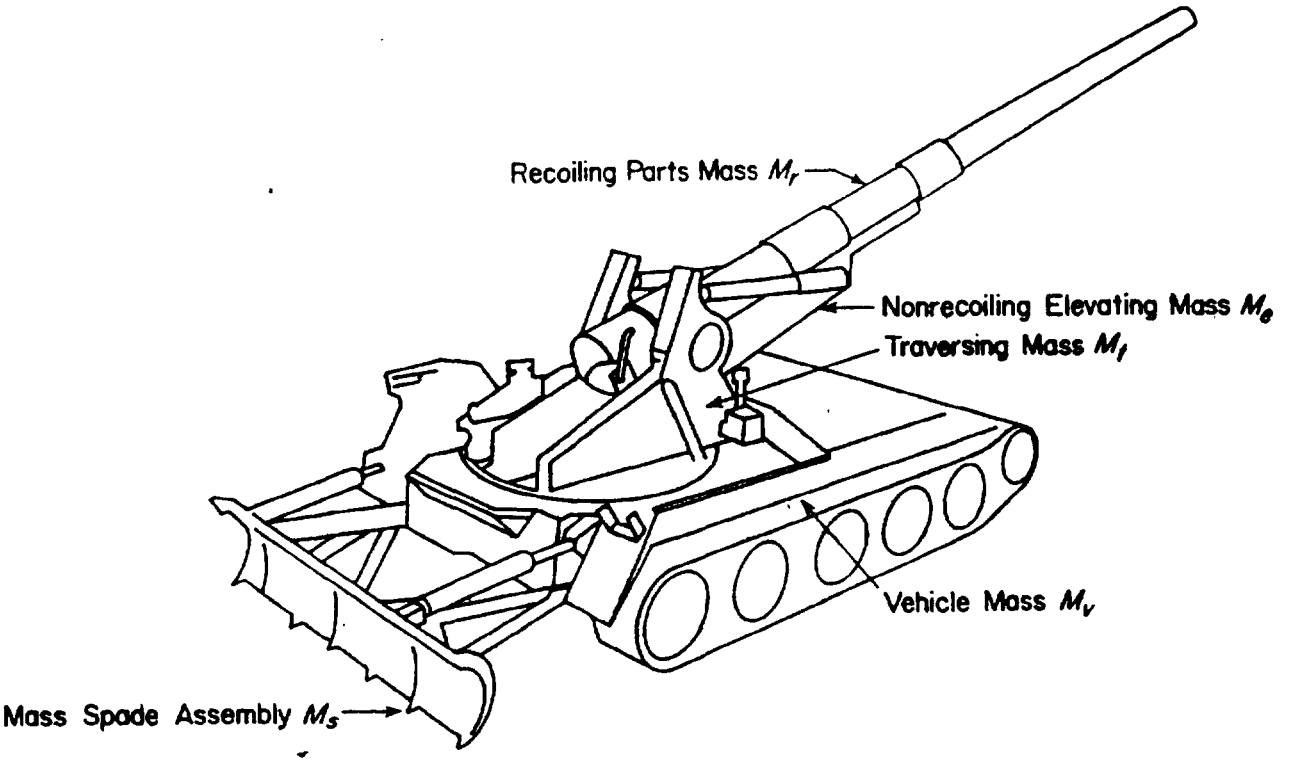

Figure 3-18. Self-Propelled M110A1 Howitzer

laterally (x), roll (θ), and yaw (ψ) as a single rigid mass; the vehicle can translate fore and aft (y), translate in a vertical direction (z) and pitch (ϕ) about its own mass center; those parts that traverse ($M_t + M_e + M_r$) can yaw (τ) relative to the vehicle; those parts that elevate ($M_e + M_r$) can pitch (γ) relative to the vehicle; the recoiling parts can translate (η) relative to the M_e parts; and, finally, the spade assembly can translate fore and aft (ν) and pitch (ν) relative to the ground. Note that the initial value of $\gamma(\gamma_0)$ is the angle of elevation, the initial value of $\tau(\tau_0)$ is the angle of traverse, and the initial value of $\eta(\eta_0)$ locates the in-battery position of the mass center of the recoiling parts relative to the trunnion.

The spades are designed to offer ground resistance to rearward motion and to pitching of the spade assembly, but they offer little resistance to roll, yaw, and translation in the lateral and vertical directions. Thus horizontal ground springs acting on the spade assembly in the longitudinal direction are sufficient to restrain the longitudinal translation and pitch of the spade assembly.

The resistance to lateral translation and yaw of the weapon system is ground friction between the ground and the vehicle tread (assumed to be at the ground contact points of the four corner roller wheels). Vertical ground springs are located at these four ground contact points, and they restrain the roll and vertical translation of the weapon system. Note that the effective spring rate goes to zero at any of the ground contact points when contact between the ground and the vehicle is lost. The braces and spade cylinders are modeled as springs and hydraulic dampers, which act primarily in the longitudinal direction between the vehicle and the spade assembly. Dampers are associated with the vertical ground springs and the braces.

The kinetic and potential energies for this model are developed in Ref. 15. The derivatives of these expressions are computed using FORMAC to formulate all the terms required in Lagrange's equations of motion for the system. For a well-written and complete presentation of the equation manipulation method of dynamic analysis, as applied to the M110 self-propelled Howitzer, refer to Ref. 15.

For large-scale system models, many parameters used in the mathematical model must be estimated by the analyst. Accurate estimates of parameters such as mass, moments of inertia, and geometric variables are usually available. Estimates for other parameters—such as coefficients of friction and stiffness of the torsional spring at the trunnion in the three- or four-degree-of-freedom models—may be difficult to obtain. As test data become available, it is necessary to "validate" and "tune" the model. If correlation between test results and predicted motion is poor and significant motion occurs, which was neglected in the model, a complete revision

THIS DOCUMENT PROVIDED BY THE ABBOTT AEROSPACE
TECHNICAL LIBRARY
ABBOTTAEROSPACE.COM

of the model may be required. However, if all significant motion has been accounted for in the model but the magnitude and timing of the predicted motion is in error, a "tuning" of the model is in order. For example, the models developed in pars. 3-2.2 and 3-2.3 require an effective spring rate for the ground-weapon interaction. The value chosen for this parameter may be poorly estimated. If varying the value of this parameter between reasonable limits greatly improves the desired correlation between model and test, the model is said to have been "tuned".

If no estimates are available for some parameter of the model, the analyst must generate estimates from experimental data. Techniques used to estimate parameters of the model are called system identification techniques. This problem can be posed as an optimal design problem by determining the parameters of the model to best match experimental performance data. To identify or determine unknown parameters, a mathematical model of the real system is formulated. An optimization technique can then be used to determine parameters to minimize deviation between the predicted and observed response of the system. The error to be minimized, i.e., the difference between experimental data and model response, can be characterized by either of the two error criteria: (1) the least square error and (2) the Chebyshev error. The least square error criterion characterizes the error to be the sum of the squares of error at each point in the interval, whereas the Chebyshev error criterion characterizes the error to be the maximum error over the interval.

Methods for error minimization are given in Refs. 10 and 11. In addition to the two methods of error characterization cited, there are other methods available for the same purpose. (See Ref. 17.)

3-4.2 DYNAMIC ANALYSIS OF LARGE-SCALE SYSTEMS

Equations of motion for artillery system models with 1 and 2 degrees of freedom were developed in par. 3-2. As was evident, even for models with 2 degrees of freedom, these equations are complex. Furthermore, adequate mathematical models of weapon systems can only be achieved by using higher degree-of-freedom models. It is virtually impossible to generate and manually solve equations of motion for such models. The only resort is to use automated techniques for generation and solution of equations of motion. Semiautomated methods, such as FORMAC (described in par. 3-4.1), have been used with success for models with intermediate levels of complexity. For models with large numbers of degrees of freedom, however, these methods become cumbersome. Computational methods for dynamic analysis of electronic circuits and structures have become well developed and user-oriented—a situation that is not enjoyed in the field of mechanical system dynamics. In most areas of mechanical design, classical Lagrangian methods of dynamic analysis are still used almost exclusively. Development of general-purpose computer programs for dynamic analysis of mechanisms and mechanical systems was initiated in the mid-1960s and has made significant progress for certain classes of mechanical systems. A comprehensive survey of computer programs and the analytical techniques on which they are based has been presented in Ref. 16. Numerous planar (2-D) mechanism analysis programs are cited, but only two 3-dimensional (3-D) analysis programs appear. The 3-D Integrated Mechanism Program (IMP) and the 2-D Dynamic Response of Articulated Machinery (DRAM) codes are both based on closed loop linkages or mechanisms that are too restrictive a class for general use in mechanical system dynamic analysis and design. A general 2- and 3-dimensional dynamic analysis and design system (DADS) method and corresponding computer programs have been developed, which are fundamentally better suited for dynamic analysis of systems that are not in closed loop configuration (Ref. 3). The basic idea of this computer-aided analysis method is outlined in Appendix A. For more details and guidance in use of such methods, the reader should consult Ref. 3.

Modeling of mechanical systems by the constrained multielement formulation is now discussed. This formulation is the basis for the DADS computer programs (Ref. 3). To determine the configuration or state of a planar mechanical system, this technique requires that generalized coordinates be defined that specify the location of each body in the system. These generalized coordinates need not be independent. As shown in Fig. 3-19, let the (x,y)-coordinate system be a fixed inertial (global) reference frame. Define a body-fixed coordinate system (ξ_i,η_i) embedded in body i, with the origin O_i at the center of mass, located by the vector r_i from the origin of the fixed inertial reference frame. The subscripts i and j refer to arbitrary body numbers. Rigid body i can be located by specifying the global coordinates x_i and y_i of point O_i and the angle ϕ_i of rotation relative to the global coordinates. The kinetic energy of body i is

$$T_i = \frac{1}{2} m_i(\dot{x}_i^2 + \dot{y}_i^2) + \frac{1}{2} J_i \dot{\phi}_i^2, \text{ J} \qquad (3\text{-}132)$$

THIS DOCUMENT PROVIDED BY THE ABBOTT AEROSPACE
TECHNICAL LIBRARY
ABBOTTAEROSPACE.COM

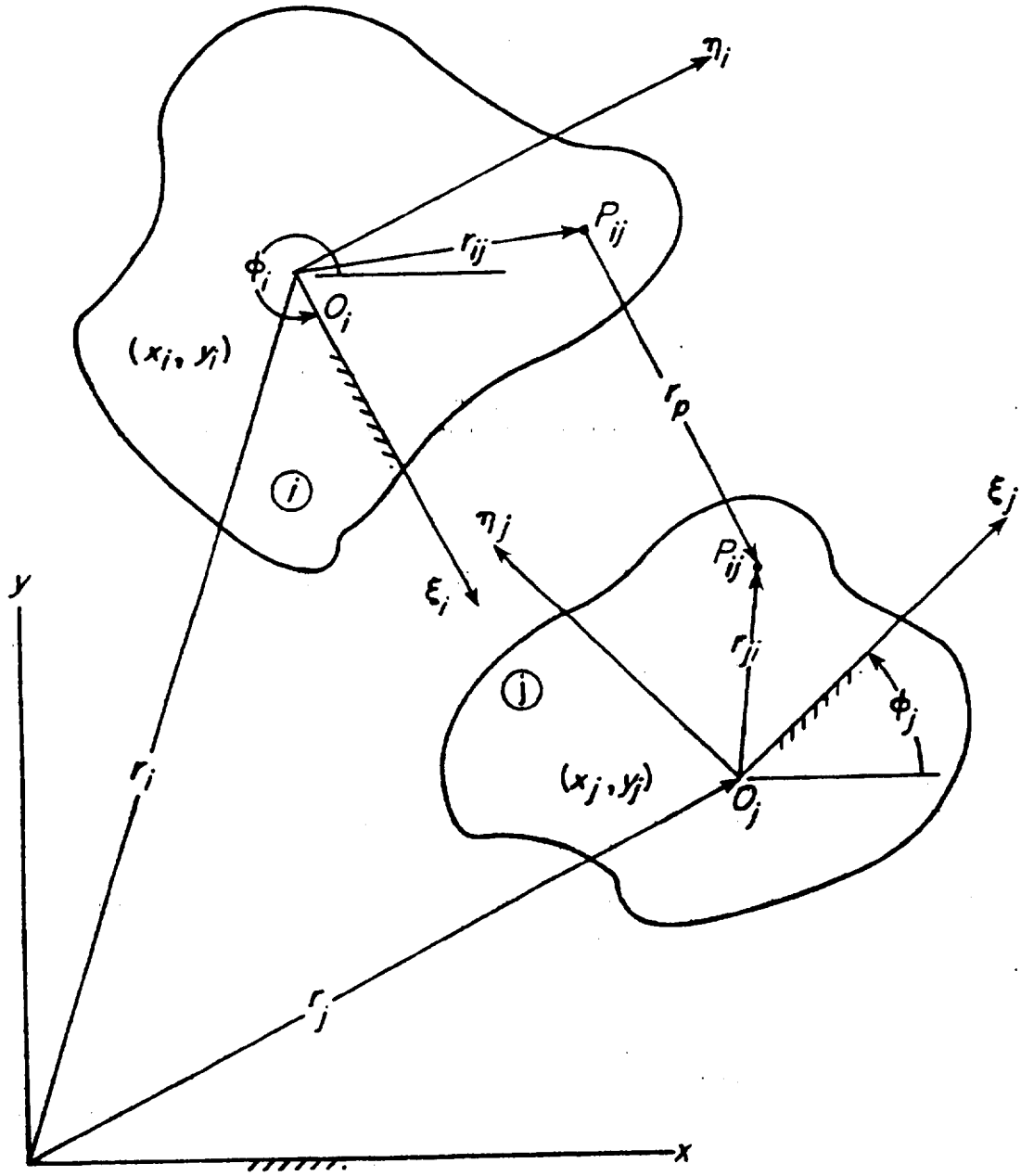

Figure 3-19. Rigid Bodies Connected by a Vector r_p and Rotational Joints

where

T_i = kinetic energy of body i, J
m_i = mass of body i, kg
x_i = x-coordinate of O_i, m
y_i = y-coordinate of O_i, m
J_i = centroidal polar moment of inertia of body i, kg·m^2
ϕ_i = angular orientation of (ξ_i,η_i)-body-fixed coordinate system relative to global system, rad.

Bodies in mechanical systems may be connected by joints. These joints are considered to be constraints on the relative motion of the bodies they connect. For the planar mechanical systems discussed here, standard constraints between rigid bodies are taken as friction-free (workless) translational and rotational joints. User-supplied constraint equations are also allowed to make provision for nonstandard constraints such as

THIS DOCUMENT PROVIDED BY THE ABBOTT AEROSPACE
TECHNICAL LIBRARY
ABBOTTAEROSPACE.COM

cams and prescribed functional relations. Arbitrary (conservative or nonconservative) internal and external forcing functions are incorporated, including spring-damper-actuator elements connecting any pair of points on different bodies of the system. Allowance is also made for arbitrary user-supplied forcing functions.

Fig. 3-19 further depicts an adjacent body j, with body-fixed coordinate system located by the vectors r_i and r_j from the origin of the global coordinate system. Let points p_{ij} on body i and p_{ji} on body j be located by vectors r_{ij} and r_{ji}, specified in the body-fixed coordinate systems by coordinates (ξ_{ij},η_{ij}) and (ξ_{ji},η_{ji}), respectively. These points are in turn connected by vector r_p,

$$r_p = r_j + r_{ji} - r_i - r_{ij}, \text{ m} \tag{3-133}$$

where

r_p = position vector of point p_{ji} relative to point p_{ij}, m
r_j = position vector of O_j, m
r_i = position vector of O_i, m
r_{ij} = position vector of p_{ij} relative to O_i, m
r_{ji} = position vector of p_{ji} relative to O_j, m.

The vector condition for a rotational joint at points p_{ij} and p_{ji} is simply $r_p = 0$. The scalar equations of a rotational joint are thus

$$\begin{aligned} x_i + \xi_{ij}\cos\phi_i - \eta_{ij}\sin\phi_i - x_j - \xi_{ji}\cos\phi_j + \eta_{ji}\sin\phi_j = 0 \\ y_i + \xi_{ij}\sin\phi_i + \eta_{ij}\cos\phi_i - y_j - \xi_{ji}\sin\phi_j - \eta_{ji}\cos\phi_j = 0 \end{aligned} \tag{3-134}$$

where

ξ_{ij} = coordinate of point p_{ij} along ξ_i-axis, m
η_{ij} = coordinate of p_{ij} along η_i-axis, m
ξ_{ji} = coordinate of point p_{ji} along ξ_j-axis, m
η_{ji} = coordinate of point p_{ji} along η_j-axis, m.

Other constraints that define joints, such as translation of recoiling parts relative to the cradle, may be formulated by a similar process.

Denote by $q^i = [x_i, y_i, \phi_i]^T$ the vector of generalized coordinates of body i and by $q = [q^{1T}, q^{2T}, ..., q^{nT}]^T$ the composite vector of all system-generalized coordinates. In this notation the constraints of Eq. 3-134 and other (perhaps time dependent) nonstandard constraints can be written in vector function form as

$$\Phi(q,t) = 0 \tag{3-135}$$

where

$\Phi(q,t) = [\Phi_1(q,t), ..., \Phi_m(q,t)]^T$ is a vector of constraint functions.

Virtual displacements δq that are consistent with constraints, i.e., with time fixed, satisfy

$$[\Phi_q]\delta q = 0 \tag{3-136}$$

where

$[\Phi_q] = \dfrac{\partial \Phi}{\partial q} \equiv \left[\dfrac{\partial \Phi_i}{\partial q_j}\right]_{m \times 3n}$, using subscript notation for differentiation with respect to a vector

δ_q = virtual displacement of generalized coordinates, m.

Differentiation of Eq. 3-135 with respect to time gives the velocity relation

$$[\Phi_q]\dot{q} + \Phi_t = 0 \tag{3-137}$$

THIS DOCUMENT PROVIDED BY THE ABBOTT AEROSPACE
TECHNICAL LIBRARY
ABBOTTAEROSPACE.COM

where

$\dot{q}$ = generalized velocities, m/s

$$\Phi_t = \frac{\partial \Phi}{\partial t} \equiv \left[\frac{\partial \Phi_i}{\partial t} \right]_{m \times 1}$$

Internal forces acting between bodies may be obtained by a process similar to the constraint equation development. For example, since springs, dampers, and actuators generally appear together, as shown in Fig. 3-20, they are incorporated into a single set of equations. The equation for spring-damper-actuator force is

$$F_{ij} = [k_{ij}(l_{ij} - l_{0_{ij}}) + c_{ij}\dot{l}_{ij} + F_{0_{ij}}]\left(\frac{r_{s_{ij}}}{l_{ij}}\right), \text{ N} \qquad (3\text{-}138)$$

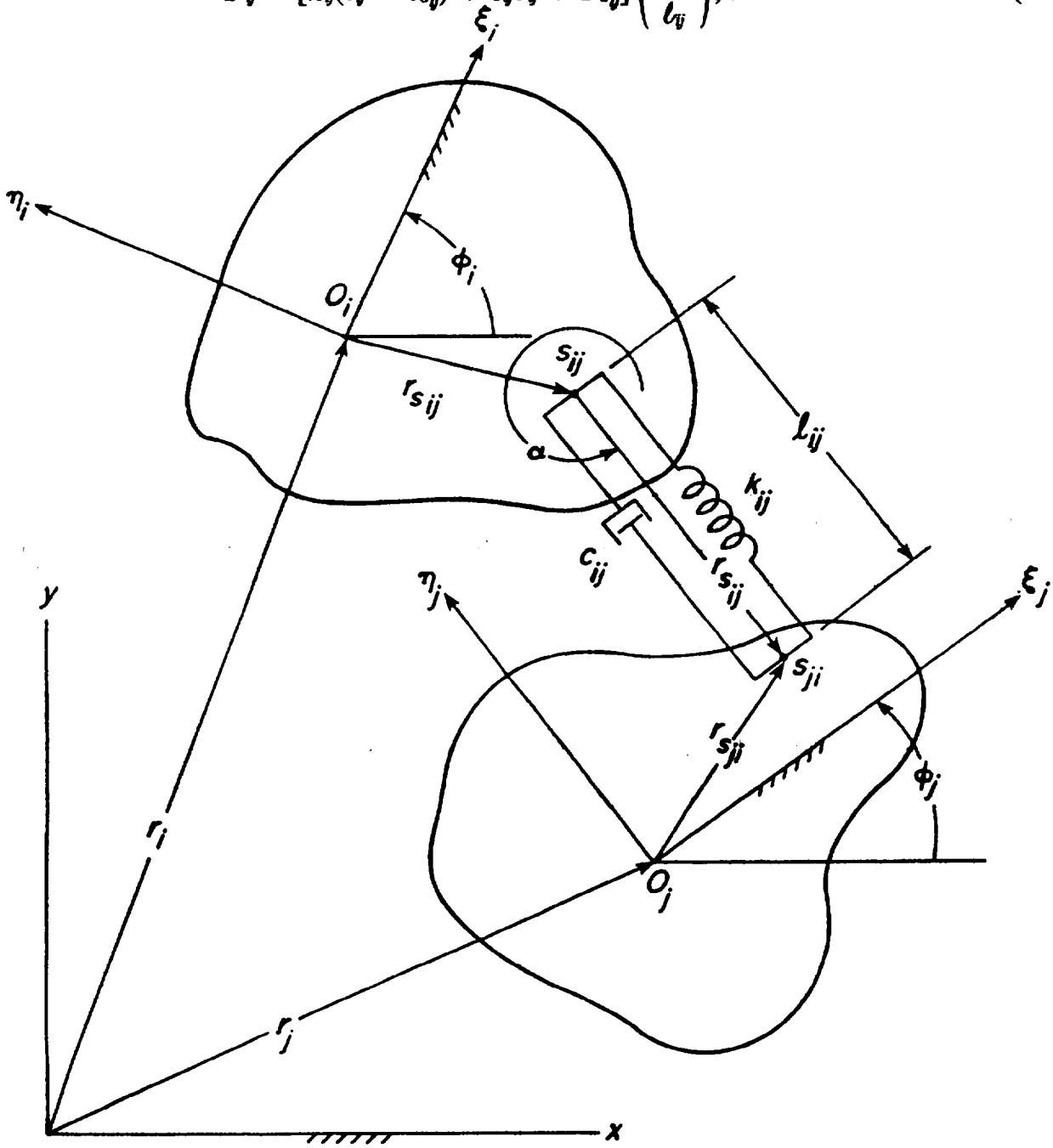

Figure 3-20. Rigid Bodies Connected by a Spring-Damper-Actuator Combination

THIS DOCUMENT PROVIDED BY THE ABBOTT AEROSPACE
TECHNICAL LIBRARY
ABBOTTAEROSPACE.COM

where

F_{ij} = resultant force vector $F_{x_{ij}}i + F_{y_{ij}}j$ in the element, N
$r_{s_{ij}}$ = vector $(\ell_{ij}\cos\alpha)i + (\ell_{ij}\sin\alpha)j$ between points s_{ij} and s_{ji}, m
$\ell_{0_{ij}}$ = undeformed spring length, m
ℓ_{ij} = deformed spring length, m
k_{ij} = elastic spring coefficient that may depend on generalized coordinates and time, N/m
c_{ij} = damping coefficient that may depend on generalized coordinates and time, N·s/m
$F_{0_{ij}}$ = actuator force applied along element that may depend upon generalized coordinates and time, N.

The unit vectors i and j are parallel to the x- and y-axes, respectively, and are dimensionless.

Contributions of forces acting on body i to the system equations of motion are determined using the principle of virtual work. The virtual work of externally applied forces and spring-damper-actuator forces acting on body i is written as

$$\delta W^i = Q_x^i(q,\dot{q},t)\delta x_i + Q_y^i(q,\dot{q},t)\delta y_i + Q_\phi^i(q,\dot{q},t)\delta\phi_i, \text{ J} \tag{3-139}$$

where

δW^i = virtual work of forces acting on body i, J
Q_x^i, Q_y^i, Q_ϕ^i = generalized forces on body i in the x-, y-, and ϕ-directions, N, N, N·m, respectively.

The vector $Q^i = [Q_x^i, Q_y^i, Q_\phi^i]^T$ of generalized forces on body i is thus defined, and $Q = \left[Q^{1^T}, Q^{2^T}, \ldots, Q^{n^T}\right]^T$ is the vector of system-generalized forces. Typical generalized forces are calculated to illustrate the procedure. Point s_{ij} on body i is located by the vector $r_i + r_{s_{ij}}$. A virtual change in the location of point s_{ij} is given by

$$\delta(r_i + r_{s_{ij}}) = \frac{\partial}{\partial x_i}(r_i + r_{s_{ij}})\delta x_i + \frac{\partial}{\partial y_i}(r_i + r_{s_{ij}})\delta y_i + \frac{\partial}{\partial \phi_i}(r_i + r_{s_{ij}})\delta\phi_i, \text{ m.} \tag{3-140}$$

Forming the dot product of F_{ij} with $\delta(r_i + r_{s_{ij}})$ determines contributions to the generalized expressions for body i as

$$\left.\begin{aligned} Q_{x_s}^i &= F_{x_{ij}}, \text{ N} \\ Q_{y_s}^i &= F_{y_{ij}}, \text{ N} \\ Q_{\phi_s}^i &= F_{x_{ij}}(-\xi_{s_{ij}}\sin\phi_i - \eta_{s_{ij}}\cos\phi_i) \\ &\quad + F_{y_{ij}}(\xi_{s_{ij}}\cos\phi_i - \eta_{s_{ij}}\sin\phi_i), \text{ N·m.} \end{aligned}\right\} \tag{3-141}$$

Generalized force contributions are summed for all externally and internally applied forces acting on body i to arrive at Q^i.

The variational form of Lagrange's equations of motion with workless constraints (Ref. 1) is, using subscript notation for differentiation with respect to a vector,

$$\left[\frac{d}{dt}(T_{\dot{q}}) - T_q - Q^T\right]\delta q = 0 \tag{3-142}$$

where

T = total kinetic energy of system, J

THIS DOCUMENT PROVIDED BY THE ABBOTT AEROSPACE
TECHNICAL LIBRARY
ABBOTTAEROSPACE.COM

$$[T_{\dot{q}}] = \frac{\partial T}{\partial \dot{q}} \equiv \left[\frac{\partial T}{\partial \dot{q}_j} \right]_{1\times 3n}$$

$$[T_q] = \frac{\partial T}{\partial q} \equiv \left[\frac{\partial T}{\partial \dot{q}_j} \right]_{1\times 3n}$$

which must hold for all δq satisfying Eq. 3-136. By Farkas' Lemma (Ref. 10), there exists an m-component vector of Lagrange multipliers λ such that

$$\frac{d}{dt}[T_{\dot{q}}]^T - [T_q]^T - [Q] + [\Phi_q]^T\lambda = 0 \tag{3-143}$$

which, with Eq. 3-135, form the constrained equations of motion of the system where

λ = Lagrange multiplier vector with m-components.

Initial conditions for system motion are given as

$$q(0) = q^0, \text{ m}$$
$$\dot{q}(0) = \dot{q}^0, \text{ m/s} \tag{3-144}$$

where

q^0 = specified initial values of generalized coordinates, m
$\dot{q}^0$ = specified initial values of generalized velocities, m/s.

It is required that q^0 and $\dot{q}^0$ are consistent with constraints—i.e., q^0 satisfies Eq. 3-135 and $\dot{q}^0$ satisfies Eq. 3-137.

The vector of Lagrange multipliers is directly related to the reaction forces of constraints (Ref. 3).

The equations of motion of Eq. 3-143 and constraint equations of Eq. 3-135 comprise a large collection of equations in many variables and are not generally practical for manual calculation. The form of these equations, however, is very systematic. This systematic format increases the feasibility of automated computer construction of the equations and subsequent automated solution to predict dynamic performance of an artillery system. Details of techniques that are used for automated computer formulation and solution of these equations are presented in Ref. 3, along with numerous examples and guidelines in applying these methods for dynamic analysis of large-scale systems. Use of these computer-automated methods, which are similar to well-developed finite element structural analysis methods, now makes detailed dynamic analysis of towed artillery systems practical during the design process. Use of this new class of techniques is recommended for support of the development of towed artillery systems.

Design requirements specify that a weapon system is to perform some task at some index of performance. Thus the design of a weapon system provides a natural setting for an optimization problem, if it is assumed that knowledge of all environmental factors influencing the design process are known. It is not satisfactory to search only for admissible design parameters that enable the system to perform its intended task. It should be required to seek design parameters that optimize performance.

The ability to analyze large-scale mechanical systems having been developed, it is natural to integrate this with techniques for optimization. This integration results in the development of a technique for computer-aided design of mechanical systems. Optimization techniques have successfully been used for the computer-aided design of large-scale systems (Refs. 10, 11, and 16). A computer-aided design technique, as proposed, can also be used for system identification in a manner similar to that described in par. 3-4.1 used to determine model parameters. Weapons could also be designed to satisfy stability criteria (Refs. 9, 10, 11, and 16.)

THIS DOCUMENT PROVIDED BY THE ABBOTT AEROSPACE
TECHNICAL LIBRARY
ABBOTTAEROSPACE.COM

REFERENCES

1. D. T. Greenwood, *Principles of Dynamics*, Prentice-Hall, Englewood Cliffs, NJ, 1965.
2. C. M. Robinder and B. L. Hofgaard, *Stress Analysis of 195-mm Towed Howitzer XM204 Serial Numbers 3 Through 8*, Technical Note R-TN-76-010, Research Directorate, General Thomas J. Rodman Laboratory, Rock Island Arsenal, IL, June 1976.
3. E. J. Haug, *Computer-Aided Kinematics and Dynamics*, Allyn & Bacon, Boston, MA, 1988.
4. J. W. Frantz and M. C. Nerdahl, *Mathematical Models for Engineering Analysis and Design of Howitzer, Medium, Towed; 155-mm, XM198*, Technical Report RE-TR-70-186, Artillery Systems Laboratory, US Army Weapons Command, Research and Engineering Directorate, Rock Island Arsenal, IL, October 1970.
5. M.C. Nerdahl and J. W. Frantz, *Mathematical Firings of 155-mm Howitzer, XM198*, Technical Report SWERR TR 72-72, Weapons Laboratory-WECOM, Artillery Weapons Systems Directorate, US Army Weapons Command, Rock Island Arsenal, IL, October 1972.
6. S. M. Selby, Ed., *CRC Abridged Mathematical Tables*, Fourteenth Edition, The Chemical Rubber Co., Cleveland, OH, 1967.
7. R. M. Coberly, *Mathematical Simulation of Carriage Motion Under Dynamic Conditions of Firing*, Technical Report 67-381, US Army Weapons Command, Research and Engineering Directorate, Rock Island Arsenal, IL, February 1967.
8. G. Lind and L. Johnston, *Stabilization Study of a Variable Recoil Howitzer Fired From Wheels*, Undesignated Report, Rock Island Arsenal, IL, March 1967.
9. T. D. Streeter, *Optimal Weapon Stability by a Steepest Descent Method*, US Army Weapons Command, Systems Analysis Directorate, Rock Island Arsenal, IL, August 1969.
10. AMCP 706-192, Engineering Design Handbook, *Computer-Aided Design of Mechanical Systems*, Vol. I, July 1973.
11. DARCOM-P 706-193, Engineering Design Handbook, *Computer-Aided Design of Mechanical Systems*, Vol. II, September 1977.
12. K. E. Atkinson, *An Introduction to Numerical Analysis*, John Wiley & Sons, Inc., New York, NY, 1978.
13. *IMSL Library Reference Manual*, 7th Edition, IMSL, Houston, TX, January 1979.
14. United Kingdom Atomic Energy Authority, Harwell Subroutine Library: *A Catalogue of Subroutines*, Report AERE 7477, Subroutine Librarian, CSS Division, Atomic Energy Research Establishment, Marwell Didcot, Oxfordshire, England, OX11 ORA, 1973.
15. T. D. Streeter and R. M. Coberly, *A Dynamic Analysis of the Self-Propelled, 8- in. M110A1, Howitzer Utilizing FORMAC*, Technical Report R-TR-77-025, Large Caliber Weapons System Laboratory, US Army Armament Research and Development Command, Rock Island Arsenal, IL, June 1977.
16. E. J. Haug, Ed., *Computer-Aided Analysis and Optimization of Mechanical System Dynamics*, Springer-Verlag, Heidelberg, Germany, 1984.
17. J. L. Junkins, *An Introduction to Optimal Estimation of Dynamical Systems*, Sijthoff & Noordhoff International Publishers, Alphen Aan den Rijn, The Netherlands, 1978.

THIS DOCUMENT PROVIDED BY THE ABBOTT AEROSPACE
TECHNICAL LIBRARY
ABBOTTAEROSPACE.COM

THIS DOCUMENT PROVIDED BY THE ABBOTT AEROSPACE
TECHNICAL LIBRARY
ABBOTTAEROSPACE.COM

CHAPTER 4
MECHANISM DESIGN

This chapter deals with design of mechanisms for towed artillery systems, with emphasis on elevating and traversing mechanisms. Weapon lowering and raising mechanisms, weapon suspension systems, and linkages for variable recoil control are also discussed. Kinematic functions of all mechanisms are defined, and alternate gearing, bearing, and actuator configurations are identified. Gear train requirements are defined, loads acting are determined, and criteria for gearing ratios in manual operation are determined. Design of clutches and no-back devices to protect the operator and gear train components from large loads that occur during weapon firing is discussed. Precision gearing design, including antibacklash techniques, is discussed for towed artillery systems.

4-0 LIST OF SYMBOLS

a = distance along ξ-axis of F_g from trunnion, m
a_K = perpendicular distance between recoil force vector K and propellant gas force vector F_g, m
b = distance along ξ-axis of F_a from trunnion, m
b_K = perpendicular distance between recoil force vector K and vector F_a of inertial forces of recoiling parts, m
d = distance along ξ-axis of CG from bore centerline, m
F_a = inertial force of recoiling parts, N
F_{bv} = total normal force on traversing bearing, N
F_g = propellant gas force, N
F_s = spring load, N
F_t = load on both trunnions, N
I_t = mass moment of inertia of tipping parts about trunnion, kg·m^2
K = recoil force, N
M_e = equilibrator moment, N·m
M_w = moment due to weight of parts, N·m
R_p = pitch radius of spring-loaded pinion, m
R_t = radius of traversing axis to CG, m
R_μ = frictional radius, m
r_b = trunnion bearing radius, m
r_i = inside radius of bearing, m
r_o = outside radius of bearing, m
T_a = torque required to accelerate tipping parts, N·m
T_b = static frictional torque, N·m
T_E = maximum torque at elevating arc, N·m
T_e = unbalanced equilibrator moment, N·m
T_f = component of firing couple affecting elevation, N·m
T_t = torque on traverse bearing due to firing couple, N·m
T_s = torque at spring-loaded pinion, N·m
W = total weight of weapon, N
W_t = weight of tipping parts, N
W_v = weight of traversing parts, N
α = maximum elevating acceleration, rad/s^2
θ = angle of elevation, rad
θ_t = slope of terrain, rad
λ = helix angle, rad
μ = coefficient of friction, dimensionless
ϕ_a = location of CG with respect to horizontal line in plane parallel to slope, rad
ω = maximum elevating velocity, rad/s.

THIS DOCUMENT PROVIDED BY THE ABBOTT AEROSPACE
TECHNICAL LIBRARY
ABBOTTAEROSPACE.COM

4-1 ELEVATING MECHANISMS

4-1.1 TYPES OF ELEVATING MECHANISMS

Elevating mechanisms are essentially gear trains with input at the power source and output at the tipping parts. The gear train frequently includes a self-locking worm and worm wheel. Otherwise, a mechanical brake or no-back device must be provided to hold the tipping parts in the prescribed position. Elevating mechanisms may be power operated. Manually operated units, in which effort is applied by a handwheel, are generally used for towed weapons. If the elevation effort is too burdensome for manual operation, the mechanism must derive its power from mechanical or electrical sources. In case of power failure, however, mechanisms are geared for handwheel operation.

4-1.1.1 Ball-Screw Type

Ball-screw elevating mechanisms are used in most modern weapon systems. There are two basic configurations in which this type of mechanism is used. In Fig. 4-1(A) a captive nut is attached to and pivoted in the cradle. Elevation is achieved in turning the screw by means of the handwheel and gear train, which causes the nut to travel in the desired direction. The base of the screw rests in a thrust bearing whose housing pivots on the top carriage. Two bevel gears, which may be enclosed in a housing, serve as drivers for the screw. One bevel gear is fixed to the screw near its lower end.

The other configuration, shown in Fig. 4-1(B), pivots the screw in the cradle and rotates the nut to provide elevation change. Thus no matter what angle is assumed by the elevating screw, proper gear mesh is assured. This second version differs from the first by having the elevating screw pivoted in the cradle with the nut free to turn and tilt.

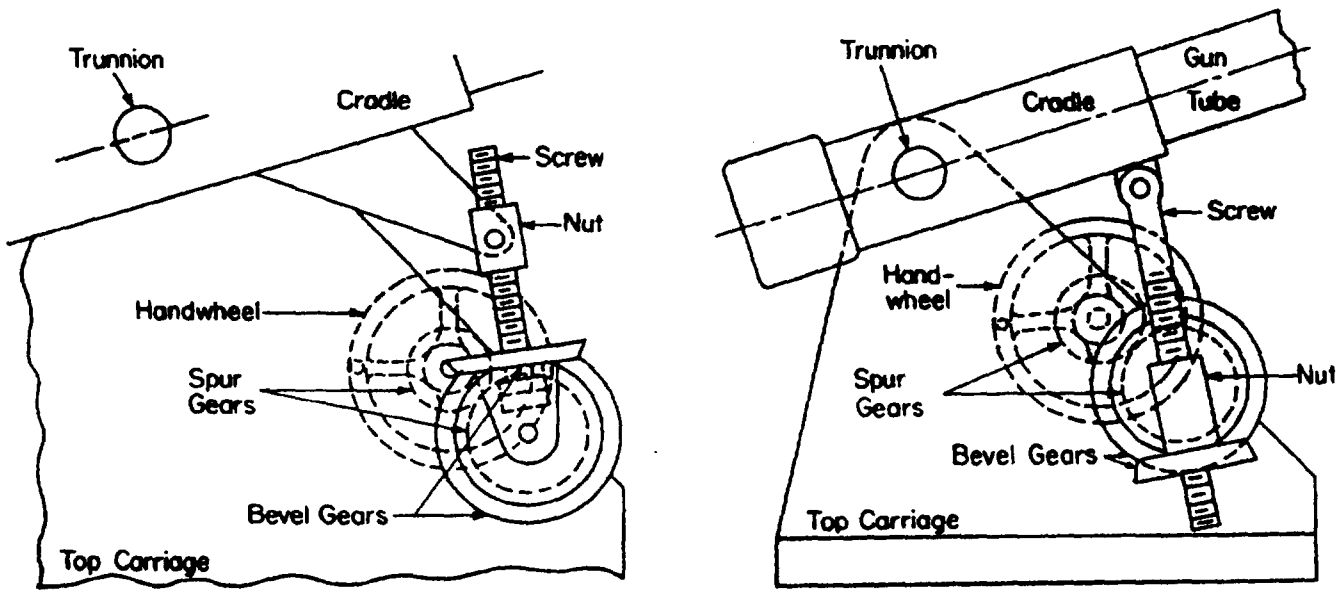

Figure 4-1. Screw- and Nut-Type Elevating Mechanisms

The ball-screw device shown in Fig. 4-2 employs balls running in a helical groove in a shaft so that the balls are recirculated in a special nut. Friction levels are reduced by at least 90%, compared to standard screw devices.

Because the ball screw is so efficient, any axial force imposed on the nonrotating nut will cause the lead screw to turn. Thus a vertically applied load can overrun the screw unless some protecting device is incorporated and the tipping parts will be lowered. A bidirectional reverse locking clutch or a manually locking clutch must be used to prevent the screw from being turned by the load but still enable it to be returned by the operator. The locking clutch, also known as a no-back device, allows torque to be transmitted through the unit from the input end but prevents torque from being transmitted through the clutch from the output end. The no-back device is mounted in a housing, and the ball-screw shaft is keyed to the clutch hub. Thrust bearings are necessary to absorb the thrust load on the mechanism and are mounted next to the clutch.

THIS DOCUMENT PROVIDED BY THE ABBOTT AEROSPACE
TECHNICAL LIBRARY
ABBOTTAEROSPACE.COM

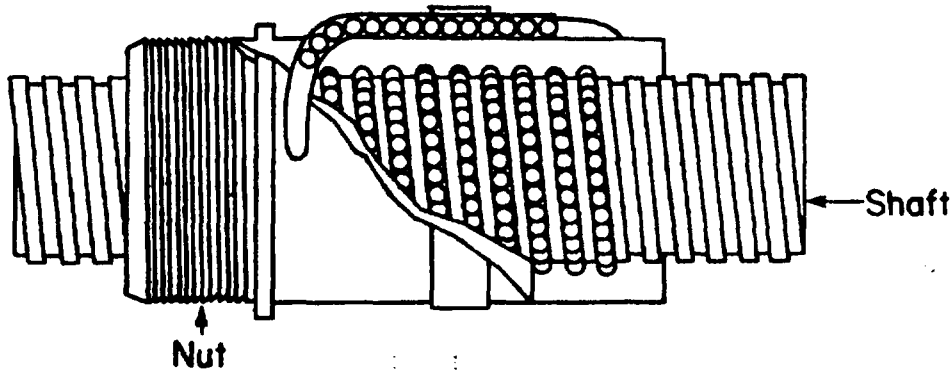

Figure 4-2. Ball-Screw Device

Ball-screw units are commercially available in sizes from 9-mm to about 250-mm. The choice of size and type of ball-screw unit can be made from manufacturers' catalogues. The two main criteria on which the designer should base his choice are the axial load capacity of the unit and the critical buckling length of the column. If the ball-screw shaft is required to rotate at a high speed, the natural frequencies of vibration of the shaft may have to be taken into consideration. Ball-screw assemblies should be loaded in a manner that will insure nut and screw are either in tension or in compression simultaneously to prevent unwanted backlash and associated error in elevation of the weapon. End play (backlash) in a ball-screw assembly, requiring precise positioning under load reversal conditions, can be minimized by preloading the ball screw.

With solid film lubricants, ball screws can be made to operate at high temperatures. With special lubricants, ball screws can be made to operate in the range of −70° to 320°C.

On elevating mechanisms with a ball-screw assembly on each side of the weapon, synchronization of the two drives is important. It may be necessary to provide an adjustable coupling in the cross drive shaft to insure that each of the ball screws in the drive takes an equal load.

4-1.1.2 Pinion and Arc Type

Pinion and arc elevation mechanisms were used in the past and may be considered for some types of weapons. They may be operated manually and may be self-locking or have a brake. Like the screw and nut type, the pinion and arc type has two versions, both identical except for the last two members—the pinion and elevating arc—of the gear train. Fig. 4-3(A) is a schematic diagram of one method of installation. It depicts the mechanism attached to the top carriage and the elevating arc attached to the cradle. Change in elevation occurs when the pinion rotates the elevating arc about the trunnions.

The second method, as shown in Fig. 4-3(B), has the arrangement reversed. Here the arc is attached to the top carriage, and the mechanism is fixed to and rides with the cradle. This second version, because of additional mass and installation difficulties, is not particularly adaptable to power drives if some or all power equipment is included with the tipping parts.

Depending on the design of the elevating mechanism, there may or may not be a no-back device in the system. As shown in Figs. 4-3(A) and (B), a worm and worm gear are part of the elevating mechanism. It is possible to design this gear set to make it irreversible. If this is done, there is no need for a no-back device in the system. The efficiency of such a gear drive depends mainly on the worm gear design.

The modern ball-screw system discussed in par. 4-1.1 can achieve much lower friction levels and is generally preferred over the pinion and arc for modern towed artillery systems.

4-1.2 ELEVATING MECHANISM COMPONENTS

Four basic design requirements are essential to any elevating mechanism, namely, control, power transmission, precision, and sensitivity. Control is prescribed by the fire control equipment, which is not considered part of the mechanism, and the limit stops and a locking device that maintain weapon elevation. The locking device, considered part of the elevating mechanism, may be a brake, a clutch, or an irreversible screw. Limit stops, usually springs or hydraulic buffers, prevent overtravel. Power, whether manual or mechanical, is transmitted by a gear train. Precision depends on the quality of manufacture, particularly in relation to backlash, whereas sensitivity involves the gear ratio. These components and considerations, plus the location of all components, become the primary factors in elevating mechanism design.

THIS DOCUMENT PROVIDED BY THE ABBOTT AEROSPACE
TECHNICAL LIBRARY
ABBOTTAEROSPACE.COM

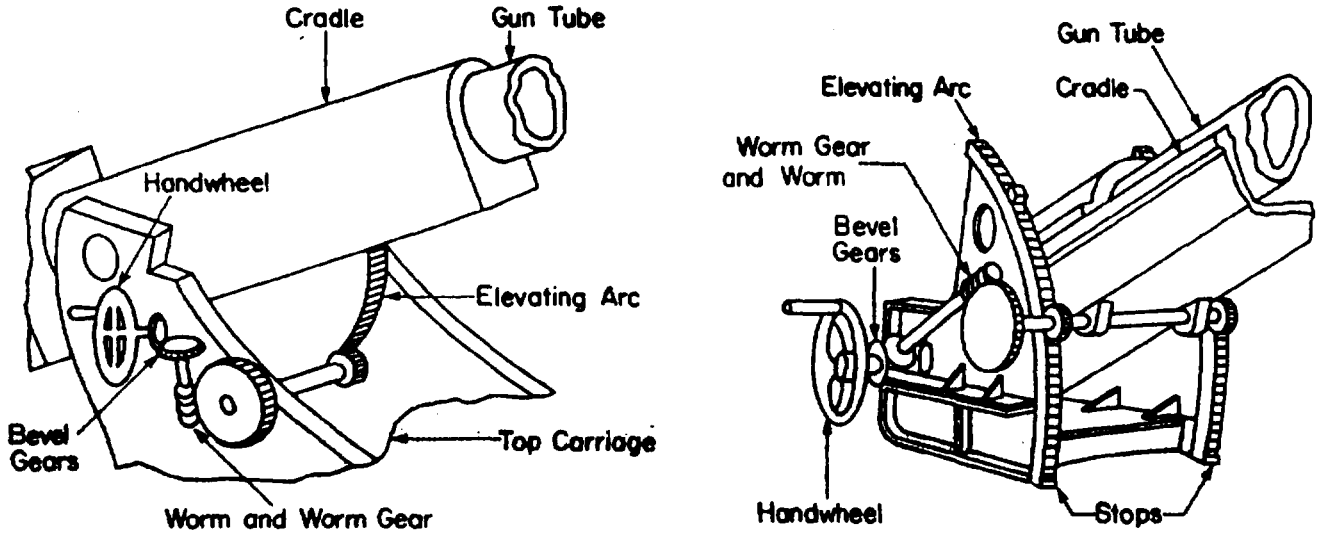

Figure 4-3. Pinion- and Arc-Type Elevating Mechanisms

4-1.2.1 Gear Trains

The gear train, no matter how simple, is the principal part of the elevating mechanism. If the train is reversible, a brake or some other type of locking device is needed to preclude reverse motion. The gear ratio should be considered first. Not only does the ratio prescribe the effort at the power source, it also affects the sensitivity. A high gear ratio means slow elevation with respect to applied motion; a low ratio means correspondingly faster action. Although a high gear ratio requires only a low torque at the power source, the energy requirement to meet identical performance specifications is unaffected. For example, assume that the torque required to elevate the weapon, incorporating the efficiency of the gear train, is 3000 N·m. A gear ratio of 640:1 reduces the torque requirement to 4.7 N·m at the handwheel; a ratio of 320:1 reduces it to 9.4 N·m. Specified handwheel effort and sensitivity requirements thus establish the gear ratio. Thereafter, type, number, size, and location of the gear train components may be determined.

In addition to the available data, the design of the gear train involves an iterative procedure. Only the efficiency needs to be estimated for a manually operated train because accelerating forces are low enough to be negligible. Final computed data must agree reasonably well with estimates before preliminary concepts are acceptable. Thus a careful analysis of the gear train is required. For detailed design of gear trains and gears, the reader can refer to standard machine design texts such as Refs. 1 and 2.

The design for manually operated systems is computed from statics of the weapon. The data required include the weight moment after equilibration and the torque due to frictional resistance of the trunnion bearings. The unbalanced equilibrator moment T_e is

$$T_e = M_w - M_e, \text{ N·m} \tag{4-1}$$

where

M_e = equilibrator moment, N·m
M_w = moment due to weight of parts, N·m.

The static frictional torque T_b in the trunnion bearing is

$$T_b = \mu F_t r_b, \text{ N·m} \tag{4-2}$$

where

F_t = load on both trunnions, N
r_b = trunnion bearing radius, m
μ = coefficient of friction, dimensionless.

THIS DOCUMENT PROVIDED BY THE ABBOTT AEROSPACE
TECHNICAL LIBRARY
ABBOTTAEROSPACE.COM

When recoil forces are present, F_i increases appreciably, which increases the torque T_b. This additional torque must be considered if the weapon fires while elevating. Another component of the torque on the elevating parts is the firing couple that is generated during firing and is due to the eccentricity of the applied and inertia forces about the trunnion axis. As shown in Fig. 4-4, the component T_f of the firing couple, which affects elevation, is

$$T_f = aF_g - bF_a, \text{ N·m} \tag{4-3}$$

where

F_a = inertial force of recoiling parts, N
F_g = propellant gas force, N
a = distance along ξ-axis of F_g from trunnion, m
b = distance along ξ-axis of F_a from trunnion, m.

Careful system design should hold T_f to a minimum, the objective being to have the trunnion axis and the mass center of the recoiling parts lie on the bore centerline. This alignment is not always possible because space limitations and required structural locations may cause an unequal distribution of weight and thus create an imbalance about the bore axis. Regardless of the care exercised, manufacturing tolerances may augment this imbalance. If the firing torque is transmitted through the gear train, the effect at the handwheel may be significant. If the gear train is locked out, only the gears between the elevating arc and the locking device will be disturbed.

The firing couple can be modified by shifting the trunnion axis, but no location can maintain a zero torque throughout the entire firing cycle. This is especially true during the propellant gas period when the gas force varies from zero to maximum. For example, consider a hypothetical gun whose recoil force is K and the propellant gas force F_g may range from $16K$ to 0; thus

$$F_a = F_g - K, \text{ N.} \tag{4-4}$$

By using the geometry of Fig. 4-4 and Eq. 4-4, when $a = 0$, the firing couple varies from $-15Kd \leq T_f \leq Kd$ where

d = distance along ξ-axis of center of gravity (CG) from bore centerline, m.

When zero torque is desired at maximum gas pressure, select

$a = 15d$, m
$b = a + d = 16d$, m.

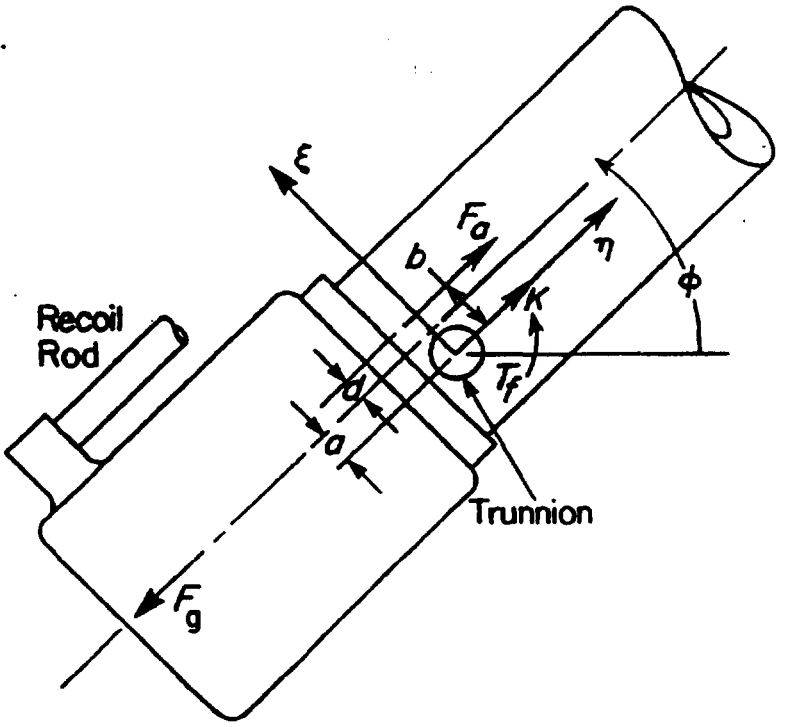

Figure 4-4. Elevation Firing Couple Diagram

THIS DOCUMENT PROVIDED BY THE ABBOTT AEROSPACE
TECHNICAL LIBRARY
ABBOTTAEROSPACE.COM

The firing torque T_f due to F_g, as can be seen in Table 4-1, thus varies from $0 \leq T_f \leq 16Kd$ for these values of a and b. For intermediate values, say $a = 7d$ and $b = 8d$, the firing torque T_f is as given in Table 4-2.

These examples show a varying firing torque during the propellant gas period regardless of where the trunnion axis is located. After this period, the inertia forces induced by the recoil mechanism act for a considerably longer period of time than the gas period. The obvious solution is to locate the trunnion axis in the plane of the recoiling mass center. Except for the gas period, the firing torque is now always zero. But, as mentioned previously, this position may not be readily available. Under such conditions, it is advisable to locate the trunnion axis in the plane of the bore center because the large inertia forces and torques due to the propellant gas period appear only briefly, whereas the sustained load and corresponding torque during recoil are considerably smaller.

The fourth component of the torque on the elevating parts is that required to accelerate the tipping parts

$$T_a = I_t\alpha, \text{ N·m} \tag{4-5}$$

where

I_t = mass moment of inertia of the tipping parts about trunnions, kg·m^2
T_a = torque required to accelerate tipping parts, N·m
α = maximum elevating acceleration, rad/s^2.

TABLE 4-1
FIRING TORQUE T_f WITH MAXIMUM DISPLACEMENT OF TRUNNION AXIS ($a = 15d$, $b = 16d$)

F_g	F_a	aF_g	bF_a	T_f
$16K$	$15K$	$240Kd$	$240Kd$	0
$15K$	$14K$	$225Kd$	$224Kd$	Kd
$14K$	$13K$	$210Kd$	$208Kd$	$2Kd$
—	—	—	—	—
—	—	—	—	—
$2K$	K	$30Kd$	$16Kd$	$14Kd$
K	0	$15Kd$	0	$15Kd$
0	$-K$	0	$-16Kd$	$16Kd$

TABLE 4-2
FIRING TORQUE T_f WITH INTERMEDIATE DISPLACEMENT OF TRUNNION AXIS ($a = 7d$, $b = 8d$)

F_g	F_a	aF_g	bF_a	T_f
$16K$	$15K$	$112Kd$	$120Kd$	$-8Kd$
$15K$	$14K$	$105Kd$	$112Kd$	$-7Kd$
$14K$	$13K$	$98Kd$	$104Kd$	$-6Kd$
—	—	—	—	—
—	—	—	—	—
$9K$	$8K$	$63Kd$	$64Kd$	$-Kd$
$8K$	$7K$	$56Kd$	$56Kd$	0
$7K$	$6K$	$49Kd$	$48Kd$	Kd
—	—	—	—	—
—	—	—	—	—
$2K$	K	$14Kd$	$8Kd$	$6Kd$
K	0	$7Kd$	0	$7Kd$
0	$-K$	0	$-8Kd$	$8Kd$

THIS DOCUMENT PROVIDED BY THE ABBOTT AEROSPACE
TECHNICAL LIBRARY
ABBOTTAEROSPACE.COM

The general expression for maximum torque T_E at the elevating arc is

$$T_E = T_a + T_b + T_f + T_e, \text{ N·m.} \tag{4-6}$$

In summary, for a level weapon that is elevated manually and not firing, $T_a \approx 0$ because accelerations are negligible and $T_f = 0$. Therefore,

$$T_E = T_b + T_e, \text{ N·m.} \tag{4-7}$$

For a weapon elevated by mechanical or electric power, but not firing,

$$T_E = T_a + T_b + T_e, \text{ N·m} \tag{4-8}$$

because $T_f = 0$.

Example 4-1:

Determine the characteristics—T_a, T_b, and T_E—for an elevating mechanism, based on the following data:

W_t = 62,275 N, weight of tipping parts
F_t = 222,400 N, load on both trunnions
T_e = 3030 N·m, unbalanced equilibrator moment
I_t = 241,520 kg·m^2, mass moment of inertia of tipping parts about trunnions
r_b = 0.0762 m, trunnion bearing radius
μ = 0.01, coefficient of friction
α = 0.10, rad/s^2, elevating acceleration
ω = 0.262 rad/s, maximum elevating velocity.

Solution:

From Eq. 4-5

$$T_a = 241{,}520 \times 0.10 = 24{,}152 \text{ N·m.}$$

From Eq. 4-2

$$T_b = 0.01 \times 222{,}400 \times 0.0762 = 169.5 \text{ N·m.}$$

From Eq. 4-8

$$T_E = 24{,}152 + 169.5 + 3030 = 27{,}351.5 \text{ N·m}$$

which is the required torque at the elevating arc.

Precision in weapon positioning can only be obtained by eliminating backlash in gear devices. There are two different ways of controlling backlash in gears. One involves specifying fine precision for manufacture of the gears, and the other uses design techniques to reduce backlash between gears of lower precision (Ref. 3). Some of the techniques are described in par. 4-2.2.2.

4-1.2.2 Clutches and No-Back Devices

Equilibrators are designed to reduce static forces on the elevating mechanism. Perfect equilibration, however, is generally impossible. The residual imbalance must thus be balanced by the elevating strut. If friction in the elevating mechanism is low, it is possible that the gun tube will depress on its own due to static forces. More important, powder couples during firing of the weapon can produce forces in the elevating

THIS DOCUMENT PROVIDED BY THE ABBOTT AEROSPACE
TECHNICAL LIBRARY
ABBOTTAEROSPACE.COM

mechanism which would cause the weapon to move in elevation. Thus it is necessary to have no-back devices in the elevating mechanism that prevent the raising or lowering of the gun tube except by rotating the elevation handwheel.

Clutches are used to link the gear train to the handwheel and to control the amount of torque transmitted. Positive clutches, such as square jaw clutches, are recommended for systems that are stopped during clutch operation. This type of clutch is small for the power it is capable of transmitting, and fabrication costs are low. Friction clutches—including cone, disk, and ring clutches—are recommended for systems in motion so that torque may be applied gradually and thus reduce the possibility of sudden loading. Slip clutches, a type of friction clutch transmitting only a limited torque, are used in no-back installations to protect the elevating mechanism from large reverse torques. Much more sensitive than brakes or other clutches, the slip clutch relies upon fairly constant frictional resistance. Because the coefficient of friction of its rubbing surfaces is influenced by atmospheric conditions, its performance may become erratic.

A special irreversible clutch, called a Smith no-back device (shown in Fig. 4-5), transmits torque in either direction from handwheel to gear train but precludes a reversal of this activity. The driving and driven shafts have overlapping ends, and a segment extending past the diameter is cut from each. The void thus formed makes room for the spring-loaded locking bar, which is the shear member that transmits the handwheel effort. The shafts and bar rotate inside the lock ring that is keyed to the housing. The locking bar, with its ends slightly off-center, bears against the inner surface of the lock ring on the driveshaft side of the shaft axis. Held firmly between the shafts by a flat spring, the locking bar rotates with them in the direction of the applied torque. Torque from the handwheel moves the locking bar toward the center so that its longest dimension lies along the diameter and releases contact with the lock ring and permits both shafts to turn. Torque from the other end moves the bar off-center and jams it against the lock ring, which stops all motion. Since its capacity is limited, a slip clutch in the gear train between the no-back device and the tipping parts yields to any excessive torque to relieve the load on the no-back device and eliminates it as a lock for the whole elevating system.

No-back devices are available commercially. The weapon system designer is thus required only to specify the load on the device and then to choose the device of appropriate size from manufacturers' catalogues.

The usual location of the no-back device is at the base of each elevating screw assembly. Under dynamic conditions, such as firing, these devices may fail to hold due to the shaking forces induced in the strut assembly. This is usually due to loads that change from compression to tension.

The desirability of achieving a safe and automatic no-back device is clear: It requires no action on the part of the crew to prevent torque feedback to the handwheel. Problems with automatic no-back devices have arisen

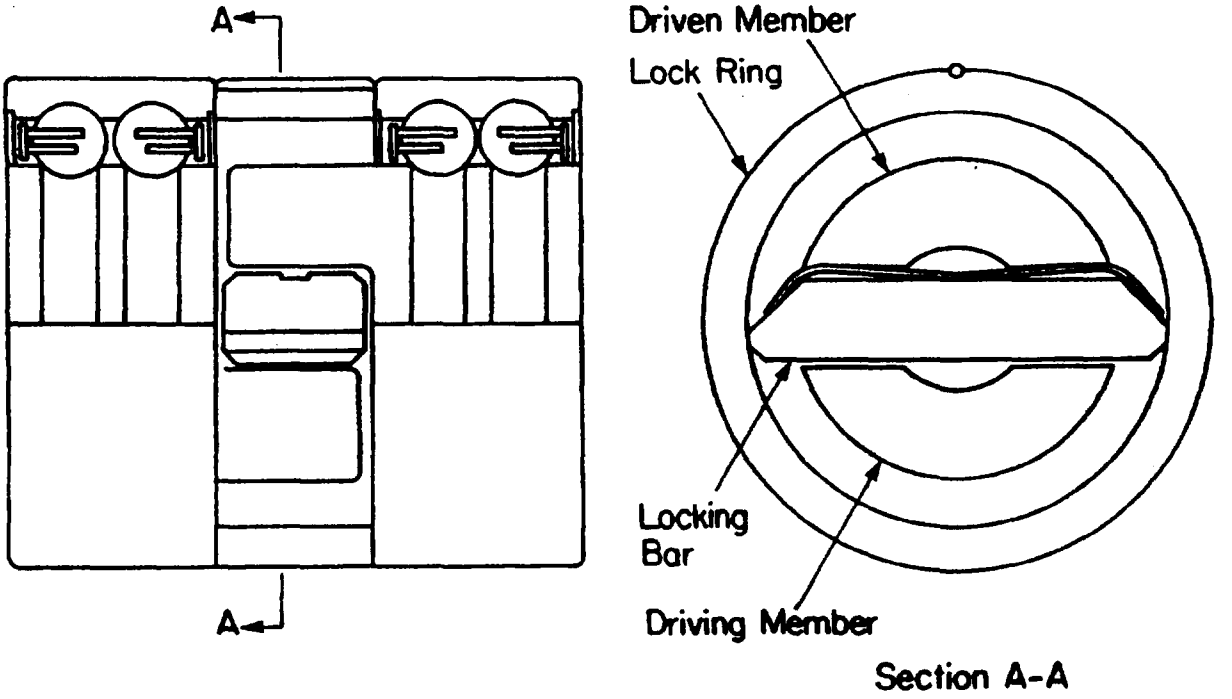

Figure 4-5. Smith No-Back Device

THIS DOCUMENT PROVIDED BY THE ABBOTT AEROSPACE
TECHNICAL LIBRARY
ABBOTTAEROSPACE.COM

in large caliber, high-impulse towed artillery systems such as the M198, 155-mm towed system. Large torques due to powder couple and vibration of lightweight, flexible carriage components in that application led to adoption of a mechanical clutch. The designer, therefore, must take great care in selecting a high-capacity no-back device that is not susceptible to vibration-induced slippage if he is to achieve reliable operation of an automatic no-back device.

4-1.2.3 Handwheels

Handwheels are normally circular, with a handle and a counterweight attached opposite to each other on the rim. Any structural material may be used including cast iron, steel, aluminum, or magnesium. Some handwheels are cut from plate stocks, others are cast. If the handwheel is of a dissimilar metal from the shaft to which it is attached, provision must be made to guard against galvanic corrosion.

Handwheels are designed on the basis of the physical effort required to overcome static loads and frictional resistance of the elevating system. Dynamics need not be considered because speeds are generally low. Much work has been done to determine a man's capacity for turning a handwheel. His best effort for sustained operation has generally been achieved while producing 5.65 N·m of torque at a turning radius of 0.18 m. For equipment that cannot meet these limits, handwheel force should not exceed 66.7 N. Where elevating loads are extreme, the mechanical advantage of the gear train must be increased to reach the required handwheel effort.

Handwheels, other sighting controls, and associated indicators must be located near each other to offer ready access and easy observation to the gunner. All manipulating equipment—such as wheels, handles, levers, and pushbuttons—must be large enough to be operated easily with gloved hands during cold weather operations. Folding handles on handwheels are highly desirable to prevent any inadvertent rotating of the handwheels by the crew and to minimize the chance of damage during towing.

Two-handed effort is conducive to smoother and more uniform operation and should be considered for large caliber weapons, provided that one hand is not needed to manipulate other controls simultaneously. The smoother action will be less tiring. It should be noted that the use of ball screws in elevating mechanisms reduces friction considerably and leads to lower handwheel loads. The lower force is required because the ball screw leads to less gear reduction and increases gun laying speed without increasing the total force required.

Although horsepower available from a motor-driven elevation drive dictates achievable elevation rates, maximum torque and the period of time a crew member can exert the torque are more critical for manually operated towed systems. For large caliber systems human factor guides should be consulted and tests planned to assure that elevation rates required can be met. A simple horsepower calculation generally is not adequate.

4-1.2.4 Cushioning of Peak Firing Loads

During firing of the weapon the components of the system experience large forces. To compensate for some of these forces, it may be necessary to have some cushioning built into assemblies such as the elevating mechanisms. One of the commonly used methods is to provide ring springs in the elevation strut.

Firing loads could also cause impulsive loads on gear drives used in the elevating mechanism. Thus it may be necessary to provide some form of slip clutch in the gear drive to absorb the shock loads. Functionally, slip clutches only allow a certain amount of torque to be transmitted, i.e., if the torque exceeds this level, the clutch slips.

4-1.2.5 Travel Locks

As explained in Chapter 3, components of a weapon experience large acceleration during cross-country transportation or airdrop. To avoid excessive loads on components, such as the elevating mechanism, due to large acceleration of the cradle and gun, it is necessary to provide travel locks. On modern weapons such as the 155-mm Howitzer, M198, a travel lock, such as that shown in Fig. 4-6, is used. It consists of a frame with members pinned on each side of the cradle. The other end of each member is pinned to the bottom carriage. The frame also has two cross members welded onto the pinned members. The joints at the bottom carriage have removable pins; to position the gun in elevation, these pins are removed.

A different device is used to lock the gun tube to the trail. A locking device, such as that shown in Fig. 4-7, consists of a cap pinned to a saddle, which is fixed on the trail. During travel the gun tube is clamped between the saddle and the cap to prevent transmission of large torques through the elevating mechanism or impact with the trail during travel.

THIS DOCUMENT PROVIDED BY THE ABBOTT AEROSPACE
TECHNICAL LIBRARY
ABBOTTAEROSPACE.COM

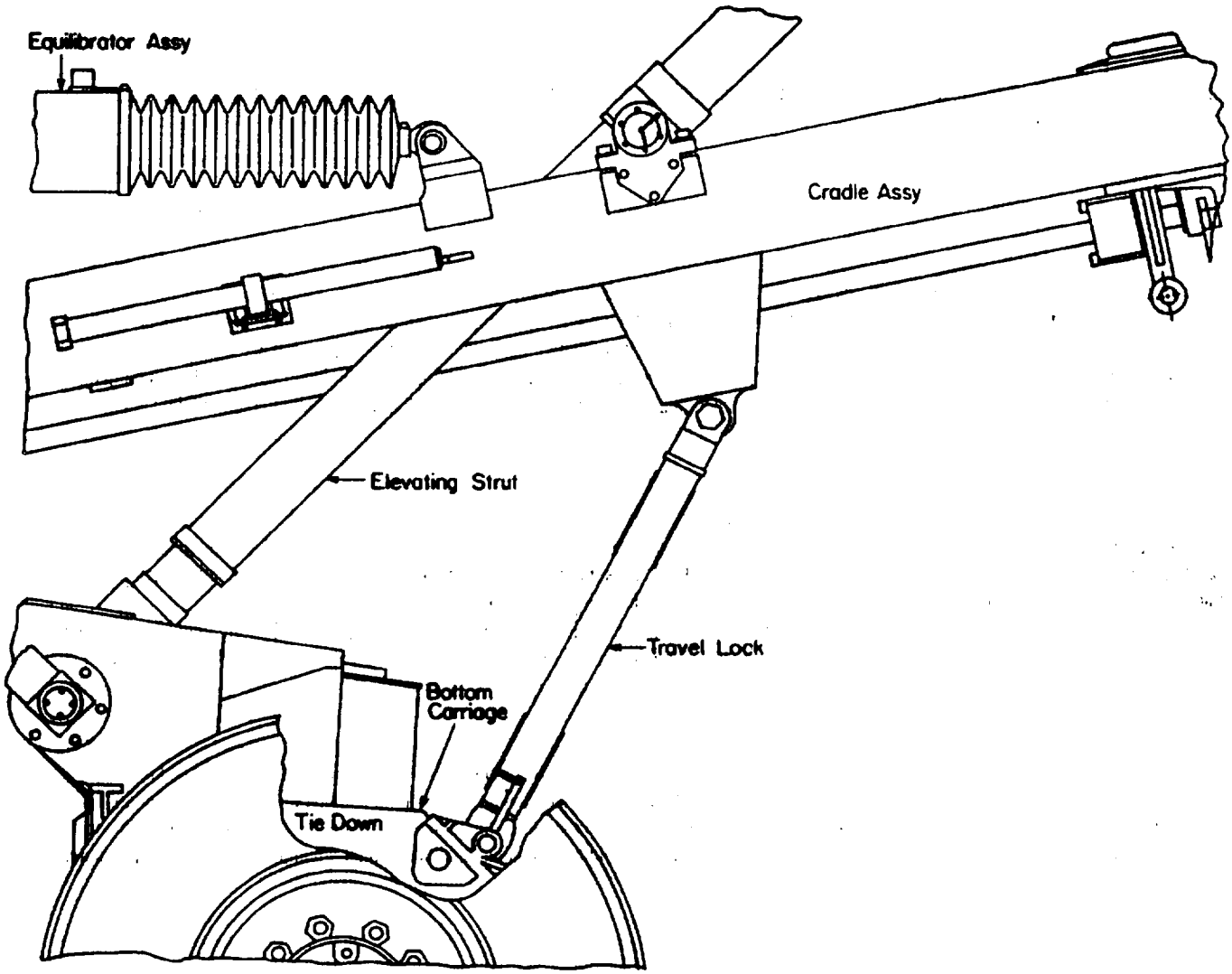

Figure 4-6. Travel Lock for Elevating Parts

THIS DOCUMENT PROVIDED BY THE ABBOTT AEROSPACE
TECHNICAL LIBRARY
ABBOTTAEROSPACE.COM

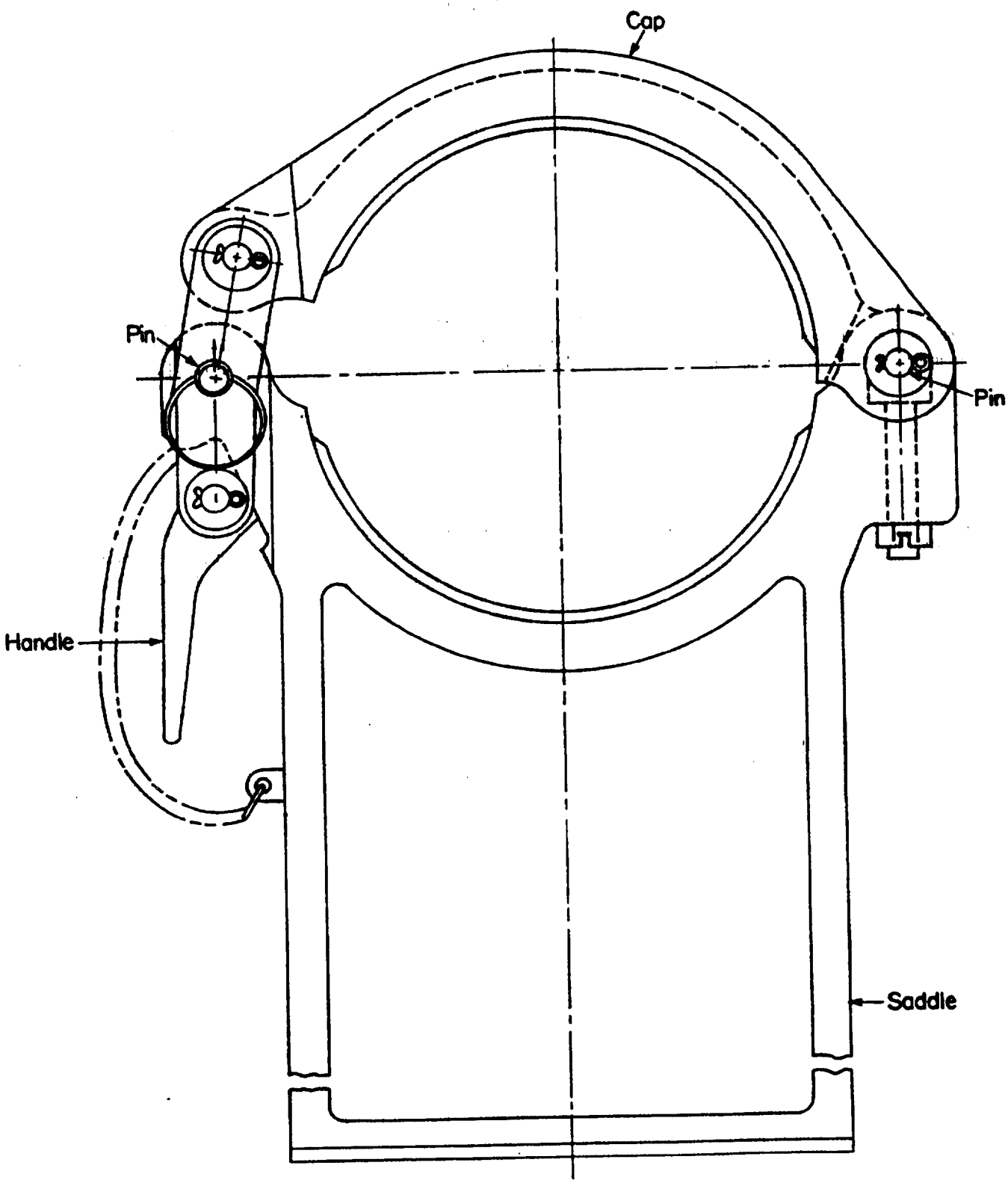

Figure 4-7. Gun Tube Travel Lock

THIS DOCUMENT PROVIDED BY THE ABBOTT AEROSPACE
TECHNICAL LIBRARY
ABBOTTAEROSPACE.COM

4-2 TRAVERSING MECHANISMS

4-2.1 TYPES OF TRAVERSING MECHANISMS

The long range of modern towed artillery systems requires extremely accurate weapon laying. Slight errors in pointing of the cannon can result in considerable deviation at the target. When aimed by direct sighting, a weapon must be moved slowly and precisely to align it accurately with the target. When aimed by a separate fire control unit, the cannon must be able to respond accurately to the direction signals of the unit. In either case, such a weapon is too heavy to be pushed by hand in the proper horizontal direction. Hence, a manual or power-operated mechanism is provided to enable a gunner to attain a precise position and to hold it during firing.

Heavy weapons such as the M198, 155-mm Howitzer have a manually operated, on-carriage traverse mechanism. Traversing of the weapon is achieved by rotating the top carriage, which supports the cradle and the gun, relative to the bottom carriage. Off-carriage traverse, as used on the M102 Howitzer shown in Fig. 4-8, has a roller at the rear end of the trails. The axis of the roller coincides with the longitudinal axis of the trails. Thus the weapon can be rotated about a pivot at the front end of the trails by rotating the roller and causing movement in azimuth.

For a weapon system with on-carriage traverse, components of the weapon that traverse are called traversing parts. They generally consist of the cannon and other tipping parts and the top carriage. The unit that controls rotation of the traversing parts and holds the cannon firmly in azimuth during firing is the traversing mechanism. For weapons with off-carriage traverse, the whole weapon traverses on the base plate to position the weapon in azimuth.

A full 360-deg traverse capability is desirable on all towed artillery systems. It is usually achieved by adopting off-carriage traverse—e.g., M102 and M204, 105-mm Howitzers. Only limited traverse is achieved with on-carriage traverse and split trails. Weapons with limited traverse, such as the M198 towed Howitzer,

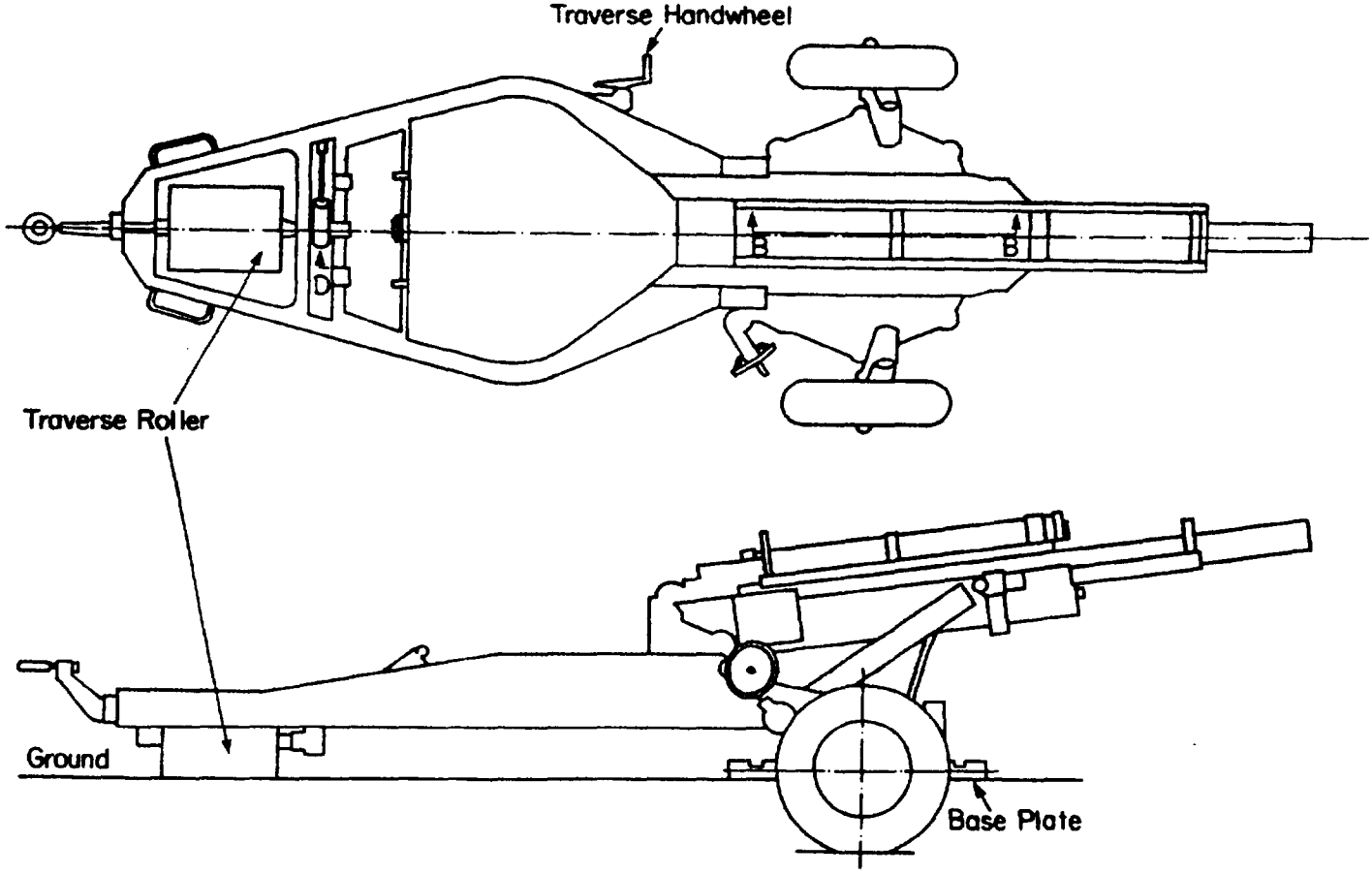

Figure 4-8. Off-Carriage Traverse for M102 Howitzer

THIS DOCUMENT PROVIDED BY THE ABBOTT AEROSPACE
TECHNICAL LIBRARY
ABBOTTAEROSPACE.COM

must be equipped with a hydraulic jack to provide a speed shift capability. The jack should be located near the weapon center of gravity to balance the weapon for speed shift by the crew.

Because of the close relationship between the forms of traverse mechanisms and the type of traverse bearing, traverse mechanisms are classified as

1. Pintle
2. Base rig and race
3. Roller
4. Axle
5. Ball joint.

Of these five types of traverse bearings, axle and ball joint are not used in modern weapon systems.

On all traversing mechanisms it is necessary to provide traversing handwheels on both sides of the weapon so that one- and two-man lay capability is provided. Weapons with off-carriage traverse usually have their traverse handles on one side of the trails. The handle is connected to the traverse roller by reduction gearing and shafts, connected by hook joints.

4-2.1.1 Pintle Traverse

A versatile mechanism that is adaptable to light weapons and provides a greater range of traverse is one in which the traversing parts pivot on the bottom carriage about a pintle. (See Fig. 4-9.) The pintle is attached to the top carriage and rotates in a bearing on the bottom carriage. The traversing parts are supported by a thrust bearing, and where clearances permit, 360-deg traverse is available. The stability of the weapon, however, usually determines this range. Weapons that are stable in all directions may have unlimited traverse; however, the split trail type is stable only within the spread of the trails, about 85-deg traverse, as shown in Fig. 4-10.

Three methods of actuation for a pintle traverse mechanism are described:

1. *Method A.* Power is transmitted through a gear train whose terminal member is the traversing gear, which may be either a large worm wheel or a spur gear. Two installations are available. The first (Fig. 4-11) has the driving gear on the bottom carriage and the traversing gear (driven) on the top carriage. Alternatively, the

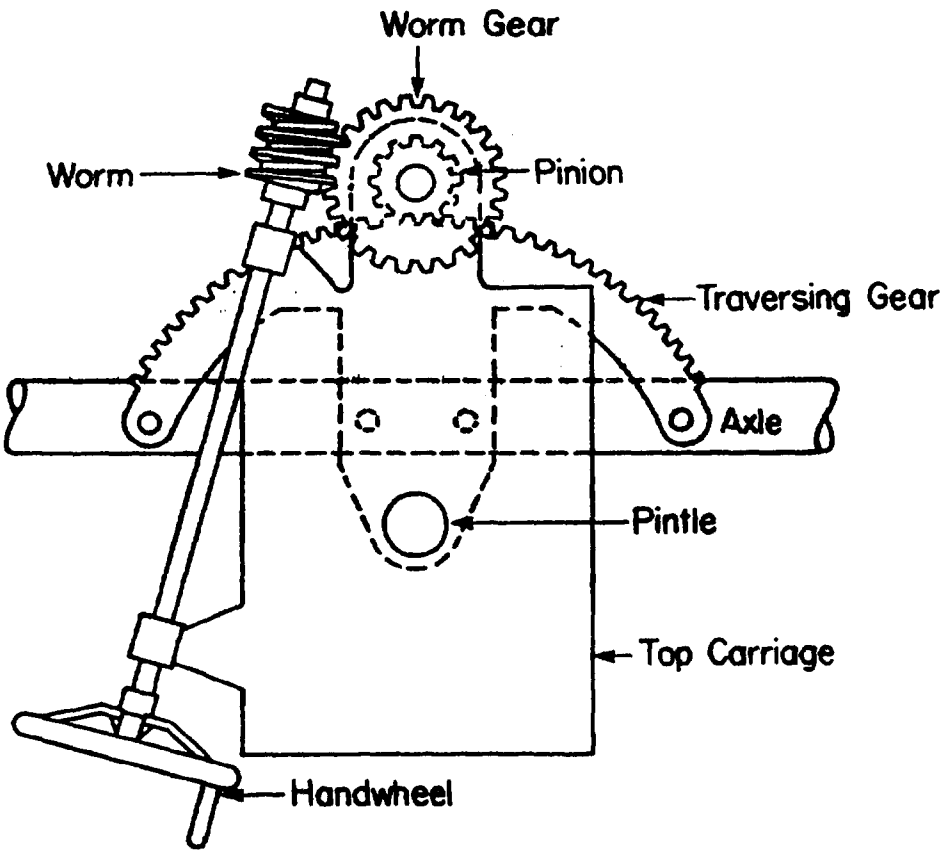

Figure 4-9. Pintle Traverse

THIS DOCUMENT PROVIDED BY THE ABBOTT AEROSPACE
TECHNICAL LIBRARY
ABBOTTAEROSPACE.COM

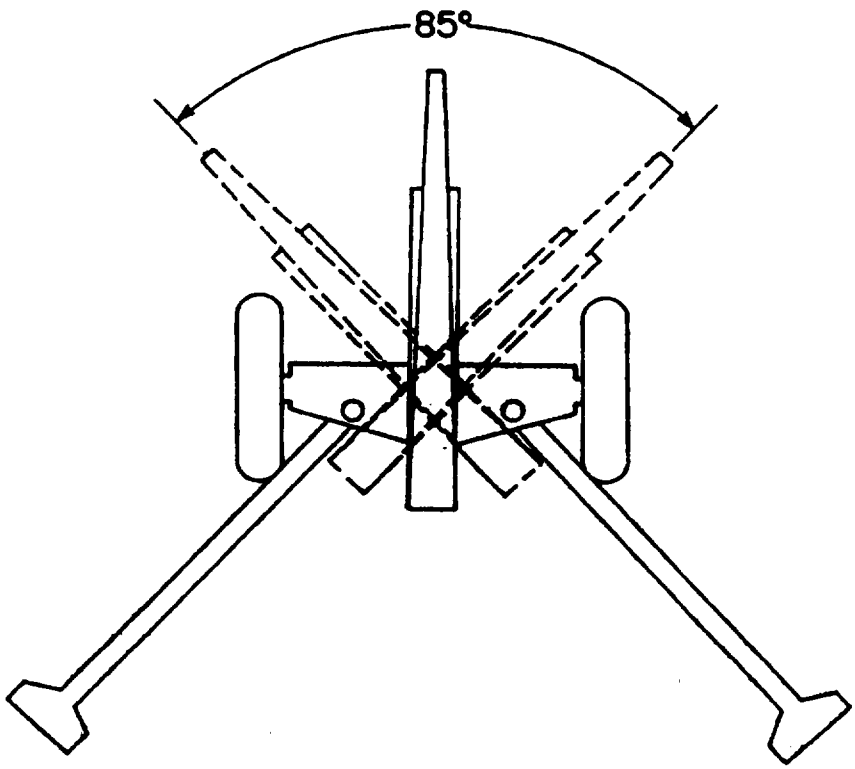

Figure 4-10. Split Trail Mount Showing Traversing Range

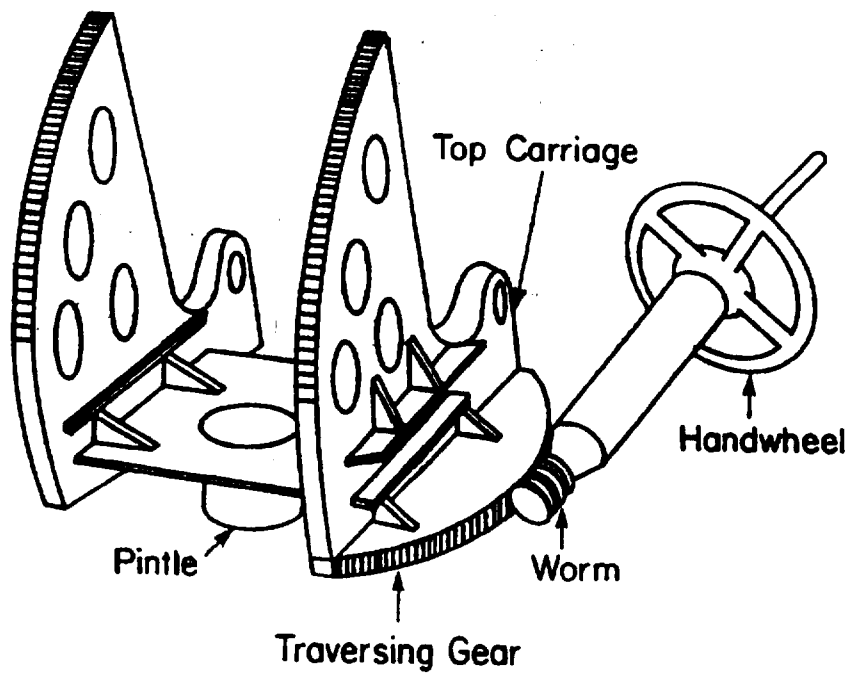

Figure 4-11. Traversing Mechanism With Gear on Top Carriage

THIS DOCUMENT PROVIDED BY THE ABBOTT AEROSPACE
TECHNICAL LIBRARY
ABBOTTAEROSPACE.COM

driving gear can be mounted on the top carriage, and the traversing gear mounted on the bottom carriage (Fig. 4-12). This second arrangement permits unlimited traverse and, with the gunner moving with the traversing parts, direct sighting is more convenient. If high traversing speeds are necessary, the gear train is powered mechanically or electrically as shown in Fig. 4-13. If high speeds are unnecessary, or in the event of power failure, manual action is provided through a handwheel.

2. *Method B.* A variation of the pintle-type traversing gear consists of a screw-nut combination that pivots on the bottom carriage near the handwheel, as shown in Fig. 4-14. The screw, turned by the handwheel, and nut pivot on the top carriage as it traverses about the pintle. Such an arrangement, however, is very limited in traverse range and is inherently lacking in rigidity.

3. *Method C.* Manually operated traversing mechanisms are relatively slow, but rapid traverse can be achieved with those weapons having a low frictional resistance of the pintle mounting. Rapid coarse traverse is available by simply disengaging the gear train and swinging the weapon by hand until pointed in the direction desired. Reengaging the gears reverts the system to its fine traverse state.

4-2.1.2 Base Ring and Race Traverse

Weapons with heavy traversing parts require large traversing bearings to supplement a broad firing base. (See Fig. 4-15.) These weapons are trained by rotating the top carriage on a base ring that is equipped with either ball or roller bearings. A large spur gear mounted on the bottom carriage, concentric with the bearing ring, serves as the traversing gear. Its pinion is mounted on the traversing parts. As the pinion turns, it tracks around the traversing gear and carries with it the top carriage and cannon. This arrangement provides unlimited traverse and can be powered either mechanically or electrically.

The top and bottom carriages are connected through the traverse bearing. Thrust and moment acting through the bearing thus act on the flexible top and bottom carriage structures. These two components, therefore, must be designed for adequate stiffness to prevent excessive twist. Design of the top carriage and bottom carriage for stiffness is carried out by the procedure described in Chapters 8 and 9, respectively.

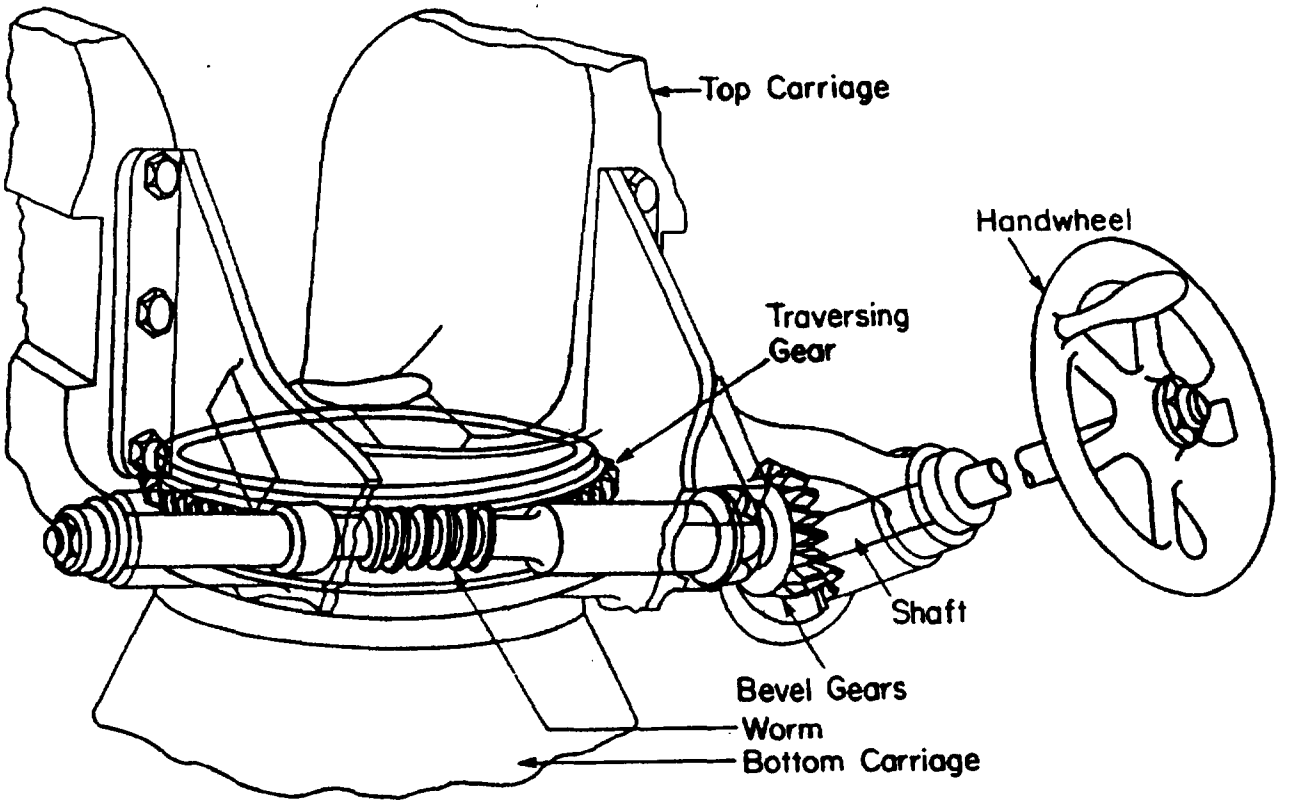

Figure 4-12. Manually Operated Traversing Mechanism

THIS DOCUMENT PROVIDED BY THE ABBOTT AEROSPACE
TECHNICAL LIBRARY
ABBOTTAEROSPACE.COM

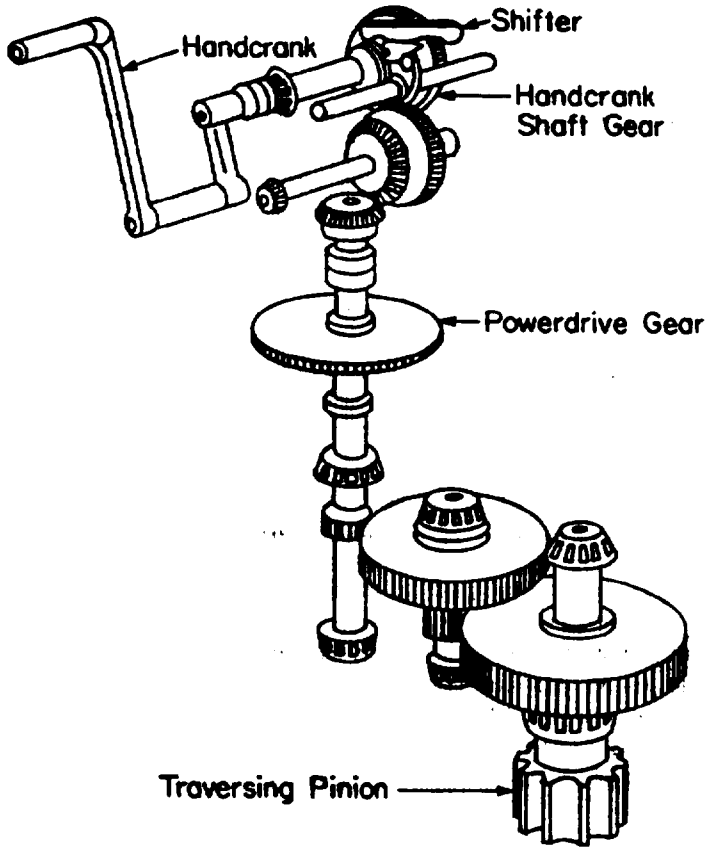

Figure 4-13. Powered Traversing Mechanism

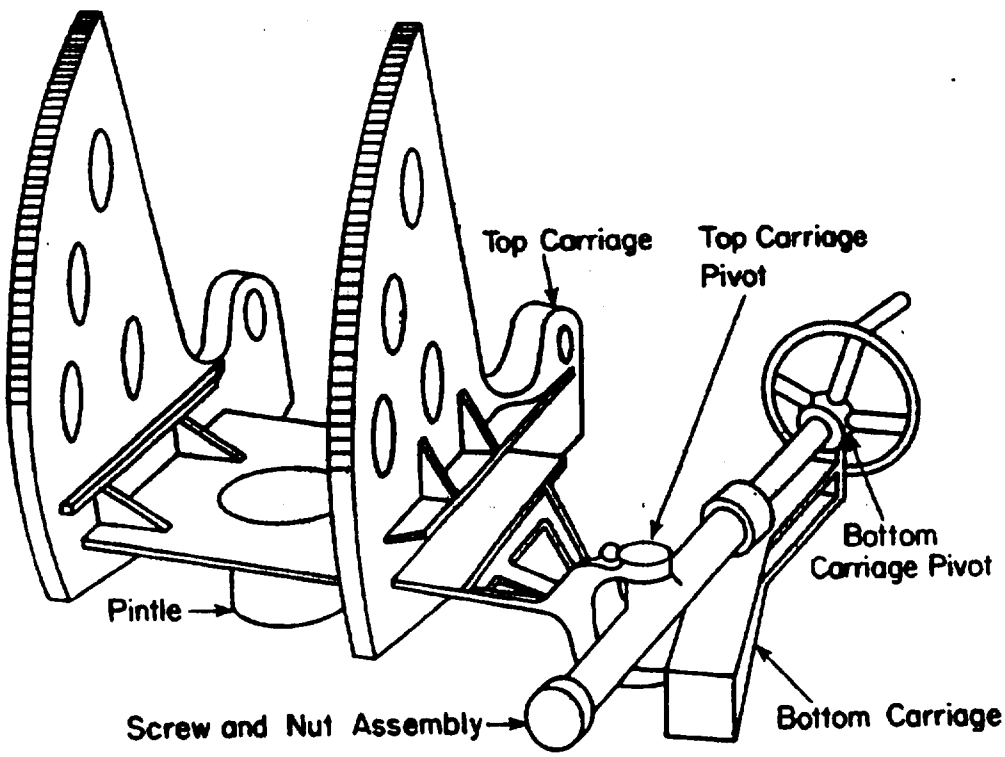

Figure 4-14. Screw and Nut Traversing Mechanism

THIS DOCUMENT PROVIDED BY THE ABBOTT AEROSPACE
TECHNICAL LIBRARY
ABBOTTAEROSPACE.COM

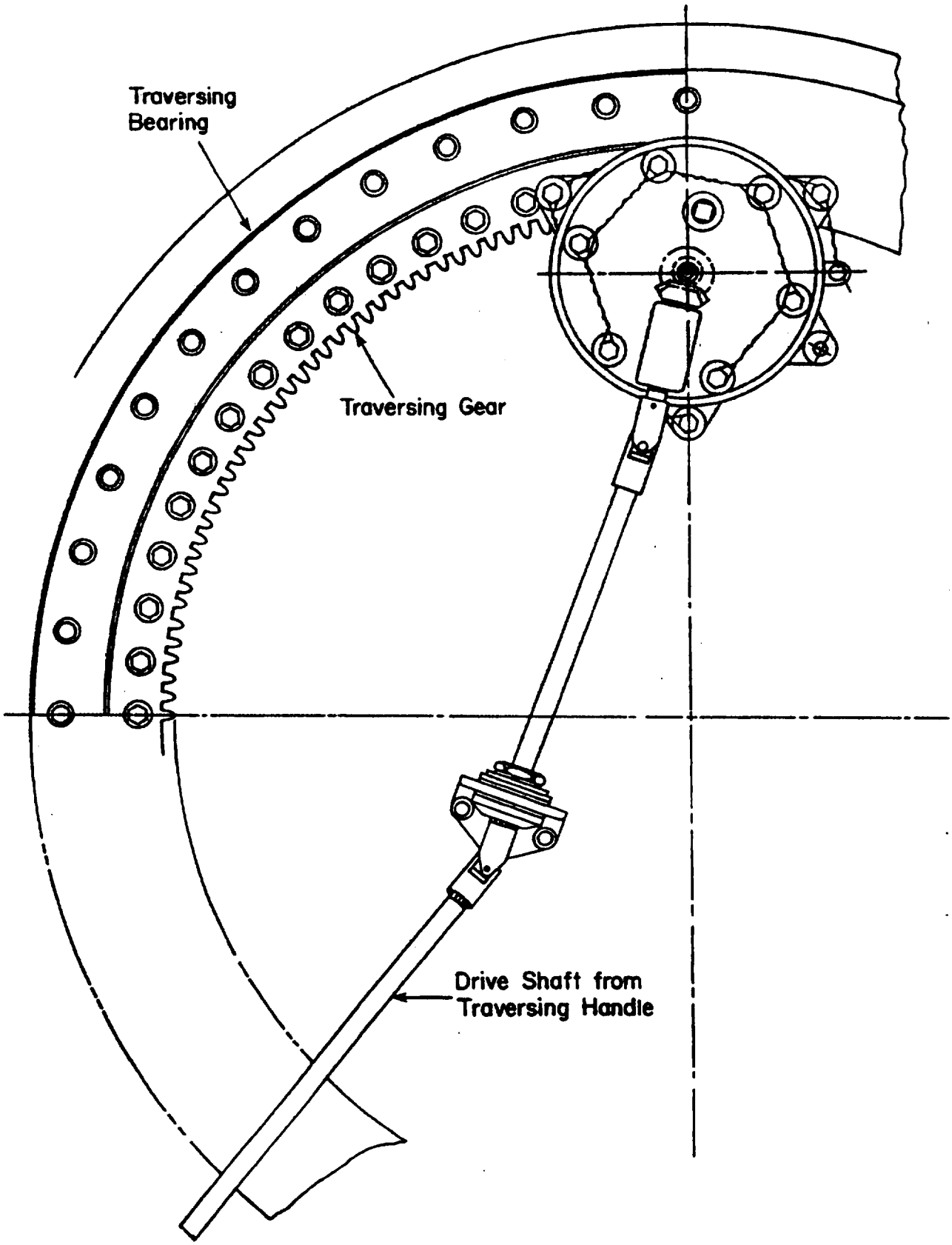

Figure 4-15. Traversing Mechanism for M198 Howitzer

THIS DOCUMENT PROVIDED BY THE ABBOTT AEROSPACE
TECHNICAL LIBRARY
ABBOTTAEROSPACE.COM

4-2.1.3 Off-Carriage Traverse

For full 360-deg traverse, off-carriage traverse systems—such as the M102, 105-mm Howitzer shown in Fig. 4-8—have come into use. Fine traverse adjustment is provided by a gearing and universal joint system that transmits traverse handwheel rotation to rotation of the traverse roller. The traverse roller then rolls on the ground and pivots the weapon about a pintle bearing in the base plate. Rapid traverse is accomplished by disengaging the handwheel gear and allowing the crew to push the trails laterally through large angles manually, with the traverse roller rotating freely.

In principle, both single and double roller configurations are possible, the double roller acting as a split trail. However, problems with weapon cant with two widely spaced rollers on uneven terrain favor the single roller configuration. The single roller configuration, unlike the split trail with its two-point contact, has only single-point contact of the trail with ground at the roller. Thus lateral stability of the weapon must be provided by the bearing between the carriage and base plate. This may be accomplished with a pintle bearing between the carriage and base plate. It may also be accomplished by a ball joint with an off-axis stud on the carriage which rides in a circular groove in the base plate. To prevent tipping, the stud and groove must be designed to provide both tensile and compressive force. Due to problems of keeping such a groove clean in a field environment, the pintle bearing design is preferred.

Because the roller bears on the ground during traverse, soil conditions and the vertical load carried by the roller influence the handwheel load required to traverse the weapon. An experimental study with the M102, 105-mm Howitzer, varying the load on the roller, has provided quantitative data for several soil conditions (Ref. 4). Fig. 4-16 is a plot of handwheel force—for concrete, mud, and sand for the M102 system—versus traverse roller load. As might be expected, sand is the most critical soil condition. Fig. 4-17 is a plot of crew

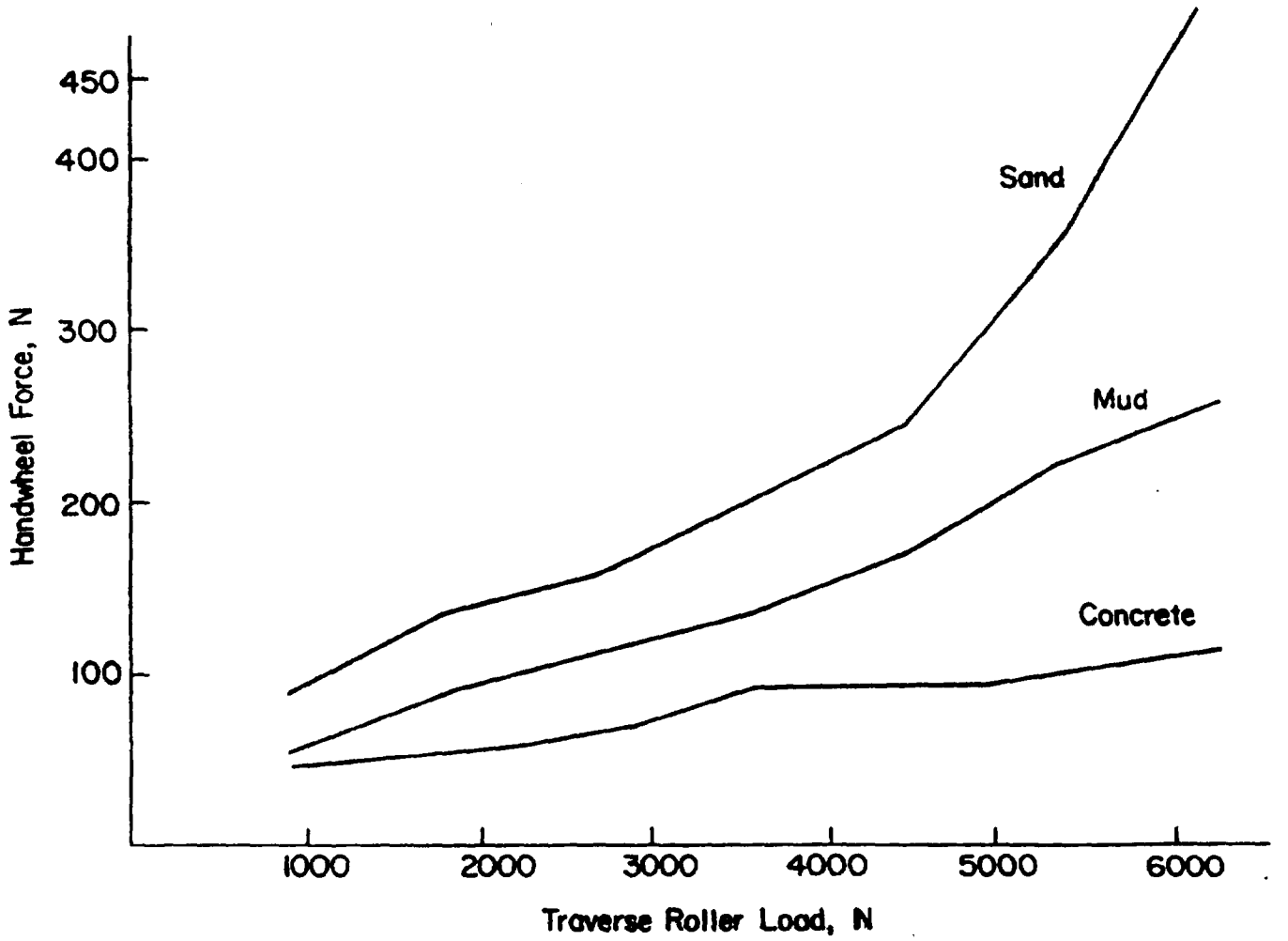

Figure 4-16. Handwheel Force vs Roller Load

THIS DOCUMENT PROVIDED BY THE ABBOTT AEROSPACE
TECHNICAL LIBRARY
ABBOTTAEROSPACE.COM

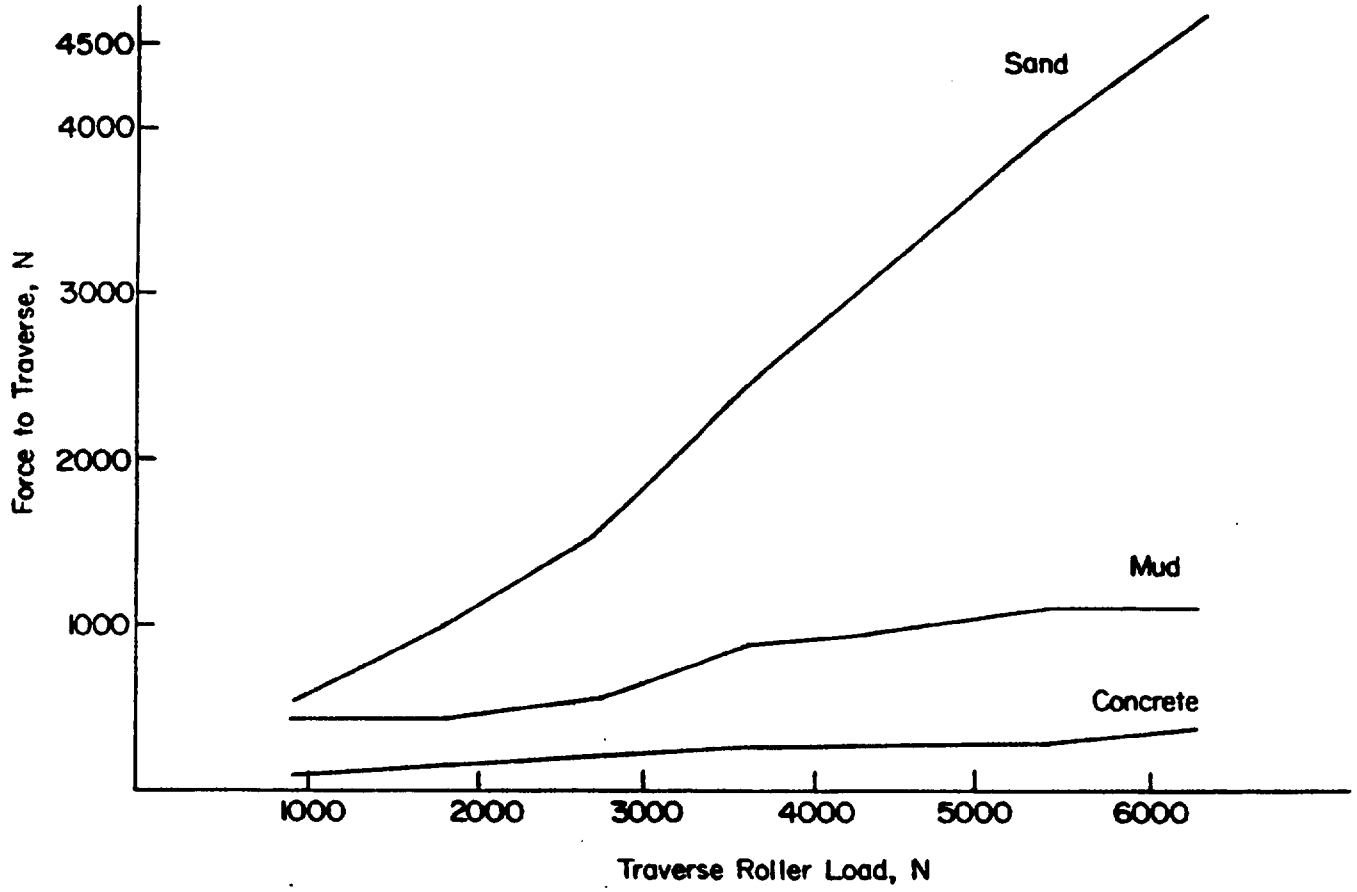

Figure 4-17. Traverse Force vs Roller Load

force required at the roller versus traverse roller load for the same soil conditions. As concluded in Ref. 4 feasibility of the roller-type off-carriage traverse system is limited to lightweight towed systems.

Design of the traverse gearing system is heavily dependent on the force required to traverse the weapon through the roller. Once the roller load is known, roller torque required can be determined by using data of the kind given in Figs. 4-16 and 4-17. Once the required roller torque is known, the gear ratio and traverse handwheel diameter may be selected.

In addition to gear design, universal joints are often required to transmit shaft rotation through the interior of a curved box trail (Fig. 4-8) to the traverse roller.

4-2.2 TRAVERSING MECHANISM COMPONENTS

4-2.2.1 Gear Trains

The gear train, no matter how simple, is the principal part of the traversing mechanism and must satisfy several basic design requirements. Its gear ratio should be considered first. Not only does the gear ratio prescribe the effort at the source, it also limits sensitivity. A high gear ratio means slow traverse with respect to applied motion. A low ratio means correspondingly faster traverse. Although a high gear ratio demands a low torque output from the power source, the power requirements alone are unaffected. For example, assume that the torque at the traversing gear, incorporating the efficiency of the gear train, is 271 N·m. For slow traverse a gear ratio of 60:1 reduces it to 4.5 N·m at the handwheel. A ratio of 30:1 reduces it to 9.0 N·m.

Design of gear trains is discussed in par. 4-1.2.1; however, traversing mechanisms place some additional performance requirements on the gear trains. These requirements are discussed here. The design of the gear train involves some trial and error procedure, particularly if mechanically powered, because preliminary estimates of both efficiency and inertia must be made. Only efficiency needs to be estimated for manually operated gear trains. Final computed data must agree reasonably well with the estimates before the preliminary results are acceptable. In short, the torque and power required to move the traversing parts, including the moving components of the traversing mechanism, must not exceed the available effort at the handwheel.

THIS DOCUMENT PROVIDED BY THE ABBOTT AEROSPACE
TECHNICAL LIBRARY
ABBOTTAEROSPACE.COM

Design data are computed from the statics and dynamics of the moving masses. Data on statics include the weight moment about the traversing axis and the torque due to frictional resistance of the traverse bearing. If the weapon is on a slope and the center of gravity of the traversing parts is not on the axis (See Fig. 4-18.), the moment M_w due to weight of parts is

$$M_w = W_{tr} R_t \sin\theta_t \cos\phi_a, \text{ N·m} \tag{4-9}$$

where

W_{tr} = weight of traversing parts, N
R_t = radius of traversing axis to CG, m
θ_t = slope of terrain, rad
ϕ_a = location of CG with respect to horizontal line in plane parallel to slope, rad.

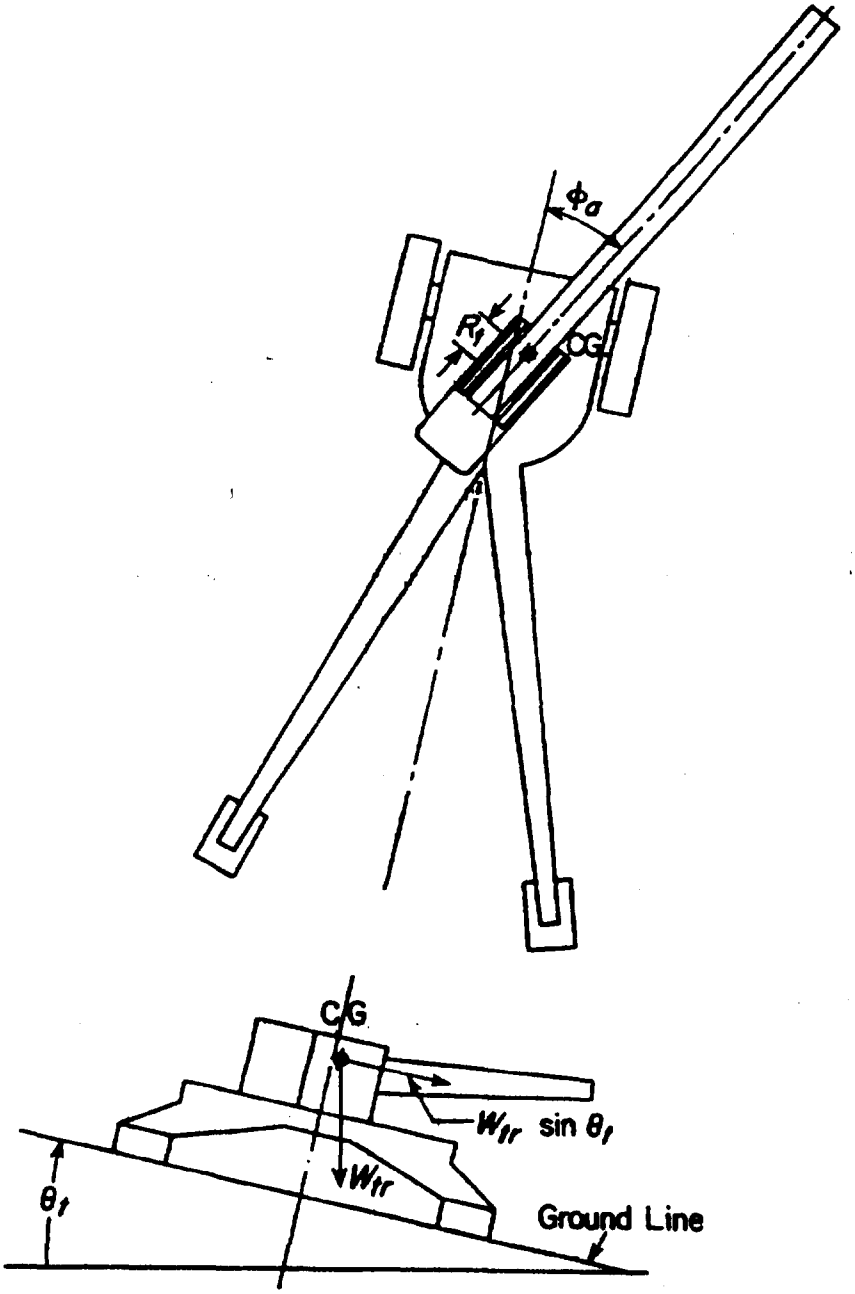

Figure 4-18. Weight Moment Diagram

THIS DOCUMENT PROVIDED BY THE ABBOTT AEROSPACE
TECHNICAL LIBRARY
ABBOTTAEROSPACE.COM

On level terrain or if leveling devices are used, θ_t and M_w are zero. Otherwise, M_w may become appreciable and reach a maximum when ϕ_e equals zero. The static frictional torque T_b occurs in the traverse bearing and is

$$T_b = \mu F_{br} R_\mu, \text{ N·m} \tag{4-10}$$

where

F_{br} = total normal force on traversing bearing, N

$$R_\mu = \frac{2}{3}\left(\frac{r_o^3 - r_i^3}{r_o^2 - r_i^2}\right) = \text{frictional radius, m (See Ref. 5.)} \tag{4-11}$$

r_i = inside radius of bearing, m
r_o = outside radius of bearing, m.

Due to the presence of recoil force, F_{br} increases appreciably, and, thereby, increases the torque T_b.

Another component of the torque at the traversing gear, the firing couple, is generated during firing and is due to the eccentricity of the recoiling parts about the traversing axis. As shown in Fig. 4-19, the component of the firing couple affecting traverse is

$$T_t = (a_K F_g - b_K F_a)\cos\theta, \text{ N·m} \tag{4-12}$$

where

T_t = torque on traverse bearing due to firing couple, N·m
a_K = perpendicular distance between recoil force vector K and propellant gas force vector F_g, m
b_K = perpendicular distance between recoil force vector K and vector F_a of inertial forces of recoiling parts, m
θ = angle of elevation, rad.

Careful design should hold this torque to a minimum. The object is to have the bore center, traversing axis, and mass center of the recoiling parts lie in a vertical plane, but this alignment is not always possible. Space

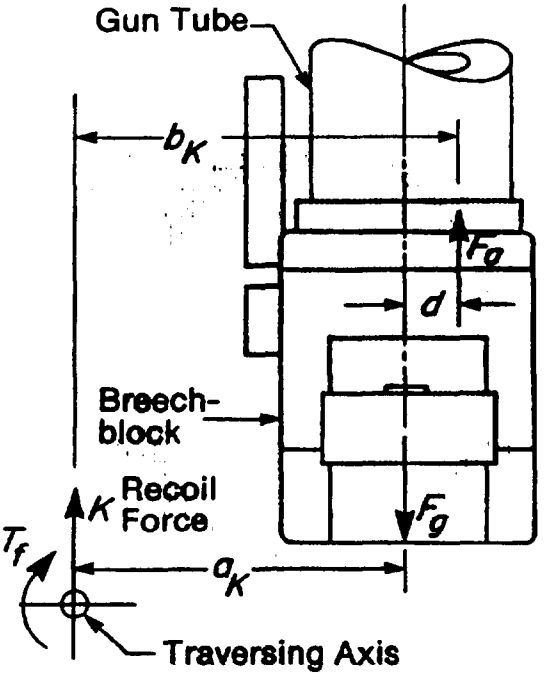

Figure 4-19. Traverse Firing Couple Diagram

THIS DOCUMENT PROVIDED BY THE ABBOTT AEROSPACE
TECHNICAL LIBRARY
ABBOTTAEROSPACE.COM

limitations and required structural locations may cause an unequal distribution of weight and create an imbalance about the bore axis. Regardless of the care exercised, manufacturing tolerances may augment this imbalance. The inertia forces of the unbalanced weight produce the firing couple. If the traversing gear train is subject to the firing torque, the effect may be significant. If locked out by any means, only the gears between the traversing gear and locking device will be disturbed.

The conventional worm gear drive used in traverse systems for towed artillery weapons has been largely replaced by a new design. Conventional worm gears offer fairly large gear reduction in a relatively small space and are self-locking; however, as in the case of an Acme screw, the self-locking worm gear has an efficiency of only about 50%. A new design that may be considered employs a unit called a Harmonic Drive, Fig. 4-20, in which a wave generator (which may be manufactured in many configurations) imparts an ellipse-like shape to a nonrigid flexspine, which is normally the output member of the unit. The shape imparted to the flexspine by the input member (wave generator) causes it to rotate slowly and leads to a reduction of 200:1 or more in a relatively small package. The advantage is a large gear reduction with low friction. The unit, however, is not self-locking.

Accuracy of the weapon depends to a great extent on the precision of its traversing mechanism; accordingly, loosely meshed gears cannot be tolerated. A small amount of backlash is, however, required to reduce friction, to compensate for thermal expansion, and to allow for manufacturing tolerances. Thus some form of antibacklash gearing is needed to meet system accuracy requirements.

Careful machining will hold backlash to a minimum. If extremely tight gearing is required, gears can be assembled tightly or even with a slight interference and then "run-in". For small gears, a light oil is generally used for the run-in process. For large gears, a mixture of household cleanser and water or a mixture of grinding compound and oil may be used. If the cost is justified, some gears may be mounted on adjustable centers. After being fitted, the assembly is doweled into place. Even these techniques, however, do not eliminate backlash indefinitely because wear will eventually cause some play between the gear teeth.

4-2.2.2 Antibacklash Devices

Antibacklash devices are designed to minimize or eliminate play between gear teeth. These devices work on the principle of preloading the last gear in the train in two directions so that tooth contact is always present regardless of the direction of motion. Fig. 4-21 shows two spring-loaded, concentric gears, A and B, on the same shaft. Gear A is keyed and gear B is free to turn, but both mesh at the same point with gear C. The springs induce a torque that tends to turn the gears in opposite directions; this turning loads two adjacent teeth on gear C in opposite directions. Backlash is precluded only when the induced spring torque is larger than the applied

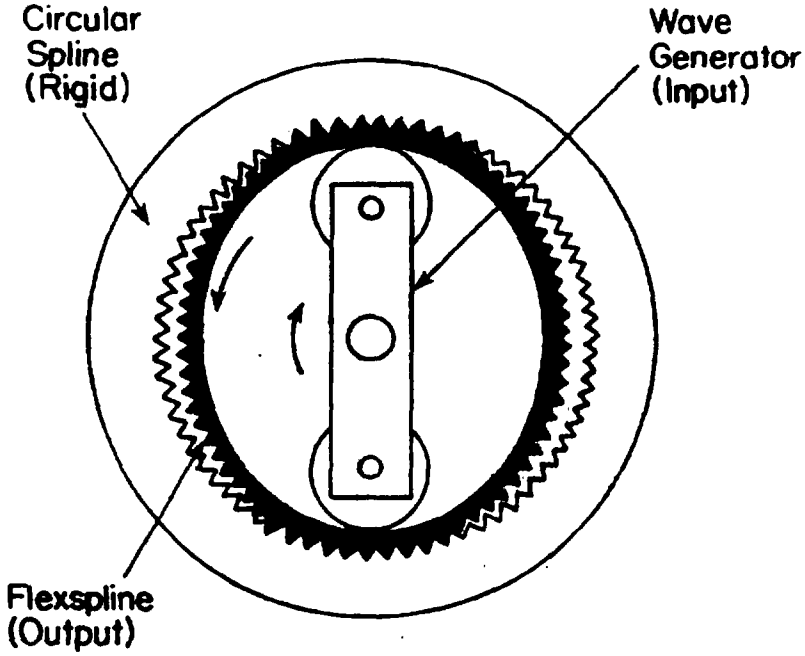

Figure 4-20. Schematic Diagram for Harmonic Drive

THIS DOCUMENT PROVIDED BY THE ABBOTT AEROSPACE
TECHNICAL LIBRARY
ABBOTTAEROSPACE.COM

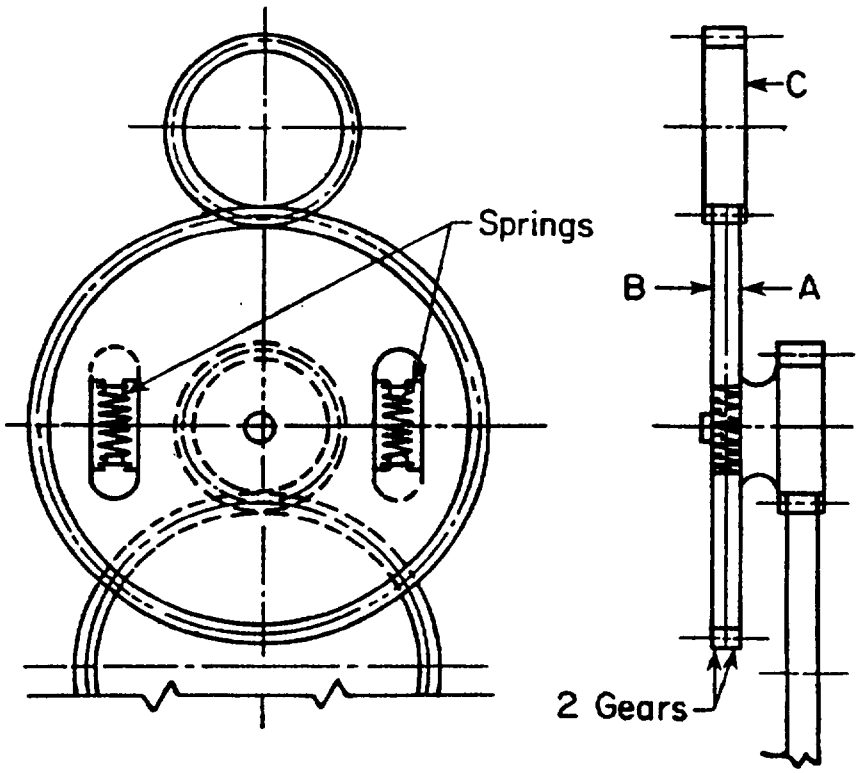

Figure 4-21. Antibacklash Device, Tangential Spring Type

torque of gear A. Because of limited spring loads, this type is suited only for small gearing and is used extensively in indicator gear trains.

Antibacklash devices requiring relatively light spring loads are also available for large gearing. (See Fig. 4-22.) For this type a coil spring provides an axial force to load the helical gear serving each pinion. The gear teeth convert the small axial load into large tangential components that provide the torque necessary to keep the traversing pinions in contact with the traversing gear at all times. The torque T_s at the spring-loaded pinion is

$$T_s = \frac{F_s}{\tan\lambda} R_p, \text{ N·m} \qquad (4\text{-}13)$$

where

F_s = spring load, N
R_p = pitch radius of the spring-loaded pinion, m
λ = helix angle, rad.

To be effective, this torque must exceed that applied through the traversing mechanism by the power source.

For example, using these techniques, backlash in gearing on the M198 Howitzer is of the order of 0.076 mm to 0.127 mm.

4-2.2.3 Clutches and No-Back Devices

Locking and no-back devices perform two functions. First, as a control measure, they hold the traversing parts in a fixed position during firing by resisting any unbalanced couples that tend to rotate the traversing parts. Second, as a safety measure, they prevent these same couples from reversing through the gear train to spin handwheels, which would endanger personnel. The simplest locking device may be a component of the gear train, namely, the irreversible worm. It should be near the traversing gear in the gear train sequence to protect gears that are designed for lighter loads from the excessive loads that occur during firing and recoil.

THIS DOCUMENT PROVIDED BY THE ABBOTT AEROSPACE
TECHNICAL LIBRARY
ABBOTTAEROSPACE.COM

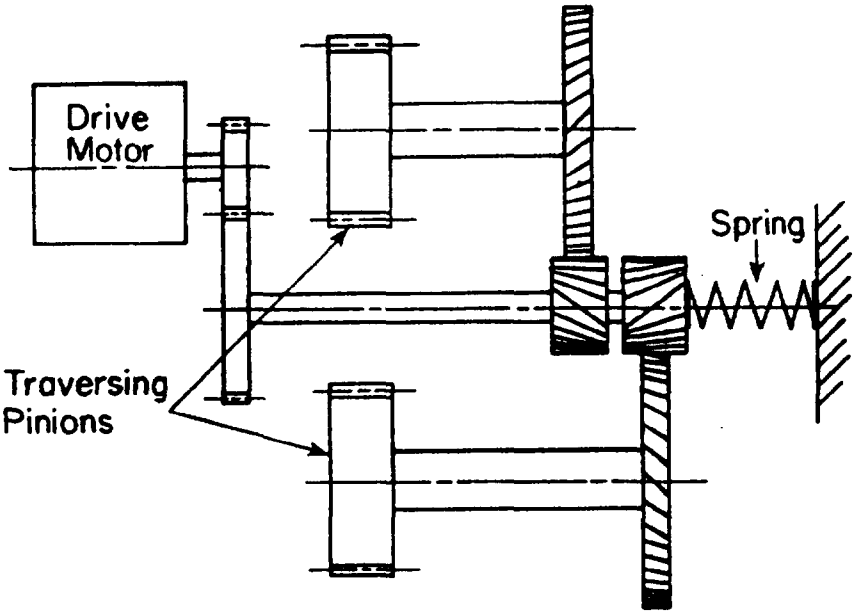

Figure 4-22. Antibacklash Device, Axial Spring Type

A gear train without an irreversible feature, such as the self-locking worm, must rely on brakes to hold the traversing parts. A brake may appear anywhere in the gear train, its capacity being governed by its proximity to the traversing gear. A large brake is needed when it is adjacent to this gear, where torques are high, whereas a relatively small brake is needed near to the handwheel, where torques are low. If near the traversing gear, a brake will relieve the gear train of some dynamic loads. Cost comparisons and availability of space determine whether brakes are to be large and gears small or whether brakes are to be small and the gears relatively large. Special couplings, such as the Smith no-back device, permit torque transmission in either direction from the handwheel to the gear train but preclude a reversal of this activity. Operation and design of these devices are described in par. 4-1.2.2.

Clutches may be used in traversing mechanisms to control the amount of torque transmitted and to disengage the gearing to allow manual rapid traverse. Considerations in par. 4-1.2.2 are valid for traversing clutches.

An additional comment on slip clutches in traversing mechanisms is in order. It the slip clutch is installed near the source of the reverse torque, the gear train does not become burdened with its own inertia. The advantage of lower gear loads obtained here is offset by the large and costly clutch required to transmit a large operating torque. On the other hand, if placed near the low-torque, high-speed end of the gear train, a much smaller and less costly clutch is needed to generate the required low frictional resistance. The advantage gained may compensate for the somewhat larger capacity gears required to carry the additional inertial loads.

4-2.2.4 Handwheels

The handwheels used in traversing mechanisms are similar to those in elevating mechanisms described in par. 4-1.2.3. The only difference is that human factors considerations indicate that the handwheel force for traversing mechanisms should be limited to 53 N.

It is desirable to plabe traversing handwheels on both sides of all towed systems to provide both one- and two-man lay capability. Traversing mechanism operation should be smooth and continuous throughout the entire traverse range. Folding handles on both traverse and elevating handwheels are desired by the user.

4-2.2.5 Travel Locks

A positive travel lock must be provided that secures the traversing parts during transport operations. This lock protects the traversing system from transport loads and severe shocks that may occur during weapon movement over uneven terrain and airdrop operation.

Clutches and no-back devices used in traversing mechanisms are similar to those used on elevating mechanisms discussed in par. 4-1.2.2.

THIS DOCUMENT PROVIDED BY THE ABBOTT AEROSPACE
TECHNICAL LIBRARY
ABBOTTAEROSPACE.COM

4-3 WEAPON-LOWERING AND -RAISING MECHANISMS

Weapon firing stability requires that a firing base attached to the bottom carriage support the weapon on the ground. Two alternative methods of lowering the firing base to the ground may be considered. The first, and most commonly used, method is shown schematically in Fig. 4-23. It has the firing base attached to the bottom carriage with a simple ball joint. With this configuration the entire weapon is lowered by raising the wheel assembly relative to the bottom carriage. Thus the center of gravity of the weapon is as low as possible when the weapon is fired. As shown in Chapter 3, this low center of gravity enhances firing stability of the system.

A second method, shown in Fig. 4-24, that may be considered is a firing base that is lowered relative to the bottom carriage, with the wheels fixed to the bottom carriage. This method is not generally employed for modern weapons because the center of gravity of the weapon is high and the loads on the firing base are high during the weapon recoil; therefore, the translational joint between the firing base and bottom carriage would have to be designed to carry high load.

With the firing base attached to the bottom carriage (Fig. 4-23), a mechanism must be designed to raise the wheels relative to the bottom carriage. The road arm must be pivoted to the bottom carriage with an antifriction bearing and a mechanism designed to rotate the road arm. Either a gear screw jack or hydraulic system may be used. If a gear drive is selected, standard gear train design techniques may be employed. For heavy weapons, care must be exercised to achieve low friction. Gear ratios and handwheel, or jack handle, dimensions must be selected with human factors accounted for. A determination of the time for the crew to raise the weapon should be made early in the design cycle to assure that user-specified weapon displacement times can be met.

Efficient hydraulic weapon-lowering and -raising mechanisms are generally preferred for large caliber towed systems as in the M198, 155-mm towed system. A hydraulic system has a secondary advantage of serving to drive the speed shift jacks when a separate speed shift axis is used. Commercially available pumps and hydraulic struts may be used for this application. Human factor considerations are again important in selecting pump hydraulic displacement and pump arm length to optimize performance within crew capabilities.

4-4 SUSPENSION SYSTEM

The suspension system used in towed artillery systems has conventionally been a rigid axle with pneumatic tires. Standard military tires and wheels are employed with specifications determined by weapon weight, loads encountered in towing, and soil conditions over which the weapon is to be towed.

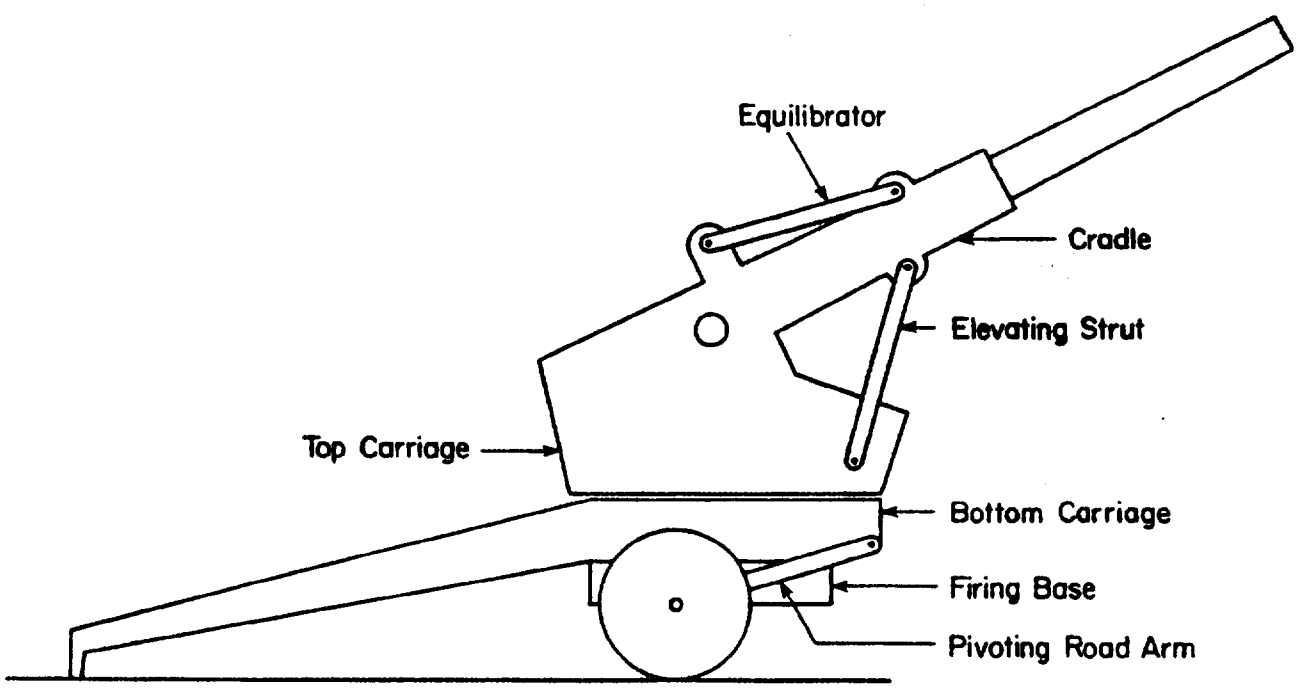

Figure 4-23. Road Arm Pivot for Firing Base Emplacement

THIS DOCUMENT PROVIDED BY THE ABBOTT AEROSPACE
TECHNICAL LIBRARY
ABBOTTAEROSPACE.COM

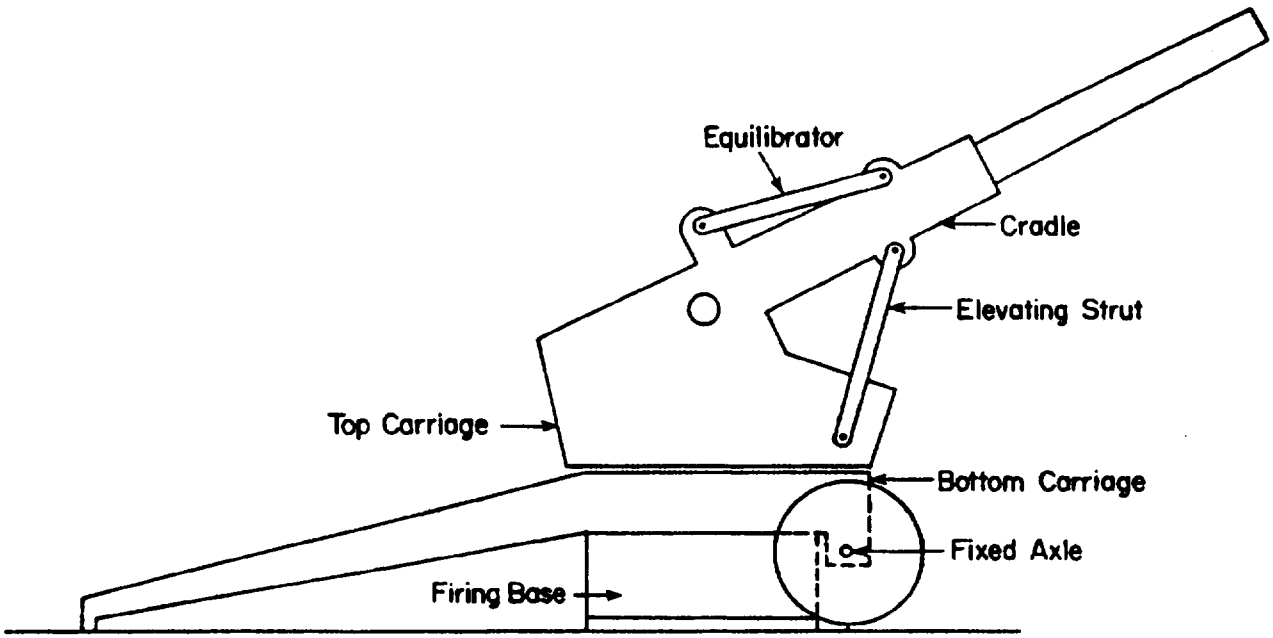

Figure 4-24. Lowering Firing Base

Commercially available wheel bearings will generally be selected based on loads to be encountered during towing. Both radial and axial bearing loads must be considered as predicted by system dynamic analysis considered in Chapter 3. For example, if a 6-*g* acceleration is encountered in towing the weapon over rough terrain, then each wheel bearing must be capable of supporting a load that is three times the total weight *W* of the weapon, as shown in Fig. 4-25. For the M198, 155-mm system, which weighs about 70,000 N, this is 210,000 N as the maximum radial load on each wheel bearing.

If during a turn the weapon slides laterally and is stopped by impact of the tire against a solid object such as a rock, a lateral acceleration of up to 3 *g* can occur. This results in a lateral load on the wheel of three times the weapon weight, as shown in Fig. 4-26. The wheel bearing must be capable of withstanding this suddenly applied torque. These radial and thrust loads form the basis for bearing specifications and procurement.

Although no cushioning devices other than the pneumatic tire have been used in towed artillery suspension in the past, higher towing speeds in the future may require some form of spring-damper suspension. Either a torsion bar or coil spring and associated damper (shock absorber) may be employed. Since most systems are lowered onto their firing base by pivoting a road arm (See par. 4-3.), a torsion bar suspension using the same road arms and pivots may be feasible.

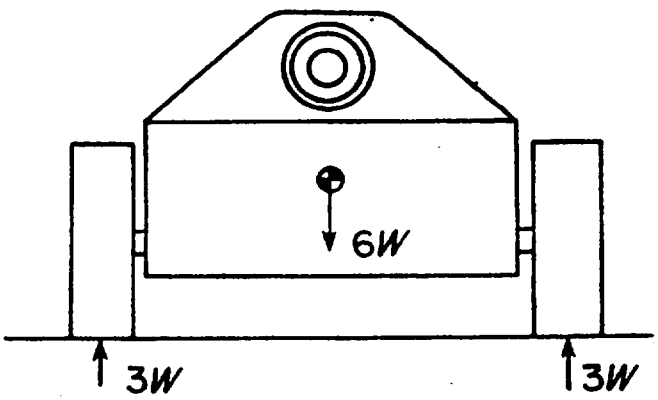

Figure 4-25. Suspension Loads at 6-*g* Vertical Acceleration

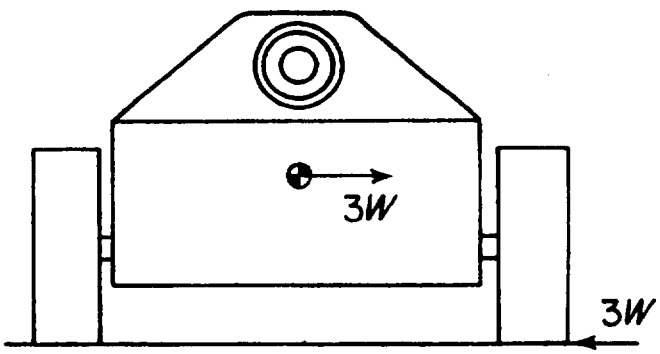

Figure 4-26. Suspension Loads at 3-*g* Lateral Acceleration

THIS DOCUMENT PROVIDED BY THE ABBOTT AEROSPACE
TECHNICAL LIBRARY
ABBOTTAEROSPACE.COM

4-5 LINKAGE FOR VARIABLE RECOIL

When firing a conventional artillery weapon at maximum elevation, the allowable recoil length is limited by the distance between the breech and the ground. When firing at lower angles of elevation, this constraint is removed and the level of the resisting force, which must be produced by the recoil mechanism, may be reduced by increasing the length of recoil. For the M198 Howitzer (using the M45 variable stroke recoil mechanism), recoil is limited to either 1.27 m or 1.78 m, depending on the angle of elevation. Variable length recoil generally is achieved by using two sets of control orifices in the recoil brake, as discussed in detail in Ref. 6. By rotating the control rod, transition from long and short recoil grooves is accomplished automatically as the weapon is elevated. A linkage is thus required that indexes the control rod as the weapon is elevated through an increment of elevation. For example, in the case of the M198, 155-mm system, the transition from long to short grooves occurs as the weapon is elevated from 100 through 900 mils.

A cam or geneva mechanism may be used to transmit rotation of the elevating parts about the trunnion to rotation of the control rod. A schematic of such a gearing system for a recoil mechanism with two recoil brakes is shown in Fig. 4-27. As the variable recoil drive gear is rotated, both control rods are simultaneously rotated from long to short recoil grooves. The angle of rotation required is dictated by design of the recoil rods. (See Ref. 6.)

A geneva or cam mechanism is required that has dwells for elevation angles below the beginning of the transition zone (long recoil) and above the transition zone (short recoil). Flow occurs through long and short recoil grooves in the transition zone and leads to intermediate recoil lengths. Input motion to the indexing mechanism may be taken from rotation about the trunnion or a link attached between the top and bottom carriages to provide a linear displacement input as the weapon is elevated. The latter approach is employed with a cam in the M198, 155-mm system.

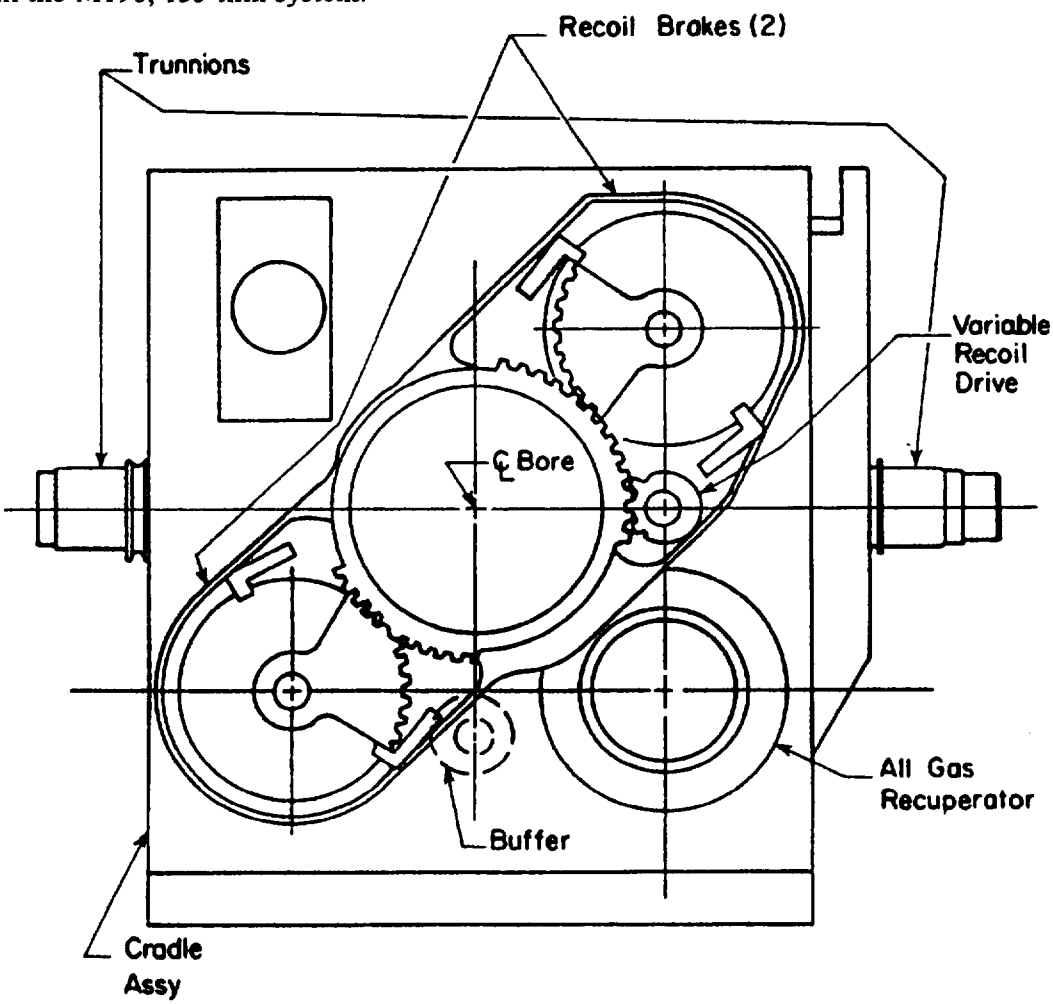

Figure 4-27. Front View of Variable Recoil Assembly

THIS DOCUMENT PROVIDED BY THE ABBOTT AEROSPACE
TECHNICAL LIBRARY
ABBOTTAEROSPACE.COM

REFERENCES

1. M. F. Spotts, *Design of Materials Elements*, 5th Edition, Prentice-Hall, Englewood Cliffs, NJ, 1978.
2. J. E. Shigley and J. J. Uicker, *Theory of Machines and Mechanisms*, McGraw-Hill, New York, NY, 1980.
3. J. W. Michalec, *Precision Gearing*, John Wiley & Sons, New York, NY, 1966.
4. Robert Toering, *Test of Roller Traverse System for Application on Towed Artillery*, Report No. ART-5-68, US Army Weapons Command, Research and Engineering Directorate, Artillery Systems Laboratory, Rock Island Arsenal, Rock Island, IL, December 1968.
5. F. B. Seely and N. E. Ensign, *Analytical Mechanics for Engineers*, 4th Edition, John Wiley and Sons, New York, NY, 1952.
6. DOD-HDBK-778(AR), *Recoil Systems*, July 1988.

THIS DOCUMENT PROVIDED BY THE ABBOTT AEROSPACE
TECHNICAL LIBRARY
ABBOTTAEROSPACE.COM

CHAPTER 5
EQUILIBRATOR DESIGN

This chapter presents information on the operating principles and design of the equilibrators, the component of an artillery system that compensates for imbalance of the tipping parts. Methods of calculating the moment about the trunnion which would lead to perfect balance in elevation are presented and illustrated. Several types of equilibrator designs are described with guides for the selection of the most desirable type. Geometry and force analysis, mechanics, and kinematics of equilibrators are discussed. Design techniques and calculations with examples are presented for both spring and pneumatic equilibrators. Techniques for optimization of equilibrators, i.e., minimizing handwheel effort in elevating and depressing the weapon, are presented and illustrated.

5-0 LIST OF SYMBOLS

A = effective piston area, m^2
a = outer radius of cylinder head, m
= dimensionless parameter, dimensionless
b = inner radius of cylinder head, m
= design variable vector, dimensionless
c = distance between points A and T, m
= spring index, dimensionless
= spring length, m
D = mean coil diameter of spring, m
= piston diameter, m
= outside diameter of packing, m
D_i = coil diameter of equilibrator concentric spring i, m
d = piston rod diameter, m
= distance from B to perpendicular from T to L (Figs. 5-13 and 5-14), m
= perpendicular distance from T to the extension of force of F_s (Fig. 5-19(C)), m
di = wire diameter of spring i, m
= wire diameter of equilibrator concentric spring i, m
d_1 = inner diameter of cylinder, m
d_2 = outer diameter of cylinder, m
E = error, m^2
E_t = total spring energy, J
e = adjusting guide travel, each direction for normal to centerline, m
F = equilibrator force, N
= load on spring, N
F_A = reaction force at A, N
F_B = reaction force at B, N
F_i = equilibrator force at ΔL_i, N
= distributed forces to equilibrator concentric spring i, N
F_j = total spring load at θ_j, N
F_{max} = maximum spring force, N
F_n = net equilibrator force, N
F_{o_j} = outer spring load at ϕ_j, N
F_p = piston friction force in packing, N

THIS DOCUMENT PROVIDED BY THE ABBOTT AEROSPACE
TECHNICAL LIBRARY
ABBOTTAEROSPACE.COM

F_R = compressive force on rod, N
F_s = spring force, N
F_u = equilibrator force at $\phi = u$, N
F_0 = equilibrator force when $\phi = 0$, N
F_1 = spring load at $\theta = 0$, N
F_2 = spring load at $\theta = 0.96$, N
F_{1_o} = outer spring load at $\theta = 0$, N
F_{2_o} = outer spring load at $\theta = 0.96$, N
$F_{\phi'}$ = equilibrator force at $\phi = \phi'$ ($\theta = 0$), N
$\bar{F}_p$ = radial force exerted by packing, N
f = imbalance between weight moment and equilibrator moment, N·m
$f(\theta_j)$ = cost function at elevation grid angle θ_j, dimensionless
f_p = packing friction force, N
G = shear modulus of spring, Pa
K = ratio of c to R, dimensionless
= curvature correction factor of spring, dimensionless
K_p = pressure factor, dimensionless
K_s = equilibrator spring rate, N/m
K_{s_i} = equilibrator spring rate of inner spring, N/m
K_{s_o} = equilibrator spring rate of outer spring, N/m
k = spring rate of stiffness, N/m
L = equilibrator length, m
L_{max} = maximum equilibrator length, m
L_0 = equilibrator length at $\phi = 0$, m
L_1 = equilibrator length at $\theta = 0$, m
L_θ = equilibrator length at θ elevation, m
L' = equilibrator length, adjusted position on either side, m
ΔL = change in equilibrator length, m
ΔL_i = deflection of equilibrator concentric spring i, m
= equilibrator travel, m
ΔL_u = equilibrator travel at $\phi = u$, m
ΔL_1 = deflection of equilibrator concentric spring 1, m
ΔL_2 = deflection of equilibrator concentric spring 2, m
ΔL_θ = equilibrator travel at θ elevation, m
ℓ = straight line, dimensionless
M_A = moment about A, N·m
M_B = moment about B, N·m
M_e = equilibrator moment about trunnion, N·m
M_{e_0} = equilibrator moment about trunnion at $\phi = 0$, N·m
M_T = moment about trunnion, N·m
M_W = weight moment of tipping parts about trunnion, N·m
M_{W_u} = weight moment of tipping parts about trunnion at $\phi = u$, N·m
M_{W_0} = weight moment of tipping parts about trunnion at $\phi = 0$, N·m
M_{W_ϕ} = weight moment of tipping parts about trunnion at $\phi = \phi'$ ($\theta = 0$), N·m
m = reciprocal of Poisson's ratio, dimensionless
n = number of active coils in spring, dimensionless
n_1 = number of active coils of equilibrator concentric spring 1, dimensionless

THIS DOCUMENT PROVIDED BY THE ABBOTT AEROSPACE
TECHNICAL LIBRARY
ABBOTTAEROSPACE.COM

n_2 = number of active coils of equilibrator concentric spring 2, dimensionless
P_A = atmospheric pressure, Pa
$P_{a_{min}}$ = minimum gas absolute pressure, Pa
P_{a_u} = absolute gas pressure at $\phi = u$, Pa
P_{a_0} = absolute gas pressure at $\phi = 0$, Pa
P_{a_θ} = absolute gas pressure at θ elevation, Pa
P_d = limit design pressure of packing, Pa
P_m = maximum fluid pressure, Pa
P_{max} = maximum gas gage pressure, Pa
P_r = radial pressure, Pa
P_s = axial pressure in packing produced by spring, Pa
= seal pressure, Pa
P_u = gas gage pressure at $\phi = u$ elevation, Pa
P_0 = gas gage pressure at $\phi = 0$, Pa
P_1 = gas gage pressure at state 1, Pa
P_2 = gas gage pressure at state 2, Pa
P_{1_a} = absolute gas pressure at state 1, Pa
P_{2_a} = absolute gas pressure at state 2, Pa
P_θ = fluid pressure at θ elevation, Pa
= gas gage pressure at θ elevation, Pa
p_i = pitch of equilibrator concentric spring i, m
p_1 = pitch of equilibrator concentric spring 1, m
p_2 = pitch of equilibrator concentric spring 2, m
R = turning radius, m
= distance between trunnion and B, m
R_t = distance between trunnion and center of gravity of tipping parts, m
r = equilibrator moment arm, m
= moment arm, normal position, m
r_A = radius of bearing at A (Fig. 5-19), m
r_B = radius of bearing at B (Fig. 5-19), m
r_i = inside radius of terminal, m
r_o = outside radius of terminal, m
r_u = equilibrator moment arm at $\phi = u$, m
r' = equilibrator moment arm, any adjusted position, m
r_0 = equilibrator moment arm when $\phi = 0$, m
r_1 = inside radius of piston ring assembly, m
r_2 = outside radius of piston ring assembly, m
$r_{\phi'}$ = equilibrator moment arm at $\phi = \phi'$ ($\theta = 0$), m
S_{max} = maximum spring deflection, m
T_A = friction torque at A (Fig. 5-19), N·m
T_B = friction torque at B (Fig. 5-19), N·m
T_e = moment provided by elevating strut, N·m
T_T = friction torque at trunnion, N·m
T_1 = absolute temperature at state 1, K
T_2 = absolute temperature at state 2, K
t = plate thickness, m
= thickness of terminal end, m

THIS DOCUMENT PROVIDED BY THE ABBOTT AEROSPACE
TECHNICAL LIBRARY
ABBOTTAEROSPACE.COM

t' = total number of grid points, dimensionless
u = ϕ at high angle of elevation, rad
V_{max} = maximum gas volume, m^3
V_{min} = minimum gas volume, m^3
V_u = gas volume at $\phi = u$, m^3
V_1 = gas volume at state 1, m^3
V_2 = gas volume at state 2, m^3
V_θ = gas volume at θ elevation, m^3
ΔV = change in gas volume, m^3
ΔV_u = change in gas volume due to equilibrator travel at $\phi = u$, m^3
W_t = weight of tipping parts, N
w = packing width, m
= seal width, m
α = angle between R_1 and R (Figs. 5-13, 5-14, and 5-20), rad
β = angle between vertical line and c (Figs. 5-13, 5-14, and 5-20), rad
γ = angle between vertical line and R (Figs. 5-13 and 5-14), rad
δ = spring deflection, m
δ_i = deviation of F_i from F, N
δ_{max} = maximum spring deflection, m
δ_1 = spring deflection at $\phi = \phi'$ ($\theta = 0$), m
ϵ = angle between c and L (Figs. 5-13 and 5-14), rad
θ = elevation angle, rad
θ_j = elevation grid angle at every grid point, rad
θ_{max} = maximum elevation, rad
θ_{min} = minimum elevation, rad
θ_u = maximum elevation angle, rad
θ_0 = minimum elevation angle, rad
θ_1 = elevation angle when equilibrator makes an angle $\pi/2$ rad with line from trunnion to B (Fig. 5-18), rad
μ = coefficient of packing-cylinder friction, dimensionless
= friction coefficient at bearings, dimensionless
ν = leakage factor, dimensionless
σ = maximum tensile stress in cylinder terminal, Pa
σ_t = circumferential stress, Pa
σ_{t_θ} = stress at inner edge of cylinder head, Pa
τ = uncorrected shear stress in spring, Pa
τ_a = allowable stress in spring wire, Pa
τ' = $K\tau$ = corrected shear stress in spring, Pa
ϕ = angle between horizontal line and OT (Figs. 5-10, 5-13, 5-14, and 5-20), rad
ϕ_D = ϕ at maximum angle of depression, rad
ϕ' = angle between OT and centerline of gun tube (Figs. 5-13, 5-14, and 5-20), rad
ψ = angle between R and c (Figs. 5-13, 5-14, and 5-20), rad
= angle between L and R (Fig. 5-32), rad
ψ_i = equality or inequality constraint functions, dimensionless
ψ' = angle between L' and R (Fig. 5-32), rad
ψ_0 = angle between R and c when $\phi = 0$ (Figs. 5-13, 5-14, and 5-20), rad
= cost function, dimenionless
ψ_θ = ψ at any angle θ, rad

THIS DOCUMENT PROVIDED BY THE ABBOTT AEROSPACE
TECHNICAL LIBRARY
ABBOTTAEROSPACE.COM

5-1 INTRODUCTION

Towed artillery weapons should have a low silhouette and low center of gravity and yet be able to fire at both high and low elevations. To provide clearance for recoil at high elevation, it is necessary to place the recoiling parts well forward of the trunnions. This placement of the recoiling parts positions the center of gravity of the tipping parts ahead of the trunnions and creates a muzzle preponderance, or weight moment, which must be balanced by a couple applied at the trunnions and by the elevating mechanism. It is desirable to eliminate, or at least reduce, the weight moment by balancing it with a mechanical device referred to as an equilibrator.

5-1.1 TYPES OF EQUILIBRATORS

The equilibrator provides its balancing force either by gas pressure or by a spring. The direction in which the force is applied determines whether it is to be a pull-type equilibrator (Fig. 5-1) or a push-type equilibrator (Fig. 5-2). With a pull type, the piston rod is in tension, whereas with a push type, the rod is in compression. The location and type of equilibrator used depend on other characteristics of the weapon, such as available space, clearances, and silhouette.

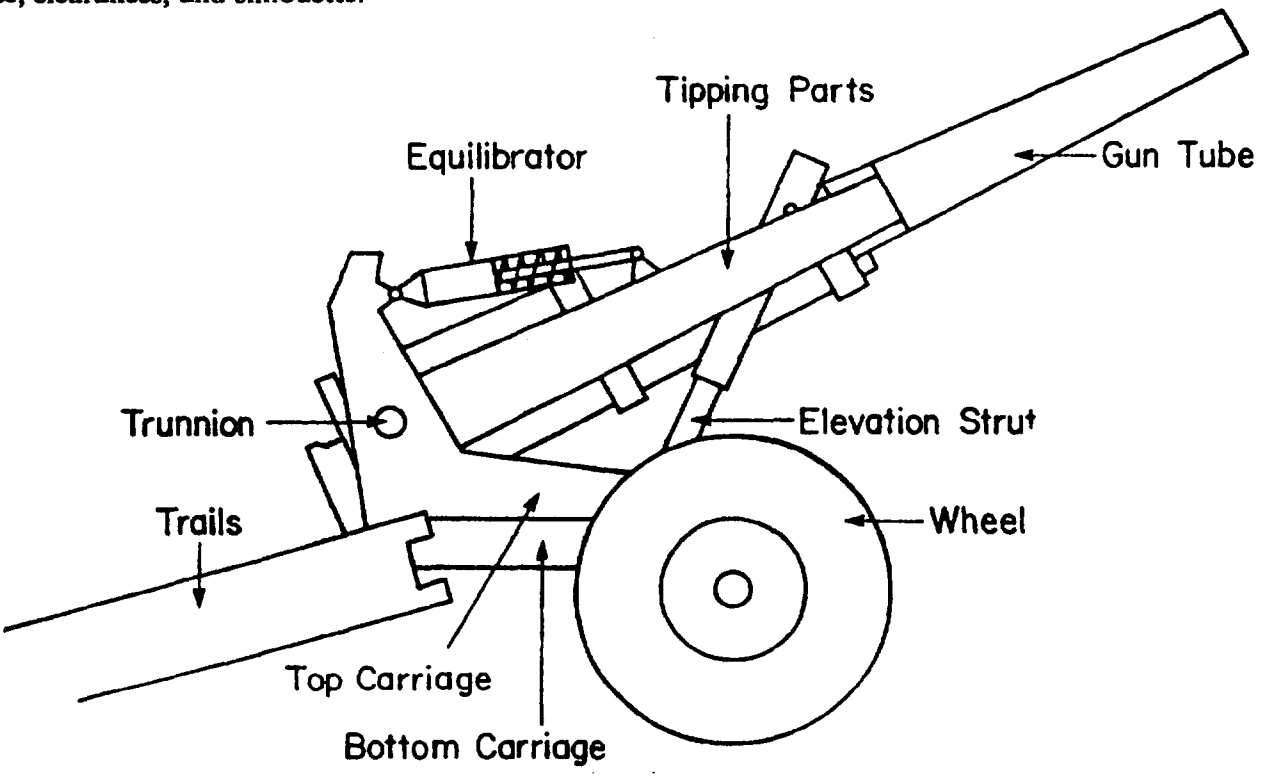

Figure 5-1. Pull-Type Equilibrator

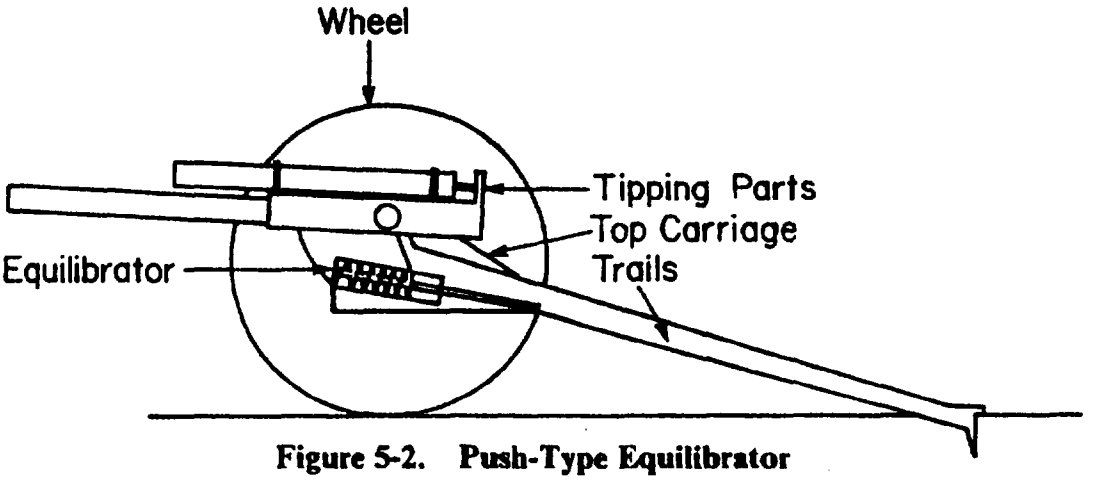

Figure 5-2. Push-Type Equilibrator

THIS DOCUMENT PROVIDED BY THE ABBOTT AEROSPACE
TECHNICAL LIBRARY
ABBOTTAEROSPACE.COM

All equilibrators must be able to apply a force over a variable distance. This application of force is accomplished by having an elastic medium in the system, of which there are three basic types. The simplest is the spring-strut equilibrator in which the spring element is self-contained. The second is a gas-strut equilibrator with a conveniently located accumulator. Both of these can be either pull or push type. In the third type, the force is carried to the tipping parts by means of a chain, as shown in Fig. 5-3. This chain may act directly or may be wrapped around a cam to control the moment arm more effectively.

Equilibrators are further identified according to their methods of producing a force. Force-generating elements may be

1. Spring
2. Pneumatic
3. Hydropneumatic
4. Spring-loaded hydraulic.

Each of these elements is described in the paragraphs that follow.

Two types of spring equilibrators may be considered—a coil spring or a torsion bar. The coil-spring type is shown in Fig. 5-4. Note that, as illustrated, this is a pull-type equilibrator. The free end of the rod is pin-connected to the tipping parts, and the end of the housing is pinned to the top carriage. Maximum compression of the spring occurs at minimum elevation. As the tipping parts are elevated, the weight moment decreases and the spring is expanded, which reduces the equilibrating force.

The torsion-bar type equilibrator shown in Fig. 5-5 uses a torsion bar and linkage instead of a coil spring to provide balancing force. One end of the bar is rigidly connected to the top carriage, and the free end is fixed to the torque arm. As the torque arm rotates during elevation, the bar unwinds to reduce the equilibrator moment. However, since this type of equilibrator is not used in modern artillery, it is not considered further.

The pneumatic equilibrator consists of a cylinder and piston, as shown in Fig. 5-6. It is similar in application to the coil-spring type, but its elastic medium is compressed gas rather than a coil spring. Maximum pressure occurs at minimum elevation. As the volume of the gas expands during elevation, pressure diminishes and the equilibrating force is reduced as desired.

In the hydropneumatic equilibrator shown in Fig. 5-7, the elastic medium is compressed gas. The system consists of a hydraulic cylinder, piston and rod, reservoir, and flexible connecting line. The pressure chamber of the hydraulic strut, all of the line, and part of the reservoir are filled with hydraulic fluid. The remainder of the reservoir is filled with gas under pressure. Maximum pressure occurs at minimum elevation. Because the size of the pressure chamber increases with elevation, fluid under pressure flows from the reservoir through the line, adapter, piston rod, and ports into the chamber. This flow of fluid changes the volumes of fluid and gas in the reservoir, which results in a reduced pressure, hence the desired reduction of equilibrating force. A single or multiple reservoir may be used. The hydropneumatic equilibrator is attractive for weapons in which weight moments are large, and space may be saved by storing the compressed gas remote from the equilibrator strut.

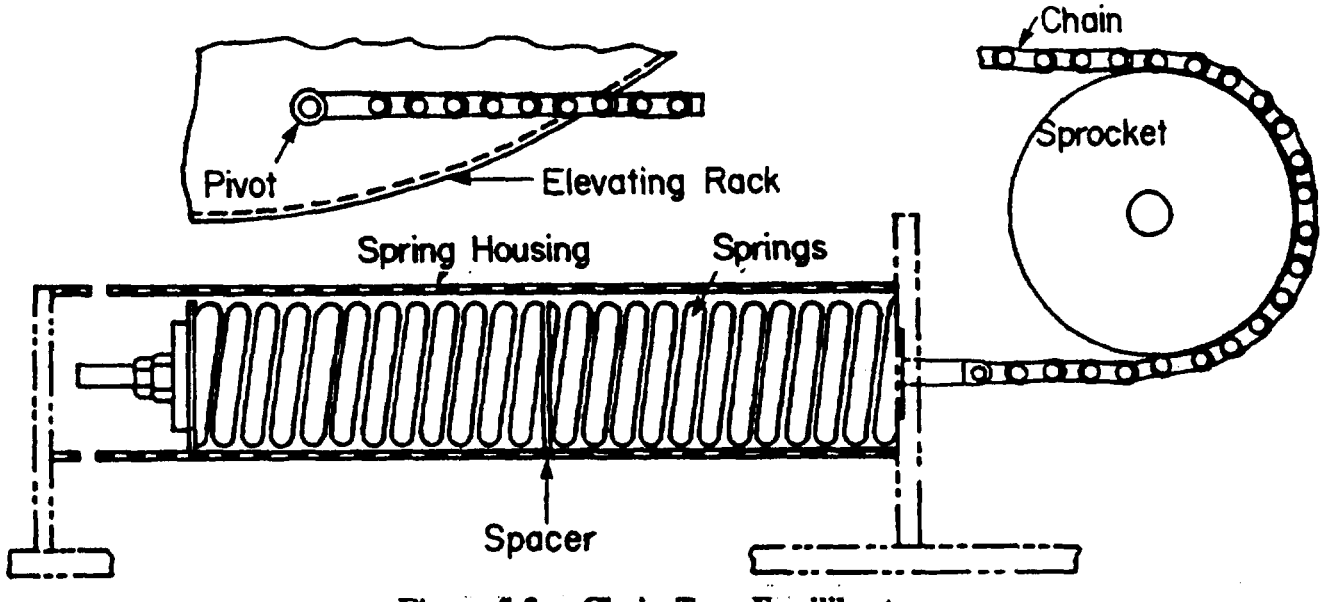

Figure 5-3. Chain-Type Equilibrator

THIS DOCUMENT PROVIDED BY THE ABBOTT AEROSPACE
TECHNICAL LIBRARY
ABBOTTAEROSPACE.COM

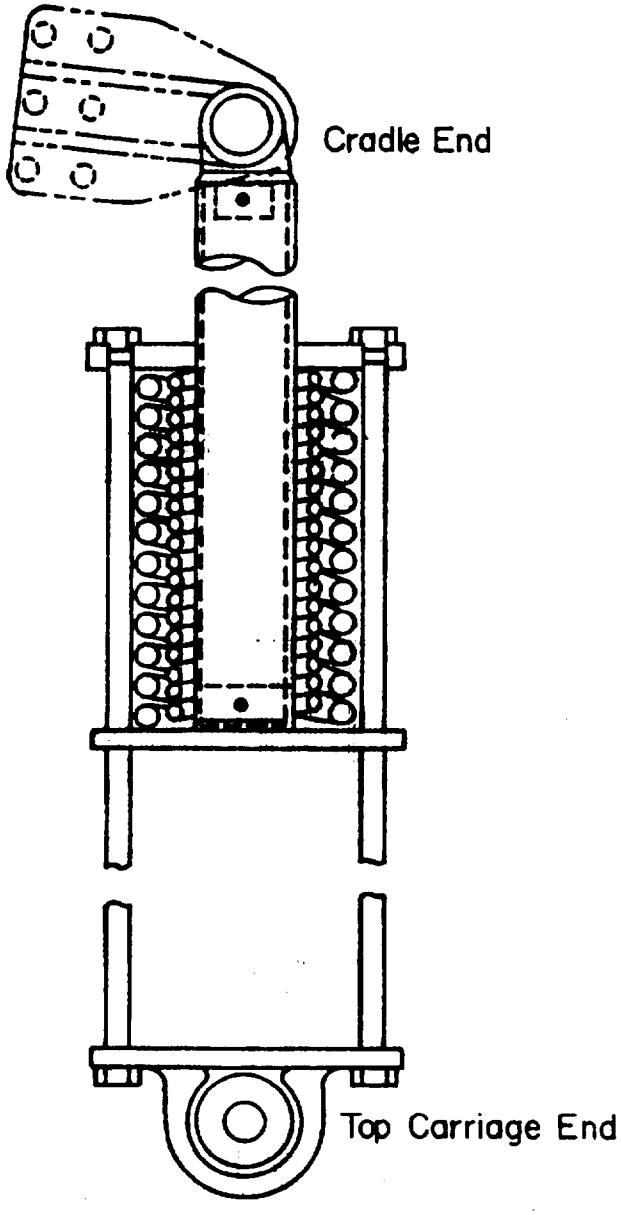

Figure 5-4. Spring Equilibrator

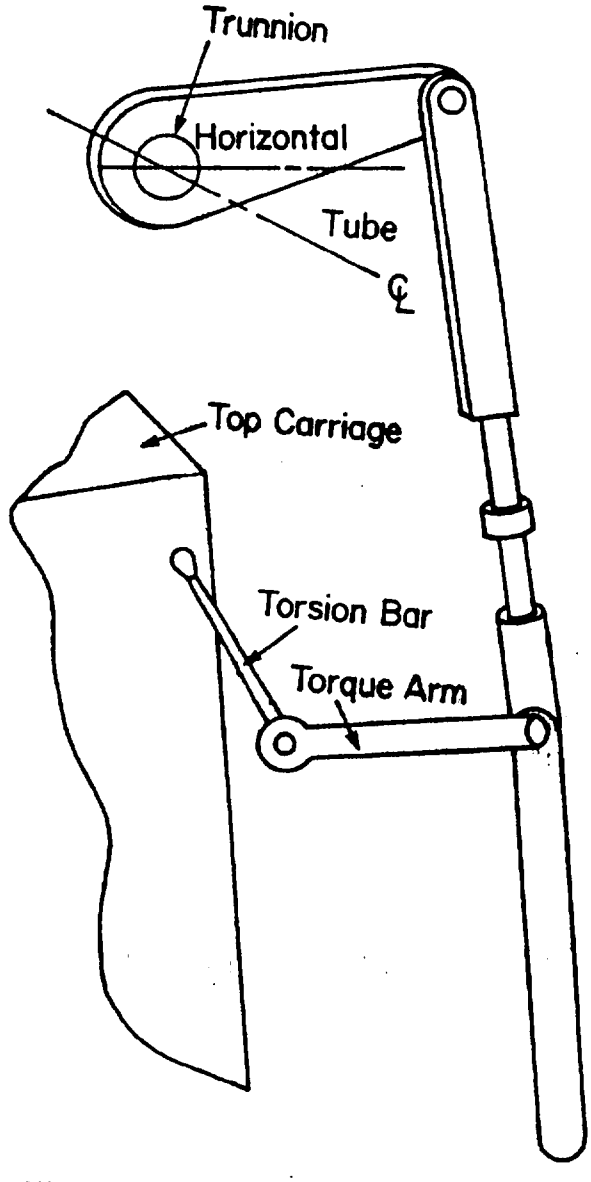

Figure 5-5. Torsion-Bar Equilibrator

THIS DOCUMENT PROVIDED BY THE ABBOTT AEROSPACE
TECHNICAL LIBRARY
ABBOTTAEROSPACE.COM

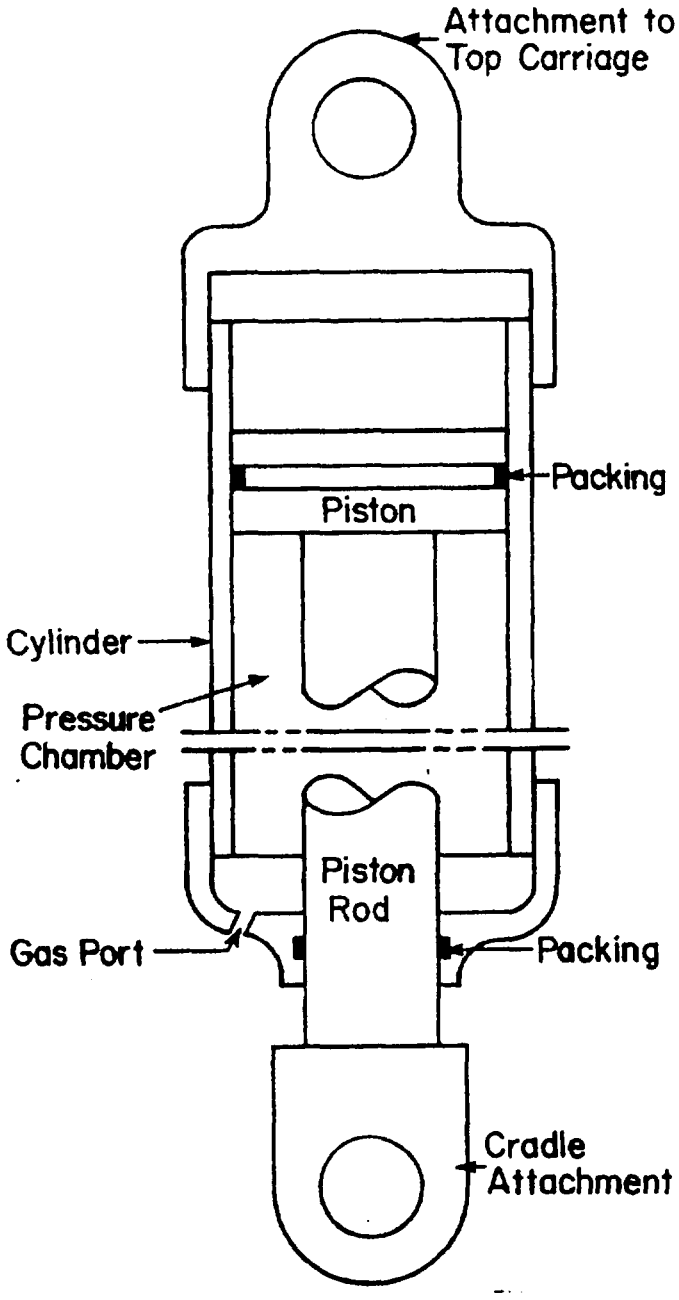

Figure 5-6. Pneumatic Equilibrator

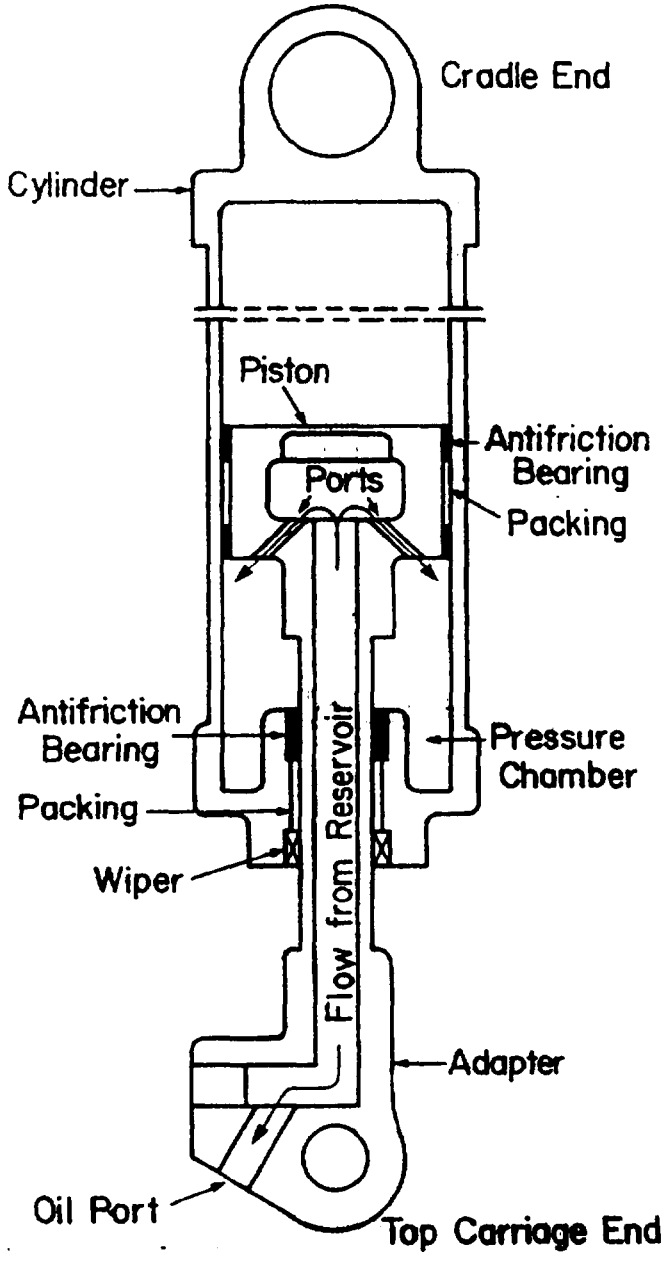

Figure 5-7. Hydropneumatic Equilibrator

The spring-loaded hydraulic equilibrator uses a coil spring to maintain hydraulic pressure, as shown in Fig. 5-8. A coil spring, instead of gas, is employed to maintain pressure in the fluid reservoir. Because this type of equilibrator has not been used for modern artillery application, it is not discussed further.

The types of equilibrators described in this paragraph are systematized; their relationship is shown in Fig. 5-9. The mechanical spring-type equilibrator is easiest to manufacture; hence it is less expensive than pneumatic and hydropneumatic types. It has the disadvantage, however, of occupying much space and being heavy. Further considerations for selecting an appropriate equilibrator type are provided in par. 5-1.3.

The potential for incorporating the equilibrator in the elevating strut may also be considered due to the advantage that can be gained by reducing the number of components of the weapon system and possibly reducing weight. Disadvantages associated with such a combination should be carefully considered. The single strut will be somewhat more complex, and its location may be dictated by gearing attachments of the elevating mechanism. Thus the optimum location of the equilibrator attachment points may be sacrificed.

THIS DOCUMENT PROVIDED BY THE ABBOTT AEROSPACE
TECHNICAL LIBRARY
ABBOTTAEROSPACE.COM

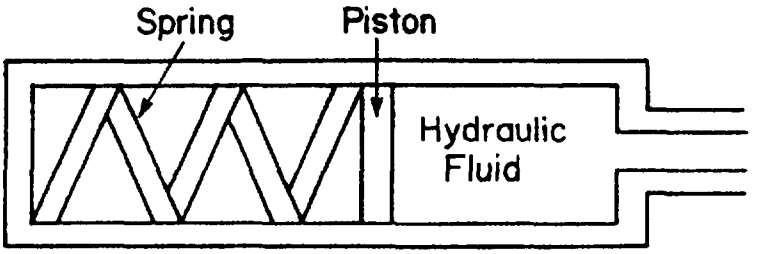

Figure 5-8. Spring-Loaded Hydraulic Reservoir

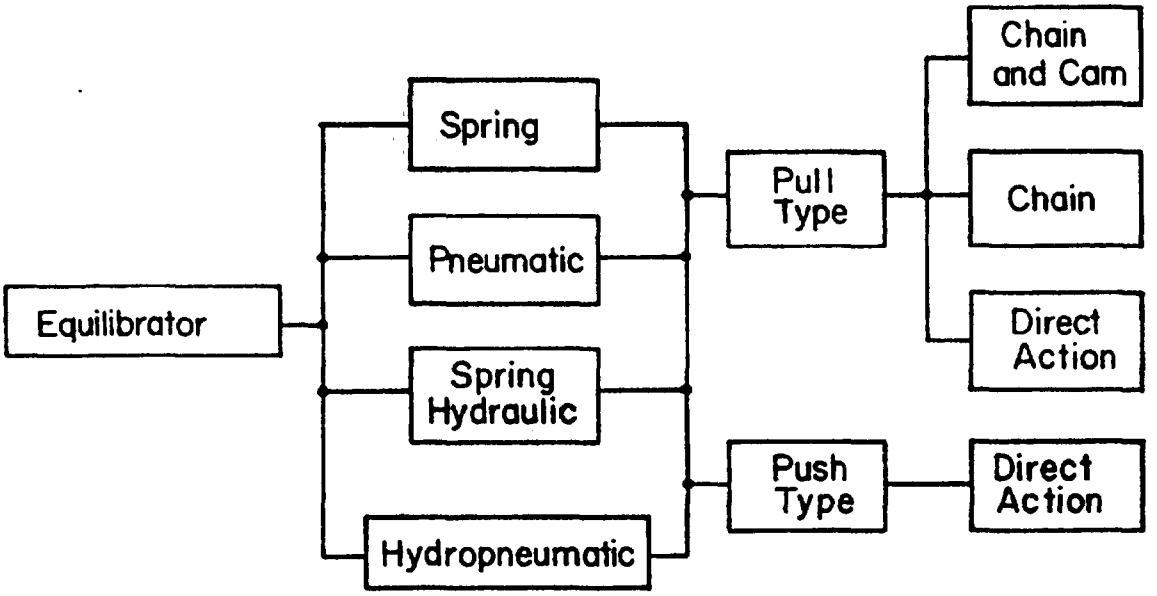

Figure 5-9. Types of Equilibrators

5-1.2 FACTORS INFLUENCING EQUILIBRATOR DESIGN

5-1.2.1 Weight Moment of Tipping Parts

The muzzle preponderance or weight moment of the tipping parts is the product of the weight of the tipping parts and the horizontal distance of their center of gravity from the trunnion axis. The tipping parts consist of all parts supported by the trunnions (Figs. 5-10 and 5-11). The weight moment M_w of tipping parts about the trunnion is

$$M_w = W_t R_t \cos\phi \qquad (5\text{-}1)$$

where

W_t = weight of tipping parts, N
R_t = distance between trunnion and center of gravity of tipping parts, m
ϕ = angle between horizontal line and OT (Fig. 5-10), rad.

By manipulating the equilibrating force or its moment arm, or both, in a manner such that their product varies as $\cos\phi$, it is theoretically possible to achieve perfect balance for any angle of elevation. This fact is particularly true of equilibrators having constant spring rates. In practice, it is usual to accept an approximate balance. If a perfect balance were attempted, other factors, such as friction, would impair its precision.

THIS DOCUMENT PROVIDED BY THE ABBOTT AEROSPACE
TECHNICAL LIBRARY
ABBOTTAEROSPACE.COM

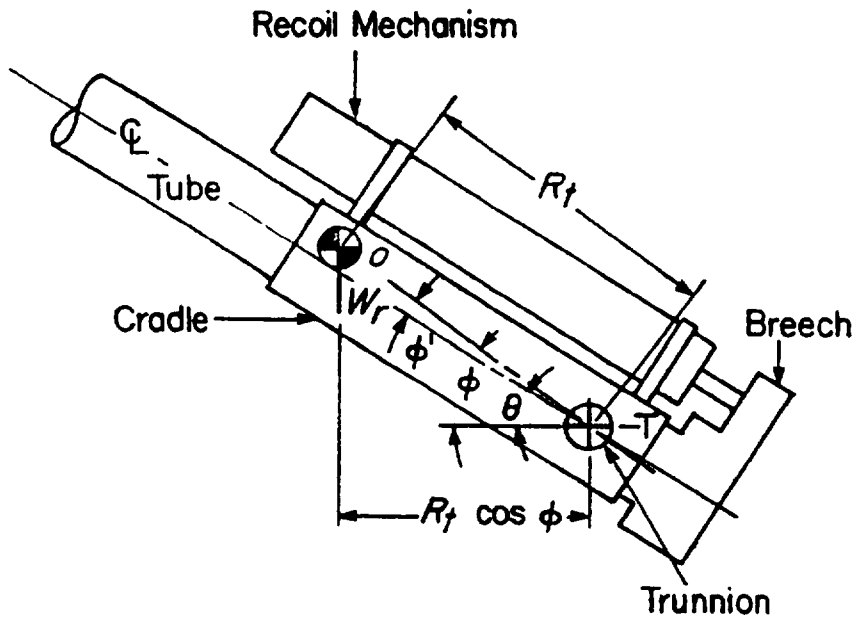

Figure 5-10. Geometry of Weight Moment of Tipping Parts

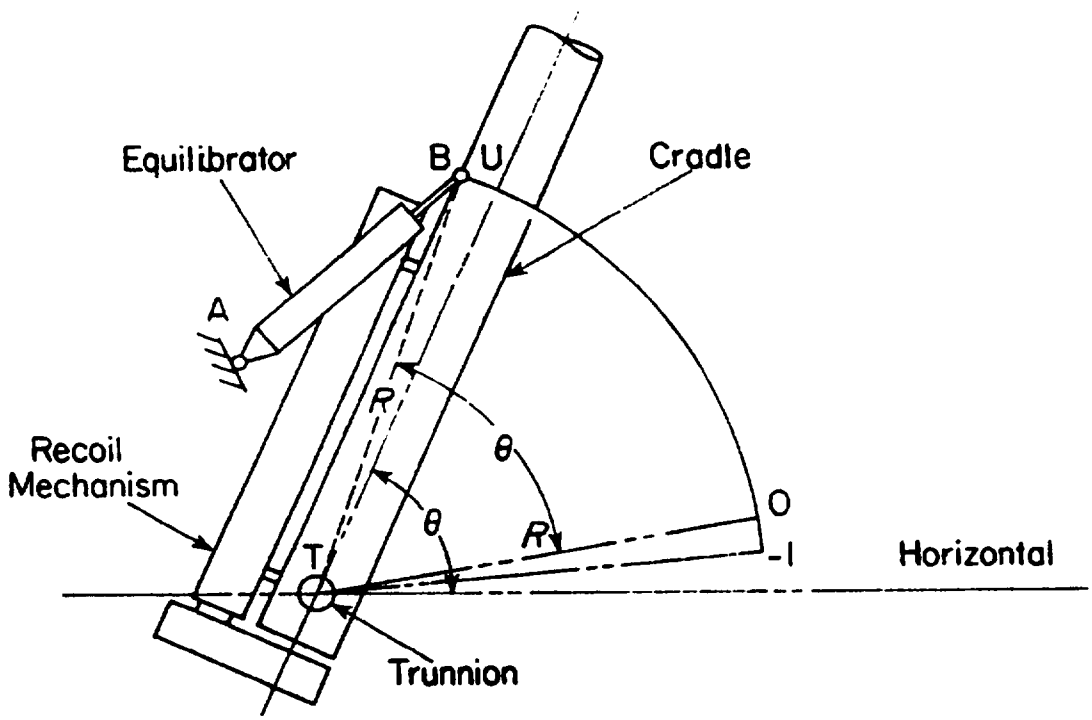

A = equilibrator attachment on carriage
B = equilibrator attachment of cradle
O = location of B at zero angle of elevation
-1 = location of B for negative angle of elevation
U = location of B at maximum angle of elevation

Figure 5-11. Equilibrator Geometry Showing Components

THIS DOCUMENT PROVIDED BY THE ABBOTT AEROSPACE
TECHNICAL LIBRARY
ABBOTTAEROSPACE.COM

5-1.2.2 Friction

Friction in the equilibrator system increases the required input forces and detracts from performance; thus friction force must be computed. Frictional forces cannot be compensated for by the equilibrator because friction forces change direction with elevation and depression. Friction also occurs in the trunnion bearings, at connections to the carriage and cradle, and in packings. Cradle trunnion friction may be neglected when low-friction bearings are used.

5-1.2.3 Packing Friction

In pneumatic and hydropneumatic equilibrators, friction of the packings in liquid or gas cylinders must be considered. Packings prevent leakage past moving parts such as pistons and piston rods. The packings are forced firmly against the moving surfaces, both by the pressure of the fluid itself and by springs.

Fig. 5-12 shows the piston seal assembly and internal pressure distribution. The fluid pressure P_θ and the seal pressure P_s make up the total pressure exerted on the leather packing ring. The seal pressure P_s is that pressure resulting from the force F_s of the spring. Because of the hydrostatic condition of the packing material, axial and radial pressures are nearly equal—a condition necessary for sealing.

The ratio of the radial pressure to the applied axial pressure is a property of the packing material called the "pressure factor".

The ratio of the radial pressure P_r to the maximum fluid pressure P_m is known as the "leakage factor". For positive sealing the leakage factor must be greater than unity, or $P_r/P_m > 1$. This insures that no leakage takes place at any time. Usually, however, changes in elevation cause both P_θ and P_s to vary and the leakage factor can dip to unity, or $P_r/P_m \geq 1$. Sometimes a small amount of leakage is desirable for lubrication. At such times the leakage factor is less than unity, or $P_r/P_m < 1$.

The packing friction force f_p is the product of the total radial force exerted by the packing and the coefficient of friction

$$f_p = \mu \bar{F}_p, \text{ N} \tag{5-2}$$

where

$\bar{F}_p$ = radial force exerted by packing, N
μ = coefficient of packing-cylinder friction, dimensionless.

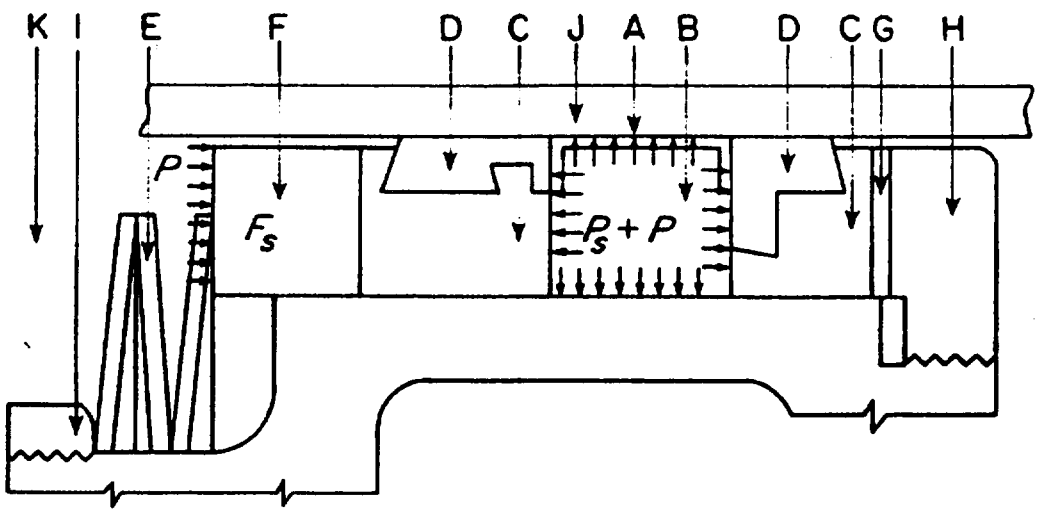

A = packing ring
B = piston ring filler
C = piston rings
D = piston ring band
E = Belleville spring
F = spring adapter
G = washer
H = retainer
I = retainer spring
J = cylinder
K = fluid under pressure

Figure 5-12. Piston Seal Assembly Showing Pressure Distribution and Applied Loads

THIS DOCUMENT PROVIDED BY THE ABBOTT AEROSPACE
TECHNICAL LIBRARY
ABBOTTAEROSPACE.COM

5-1.2.4 Geometric Considerations

As noted in par. 5-1.2.1, perfect equilibration is theoretically possible if the designer is free to select any equilibrator force and attachment points on the cradle and top carriage. Due to interference with other components, weapon profile limitations, and vulnerability considerations, the designer is seldom completely unconstrained in positioning of the equilibrator.

In locating the equilibrator in the position for best performance, the designer may place it where it is vulnerable to enemy artillery fragments. If this is the case, a coil-spring or hydropneumatic equilibrator should be chosen to enhance survivability. The coil-spring equilibrator is inherently rugged, and with the large gas recuperator of the hydropneumatic equilibrator located in a protected space, it is less vulnerable than a pneumatic equilibrator.

5-1.3 SELECTING AN EQUILIBRATOR TYPE

Table 5-1 presents a comparative evaluation of three basic types of equilibrators according to their desirable characteristics. The lower the index in Table 5-1, the higher the rating. The selection of an equilibrator type is not simply a matter of free choice; it is dictated by the problems encountered and system characteristics. A spring type is most desirable because of its simplicity. However, the designer may find it necessary to use one of the other types because of space, length of stroke, force required, or other factors.

When mechanical springs are used, small variations in dimensions, such as manufacturing tolerances, affect the spring rate. On the other hand, the rate is not affected by the speed of operation or the atmospheric temperature. These factors, however, do affect pneumatic equilibrators.

Spring-type equilibrators are generally limited to applications in which tipping moment imbalance is small, such as in 105-mm systems. For larger caliber weapons with large moment imbalance, long, large wire diameter coil springs are required. Such springs are physically large and very heavy. Further, with large compressive spring force, spring buckling becomes a severe problem. For such weapons, compressed gas is a much more weight efficient medium for generating the force required for equilibration. Also the combination of a hydraulic piston drive equilibrator with a remote pneumatic reservoir leads to a compact equilibrator strut that simplifies weapon design.

TABLE 5-1
COMPARATIVE EVALUATION OF EQUILIBRATORS

Parameter	Spring	Pneumatic	Hydropneumatic
Simplicity	1*	2	3
Space	3	1	2
Length of Stroke	3	2	1
Minimum Weight	3	1	2
Dependability	1	3	2
Ease of Maintenance	1	2	2
Flexibility of Operation	2	1	1
Versatility	2	1	1
Minimum Cost	1	2	3
Invulnerability	1	3	2

*1 indicates highest rating

5-2 MECHANICS OF EQUILIBRATORS

5-2.1 GEOMETRY AND FORCE ANALYSIS

The equilibrator force applied to the tipping parts to counterbalance the weight moment must vary with elevation because, as the tipping parts are elevated, the weight moment decreases. Sometimes it is impractical to strive for perfect balance at all angles of elevation, but it is feasible to keep the imbalance very small. The criterion for permissible imbalance is that it must be easily overcome by the elevating handwheel.

The position of the equilibrator on the mount is a critical design feature. A layout must be made of the gun carriage in the initial design stage to show the space available at all angles of elevation. The most effective geometry, including the proper turning radius, is determined so that the equilibrator can provide the required

THIS DOCUMENT PROVIDED BY THE ABBOTT AEROSPACE
TECHNICAL LIBRARY
ABBOTTAEROSPACE.COM

torque about the trunnions. The geometry is determined first for a perfectly balanced system. If the geometry is not compatible with the available space, it is modified only to the extent that it still closely approximates the ideal system. This approximation requires an iterative approach.

A method has been established and used extensively to determine the geometric properties necessary for a spring equilibrator. This method can be used for layout purposes of other types not having constant spring rates, but in these some imbalance will exist. The force required of an equilibrator depends on the moment arm and stroke available. See Figs. 5-13 and 5-14 for definition of geometry and variables associated with equilibrators located below and above the trunnions.

The turning radius R should be as large as the dimensions of the cradle permit. The ratio of c/R determines the efficiency of the spring the optimum being 1.0, although a ratio as high as 3.0 is not unduly inefficient. The length L_θ of the equilibrator, at any angle of elevation θ, may be found by the law of cosines as (See Fig. 5-13 or 5-14.)

$$L_\theta^2 = c^2 + R^2 - 2cR\cos\psi, \text{ m}^2 \tag{5-3}$$

where

θ = elevation angle, rad
L_θ = equilibrator length at θ elevation, m
c = distance between points A and T (Figs. 5-13 and 5-14), m
R = turning radius, m
ψ = angle between R and c (Figs. 5-13 and 5-14), rad.

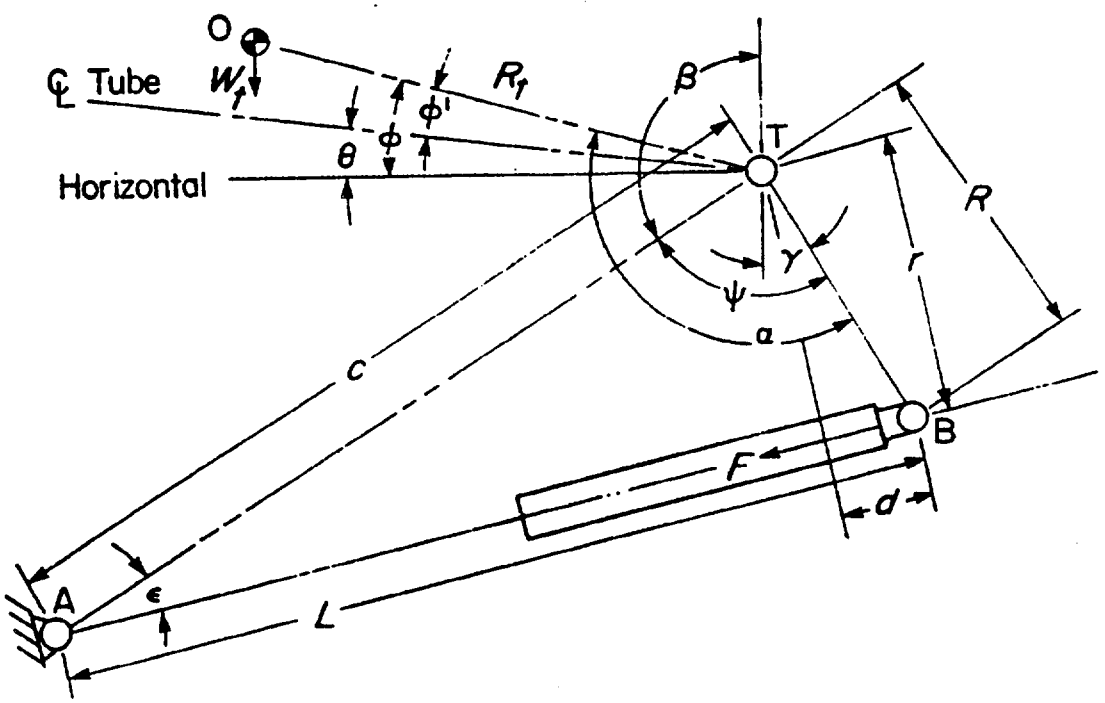

A = pivot point of equilibrator on carriage
B = pivot point of equilibrator on cradle, rotates about T
O = position of CG of tipping parts
T = center of trunnions, pivot point of tipping parts

Figure 5-13. Geometry of Equilibrator Shown Below Trunnions

THIS DOCUMENT PROVIDED BY THE ABBOTT AEROSPACE
TECHNICAL LIBRARY
ABBOTTAEROSPACE.COM

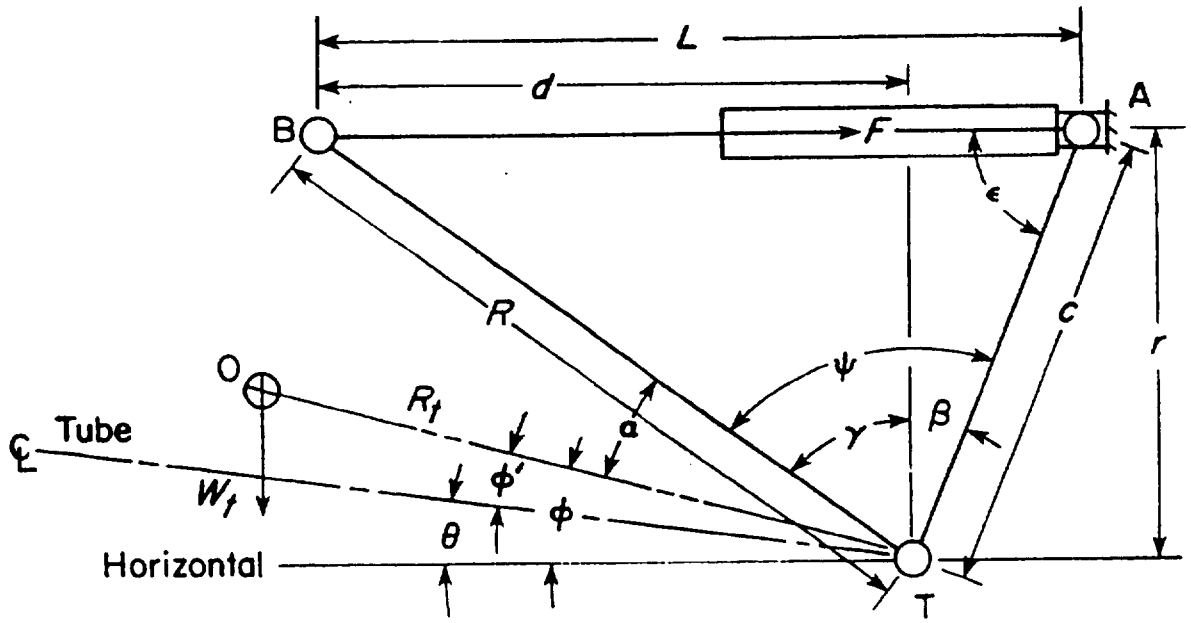

A = pivot point of equilibrator on carriage
B = pivot point of equilibrator on cradle, rotates about T
O = position of CG of tipping parts
T = center of trunnions, pivot point of tipping parts

Figure 5-14. Geometry of Equilibrator Shown Above Trunnions

By the law of sines, R and L_θ are related as (See Fig. 5-13 or 5-14.)

$$\frac{R}{\sin\epsilon} = \frac{L_\theta}{\sin\psi} \tag{5-4}$$

where

ϵ = angle between c and L_θ (Figs. 5-13 and 5-14), rad.

But, $\sin\epsilon$ may be written as

$$\sin\epsilon = \frac{r}{c} \tag{5-5}$$

where

r = equilibrator moment arm, m.

From Eqs. 5-4 and 5-5, the equilibrator moment arm is

$$r = \frac{cR}{L_\theta}\sin\psi, \text{ m} \tag{5-6}$$

and the stroke is

$$\Delta L = L_0 - L_\theta, \text{ m} \tag{5-7}$$

where

ΔL = change in equilibrator length, m
L_0 = equilibrator length at $\phi = 0$, m
ϕ = angle between horizontal line and OT (Figs. 5-13, 5-14, and 5-20), rad.

THIS DOCUMENT PROVIDED BY THE ABBOTT AEROSPACE
TECHNICAL LIBRARY
ABBOTTAEROSPACE.COM

The reader should note that the reference angle for equilibration design is $\phi = 0$, where the maximum moment of tipping parts about the trunnion occurs. This angle will generally not coincide with zero elevation, $\theta = 0$, since the center of gravity of the tipping parts is seldom on the centerline of the tube, as shown in Figs. 5-13 and 5-14.

It should be noted that if the geometry is maintained, the equilibrator pin joint on the tipping parts may be located at any point on the circle described by point B about the trunnion T.

Perfect balance may be achieved by analyzing the mechanics of the equilibrator system. From Figs. 5-13 and 5-14 and Eq. 5-1, for perfect balance, the equilibrator moment equals the weight moment at all angles of elevation, i.e.,

$$M_W = W_t R_t \cos\phi, \text{ N·m}$$

where

M_W = weight moment of tipping parts about trunnion, N·m
W_t = weight of tipping parts, N
R_t = distance between trunnions and center of gravity of tipping parts, m.

When $\phi = 0$, by Eq. 5-1,

$$M_{W_0} = W_t R_t, \text{ N·m} \tag{5-8}$$

where

M_{W_0} = weight moment of tipping parts about trunnion at $\phi = 0$, N·m.

Eq. 5-8 is just the evaluation of Eq. 5-1 at $\phi = 0$; therefore,

$$M_{W_0} = M_W, \text{ N·m.}$$

The equilibrator moment M_e about the trunnion is

$$M_e = rF, \text{ N·m} \tag{5-9}$$

where

F = equilibrator force, N.

By equating moments from Eqs. 5-1 and 5-9 for perfect equilibration,

$$Fr = W_t R_t \cos\phi, \text{ N·m.} \tag{5-10}$$

According to Fig. 5-13, the angle ψ between R and c is

$$\psi = \alpha - \phi - (\beta - \pi/2) = \pi/2 - (\phi - \alpha + \beta), \text{ rad} \tag{5-11}$$

or, from Fig. 5-14,

$$\psi = \pi/2 - \phi - \alpha + \beta = \pi/2 - (\phi + \alpha - \beta), \text{ rad} \tag{5-12}$$

where

α = angle between R_t and R (Figs. 5-13, 5-14, and 5-20), rad
β = angle between vertical line and c (Figs. 5-13 and 5-14), rad.

THIS DOCUMENT PROVIDED BY THE ABBOTT AEROSPACE
TECHNICAL LIBRARY
ABBOTTAEROSPACE.COM

When $\alpha = \beta$ in both Eqs. 5-11 and 5-12,

$$\psi = \pi/2 - \phi, \text{ rad.} \tag{5-13}$$

Therefore,

$$\sin\psi = \cos\phi. \tag{5-14}$$

By substitution of Eqs. 5-6 and 5-14 into Eq. 5-10, the condition for perfect equilibration (with $\alpha = \beta$) becomes

$$F\left(\frac{cR}{L_\theta}\right)\cos\phi = W_t R_t \cos\phi, \text{ N·m} \tag{5-15}$$

and the force F required for perfect equilibration is

$$F = \left(\frac{W_t R_t}{cR}\right) L_\theta, \text{ N.} \tag{5-16}$$

That is, the equilibrator spring force is directly proportional to the length of the equilibrator. Thus the spring force at any position may be written as

$$F_s = K_s L_\theta, \text{ N} \tag{5-17}$$

where the equilibrator spring rate K_s is

$$K_s = \frac{W_t R_t}{cR}, \text{ N/m.} \tag{5-18}$$

Now consider the position of the equilibrator when $\phi = 0$. The general equation

$$\psi = \psi_0 - \phi, \text{ rad} \tag{5-19}$$

where

ψ_0 = angle between c and R when $\phi = 0$

becomes

$$\psi = \psi_0, \text{ rad} \tag{5-20}$$

where, when $\phi = 0$, r becomes (Eq. 5-6)

$$r_0 = \left(\frac{cR}{L_0}\right)\sin\psi_0, \text{ m} \tag{5-21}$$

where

r_0 = equilibrator moment arm when $\phi = 0$, m
L_0 = equilibrator length when $\phi = 0$, m.

Likewise,

$$M_{W_0} = M_{e_0} = r_0 F_0 = W_t R_t, \text{ N·m} \tag{5-22}$$

THIS DOCUMENT PROVIDED BY THE ABBOTT AEROSPACE
TECHNICAL LIBRARY
ABBOTTAEROSPACE.COM

and

$$F_0 = \frac{M_{e0}}{r_0}, \text{ N} \tag{5-23}$$

where

F_0 = equilibrator force when $\phi = 0$
M_{e0} = equilibrator moment about trunnion when $\phi = 0$.

The spring force F_s at any angle ϕ is now

$$F_s = F_0 - K_s \Delta L, \text{ N} \tag{5-24}$$

where ΔL is given by Eq. 5-7.

Substitution of Eqs. 5-23 and 5-7 into Eq. 5-24 yields

$$F_s = \frac{M_{e0}}{r_0} - K_s(L_0 - L_\theta), \text{ N} \tag{5-25}$$

or substituting for M_{e0} and r_0,

$$F_s = \frac{M_{w0} L_0}{cR \sin\psi_0} - K_s(L_0 - L_\theta), \text{ N}. \tag{5-26}$$

Multiplication of both sides of Eq. 5-26 by r and substitution of the value for Fr from Eq. 5-10, the value for r from Eq. 5-6, and the value for ψ from Eq. 5-19 yield

$$M_{w0}\cos\phi = \frac{cR}{L_\theta} \sin(\psi_0 - \phi) \left[\frac{M_{w0} L_0}{cR \sin\psi_0} - K_s(L_0 - L_\theta) \right], \text{ N·m}. \tag{5-27}$$

Rearrangement of Eq. 5-27 gives the relation

$$M_{w0} \left[- \frac{L_\theta \cos\phi}{\sin(\psi_0 - \phi)} + \frac{L_0}{\sin\psi_0} \right] = cRK_s(L_0 - L_\theta), \text{ N·m}^2. \tag{5-28}$$

Eq. 5-28 is the perfect balance equation. By inspection, $\pi/2$ is the only value of ψ_0 that will make Eq. 5-28 independent of the variable angle ϕ. Insertion of this value into Eq. 5-28 yields

$$M_{w0} \left[- \frac{L_\theta \cos\phi}{\sin(\pi/2 - \phi)} + \frac{L_0}{\sin\pi/2} \right] = cRK_s(L_0 - L_\theta), \text{ N·m}^2. \tag{5-29}$$

But $\sin(\pi/2 - \phi) = \cos\phi$, which reduces Eq. 5-29 to

$$M_{w0} - cRK_s, \text{ N·m}. \tag{5-30}$$

THIS DOCUMENT PROVIDED BY THE ABBOTT AEROSPACE
TECHNICAL LIBRARY
ABBOTTAEROSPACE.COM

5-2.2 MECHANICS AND KINEMATICS OF PERFECT EQUILIBRATION

Two conditions are necessary to obtain perfect balance throughout the operating range of spring equilibrators. To make Eq. 5-28 true for all ϕ, i.e., perfect equilibration, it is required that

$$\psi_0 = \pi/2, \text{ rad} \tag{5-31}$$

and from Eq. 5-30, the spring rate K_s is

$$K_s = \frac{Mw_0}{cR}, \text{ N/m.} \tag{5-32}$$

The spring rate equation of Eq. 5-32 has two independent variables: the dimensions c and R shown for equilibrator positions below and above the trunnions in Figs. 5-13 and 5-14, respectively. The turning radius R is selected to conform in size to the rest of the structure as discussed in par. 5-2.1.

Consideration of spring efficiency shows how to find a practical spring length c. Fig. 5-15 shows the force-deflection curve of a spring. By substituting for M_{e_0} and r_0, Eq. 5-23 may be written as

$$F_0 = \frac{Mw_0L_0}{cR\sin\psi_0}, \text{ N.} \tag{5-33}$$

By substituting from Eq. 5-31 for ψ_0 and from Eq. 5-30 for M_{w_0}, Eq. 5-33 yields

$$F_0 = \frac{Mw_0L_0}{cR} = K_sL_0, \text{ N.} \tag{5-34}$$

The maximum spring deflection S_{max} occurs at the maximum angle of depression. Written in terms of the maximum spring force F_{max} and the spring rate K_s, S_{max} becomes

$$S_{max} = \frac{F_{max}}{K_s}, \text{ m} \tag{5-35}$$

where

F_{max} = maximum spring force, N.

The area under the curve of Fig. 5-15 represents the total spring energy E_t, which is, by substituting the value of S_{max} from Eq. 5-35,

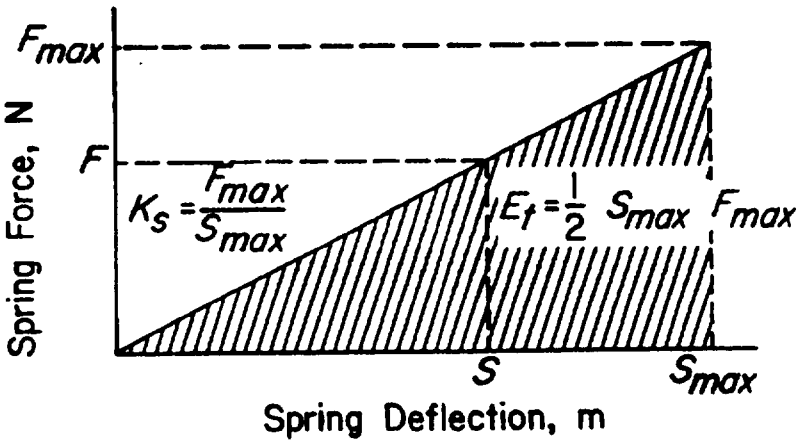

Figure 5-15. Force-Deflection Curve of a Spring

THIS DOCUMENT PROVIDED BY THE ABBOTT AEROSPACE
TECHNICAL LIBRARY
ABBOTTAEROSPACE.COM

$$E_t = \frac{S_{max}F_{max}}{2} = \frac{F_{max}^2}{2K_s}, \text{ J.} \tag{5-36}$$

From Eqs. 5-24 and 5-7, .

$$F_{max} = F_0 - K_s(L_0 - L_{max}), \text{ N} \tag{5-37}$$

where

L_{max} = maximum equilibrator length, m.

By substituting the value for F_0 from Eq. 5-34 and collecting terms, Eq. 5-37 becomes simply

$$F_{max} = K_s L_{max}, \text{ N.} \tag{5-38}$$

It should be noted that the values of L_{max} and S_{max} are identical. By substituting for F_{max} from Eq. 5-38 and for K_s from Eq. 5-32 into Eq. 5-36, the total energy E_t is

$$E_t = \frac{K_s^2 L_{max}^2}{2K_s} = \frac{M_{W_0} L_{max}^2}{2cR}, \text{ J.} \tag{5-39}$$

From Eq. 5-3, where $L_\theta = L_{max}$,

$$L_{max}^2 = c^2 + R^2 - 2cR\cos\psi, \text{ m}^2 \tag{5-40}$$

but $\psi = \psi_0 - \phi_D$, and since $\psi_0 = \pi/2$, then

$$\cos\psi = \cos(\psi_0 - \phi_D) = \sin\phi_D$$

where

$\phi_D = \phi$ at maximum angle of depression, rad.

By using this expression for $\cos\psi$ in Eq. 5-40, Eq. 5-39 becomes

$$E_t = M_{W_0}\left(\frac{c^2 + R^2 - 2cR\sin\phi_D}{2cR}\right), \text{ J.} \tag{5-41}$$

By rearrangement of terms, Eq. 5-41 may be written as

$$E_t = \frac{M_{W_0}}{2}\left(\frac{c}{R} + \frac{R}{c} - 2\sin\phi_D\right), \text{ J.} \tag{5-42}$$

Eq. 5-42 is the general equation for the required spring energy. It shows that the total energy requirement of the equilibrator spring is dependent on M_{W_0}, the weight moment when $\phi = 0$, on the maximum depression angle, and on the ratio of c to R, which is the only variable. By defining

$$K = \frac{c}{R}, \text{ dimensionless} \tag{5-43}$$

where

K = ratio of c to R (Figs. 5-13 and 5-14), dimensionless,

THIS DOCUMENT PROVIDED BY THE ABBOTT AEROSPACE
TECHNICAL LIBRARY
ABBOTTAEROSPACE.COM

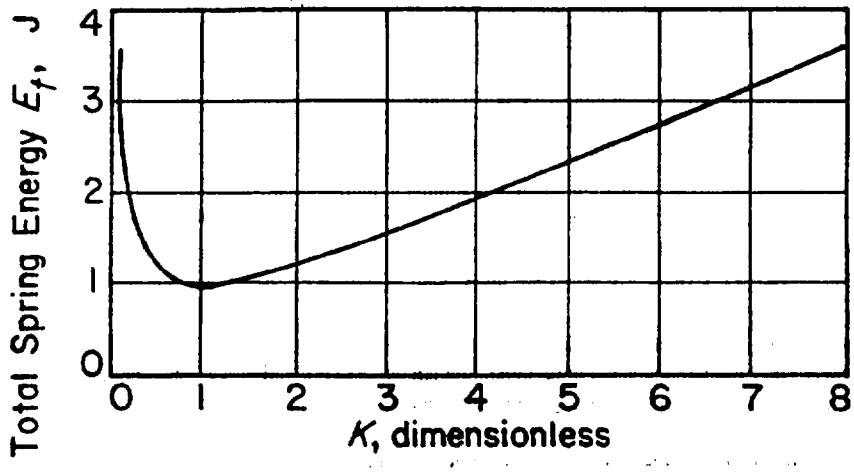

Figure 5-16. Trend Curve of Total Spring Energy

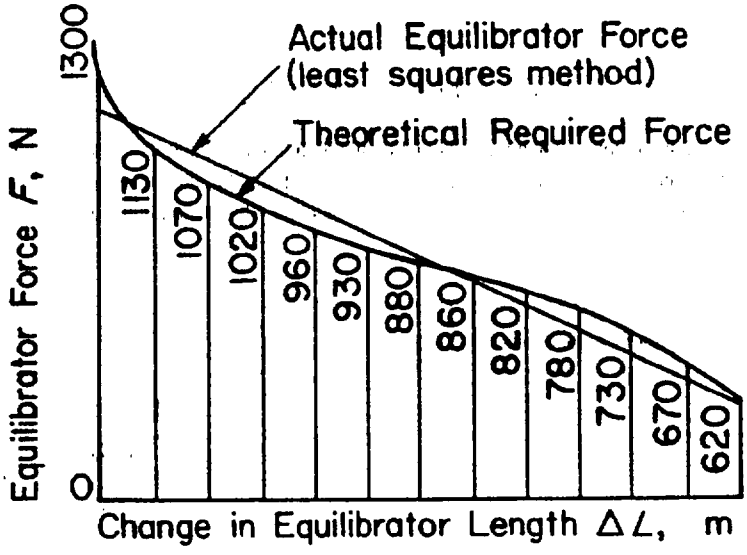

Figure 5-17. Equilibrator Force Curve

range is slight enough to be acceptable. Ordinarily, the low angle is selected as zero and the high angle is slightly less than maximum elevation. For example, assume that the two angles selected are $\phi = 0$ and $\phi = u$. The weight moments at these elevations are calculated as M_{W_0} and M_{W_u}, so

$$F_0 = \frac{M_{W_0}}{r_0}, \text{ N} \tag{5-50}$$

$$F_u = \frac{M_{W_u}}{r_u}, \text{ N} \tag{5-51}$$

where

$u = \phi$ at high angle of elevation, rad
F_u = equilibrator force at $\phi = u$, N
M_{W_u} = weight moment of tipping parts about trunnion at $\phi = u$, N·m
r_u = equilibrator moment arm at $\phi = u$, m.

THIS DOCUMENT PROVIDED BY THE ABBOTT AEROSPACE
TECHNICAL LIBRARY
ABBOTTAEROSPACE.COM

The spring rate is now calculated from Eq. 5-24 as

$$K_s = \frac{F_0 - F_u}{\Delta L} \text{ , N/m.} \tag{5-52}$$

After the spring rate is known, the equilibrator force at any angle of elevation may be found.

2. *Method 2.* Draw a straight line that most closely fits the theoretical force versus elevation curve, as shown in Fig. 5-17. The initial force F_0 is read directly from the curve, and the slope of the straight line determines the spring constant.

3. *Method 3.* The most accurate method of approximate equilibrator design is to apply the theory of optimization to the forces on the equilibrator which are required to balance the weight moments at all angles of elevation. Optimization methods are presented in par. 5-5.

5-2.4 FRICTION EFFECTS ON EQUILIBRATION

Equilibrator performance, including the effect of friction, during elevation and depression should be computed. Friction is considered in the end of connection bearings and in the trunnion bearing. Fig. 5-18 shows the kinematics of the equilibrator and defines rotational directions at the bearings and also defines the direction of frictional torques and reaction forces at each bearing.

The rotations at bearings A and B (Fig. 5-18) are as follows:

1. During Elevation:
   a. $\theta_0 \leq \theta < \theta_1$ Equilibrator rotates clockwise at A and counterclockwise at B
   b. $\theta_1 \leq \theta \leq \theta_u$ Equilibrator rotates counterclockwise at A and counterclockwise at B
2. During Depression. Directions of rotation are opposite those in elevation

where

θ_0 = minimum elevation angle, rad
θ_1 = elevation angle when equilibrator makes an angle $\pi/2$ rad with line from trunnion to B, rad
θ_u = maximum elevation angle, rad.

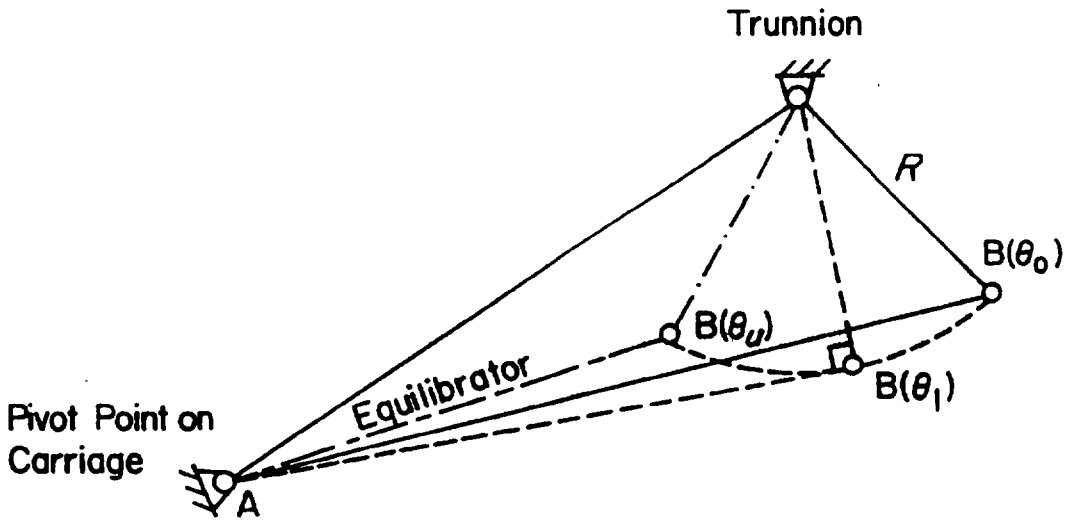

Figure 5-18. Kinematics of Equilibrator; Point B = B(θ) at Elevation θ

Fig. 5-19(A) shows a free-body diagram of the equilibrator during elevation when the elevation angle θ is in the range $\theta_0 \leq \theta \leq \theta_1$. The equilibrator force is acting parallel to the equilibrator and reaction forces are acting perpendicular to the equilibrator. By summing moments about points A and B, two equilibrium equations are obtained as

$$\Sigma M_A = T_A - T_B - F_B L = 0 \tag{5-53}$$

THIS DOCUMENT PROVIDED BY THE ABBOTT AEROSPACE
TECHNICAL LIBRARY
ABBOTTAEROSPACE.COM

$$\Sigma M_B = T_A - T_B + F_A L = 0 \tag{5-54}$$

where

M_A, M_B = moments about A and B, respectively, N·m
T_A, T_B = frictional torques at A and B, respectively, N·m
F_A, F_B = reaction forces at A and B, respectively, N
L = equilibrator length, m.

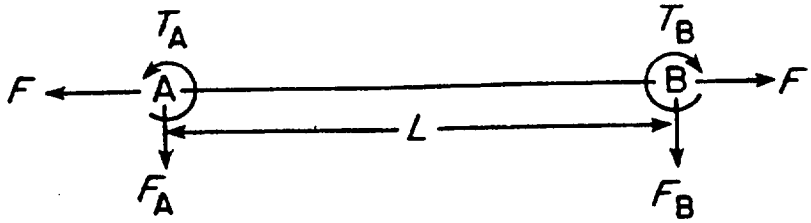

(A) $\theta_0 \leq \theta < \theta_1$, Elevation

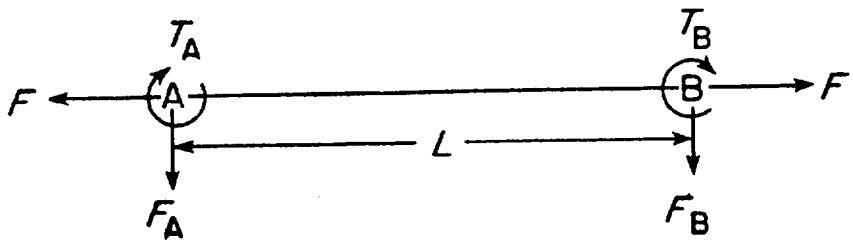

(B) $\theta_1 \leq \theta \leq \theta_u$, Elevation

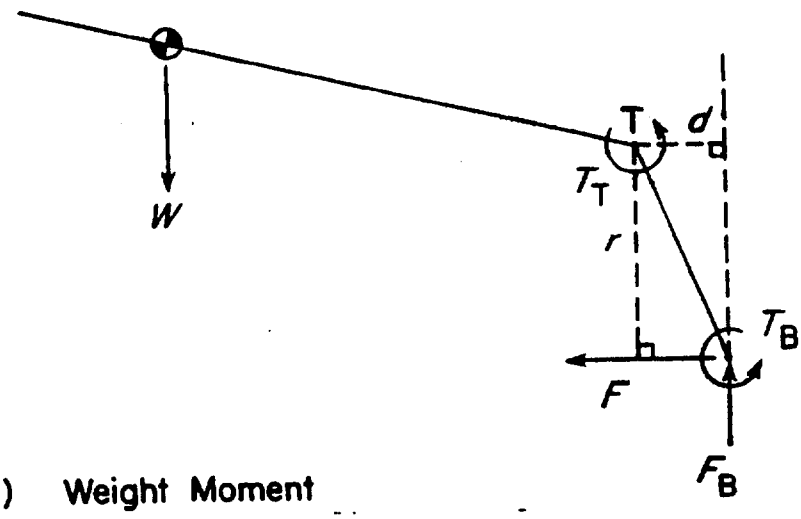

(C) Weight Moment

Figure 5-19. Free-Body Diagrams

Subtract Eq. 5-54 from Eq. 5-53, then

$$F_A = -F_B, \text{ N.} \tag{5-55}$$

The frictional torques T_A and T_B are

$$T_A = \mu r_A \sqrt{F^2 + F_A^2}, \text{ N·m} \tag{5-56}$$

THIS DOCUMENT PROVIDED BY THE ABBOTT AEROSPACE
TECHNICAL LIBRARY
ABBOTTAEROSPACE.COM

$$T_B = \mu r_B \sqrt{F^2 + F_B^2}\ , \text{N·m} \tag{5-57}$$

where

μ = friction coefficient at bearings, dimensionless
F = equilibrator force, N
r_A, r_B = radii of bearings at A and B, respectively, m.

With Eq. 5-55, substituting T_A and T_B from Eqs. 5-56 and 5-57 into Eq. 5-53 yields

$$\frac{F_B}{F} = \frac{\mu(r_A - r_B)}{\sqrt{L^2 - \mu^2(r_A - r_B)^2}}\ , \text{dimensionless.} \tag{5-58}$$

When $r_A = r_B$, $F_B/F = 0$, i.e., $F_B = 0$ and accordingly $F_A = 0$. Even when $r_A \neq r_B$, $(r_A - r_B)/L << 1$ and $\mu << 1$. Thus from Eqs. 5-56 and 5-57 and since $F_A = F_B \approx 0$,

$$T_A = \mu F r_A, \text{ N·m} \tag{5-59}$$

$$T_B = \mu F r_B, \text{ N·m} \tag{5-60}$$

are good approximations.

In case $\theta_1 \leq \theta \leq \theta_u$ in elevation, the friction torques and reaction forces have the directions shown in Fig. 5-19(B). By calculations similar to those in the range $\theta_0 \leq \theta < \theta_1$, in this case

$$\frac{F_B}{F} = \frac{\mu(r_A + r_B)}{\sqrt{L^2 - \mu^2(r_A - r_B)^2}}\ . \tag{5-61}$$

By similar reasoning, the approximations of Eqs. 5-59 and 5-60 are adequate for this case also.

Fig. 5-19(C) shows a free-body diagram of the tipping parts when the elevation angle θ is in the range $\theta_0 \leq \theta < \theta_1$ and is elevating. Consider summation of moments at the trunnion; equilibrium requires

$$\Sigma M_T = M_W - rF + F_B d + T_B - T_e + T_T = 0 \tag{5-62}$$

where

M_T = moment about trunnion, N·m
r = equilibrator moment arm, m
T_e = moment provided by elevating strut, N·m
T_T = friction torque at trunnion, N·m
d = perpendicular distance from T to the extension of force F_B, m.

The torque T_T is obtained by multiplication of a friction coefficient, radius, and reaction force at the trunnion. From Eq. 5-62, the clockwise torque that must be provided by the elevating strut for elevation in the range $\theta_0 \leq \theta < \theta_1$ is

$$T_e = M_W - rF + F_B d + T_B + T_T, \text{ N·m.} \tag{5-63}$$

The clockwise torque that must be provided by the elevating strut for $\theta_1 \leq \theta \leq \theta_u$, in elevation, is

$$T_e = M_W - rF + F_B d - T_B + T_T, \text{ N·m.} \tag{5-64}$$

THIS DOCUMENT PROVIDED BY THE ABBOTT AEROSPACE
TECHNICAL LIBRARY
ABBOTTAEROSPACE.COM

The counterclockwise torque required for $\theta_0 \leq \theta < \theta_1$, in depression, is

$$T_c = -M_W + rF + F_s d + T_s + T_T, \text{ N·m} \tag{5-65}$$

and for $\theta_1 \leq \theta \leq \theta_u$, in depression, is

$$T_c = -M_W + rF - F_s d - T_s + T_T, \text{ N·m.} \tag{5-66}$$

5-3 SPRING EQUILIBRATOR DESIGN

Coil springs provide an equilibrator with a simple, efficient, force-producing device. Although bulky, coil springs are applicable to any mount that has sufficient space and weight allowance. Sometimes, to conserve space, two concentric springs are used. Fig. 5-4 illustrates such an installation. The sum of the individual spring rates equals the effective spring rate. The springs are wound counter to each other to preclude binding. The inner spring generally provides about 40% of the outer spring force.

Compression springs are used in equilibrators for the following reasons:

1. They cannot be stressed higher than their solid heights permit.
2. They need no additional strength for end loops as do extension springs.
3. In case of breakage, a compression spring will still function, although at reduced load.

A spring having a slenderness ratio (free length divided by mean coil diameter) greater than four may tend to buckle like a column. The ends must be restrained from lateral movement or buckling may occur at lengths less than should be expected. If a spring is so long that it is unstable, several shorter lengths may be used with spacers in between. The total number of active coils of the several shorter springs, however, must be equal to that of the full-length spring, and the spacers must be guided. In some equilibrator designs, the spring housing offers sufficient restraint to prevent buckling. For a detailed discussion of spring buckling, see Chapter 6 of Ref. 1.

5-3.1 A PERFECT BALANCE EQUILIBRATOR

To illustrate the procedure for calculating the parameters of a perfectly balanced spring equilibrator system, consider the configuration shown in Fig. 5-20 with the following data:

$\alpha = \beta$ (implies $\phi = 0$ since $\psi_0 = \pi/2$)
$\psi_0 = \pi/2$ rad (required for perfect equilibration)
$\phi' = 0.0873$ rad
$c = 0.309$ m
$R = 0.922$ m
$R_t = 0.457$ m
$W_t = 8896$ N

where, as shown in Figs. 5-10, 5-13, 5-14, and 5-20,
$\phi' = \phi - \theta$, angle between R_t and centerline of gun tube, rad.

From Eq. 5-8

$$M_{W_0} = R_t W_t = 4065 \text{ N·m.}$$

From Eq. 5-32

$$K_s = \frac{M_{W_0}}{cR} = 14{,}268 \text{ N/m.}$$

THIS DOCUMENT PROVIDED BY THE ABBOTT AEROSPACE
TECHNICAL LIBRARY
ABBOTTAEROSPACE.COM

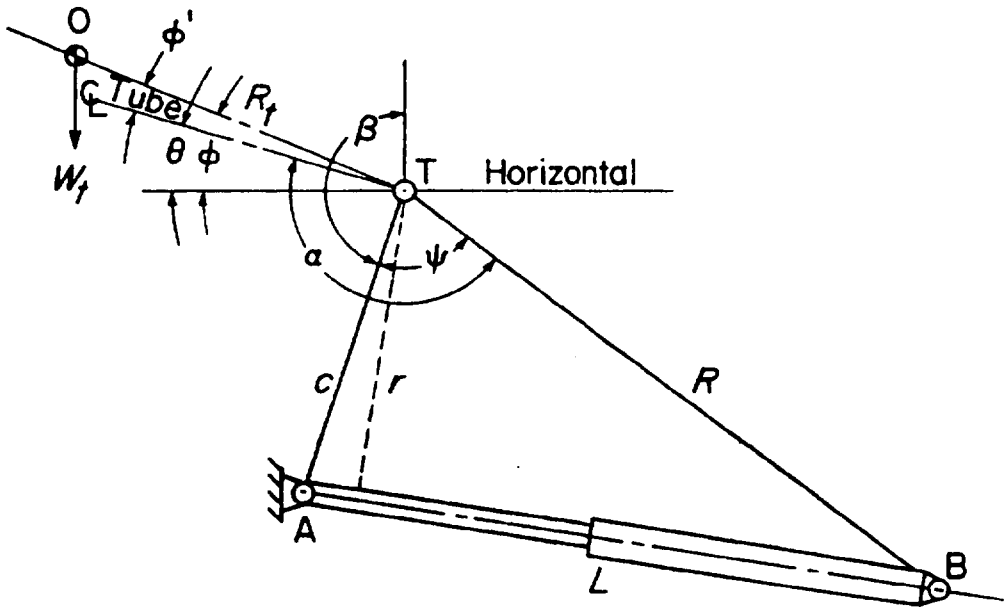

T = center of trunnions, pivot point of tipping parts
A = pivot point of equilibrator on carriage
B = pivot point on tipping parts
O = CG of tipping parts

Figure 5-20. Geometry of Spring Equilibrator

The maximum spring force will occur at the minimum angle of elevation, $\theta_0 = -0.0873$ rad and $\phi = 0$. From Eq. 5-3

$$L_{max}^2 = 0.946 \text{ m}^2$$

or

$$L_{max} = 0.973 \text{ m}.$$

From Eq. 5-17, the maximum spring force is

$$F_{max} = K_s L_{max} = 13{,}882 \text{ N}.$$

Sufficient information is now available to design the spring. An example of spring design appears in par. 5-3.3. If desired, perfect balance can be shown throughout the elevation cycle by substituting numerical values into Eqs. 5-9 and 5-10.

5-3.2 AN APPROXIMATE BALANCE EQUILIBRATOR

When space limitations preclude the installation of a perfect balance equilibrator, an approximate equilibrator must be designed which will closely approximate the ideal. To illustrate calculations for approximate equilibration, consider again the geometry of Fig. 5-20 with the following data (for a more detailed example of calculations refer to Ref. 2):

$\alpha = \beta + 0.4363$
$\psi = 2.068$ rad, when $\theta = 0$ (note perfect equilibration requires $\psi = \pi/2$)
$\phi' = 0.061$ rad

THIS DOCUMENT PROVIDED BY THE ABBOTT AEROSPACE
TECHNICAL LIBRARY
ABBOTTAEROSPACE.COM

$c = 0.309$ m
$R = 0.922$ m
$R_t = 0.457$ m
$W_t = 8896$ N.
From Eq. 5-3

$$L_\theta^2 = 0.9452 - 0.5698\cos\psi, \text{ m}^2.$$

From Eq. 5-6

$$r = (0.285\sin\psi)/L_\theta, \text{ m}$$

where, from Eq. 5-19 and $\phi = \theta + \phi'$ (See Fig. 5-20.),

$$\psi_\theta = \psi - \theta - \phi' = 2.007 - \theta, \text{ rad.}$$

The moment arm may now be calculated for a range of angles θ. Results of such a calculation are given in Table 5-2.

The weight moment M_W can be calculated from Eq. 5-1, as

$$M_W = W_t R_t \cos\phi, \text{ N·m}$$

where from Fig. 5-20,

$$\phi = \theta + \phi' = \theta + 0.061, \text{ rad.}$$

The given data and this equation provide the values presented in Table 5-3.

Characteristics of the springs to be used in approximate equilibration are determined by equating the equilibrator and weight moments at 0 rad and 0.96 rad elevation and then solving for the spring rate. For this analysis, two concentric springs are considered, and the inner spring supports 40% of the outer spring load. The total spring loads at $\phi = \phi'$ ($\theta = 0$) and ($\theta = 0.96$) rad are from Eqs. 5-50 and 5-51, respectively,

$$F_1 = \frac{M_W}{r} = \frac{W_t R_t \cos\phi}{r} = \frac{8896 \times 0.457 \times 0.9981}{0.2368} = 17{,}136 \text{ N}$$

and

$$F_2 = \frac{M_W}{r} = \frac{W_t R_t \cos\phi}{r} = \frac{8896 \times 0.457 \times 0.5225}{0.3031} = 7008 \text{ N.}$$

Values for ϕ and r for these calculations were obtained from Tables 5-3 and 5-2, respectively. The portions of these loads borne by the outer spring are, therefore,

$$F_{1_o} = \frac{F_1}{1.4} = \frac{17{,}136}{1.4} = 12{,}240 \text{ N}$$

$$F_{2_o} = \frac{F_2}{1.4} = \frac{7008}{1.4} = 5006 \text{ N.}$$

THIS DOCUMENT PROVIDED BY THE ABBOTT AEROSPACE
TECHNICAL LIBRARY
ABBOTTAEROSPACE.COM

The corresponding spring deflections are taken from Table 5-2 and

$$\Delta L = 1.0889 - 0.8128 = 0.2761 \text{ m}$$

which yields the outer spring rate, by Eq. 5-52,

$$K_{s_o} = \frac{F_{1_o} - F_{2_o}}{\Delta L} = \frac{12{,}240 - 5006}{0.2761} = 26{,}201 \text{N/m}.$$

The spring rate for the inner spring is then 40% of this quantity. Data needed to design the springs are now available.

TABLE 5-2
MOMENT ARM CALCULATIONS—SPRING EQUILIBRATOR DESIGN

θ, rad	ψ, rad	$\sin\psi$	$\cos\psi$	L^2, m^2	L, m	r, m
−0.087	2.094	0.8862	−0.4997	1.2297	1.1089	0.2223
0	2.007	0.9064	−0.4225	1.1858	1.0889	0.2368
0.175	1.832	0.9661	−0.2582	1.0923	1.0451	0.2630
0.349	1.658	0.9962	−0.0871	0.9949	0.9975	0.2842
0.524	1.483	0.9961	0.0877	0.8955	0.9463	0.2995
0.698	1.309	0.9659	0.2588	0.7961	0.8933	0.3077
0.785	1.222	0.9398	0.3418	0.7509	0.8665	0.3086
0.873	1.134	0.9061	0.4230	0.7046	0.8394	0.3072
0.960	1.047	0.8659	0.5002	0.6607	0.8128	0.3031
1.047	0.960	0.8192	0.5735	0.6190	0.7868	0.2963
1.134	0.873	0.7663	0.6425	0.5797	0.7614	0.2864

TABLE 5-3
WEIGHT MOMENT CALCULATIONS—SPRING EQUILIBRATOR DESIGN

θ, rad	ϕ, rad	$\cos\phi$	$R_t\cos\phi$, m	M_w, N
−0.087	−0.026	0.9997	0.4570	4064
0	0.061	0.9981	0.4563	4057
0.175	0.236	0.9723	0.4445	3952
0.349	0.410	0.9171	0.4193	3728
0.524	0.585	0.8337	0.3812	3389
0.698	0.759	0.7255	0.3317	2949
0.785	0.846	0.6630	0.3031	2695
0.873	0.934	0.5946	0.2719	2417
0.960	1.021	0.5225	0.2389	2124
1.047	1.108	0.4465	0.2041	1815
1.134	1.195	0.3670	0.1678	1492

5-3.3 COMPONENT DESIGN AND MANUFACTURING PROCESS

5-3.3.1 Spring Design

The most common type of mechanical spring used in equilibrators is the helical compression spring because it is simplest and easiest to install. The following commonly used equations are fundamental in the design of helical compression springs (See Chapter 6 of Ref. 1 or Chapter 5 of Ref. 7.):

$$\tau = \frac{8FD}{\pi d^3}, \text{ Pa} \qquad (5\text{-}67)$$

THIS DOCUMENT PROVIDED BY THE ABBOTT AEROSPACE
TECHNICAL LIBRARY
ABBOTTAEROSPACE.COM

$$F = \frac{\pi d^3 \tau}{8D}, \text{ N} \tag{5-68}$$

$$\delta = \frac{8FD^3 n}{Gd^4}, \text{ m} \tag{5-69}$$

$$\delta = \frac{\pi D^2 n \tau}{Gd}, \text{ m} \tag{5-70}$$

$$k = \frac{Gd^4}{8D^3 n}, \text{ N} \tag{5-71}$$

$$k = \frac{F}{\delta}, \text{ N/m} \tag{5-72}$$

$$\tau = \frac{\delta G d}{\pi D^2 n}, \text{ Pa} \tag{5-73}$$

$$\tau' = K\tau = \frac{8FDK}{\pi d^3}, \text{ Pa} \tag{5-74}$$

$$K = \frac{4c - 1}{4c - 4} + \frac{0.615}{c}, \text{ dimensionless} \tag{5-75}$$

$$c = \frac{D}{d} = \text{spring index, dimensionless} \tag{5-76}$$

where

F = load on spring, N
d,D = wire and mean coil diameters of spring, respectively, m
δ = spring deflection, m
τ = uncorrected shear stress in spring, Pa
$\tau' = K\tau$ = corrected shear stress in spring, Pa
K = curvature correction factor of spring, dimensionless
n = number of active coils in spring, dimensionless
$k = F/\delta$ = spring rate or stiffness, N/m
G = shear modulus of spring, Pa.

If compression springs are too long, instability may occur due to column action under load. When this occurs, the spring may fly out laterally. In design, it is necessary to guard against this condition by choosing the spring proportions so that the working load will always be less than the critical buckling load. If this is not practical, guides must be provided to prevent lateral moment. In equilibrator design the spring housing may act as a guide. Buckling criteria for compression coil springs are given in Chapter 6 of Ref. 1 and in Ref. 7.

As a sample spring design calculation, consider the outer spring of the equilibrator of par. 5-3.2. Assume that the mean diameter D of the spring is selected, based on space availability, as

$$D = 0.1334 \text{ m}$$

THIS DOCUMENT PROVIDED BY THE ABBOTT AEROSPACE
TECHNICAL LIBRARY
ABBOTTAEROSPACE.COM

and also that the allowable stress τ_a in the spring wire is

$$\tau_a = 8.274 \times 10^8 \text{ Pa.}$$

Then, the wire diameter is given by Eq. 5-68 as

$$d^3 = \frac{8F_{l_o}D}{\pi\tau_a} = \frac{8 \times 12{,}240 \times 0.1334}{3.14 \times 8.274 \times 10^8} = 5.025 \times 10^{-6}, \text{ m}^3$$

or

$$d = 0.0171 \text{ m.}$$

The deflection δ_1 of the assembled equilibrator spring at $\phi = \phi'$ ($\theta = 0$) deg is, by Eq. 5-72,

$$\delta_1 = \frac{F_{l_o}}{K_{s_o}} = \frac{12{,}240}{26{,}201} = 0.467 \text{ m.}$$

The number of active coils n in the spring is given by Eq. 5-69 as

$$n = \frac{\delta_1 G d^4}{8F_{l_o}D^3}$$

$$= \frac{0.467 \times 7.929 \times 10^{10} \times (0.0171)^4}{8 \times 12{,}240 \times (0.1334)^3}$$

$$= 13.6$$

where

G = shear modulus of spring, Pa
= 7.929×10^{10} Pa.

To compute the maximum spring stress, the maximum deflection and maximum load must first be determined. The maximum spring deflection δ_{max} occurs at extreme weapon depression, (L values are taken from Table 5-2)

$$\delta_{max} = \delta_1 + (L_{-0.087} - L_1) = 0.467 + (1.1089 - 1.0889) = 0.487 \text{ m.}$$

The maximum load (at −0.087 rad elevation) in the outer spring is given by Eq. 5-72 as

$$F_{max} = K_{s_o}S_{max} = 26{,}201 \times 0.487 = 12{,}760 \text{ N.}$$

Therefore, the uncorrected maximum shear stress is, by Eq. 5-68,

$$\tau = \frac{8F_{max}D}{\pi d^3} = 8.67 \times 10^8 \text{ Pa.}$$

Maximum stress for alloy steel wire that is heat treated after coiling, for a wire of 0.0170 m diameter, is 9.1×10^8 Pa (See Ref. 7.), which renders the calculated stress of 8.67×10^8 Pa acceptable.

THIS DOCUMENT PROVIDED BY THE ABBOTT AEROSPACE
TECHNICAL LIBRARY
ABBOTTAEROSPACE.COM

The characteristics of the inner spring are found in the same manner as that shown for the outer spring. Since the inner spring rate K_{s_i} is 40% of the outer spring rate,

$$K_{s_i} = 0.4 \times 26{,}201 = 10{,}480 \text{ N/m}.$$

The remaining task is to compute the performance of the double spring equilibrator of par. 5-3.2. The total spring rate K_s is

$$K_s = 26{,}201 + 10{,}480 = 36{,}681 \text{ N/m}.$$

The spring force F_s on the rod is

$$F_s = K_s (\delta_1 - \Delta L), \text{ N}.$$

The equilibrator moment M_e, when friction is neglected, is given by Eq. 5-9 as

$$M_e = F_s r, \text{ N·m}$$

and the imbalanced moment T_e is

$$T_e = M_e - M_w, \text{ N·m}.$$

The spring equilibrator performance is then indicated by the numerical data from Tables 5-2 and 5-3 of par. 5-3.2, which were calculated using the foregoing equations. Results are tabulated in Table 5-4. Thus the approximate spring equilibrator designed in par. 5-3.2 and in this paragraph has a maximum imbalance of 189 N·m, which must be provided by the elevating mechanism (neglecting friction effects).

5-3.3.2 Manufacturing Processes

Manufacturing practices for spring equilibrators involve only standard processes and procedures. The most critical component is the coil spring, which is manufactured according to procedures presented in Chapter 6 of Ref. 1.

TABLE 5-4
SPRING PERFORMANCE CALCULATIONS—PNEUMATIC EQUILIBRATOR DESIGN

θ, rad	ΔL, m	$\delta_{\phi'} - \Delta L$, m	F_s, N	r, m	M_e, N·m	M_w, N·m	T_e, N·m
−0.087	−0.0200	0.4870	17,880	0.2223	3975	4064	−91
0	0	0.4670	17,146	0.2368	4060	4057	0
0.175	0.0438	0.4232	15,538	0.2630	4086	3952	131
0.349	0.0914	0.3756	13,790	0.2842	3919	3728	189
0.524	0.1426	0.3244	11,910	0.2995	3567	3389	176
0.698	0.1956	0.2714	9,964	0.3077	3066	2949	115
0.785	0.2224	0.2446	8,980	0.3086	2771	2695	74
0.873	0.2495	0.2175	7,986	0.3072	2453	2417	34
0.960	0.2761	0.1909	7,009	0.3031	2124	2124	−1
1.047	0.3021	0.1649	6,054	0.2963	1794	1815	−22

Maximum stress for alloy steel wire that is heat treated after coiling, for a wire of 0.0170 in diameter, is 9.1×10^8 Pa (See Ref. 7.), which renders the calculated stress of 8.67×10^8 Pa acceptable.

THIS DOCUMENT PROVIDED BY THE ABBOTT AEROSPACE
TECHNICAL LIBRARY
ABBOTTAEROSPACE.COM

5-4 PNEUMATIC EQUILIBRATOR DESIGN

5-4.1 APPROXIMATE BALANCE EQUILIBRATOR

5-4.1.1 Force Versus Gas Volume Relation

In a pneumatic equilibrator, force is provided by gas pressure. The design should be based on minimum handwheel loads. Since manual operation is a slow process, the gas is assumed to behave isothermally. The gas volume is determined by equating the equilibrator moments and the weight moments at $\phi = 0$ and at $\phi = u$ (near maximum elevation), solving for the corresponding forces and pressures, and subsequently solving for the initial gas volume.

The conditions of balance at $\phi = 0$ and $\phi = u$ (See Eq. 5-9.) are

1. At $\phi = 0$ ($M_e = M_w$),

$$F_0 = \frac{M_{w_0}}{r_0}, \text{ N} \tag{5-77}$$

$$P_0 = \frac{F_0}{A}, \text{ Pa} \tag{5-78}$$

and

2. At $\phi = u$ ($M_e = M_w$),

$$F_u = \frac{M_{w_u}}{r_u}, \text{ N} \tag{5-79}$$

$$P_u = \frac{F_u}{A}, \text{ Pa} \tag{5-80}$$

where

M_{w_0} = weight moment of tipping parts about trunnion at $\phi = 0$, N·m
F_0 = equilibrator force at $\phi = 0$, N
P_0 = gas gage pressure at $\phi = 0$, Pa
P_u = gas gage pressure at $\phi = u$, Pa
A = effective piston area, m^2.

The change in volume of gas in the cylinder due to a change in equilibrator length, at the upper elevation, is

$$\Delta V_u = A \Delta L_u, \text{ m}^3 \tag{5-81}$$

where

ΔV_u = change in gas volume due to equilibrator travel at $\phi = u$, m^3
ΔL_u = equilibrator travel at $\phi = u$ elevation, m.

Thus

$$V_u = V_0 + \Delta V_u, \text{ m}^3 \tag{5-82}$$

where

V_0 = gas volume at $\phi = 0$, m^3
V_u = gas volume at $\phi = u$, m^3.

THIS DOCUMENT PROVIDED BY THE ABBOTT AEROSPACE
TECHNICAL LIBRARY
ABBOTTAEROSPACE.COM

The absolute gas pressure at elevation θ is

$$P_{a_\theta} = P_\theta + P_A, \text{ Pa} \tag{5-83}$$

where

P_θ = gas gage pressure at θ elevation, Pa
P_A = atmospheric pressure = 101,300 Pa
P_{a_θ} = absolute gas pressure at θ elevation, Pa.

According to Boyle's law of isothermal expansion (See Ref. 8.), gas pressure and volume are related according to

$$P_{a_0} V_0 = P_{a_u} V_u, \text{ J} \tag{5-84}$$

so, by substituting the expression for V_u from Eq. 5-82,

$$V_0 = \left(\frac{P_{a_u}}{P_{a_0}}\right) V_u = \left(\frac{P_{a_u}}{P_{a_0}}\right)(V_0 + \Delta V_u), \text{ m}^3 \tag{5-85}$$

where

P_{a_0} = absolute gas pressure at $\phi = 0$, Pa
P_{a_u} = absolute gas pressure at $\phi = u$, Pa.

When P_{a_u} and P_{a_0} are known, V_0 can be determined.

The equilibrator displacement at any angle of elevation yields

$$\Delta V_\theta = A \Delta L_\theta, \text{ m}^3 \tag{5-86}$$

where

ΔV_θ = change in gas volume at θ elevation, m^3
ΔL_θ = equilibrator travel at θ elevation, m.

The gas volume at any angle of elevation is

$$V_\theta = V_0 + \Delta V_\theta, \text{ m}^3 \tag{5-87}$$

where

V_θ = gas volume at θ elevation, m^3.

The gas gage pressure P_θ at any angle can be found from Boyle's law as

$$P_\theta = P_{a_0}\left(\frac{V_0}{V}\right) - P_A, \text{ Pa} \tag{5-88}$$

where

P_{a_0} = absolute gas pressure at $\phi = 0$, Pa.

Now, the equilibrator force at any angle of elevation is

$$F_\theta = P_\theta A, \text{ N} \tag{5-89}$$

where

F_θ = equilibrator force at θ elevation, N.

THIS DOCUMENT PROVIDED BY THE ABBOTT AEROSPACE
TECHNICAL LIBRARY
ABBOTTAEROSPACE.COM

The equilibrator moment is thus

$$M_e = rF, \text{ N·m} \tag{5-90}$$

where

M_e = equilibrator moment about the trunnion, N·m
r = equilibrator moment arm, m.

The moment T_e that must be provided by the elevating strut is thus

$$T_e = M_W - M_e, \text{ N·m.} \tag{5-91}$$

The maximum gas pressure for pneumatic equilibrators is limited to the capacity of the packings in the cylinders. The initial pressure at $\phi = 0$ must be selected so that P will not exceed this limit. This requires a trial-and-error solution since the displacements, volumes, and piston area are interdependent. The greatest increase in pressure under normal operation takes place during compression of the gas from maximum to minimum volume, i.e., as the gun depresses from maximum to minimum elevation. Assume adiabatic compression so that (See Ref. 3.)

$$P_{max} = P_{a_{min}} \left(\frac{V_{max}}{V_{min}} \right)^{1.4} - 101{,}300 = P_d, \text{ Pa} \tag{5-92}$$

where

P_{max} = maximum gas gage pressure, Pa
$P_{a_{min}}$ = minimum gas absolute pressure, Pa
V_{max} = maximum gas volume, m^3
V_{min} = minimum gas volume, m^3
P_d = limit design pressure of packing, Pa.

By Boyle's law (Eq. 5-84)

$$P_0 = P_{a_{min}} \left(\frac{V_{max}}{V_0} \right) - 101{,}300, \text{ Pa.} \tag{5-93}$$

The effective area A of the piston may now be written as

$$A = \frac{F_0}{P_0}, \text{ m}^2. \tag{5-94}$$

Once the piston area A is determined, appropriate sizes are selected for the piston and piston rod.

As an illustration, two pneumatic equilibrators performing as one unit in a hypothetical weapon have been chosen. The equilibrator geometry is shown in Fig. 5-21. For calculating the moment arm, data given are when $\phi = \phi' (\theta = 0)$:

ψ = 1.515 rad
c = 1.4478 m
θ_{max} = 1.134 rad (maximum elevation)
R = 0.4826 m
β = 2.150 rad
θ_{min} = −0.0873 rad (minimum elevation).

From Eq. 5-3, equilibrator length L at elevation θ is

$$L_\theta = (c^2 + R^2 - 2cR\cos\psi)^{1/2} = (2.3290 - 1.3974\cos\psi)^{1/2}, \text{ m.}$$

THIS DOCUMENT PROVIDED BY THE ABBOTT AEROSPACE
TECHNICAL LIBRARY
ABBOTTAEROSPACE.COM

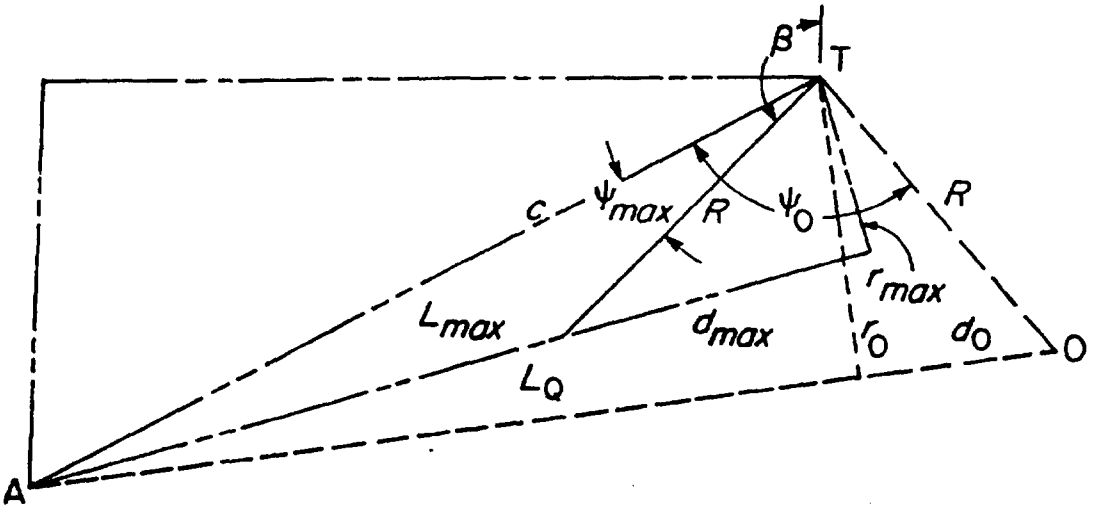

Figure 5-21. Geometry of a Typical Pneumatic Equilibrator

From Eq. 5-6, the equilibrator moment arm r is

$$r = (cR\sin\psi)/L_\theta = 0.69871(\sin\psi)/L_\theta, \text{ m}$$

and the distance d shown in Fig. 5-21 is (since $\theta = 0$, $r_0 \equiv r$ and $d_0 \equiv d$)

$$d = \sqrt{R^2 - r^2} = \sqrt{0.23290 - r^2}, \text{ m}.$$

The moment arm calculations by these equations are given in Table 5-5.

The tipping parts of the weapon weigh 44,482 N, and the configuration of the tipping parts is shown in Fig. 5-22. Data for the tipping parts are

$W_t = 44{,}482$ N
$R_t = 0.7465$ m
$\phi' = 0.0605$ rad.

TABLE 5-5
MOMENT ARM CALCULATIONS—PNEUMATIC EQUILIBRATOR DESIGN

θ, rad	ψ, rad	$\sin\psi$	$\cos\psi$	L_θ^2, m^2	L_θ, m	r, m	d, m
−0.0873	1.6023	0.9995	−0.0315	2.3730	1.5405	0.4533	0.1655
0	1.5150	0.9984	0.0558	2.2511	1.5004	0.4650	0.1293
0.1745	1.3405	0.9736	0.2283	2.0100	1.4178	0.4798	0.05178
0.3491	1.1659	0.9191	0.3939	1.7786	1.3336	0.4816	0.03174
0.5236	0.9914	0.8368	0.5475	1.5639	1.2506	0.4675	0.11967
0.6981	0.8169	0.7290	0.6845	1.3725	1.1715	0.4348	0.20943
0.7845	0.7305	0.6672	0.7448	1.2882	1.1350	0.4108	0.25333
0.8727	0.6423	0.9990	0.8007	1.2101	1.1000	0.3805	0.29687
0.9599	0.5551	0.5270	0.8499	1.1414	1.0684	0.3447	0.33779
1.0470	0.4680	0.4511	0.8925	1.0819	1.0401	0.3030	0.37560
1.1340	0.3810	0.3719	0.9283	1.0318	1.0158	0.2558	0.40924

THIS DOCUMENT PROVIDED BY THE ABBOTT AEROSPACE
TECHNICAL LIBRARY
ABBOTTAEROSPACE.COM

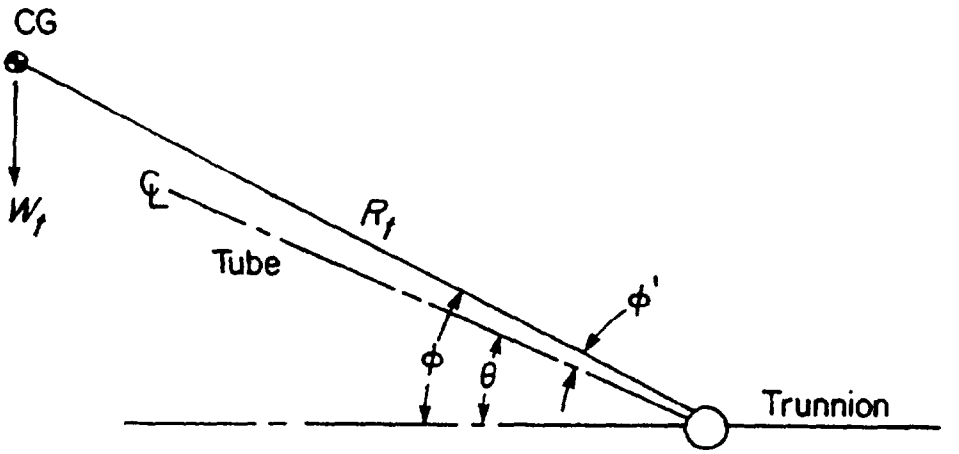

Figure 5-22. Geometry for Weight Moment

From Eq. 5-1, the imbalance of the tipping parts about the trunnion is

$$M_W = W_t R_t \cos\phi, \text{ N·m}$$

and the change of length of the equilibrator is

$$\Delta L = L_1 - L_\theta, \text{ m}$$

where L_1 and L_θ are given in Table 5-5, and $\phi = \theta + \phi'$. Weight moment calculations are illustrated in Table 5-6.

Gas volume is determined by equating the equilibrator and weight moments at 0 and 0.9599 rad elevation, respectively, and then solving for the initial gas volume. If it is assumed that for this equilibrator the piston diameter is $D = 0.09525$ m and the piston rod diameter is $d = 0.03175$ m, then the effective pressure area of the two pistons combined is

$$A = 2\times\frac{\pi}{4}(D^2 - d^2) = 0.01267 \text{ m}^2.$$

Equating the weight moment to the equilibrator moment at two elevations, by using data calculated in Tables 5-5 and 5-6, gives the following relations:

TABLE 5-6
WEIGHT MOMENT CALCULATIONS

θ, rad	ΔL, m	ϕ, rad	$\cos\phi$	$R_t\cos\phi$, m	M_w, N·m
−0.0873	−0.0401	−0.0268	0.9996	0.7462	33,193
0	0	0.0605	0.9982	0.7451	33,145
0.1745	0.0826	0.2350	0.9725	0.7260	32,293
0.3491	0.1668	0.4096	0.9173	0.6848	30,460
0.5236	0.2498	0.5841	0.8342	0.6227	27,700
0.6981	0.3289	0.7586	0.7258	0.5418	24,101
0.7845	0.3654	0.8450	0.6637	0.4955	22,039
0.8727	0.4004	0.9333	0.5952	0.4443	19,764
0.9599	0.4320	1.0204	0.5230	0.3904	17,367
1.047	0.4603	1.1075	0.4469	0.3336	14,840
1.134	0.4846	1.1945	0.3575	0.2743	11,871

THIS DOCUMENT PROVIDED BY THE ABBOTT AEROSPACE
TECHNICAL LIBRARY
ABBOTTAEROSPACE.COM

1. At $\phi = \phi'$ ($\theta = 0$) rad elevation,

$$F_1 = \frac{M_W}{r} = \frac{33{,}145}{0.4650} = 71{,}280 \text{ N}$$

2. At 0.9599 rad elevation,

$$F_2 = \frac{M_W}{r} = \frac{17{,}367}{0.3447} = 50{,}382 \text{ N.}$$

With the area A known ($A = 0.01267$ m^2), the respective gage gas pressures are from Eq. 5-94

$$P_1 = \frac{F}{A} = 5{,}626{,}000 \text{ Pa}$$

$$P_2 = \frac{F_2}{A} = 3{,}976{,}000 \text{ Pa}$$

or, in terms of absolute pressure, from Eq. 5-83

$$P_{1_a} = 5{,}626{,}000 + 101{,}300 = 5{,}727{,}300 \text{ Pa}$$

$$P_{2_a} = 3{,}976{,}000 + 101{,}300 = 4{,}077{,}300 \text{ Pa.}$$

To determine the initial gas volume, first compute the gas volume at 0.9599 rad elevation by Eq. 5-87, i.e.,

$$V_2 = V_1 + \Delta V, \text{ m}^3.$$

From Table 5-7

$$\Delta L = L_2 - L_1 = 0.432 \text{ m}$$

so, by Eq. 5-88

$$\Delta V = A\Delta L = 0.01267 \times 0.432 = 0.005473 \text{ m}^3.$$

TABLE 5-7
TORQUE REQUIRED TO ELEVATE (FRICTION NOT CONSIDERED)

ϑ, rad	ΔL, m	ΔV, m^3	V_θ, m^3	P_{θ_a}, Pa	P_θ, Pa	F, N	r, m	M_e, N·m	M_w, N·m	T_e, N·m
−0.0873	−0.0401	−0.0005081	0.01302	5,952,000	5,851,000	74,132	0.4533	33,604	33,193	−411
0	0	0	0.01353	5,727,300	5,626,000	71,281	0.4650	33,146	33,145	− 1
0.1745	0.0826	0.0010465	0.01458	5,315,000	5,214,000	66,061	0.4798	31,696	32,293	597
0.3491	0.1668	0.0021134	0.01564	4,955,000	4,854,000	61,500	0.4816	29,618	30,460	842
0.5236	0.2498	0.0031650	0.01670	4,640,000	4,539,000	57,509	0.4675	26,885	27,700	815
0.6981	0.3289	0.0041672	0.01770	4,378,000	4,277,000	54,190	0.4348	23,562	24,101	539
0.7845	0.3654	0.0046296	0.01816	4,267,000	4,166,000	52,783	0.4108	21,683	22,039	356
0.8727	0.4004	0.0050731	0.01860	4,166,000	4,065,000	51,504	0.3805	19,597	19,764	167
0.9599	0.4320	0.0054734	0.01900	4,078,000	3,977,000	50,389	0.3447	17,369	17,367	2
1.047	0.4603	0.0058320	0.01936	4,003,000	3,902,000	49,438	0.3030	14,980	14,840	−140
1.134	0.4846	0.0061399	0.01967	3,940,000	3,839,000	48,636	0.2558	12,441	12,203	−238

THIS DOCUMENT PROVIDED BY THE ABBOTT AEROSPACE
TECHNICAL LIBRARY
ABBOTTAEROSPACE.COM

Finally, from Boyle's law, Eq. 5-84

$$P_{1_a} V_1 = P_{2_a} V_2$$

or

$$5{,}727{,}300\ V_1 = 4{,}077{,}300\ (V_1 + 0.005473)$$

Solving this equation, the initial gas volume V_1 is

$$V_1 = 0.01353\ \text{m}^3.$$

If friction is neglected, the following equations are sufficient for calculating the torque required to elevate—$T_e = M_w - M_e$ (Eq. 5-91):

1. The change in gas volume at any elevation is given by Eq. 5-86 as

$$\Delta V = A\Delta L = 0.01267\Delta L,\ \text{m}^3.$$

2. Gas volume at any elevation is given by Eq. 5-87 as

$$V_\theta = V_1 + \Delta V = 0.01353 + \Delta V_\theta,\ \text{m}^3.$$

3. Absolute pressure at any elevation is, by Boyle's law (Eq. 5-84),

$$P_{a_\theta} = \frac{P_{1_a} V_1}{V_\theta} = \frac{5{,}727{,}300 \times 0.01353}{V_\theta} = \frac{77{,}490}{V_\theta},\ \text{Pa}$$

so the gage gas pressure is, by Eq. 5-83,

$$P_\theta = P_{a_\theta} - 101{,}300,\ \text{Pa}.$$

The equilibrator force F is now calculated by Eq. 5-89 as

$$F = P_\theta A = 0.01267 P_\theta,\ \text{N}$$

and the equilibrator moment M_e is, by Eq. 5-9,

$$M_e = Fr,\ \text{N·m}.$$

The torque T_e that must be exerted by the elevating strut is thus, by Eq. 5-91,

$$T_e = M_w - M_e,\ \text{N·m}.$$

These calculations are tabulated in Table 5-7 by using data from Tables 5-5 and 5-6. Fig. 5-23 shows the relation between the weight moment M_w and equilibrator moment M_e about the trunnion during the frictionless elevation.

THIS DOCUMENT PROVIDED BY THE ABBOTT AEROSPACE
TECHNICAL LIBRARY
ABBOTTAEROSPACE.COM

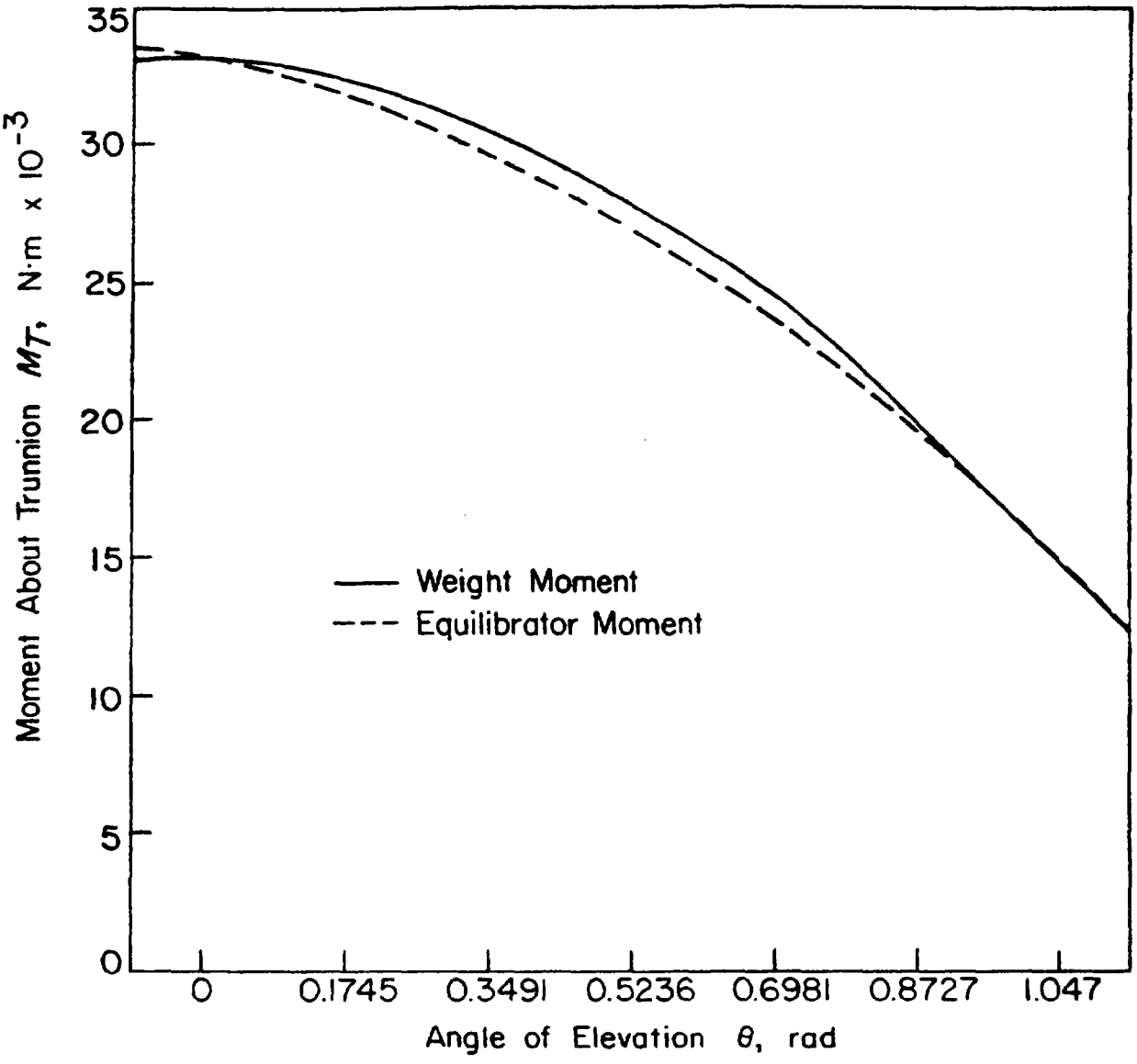

Figure 5-23. Equilibrator Performance Curves for a Frictionless System

5-4.1.2 Performance of the Equilibrator Including Friction

The pressure in the equilibrator cylinder packing is only slightly greater than P_θ; therefore, piston friction F_p is approximately (See par. 5-4.2.4 for details.)

$$F_p = \mu P_\theta \pi D w, \text{ N} \tag{5-95}$$

where

D = piston diameter = 0.09525 m
w = seal width = 0.01588 m
μ = coefficient of packing-cylinder friction = 0.05, dimensionless.

The piston rod friction is usually ignored, but if there is a rod seal and the value of rod friction is not trivial, it should be included.

The net equilibrator force F_n is

$$F_n = F_\theta - F_p, \text{ N}. \tag{5-96}$$

THIS DOCUMENT PROVIDED BY THE ABBOTT AEROSPACE
TECHNICAL LIBRARY
ABBOTTAEROSPACE.COM

From Eqs. 5-95 and 5-96, the net equilibrator force can be rewritten as

$$F_n = P_\theta A - \mu \pi D w P_\theta, \text{ N.} \tag{5-97}$$

The equilibrator performance analysis with friction is carried out in the same way as for the linear mechanical spring equilibrator in par. 5-2.4. The same elevation strut torque expressions as in Eqs. 5-63 through 5-66 can be used by substituting F_n (Eq. 5-97) for F.

An example of equilibrator performance, including friction, is shown in Fig. 5-24.

5-4.2 COMPONENT DESIGN AND MANUFACTURING PROCESSES

The forces of an equilibrator are usually treated as being confined to one unit. If only one equilibrator is used, it is located in a vertical plane passing through the centerline of a gun tube to preclude eccentric loads. However, a weapon will generally have two identical equilibrators. The total equilibrator force is divided into two equal parts; each half represents the design load for an equilibrator. The pair is arranged symmetrically about the center of the mount to preclude unwanted moments.

No special techniques are needed in pneumatic equilibrator fabrication because they can be constructed by ordinary machine methods. It should be pointed out, however, that cylinders are generally honed and pistons are fitted on assembly.

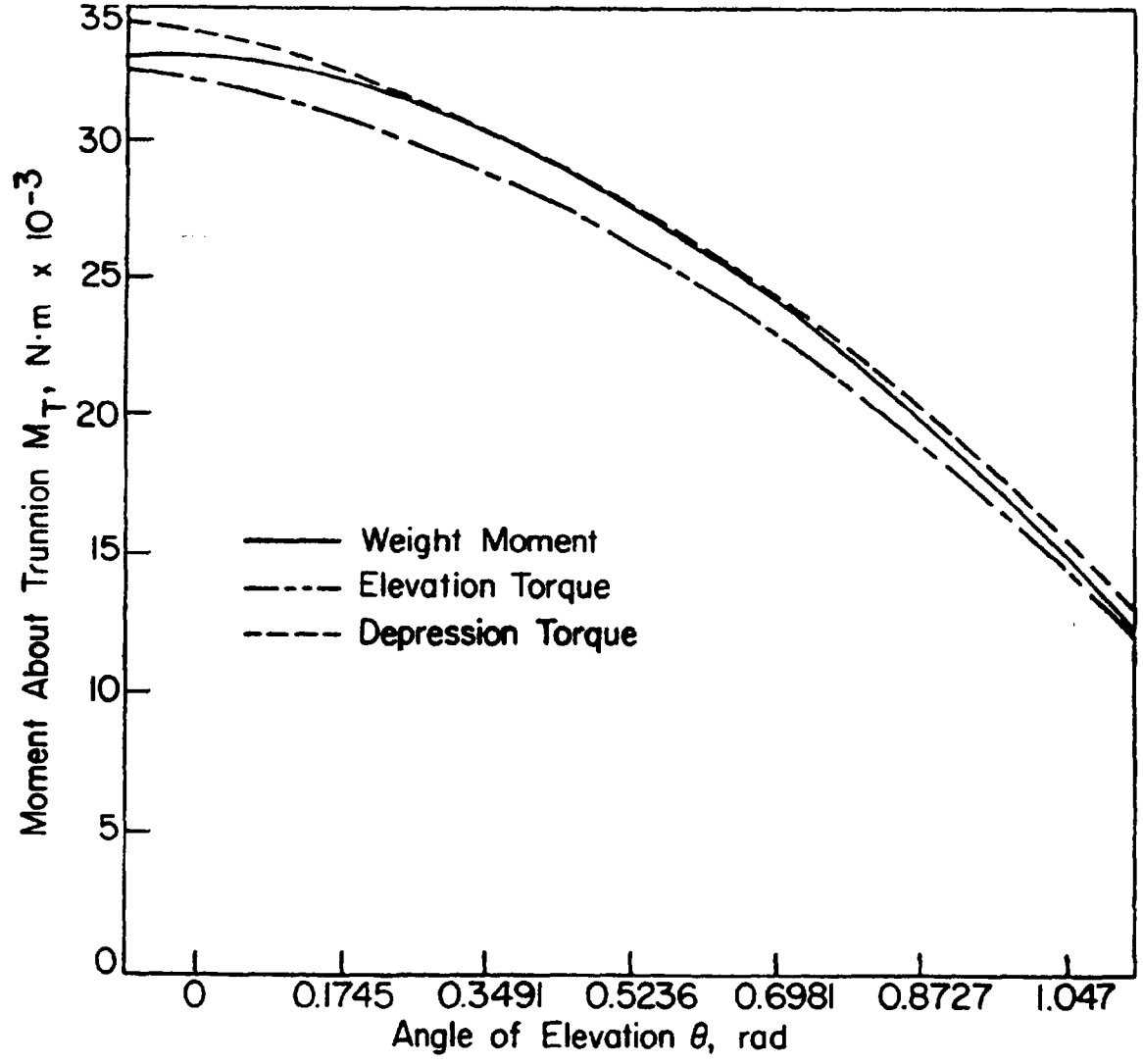

Figure 5-24. Equilibrator Performance Curves Including Friction

THIS DOCUMENT PROVIDED BY THE ABBOTT AEROSPACE
TECHNICAL LIBRARY
ABBOTTAEROSPACE.COM

Adequate care of the equilibrator usually insures that it will be in working order at all times. Periodic inspection, lubrication of sliding surfaces, and adjustments to compensate for temperature changes constitute preventive maintenance. The adjustment of spring tension, gas pressure, or oil volume and the replacement of broken parts or the repair of slightly damaged parts constitute corrective maintenance. The gun crew attends to preventive maintenance, but only skilled maintenance personnel, unless directives state otherwise, perform corrective maintenance.

5-4.2.1 Cylinder Design

The inside dimensions of the cylinder are determined by the piston size and the length of stroke. The wall and head thicknesses are determined by the pressures to be withstood. As shown in Fig. 5-25, the cylinder may be either closed or open-ended, depending on which side of the piston is pressurized.

The circumferential stress σ_t in the cylinder wall (due to fluid or packing) is found using the Lamé equation for thick-walled cylinders (See Ref. 1 of Chapter 6.) as

$$\sigma_t = P_{max}\left(\frac{d_2^2 + d_1^2}{d_2^2 - d_1^2}\right), \text{ Pa} \tag{5-98}$$

where

P_{max} = maximum gage pressure, Pa
d_1 = inner diameter of cylinder, m
d_2 = outer diameter of cylinder, m.

The cylinder may be constructed of medium strength steel. Rigidity is required to minimize the possibility of local damage and to prevent excessive dilation, which makes the seals less effective. For calculation of radial deflection, see par. 2-4 in which radial expansion of recoil cylinders is discussed in detail.

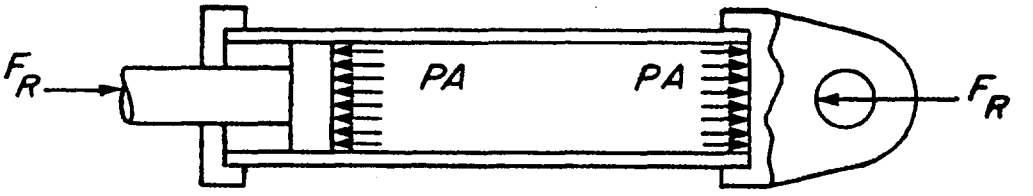

(A) Pressure on Head End (Open End)

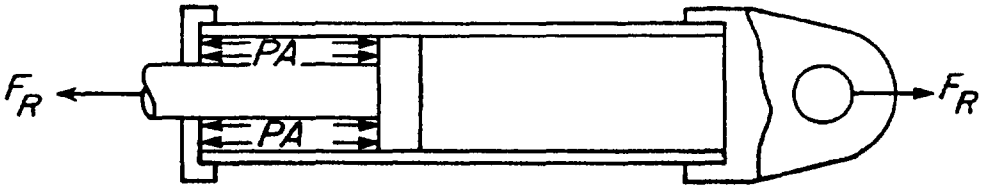

(B) Pressure on Rod End (Closed End)

Figure 5-25. Two Methods of Applying Pressure in a Cylinder

The cylinder head at the rod end, when this end is pressurized, is treated as a flat plate with a concentric hole. The outer edge of the cylinder head is fixed, and a uniform load acts over the entire actual surface, as shown in Fig. 5-26. The maximum stress occurs at the inner edge (See Ref. 4.) and is

$$\sigma_{t_\theta} = \left[\frac{3P_\theta(m^2 - 1)}{4mt^2}\right]\left[\frac{a^4 - b^4 - 4a^2b^2\log(a/b)}{a^2(m-1) + b^2(m+1)}\right], \text{ Pa} \tag{5-99}$$

where

σ_{t_θ} = stress at inner edge of cylinder head, Pa
a = outer radius of cylinder head, m
b = inner radius of cylinder head, m

THIS DOCUMENT PROVIDED BY THE ABBOTT AEROSPACE
TECHNICAL LIBRARY
ABBOTTAEROSPACE.COM

m = reciprocal of Poisson's ratio, dimensionless
P_θ = gas gage pressure at θ elevation, Pa
t = plate thickness, m.

The cylinder head at the terminal end is more than adequately reinforced by the lug and, therefore, requires no special stress analysis.

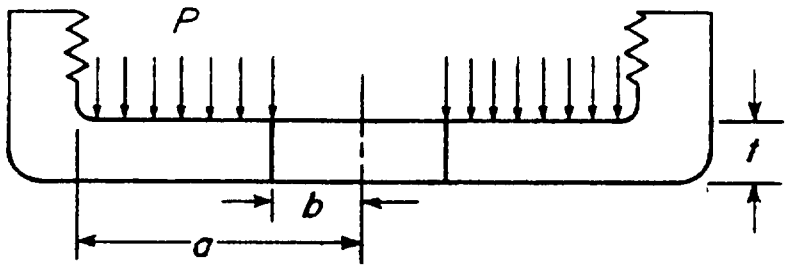

Figure 5-26. Cylinder Head, Rod End

5-4.2.2 Piston Rod

If the equilibrator is a pull type, the piston rod will be subjected to a tension load and the stresses can be calculated accordingly. Note that if the rod is threaded, the critical section is at the root of the thread. If the equilibrator is a push type, as shown in Fig. 5-27, the rod is subjected to compression F_R and column action must be considered.

In addition to axial load F_R, the rod is subjected to a bending moment because of the frictional torque T_A shown in Fig. 5-27. Usually T_A is small enough to be ignored, but it must not be forgotten. With a long, slender rod, there is a possibility that this bending might become appreciable. In this case, beam bending analysis of the rod is required.

5-4.2.3 Terminals

The equilibrator is pin-connected to the tipping parts at one end and to the top carriage at the other. The terminals should be bushed and lubricated to reduce friction. Intermittent lubrication is considered satisfactory. If the bearing is a free-fit with frequent relative motion, but is unprotected from dirt, the allowable bearing stress is approximately 55.16 MPa. (See Ref. 5.) If the bearing is protected, the allowable bearing stress becomes 82.74 MPa. (See Ref. 5.)

The maximum tensile stress σ in the cylinder terminal of Fig. 5-28 occurs at point m and is (See Ref. 6.)

$$\sigma = a\left(\frac{8F_R}{\pi r_o^2 t}\right), \text{ Pa} \qquad (5\text{-}100)$$

where

a = 4.35 when $2 \leq r_o/r_i \leq 4$ = dimensionless parameter, dimensionless
r_o = outside radius of terminal, m
r_i = inside radius of terminal, m
t = thickness of terminal end, m.

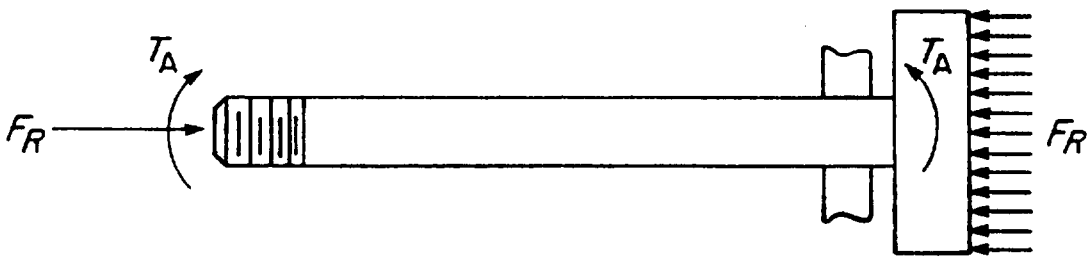

Figure 5-27. Piston Rod Showing Applied Loads and Moments

THIS DOCUMENT PROVIDED BY THE ABBOTT AEROSPACE
TECHNICAL LIBRARY
ABBOTTAEROSPACE.COM

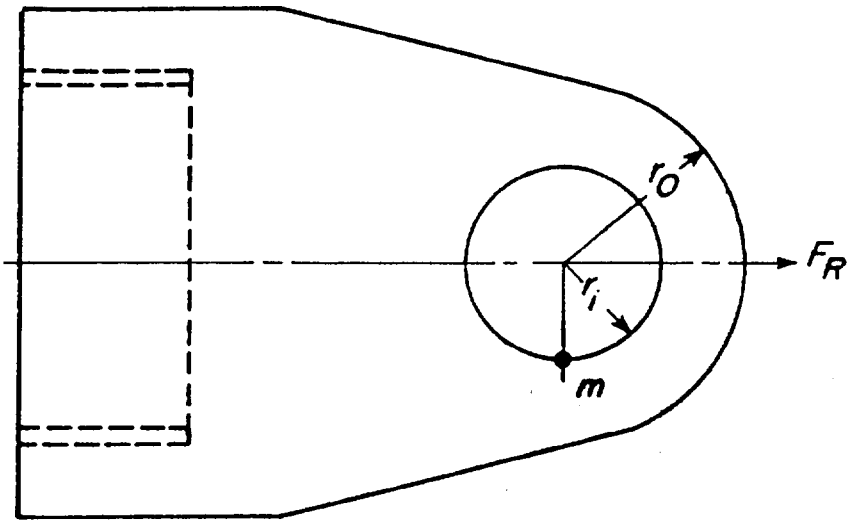

Figure 5-28. Cylinder Terminal

The terminal end must satisfy both bearing and tensile strength requirements. The hole radius used in Eq. 5-100 is that of the lug terminal end and not that of the bushing.

Pins are made of high tensile strength steel because they are subjected to shear and bending stresses. The load distribution on the pin is shown in Fig. 5-29. Both shear and bending should be checked. Bearing pressure also may be critical because of its low permissible value of 55.16 MPa. Whichever of these three conditions is most critical will determine the size of the pin.

5-4.2.4 Packing Design

Fig. 5-30 shows a typical packing assembly for an equilibrator. The packing illustrated is proportioned after that already in use. (Previous experience is helpful in its design.) The Belleville spring and fluid pressure force the piston ring against the rubber filler. The pressure developed in the rubber then presses the packing ring

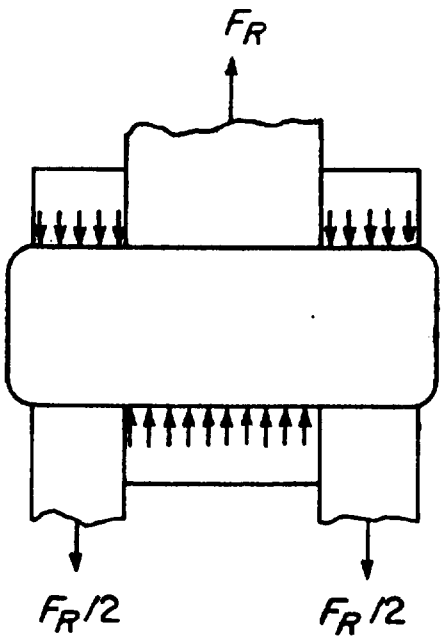

Figure 5-29. Loading Diagram of Pin and Bearing

THIS DOCUMENT PROVIDED BY THE ABBOTT AEROSPACE
TECHNICAL LIBRARY
ABBOTTAEROSPACE.COM

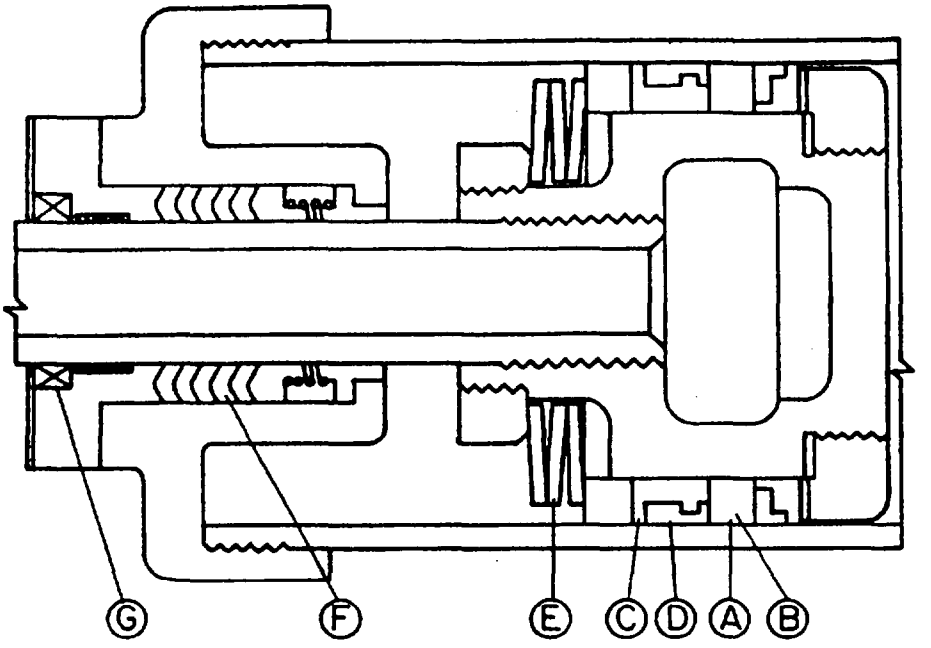

A = packing ring
B = piston ring filler
C = piston ring, steel
D = piston ring band, antifriction metal
E = Belleville spring
F = chevron pack
G = oil seal

Figure 5-30. Typical Packing Assembly

against the cylinder wall to provide a seal. The sealing pressure to be produced by the Belleville spring must be determined to assure a tight seal. The radial force $\bar{F}_p$ in the packing is

$$\bar{F}_p = \pi D w K_p (P + P_s), \text{ N} \tag{5-101}$$

where

D = outside diameter of packing, m
w = packing width, m
K_p = pressure factor, dimensionless
P_s = axial pressure in packing produced by spring, Pa.

The pressure factor K_p is the ratio of the radial pressure to the applied axial pressure and is somewhat analogous to Poisson's ratio. The pressure factor would be 1.0 if the packing behaved hydrostatically. For rubber filler, $K_p = 0.73$.

If the radial pressure is expressed in terms of fluid pressure,

$$K_p(P_m + P_s) = \nu P_m, \text{ Pa}, \tag{5-102}$$

THIS DOCUMENT PROVIDED BY THE ABBOTT AEROSPACE
TECHNICAL LIBRARY
ABBOTTAEROSPACE.COM

then the required spring pressure P_s is

$$P_s = \left(\frac{\nu - K_p}{K_p}\right) P_m, \text{ Pa} \tag{5-103}$$

where

ν = leakage factor, dimensionless
P_m = maximum fluid pressure, Pa.

The value of ν is selected to be greater than unity for complete sealing. If it is desired that some fluid flow pass the packing for lubrication, ν is selected to be less than one. Aluminum alloy rings may be used to confine the corner of the packing to prevent it from extruding between the piston ring and the cylinder. Teflon is a commonly used packing material.

Springs are used to augment the packing pressure. Belleville springs are selected because they require little space and provide large loads at small deflections. The design of Belleville springs is outlined in Chapter 6 of Ref. 1 and in Ref. 7. These springs are extremely sensitive to small changes in dimensions, so manufacturing variations can produce large load differences. Therefore, each spring assembly should be tested for load before installation. The spring load F_s required to cause the desired packing pressure P_s is

$$F_s = \pi(r_2^2 - r_1^2)P_s, \text{ N} \tag{5-104}$$

where

F_s = spring force, N
r_1 = inside radius of piston ring assembly, m
r_2 = outside radius of piston ring assembly, m.

5-4.2.5 Equilibrator Adjustment

Adjustment devices may be required to compensate for changes in gas pressure that occur due to temperature changes. The devices eliminate the requirement for frequently adding and releasing gas to adjust the pressure. With the volume of gas being held constant, the pressure varies directly as the absolute temperature, i.e.,

$$\frac{P_1}{P_2} = \frac{T_1}{T_2}, \text{ dimensionless} \tag{5-105}$$

where

P_1 = absolute gas pressure at state 1, Pa
T_1 = absolute temperature at state 1, K
P_2 = absolute gas pressure at state 2, Pa
T_2 = absolute temperature at state 2, K.

At 21°C, T_1 = 294 K. Thus a variation of 14 deg K represents a variation in pressure of about 5%. This deviation is reflected in the equilibrator force and equilibrator moment about the trunnion. An adjustment is designed to compensate for this amount of deviation. If further adjustment is needed, gas is either added to or released from the equilibrator. The adjustment may be achieved by varying the moment arm or the gas pressure.

The variable-moment-arm method of adjusting for temperature variations is illustrated in Fig. 5-31. The top carriage end of the equilibrator is pin-connected to a slide or adjusting guide that is housed in a machined guide housing that is attached to the top carriage. The guide includes an adjusting screw that is used to position the guide in the housing. This shifts the line of action of the equilibrator and increases or decreases the length of the moment arm, as may be required. A scale, calibrated in degrees, indicates what the temperature setting should be.

THIS DOCUMENT PROVIDED BY THE ABBOTT AEROSPACE
TECHNICAL LIBRARY
ABBOTTAEROSPACE.COM

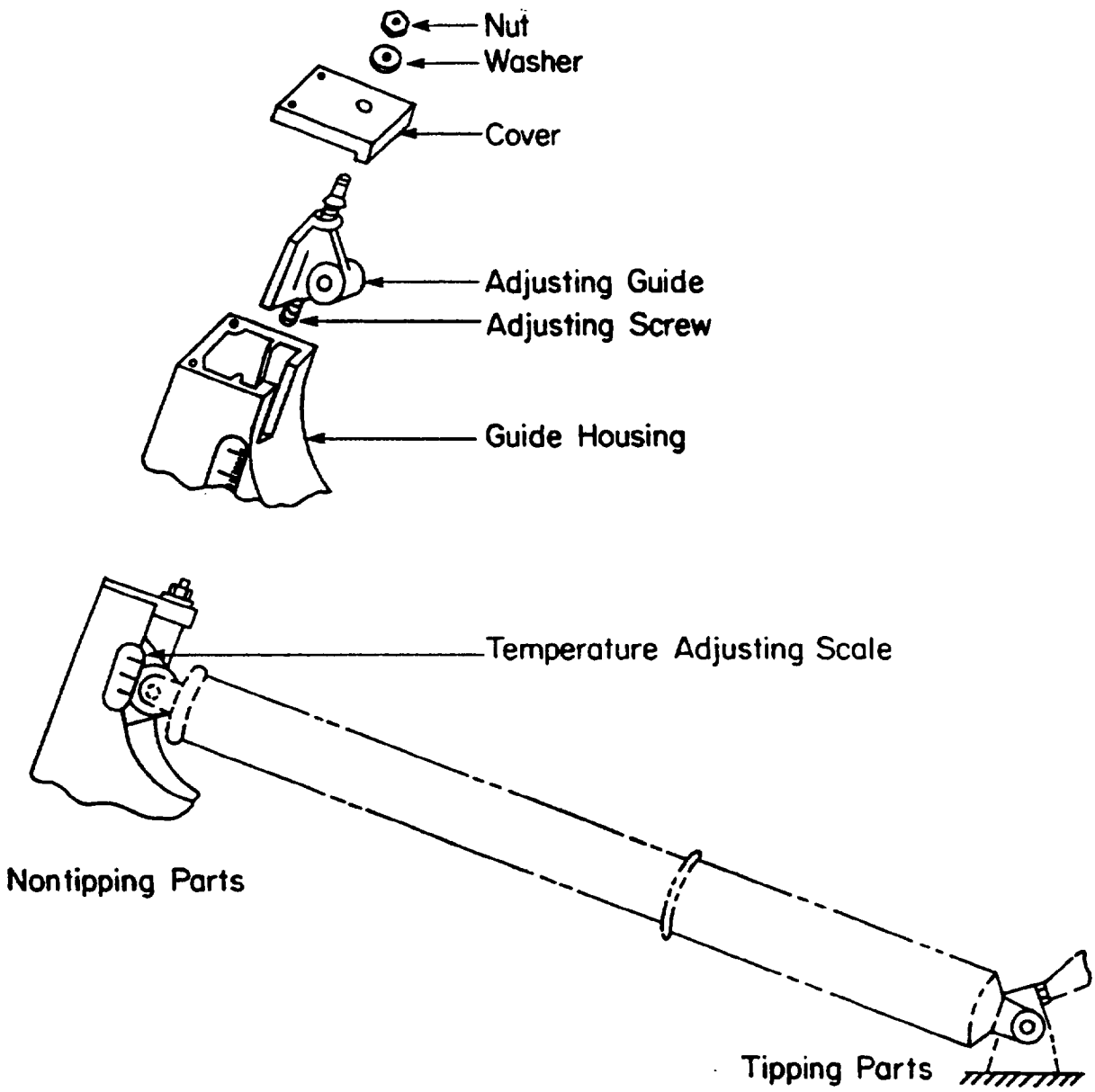

Figure 5-31. Variable Moment-Arm Adjustment

THIS DOCUMENT PROVIDED BY THE ABBOTT AEROSPACE
TECHNICAL LIBRARY
ABBOTTAEROSPACE.COM

The procedure for determining the direction and length of travel of the adjusting guide will now be described. Fig. 5-32 is a schematic sketch of the system. The adjusting movement of the guide is perpendicular to the normal position of the equilibrator. Because only 5% variation in equilibrator force (hence moment) is required, the limits of the adjusted moment arm r' are $0.95r$ and $1.05r$. At the limits of r', geometrical relations from Fig. 5-32 are

$$\left.\begin{aligned} \psi &= \mathrm{Sin}^{-1}\left(\frac{r}{R}\right), \text{ rad} \\ r' &= 0.95r \text{ and } 1.05r, \text{ m} \\ \psi' &= \mathrm{Sin}^{-1}\left(\frac{r'}{R}\right), \text{ rad} \\ e &= L\tan(\psi - \psi'), \text{ m} \\ L' &= \frac{L}{\cos(\psi - \psi')}, \text{ m} \end{aligned}\right\} \quad (5\text{-}106)$$

where

e = adjusting guide travel, each direction for normal to centerline, m
L' = equilibrator length, adjusted position on either side, m
r = equilibrator moment arm, normal position, m
r' = equilibrator moment arm, any adjusted position, m
R = turning radius, m
ψ = angle between L and R (Fig. 5-32), rad
ψ' = angle between L' and R (Fig. 5-32), rad.

A change in the equilibrator travel length L means a change in gas volume and pressure. Thus the equilibrator moment changes in two respects—a change in moment arm and a change in force. The change in force is negligible, and its effect may be ignored.

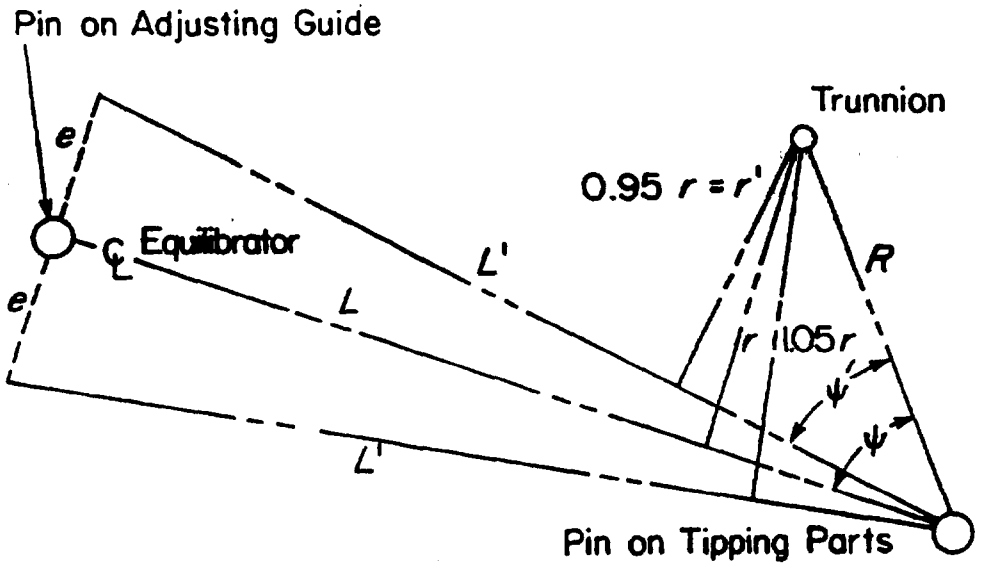

Figure 5-32. Equilibrator Geometry for Adjustment

THIS DOCUMENT PROVIDED BY THE ABBOTT AEROSPACE
TECHNICAL LIBRARY
ABBOTTAEROSPACE.COM

The adjusting guide travel having been determined, the adjusting scale can now be calibrated in terms of temperature change. At points along the travel line on both sides of the normal position, small increments e are selected for which L' and r' are calculated from Eq. 5-106. From the change in equilibrator length, $\Delta L = L - L'$, the new gas volumes are determined as in par. 5-4.1.

The equilibrator moment is found first for normal temperature and position. Next, the moment is calculated for the changes in pressure and moment arm caused by the change in position. These results determine how much the pressure must be increased or decreased to provide a moment equal to the normal one. The change in pressure is indicative of the change in temperature necessary to produce it. This change in temperature is marked on the scale at the appropriate point. This process is repeated until the required temperature range is spanned.

The pressure control method of adjustment entails adding fluid to the reservoir to raise the gas pressure or removing fluid to lower the pressure. The correct pressure usually is indicated by a specified handwheel torque at a given elevation. A hand pump may be used to add fluid if this is required. The adjustment range is limited by the amount of reserve fluid in the accumulator. Calibration of the pressure controller is based on volume changes, instead of distance as in the preceding discussion. The calculations outlined in the preceding discussion provide the volume-temperature relation needed for calibration; accordingly, they need not be repeated.

5-5 OPTIMIZATION OF APPROXIMATE EQUILIBRATOR IMBALANCE

5-5.1 MINIMIZATION OF APPROXIMATE EQUILIBRATOR IMBALANCE

The optimization objective in equilibrator design is to minimize the equilibrator imbalance by varying equilibrator (mechanical or pneumatic) characteristics such as spring rate, spring-free length, and attachment point locations of the equilibrator to the tipping parts and top carriage.

Perfect balance cannot be expected during the entire range of elevation because the force necessary to equilibrate is nonlinear, whereas the force exerted by the equilibrator is linear. This fact leads to the optimization objective of minimizing the maximum equilibrator imbalance occurring in the range of motion.

5-5.2 LEAST SQUARE IMBALANCE MINIMIZATION

The least square method for selection of a spring constant and preload of a spring-type equilibrator for fixed geometry is discussed briefly in par. 5-2.3. Here, the basic least square minimization technique is derived and illustrated. Define

F_i = equilibrator force at ΔL_i, N
F_0 = equilibrator force when $\phi = 0$, N
K_s = equilibrator spring rate, N/m
ΔL_i = equilibrator travel, m.

Suppose that a straight line ℓ whose equation is

$$F = F_0 - K_s \Delta L, \text{ N} \tag{5-107}$$

is to pass as nearly as possible through the points $(\Delta L_1, F_1)$, $(\Delta L_2, F_2)$, ..., $(\Delta L_n, F_n)$. Because two points completely determine a straight line, it will in general be impossible for the required line to pass through more than two of the given points. Hence the coordinates of the general point $(\Delta L_i, F_i)$ will not satisfy Eq. 5-107. That is, when ΔL_i is substituted into Eq. 5-106, the value obtained is not F_i, but the ordinate of ℓ, which, as seen from Fig. 5-33, differs from F_i by δ_i. In other words,

$$F_i - (F_0 - K_s \Delta L_i) = \delta_i \neq 0 \tag{5-108}$$

where

δ_i = deviation of F_i from F, N.

The deviation δ_i is computed for each point ΔL_i, and then the sum of the squares of these quantities (in order to prevent large positive and large negative δ_i's cancelling each other and thereby giving an unwarranted impression of accuracy) are computed. The result is the error E

THIS DOCUMENT PROVIDED BY THE ABBOTT AEROSPACE
TECHNICAL LIBRARY
ABBOTTAEROSPACE.COM

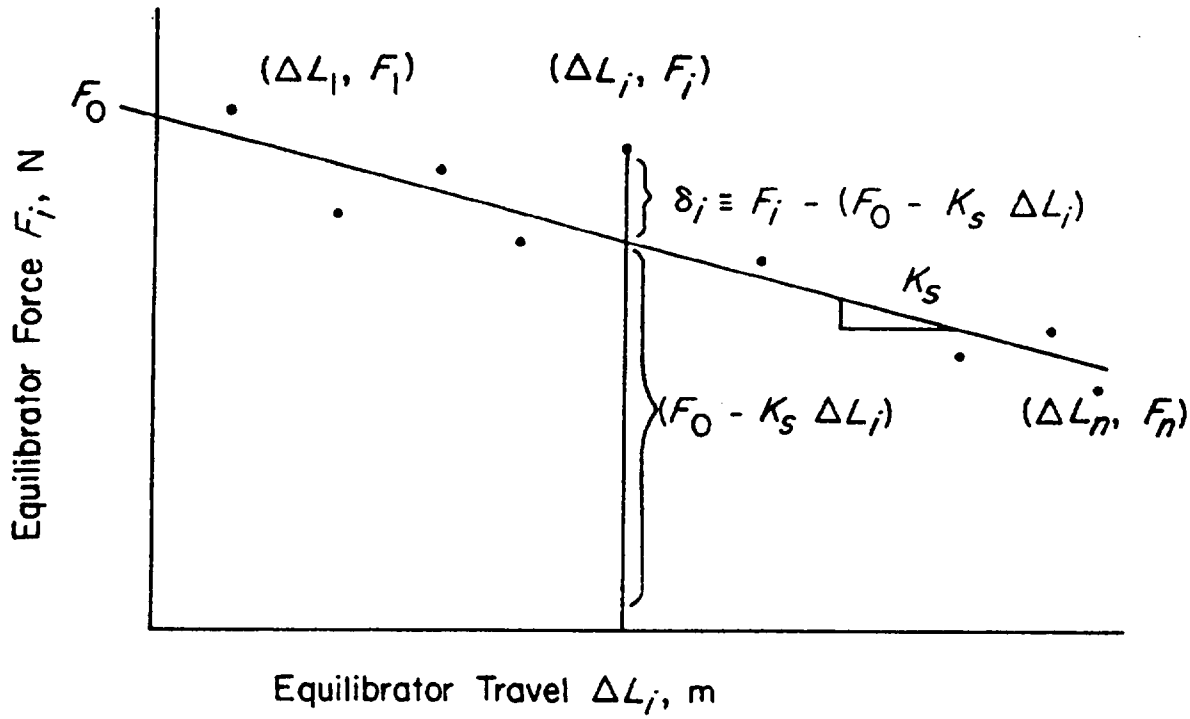

Figure 5-33. Approximate Fitting of a Straight Line to a Set of Points

$$E = \sum_{i=1}^{n} \delta_i^2 = (F_1 - F_0 + K_s\Delta L_1)^2 + (F_2 - F_0 + K_s\Delta L_2)^2 + \cdots + (F_n - F_0 + K_s\Delta L_n)^2, \text{ m}^2. \quad (5\text{-}109)$$

The quantity E is a measure of how well the line ℓ fits the set of points. The error E will be zero if, and only if, each of the points lies on ℓ. The larger E is, the farther the points are, on the average, from ℓ. The least square criterion is that the parameters F_0 and K_s should be chosen to make E as small as possible. To do this, the usual conditions for minimizing a function of several variables are applied.

To find F_0 and K_s to minimize E, the two first partial derivatives $\partial E/\partial F_0$ and $\partial E/\partial K_s$ are set equal to zero. This gives the two equations

$$\frac{\partial E}{\partial F_0} = 2(F_1 - F_0 + K_s\Delta L_1)(-1) + 2(F_2 - F_0 + K_s\Delta L_2)(-1) + \cdots + 2(F_n - F_0 + K_s\Delta L_n)(-1) = 0 \quad (5\text{-}110)$$

$$\frac{\partial E}{\partial K_s} = 2(F_1 - F_0 + K_s\Delta L_1)(\Delta L_1) + 2(F_2 - F_0 + K_s\Delta L_2)(\Delta L_2) + \cdots + 2(F_n - F_0 + K_s\Delta L_n)(\Delta L_n) = 0. \quad (5\text{-}111)$$

By dividing Eqs. 5-110 and 5-111 by 2 and collecting terms on the unknown variables F_0 and K_s, these equations become

$$nF_0 - K_s \sum_{i=1}^{n} \Delta L_i = \sum_{i=1}^{n} F_i \quad (5\text{-}112)$$

THIS DOCUMENT PROVIDED BY THE ABBOTT AEROSPACE
TECHNICAL LIBRARY
ABBOTTAEROSPACE.COM

THIS DOCUMENT PROVIDED BY THE ABBOTT AEROSPACE
TECHNICAL LIBRARY
ABBOTTAEROSPACE.COM

limitations. For example, allocation of space for artillery components may impose geometric restrictions on the attachment points of the equilibrator. Thus the designer must choose design variables that satisfy these restrictions, which are called constraints. Among the constraints there can also be relations between the design variables. These constraints can be termed equality constraints.

The general nonlinear programming problem is defined as find design variables b to minimize cost ψ_0, i.e.,

$$\text{minimize } \psi_0(b) \tag{5-114}$$

subject to constraints

$$\psi_i(b) = 0, \quad i = 1, ..., n \tag{5-115}$$

$$\psi_i(b) \leq 0, \quad i = n + 1, ..., m \tag{5-116}$$

where

ψ_0 = cost function, dimensionless
b = design variable vector, dimensionless
ψ_i, for $i = 1, ..., n$ = equality constraint functions, dimensionless
ψ_i, for $i = n + 1, ..., m$ = inequality constraint functions, dimensionless.

For a detailed discussion of nonlinear programming problems and their application to design, the reader is referred to Refs. 9 and 10.

5-5.3.2 Optimization Methods

Many optimization methods are available for solution of the nonlinear programming problem. In this paragraph the gradient projection method is briefly described. This method uses only first derivative, or gradient information, to make successive improvements in an estimated solution of a nonlinear programming problem. Geometrically, this method first determines the direction of most rapid decrease in the cost function. This direction is then projected onto the tangent plane to the boundary of the constraint set at the design b. A small move in the resulting direction will then decrease the cost function and will not cause excessive violation of constraints. This process is repeated as long as the cost function can be decreased. The reader may refer to Ref. 9 for details.

In equilibrator design the imbalance to be minimized varies in magnitude as the tipping parts move. The tipping parts move over a certain range, and the constraints should be satisfied at every position. Although this requirement seems to cause difficulty in solving the problem, discretization of the range of motion allows the problem to be solved. Placing a grid along the range of motion leads to the worst-case optimization technique. (See Ref. 9.) The idea of worst-case optimization is to choose the worst case of the cost function, over the range of motion, and then to minimize the worst-case cost function. The cost function can be restated as

$$\psi_0 = \max_j f(\theta_j), \quad j = 1, ..., t' \tag{5-117}$$

where

t' = total number of grid points, dimensionless
$f(\theta_j)$ = cost function at elevation grid angle θ_j, dimensionless.

5-5.3.3 Example of Nonlinear Programming Method

As an example of discussion in pars. 5-5.3.1 and 5-5.3.2, consider the problem that follows. For an example of equilibrator optimization, the gradient projection method of Ref. 9 is used. Consider the equilibrator of Fig. 5-34. Data for this example are as follows:

$\alpha = \beta + 0.4363$ rad
$\psi_0 = 2.007$ rad
$\phi' = 0.0605$ rad
$c = 0.3086$ m
$R = 0.9228$ m
$R_t = 0.4572$ m
$W_t = 8896$ N.

THIS DOCUMENT PROVIDED BY THE ABBOTT AEROSPACE
TECHNICAL LIBRARY
ABBOTTAEROSPACE.COM

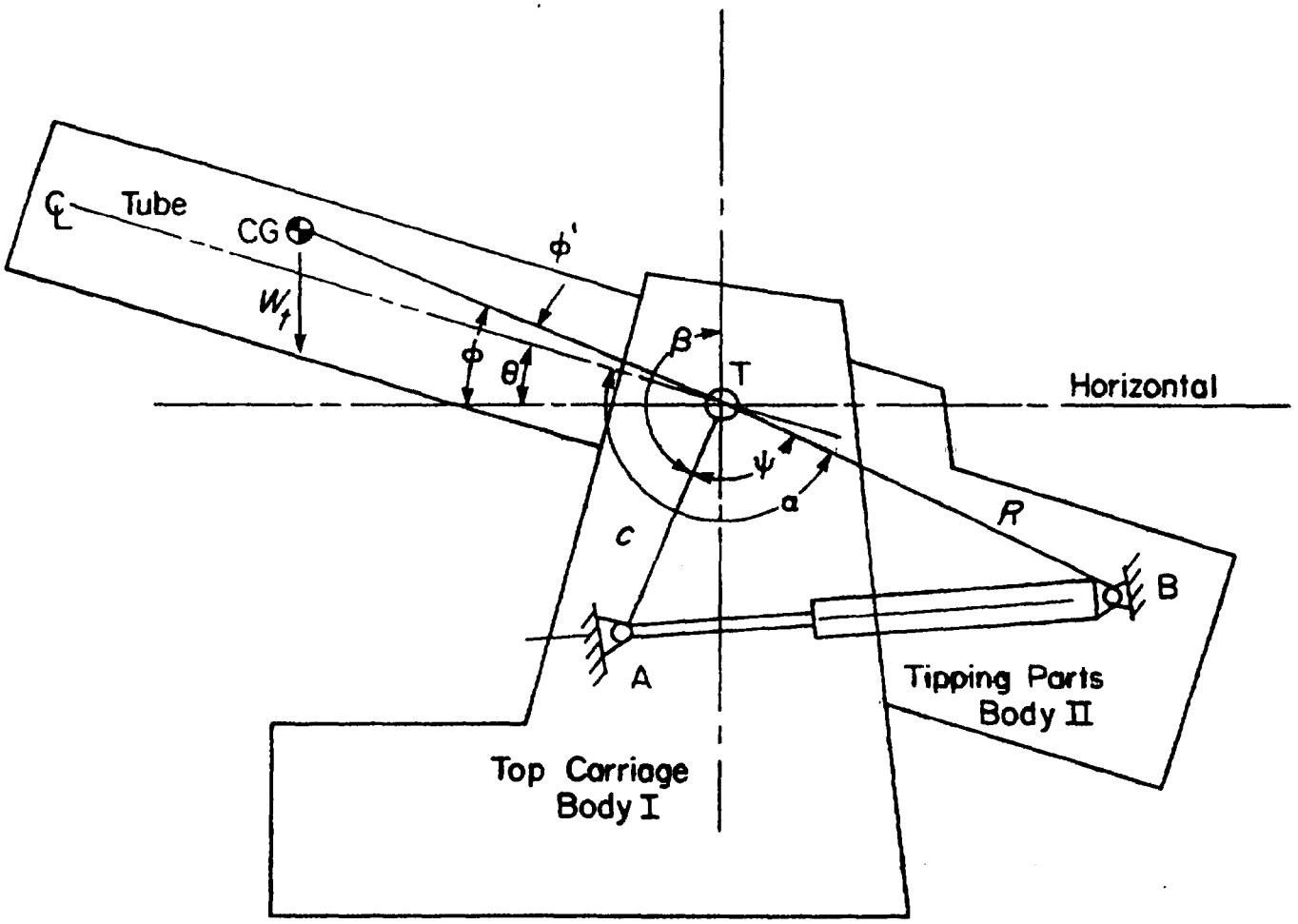

Figure 5-34. Equilibrator Configuration

The equilibrator consists of two concentric springs whose coil diameters are $D_1 = 0.1334$ m and $D_2 = 0.0889$ m, respectively. The spring rates and free lengths depend only on wire diameter, number of active coils, and pitch. Thus the design variables are d_1, d_2, n_1, n_2, p_1, and p_2 where

d_1, d_2 = wire diameters of equilibrator concentric springs 1 and 2, respectively, m
n_1, n_2 = numbers of active coils of equilibrator concentric springs 1 and 2, respectively
p_1, p_2 = pitches of equilibrator concentric springs 1 and 2, respectively, m.

The cost function is

$$\psi_0 = \max f, \quad j = 1, \ldots, t' \tag{5-118}$$

where

f = imbalance between weight moment and equilibrator moment, N·m
t' = total number of grid points, dimensionless.

The motion of the system is decided at every grid point as

$$\theta = \theta_j, \text{ rad} \tag{5-119}$$

where

θ_j = elevation angle at each grid point, rad.

THIS DOCUMENT PROVIDED BY THE ABBOTT AEROSPACE
TECHNICAL LIBRARY
ABBOTTAEROSPACE.COM

The equilibrator force is distributed so that the inner spring supports 40% of the outer spring load. This force distribution is defined by the relation

$$0.4F_1 - F_2 = 0 \tag{5-120}$$

where

F_1, F_2 = distributed equilibrator forces to equilibrator concentric springs 1 and 2, respectively, N.

By applying Eq. 5-71, Eq. 5-120 becomes

$$0.4\left(\frac{Gd_1^4}{8D_1^3 n_1}\right)\Delta L_1 - \left(\frac{Gd_2^4}{8D_2^3 n_2}\right)\Delta L_2 = 0 \tag{5-121}$$

where

$\Delta L_1, \Delta L_2$ = deflection of equilibrator concentric springs 1 and 2, respectively, m

G = shear modulus, Pa.

Stress constraints for each spring are

$$\left.\begin{aligned} \max_j \frac{8F_1 D_1}{\pi d_1^3} - 9.1\times10^8 \le 0 \\ \max_j \frac{8F_2 D_2}{\pi d_2^3} - 9.1\times10^8 \le 0 \end{aligned}\right\} \quad j = 1, \ldots, t'. \tag{5-122}$$

Numerical results obtained using the foregoing data and the nonlinear programming methods of Ref. 9 are tabulated in Table 5-9 and compared with the design obtained in par. 5-3.2.1.

The maximum imbalance between weight moment of tipping parts and equilibrator torque—using the method of nonlinear programming—reduces to 49.9% of that computed in par. 5-3.3.1.

TABLE 5-9
COMPARISON OF NONLINEAR PROGRAMMING DESIGN TO CONVENTIONAL DESIGN

	Design in Par. 5-3.3.1	Design Using Nonlinear Programming
d_1	0.0171 m	0.01663 m
n_1	13.7	13.84
P_1	–	0.06247 m
d_2	0.0108 m	0.0109 m
n_2	18.1	19.83
P_2	–	0.04232 m
max imbalance of equilibrator torque	189 N·m	94.3 N·m

THIS DOCUMENT PROVIDED BY THE ABBOTT AEROSPACE
TECHNICAL LIBRARY
ABBOTTAEROSPACE.COM

REFERENCES

1. DOD-HDBK-778(AR), *Recoil Systems*, July 1988.
2. *The Design of Elevating, Traversing, and Equilibrator Components for 105-mm Howitzer Weapon, XM164*, TN 11-67, Rock Island Arsenal, Rock Island, IL, March 1967.
3. R. E. Balzhiser and M. R. Samuels, *Engineering Thermodynamics*, Prentice-Hall, Inc., Englewood Cliffs, NJ, 1977.
4. R. J. Roarck, *Formulas for Stress and Strain*, 5th Edition, McGraw-Hill Book Co., New York, NY, 1975.
5. *Strength of Metal Aircraft Elements*, ANC-5 Bulletin, issued jointly by Department of the Air Force (Air Research and Development Command), Department of the Navy (Bureau of Aeronautics), and Department of Commerce (Civil Aeronautics Administration), March 1955.
6. S. Timoshenko, *Strength of Materials*, 3rd Edition, D. Van Nostrand Company, Inc., New York, NY, 1955.
7. A. M. Wahl, *Mechanical Springs*, 2nd Edition, McGraw-Hill Book Co., New York, NY, 1963.
8. R. Resnick and D. Halliday, *Physics*, John Wiley and Sons, New York, NY, 1966.
9. AMCP 706-192, Engineering Design Handbook, *Computer-Aided Design of Mechanical Systems*, July 1973.
10. DARCOM-P 706-193, Engineering Design Handbook, *Computer-Aided Design of Mechanical Systems, Part Two*, September 1977.

THIS DOCUMENT PROVIDED BY THE ABBOTT AEROSPACE
TECHNICAL LIBRARY
ABBOTTAEROSPACE.COM

CHAPTER 6
BEARING DESIGN

Bearing design for trunnion and traverse bearings is discussed. Alternate configurations of ball, roller, and journal bearings are defined and the advantages and disadvantages of each are identified. Design methods for journal bearings are presented. Load determination for antifriction bearings is discussed as input to procurement of commercially available bearings. Special considerations in the design of trunnion and traverse bearings also are presented.

6-0 LIST OF SYMBOLS

A_{br} = projected area of trunnion bearing, m^2
C = radial clearance in journal bearing (bearing radius − journal radius), m
$\bar{C}$ = specific dynamic capacity, N
c = difference between diameter of bushing and diameter of journal, m
d = diameter of journal, m
F = summation over bearing area of shear force exerted by lubricant, N
F_r = radial load, N
F_T = trunnion load, N
F_t = thrust load, N
L = length of bearing, m
L_n = life, millions of revolutions
P = load supported by bearing [load on journal/(bearing length × diameter)]
P_e = equivalent load, N
p = pressure on projected bearing area, Pa
R = radius of journal, m
S = bearing characteristic number, dimensionless
S_f = safety factor, dimensionless
T = torque required to overcome journal friction, N·m
Z = absolute viscosity of lubricant, centipoise
σ_{br} = bearing stress, Pa
μ = coefficient of friction in journal bearings, dimensionless
ϕ = functional relationship, dimensionless
ω = angular velocity of journal, rps

6-1 INTRODUCTION

6-1.1 BEARING FUNCTIONS AND LOADS

In almost every machine the designer is confronted with the relative motion of machine parts and the abrasive wear that may result from this motion. A bearing confines or constrains the relative motion of those machine elements that depend upon it for support. The relative motion between the members may be classified as either translation or rotation. By this classification it may be seen that there are many types of bearings. The principal bearings in a towed artillery system are the trunnion bearing, traverse bearing, and translational bearing between the recoiling parts and the cradle.

The trunnion and traverse bearings provide low-friction rotating elements that are essential to enhance ease and speed of weapon elevation and traverse. They also transmit firing loads from the cradle to the top and bottom carriages. The traverse bearing is particularly critical because it must provide a low frictional means for rotating the traversing parts and also is subjected to both radial and thrust loads. The radial component supports the weapon laterally, whereas the thrust component supports the weapon weight and vertical firing loads. Firing loads are transmitted through the bearing to the bottom carriages, although in some weapons the vertical components of these loads are transmitted directly from the top to bottom carriage.

THIS DOCUMENT PROVIDED BY THE ABBOTT AEROSPACE
TECHNICAL LIBRARY
ABBOTTAEROSPACE.COM

Structurally, the trunnion bearings must be strong enough to support large firing loads and still permit the trunnions to rotate freely as the weapon is elevated. A cutaway of a trunnion bearing is shown in Fig. 6-1. Whether of ball or roller type, each bearing is selected according to the manufacturer's specifications.

Bearings with rolling elements have a basic static load rating defined as the maximum static load that will lead to a combined permanent deformation of ring and rolling elements of less than 0.0001 times the rolling element diameter (Ref. 1).

Translational bearings are treated in detail in Ref. 2. Translational bearings are available for use with both flat and cylindrical surfaces. Those for flat surfaces most often use rollers, and those for cylindrical surfaces use balls as the rolling elements. The rolling elements must circulate, i.e., they must roll to the end of the bearing and then in some manner return. The type for use with a shaft, known as a ball bushing, is shown in Fig. 6-2.

The surface in contact with the rolling element must be hardened and must be smooth to develop the full capacity of the bearing. Translational bearings, like all rolling bearings, are adversely affected by dirt. Because the surface upon which they roll is a part of the bearing, preventing the accumulation of dirt or removing it before the bearing arrives is essential. Another factor to be remembered when considering a ball bushing is that it is intended only for linear motion and should not be subjected to rotation.

For trunnion and traverse bearings with rough surfaces, friction involves the tendency of the peaks and valleys of surfaces to interlock. If the surfaces are sufficiently rough, the interlocking may be of such magnitude that sliding or rolling will not maintain small deformation, as was the case with friction, but will cause parts of the surfaces to be torn off. This is wear that will also increase the friction force. On the other hand, if the surfaces of a bearing are separated at all times by a layer of lubricant, there may be practically no wear.

If the deformation, even the tearing off of minute particles, is not too pronounced, it may be regarded as "wearing in". The immediate performance of the bearing will be improved. Such a bearing, however, will not have the combination of load-carrying capacity and life of a bearing which, because of smoother surfaces, did not undergo "wearing in". The production of bearings with smoother surfaces is more expensive. Thus designing for "wearing in" is a reasonable practice if the bearing can be made large enough to compensate for the reduced capacity or if a shorter life is acceptable.

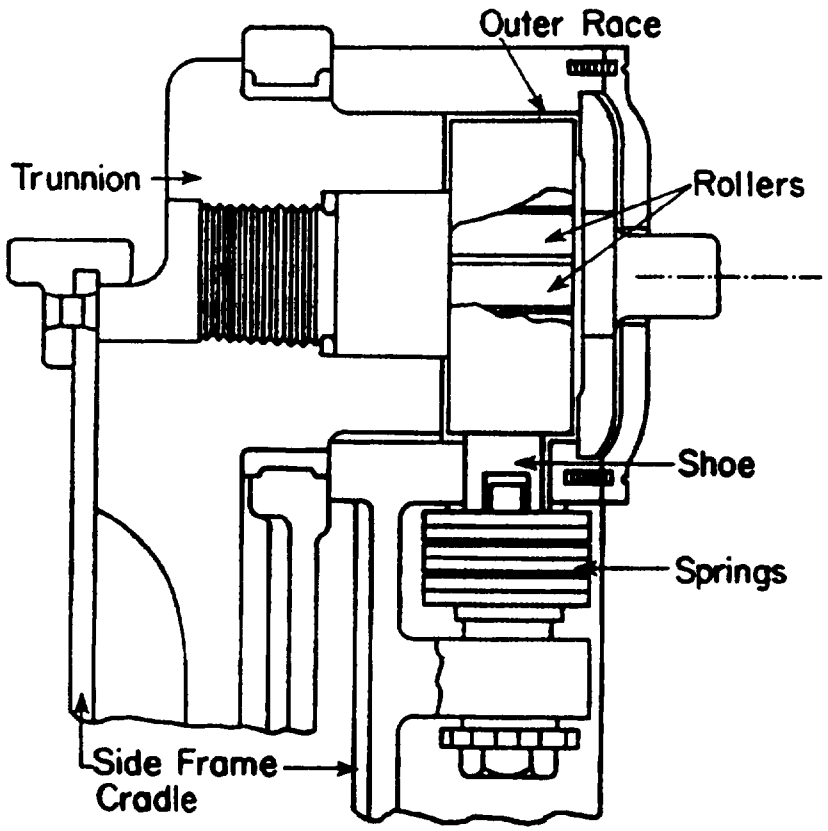

Figure 6-1. Trunnion Bearing (Antifriction Type)

THIS DOCUMENT PROVIDED BY THE ABBOTT AEROSPACE
TECHNICAL LIBRARY
ABBOTTAEROSPACE.COM

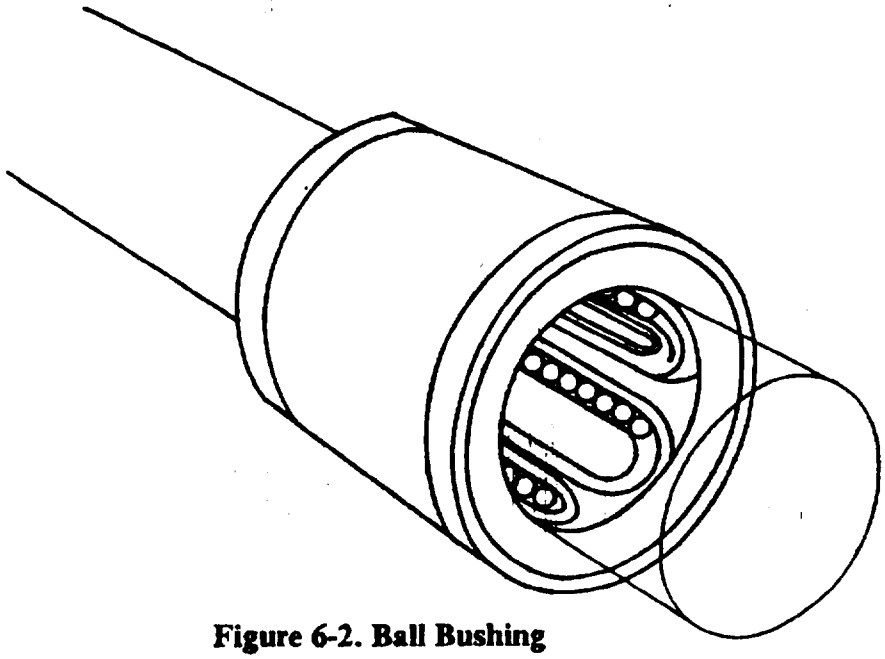

Figure 6-2. Ball Bushing

Excessive friction in the trunnion and traverse bearings leads to large elevating and traverse handwheel loads. Design calculations relating bearing friction to handwheel effort are presented and illustrated in Chapter 4. These calculations should be carried out to determine an acceptable level of friction in the trunnion and traverse bearings. The resulting acceptable levels of bearing friction will then form a specification for the design or procurement of the bearings.

Because of the elastic deformations of the surfaces at the regions of contact between a ball or roller and the races, the contact pressure is distributed over the areas in contact. The extent of these areas depends on the elastic properties of the materials, on the size of the balls or rollers, and on the form of the raceways. To provide a large area and in turn to reduce the pressure in a ball bearing and to permit the bearing to carry axial loads (in addition to radial loads), the raceways are formed as shown schematically in Fig. 6-3.

In a ball or roller bearing, the load-carrying capacity is based mainly on the surface endurance limit of the material. The rated load of a bearing is the load it will carry for a specific life of the bearing when operating at a definite speed. Therefore, for other expected periods of life and for other speeds, the load that the bearing is required to carry must be altered accordingly.

Load prediction, as an input to bearing design, for towed artillery design is addressed in considerable detail in Chapter 3. The dynamic nature of the artillery system dictates that analyses of the kind presented in Chapter 3 be carried out prior to sizing of bearings and components. The bearing designer is advised to work closely with dynamic analysts to determine loads that must be supported by the bearings. This is particularly important in design of trunnion, traverse, and wheel bearings.

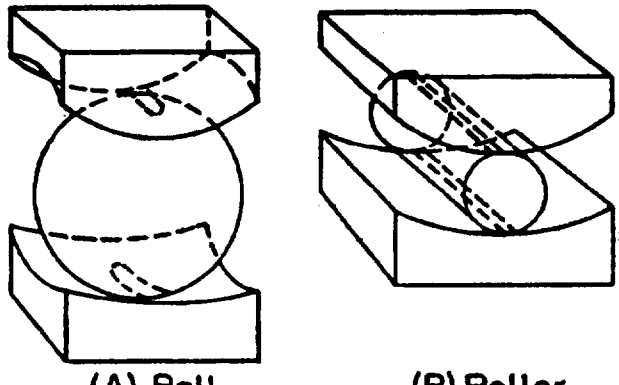

Figure 6-3. Contact Area in Ball and Roller Bearings

THIS DOCUMENT PROVIDED BY THE ABBOTT AEROSPACE
TECHNICAL LIBRARY
ABBOTTAEROSPACE.COM

6-1.2 ANTIFRICTION BEARING TYPES AND AVAILABILITY

Bearings are manufactured to support pure radial loads, pure thrust loads, or a combination of the two. A typical ball bearing is illustrated in Fig. 6-4, which also shows the four essential parts of the bearing, i.e., outer ring, inner ring, balls, and separator. The separator has the important function of separating the rolling elements so that rubbing contact will not occur. Some types of standardized ball bearings are shown in Fig. 6-5.

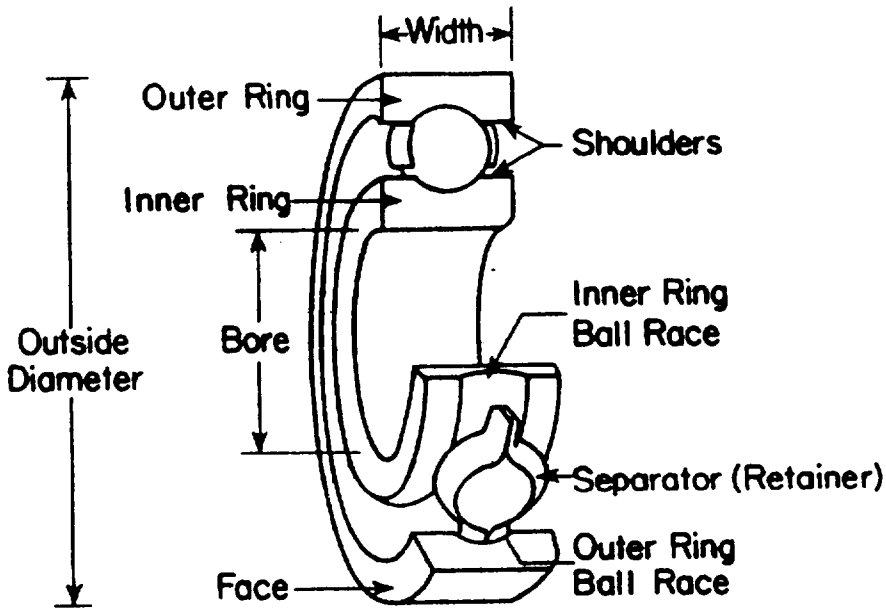

Figure 6-4. Nomenclature of a Ball Bearing

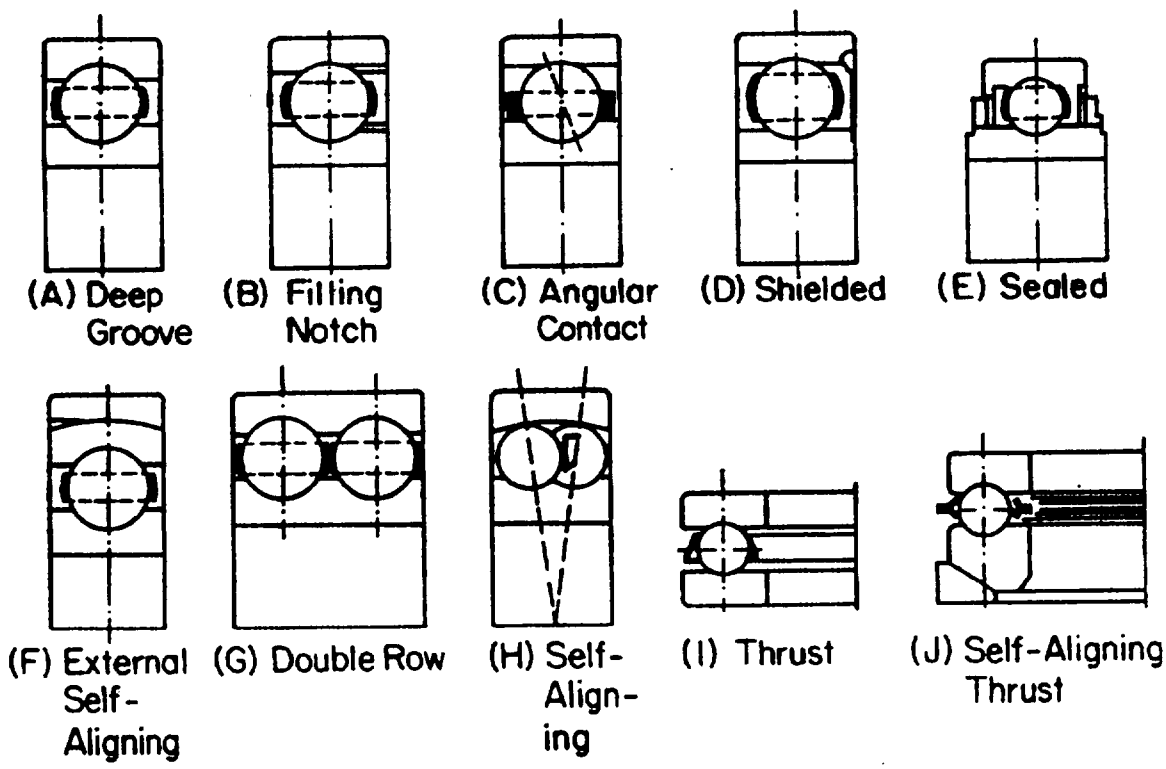

Figure 6-5. Types of Ball Bearings

THIS DOCUMENT PROVIDED BY THE ABBOTT AEROSPACE
TECHNICAL LIBRARY
ABBOTTAEROSPACE.COM

The single-row, deep-groove bearing (Fig. 6-5(A)) will carry a radial load and some thrust load. The use of a filling notch (Fig. 6-5(B)) in the inner and outer rings enables a greater number of balls to be inserted and thereby increases the load capacity of the bearing; the thrust capacity is decreased, however. The angular-contact bearing (Fig. 6-5(C)) provides a greater thrust capacity.

All bearings indicated in Fig. 6-5 may be obtained with shields on one or both sides, as illustrated by Figs. 6-5(D) and 6-5(E). The shields are not a complete closure but do offer a measure of protection against dirt. A variety of bearings is manufactured with seals on one or both sides. When the seals are on both sides, the bearings are lubricated at the factory, and although a sealed bearing is supposed to be lubricated for life, a method of relubrication is provided sometimes.

Single-row bearings will withstand a small amount of shaft misalignment or deflection. When misalignment is severe, self-aligning or double-row bearings may be used (Figs. 6-5(F), (G), and (H)). Double-row bearings are made in several types and are sized to carry heavier radial and thrust loads. Two single-row bearings may be used together for the same reason, although a double-row bearing will generally require fewer parts and occupy less space. The one-way ball thrust bearings shown in Figs. 6-5(I) and (J) are also made in many types and sizes.

Some of the large variety of available standard roller bearings are illustrated in Fig. 6-6. Straight roller bearings (Fig. 6-6(A)) will carry a greater radial load than ball bearings of the same size because of the greater contact area. Straight roller bearings, however, have the disadvantage of requiring almost perfect geometry of the raceways and rollers. A slight misalignment will cause the rollers to skew and get out of line. For this reason, the retainer must be heavy. Straight roller bearings will not, of course, carry thrust loads.

The spherical-roller thrust bearing of Fig. 6-6(B) is useful where heavy loads and misalignment occur. The spherical elements have the advantage of increasing their contact area as the load is increased. Needle bearings (Fig. 6-6(C)) are very useful where radial space is limited. They have a high load capacity when separators are used, but may be obtained without separators, and are furnished both with and without races. Tapered roller bearings (Figs. 6-6(D), (E), and (F)) combine the advantages of ball and straight roller bearings because they can take either radial or thrust loads or any combination of the two. In addition, they have the high load-carrying capacity of straight roller bearings. The tapered roller bearing is designed so that all elements in the roller surface and raceways intersect at a common point on the bearing axis.

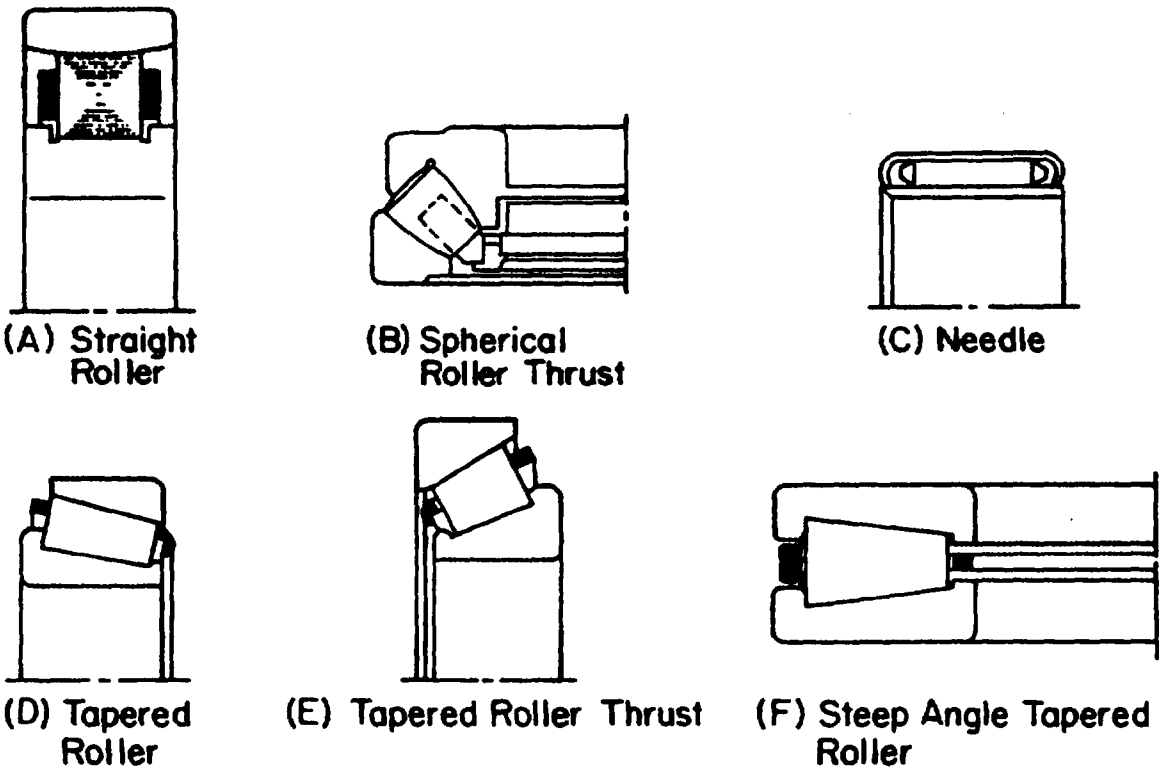

Figure 6-6. Types of Roller Bearings

THIS DOCUMENT PROVIDED BY THE ABBOTT AEROSPACE
TECHNICAL LIBRARY
ABBOTTAEROSPACE.COM

Many of the bearing types discussed are available as either standard or precision bearings. Actually, all antifriction bearings are precision bearings, i.e., they are made to a tolerance of a few ten-thousandths of an inch. All these bearings are commercially available in a variety of sizes and load-carrying capacities. Modern artillery design practice requires that the artillery designer carefully determine loads that the bearing must carry in-service. A standard bearing, with the precision needed, is then selected to perform the required load-carrying function. Dynamic load prediction, discussed in Chapter 3, thus plays a key role in the definition of bearing load requirements and, hence, bearing selection.

Since solid bearings are not wholly satisfactory because of the inability to adjust them, similar bearings are designed that may be split into two pieces. The halves are parted in such a manner as to avoid excessive pressure on the parting line. For this reason, it is sometimes necessary to use angle-type adjustable bearings, in which adjustment of bearing size can be provided by means of shims, i.e., multiple layers of thin sheets of brass or copper placed between the two halves. As wear takes place, a layer of shim stock may be removed to make it possible to bring the bearing halves closer together.

There are many ways in which bearings of this type are lubricated. On slower moving parts, lubrication may be obtained from an oil hole and small reservoir in the cap of the bearing. In higher speed applications, forced-feed lubrication is employed. Ring oiling is sometimes used for lubricating the bearings of electric motors and generators; this type of lubrication, however, cannot be used on small journals running at high speed because ring slippage tends to prevent adequate lubrication.

6-2 TRUNNION BEARINGS

For trunnion bearings, either journal or roller bearings are used. Roller bearings offer two advantages: (1) lower frictional properties and (2) adaptability to self-alignment. Their high cost and comparatively large size, requiring housings that are larger than those necessary for a journal bearing, are their main disadvantages. Journal bearings are smaller and cost less, but in this type of installation they do not have the low frictional properties that can be achieved with roller bearings.

6-2.1 JOURNAL BEARINGS

The journal bearing consists of the turning element and the bearing that supports and holds the turning element. The portion of the shaft, or turning element, that rotates within the bearing is known as the journal. Journal bearings may be used as trunnion bearings for smaller caliber artillery that use hydrodynamic lubrication even though the relative speed between the journal and the bearing is small. The journal bearing in the presence of good lubrication is discussed first and is followed by considerations of bearing loads and material selection. Design considerations for journal bearings are also discussed.

6-2.1.1 Friction in Journal Bearings

The coefficient of friction μ in journal bearings is defined as

$$\mu = \frac{F}{P} = \frac{T}{PR}, \text{ dimensionless} \tag{6-1}$$

where

P = load supported by bearing, N
F = summation over bearing areas of shear force exerted by lubricant, N
T = torque required to overcome journal friction, N·m
R = radius of journal, m.

By the use of dimensional analysis (See Ref. 3.), the coefficient of friction μ can be expressed as the functional relationship

$$\mu = \phi\left(\frac{Z\omega}{p}, \frac{d}{c}, \frac{L}{d}\right), \text{ dimensionless} \tag{6-2}$$

where

ϕ = functional relationship, dimensionless
Z = absolute viscosity of lubricant, centipoise
ω = angular velocity of journal, rps

THIS DOCUMENT PROVIDED BY THE ABBOTT AEROSPACE
TECHNICAL LIBRARY
ABBOTTAEROSPACE.COM

p = pressure on projected bearing area [load on journal/(bearing length × diameter)], Pa
d = diameter of journal, m
c = difference between diameter of bushing and diameter of journal, m
L = length of bearing, m.

The quantity $Z\omega/p$ is termed the bearing characteristic number. The variation of the coefficient of friction with operating values of $Z\omega/p$ is shown in Fig. 6-7. The part of the curve ab in Fig. 6-7 represents the region of fluid-film lubrication (stable operating conditions) that is a straight line only for the full journal bearing. Between points b and c on the curve, the viscosity Z or the angular velocity ω is so low, or the pressure p is so great, that their combination $Z\omega/p$ will reduce the film thickness so that partial metal-to-metal contact will result. Between points c and d on the curve, imperfect boundary lubrication exists. In this case, the operating value of $Z\omega/p$ is too low to insure fluid-film lubrication.

6-2.1.2 Bearing Loads

Breakdown of the lubrication film occurs at operating conditions between points b and c on Fig. 6-7. The conditions affecting breakdown are important to consider in the design of a journal bearing.

Factors that affect lubricating film breakdown include

1. Clearance. The clearance in a bearing should be small enough to provide the necessary velocity gradient so that the built-up pressure will support the load. Allowance must be made for manufacturing tolerances in the journal and the bushing, for deflection of the shaft, and for space to permit foreign particles, such as grit and flakes of metal, to pass through the bearing. These latter considerations require large clearances.

2. Length-to-Diameter Ratio L/d. From the standpoint of side leakage, a bearing with a large L/d is preferable. Space requirements, manufacturing tolerances, and shaft deflections, however, are better met with a bearing of short length.

3. Surface Finish. Although the degree of smoothness of the surfaces of the journal and the bushing does not have a marked effect on a bearing operating with fluid-film lubrication, it does have an effect on the point of breakdown of the film.

6-2.1.3 Strength and Stiffness of Journal Bearings

The diameter of the journal is somewhat larger than the diameter of the shaft. In most cases, the shaft diameter is determined from consideration of strength and stiffness. Deflection of the journal in the bushing is also an important consideration because a large deflection will cause undue wear and failure of the oil film. A perfectly aligned bearing is shown in Fig. 6-8(A). The effect of shaft deflection, shown in Fig. 6-8(B), may require the use of a self-aligning bearing (Fig. 6-8(C)) in some instances.

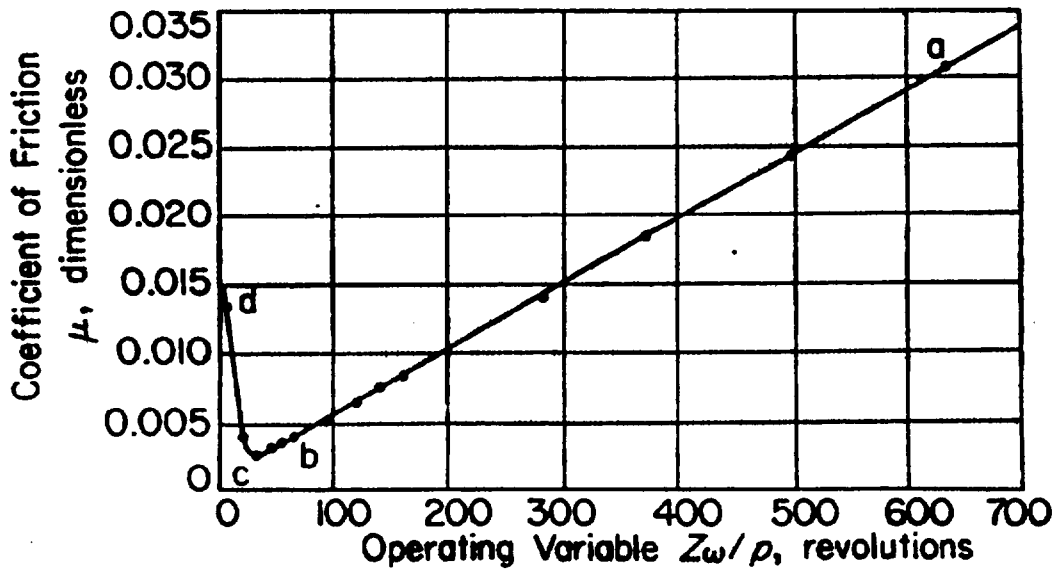

Figure 6-7. Journal-Bearing Friction as a Function of $Z\omega/p$

THIS DOCUMENT PROVIDED BY THE ABBOTT AEROSPACE
TECHNICAL LIBRARY
ABBOTTAEROSPACE.COM

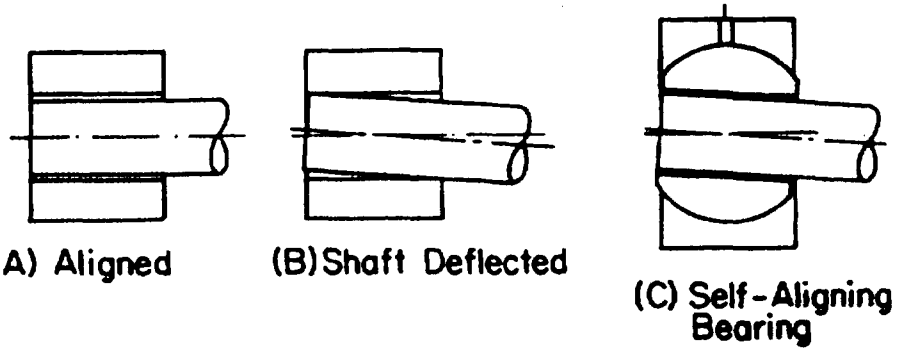

Figure 6-8. Effect of Shaft Deflection on Bearing Alignment

The material strength is also a consideration in bearing design. The bearing stress σ_{br} is

$$\sigma_{br} = \frac{F_T}{A_{br}}, \text{ Pa} \tag{6-3}$$

where

F_T = trunnion load, N
A_{br} = projected area of trunnion, m^2.

For firing, when the trunnions are not turning, the bearing stress should show a substantial safety factor S_f determined by stress correction factors for journal bearings. (See Ref. 1.)

6-2.1.4 Materials

When referring to a lubricated assembly, it is necessary to distinguish between the following elements:

1. The journal, or moving member
2. The lubricant, if it exists
3. The bearing, or fixed member
4. The housing in which the bearing is assembled.

Good bearing material (1) must have adequate compressive and fatigue strength to resist externally applied loads, (2) must be soft, and (3) must have a low melting point and a low modulus of elasticity. The second set of requirements is necessary to permit the material to wear in since the material can conform to slight irregularities and absorb and release foreign particles. The resistance to wear and the coefficient of friction are also important because all bearings must operate, at least for part of the time, with thin-film lubrication.

Additional considerations in the selection of a good bearing material are its ability to resist corrosion and the cost of producing the bearing. Some of the commonly used materials are listed in Table 6-1, together with their composition and characteristics.

Bearing life can be increased very substantially by depositing a layer of babbitt, or other white metal, in thicknesses from 0.025 mm to 0.356 mm over a steel backup material. A copper-lead deposit on steel provides strength, and a babbitt overlay provides surface and corrosion characteristics—making an excellent bearing.

Small bushings and thrust collars may operate with thin-film lubrication. When this is the case, improvements over a solid bearing material can be made by using powder metallurgy techniques to add significantly to the life of the bearing. A powder metallurgy bushing is porous, which permits oil to penetrate into the bushing material. Such a bushing may be enclosed in an oil-soaked material to provide backup lubrication. Bearings are frequently ball-indented to provide small basins for the storage of lubricant while the journal is at rest. This design feature supplies some lubrication during starting. Another method of reducing friction is to indent the bearing wall and to fill these indentations with graphite.

6-2.1.5 Bearing Design

Because of the large number of variables involved, design of a journal bearing usually requires making reasonable assumptions and then applying available relations to establish their validity. Two methods of journal bearing design are considered here. The first applies dimensional analysis to an infinitely long bearing with a side-flow correction factor that is determined experimentally. The resulting values for frictional

THIS DOCUMENT PROVIDED BY THE ABBOTT AEROSPACE
TECHNICAL LIBRARY
ABBOTTAEROSPACE.COM

TABLE 6-1
COMPOSITION AND CHARACTERISTICS OF BEARING ALLOYS

Alloy	Material Thickness, mm	SAE‡ No.	Cu, %	Sn, %	Pb, %	Sb, %	Corrosion Resistance
Tin-base babbitt	0.559	12	3.25	89	–	7.5	Excellent
Lead-base babbitt	0.559	15	–	1	83	15	Very Good
Tin-base babbitt	0.102	12	3.25	89	–	7.5	Excellent
Lead-base babbitt	0.102	15	–	1	83	15	Very Good
Leaded bronze	Solid	792	80	10	10	–	Very Good
Copper-lead	0.559	480	65	–	35	–	Good
Aluminum alloy	Solid	–	1	6	–	–	Excellent
Silver plus overlay	0.33	17P	–	–	–	–	Excellent
Cadmium (1.5% Ni)	0.559	18	–	–	–	–	Good
Trimetal 88*	–	–	–	–	–	–	Excellent
Trimetal 77†	–	–	–	–	–	–	Excellent

* This is a 0.2-mm layer of copper-lead on a steel back plus 0.0254 mm of tin-base babbitt.
† This is a 0.33-mm layer of copper-lead on a steel back plus 0.0254 mm of lead-base babbitt.
‡ See Ref. 3.

resistance compare favorably with results based on the hydrodynamic theory for bearings operating under high Sommerfeld numbers. The analysis assumes that the bearing load is essentially constant in magnitude and direction and that speed is constant. If these conditions do not exist, the designer must consider the variations carefully and arrive, based on experience, at a prediction of probable conditions of service.

The second method of journal bearing design is more precise and is based directly on the hydrodynamic equation of Reynold. (See Ref. 4.) Since a general solution to Reynold's equation does not exist, this method employs the work of Raimondi and Boyd (See Ref. 4.) for determining film thickness and its extent, film pressure and its distribution, flow characteristics, and temperature rise. These characteristics are expressed in terms of the Sommerfeld number and various ratios of bearing length-to-diameter.

The Sommerfeld number, or bearing characteristic number S, was proposed by Sommerfeld in 1904 as a dimensionless quantity and is defined by the equation

$$S = \left(\frac{R}{C}\right)^2 \frac{Z\omega}{p} \text{ , dimensionless} \qquad (6\text{-}4)$$

where

C = radial clearance in journal bearing (bearing radius − journal radius), m.

6-2.2 STRESS DISTRIBUTION IN JOURNAL BEARINGS

6-2.2.1 Force Distribution

During recoil the journal and trunnion bearings are subject to direct contact. When two bodies come into contact, a force distribution over the surfaces arises and high contact stresses may occur over subsets of the contact region. This is undesirable because high normal forces may lead to wear or fatigue. Therefore, a technique is necessary for adjusting the contour of one or both of the bodies to achieve a minimum peak contact stress between the bodies.

6-2.2.2 Contact Stress Analysis

A common case of bearing contact stress occurs along an axial line between two parallel cylinders in contact. The usual method for determining stresses in the contact zone of two elastic bodies was first established by Hertz by using the theory of elasticity. The distribution of pressure on the contact area is an elliptical distribution shown in Fig. 6-9. The parabolic distribution of stress over the contact zone leads to the highest contact stress at the center of the contact zone. These stress variations should be used in design of trunnion bearings to complement considerations presented in par. 6-2.1.3.

THIS DOCUMENT PROVIDED BY THE ABBOTT AEROSPACE
TECHNICAL LIBRARY
ABBOTTAEROSPACE.COM

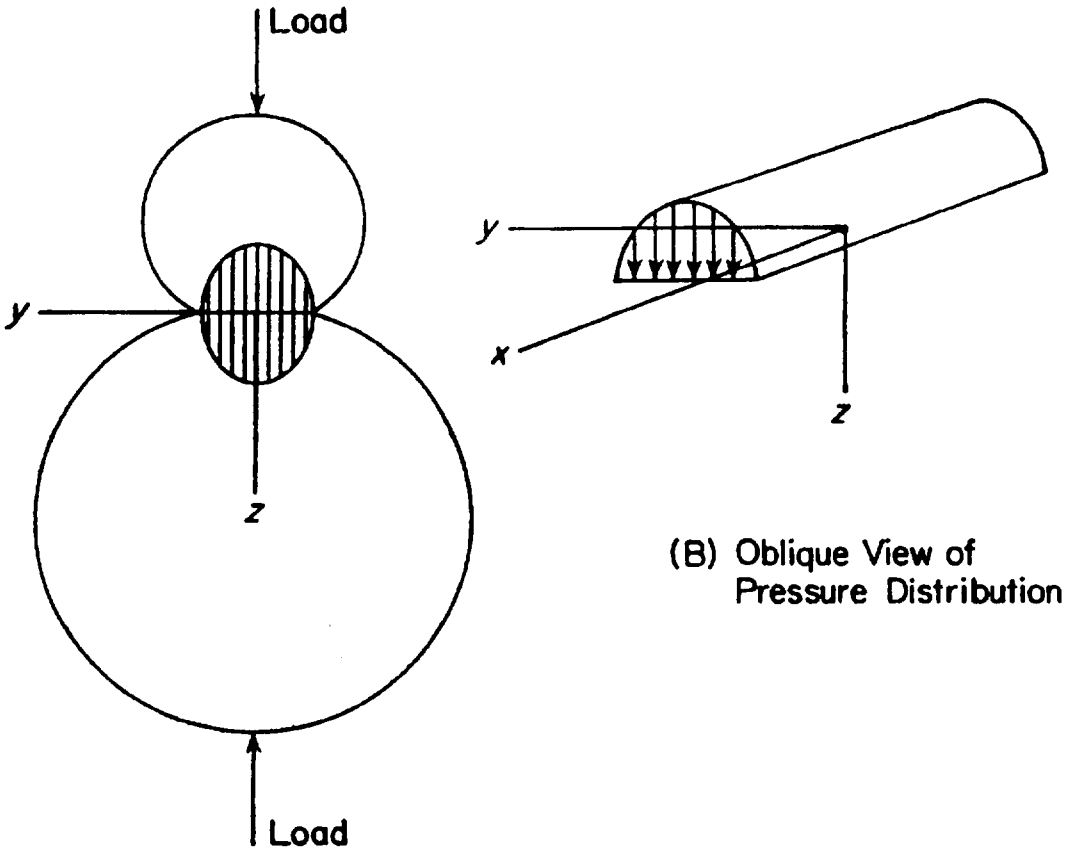

Figure 6-9. Pressure Distribution Across Contact Surfaces of Two Cylinders

The finite element stress analysis and computer-aided design methods presented in Ref. 5 may be used in detailed contact stress analysis. Furthermore, bearing contour shape can be designed to minimize stress concentration effects. For details on such methods, the reader may consult Ref. 5.

6-2.3 ANTIFRICTION ROLLER BEARINGS

Instead of having point contact between the rolling elements and the races, as in the ball bearing, there is line contact in a roller bearing. This contact means that there is greater surface under pressure, and consequently, greater loads may be carried by roller bearings of the same size than is possible by ball bearings. Roller bearings are ideally suited for applications that involve varying load conditions, shock loads, and overloading. Types of antifriction roller bearings were discussed in par. 6-1.2.

6-2.3.1 Bearing Capacity

The capacity of a bearing involves its capability with respect to load, speed, and life—all of which are interrelated. There is an exponential relationship between the magnitude of the load on the bearing and its expected life. The relationship among load, life, and capacity is (Ref. 4)

$$L_n = \left(\frac{\bar{C}}{P_e} \right)^3, \text{ millions of revolutions} \qquad (6\text{-}5)$$

where

L_n = life, millions of revolutions
$\bar{C}$ = specific dynamic capacity, N
P_e = equivalent load, N.

THIS DOCUMENT PROVIDED BY THE ABBOTT AEROSPACE
TECHNICAL LIBRARY
ABBOTTAEROSPACE.COM

The specific dynamic capacity $\bar{C}$ is the load that 90% of a group of bearings can carry for one million revolutions before the first evidence of fatigue develops. Some manufacturers use an average life for which 50% of a group of bearings, rather than 90%, is specified.

A number of factors must be taken into account when determining the size of a bearing for a particular application. A bearing often is subjected to both radial and thrust loads, a combination that is converted to an equivalent load. Definition of an equivalent load depends on the manufacturer as well as on the type of bearing. A rough, though conservative, approximation can be made by (Ref. 6)

$$P_e = 0.5F_r + 1.7F_t, \text{ N} \tag{6-6}$$

where

F_r = radial load, N
F_t = thrust load, N.

If Eq. 6-6 produces an equivalent load less than the radial load, the radial load is used as the equivalent load.

6-2.3.2 Self-Aligning Bearings

The purpose of a self-aligning bearing is to allow for inaccuracies in shaft alignment and deflections of the shaft or its supports. When deflections are provided for in this manner, stresses that otherwise would be induced are avoided.

Both single-row and double-row self-aligning roller bearings are available in several forms. One form of each is shown in Fig. 6-10. Both forms are internally self-aligning; however, the load-carrying capacity is not affected.

Roller bearings are often used as thrust bearings. The cylindrical roller has the disadvantage that because the outer end must travel farther than the inner end, considerable sliding takes place. This effect is reduced by making the rollers short. This roller type is available with a self-aligning feature that compensates for slight misalignment. Any misalignment would result in only a few of the rolling elements carrying the entire load and thus shortening the life of the bearing.

6-2.3.3 Bearing Shields and Seals

Some bearings are available with shields or seals as part of the bearing assembly. The purpose of the shield or seal is to protect the bearing. Generally, shields are attached permanently to the outer race and fit into a notch in the inner race, with a slight clearance. The shields exclude all but the finest grit. Bearings are available with a shield on one or both sides.

Because it rubs against the race, a bearing seal provides protection from all contaminants. The seal also may retain the lubricant placed in the bearing by the manufacturer and may be used on one or both sides. Bearings also are available with a shield on one side and a seal on the other.

6-2.3.4 Lubrication

The principles involved in lubrication of roller bearings are different from those that apply to sliding bearings. Because of the extremely high pressure between the roller and the race, any lubricant is squeezed out

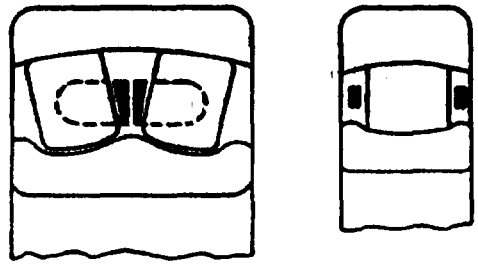

(A) Double Row (B) Single Row

Figure 6-10. Self-Aligning Roller Bearings

THIS DOCUMENT PROVIDED BY THE ABBOTT AEROSPACE
TECHNICAL LIBRARY
ABBOTTAEROSPACE.COM

and there is metal-to-metal contact. A lubricant is, nevertheless, essential to the operation of a roller bearing for the following reasons:

1. To reduce the friction at the points where sliding takes place
2. To control heat generated by friction and deformation
3. To prevent corrosion
4. To aid in protecting the bearing from dirt.

If heat removal is not involved, a fraction of a drop of oil per hour will provide adequate lubrication for a moderate-size bearing. Oil is the better lubricant, but grease is used more often because it permits a simpler installation design and the problem of leakage is practically eliminated.

It would be an error to conclude that because of the great latitude allowed in lubricating roller bearings and the small amount of lubricant necessary, lubrication is not important. Lack of lubrication usually will cause destruction of the bearing.

Because journal bearings must be extremely large when used in artillery applications with high trunnion forces and because friction is much lower for roller bearings, roller bearings generally are used for large caliber towed artillery weapons. The lower friction of roller bearings is especially critical for large caliber weapons because the elevation handwheel torque that can be supplied by the crew is already a limiting factor in meeting laying time requirements. Thus the larger friction associated with a journal bearing generally is unacceptable. Since torques required to elevate small caliber weapons often are not limited by human factors, journal bearings may be acceptable for this application.

6-3 TRAVERSE BEARINGS

The traverse bearing is generally of the rolling contact type. The roller bearing is used where running loads are small and, therefore, frictional resistance is inherently low. Since this bearing must support the weight of the top carriage plus the vertical component of trunnion force, it must be capable of supporting a large thrust load. The thrust load normally is supported by the main bearing, but a separate thrust bearing may also be considered. Some medium and heavy artillery have been designed with thrust bearings supported by springs, usually Belleville, which are stiff enough to carry the weight. Firing loads compress the springs and force the top and bottom carriages into direct contact, which relieves the load on the rolling elements of the bearing.

6-3.1 PINTLE BEARINGS

As mentioned in par. 6-1, the traverse bearing supports both radial and thrust loads. Pintle bearings may be used for light weapons, in which the radial component supports the weapon laterally through its pintle, whereas the thrust component supports its weight. Firing loads are transmitted through the bearing to the bottom carriage. The bearing may be a ball or roller bearing.

Antifriction rotation-thrust bearings may be used to carry only a thrust load. The flat-race type shown in Fig. 6-11 develops a small contact area and thus has low load-carrying capacity. The advantages are the low friction and the fact that an eccentric shaft has no effect on performance. Ball-thrust bearings are also made with grooved races and with two rows of balls. Rollers are often used in thrust bearings. The cylindrical roller has the disadvantage that because the outer end must travel farther than the inner end, considerable sliding takes place. This is reduced by making the rollers short. A tapered roller can have pure rolling.

Both ball and roller bearings are available with a self-aligning feature that compensates for slight misalignment. Without this feature any misalignment would cause only a few of the rolling elements to carry the entire load and thus shorten the life of the bearing. The outside face of one of the races is spherical and rests against a washer with a corresponding spherical surface, as shown in Fig. 6-12.

A pintle traverse bearing must support a substantial moment during recoil; the magnitude of the moment predicted by the dynamic analysis of Chapter 3. Two problems arise with pintle bearings as this moment

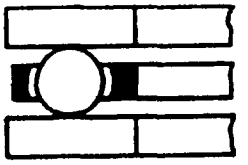

Figure 6-11. Flat-Race Thrust Bearing

THIS DOCUMENT PROVIDED BY THE ABBOTT AEROSPACE
TECHNICAL LIBRARY
ABBOTTAEROSPACE.COM

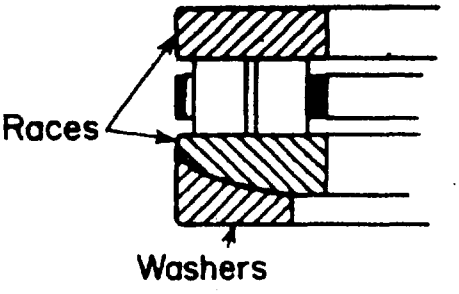

Figure 6-12. Self-Aligning Roller Thrust Bearing

increases. First, a large vertical spacing of ball or roller elements is required to support the moment with acceptable radial bearing loads. Second, the pintle itself must be large and rigidly fastened to the bottom carriage to transmit the moment. These difficulties generally limit applicability of pintle traverse bearings and lead to adoption of large diameter traverse bearings.

6-3.2 LARGE DIAMETER TRAVERSE BEARINGS

Large diameter roller traverse bearings have generally been adopted for large caliber towed artillery systems with on-carriage traverse, e.g., the M198 and FH-70 155-mm towed systems. This type of bearing is particularly attractive in supporting the large pitch moments that occur during weapon recoil. The schematic load diagram of Fig. 6-13 illustrates thrust force distribution across the bearing that balances the recoil force moment.

The traverse bearing for the M198 155-mm system, for example, is 1.12 m in diameter. Thus the thrust force that must be supported by each roller element is moderate. A linear force distribution as a function of distance from the bearing center, shown in Fig. 6-13, is a good approximation for preliminary bearing design. This force variation arises due to the elastic deformation of carriage components. The magnitude of recoil force is determined from dynamic analysis and preliminary system design, as presented in Chapters 2 and 3. With dimensions available from the weapon layout, the moment that must be supported by the traverse bearing is thus defined. The bearing designer may not use the linear bearing force variation to determine roller loads for several diameters of the traverse bearing. A sufficiently large diameter may be selected so that bearing forces are within allowable limits.

Although the linear force variation assumption, shown in Fig. 6-13, is reasonable for preliminary bearing design, a more refined calculation is needed to account for exact deformation of the carriage components during recoil. Finite element models of the top and bottom carriages (See Chapters 8 and 9.), with bearing races considered, can provide a much more precise definition of the actual loads in the bearing. These loads may then be used as technical specifications for procurement of the traverse bearing.

6-3.3 BALL JOINT AND FOLLOWER BEARINGS FOR 360-DEG TRAVERSE

An alternative to the pintle and large diameter traverse bearings is a ball joint and follower bearing. This configuration, shown in Fig. 6-14, is particularly attractive for off-carriage traverse systems, such as the M102

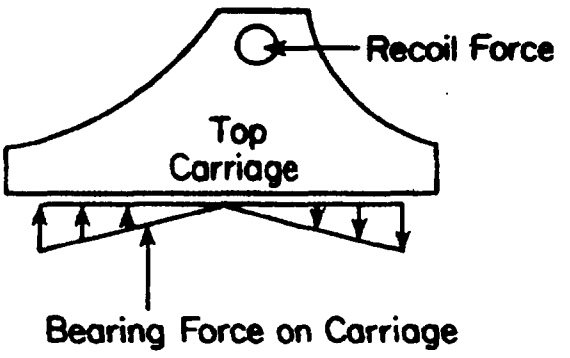

Figure 6-13. Large Diameter Traverse Bearing Force Distribution

THIS DOCUMENT PROVIDED BY THE ABBOTT AEROSPACE
TECHNICAL LIBRARY
ABBOTTAEROSPACE.COM

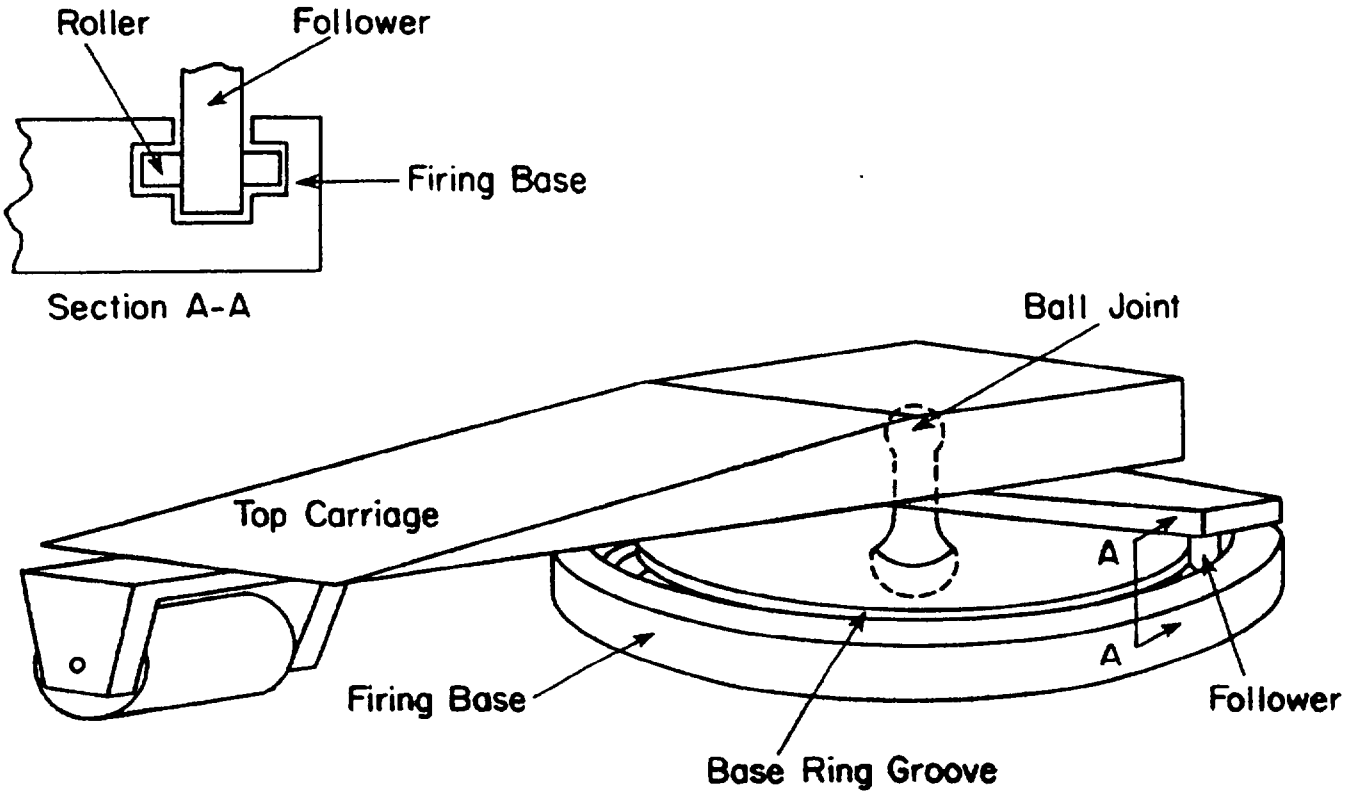

Figure 6-14. Ball Joint and Follower Traverse Bearing

and M204 105-mm towed systems, that employ a firing base and top carriage configuration. A ball joint connects the top carriage and firing base at its center, which allows full 360-deg traverse. To provide lateral stability of the weapon, a follower attached to the top carriage rides in a base ring groove in the firing base. If only one follower is employed, it must have a roller assembly, as shown schematically in Section A-A of Fig. 6-14, to prevent either upward or downward movement.

This type of traverse bearing tends to be limited to small caliber artillery application since, as shown in Chapter 4, the off-carriage traverse system is limited primarily to light weapons. Further, inherent difficulties associated with keeping the base ring groove clean in field operations must be accepted if this traverse bearing is employed.

REFERENCES

1. V. M. Faires, *Design of Machine Elements*, 4th ed., Macmillan Co., New York, NY, 1965.
2. DOD-HDBK-778 (AR), *Recoil Systems*, July 1988.
3. J. E. Shigley, *Mechanical Engineering Design*, 2nd ed., McGraw-Hill Book Co., New York, NY, 1977.
4. P. H. Black and O. E. Adams, Jr., *Machine Design*, McGraw-Hill Book Co., New York, NY, 1968.
5. DARCOM-P 706-193, Engineering Design Handbook, *Computer-Aided Design of Mechanical Systems, Part Two*, September 1977.
6. R. E. Parr, *Principles of Mechanical Design*, McGraw-Hill Book Co., New York, NY, 1970.

THIS DOCUMENT PROVIDED BY THE ABBOTT AEROSPACE
TECHNICAL LIBRARY
ABBOTTAEROSPACE.COM

CHAPTER 7
CRADLE DESIGN

This chapter presents procedures for designing cradles for towed artillery systems. The equipment associated with cradles is described, and materials used to manufacture cradles and manufacturing procedures are discussed. There are two types of cradles—the O-type and the U-type. U-type cradles are associated with towed artillery systems and, therefore, are discussed in detail in this handbook. O-type cradles, however, are used with self-propelled systems and are described only generally in this handbook. Detailed procedures for design of the O-type cradle are deferred for coverage in the handbook on self-propelled systems. Procedures for preliminary design of cradles are presented. These include procedures for estimating loads and strength requirements for various parts of the cradle. These procedures are based on basic mechanics of deformable bodies concepts. Sample design calculations are presented for an example cradle structure and for the cradle structure for the M198 towed Howitzer. Finally, advanced design techniques that incorporate the modern finite element method and associated software are discussed. Modeling for the finite element method and its advantages in the design process are emphasized.

7-0 LIST OF SYMBOLS

A = cross-sectional area, m^2
= area of cross section in tension, m^2
= total root area, m^2
= cross-sectional area of trunnion above neutral axis, m^2
A_b = bore area (less rifling groove area), m^2
A_{br} = bearing area, m^2
A_M = area of M/I diagram (see Fig. 7-25), MPa
A_n = area above line q, m^2
A_s = shear area, m^2
a = linear acceleration of projectile, m/s^2
= width of cross section at the level where τ is evaluated, m
= moment arm (see Fig. 7-11), m
= lever arm of force F_A from cradle (see Fig. 7-12), m
= dimension (see Fig. 7-5), m
= width of section A-A (see Fig. 7-18(A)), m
a_t = peripheral acceleration of projectile at bore, m/s^2
BF = counterrecoil buffing force, N
b = cross section width, m
= width of loaded edge, m
= moment arm (see Fig. 7-11), m
= length of gusset along cradle (see Fig. 7-12), m
= dimension (see Fig. 7-5), m
CF = force due to breech opening cam, N
c = distance to extreme fiber, m
= dimension (see Fig. 7-5), m
= height of gusset along trunnion, m
D_b = bore diameter, m
D_i = inner diameter of tube, m
D_o = outer diameter of tube, m
D_s = depth of section, m

THIS DOCUMENT PROVIDED BY THE ABBOTT AEROSPACE
TECHNICAL LIBRARY
ABBOTTAEROSPACE.COM

d = dimension (see Fig. 7-5), m
= dimension (see Fig. 7-18), m
= lever arm of force F, m
= distance from baseline to neutral axis of part, m
d_r = distance between reactions on rails (or center-to-center distance between rails), m
d_t = distance between trunnion reactions (center to center) or span of trunnion bearings, m
$\bar{d}$ = distance between the neutral axis of section and neutral axis of A_n, m
= distance from baseline to neutral axis of section, m
E = modulus of elasticity, Pa
e = dimension (see Fig. 7-5), m
= dimension (see Fig. 7-18), m
F = total load, N
$\boldsymbol{F}$ = force vector, N
F_A = trunnion reaction parallel to bore centerline, N
F_a = inertia force of recoiling parts, N
F_a' = maximum inertia force, N
F_E = equilibrator force, N
F_g = elevating gear load, N
= propellant gas force, N
F_g' = maximum propellant gas force, N
F_H = horizontal force, N
F_N = trunnion reaction normal to bore centerline, N
F_r = trunnion load due to rifling torque, N
F_r' = load on rails due to rifling torque, N
F_r'' = reaction on trunnion housing bolts due to rifling torque, N
F_s = force on elevating strut, N
F_T = resultant shear at section (see Fig. 7-8), N
= maximum trunnion load, N
F_V = vertical force, N
ΣF_V = total shear at cross section, N
f_1 = frictional force due to rear-end clip reaction, N
= frictional resistance of front bearing, N
f_2 = frictional force due to front-end clip reaction, N
= frictional resistance of rear bearing, N
g = acceleration due to gravity, m/s^2
h = dimension (see Fig. 7-5), m
= cross section height, m
I = moment of inertia of cross section, m^4
I_{BL} = moment of inertia at baseline, m^4
I_c = moment of inertia of cradle section, m^4
I_p = mass moment of inertia of projectile, $kg \cdot m^2$
I_T = moment of inertia of tube, m^4
I_0 = moment of inertia of part about its own neutral axis, m^4
K = total recoil resistance, N
K_R = force provided by recoil mechanism, N
K_e = fixity factor determined from the width-to-length ratio, dimensionless
k = radius of gyration of projectile, m

THIS DOCUMENT PROVIDED BY THE ABBOTT AEROSPACE
TECHNICAL LIBRARY
ABBOTTAEROSPACE.COM

L = moment arm of trunnion measured to center of bearing (see Fig. 7-13), m
= distance between stations, m
= dimensions (see Fig. 7-5), m
L_R = length of rail, m
L_1 = distance to centroid of distributed load, m
M = moment, N·m
M = moment vector, N·m
M_B = mass of elevating (but nonrecoiling) parts, kg
M_{ci} = bending moment of cradle at section i, N·m
M_{max} = maximum bending moment at various sections, N·m
M_R = couple of recoiling parts, N·m
M_T = moment about trunnion, N·m
M_W = weight moment about trunnions, N·m
M_x = moment of vertical force, N·m
M_y = moment of horizontal force, N·m
M_z = moment along z-axis, N·m
m_p = mass of projectile, kg
N_r = twist of rifling, calibers per turn
n = number of gussets parallel to F_A, dimensionless
P = axial force, N
P_g = propellant gas pressure, Pa
P_i = axial force at section i, N
P_{max} = maximum axial stress at various sections, N
p = pressure at interface due to shrink fit, Pa
Q = first moment about neutral axis of area above level where τ is evaluated, m^3
$R(t)$ = rod pull, N
R_b = radius of bore, m
R_c = shear between gusset and cradle body, N
R_c' = maximum bolt load (see Fig. 7-21), N
R_E = load on primary cradle structure (see Fig. 7-22), N
R_G = distributed horizontal reaction of gusset, N
R_g = elevating gear load, N
R_h = shear between gusset and hub, N
R_p = pitch radius of elevating gear, m
R_{RH} = shear reaction on key (see Figs. 7-9 and 7-22), N
R_{RL} = left bolt reaction (see Figs. 7-9 and 7-22), N
R_{RR} = right bolt reaction (see Figs. 7-9 and 7-22), N
R_s = load on key, N
R_t = maximum bolt load (see Fig. 7-22), N
R_t' = maximum bolt load (see Fig. 7-21), N
R_v = distributed vertical reaction of gusset, N
R_1 = normal reaction of front bearing, N
R_2 = normal reaction of rear bearing, N
R_1', R_2' = reactions to couple M_R of recoiling parts, N
R_3, R_4 = loads on the primary cradle structure (see Fig. 7-22), N

THIS DOCUMENT PROVIDED BY THE ABBOTT AEROSPACE
TECHNICAL LIBRARY
ABBOTTAEROSPACE.COM

r = distance between center of trunnion and centerline of equilibrator, m
= radius at contact surfaces of concentric cylinders, m
$\mathbf{r}$ = vector from centerline of a section to point of application of force F, m
r_c = distance between CG of cradle and center of trunnion, m
= moment arm from trunnion to W_c, m
r_h = radius of the hub or socket holding trunnion, m
r_1 = distance between CG of recoiling parts and center of trunnion, m
= moment arm from trunnion to W_1, m
= inner radius of inner cylinder, m
r_2 = outer radius of outer cylinder, m
S_b = tensile stress in cradle section due to bending moment, Pa
S_c = tensile stress in cradle section due to axial force, Pa
S_f = factor of safety, dimensionless
S_1 = clip reaction at rear end, N
S_2 = clip reaction at front end, N
T = torque on cradle arm, N·m
T_r = rifling torque, N·m
T_V, T_H = trunnion reactions perpendicular to and along barrel, respectively, N
t = thickness of section, m
= thickness of section at q, m
= thickness of gusset, m
= diameter of trunnion, m
W_c = weight of cradle, N
W_R = width of rails, m
W_t = weight of tipping parts, N
W_1 = weight of recoiling parts, N
w = unit load, maximum intensity, N/m
= total uniformly distributed load, N
= maximum unit load on gusset, N/m
w_r = uniformly distributed load, N
w_2 = equivalent uniformly distributed load on rails, N/m
X = distance to section from trunnion centerline, m
$\bar{x}$ = centroid, m
$\bar{y}$ = distance of centroid of cross section above neutral axis from neutral axis, m
Z = section modulus, m^3
Z_x = section modulus about x-axis, m^3
Z_1 = section modulus of lower side of cradle, m^3
Z_2 = section modulus of upper side of cradle, m^3
α = angular acceleration of projectile, rad/s^2
= $f(b/h)$, dimensionless
β = pressure angle of gear, deg
β_1 = ζ-coordinate of rear-end frictional force, m
β_2 = ζ-coordinate of front-end frictional force, m
γ = original angle of elevation, deg
$\gamma + \theta$ = angle between gun tube and horizontal, deg
ζ_B = ζ-coordinate of center of mass, m
ζ_{EL} = ζ-coordinate of elevating strut, m

THIS DOCUMENT PROVIDED BY THE ABBOTT AEROSPACE
TECHNICAL LIBRARY
ABBOTTAEROSPACE.COM

ζ_{EQ} = ζ-coordinate of equilibrator, m
ζ_2 = ζ-coordinate of rod pull force, m
ζ_5 = ζ-coordinate of counterrecoil buffing force, m
ζ_6 = ζ-coordinate of breech opening cam force, m
η = angle as shown in Fig. 7-9, deg
η_β = η-coordinate of center of mass, m
η_{EL} = η-coordinate of elevating strut, m
η_{EQ} = η-coordinate of equilibrator, m
η_F = η-coordinate of front clip reaction, m
η_R = η-coordinate of rear clip reaction, m
θ = relative rotation between masses M_B and M_D (nonelevating mass), deg
= angle of elevation, deg
θ_r = helix angle of rifling, deg
θ_1 = angular deflection at station −0.381 m, deg
θ_2 = angle through which tube rotates due to rail clearance, deg
Δ = radial interference, m
= deflection at a station, m
λ = angle between equilibrator and barrel, deg
= angle between equilibrator and horizontal axis in Fig. 7-8, deg
= angle between equilibrator and ($\phi - \eta$)-axis, deg
μ = coefficient of friction, dimensionless
ν = Poisson's ratio, dimensionless
σ = combined stress, Pa
= bending stress, Pa
σ_{br} = bearing pressure (stress), Pa
σ_c = compressive stress, Pa
σ_e = equivalent stress, Pa
= effective stress, Pa
σ_t = tensile stress, Pa
σ_y = yield stress, Pa
σ_1 = maximum principal stress, Pa
σ_2 = minimum principal stress, Pa
τ = shear stress, Pa
= angle between elevating strut and barrel, deg
= angle between elevating strut and ($\phi - \eta$)-axis, deg
ϕ = rotation of M_D around ground pivot, deg
ϕ_1 = angle between line of action of force F_a and centerline of bore (see Fig. 7-8), deg
ϕ_2 = angle between line joining CG of cradle and center of trunnion and centerline of bore (see Fig. 7-8), deg

7-1 INTRODUCTION

The cradle is a nonrecoiling structure of the weapon. It houses the recoiling parts and rotates about the trunnions to elevate the weapon. The perspective view of a cradle structure is shown in Fig. 7-1. The primary function of the cradle is to support the gun tube and provide the guides on which the tube slides during recoil and counterrecoil. The cradle also prevents the tube from rotating about its axis due to rifling torque and transmits firing loads to the top carriage.

With an estimate of the weight and dimensions of the cradle known from a preliminary design, an iterative procedure is used to design the final structure. For the first few design iterations, the structure is rendered determinate by making some simplifying assumptions. Once the simplified design is found to be acceptable, more refined methods can be used to obtain better estimates for forces and stresses and to redesign the

THIS DOCUMENT PROVIDED BY THE ABBOTT AEROSPACE
TECHNICAL LIBRARY
ABBOTTAEROSPACE.COM

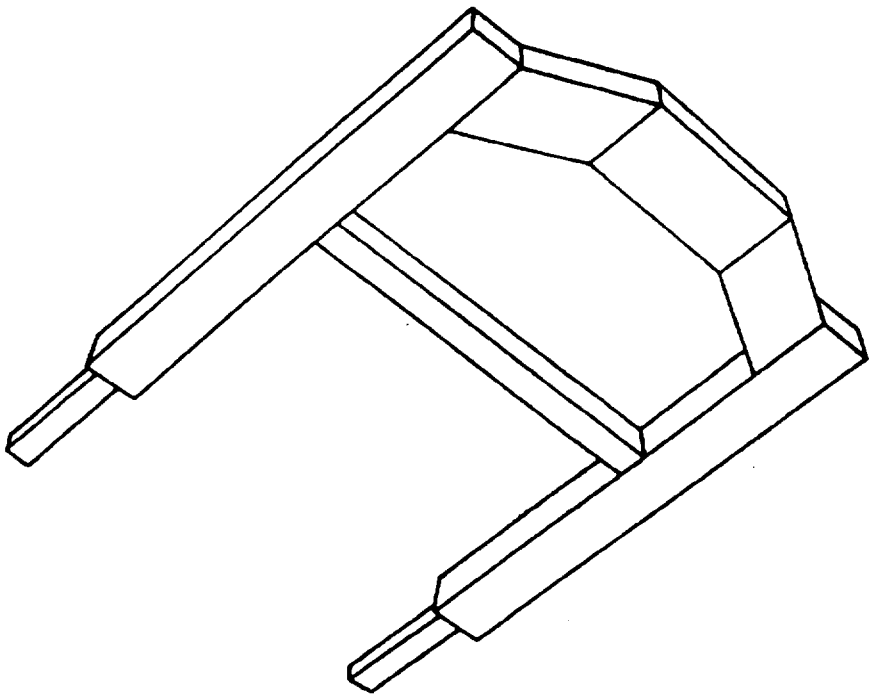

Figure 7-1. Perspective View of Cradle Structure

structure if necessary. This philosophy was used in the design of the cradle structure for the M198 towed Howitzer. One of the refined methods of stress analysis is the finite element technique (Refer to Appendix C.), and the use of this technique for the analysis of the cradle is described.

7-2 EQUIPMENT ASSOCIATED WITH CRADLES

Various components that affect cradle design are described in the subparagraphs that follow. These are the recoil mechanism, trunnions, elevating mechanism, and equilibrator.

7-2.1 RECOIL MECHANISM

The fixed part of the recoil mechanism is attached to the cradle, and the movable portions are attached to the recoiling parts. There are, in general, two basic arrangements for the recoil mechanism. One has the recoil cylinder and recuperator fixed to the cradle and the piston rod fixed to the gun lug or breechblock. The other arrangement fixes the recoil cylinder and the recuperator to the gun and the rod to the cradle. In the first case, the cylinder and recuperator are either integral parts of the cradle or separate parts rigidly attached to it. It is well to have the recoil mechanism installed as near as possible to the tube, not only for compactness but also for lower bending moments on the cradle, which are axiomatic for lower stresses and, therefore, lighter structure. The design of recoil mechanisms is covered in a separate handbook (Ref. 1).

7-2.2 TRUNNIONS

The trunnions are considered to be components of the cradle whether the trunnion bearings are located on the side frames or in the cradle itself. The trunnions, through which the firing loads are transmitted, are the main attachment to the top carriage and also serve as the pivot about which the tipping parts rotate during elevation. In the top view, their axis should be normal to the direction of recoil. In the side view, the trunnion axis should be located on or near the line parallel to the bore and passing through the center of gravity of the recoiling parts. This geometry reduces tipping moments during firing and relieves the elevating arc of large loads. The design of trunnion bearings is covered in Chapter 6.

THIS DOCUMENT PROVIDED BY THE ABBOTT AEROSPACE
TECHNICAL LIBRARY
ABBOTTAEROSPACE.COM

7-2.3 ELEVATING MECHANISM

The elevating mechanism terminates at the elevating arc, which is a gear segment rigidly attached to the cradle. It is here that the torque required to elevate is applied to the tipping parts. The pitch radius of the elevating arc is centered at the trunnions and should be as large as possible and still remain compatible with the size of the rest of the structure. A large radius results in small gear tooth loads and less effort to elevate the gun. Also, if the arc is large, the attachments to the cradle can be located farther apart, and although the torque transmitted to the tipping parts remains unaffected, the corresponding loads at the attachment points are decreased.

In the M198 towed Howitzer, the elevating mechanism consists of two struts. One end of the strut is attached to the top carriage and the other is attached to the cradle. These struts can be extended or shortened, depending upon whether the gun tube is to be raised or lowered in the firing plane.

The design of elevating mechanisms is covered in Chapter 4.

7-2.4 EQUILIBRATOR

One end of the equilibrator is attached to the top carriage and the other to the cradle. A large turning radius about the trunnion is desirable for the equilibrator because it lowers the forces; hence a more efficient design results. The attachment on the cradle may be at any convenient location on the structure or on the elevating arc, provided that clearances and strength requirements are met. The equilibrator design is covered in Chapter 5.

7-3 TYPES OF CRADLE

There are two basic types of cradle, designated according to the general form of cross section as the U-type and the O-type. Each has its own method of seating the gun tube. The U-type seats the tube on top or in the sides and retains it by guides, whereas the O-type holds the tube in a hollow cylinder whose inner wall conforms to the mating portion of the tube.

7-3.1 U-TYPE CRADLE

The degree of resemblance between the U-type cradle and the letter "U" depends on construction features. If the recoil cylinder and recuperator are attached to the gun tube so that they become part of the recoiling system, the cradle may be approximately U-shaped with provisions for accommodating the rails and trunnions. On the other hand, if the recoil cylinder and recuperator are integral with the cradle, the resemblance to a U-section is lost. However, the terminology is still retained in the latter case. Figs. 7-2 and 7-3 show construction for a U-type cradle. If the recoil cylinder and recuperator are attached to recoil with the gun tube, the structure that supports them is called a sleigh. The sleigh carries the rails and thus supports the tube in the cradle.

The sliding surfaces of the recoiling parts are called rails. Either the rails or their supporting guides may be channel-shaped to prevent them from separating due to the upsetting moments and rifling torque. Either, but not both, may be discontinuous (made of several shorter lengths spaced at convenient distances). Rails may be attached to the sleigh. For any type of construction, either the rail assembly or the sleigh, these parts are treated as constituents of the cradle.

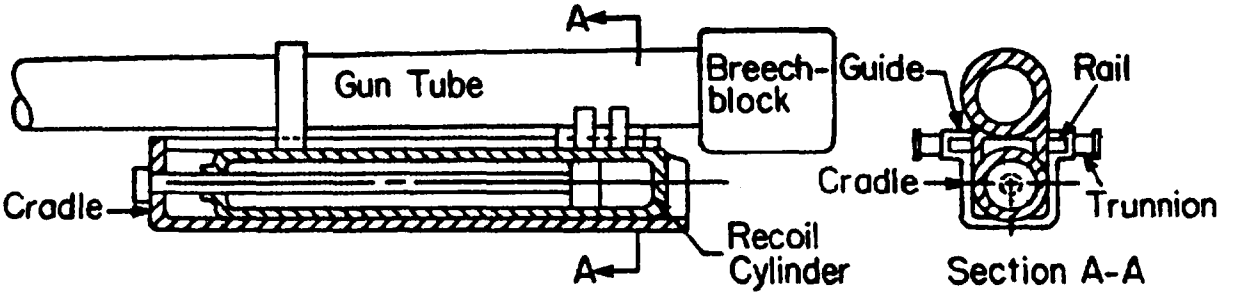

Figure 7-2. U-Type Cradle With Attached Recoil Mechanism

THIS DOCUMENT PROVIDED BY THE ABBOTT AEROSPACE
TECHNICAL LIBRARY
ABBOTTAEROSPACE.COM

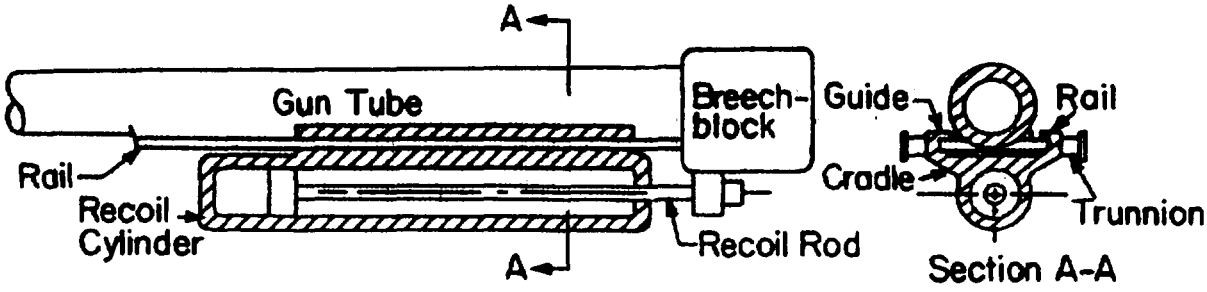

Figure 7-3. U-Type Cradle With Integral Recoil Mechanism

The equilibrator, which provides the moment about the trunnions, is attached to the body of the top carriage on the rear end and to the cradle at the front end. The elevating struts, if used, pass through the arms of the cradle, and a mechanism lowers and raises the gun tube and cradle.

The U-type cradle has several advantages. With a sleigh, the added weight of the recoiling parts reduces either the recoil force or the length of recoil. Ordinarily, the height of the weapon is decreased (lower silhouette) by having the recoil mechanism below the gun tube. The design of the gun tube is not influenced to any great extent by the fixtures that hold it in the cradle. Because the gun tube does not form the sliding surfaces for recoil, its contour, and hence wall thickness, needs only to conform to the gas pressure distribution along its length.

Several disadvantages associated with the U-type cradle follow:

1. Fabrication is difficult. The structure is complex, and a high degree of accuracy is required to machine the slides and rails to the proper alignment and fit. Therefore, production costs are high.
2. If clearances are not sufficient for an underslung recoil mechanism, the trunnion height must be increased. This increased height results in an accompanying increase in overturning moment and a higher silhouette.
3. It is difficult to arrange the ideal loading pattern with the resultant of the recoil forces passing through the centerline of the trunnions. This arrangement is, however, always attempted in order to minimize the elevating gear loads during recoil.
4. During extended firing, heat transmitted from gun tubes to rails may cause warpage and eventual binding.
5. Misalignment may occur in discontinuous rails or slides and cause them to bind during recoil and counterrecoil. Binding of this nature may prevent the gun tubes from returning to the in-battery position.

7-3.2 O-TYPE CRADLE

This type of cradle has a cylindrical tube for its basic structural element. Each end contains suitable bearings in which the gun tube slides. The outside surface of the tube is cylindrical for a considerable length forward of the breech. This surface is machined smooth, and the tube itself serves as its own slide—the bearings function as guides during recoil and counterrecoil. A key transmits the rifling torque to the cradle to prevent rotation of the tube. Brackets or some similar structure are provided on the cylindrical portion of the cradle to attach the recoil mechanism, the trunnions, and the elevating arc. Fig. 7-4 shows construction of the O-type cradles.

The use of an O-type cradle offers several advantages:

1. It is convenient to locate the trunnions on the line of action of the recoiling parts to relieve the elevating gear of firing loads.
2. The structure is comparatively light, which helps to increase mobility.
3. The use of the O-type cradle does not require the sliding surfaces to be attached to the gun tube, which eliminates this fabrication problem.
4. The cylindrical surfaces reduce machining problems and provide more accurate alignment.
5. A choice of a favorable location is available for the recoil mechanism.
6. When the recoil mechanism is on the top of the tube, it does not present clearance problems while the tipping parts are being elevated.

There are several disadvantages inherent to the O-type cradle:

1. The sliding surface of the gun tube is exposed to the weather, although this can be eliminated by the installation of a shield.

THIS DOCUMENT PROVIDED BY THE ABBOTT AEROSPACE
TECHNICAL LIBRARY
ABBOTTAEROSPACE.COM

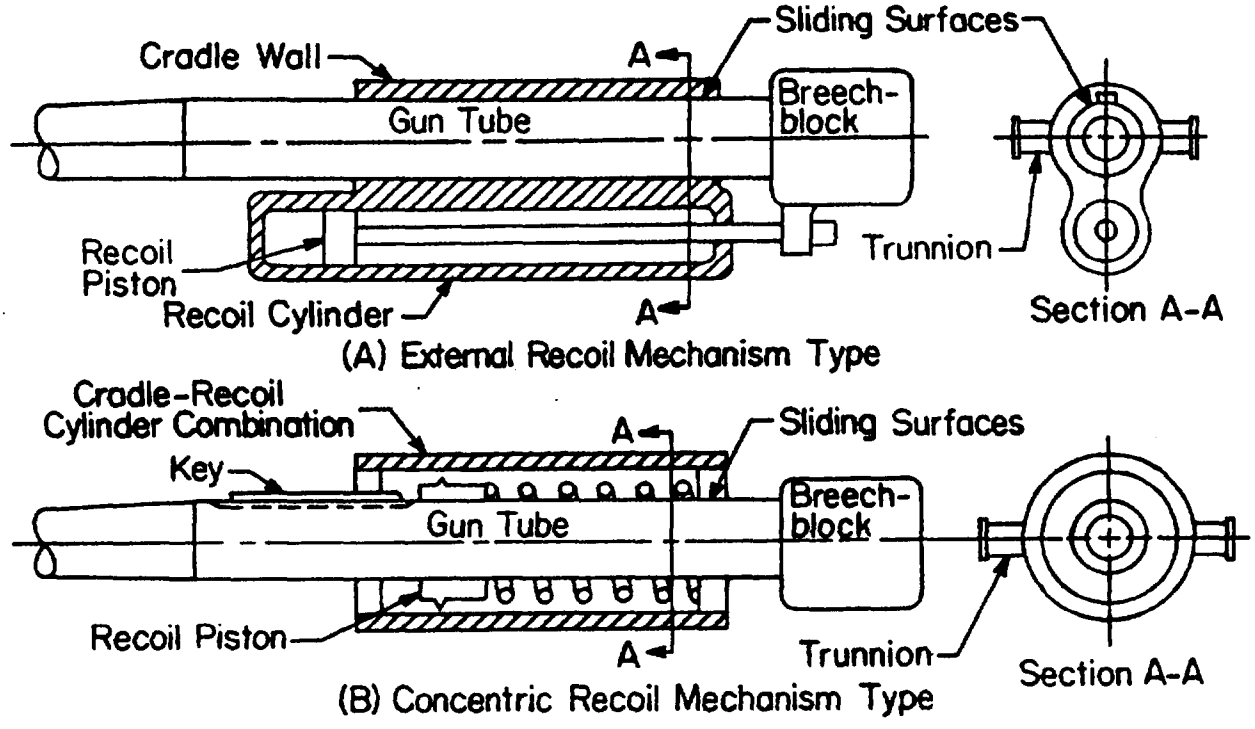

Figure 7-4. O-Type Cradles

2. It dictates, to some extent, the diameter of the tube forward of the chamber because it cannot be tapered along the sliding surface.
3. If the forward position of the sliding surface is made smaller in diameter, two sleeve bearings of different diameters are necessary.
4. The effects of heating the gun tube can be serious if the expansion exceeds the clearances in the bearings.
5. The clearances that must be provided to avoid binding may result in sloppy fits while the gun is cold. Another clearance problem stems from the transport condition, where road clearances may be critical with the recoil mechanism attached to the top of the gun tube.

The O-type cradle generally has been used in self-propelled artillery systems; consequently, detailed design of this type of a cradle is not discussed in this handbook.

7-3.3 EFFECT OF FRICTION ON SLIDING SURFACES

Frictional forces, as such, are not a serious design criterion with respect to the structural strength. In other aspects, however, they present serious problems. For design analysis the present practice is to use a coefficient of friction of 0.15. Friction resists recoil and thus forms part of the recoil force, but it is desirable to keep friction to a minimum through proper lubrication because wear and eventual damage to the sliding surfaces are less likely to occur. Also frictional forces are somewhat of an unknown value on exposed surfaces and may vary considerably. If their maximum value is small, friction forces will constitute only a small part of the total recoil force and will have only a slight effect on the functioning of the recoil mechanism.

7-3.4 EFFECT OF TEMPERATURE VARIATION ON SLIDING SURFACES

Artillery is employed in both desert and arctic climates. Changes in the ambient temperature will shrink or expand the structure. If made of like material, all components will be affected equally and there will be no relative displacement among them. However, if the structural members are of unlike material, their rates of expansion will differ, which may prove deleterious simply by reducing clearances between moving parts to the extent that binding impends. The sliding surfaces of cradles must be of different materials because two mating surfaces of like material seldom provide compatible sliding properties. Bronze makes an excellent sliding

THIS DOCUMENT PROVIDED BY THE ABBOTT AEROSPACE
TECHNICAL LIBRARY
ABBOTTAEROSPACE.COM

surface for steel. The coefficient of linear expansion for bronze is 6.3×10^{-6} m/m·°C, which is larger than that for steel. This value is computed from the coefficients in the centigrade scale of 16.8×10^{-6} for phosphor bronze and 10.5×10^{-6} for 1.2% carbon steel. Based on an ambient temperature of 21°C, the extreme ranges will show a difference in dimensions for bronze and steel of 0.00033 m/m at 73.8°C and of −0.00047 m/m at −53.9°C. The lower limit of the temperature extremes, because of climatic conditions, has the greater effect. However, neither extreme requires excessively loose fits to compensate for the thermal activity.

7-3.5 SUGGESTED MATERIALS FOR CRADLE

The predominant requirements for the cradle are strength and rigidity. For its main structure an inherently strong material with a high modulus of elasticity is preferred. This preference suggests steel, although it does not exclude other materials, such as aluminum alloys, having the required physical properties. For the sliding surfaces, hardness and compatibility are required to preclude galling of the contacting surfaces. Steel slides, rails, and guides—as components of the main structure—provide strength and rigidity and, as sliding members, provide a hardened surface. Hard bearing bronze, covering one member, also provides a hardened surface, and in conjunction with the bare steel of the other member, the two constitute adjacent materials that can provide the compatibility requirement. Bronze is preferred to brass because of the tendancy of brass to form zinc oxide, a substance that promotes galling.

7-3.6 MANUFACTURING PROCEDURES

Standard production practices are followed in constructing cradles regardless of whether castings, forgings, or weldments form the basic structure. If there are deviations from this practice, it is only in the manner in which the cradles are handled. Basic fabrication activities remain undisturbed. If necessary, standard machines are adapted for convenient operation. Warpage is corrected by stress relief through heat treatment. Those members of the cradle that require finished surfaces are made oversize so that residual irregularities may be removed when the part is machined to size.

The decision whether forgings, castings, or weldments should be used usually is reached by the nature of the structure. If high strength-to-weight ratios are needed, forgings are used; however, forgings are costly. If weight is not important, castings may be applicable. They provide large fillets and thus create stress concentrations at reentrant angles. Forgings and castings are less susceptible to warpage than weldments, although all should be stress relieved to insure dimensional stability. The main disadvantages of castings include bulkiness and a lengthy manufacturing process. Welded assemblies should be used where applicable because

1. The buildup structure is relatively simple and light.
2. Joints are permanent and provide a more rigid structure than if bolted or riveted.
3. Weldments can be made from available stock material to permit construction at low cost in a relatively short time.

Although weldments are prone to warp, this tendency is overcome by stress relief through heat treatment.

7-4 PRELIMINARY DESIGN OF CRADLES

The design of components of the cradle is an iterative process, as discussed in Chapter 2. Based on a mixture of intuition, experience, and historical data, the designer estimates the weight and dimensions for the preliminary design. In Chapter 3 these quantities are used in the dynamic analysis and load determination.

This paragraph describes load and stress analysis for the cradle structure at the preliminary design stage. Very little data are available for the cradle at this stage. Therefore, the designer must rely on historical data and his experience and intuition to arrive at a preliminary design of the cradle structure or, for that matter, any component of the weapon system. Also, at the preliminary design stage highly idealized models for the cradle structure must be used for quick stress analysis and checking of failure conditions. The basic mechanics of deformable bodies concepts are used. The Maximum Shear Stress Theory, Ref. 2, is used as a failure criterion in preliminary design. After an acceptable structure has been obtained by the use of these preliminary design procedures, design improvements are possible by using the test data for a prototype system. This is explained in par. 7-4.3.

The design practice follows a set of simple guidelines. The structure should be simple and symmetrical. Simplicity and symmetry offer several advantages—fabrication is easier and they tend to keep the weight down—and a stronger, more compact and efficient unit is the ultimate result. If a material of large strength-to-weight ratio is needed, high strength is indicated. However, if rigidity is also essential, low weight must be

THIS DOCUMENT PROVIDED BY THE ABBOTT AEROSPACE
TECHNICAL LIBRARY
ABBOTTAEROSPACE.COM

sacrificed and the necessary strength derived from a bulkier structure. Cradles must be rigid to insure an accurate weapon; therefore, the overall design should be directed toward this end.

A well-designed structure embodies good maintenance features; hence ease of maintenance, both preventive and corrective, begins on the drawing board. Inspecting, cleaning, and lubricating are activities usually associated with preventive maintenance. Of these activities, lubrication is the most important because it not only reduces friction and the accompanying wear or galling, but it also protects the sliding surfaces from corrosion. A good lubricant for sliding surfaces is MIL-G-10924A grease, which lubricates effectively through the temperature range of −53.8° to 51.7°C. Lubrication should be a simple task requiring only a short time to perform; therefore, fittings must be readily accessible on the assembled weapon but should not be located in highly stressed regions of the cradle because small holes introduced into the structure cause stress concentrations. If location in highly stressed regions is unavoidable, the lubrication holes should be heavily bossed for reinforcement.

A cradle functions best when clean; any dirt or other foreign substance on slides or trunnions will impede recoil and elevation. Maintenance here is a continuous effort to keep the cradle and its attachments clean: Sand, mud, water, snow, or ice must not accumulate in it. Pockets created by structural members should have drain holes or should be easily reachable for cleaning; otherwise water, from rain or melting snow, accumulates in these pockets and may later freeze and thus damage even equipment that is well-designed in other respects. Dirt must be kept off sliding surfaces. Cover plates are effective dirt seals at the trunnion, and wipers, located where the initial contact begins between sliding surfaces, remove dirt and grit from the exposed portions of the slide.

Corrective maintenance is a repair or replacement activity that may require disassembly of the cradle. In many instances this work must be performed in the field where regular handling equipment normally is not available; this lack of equipment increases the burden on maintenance crews. If feasible, each subassembly should be designed so that it will not interfere with the dismantling of other components. When this practice is followed, only those parts requiring attention need be removed, i.e., the undamaged ones are undisturbed. Also following this practice will expedite maintenance in the field, particularly from the handling viewpoint.

Failure of the primary structure often can be repaired by welding. Hence the selection of a weldable material while the cradle is still in the design stage may prove to be an asset. Other repairs involve sliding surfaces. Scored or galled surfaces can be scraped and hand polished until smooth. If damage is too extensive, the surfaces must be replaced—a relatively easy operation if bronze liners are used. If the damage is on the steel surface of a slide integral with the main structure, however, the entire cradle may have to be scrapped. This fact emphasizes the need for good design practice with respect to maintenance. Those members of a structure that have a critical function and are prone to damage should be detachable.

More discussion on design for maintainability is given in Chapter 10. Human factors to be considered in design are discussed in Chapter 11.

7-4.1 LOAD ANALYSIS FOR CRADLE STRUCTURE

There are three types of loads that act on the cradle—firing loads, traveling loads, and lifting loads. These loads are functions of time; however, time generally is not considered a variable in design and analysis. Because maximum values are used, this design procedure is conservative since maximum values of these forces often occur at different times. To determine loads that are transmitted to the cradle due to firing, traveling, and lifting, a dynamic model for the weapon system is needed. As explained in par. 7-4, a preliminary design of the weapon system based on a combination of experience and historical data is necessary. The iterative process of estimating component sizes, carrying out the dynamic analysis, and computing the stresses refines the model by estimating loads and stresses more accurately. Many times, it is not possible to analyze the structure for all loading cases because of the constraints on time and computing effort. The designer should select a few loading cases that are critical and should include only these in the analysis and design process.

7-4.1.1 Firing Loads

The firing loads for the cradle are obtained from a dynamic analysis of the model. If field data from a prototype model testing are available, these data can be used to predict loads for various components. As a result of the interaction of several forces, it may be necessary to use a trial and error procedure to compute the maximum bending moment.

The firing loads consist of loads from the recoil mechanisms, equilibrator, elevating mechanism, and rifling torque. For any angle of elevation the equilibrator force is the one required to produce the moment that balances the weight moment of the tipping parts. The elevating arc (or strut) is attached to the cradle through a

THIS DOCUMENT PROVIDED BY THE ABBOTT AEROSPACE
TECHNICAL LIBRARY
ABBOTTAEROSPACE.COM

well-fitting rigid joint because meshing of gear teeth is involved. A detailed description of the loads on different parts is given in par. 7-5.

The loads transmitted to the cradle are shown in Fig. 7-5. Note that for the preliminary analysis the structure is rendered determinate using the analysis philosophy discussed in Chapter 2. The preliminary load analysis also does not include the travel and lifting loads that are considered when refined load and stress analyses are carried out. Therefore, effects due to travel and lifting loads are discussed later.

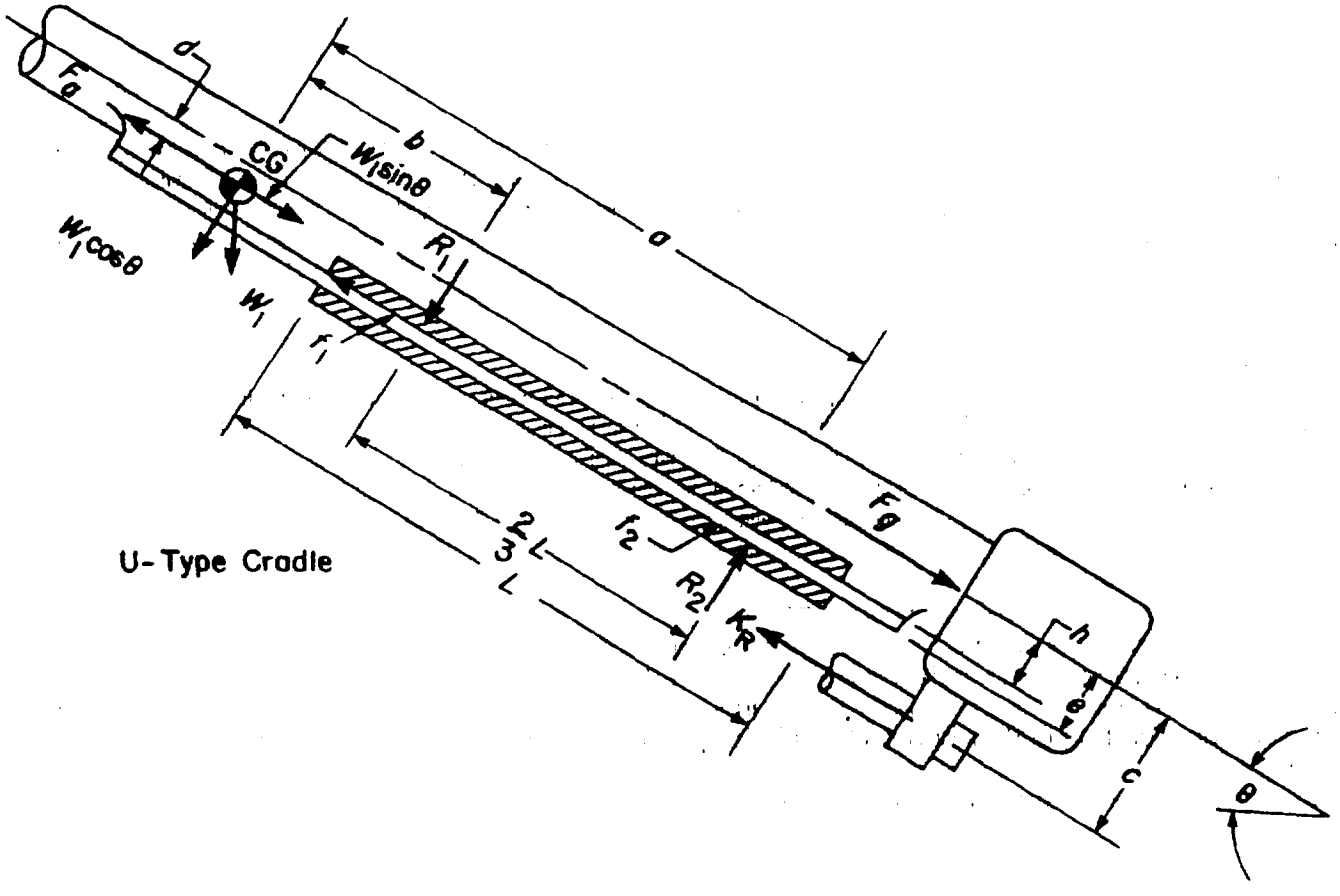

Figure 7-5. Loads Transmitted to Cradle

7-4.1.2 Loads on Various Components of Cradle Structure

For the first iteration an approximate model for the structure is assumed. This model is then used in load and stress analysis of the structure. In this subparagraph, analysis and design of four components—recoil attachment, equilibrator attachment, elevating arc, and attachment for transmitting rifling torque—of the cradle structure are described.

7-4.1.2.1 Recoil Attachment to Cradle

When the recoil mechanism housing is integral with the cradle, the recoil forces are applied through it and no additional supporting structure is necessary. If it is merely attached to the cradle, appropriate yokes or similar structures are needed to transmit its force to the cradle. If the recoil mechanism is attached to and moves with the recoiling parts, the recoil rod is fixed to the cradle, sometimes by an adapter or sometimes by a nut threaded to the end of the rod. The rod, in this case, is attached to the front of the cradle where local reinforcement of the structure may be necessary to carry the load.

To determine loads for the recoil attachment, it is necessary to analyze the loads during a recoil cycle. Consider the free-body diagram shown in Fig. 7-5 for a typical U-type cradle during a recoil stroke. For any

THIS DOCUMENT PROVIDED BY THE ABBOTT AEROSPACE
TECHNICAL LIBRARY
ABBOTTAEROSPACE.COM

variation for the cradle from that shown in Fig. 7-5, a similar free-body diagram must be developed. The procedure to be outlined can then be used for other constructions of a U-type cradle.

In the free-body diagram of Fig. 7-5, values of R_1, R_2, and K_R are unknown and must be determined by solving the three equations of static equilibrium:

$$\Sigma F_H = 0, \text{ N} \tag{7-1}$$

$$\Sigma F_V = 0, \text{ N} \tag{7-2}$$

$$\Sigma M = 0, \text{ N·m} \tag{7-3}$$

where

F_H = horizontal force, N
F_V = vertical force, N
M = moment, N·m.

In Eqs. 7-1 and 7-2 the forces are summed along the horizontal and vertical directions or along any two convenient orthogonal directions. In Eq. 7-3 moments are computed at a convenient point, such as the intersection of f_2 and R_2. The location of reactions R_1 and R_2 depends on the type of rail guide construction. If there is continuous contact between the rail and guide, the pressure distribution between them is assumed to be triangular and the reactions are located appropriately. This point is discussed further in par. 7-4.2.2, in which the design of sliding surfaces is discussed. If bronze bearing pads are used at some locations, the reaction forces R_1 and R_2 are applied only at these points and are assumed to be uniformly distributed on the bearing surface.

A method for calculating total recoil resistance force K is given in Ref. 1. This force comprises the sliding frictional resistance of the recoiling parts and the resistance provided by the recoil mechanism.

Note that

$$f_1 = \mu R_1, \text{ N} \tag{7-4}$$

$$f_2 = \mu R_2, \text{ N} \tag{7-5}$$

$$K = K_R + f_1 + f_2, \text{ N} \tag{7-6}$$

where

μ = coefficient of friction, dimensionless
K_R = force provided by recoil mechanism, N
R_1 = normal reaction of front bearing, N
R_2 = normal reaction of rear bearing, N
f_1 = frictional resistance of front bearing, N
f_2 = frictional resistance of rear bearing, N.

Summation of the forces in directions parallel and perpendicular to the bore axis yields, respectively,

$$F_a = F_g + W_1 \sin\theta - K, \text{ N} \tag{7-7}$$

and

$$W_1 \cos\theta + R_1 = R_2, \text{ N} \tag{7-8}$$

where

F_a = inertial force of recoiling parts, N
F_g = propellant gas force, N
W_1 = weight of recoiling parts, N
θ = angle of elevation, deg.

THIS DOCUMENT PROVIDED BY THE ABBOTT AEROSPACE
TECHNICAL LIBRARY
ABBOTTAEROSPACE.COM

Also taking moments of all the forces about the intersection of f_2 and R_2 yields

$$(F_a - W_1\sin\theta)(e - d) + (W_1\cos\theta)a + R_1(a - b) + f_1(e - h) = F_g e + K_R(c - e), \text{ N·m} \quad (7\text{-}9)$$

where the distances a, b, c, d, e, and h are defined in Fig. 7-5. Note that $(a - b) = 2L/3$ in Eq. 7-9. These last three equations are solved for R_1, R_2, and K_R.

7-4.1.2.2 Equilibrator Attachment

Each equilibrator, whether one or two per weapon, pivots on a shaft attached to the cradle. If two are used, the shafts are usually cantilevered from each side of the structure (Fig. 7-6(A)) or the elevating arc (Fig. 7-6(B)). If one is used, each end of the shaft is supported by the structure as shown in Fig. 7-7.

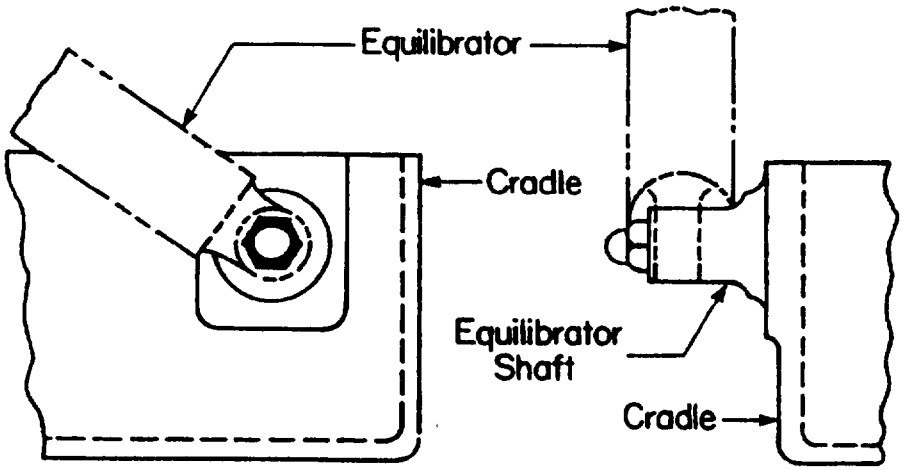

(A) Equilibrator Attachment on Cradle Structure

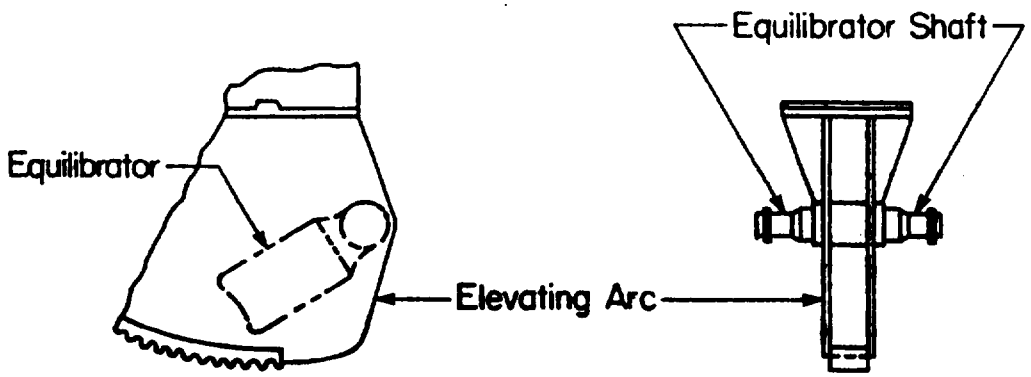

(B) Equilibrator Attachment on Elevating Arc

Figure 7-6. Equilibrator Attachments, Cantilever Type

For any given angle of elevation the equilibrator force is the one required to produce the moment that balances the weight moment of the tipping parts. Although actual equilibrator forces do not always equal the theoretically required ones, differences are small enough that the structure is not affected. Hence for design purposes the theoretical value is used to simplify the load analysis. All external loads on the cradle are shown in

THIS DOCUMENT PROVIDED BY THE ABBOTT AEROSPACE
TECHNICAL LIBRARY
ABBOTTAEROSPACE.COM

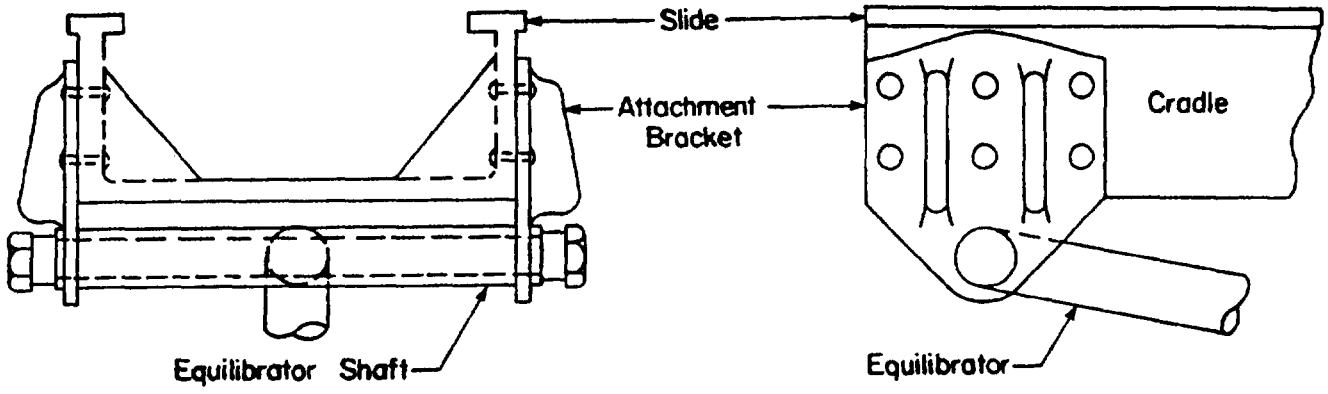

Figure 7-7. Equilibrator Attachment, Simple Beam Type

Fig. 7-8. The equilibrator force is determined from the condition that it balances the moment about the trunnions of the forces due to the weights of the recoiling parts and cradle. By taking moments about the trunnion, the equilibrator force F_E is given as

$$F_E = \frac{W_1 r_1 \cos(\theta + \phi_1) + W_c r_c \cos(\theta + \phi_2)}{r}, \text{ N.} \qquad (7\text{-}10)$$

Note that in Fig. 7-8 ϕ_2 is negative.

It is apparent that, before the preliminary design of the cradle is completed, the equilibrator geometry, at least a preliminary one, must be determined in order to compute the equilibrator force. This is discussed in Chapter 5.

7-4.1.2.3 Elevating Arc

The attachment of the elevating arc to the cradle should be through a well-fitting, rigid joint because the meshing of gear teeth is involved. Improper meshing of the gears will prove detrimental in one or all of three ways, i.e., poor load distribution may overstress the teeth; excessive wear may occur; and gear efficiency may decrease, which would require an increased torque at the handwheel. The attachment then must be secured in a manner that will preclude objectionable misalignment under load, which requires close-fitting machined surfaces held together by shear connections, such as body-bound bolts, keys, pins, or shafts. Fig. 7-9 shows the loads on the attachments between arc and cradle.

The action of equilibrators practically eliminates the gear load except during elevation and recoil. The largest load usually occurs during recoil, and only if the trunnions and the CG of the recoiling parts lie on the bore axis will no additional gear load be applied during recoil. Fig. 7-8 illustrates the applied external loads on the cradle for a single recoil system. The reaction R_g on the gear is computed by taking moments about the trunnions. The trunnion reactions, parallel and normal to the bore axis, are found by bringing the force system into equilibrium.

For the M198 towed Howitzer, the elevating mechanism consists of two elevating struts. One end of these struts is attached to the top carriage, and the other end is attached to the cradle. It should be noted that if the elevating strut is present, there is no necessity for an elevating arc. The gear attachment is contained at the connection point on the top carriage. The struts pass through the arms of the cradle and are connected by a threaded ball-screw arrangement. To raise or lower the gun tube, the system of gears located in the top carriage turns the elevating struts through the threaded ball-screw arrangement.

7-4.1.2.4 Attachment for Transmitting Rifling Torque

In addition to supporting the tube, the cradle must also transmit the rifling torque to the top carriage. Fig. 7-10 shows the torque reactions on the cradle and the distances between the load centers. The approximate rifling torque equation,

THIS DOCUMENT PROVIDED BY THE ABBOTT AEROSPACE
TECHNICAL LIBRARY
ABBOTTAEROSPACE.COM

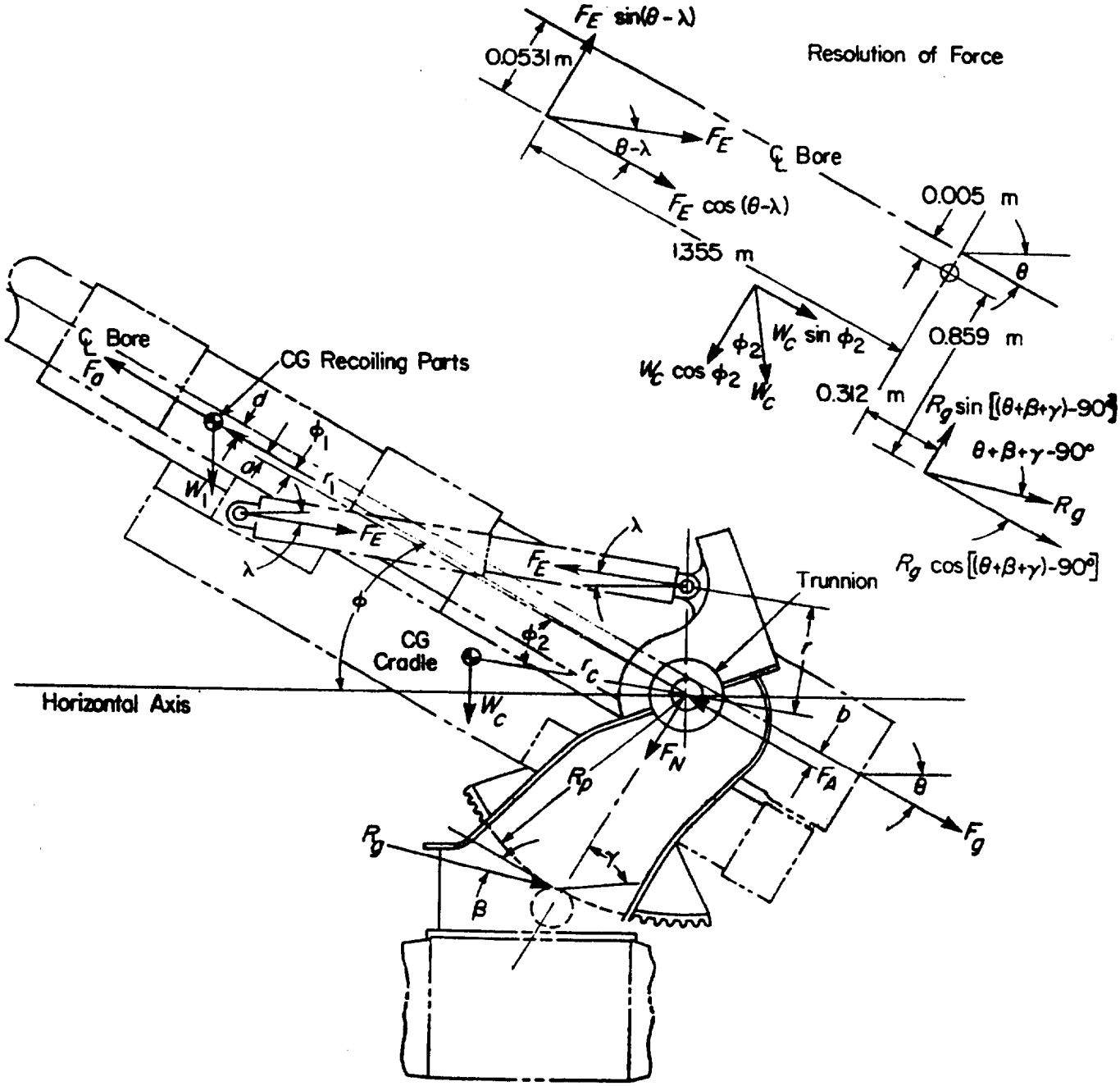

F_o = inertia force of recoiling parts, N

F_E = equilibrator force, N

F_g = propellant gas force, N

F_A = trunnion reaction parallel to bore centerline, N

F_N = trunnion reaction normal to bore centerline, N

(cont'd on next page)

Figure 7-8. External Loads on Cradle for Single Recoil System

THIS DOCUMENT PROVIDED BY THE ABBOTT AEROSPACE
TECHNICAL LIBRARY
ABBOTTAEROSPACE.COM

R_p = pitch radius of elevating gear, m
R_g = elevating gear load, N
W_1 = weight of recoiling parts, N
W_c = weight of cradle, N
β = pressure angle of gear, deg
θ = angle of elevation, deg
γ = elevation of F_N, deg
λ = equilibrator elevation, deg
r = distance between center of trunnion and centerline of equilibrator, m
r_1 = distance between CG of recoiling parts and center of trunnion, m
r_c = distance between CG of cradle and center of trunnion, m
ϕ_1 = angle between line of action of force F_d and centerline of bore, deg
ϕ_2 = angle between line joining CG of cradle and center of trunnion and centerline of bore, deg

Figure 7-8. (cont'd)

$$T_r = \frac{0.6\pi^2 R_b^3 P_g}{N_r}, \text{ N·m}, \tag{7-11}$$

is derived—with the aid of Eqs. 7-13 through 7-20—from the basic torque equation

$$T_r = I_p \alpha, \text{ N·m} \tag{7-12}$$

where

I_p = mass moment of inertia of projectile, kg·m^2
α = angular acceleration of projectile, rad/s^2
T_r = rifling torque, N·m
N_r = twist of rifling, calibers per turn
P_g = propellant gas pressure, Pa
R_b = radius of bore, m.

The terms used in the equations that follow are defined, i.e.,

a = linear acceleration of projectile, m/s^2
a_t = peripheral acceleration of projectile at bore, m/s^2
k = radius of gyration of projectile, m
m_p = mass of projectile, kg
θ_r = helix angle of rifling, deg
F_g = propellant gas force, N

THIS DOCUMENT PROVIDED BY THE ABBOTT AEROSPACE
TECHNICAL LIBRARY
ABBOTTAEROSPACE.COM

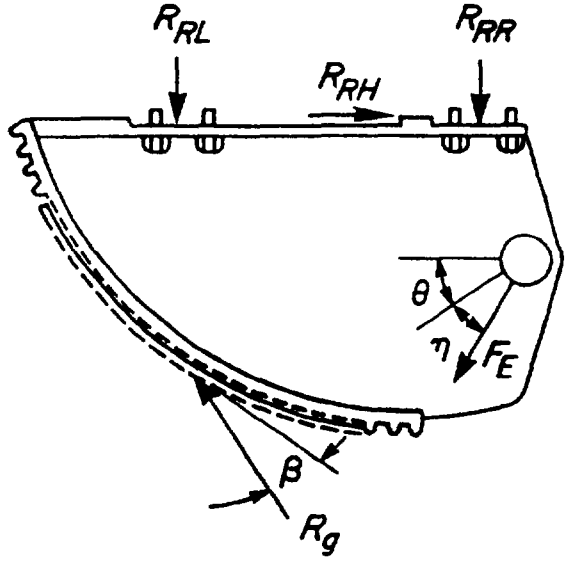

β = pressure angle of gear, deg
η = elevation of F_E $-\theta$, deg
F_E = equilibrator force, N
R_g = elevating gear load, N
R_{RH} = shear reaction on key, N
R_{RL} = left bolt reaction, N
R_{RR} = right bolt reaction, N

Figure 7-9. Elevating Arc

$$A_b = \pi R_b^2 = \text{bore area (less rifling groove area), m}^2 \tag{7-13}$$

$$F_g = A_b P_g, \text{ N.} \tag{7-14}$$

From the general expression, $F_g = m_p a$,

$$a = \frac{F_g}{m_p}, \text{ m/s}^2 \tag{7-15}$$

$$\tan\theta_r = \frac{\pi}{N_r} \tag{7-16}$$

$$a_t = a\tan\theta_r, \text{ m/s}^2. \tag{7-17}$$

Substitution of the appropriate terms of Eqs. 7-13 to 7-15 into Eq. 7-17 and collection of terms give

$$a_t = \frac{\pi^2 R_b^2 P_g}{m_p N_r}, \text{ m/s}^2 \tag{7-18}$$

THIS DOCUMENT PROVIDED BY THE ABBOTT AEROSPACE
TECHNICAL LIBRARY
ABBOTTAEROSPACE.COM

U-Type Cradle

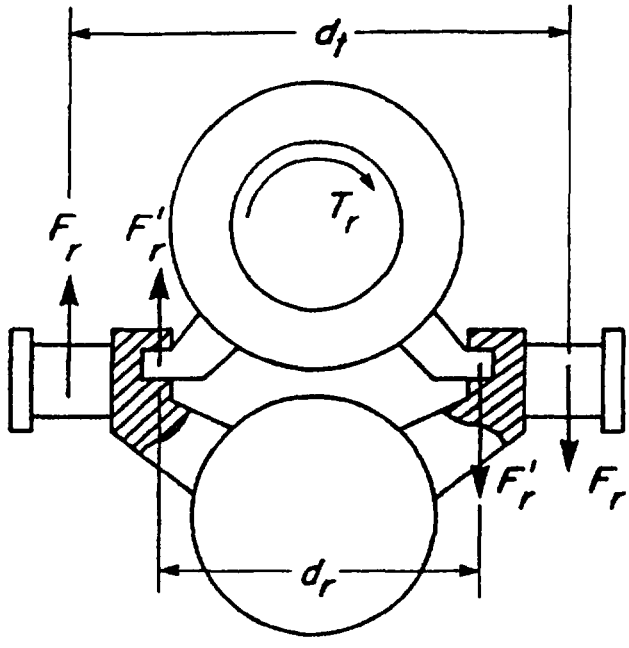

d_r = distance between reaction on rails (or center-to-center distance between rails), m

d_t = distance between trunnion reactions (center-to-center), or span of trunnion bearings, m

T_r = rifling torque, N·m

d_r = distance between reactions on rails (or center-to-center distance between rails), m

F_r = load on trunnions due to rifling torque, N

F_r' = load on rails due to rifling torque, N

Figure 7-10. Forces Due to Rifling Torque

$$\alpha = \frac{a_t}{R_b} = \frac{\pi^2 P_g R_b}{m_p N_r}, \text{ rad/s}^2. \tag{7-19}$$

The value $k^2 = 0.6R_b^2$ generally is accepted as an approximate value; therefore,

$$I_p = m_p k^2 = 0.6 m_p R_b^2, \text{ kg·m}^2. \tag{7-20}$$

Eq. 7-11 is obtained by substituting the terms of Eqs. 7-19 and 7-20 into Eq. 7-12. From Fig. 7-10 the load F_r on the trunnions due to rifling torque is

$$F_r = \frac{T_r}{d_t}, \text{ N} \tag{7-21}$$

THIS DOCUMENT PROVIDED BY THE ABBOTT AEROSPACE
TECHNICAL LIBRARY
ABBOTTAEROSPACE.COM

and, correspondingly, the load F_r' on the rails or on the key is

$$F_r' = \frac{T_r}{d_r}, \text{ N.} \tag{7-22}$$

Note that the maximum torque occurs when the propellant gas pressure is maximum. For the U-type cradle the torque is transmitted directly to the guides through the rails or the sleigh in the form of vertical forces having a moment arm equal to the distance from their lines of action to the bore axis, as shown in Fig. 7-10.

7-4.2 STRENGTH REQUIREMENTS

In this paragraph strength requirements for various components of the cradle structure are discussed. Stresses are calculated for a cradle that is assumed to be completely isolated from all other components of the gun. This approach is conservative because the stiffness associated with the gun tube and structural members, which ordinarily would lend strength to the cradle, is ignored.

The general stresses of the main cradle structure are due to bending and direct shear. However, at each point of load application local stresses are present that may be greater than or may augment the general stress. The local areas are loaded by the recoil mechanism, the trunnion, and the elevating mechanism through their attachments to the cradle. After the principal stresses have been determined by conventional methods of stress analysis, the equivalent stress is determined. Modern methods of stress analysis, such as the finite element method, may also be used to calculate principal stresses at this stage. Such methods are discussed in par. 7-6 and Appendix C. An accepted method for computing the equivalent stress comes from the maximum shear stress theory of Tresca and Saint Venant, which states that yielding begins when the largest difference of two principal stresses equals the yield strength of the material, or

$$\sigma_1 - \sigma_2 = \sigma_y, \text{ Pa} \tag{7-23}$$

where

σ_1 = maximum principal stress, Pa
σ_2 = minimum principal stress, Pa
σ_y = yield stress, Pa.

To be compatible with other components of the gun carriage, a factor of safety of 1.5 is recommended for the cradle. Now, if $\sigma_1 = \sigma_t$ and $\sigma_2 = \sigma_c$, the equivalent stress σ_e is

$$\sigma_e = \sigma_t - \sigma_c, \text{ Pa} \tag{7-24}$$

where

σ_t = tensile stress, Pa
σ_c = compressive stress, Pa.

The factor of safety S_f is

$$S_f = \frac{\sigma_y}{\sigma_e}, \text{ dimensionless.} \tag{7-25}$$

7-4.2.1 Location and Design of Trunnions

The location of the trunnions in the vertical plane directly influences the reaction of the elevating gear during the recoil cycle. In single recoil systems, the reaction is due solely to the moment about the trunnions produced by the propellant gas force and the inertia force of the recoiling parts. Fig. 7-11 shows these forces and the perpendicular distance from their lines of action to the trunnions. The position of the trunnions with respect to these lines of action determines the moment. Thus from Fig. 7-11

THIS DOCUMENT PROVIDED BY THE ABBOTT AEROSPACE
TECHNICAL LIBRARY
ABBOTTAEROSPACE.COM

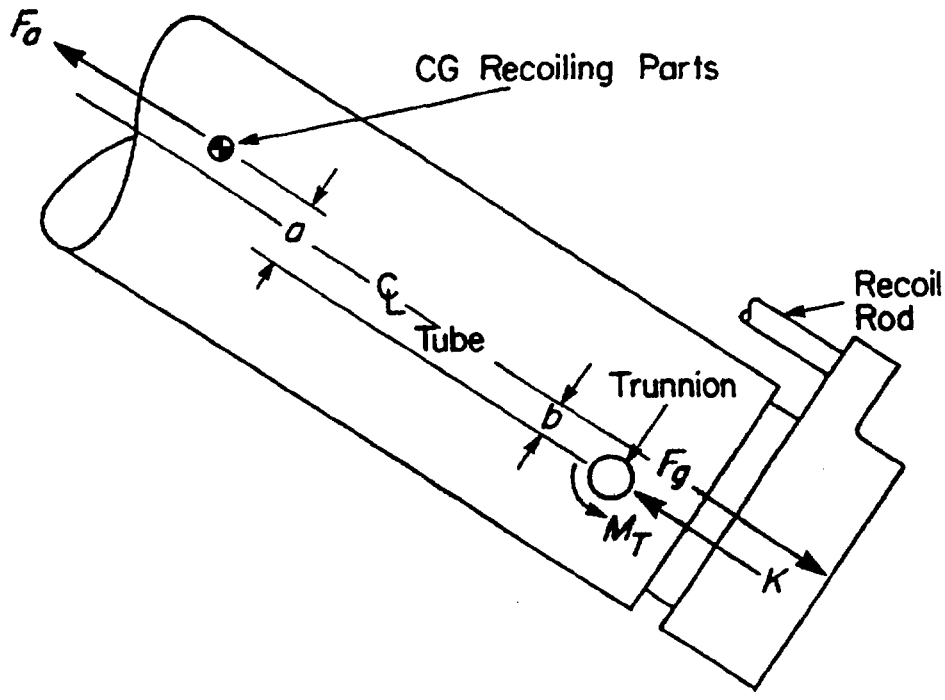

F_a = inertia force of recoiling parts, N
F_g = propellant gas force, N
K = total recoil resistance, N
M_T = moment about trunnions, N·m
a, b = moment arm, m

Figure 7-11. Trunnion Location With Respect to Recoil Forces

$$\left.\begin{aligned} M_T &= bF_g - aF_a \text{ , N·m} \\ F_a &= F_g - K, \text{ inertial force at CG, N} \end{aligned}\right\} \qquad (7\text{-}26)$$

where
a and b = moment arms, m
M_T = trunnion moment, N·m.

If F_a' and F_g' represent the maximum inertia and maximum propellant gas forces, respectively, the ideal trunnion location distance a lies between the values of b and $(F_a'/F_g')b$. It is not always feasible to have this arrangement. If a extends beyond these limits or if a and b lie on opposite sides of the trunnion, the moment will increase and vary as the distances. When $a=(F_g'/F_a')b$, the moment M_T becomes zero when the gas force becomes maximum. It gradually increases as the gas force diminishes and reaches the maximum of

$$M_T = -aF_a = -aK \text{ , N·m} \qquad (7\text{-}27)$$

when the gas force becomes zero. Thus to minimize the moment after the gas ejection period, a should be as small as possible. Also a and b should be selected to minimize the moment during the gas ejection period given by the first equation of Eq. 7-26.

THIS DOCUMENT PROVIDED BY THE ABBOTT AEROSPACE
TECHNICAL LIBRARY
ABBOTTAEROSPACE.COM

The trunnion loads are composed of five components that are derived from the weight of tipping parts, recoil force, equilibrator force, force due to the rifling torque, and elevating gear reaction. The first four components do not vary with trunnion location but form the bulk of the maximum trunnion loads. Consequently, any change in the elevating gear reaction will not materially affect the trunnions; however, small shifts in trunnion location may greatly influence elevating gear reactions.

Sometimes the location of the trunnion is adjusted in the vertical plane to satisfy some structural requirement. For example, when located below the bore centerline, more space will be provided for an underslung recoil mechanism. Or if the trunnions are located on the centerline, structural symmetry is preserved. Also if the trunnions are on the centerline, the sighting equipment will not have to be corrected for discrepancies due to an off-center location.

In the horizontal plane it is advantageous to have the trunnions located equidistant from the centerline of the gun bore. Here the object is mainly one of symmetry. If symmetry cannot be achieved, the cradle will be subjected to a direct load and a couple equal to the recoil force multiplied by the offset, that is, the vertical component tends to turn the weapon on its side, and the horizontal component tends to rotate the cradle and top carriage. However, the base supporting the top carriage is symmetrical with respect to the bore, and the loads revert to a symmetrical condition at this point. If any residual horizontal moment persists, it is resisted at the traversing gear. (This discussion does not include the rifling torque that is transmitted through the structure while the projectile travels in the bore.)

When the distances from the bore to the trunnions are unequal, the cradle must be larger to offset the effects of the unsymmetrical loads, which eventually lead to a heavier structure. In considering deflections, symmetry becomes definitely desirable. If both sides of the cradle deflect equally, compensation for misalignment during firing presents lesser problems in fire control than if the two sides of the cradle deflected unequally. In the first case, the gun tube would remain essentially in line, whereas in the latter it would turn slightly askew.

The size of the trunnion is usually dictated by the dimensions of the required bearings. The size, however, should be investigated to determine its strength in bending and shear. As a rule, the trunnion may be considered a short beam, and the stresses calculated according to the equations that follow (which can be found in any text on strength of materials) (Refs. 2 and 3). The bending stress σ is

$$\sigma = \frac{Mc}{I}, \text{ Pa} \tag{7-28}$$

where

c = distance to extreme fiber, m
I = moment of inertia of cross section, m^4

and the shear stress τ at any line q either on, or at a distance from, the neutral axis of the total section is

$$\tau = \frac{F_T A_n \bar{d}}{It}, \text{ Pa} \tag{7-29}$$

where

A_n = area above line q, m^2
t = thickness of section at q, m
$\bar{d}$ = distance between neutral axis of section and neutral axis of A_n, m
$F_T = \sqrt{F_N^2 + F_A^2}$ = resultant shear at section (See Fig. 7-8.), N.

The hubs or sockets holding the trunnions are either welded or bolted to the cradle. Reinforcements at the hub are sometimes necessary to distribute the loads and prevent local failure. If the trunnion shank fits the hub freely, the hub is stressed in shear and bending. However, if the joint is a shrink fit, the interface pressure p—due to the shrink fit—produces hoop stresses in both the trunnion shank and the hub. This pressure is determined by equating the interference to the total deflection of the concentric cylinders at their interface (Ref. 2). Thus

THIS DOCUMENT PROVIDED BY THE ABBOTT AEROSPACE
TECHNICAL LIBRARY
ABBOTTAEROSPACE.COM

$$p = \frac{E\Delta}{r}\left(\frac{r_2^2 + r^2}{r_2^2 - r^2} + \frac{r^2 + r_1^2}{r^2 - r_1^2}\right)^{-1}, \text{Pa} \qquad (7\text{-}30)$$

where

E = modulus of elasticity, Pa
r = radius at contact surfaces of concentric cylinders, m
r_1 = inner radius of inner cylinder, m
r_2 = outer radius of outer cylinder, m
Δ = radial interference, m.

The strength of the gussets supporting the hub is based on the loading arrangement shown in Fig. 7-12. The gussets are assumed to be the only support for the hub. The load distribution of the reactions R_G and R_v is assumed triangular and is balanced on the load parallel to the cannon bore.

Each structural member, whether gusset or hub, must be statically balanced. Therefore, by isolating the hub

$$R_G = \frac{F_A}{n}, \text{N} \qquad (7\text{-}31)$$

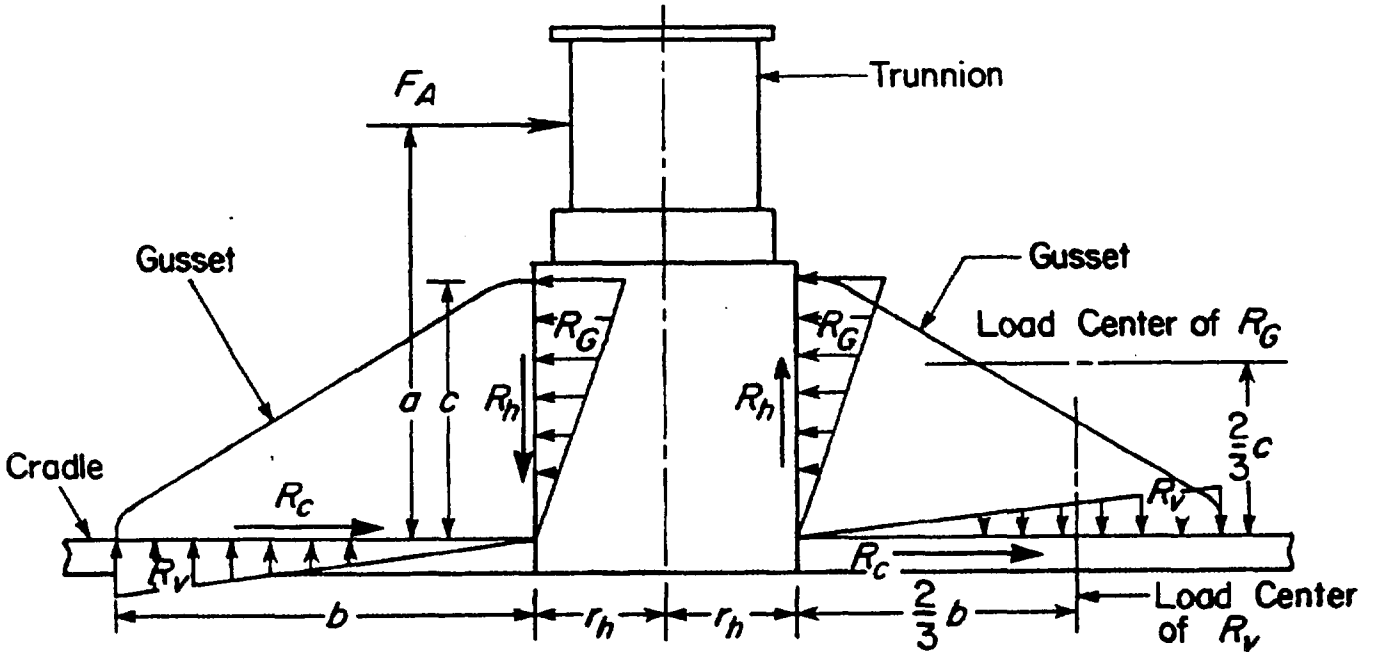

F_A = trunnion load parallel to bore centerline, N
R_c = shear between gusset and cradle body, N
R_G = distributed horizontal reaction of gusset, N
R_h = shear between gusset and hub, N
R_v = distributed vertical reaction of gusset, N

Figure 7-12. Load Distribution on Trunnion Structure

THIS DOCUMENT PROVIDED BY THE ABBOTT AEROSPACE
TECHNICAL LIBRARY
ABBOTTAEROSPACE.COM

$$r_h R_h + \frac{2cR_G}{3} = \frac{aF_A}{n}, \text{ N·m} \tag{7-32}$$

where

n = number of gussets parallel to F_A, dimensionless
r_h = radius of hub or socket holding trunnion, m
c = height of gusset along trunnion, m
a = lever arm of force F_A from cradle, m
b = length of gusset along cradle, m.

When a gusset is isolated,

$$R_v = R_h, \text{ N} \tag{7-33}$$

$$R_c = R_G, \text{ N} \tag{7-34}$$

$$bR_v = cR_G, \text{ N·m.} \tag{7-35}$$

Substituting the value of R_G of Eq. 7-31 into Eq. 7-32 and solving for R_h give

$$R_h = \left(\frac{a - \frac{2c}{3}}{r_h} \right) \frac{F_A}{n}, \text{ N.} \tag{7-36}$$

Since $R_v = R_h$, substituting the expressions for R_G and R_v from Eqs. 7-31 and 7-36 into Eq. 7-35 and solving for b give

$$b = \frac{cr_h}{a - \frac{2c}{3}}, \text{ m.} \tag{7-37}$$

This is the gusset length b required to substantiate the assumption of the triangular load distribution. If R_G represents the area of the triangle, the maximum unit load w on the gusset is

$$w = \frac{2R_G}{c}, \text{ N/m} \tag{7-38}$$

and the maximum direct tensile or compressive stress σ becomes

$$\sigma = \frac{w}{t}, \text{ Pa} \tag{7-39}$$

where

t = thickness of gusset, m.

The elastic stability is checked by assuming that the gusset is a rectangular plate loaded in compression on the two opposite edges. This assumption, although approximate, is conservative. The critical compressive stress σ_c is given (Ref. 2) as

$$\sigma_c = K_s \left(\frac{E}{1 - \nu^2} \right) \left(\frac{t}{b} \right)^2, \text{ Pa} \tag{7-40}$$

THIS DOCUMENT PROVIDED BY THE ABBOTT AEROSPACE
TECHNICAL LIBRARY
ABBOTTAEROSPACE.COM

where

b = width of loaded edge, m
K_s = fixity factor determined from width-to-length ratio, dimensionless
ν = Poisson's ratio, dimensionless.

Gussets should be arranged so that the transmitted loads will not unduly aggravate the stresses and deflections of the cradle wall. An approximate analysis of the region around the connection of the gusset plate to the cradle body should be carried out. When the finite element method is used for final stress analysis, the finite element model should include gussets as load-carrying members.

7-4.2.2 Sliding Surfaces of U-Type Cradle

There are two types of force on the slides, i.e., the normal forces and the frictional forces derived from the normal forces. The normal forces are obtained as reactions to the rifling torque, to the couple created by the recoil forces and the inertia of the recoiling parts, and to the weight of the recoiling parts. Thus the shorter the distance between the forces parallel to the bore axis and the closer the center of gravity is to the midspan of the slides, the smaller will be the forces on the slides. Actually, in single recoil systems the weight contributes little to the maximum forces; therefore, the center of gravity may fall outside the slides without deleterious effects.

When calculating the loads on rails and guides, the distribution of bearing pressure should be considered. If the two mating slide surfaces are continuous, a triangular load distribution is assumed. Triangular load distribution implies zero clearance and linear compliance of rails and guides. The assumption of triangular load distribution is subject to change for unusual constructions. If the sliding surfaces are discontinuous, a trapezoidal distribution is assumed, or if the pads are spaced sufficiently far apart, a uniform load distribution is assumed. Fig. 7-13 illustrates these effects. The diagrams represent the reactions to the couple M_R of the recoiling parts. The reactions R_f' and R_f'' are calculated by assuming that they are concentrated at the center of the area that represents the distributed load. After the reactions to the couple are determined, those resulting from the rifling torque and the normal component of the weight are added algebraically as uniformly distributed loads.

The maximum bearing pressure is then determined from the completed load diagram. A bearing pressure of 1.379 to 2.068 MPa is recommended for continuous motion, but since motion is not continuous, bearing pressures as high as 3.447 MPa are permissible. If pressures exceed this limit, there is danger of severe wear on the sliding surfaces, which leads to early replacement. This condition must be tolerated; if it cannot be, other design solutions are available, but they usually mean added maintenance and should be avoided if at all possible.

The sliding structure that supports the recoiling parts consists of male and female members. The male members are called rails or slides, and the female members are called guides. The guides are similar to channels in cross section so that bearing surfaces will support the rails against either upward or downward loads. Bronze liners with surface finishes between 0.8 and 1.6 microns root mean square (rms) cover the rails and slides to provide the bearing surface as shown in Fig. 7-14. The guides are unlined, but their surfaces are machined to the same finish as the rails and slides.

Rails usually are secured to the tube. The front attachment is to a sleeve or flat ring, either clamped or shrunk on the tube. The rear attachment is to a similar ring or it may be to the breech ring. Fig. 7-15 shows a typical installation. The rails or guides may be continuous or discontinuous. If the guides are discontinuous, they sometimes are called clips. Discontinuity in the sliding surfaces is not recommended if contact between them is broken during the recoil stroke because of the difficulty in reentering the guides during counterrecoil. The present trend in design is to have continuous rails on the gun tube.

When a sleigh is used, the gun tube is held securely to it by collars or yokes, as shown in Fig. 7-16. Fig. 7-17 shows another type of sleigh that has the recoil cylinders integral with the sleigh body. Close-fitting mating lugs on the tube and sleigh preclude tipping, and locking wedges preclude relative longitudinal motion. The wedges move laterally and fit into recesses machined in the tube structure. The structure forming the sliding surfaces may be bolted or welded to the sleigh. Sometimes the sliding surfaces form an integral part, being machined from the sleigh or cradle structure.

The strength of the rail, slide, or guide is determined by the conservative method of analysis that follows. Assume that the maximum distributed load is constant for a distance of 0.0254 m. Isolate a 0.0254-m length of structure with this load and investigate its strength. Thus the stress in Section A-A of Fig. 7-18(A), which is 0.0254 m deep, is

THIS DOCUMENT PROVIDED BY THE ABBOTT AEROSPACE
TECHNICAL LIBRARY
ABBOTTAEROSPACE.COM

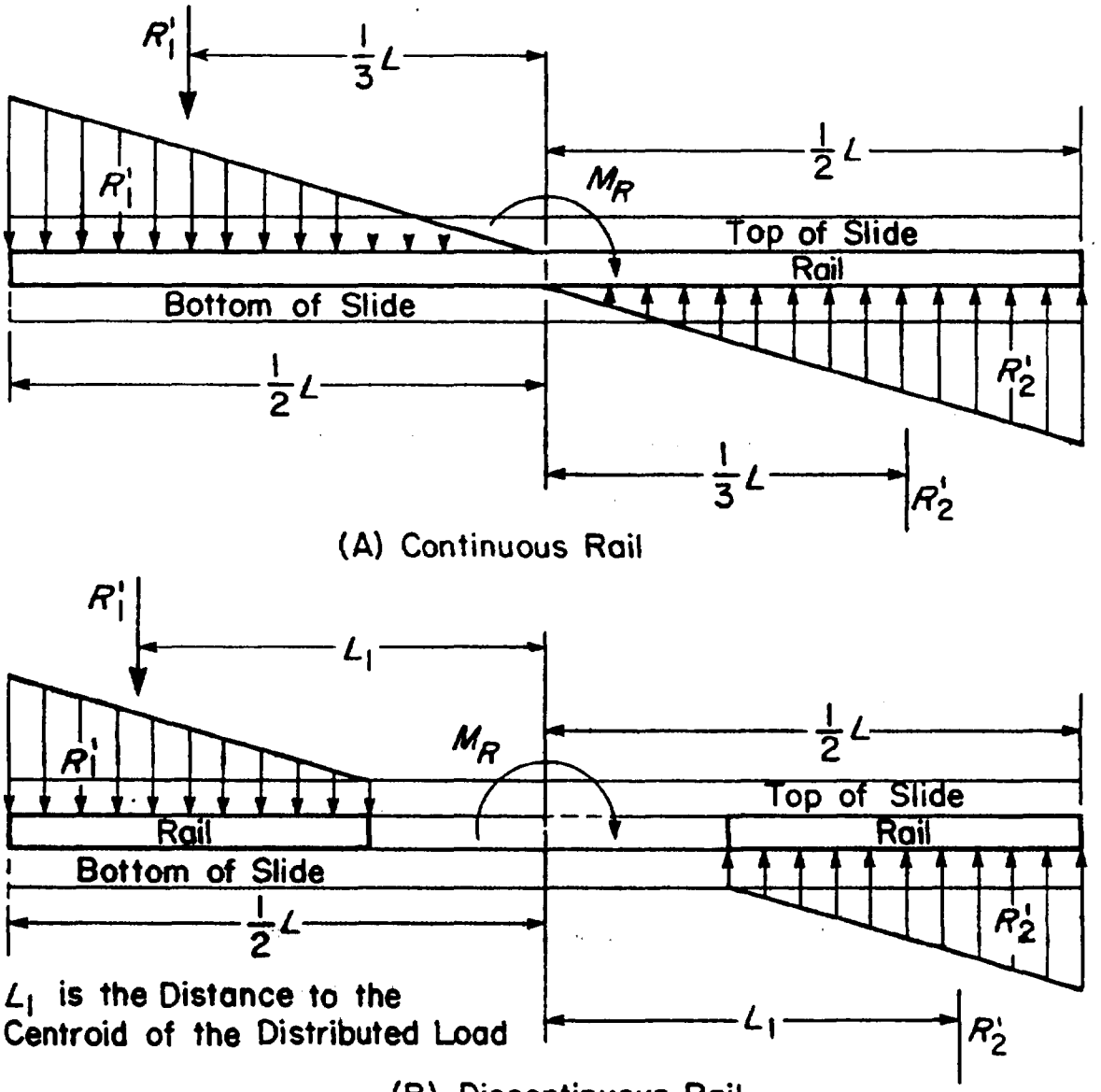

Figure 7-13. Load Distribution on Rails, U-Type Cradle

$$\sigma_t = \frac{Mc}{I} + \frac{F}{A}, \text{ tensile stress in section, Pa} \qquad (7\text{-}41)$$

where

$M = Fd$, moment, N·m
c = distance to extreme fiber, m
$F = 1 \times w$, total load, N
$A = 1 \times a$, area of cross section in tension, m^2
d = lever arm of force F, m
a = width of section A-A of Fig. 7-18(A), m
w = unit load, maximum intensity, N/m.

(The unit 1 in the expressions for F and A defines these terms for a unit length of the member under consideration.)

THIS DOCUMENT PROVIDED BY THE ABBOTT AEROSPACE
TECHNICAL LIBRARY
ABBOTTAEROSPACE.COM

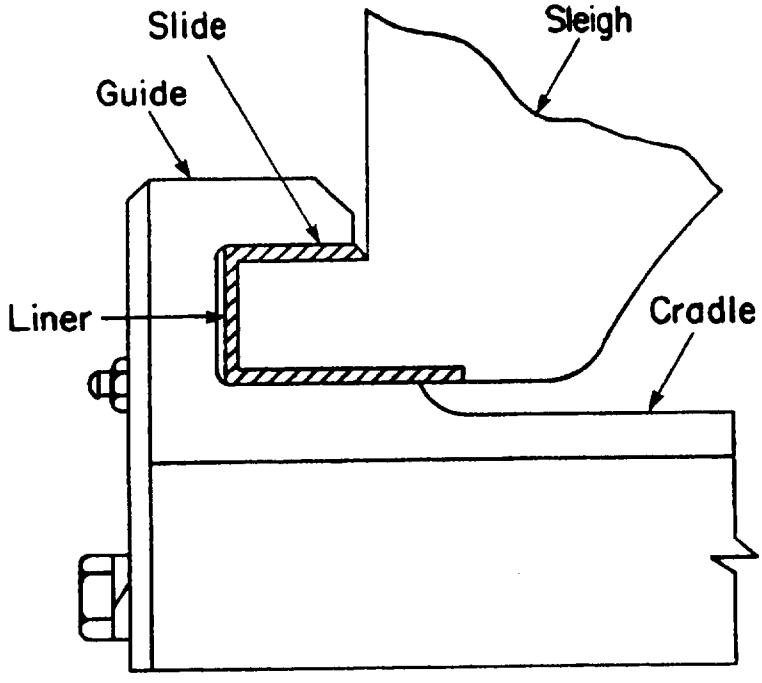

Figure 7-14. End View of Sliding Structure Showing Bearing Liner

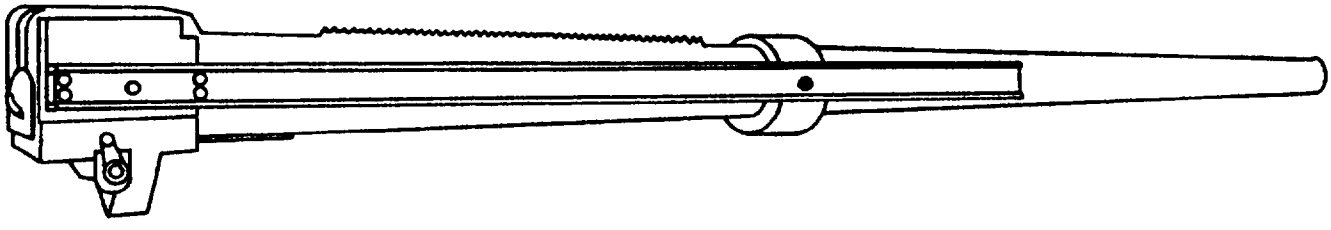

Figure 7-15. Tube Assembly Showing Rails

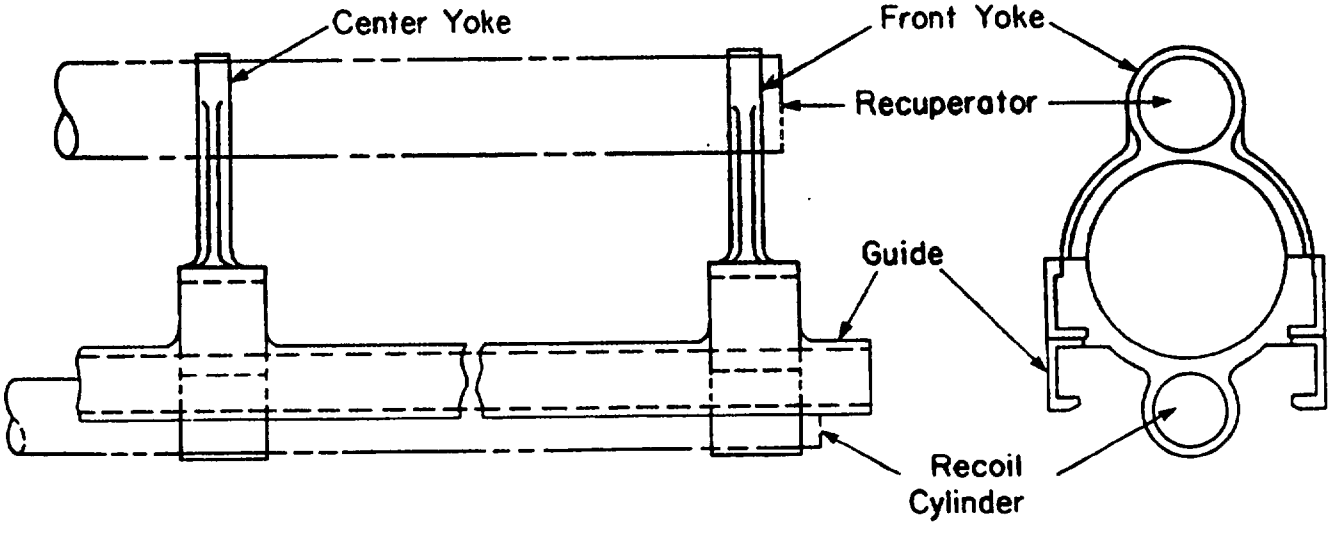

Figure 7-16. Sleigh With Attached Recoil Cylinders, Gun Tube Secured With Yokes

THIS DOCUMENT PROVIDED BY THE ABBOTT AEROSPACE
TECHNICAL LIBRARY
ABBOTTAEROSPACE.COM

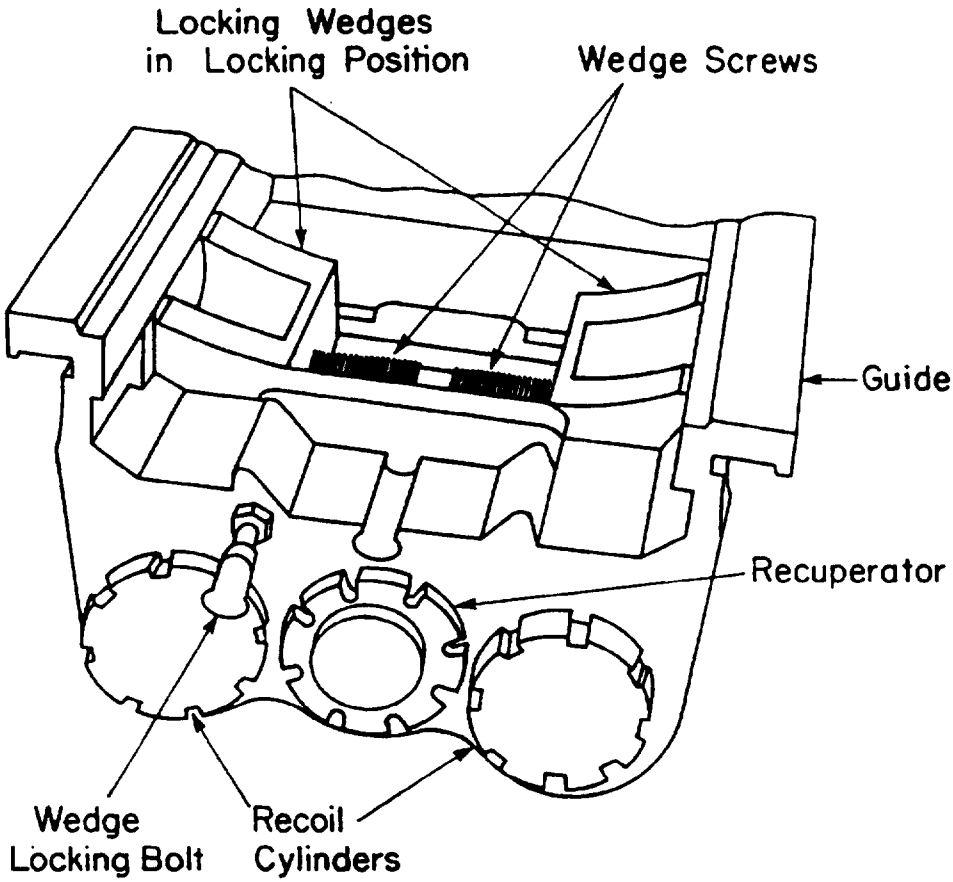

Figure 7-17. Sleigh With Integral Recoil Cylinders

In addition to strength requirements, the sliding members must have ample contact surfaces to insure a reasonable bearing pressure. Large area alone, however, may not achieve a reasonable pressure if ensuing deflections cause a reduction in the contact area and thereby intensify the pressure. Two types of deflection may occur. One involves bending of the vertical members, which causes the contacting areas to rotate and thus overload the edges of the bearing. This is illustrated by the phantom member in Fig. 7-18(A). If both members are identically constructed, however, angular deflections will be equal and the whole contact area remains intact. The other deflection concerns the equivalent cantilever beam of the bearing members, as illustrated by the sectional view in Fig. 7-18(B). This deflection poses a difficult problem because, as the beam deflects, the load immediately becomes redistributed over a smaller space with accompanying higher pressures. Since the mating parts are of similar construction, they deflect similarly with the result that the contact area becomes progressively smaller and theoretically approaches a line. Actually, line contact never materializes, but pressure will peak excessively because of the deflections. A means of circumventing peak pressures employs the practice of providing enough flexibility in the structure to enable the deflection of one mating surface to conform to the deflection of the other and thus maintain the original contact area. This type of structure, however, is not always feasible and may not be applicable to cradle design. If not, it is necessary to resort to approximation methods that are available for determining the required bearing area. One such method assumes a uniform load distribution with the maximum design pressure limited to 3.447 MPa, as noted earlier.

7-4.2.3 Design of Cradle Body

The cradle is a long, thin structural member that is subjected to bending, shearing, twisting, and axial loads. Therefore, during the preliminary design stage, it is modeled as a beam element subjected to general three-dimensional loads. Simple beam theory is used to calculate stresses in the cradle body. To calculate stresses at a section, the resultant shear, moments, and direct forces must be known. The general procedure for

THIS DOCUMENT PROVIDED BY THE ABBOTT AEROSPACE
TECHNICAL LIBRARY
ABBOTTAEROSPACE.COM

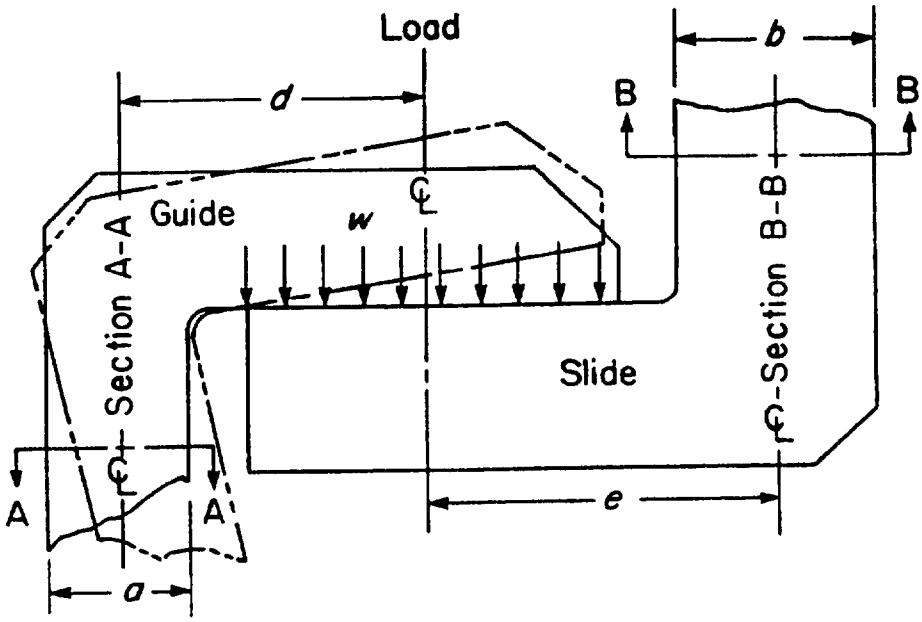

(A) Loading Diagram

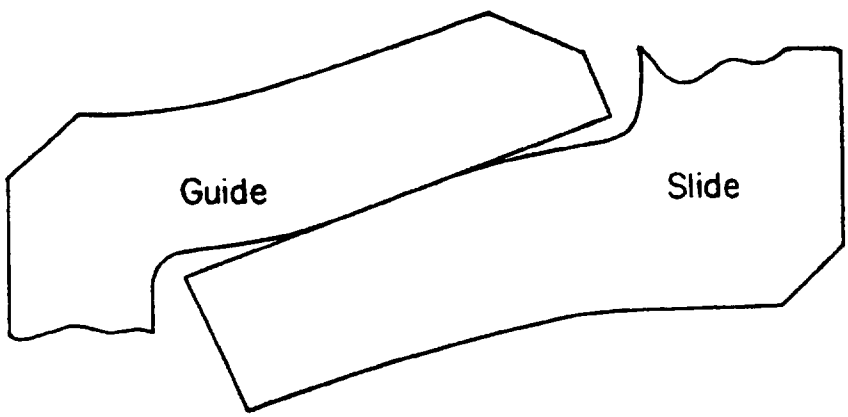

(B) Cantilever Beam Analogy

Figure 7-18. Slide and Guide Showing Assumed Deflections

calculating these forces and moments calls for developing free-body diagrams for those portions of the cradle under consideration. Static equilibrium conditions, Eqs. 7-1 through 7-3, are then used to solve for the unknown forces and moments.

To calculate moments at a point, a general vector equation is used:

$$M = r \times F, \text{ N·m} \tag{7-42}$$

where

M = moment vector, N·m
r = vector from centerline of a section to point of application of force F, m
F = force vector, N.

THIS DOCUMENT PROVIDED BY THE ABBOTT AEROSPACE
TECHNICAL LIBRARY
ABBOTTAEROSPACE.COM

The moment vector in Eq. 7-42 gives two moment components that cause bending of the section, and the third component gives the torque (or twisting moment about the centroidal axis). These moment components are then used to calculate bending and torsional stresses.

The stresses are evaluated at only a few points along the length of the cradle, i.e., where they are anticipated to reach their local maximum values or change signs.

Since there is more than one type of load acting on the structure, the designer should calculate stresses separately at each cross section for each type of load. By suitably choosing a combination of loads, the designer can then evaluate critical stresses. At a preliminary design stage it may be assumed that the loads due to firing, travel, and lifting all act in the same plane. Bending stress σ is calculated using the equation

$$\sigma = \frac{Mc}{I}, \text{ Pa} \tag{7-43}$$

and the average shearing stress τ is calculated from

$$\tau = \frac{\Sigma F_V}{A}, \text{ Pa} \tag{7-44}$$

where

c = distance to extreme fiber, m
ΣF_V = total shear at cross section, N
A = cross-sectional area, m^2.

The equation for shearing stress is not exact but is adequate for a preliminary analysis. A better estimate of the shearing stress (Ref. 3) can be obtained by using the equation

$$\tau = \frac{\Sigma F_V Q}{Ia}, \text{ Pa} \tag{7-45}$$

where

Q = first moment about neutral axis of area above level at which τ is evaluated, m^3
a = width of cross section at level where τ is evaluated, m.

Eq. 7-44 is similar to Eq. 7-29. Usually the shearing stresses are very small compared to the bending stresses and may be neglected. Note also that the rifling torque induces torsional shear stresses in the cradle body. By use of the theory of torsion of thin-walled sections (Ref. 3), there can be verification that these shear stresses too are low compared to the bending stresses. Therefore, shear stresses are also neglected at the preliminary design stage.

7-4.3 REFINED LOAD ANALYSIS AND STRESS CALCULATIONS

Once preliminary analysis yields an acceptable design based on strength and other requirements, a more refined analysis and design of the system are possible. Usually, a model of the system based on the preliminary design is constructed and subjected to field tests. Data from the field tests, e.g., reaction forces and deflections, are used to refine the preliminary design models. It should be noted that the test model is designed with a relatively high factor of safety. This practice is necessary to account for the uncertainty that the preliminary modeling introduces in stress analysis. As noted in Chapter 3 the model cannot be subjected to a wide spectrum of load tests. Tests for only those cases that are considered to be critical by the designer are carried out. The remaining tests are simulated by a static and a dynamic mathematical model. These data too are used for the refined load and stress analyses.

The dynamic model developed in Chapter 3 provides a general approach to evaluating firing loads, such as clip reactions, equilibrator and elevating strut loads, and trunnion reactions. Accuracy of forces depends on how closely the mathematical model describes the actual weapon. Once these forces and loads are known, Eqs. 7-1, 7-2, and 7-3 can be used to determine unknown direct forces, bending moments, torques, and shear forces

THIS DOCUMENT PROVIDED BY THE ABBOTT AEROSPACE
TECHNICAL LIBRARY
ABBOTTAEROSPACE.COM

at various cross sections. These parameters are then used for further stress analysis. It should be noted that design features and functional characteristics peculiar to each individual weapon have a significant effect on modeling the system. Therefore, the use of a universal model in the evaluation of artillery weapons is impractical. Instead, the model must be tailored to the specific design of the system.

The same model, however, can be used to predict forces that act on the weapon due to travel loads. Once the ground reactions have been evaluated, the loads that act on the cradle can be found by a successive series of free-body diagrams of the trails, bottom carriage, and top carriage. Free-body diagrams similar to the one shown in Fig. 7-19 for the cradle structure of the M198 towed Howitzer (Refs. 4 and 5) are developed for other

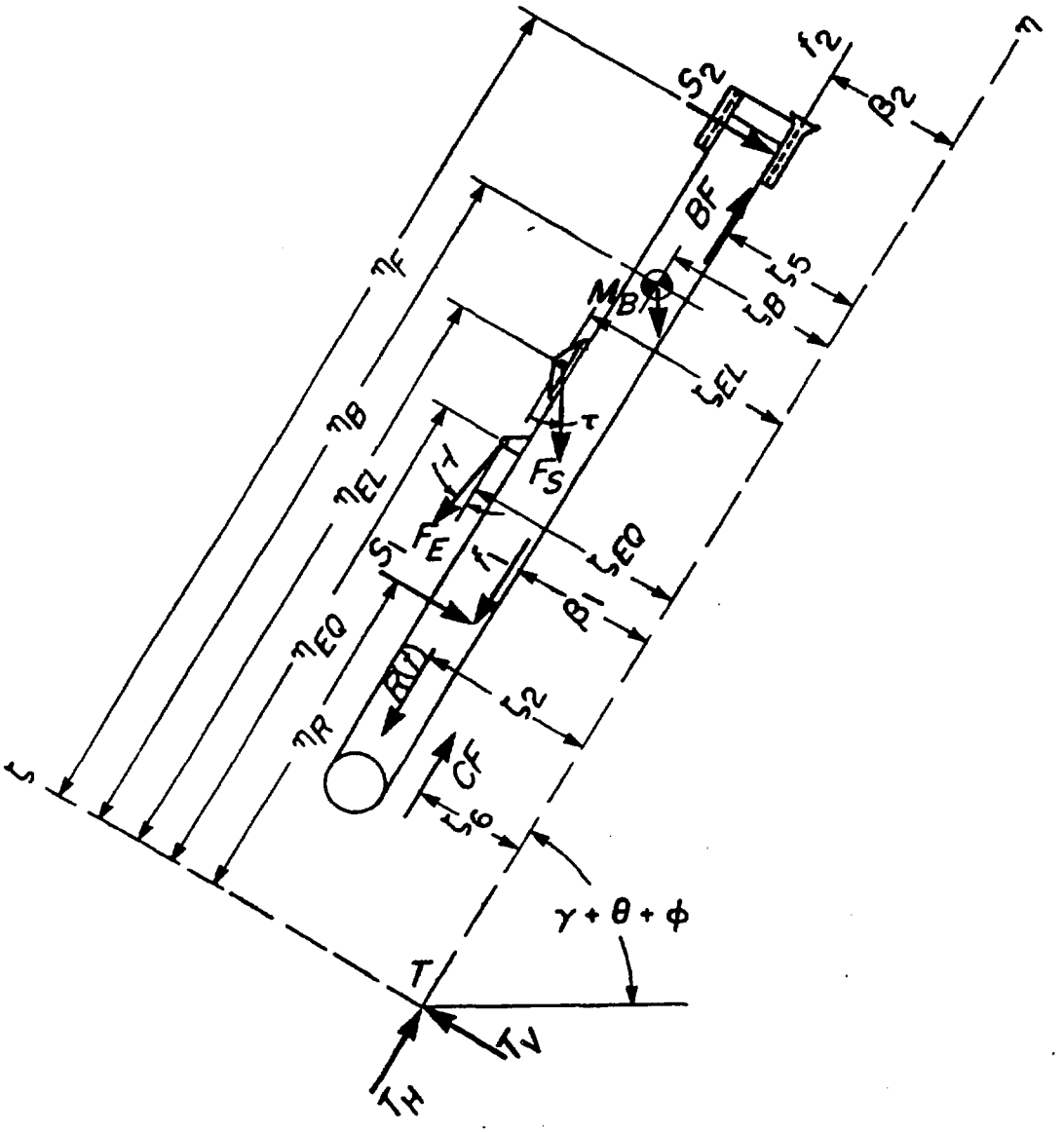

η_F = η-coordinate of front clip reaction, m

η_B = η-coordinate of center of mass, m

η_{EL} = η-coordinate of elevating strut, m

η_{EQ} = η-coordinate of equilibrator, m

(cont'd on next page)

Figure 7-19. Free-Body Diagram of Cradle Structure (M198)

THIS DOCUMENT PROVIDED BY THE ABBOTT AEROSPACE
TECHNICAL LIBRARY
ABBOTTAEROSPACE.COM

η_R = η-coordinate of rear clip reaction, m

ζ_6 = ζ-coordinate of breech opening cam force, m

ζ_2 = ζ-coordinate of rod pull force, m

ζ_{EL} = ζ-coordinate of elevating strut, m

ζ_{EQ} = ζ-coordinate of equilibrator, m

ζ_5 = ζ-coordinate of counterrecoil buffing force, m

ζ_B = ζ-coordinate of center of mass, m

β_2 = ζ-coordinate of front end frictional force, m

β_1 = ζ-coordinate of rear end frictional force, m

θ = relative rotation between masses M_B and M_D (nonelevating mass), deg

ϕ = rotation of M_D around ground pivot, deg

γ = original angle of elevation, deg

F_S = force on elevating strut, N

F_E = force on equilibrator, N

CF = force due to breech opening cam, N

BF = counterrecoil buffing force, N

$R(t)$ = rod pull, N

S_1 = clip reaction (rear end), N

S_2 = clip reaction (front end), N

f_1 = frictional force due to clip reaction (rear end), N

f_2 = frictional force due to clip reaction (front end), N

M_B = mass of elevating (but nonrecoiling) mass, kg

T_H, T_V = trunnion reactions along and perpendicular to barrel, respectively, N

τ = angle between elevating strut and $(\phi-\eta)$-axis, rad

λ = angle between equilibrator and $(\phi-\eta)$-axis, rad

Figure 7-19. (cont'd)

THIS DOCUMENT PROVIDED BY THE ABBOTT AEROSPACE
TECHNICAL LIBRARY
ABBOTTAEROSPACE.COM

structural components and used in analysis. When simulation of the terrain and ground movement is difficult, a quasi-static approach is used (as is done for the design of M204 soft recoil system) to determine travel loads. Typically two loading arrangements are considered (Refs. 4 and 5): a 6-*g* load acting through the center of the wheels at an angle of 45 deg with the ground line and a 3-*g* vertical load. These loads produce high stresses in the carriage structure. This is a statically indeterminate force analysis; therefore, an assumption that has yielded satisfactory results is made to simplify the analysis. The assumption is that the elevating screw and equilibrator forces can be determined from the condition that a 1-*g* load should be supported.

The lifting load analysis can be carried out by closely examining the lifting arrangement. Lifting brackets usually are located on the front of the cradle and the rear of the carriage, as shown in Fig. 7-20 for the M198 towed Howitzer. The division of the lifting loads between the cradle and the carriage depends on the geometry of the lifting arrangement, i.e., length of the cables and the angles. The length of the cables should be taken so that the bore of the weapon is horizontal and the forward cable makes an angle of 45 deg with the cradle. A 3-*g* lifting load is used to determine various forces.

7-5 SAMPLE CRADLE DESIGN PROBLEM

The ideas and techniques presented in par. 7-4 are used in this paragraph for the design of cradle structures. This paragraph is further divided into two subparagraphs. In par. 7-5.1 use of preliminary design procedures is demonstrated, and in par. 7-5.2 use of the refined load and stress analysis procedures presented in par. 7-4.3 is demonstrated. The cradle structure for the M198 towed Howitzer is taken as an example (Refs. 4 and 5). Test data for this system are used to carry out redesign of the cradle and its other structural components.

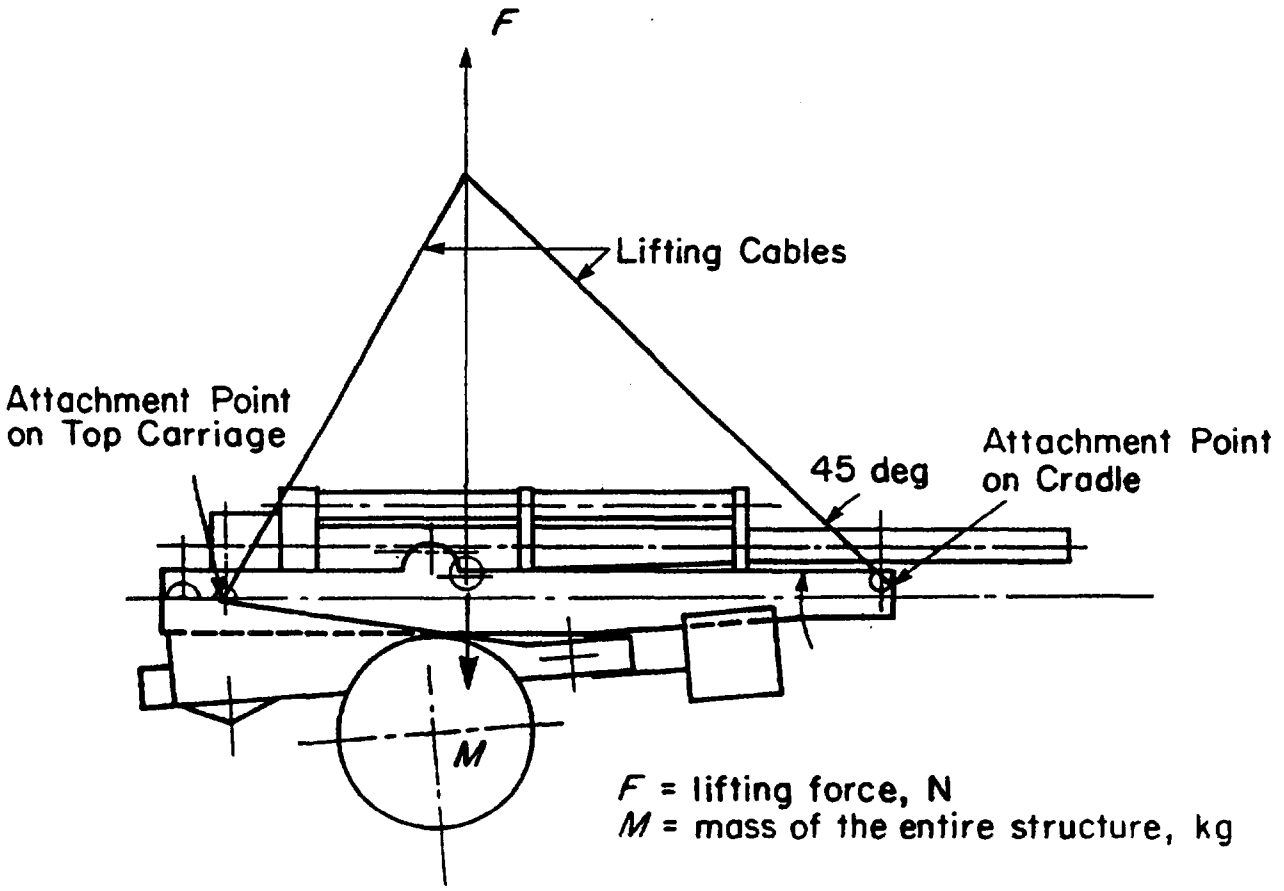

THIS DOCUMENT PROVIDED BY THE ABBOTT AEROSPACE
TECHNICAL LIBRARY
ABBOTTAEROSPACE.COM

7-5.1 PRELIMINARY DESIGN CALCULATIONS

7-5.1.1 Load Analysis

With reference to Fig. 7-5, let

$a = 2.032$ m
$b = 0.508$ m
$c = 0.406$ m
$W_1 = 44{,}482$ N
$F_g = 8.05\times10^6$ N
$d = 0.0025$ m
$e = 0.203$ m
$h = 0.178$ m
$\theta = 60$ deg.

Let

$K = 667{,}230$ N
$\mu = 0.15$.

Eqs. 7-4 through 7-7 give, respectively,

$$f_1 = 0.15R_1, \text{ N}$$

$$f_2 = 0.15R_2, \text{ N}$$

$$K_R = K - f_1 - f_2 = 667{,}230 - 0.15R_1 - 0.15R_2$$

$$F_a = F_g + W_1\sin\theta - K, \text{ N}$$

$$= 8.05\times10^6 + 44{,}482\sin60° - 667{,}230$$

$$= 7{,}421{,}293 \text{ N}.$$

Eq. 7-8 gives

$$R_2 = R_1 + W_1\cos\theta$$

$$= R_1 + 22{,}241, \text{ N}.$$

$$(7{,}421{,}293 - 44{,}482\sin60°)(0.203 - 0.0025) + (44{,}482\cos 60°)\,2.032$$

$$+ (2.032 - 0.508)R_1 + 0.015R_1(0.203 - 0.178)$$

$$= 8.05\times10^6\times0.203 + K_R(0.406 - 0.203)$$

$$(7{,}421{,}293 - 38{,}522)(0.2005) + 45{,}193.7 + 1.524R_1 + 0.00375R_1$$

$$= 1{,}634{,}150 + 0.203K_R$$

or

$$7.526R_1 - K_R = 535{,}521 \text{ N}.$$

THIS DOCUMENT PROVIDED BY THE ABBOTT AEROSPACE
TECHNICAL LIBRARY
ABBOTTAEROSPACE.COM

Solving these simultaneous equations gives

$$R_1 = 153{,}064 \text{ N}$$

$$R_2 = 175{,}501 \text{ N}$$

$$K_R = 617{,}914 \text{ N}$$

$$f_1 = 22{,}960 \text{ N}$$

$$f_2 = 26{,}325 \text{ N}.$$

7-5.1.2 Rails and Slides

The reactions R_1 and R_2 are carried equally by two rails; the length L_R of each rail is 2.286 m. These reactions have been assumed to be triangular, but the reactions due to rifling torque T_r are distributed uniformly. (Refer to par. 7-4.2.2.) The width W_R of the rails is 0.0762 m, and their center-to-center distance d_r is 0.4318 m. From Eq. 7-11

$$T_r = \frac{0.6\pi^2(0.102)^3 248\times10^6}{25} = 62{,}339 \text{ N·m}$$

where

N_r = 25 cal/turn, twist of rifling
P_g = 248 MPa, maximum propellant gas pressure
R_b = 0.102 m, radius of bore.

The trunnion load F_r due to the torque from Eq. 7-21, given the span d_t of the trunnion bearings as 0.711 m, is

$$F_r = \frac{62{,}339}{0.711} = 87{,}678 \text{ N}.$$

The load F_r' on the rails from Eq. 7-22 is

$$F_r' = \frac{62{,}339}{0.4318} = 144{,}370 \text{ N}.$$

Therefore, the uniformly distributed load w_r on rails due to rifling torque is

$$w_r = \frac{F_r'}{L_R} = \frac{144{,}370}{2.286} = 63{,}154 \text{ N/m} \qquad (7\text{-}46)$$

where

L_R = length of rails, m.

Let $R_2/2$ represent the triangular portion of R_2' shown in Fig. 7-13 for each rail. The equivalent uniformly distributed load w_2 is calculated as

$$\frac{1}{2}\left(\frac{L_R}{2}\right) w_2 = \frac{R_2}{2} \text{ , N} \qquad (7\text{-}47)$$

THIS DOCUMENT PROVIDED BY THE ABBOTT AEROSPACE
TECHNICAL LIBRARY
ABBOTTAEROSPACE.COM

or

$$w_2 = \frac{175{,}501 \times 2}{2.286} = 153{,}544 \text{ N/m.}$$

Therefore, the total uniformly distributed load w is

$$w = w_2 + w_r = 153{,}544 + 63{,}154 = 216{,}698 \text{ N/m.} \tag{7-48}$$

The maximum bearing pressure σ_{br} becomes

$$\sigma_{br} = \frac{w}{W_R} = \frac{216{,}698}{0.0762} = 2.84 \text{ MPa.} \tag{7-49}$$

This pressure is acceptable.

Assume that rail and slide have identical cross-sectional dimensions, as shown in Fig. 7-18, i.e.,

$$a = b = 0.019 \text{ m}$$

$$d = e = 0.057 \text{ m}$$

and the section depth D_s is, as previously given, 0.0254 m. Therefore,

1. Total load F is

$$F = D_s w, \text{ N} \tag{7-50}$$

$$= 0.0254 \times 216{,}698 = 5504 \text{ N.}$$

2. Area A of cross section in tension is

$$A = D_s a, \text{ m}^2 \tag{7-51}$$

$$= 0.0254 \times 0.019 = 0.00048 \text{ m}^2.$$

3. Section modulus Z is

$$Z = \frac{D_s a^2}{6}, \text{ m}^3 \tag{7-52}$$

$$= \frac{0.0254\,(0.019)^2}{6} = 1.53 \times 10^{-6} \text{ m}^3.$$

4. Bending moment M is

$$M = eF, \text{ N·m} \tag{7-53}$$

$$= 0.057 \times 5504 = 314 \text{ N·m.}$$

From Eq. 7-41 the tensile stress σ_t is given as (Note that the section modulus $Z = I/c$.)

THIS DOCUMENT PROVIDED BY THE ABBOTT AEROSPACE
TECHNICAL LIBRARY
ABBOTTAEROSPACE.COM

$$\sigma_t = \frac{M}{Z} + \frac{F}{A} = \frac{314}{1.53\times10^{-6}} + \frac{5504}{0.00048} = 217 \text{ MPa}$$

and the factor of safety S_f, assuming a yield strength of 415 MPa, is given by Eq. 7-25 as

$$S_f = \frac{415}{217} = 1.91.$$

7-5.1.3 Equilibrator Load

The equilibrator force F_E is calculated by balancing the weight moment M_W of the tipping parts about the trunnions. By referring to Fig. 7-8,

$$M_W = r_1 W_1 \cos(\theta + \phi_1) + r_c W_c \cos(\theta + \phi_2), \text{ N·m} \quad (7\text{-}54)$$
$$= 52{,}070 \text{ N·m}$$

where

r_1 = moment arm from trunnion to W_1 = 1.905 m
r_c = moment arm from trunnion to W_c = 0.635 m
W_1 = weight of recoiling parts = 44,480 N
W_c = weight of cradle = 17,800 N
θ = 60 deg, angle of elevation
ϕ_1 = 4 minutes
ϕ_2 = −30 deg.

The equilibrator force F_E is determined by equating the equilibrator moment to the weight moment, i.e.,

$$rF_E = M_W = 52{,}070 \text{ N·m}. \quad (7\text{-}55)$$

Therefore, when the moment arm r from trunnion to F_E is 0.3048 m, the equilibrator force is

$$F_E = \frac{52{,}070}{0.3048} = 170{,}833 \text{ N}.$$

The equilibrator attachment to the cradle is similar to the trunnion housing of Fig. 7-21. Details of the attachment are shown in Figs. 7-8 and 7-22. Since the equilibrator force is transmitted at a distance of 0.0993 m above the cradle top, it must be transferred to the top of the cradle to determine the imposed loads. Thus the equivalent loads R_4 and R_3 are calculated as

$$0.3048R_4 = -0.524F_E \sin(\theta - \lambda) + 0.0993F_E \cos(\theta - \lambda), \text{ N} \quad (7\text{-}56)$$

$$R_4 = \frac{-0.1524(170{,}833)\sin 15^\circ}{0.3048} + \frac{0.0993(170{,}833)\cos 15^\circ}{0.3048}$$

$$= 31{,}651 \text{ N}.$$

THIS DOCUMENT PROVIDED BY THE ABBOTT AEROSPACE
TECHNICAL LIBRARY
ABBOTTAEROSPACE.COM

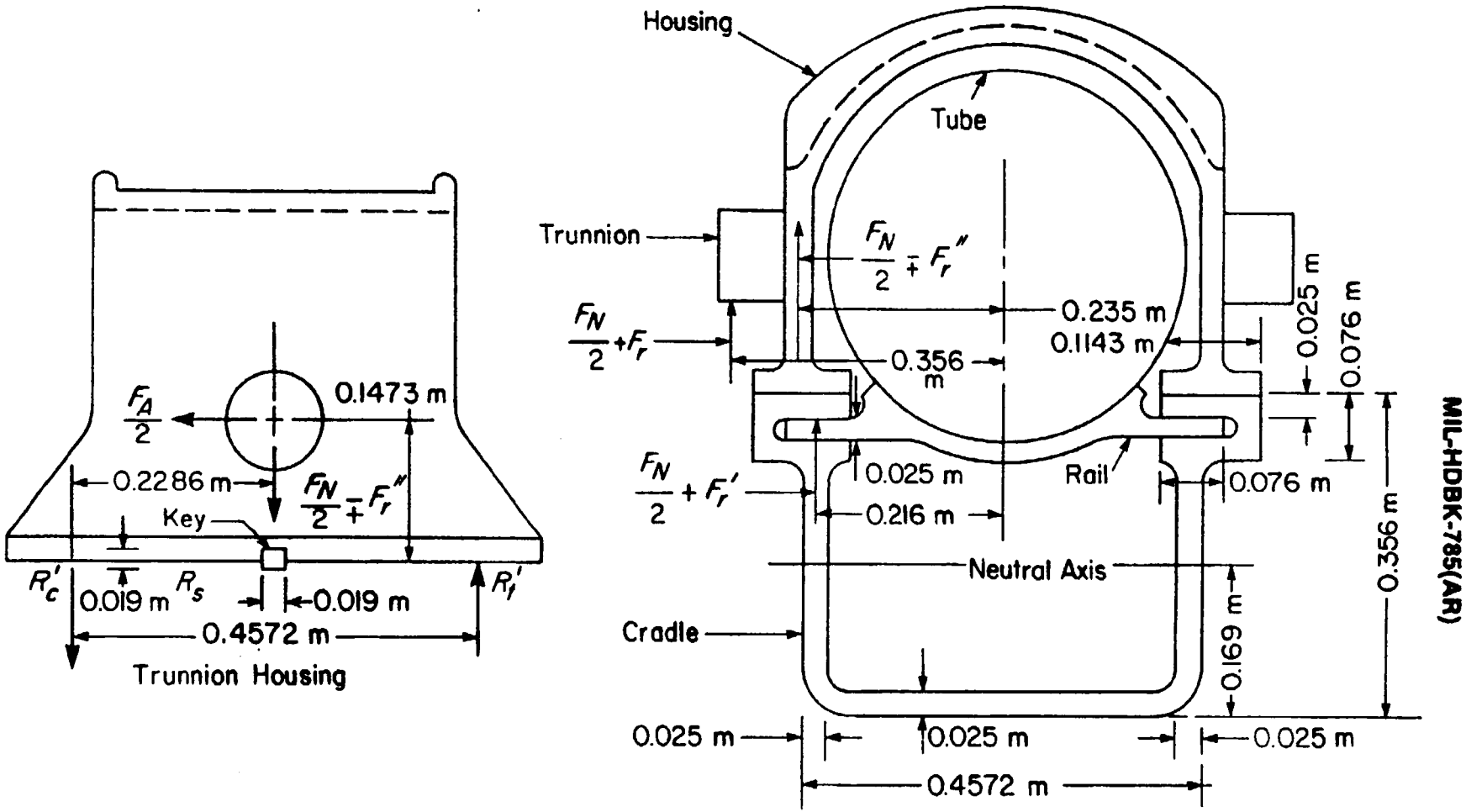

F_N = trunnion reaction normal to bore centerline, N
F_r' = load on rails due to rifling torque, N
R_s = load on key, N
R_c' and R_t' = maximum bolt loads, N
F_r'' = reaction on trunnion housing bolts due to rifling torque, N

Figure 7-21. Trunnion Housing and Cross Section of Cradle

THIS DOCUMENT PROVIDED BY THE ABBOTT AEROSPACE
TECHNICAL LIBRARY
ABBOTTAEROSPACE.COM

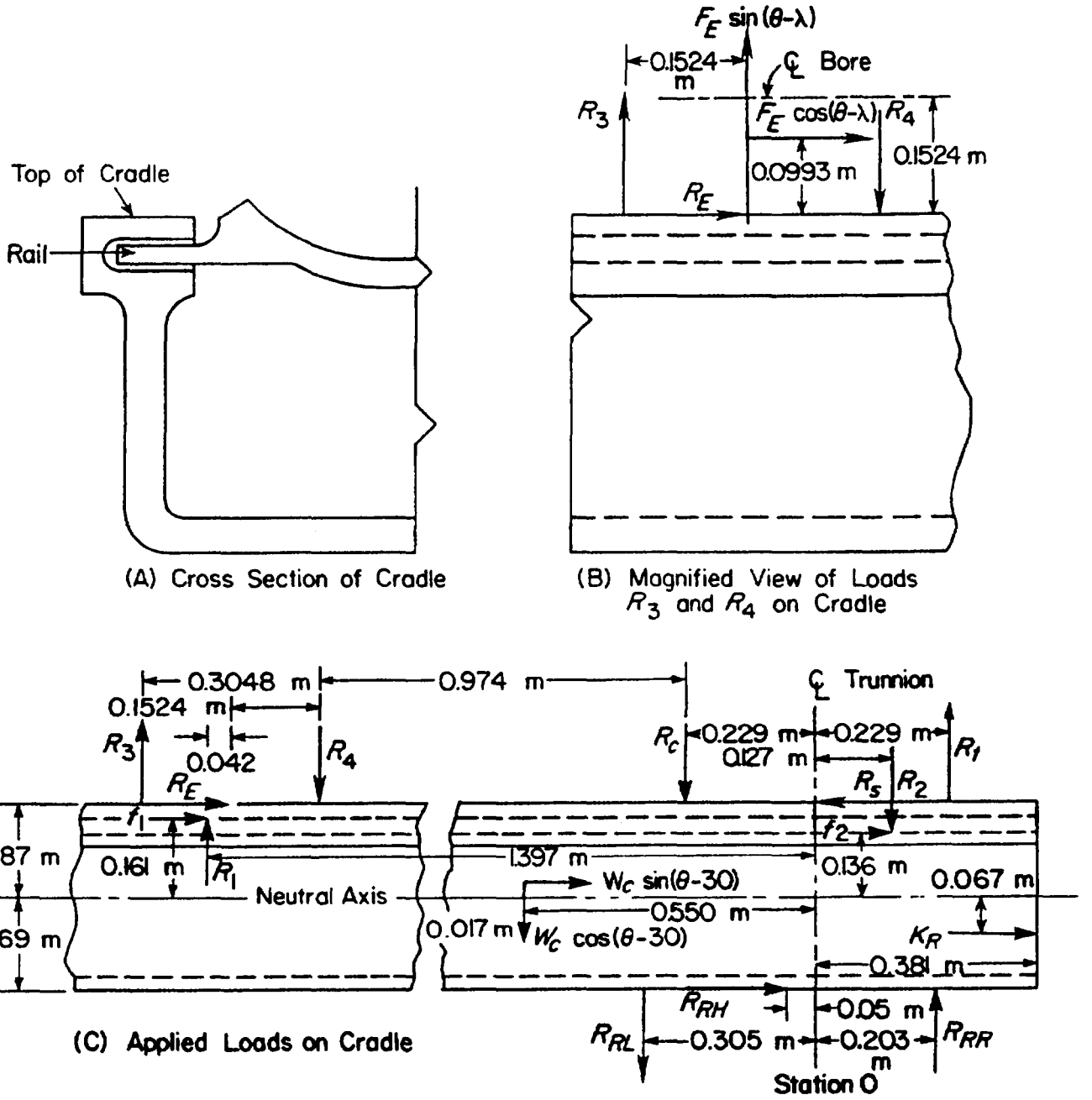

R_1 = normal reaction of front bearing, N
R_2 = normal reaction of rear bearing, N
R_E, R_3, R_4 = loads on primary cradle structure, N
W_c = weight of cradle, N
R_{RH} = shear reaction on key, N
R_{RR} = right bolt reaction, N
R_{RL} = left bolt reaction
R_t = maximum bolt load

Figure 7-22. Longitudinal Section and Applied Loads on Cradle

THIS DOCUMENT PROVIDED BY THE ABBOTT AEROSPACE
TECHNICAL LIBRARY
ABBOTTAEROSPACE.COM

Similarly,

$$0.3048R_3 = 0.0993F_E\cos(\theta - \lambda) + 0.1524F_E\sin(\theta - \lambda), \text{ N}$$

$$R_3 = \frac{0.0993(170{,}833)\cos 15°}{0.3048} + \frac{0.1524(170{,}833)\sin 15°}{0.3048}$$

$$= 75{,}866 \text{ N}.$$

The force R_E in Fig. 7-22 along the cradle is given as

$$R_E = F_E\cos(\theta - \lambda) = 165{,}012 \text{ N} \tag{7-57}$$

where

$\lambda = 45$ deg. (See par. 7-5.1.4.)

7-5.1.4 Elevating Gear Load

The reaction R_g on the elevating gear arc is found by balancing the moment about the trunnions. Additional dimensions for Fig. 7-8 are

$\lambda = 45$ deg
$\gamma = 50$ deg
$\beta = 20$ deg
$R_p = 0.9144$ m
$a = 0.0025$ m
$b = 0.0051$ m.

With reference to Fig. 7-8, summation of moments about the trunnion gives

$$F_g b + F_E r = F_a a + W_1 r_1\cos(\theta + \phi_1) + W_c r_c\cos(\theta + \phi_2) + R_p R_g\cos\beta, \text{ N·m} \tag{7-58}$$

(It is important to note that ϕ_2 is negative as given in par. 7-5.1.3.)
Based on given data and previous calculations

$$R_p R_g\cos\beta = 0.9144\times 0.940 R_g = 0.86 R_g, \text{ N·m}$$

$$rF_E = 0.3048\times 170{,}833 = 52{,}070 \text{ N·m}$$

$$W_c r_c\cos(\theta + \phi_2) = 17{,}800\times 0.635\times 0.866 = 9788 \text{ N·m}$$

$$W_1 r_1\cos(\theta + \phi_1) = 44{,}482\times 1.905\times 0.499 = 42{,}284 \text{ N·m}$$

$$F_a a = 7{,}421{,}293\times 0.0025 = 18{,}553 \text{ N·m}$$

$$F_g b = 8.05\times 10^6\times 0.0051 = 41{,}055 \text{ N·m}.$$

Substituting these values into Eq. 7-60 gives

$$41{,}055 + 52{,}070 = 18{,}553 + 42{,}284 + 9788 + 0.86 R_g$$

$$0.86 R_g = 22{,}500$$

THIS DOCUMENT PROVIDED BY THE ABBOTT AEROSPACE
TECHNICAL LIBRARY
ABBOTTAEROSPACE.COM

$$R_g = 26{,}162 \text{ N.}$$

With reference to Figs. 7-8 and 7-23, the loads at the attachments of the elevating arc to the cradle are calculated by resolving the gear tooth load about these attachments. Take moments about the intersection of R_{RR} and R_{RH}, the shear reaction on the key, and solve for R_{RL} (Note: angles θ, β, and γ are shown in Fig. 7-8.), i.e.,

$$0.508R_{RL} = 0.109R_g\sin[(\theta + \beta + \gamma) - 90°] + 0.356R_g\cos[(\theta + \beta + \gamma) - 90°], \text{ N} \quad (7\text{-}59)$$

$$= 0.109R_g[-\cos(\theta + \beta + \gamma)] + 0.356R_g\sin(\theta + \beta + \gamma)$$

$$= 0.109(26{,}162)(-\cos 130°) + 0.356(26{,}162)\sin 130°$$

$$= 1833 + 7135 = 8968$$

$$R_{RL} = 17{,}654 \text{ N}$$

$$R_{RR} = R_{RL} + R_g[-\cos(\theta + \beta + \gamma)], \text{ N} \quad (7\text{-}60)$$

$$= 17{,}654 + 26{,}162\,(-\cos 130°) = 17{,}654 + 16{,}817$$

$$= 34{,}471 \text{ N}$$

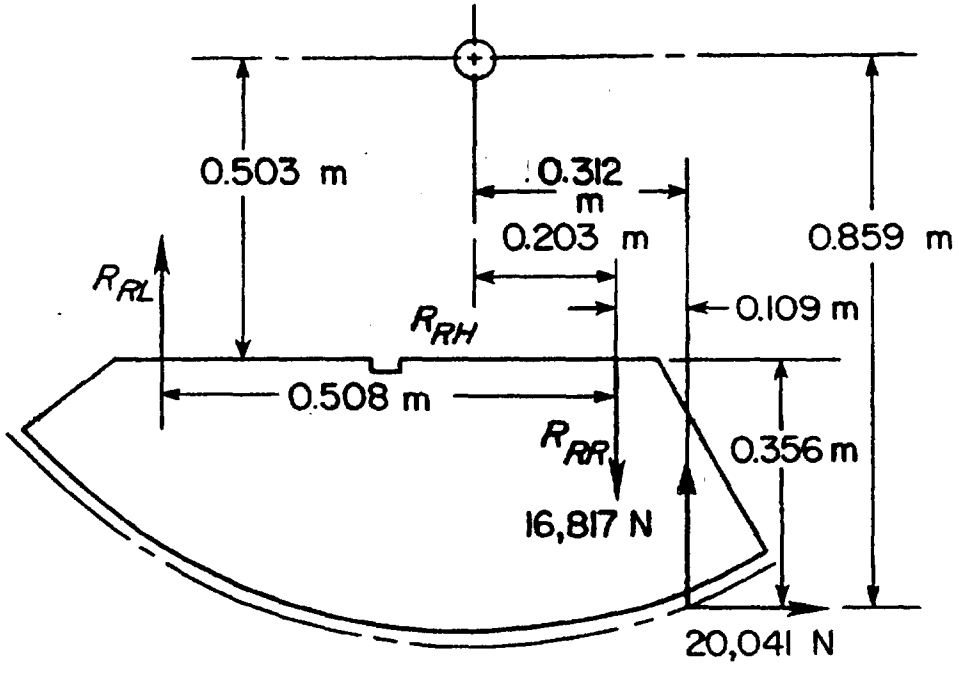

R_{RH} = shear reaction on key, N
R_{RL} = left bolt reaction, N
R_{RR} = right bolt reaction, N

Figure 7-23. Loads on Elevating Arc

THIS DOCUMENT PROVIDED BY THE ABBOTT AEROSPACE
TECHNICAL LIBRARY
ABBOTTAEROSPACE.COM

$$R_{RH} = R_g \sin(\theta + \beta + \gamma) = 26{,}162(\sin 130°) = 20{,}041 \text{ N.} \quad (7\text{-}61)$$

7-5.1.5 Trunnion Loads

The trunnion reactions F_A and F_N are determined, respectively, by the summation of forces parallel and perpendicular to the centerline of the bore, as shown in Fig. 7-8. The equation for the forces perpendicular to the centerline is

$$F_N = F_E \sin(\theta - \lambda) + R_g \sin\beta - W_1 \cos\theta - W_c \cos\theta, \text{ N} \quad (7\text{-}62)$$

$$= 170{,}833 \sin 15° + 26{,}162 \sin 20° - 44{,}482 \cos 60° - 17{,}800 \cos 60°$$

$$= 44{,}214 + 8948 - 22{,}241 - 8900 = 22{,}021 \text{ N.}$$

The equation for the forces parallel to the centerline is

$$F_A = F_E \cos(\theta - \lambda) + W_1 \sin\theta + W_c \sin\theta + R_g \cos\beta + F_g - F_a, \text{ N} \quad (7\text{-}63)$$

$$= 170{,}833 \cos 15° + 44{,}482 \sin 60° + 17{,}800 \sin 60° + 26{,}162 \cos 20°$$

$$+ 8{,}050{,}000 - 7{,}421{,}293 = 872{,}241 \text{ N.}$$

The maximum load on the trunnion housing bolts is applied when the rifling torque is maximum, i.e., $T_r = 62{,}339$ N·m as calculated in par. 7-5.1.2. The reaction F_r'' on the trunnion housing bolts due to T_r is (See Fig. 7-21.)

$$F_r'' = \frac{T_r}{2 \times 0.235} = 132{,}636 \text{ N}$$

$$\frac{F_N}{2} = \frac{22{,}021}{2} = 11{,}011 \text{ N}$$

$$\frac{F_A}{2} = \frac{872{,}241}{2} = 436{,}121 \text{ N.}$$

With reference to Fig. 7-21, and taking moments about reaction R_c', the maximum bolt load R_t' is

$$R_t' = \frac{0.1473}{0.4572}\left(\frac{F_A}{2}\right) - \frac{1}{2}\left(\frac{F_N}{2} - F_r''\right), \text{ N}$$

$$= 201{,}321 \text{ N.}$$

Assume that there are four bolts, each with a root area of 0.00013 m^2. Therefore,

1. The total root area A over which the load acts is

$$A = 4 \times 0.00013 = 0.00052 \text{ m}^2.$$

2. The tensile stress σ_t is

THIS DOCUMENT PROVIDED BY THE ABBOTT AEROSPACE
TECHNICAL LIBRARY
ABBOTTAEROSPACE.COM

$$\sigma_t = \frac{R_t'}{A} = \frac{201{,}321}{0.00052} = 387 \text{ MPa.}$$

3. The safety factor S_f, assuming a yield strength of the material = 690 MPa, is

$$S_f = \frac{690}{387} = 1.78.$$

The load R_s on each key—since there are two keys (See Fig. 7-21.)—is

$$R_s = \frac{F_A}{2} = 436{,}121 \text{ N.} \tag{7-64}$$

The shear area A_s is (length of the key 0.1143 m multiplied by its width 0.019 m in Fig. 7-21)

$$A_s = 0.1143 \times 0.019 = 0.0022 \text{ m}^2.$$

and the shear stress τ is

$$\tau = \frac{R_s}{A_s} = 198 \text{ MPa.}$$

The bearing area A_{br} is (length of the key×half of the depth, Fig. 7-21)

$$A_{br} = 0.1143 \times 0.0095 = 0.0011 \text{ m}^2$$

and the bearing stress σ_{br} is

$$\sigma_{br} = \frac{R_s}{A_{br}} = 396 \text{ MPa.}$$

The trunnion bearings are designed for the loads that are present when the rifling torque is maximum. Only this condition is investigated here. Other conditions may also be investigated. By previous calculations

$F_r = 87{,}678$ N
$F_N = 22{,}021$ N
$F_A = 872{,}241$ N.

Therefore, the maximum trunnion load F_T is

$$F_T = \sqrt{(F_A/2)^2 + (F_N/2 + F_r)^2} = 447{,}147 \text{ N.} \tag{7-65}$$

The trunnion in the hub is shown in Fig. 7-24. Assume triangular distributions for the reactions in the housing cylinder. Then

1. The moment of inertia $I = \pi d^4/64$, where d = diameter of the trunnion, is

$$I = \frac{\pi}{64}(0.0701)^4 = 1.19 \times 10^{-6} \text{ m}^4.$$

THIS DOCUMENT PROVIDED BY THE ABBOTT AEROSPACE
TECHNICAL LIBRARY
ABBOTTAEROSPACE.COM

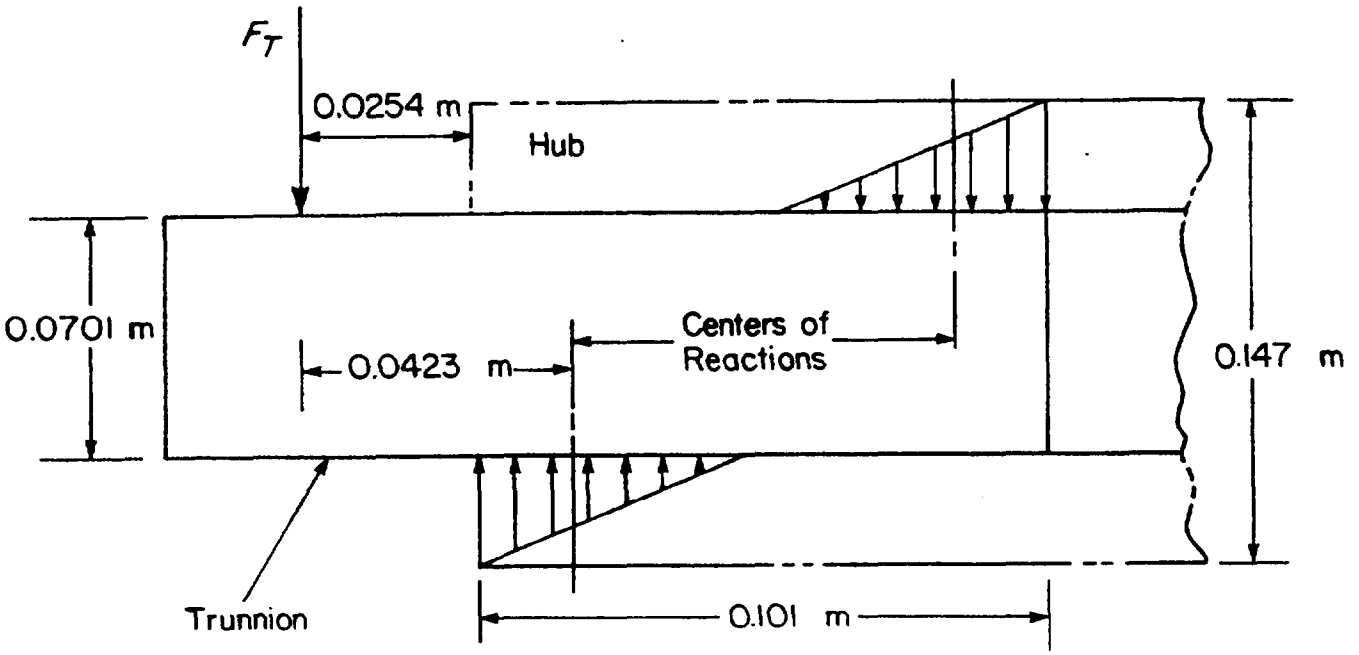

Figure 7-24. Trunnion Loads and Reactions

2. The bending moment M is

$$M = 0.0423F_T = 18{,}914 \text{ N·m.}$$

3. The bending stress σ is by Eq. 7-44

$$\sigma = \frac{Mc}{I} = \frac{18{,}914 \times 0.03505}{1.19 \times 10^{-6}} = 557 \text{ MPa}$$

where $c = 0.0701/2 = 0.03505$ m (distance of the extreme fiber from the neutral axis is half the diameter of the trunnion).
Since this is a short beam, the shear stress τ may be severe and, therefore, must be determined by the equation (Ref. 3)

$$\tau = \frac{F_T A\bar{y}}{It}, \text{ Pa} \qquad (7\text{-}66)$$

$$= 152 \text{ MPa}$$

where

$A\bar{y}$ = moment about neutral axis of cross-sectional area of trunnion above neutral axis, m^3

$A = \frac{1}{2} \times \frac{\pi}{4} \times 0.0701^2 = 0.0019$ m^2 (cross-sectional area of trunnion above neutral axis, m^2)

$t = 0.0701$ m (diameter of trunnion, m)

$\bar{y} = 0.0149$ m (distance of centroid of cross section above neutral axis from neutral axis, m).

THIS DOCUMENT PROVIDED BY THE ABBOTT AEROSPACE
TECHNICAL LIBRARY
ABBOTTAEROSPACE.COM

The reactions produced by the rifling torque are transmitted directly from the slides to the trunnion housing and, therefore, do not enter into the analysis of the primary cradle structure. All the remaining normal and axial loads and reactions are considered. With reference to Figs. 7-21 and 7-22, the reactions now become

$$R_l = \left(\frac{0.147}{0.457}\right) F_A - \frac{F_N}{2}, \text{ N} \tag{7-67}$$

$$= 269{,}557 \text{ N}$$

$$R_c = \left(\frac{0.147}{0.457}\right) F_A + \frac{F_N}{2}, \text{ N} \tag{7-68}$$

$$= 291{,}578 \text{ N}$$

$$R_s = F_A, \text{ N}$$

$$= 872{,}241 \text{ N}.$$

To compute stresses and deflections, the bending moment, axial force, and shear force acting at every section must be calculated. Fig. 7-22 shows loads applied on the cradle. Since all the forces have been determined, the equations of equilibrium, Eqs. 7-1 through 7-3, are not required to determine unknown forces. For any section, however, the three quantities—bending moment M, axial (horizontal) force F_H, and shear (vertical) force F_V—are unknowns and must be determined by the use of the equilibrium equations. Eq. 7-1 can be used to determine the axial force F_H. Eq. 7-2 can be used to determine the shear force F_V. Eq. 7-3 can be used to determine the bending moment M. By making use of these equations and Fig. 7-22, the three quantities are determined for some important cross sections along the length of the cradle. These results are summarized and tabulated in Table 7-1.

7-5.1.6 Stress and Deflection

Eq. 7-43 is used to determine the maximum stress due to bending that occurs in the cradle body. The effects due to shearing and axial forces are neglected because the bending component is dominant. The calculations presented in Table 7-2 are used to compute the moment of inertia I_c of the cradle cross section. The moment of inertia is composed principally of two parts—that of the cradle section I_c and that of the gun tube I_T. Fig. 7-21 is used to compute the values of M/I.

$$I = I_c + I_T, \text{ m}^4 \tag{7-69}$$

$$= 0.0019 \text{ m}^4.$$

The moment of inertia I_{BL} at the baseline BL is from Table 7-2

$$I_{BL} = \Sigma A d^2 + \Sigma I_0, \text{ m}^4 \tag{7-70}$$

$$= 0.0017 \text{ m}^4$$

where

I_0 = moment of inertia of part about its own neutral axis, m^4.

THIS DOCUMENT PROVIDED BY THE ABBOTT AEROSPACE
TECHNICAL LIBRARY
ABBOTTAEROSPACE.COM

TABLE 7-1
SUMMARY OF F_V, ΣF_V, M_x, M_y, AND M[a]

Station, m	x, m	F_V, N	ΣF_V, N	F_H, N	y, m	M_x, N·m	M_y, N·m	M, N·m
1.507	0	75,866(R_3)	75,866	0	0	0	0	0
1.397	0.110	153,064(R_1)	228,930	0	0	−8,345	0	−8,345
				22,960(f_1)	0.161		−3,696	−12,041
1.355	0.042	0	228,930			−9,615		−21,656
				165,080(R_E)	0.187		−30,870	−52,526
1.203	0.152	−31,651(R_4)	197,279	0		−34,798	0	−87,324
0.550	0.653	−15,415[b]	181,864			−128,823		−216,147
				8,900[c]	0.017		151	−215,996
0.305	0.245	−17,654(R_{RL})	164,210	0		−44,557	0	−260,553
0.229	0.076	−291,578(R_c)	−127,368	0		−12,480	0	−273,033[d]
0.051	0.178	0	−127,368			22,671		−250,362
				20,041(R_{RR})	0.169		3,387	−246,975
0	0.051	0	−127,368			6,496		−240,479
				872,578(R_s)	0.187		163,172	−77,307
−0.127	0.127	−175,501(R_2)	−302,869			16,176		−61,131
				26,325(f_2)	0.136		−3,580	−64,711
−0.203	0.076	34,471(R_{RR})	−268,398	0		23,018		−41,693
−0.229	0.026	269,557(R_t)	1,159[e]	0		6,978		−34,715
−0.381	0.152	0	1,159[e]	617,914(K_R)	0.067		41,400	6,685

[a] $M = M_x + M_y$ up to and including the station under consideration.
[b] $W_v \cos(\theta - 30) = -15{,}415$ N
[c] $W_v \sin(\theta - 30) = 8{,}900$ N
[d] Maximum bending moment occurs 0.229 m in front of the trunnion.
[e] ΣF_V should be zero. A value of 1,159 N results from rounding off.

Moment of inertia is based on Fig. 7-21.

TABLE 7-2
DATA FOR COMPUTING I_c*

Dimension, m	A, m^2	d, m	Ad, m^3	Ad^2, m^4	I_o, m^4
0.4572×0.2794	0.1277	0.140	0.0179	0.0025	0.0008
0.4064×0.254	−0.1032	0.152	−0.0157	−0.0024	−0.0006
0.2286×0.0762	0.0174	0.318	0.0055	0.0018	0.000008
0.1524×0.0254	−0.0039	0.318	−0.0012	−0.0004	—
Σ	0.0380		0.0065	0.0015	0.0002

*Note:
Dimension = base × height of parts of the section
d = distance from baseline to neutral axis of part, m
I_o = moment of inertia of part about its own neutral axis, m^4

The distance $\bar{d}$ from the baseline to the neutral axis of the section—using the data from Table 7-2—is

$$\bar{d} = \frac{\Sigma Ad}{\Sigma A}, \text{ m} \tag{7-71}$$

$$= \frac{0.0065}{0.038} = 0.1711 \text{ m}$$

THIS DOCUMENT PROVIDED BY THE ABBOTT AEROSPACE
TECHNICAL LIBRARY
ABBOTTAEROSPACE.COM

and

$$\Sigma A\bar{d}^2 = 0.0011 \text{ m}^4.$$

Therefore, by Eq. 7-72—where $\Sigma I_0 = I_c$ and $\Sigma Ad^2 = \Sigma A\bar{d}^2$—the moment of inertia I_c of the cradle section is

$$I_c = I_{BL} - \Sigma A\bar{d}^2, \text{ m}^4 \tag{7-72}$$

$$= 0.0017 - 0.0011 = 0.0006 \text{ m}^4.$$

Accordingly, the distance c from the extreme fiber to the neutral axis is

$$c = 0.356 - \bar{d}, \text{ m (See Fig. 7-23.)} \tag{7-73}$$

$$= 0.356 - 0.1711 = 0.1849 \text{ m.}$$

Therefore, the bending stress σ by Eq. 7-44 is

$$\sigma = \frac{Mc}{I_c} = \frac{273{,}033 \times 0.1849}{0.0006} = 84.14 \text{ MPa.}$$

The bending stress σ of 84.14 MPa falls far below the stress that would yield a factor of safety of 1.5. Rigidity, however, is a property of higher priority because large deflections eventually result in poor accuracy. Thus greater rigidity should be maintained to promote better accuracy.

Deflections are determined by the moment area method. First, the deflection for the breech end is determined by computing the moment of the M/I diagram at this point, Station −0.381 m. (See Table 7-1 and Fig. 7-25.) This deflection is normal to the tangent of the elastic line at Station 1.507 m. The calculations that follow, which are summarized in Table 7-3, refer to Station −0.381 m.

The moment of inertia I_T of the tube is

$$I_T = \frac{\pi}{64}(D_o^4 - D_i^4) \tag{7-74}$$

$$= 0.0013 \text{ m}^4$$

given

$D_o = 0.4064$ m, outer diameter of tube
$D_i = 0.2032$ m, inner diameter of tube.

The areas A_m between stations are computed and their centroids $\bar{x}$ determined. For example, consider the computation of a typical centroid $\bar{x}$ for Fig. 7-25. The centroid of the first area is $0.152/2 = 0.076$ m from the Station −0.381 m. The second area is a trapezoid whose centroid is $h(a + 2b)/[3(a + b)] = 0.0133$ m from the short parallel arm. Here, a is the short parallel arm, b is the long parallel arm, and h is the width of the trapezoid between the two parallel arms. Thus the centroid of the second area from the Station −0.381 m is $0.0133 + 0.152 = 0.1653$ m, as shown in Table 7-3. Table 7-3 shows the moment of each area about Station −0.381 m. Values of $\bar{x}A_M$ were calculated from the metric values of $\bar{x}$ and A_M and rounded to the allowable number of significant figures. From Table 7-3

$$\Sigma \bar{x} A_M = 120{,}586 \text{ kN/m.}$$

THIS DOCUMENT PROVIDED BY THE ABBOTT AEROSPACE
TECHNICAL LIBRARY
ABBOTTAEROSPACE.COM

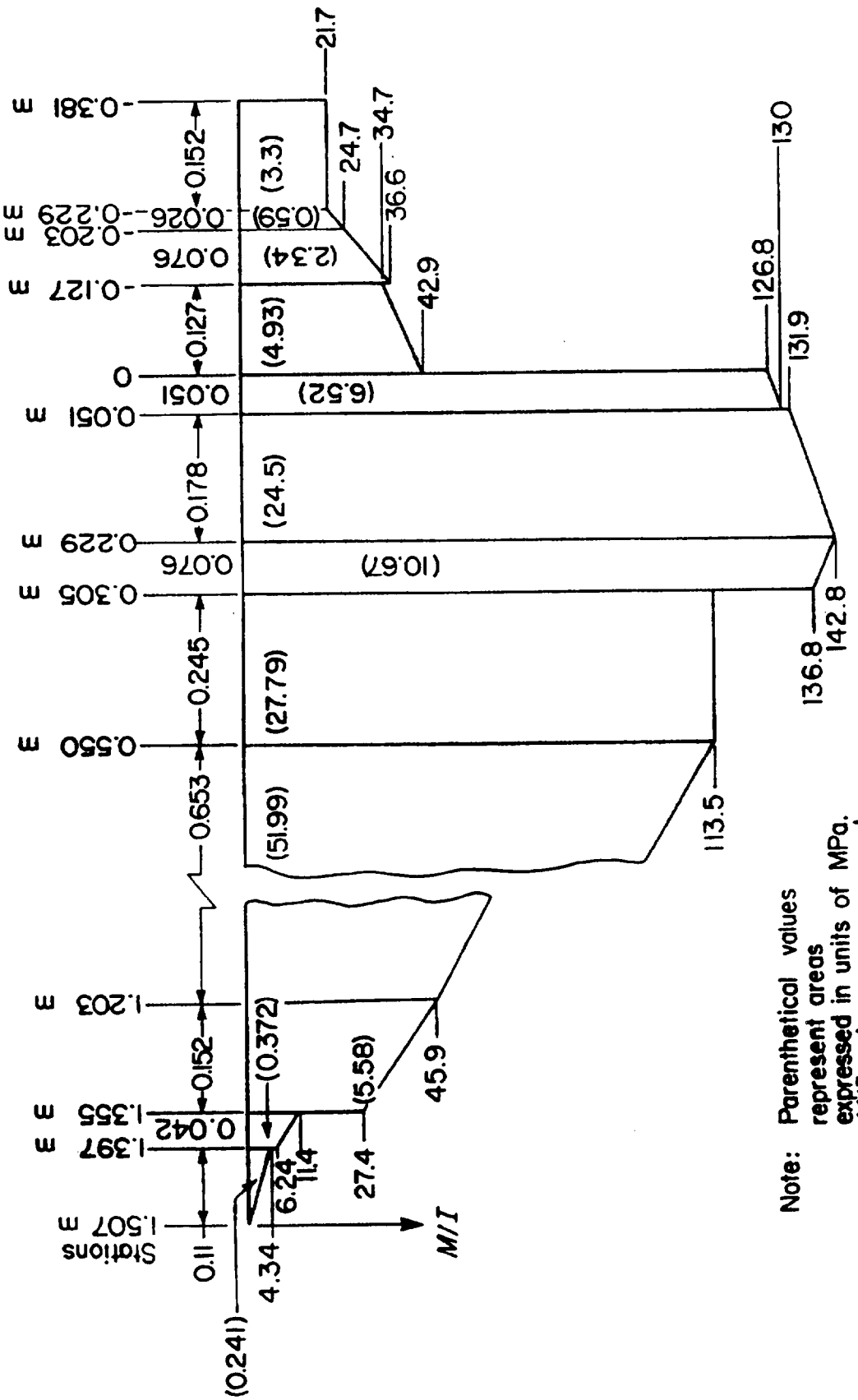

Figure 7-25. *M/I* Diagram

THIS DOCUMENT PROVIDED BY THE ABBOTT AEROSPACE
TECHNICAL LIBRARY
ABBOTTAEROSPACE.COM

TABLE 7-3
MOMENTS OF AREAS ABOUT STATION —0.381 m

$\bar{x}$, m	A_M, MPa	$\bar{x}A_M$, kN/m	$\bar{x}$, m	A_M, MPa	$\bar{x}A_M$, kN/m
0.0761	3.3	251	0.6474	10.67	6,910
0.1653	0.593	98.0	0.8085	27.79	22,470
0.2184	2.34	511	1.212	51.99	63,010
0.3198	4.93	1,577	1.654	5.58	9,230
0.4064	6.52	2,650	1.754	0.372	652
0.5220	24.5	12,790	1.815	0.241	437

Therefore, the deflection Δ at Station —0.381 is

$$\Delta = \frac{\Sigma \bar{x} A_M}{E} \tag{7-75}$$

$$= \frac{120{,}586 \times 10^3}{200{,}000 \times 10^6} = 0.0006 \text{ m}$$

where the modulus of elasticity $E = 200{,}000$ MPa. The corresponding angular deflection θ_1 at Station —0.381 is

$$\theta_1 = \frac{\Delta}{L}, \text{ rad} \tag{7-76}$$

$$= \frac{0.0006}{1.507 - (-0.381)} = \frac{0.0006}{1.888} = 0.0003 \text{ rad}$$

where

L = distance between stations, i.e., between Stations —0.381 m and 1.507 m, m.

Assume that the clearance between the rail and slide is 0.00025 m extending along the entire length. This clearance permits the tube to rotate through a small angle until the rails become cocked in the slides. In this example, the length of the slides is 2.286 m. Thus the angle θ_2 through which the tube rotates because of rail clearance is

$$\theta_2 = \frac{0.00025}{2.286} = 0.00011 \text{ rad.}$$

Therefore, the total angular deflection of the gun tube that is attributable to the cradle structure is

$$\theta = \theta_1 + \theta_2 \tag{7-77}$$

$$= 0.00043 \text{ rad.}$$

7-5.2 REFINED DESIGN CALCULATIONS AT SEVEN SELECTED CROSS SECTIONS

Once the preliminary design has been determined to be satisfactory, estimates of the areas and moments of inertia of various cross sections along the cradle body are available. The techniques discussed in this paragraph and in par. 7-4.3 for a refined design calculation can now be applied.

THIS DOCUMENT PROVIDED BY THE ABBOTT AEROSPACE
TECHNICAL LIBRARY
ABBOTTAEROSPACE.COM

Table 7-4 shows the cross-sectional properties of the cradle body. Since this example illustrates design calculations specifically related to the M198 Howitzer, data from par. 7-5.1 are not used here. Table 7-5 shows the forces that act on the cradle body for various angles of elevation.

TABLE 7-4
CROSS-SECTIONAL PROPERTIES OF CRADLE BODY FOR M198 TOWED HOWITZER

X, m	A, m^2	Z_1, m^3	Z_2, m^3
0-0.152	0.0155	0.00052	0.00052
0.152-0.343	0.0155	0.00051	0.00051
0.343-0.396	0.0155	0.00052	0.00052
0.396-0.645	0.0121	0.00088	0.00088
0.645-1.067	0.0097	0.00058	0.00058
1.067-1.295	0.0129	0.00064	0.00066
1.295-1.448	0.0187	0.00066	0.00078
1.448-1.524	0.0170	0.00057	0.00057
1.524-1.626	0.0170	0.00077	0.00066
1.626-1.676	0.0174	0.00076	0.00066
1.676-1.715	0.0239	0.00071	0.00120
1.715-1.905	0.0219	0.00080	0.00169
1.905-2.419	0.0097	0.00058	0.00058
2.419-2.959	0.0097	0.00057	0.00057

X = distance to section from trunnion centerline, m
A = area of cross section in tension, m^2
Z_1 = section modulus on lower side of cradle, m^3
Z_2 = section modulus on upper side of cradle, m^3

Note: The values of area and section moduli represent average values in the range of the cross sections given in the first column and are only for one side of the cradle body.

TABLE 7-5
FORCES ACTING ON CRADLE FOR M198 TOWED HOWITZER

$\gamma + \theta$, deg	λ, deg	τ, deg	T_V, N	T_H, N	S_1, N	S_2, N
0	−10.97	14.4	26,580	224,200	9,475	−3,150
35	11.39	2.97	21,430	206,205	140	1,270
45	9.85	−0.30	24,450	209,675	9,245	5,720
50	8.65	−1.93	37,565	277,120	25,230	−10,730
75	−0.57	−9.8	31,875	275,770	38,260	30,190

γ = original angle of elevation, deg
$\gamma + \theta$ = angle between barrel and horizontal, deg
λ = angle between equilibrator and barrel, deg
τ = angle between elevating strut and barrel, deg
T_V, T_H = trunnion reactions perpendicular to and along the barrel, respectively, N
S_1 = clip reaction at rear end, N
S_2 = clip reaction at front end, N

The data given in Table 7-5 can be obtained either from field tests or from mathematical models. By referring to Fig. 7-26 (A), it is seen from the free-body diagram that the data in Table 7-5 render the structure determinant. By applying Eqs. 7-1 through 7-3, the unknown forces F_E and F_s are obtained. Also note that the frictional forces f_1 and f_2, which depend on S_1 and S_2, respectively, are obtained by applying Eqs. 7-1 through 7-5. Results of the analysis described are shown in Table 7-6. Sufficient data now exist to calculate the stresses and forces at various cross sections along the cradle body.

THIS DOCUMENT PROVIDED BY THE ABBOTT AEROSPACE
TECHNICAL LIBRARY
ABBOTTAEROSPACE.COM

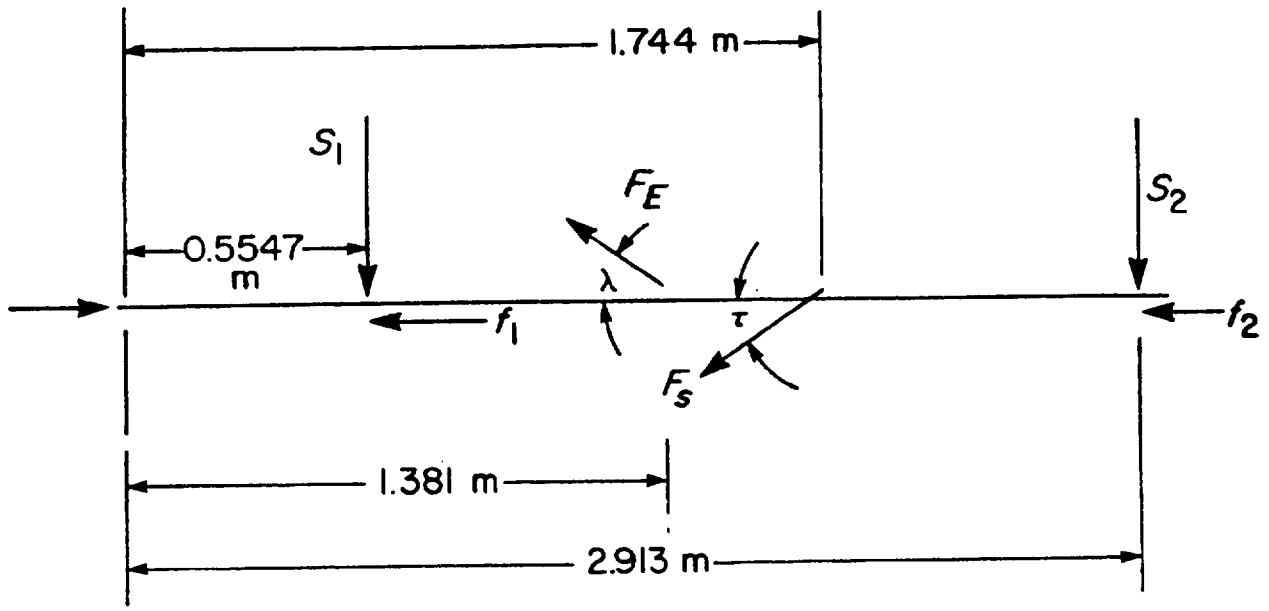

(A) Free-Body Diagram of Cradle Structure

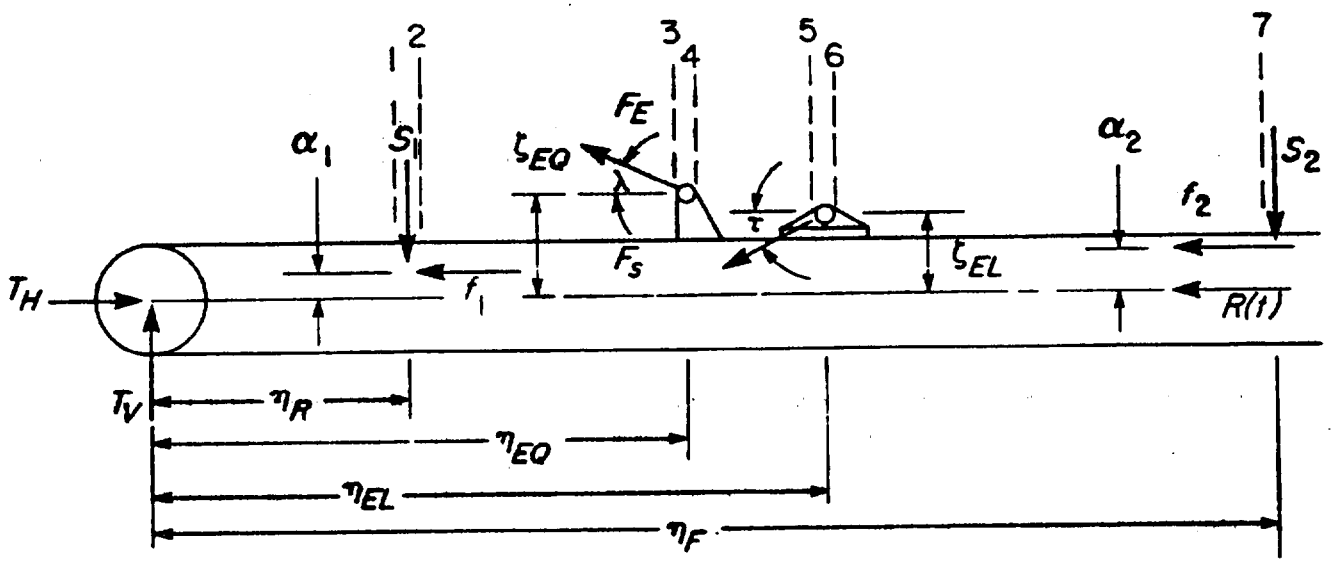

(B) Refined Free-Body Diagram of Cradle Structure

Figure 7-26. Free-Body Diagrams of M198 Howitzer Cradle Structure

Before the stress analysis can be carried out, the cross-sectional properties of the cradle body are required. Fig. 7-26(A) shows the side view of the cradle body. Table 7-4 summarizes the cross-sectional properties of the cradle for various cross sections. There are five angles of elevation for which the forces have been evaluated. Stress analysis is carried out for each case separately. Since all the forces are coplanar, the stresses are evaluated by using the equation

THIS DOCUMENT PROVIDED BY THE ABBOTT AEROSPACE
TECHNICAL LIBRARY
ABBOTTAEROSPACE.COM

TABLE 7-6
FORCES ACTING ON THE CRADLE BODY FOR M198 TOWED HOWITZER

$\gamma + \theta$, deg	F_E, N	F_z, N	f_1, N	f_2, N
0	82,848	144,890	1890	631
35	63,725	143,600	28	250
45	59,995	147,575	1850	1140
50	58,270	212,450	5049	2145
75	53,165	212,020	7650	6036

F_E = equilibrator force, N
F_z = force in elevating strut, N
f_1 = frictional force due to rear end clip reaction, N
f_2 = frictional force due to front end clip reaction, N
Note: The coefficient of friction $\mu = 0.2$.

$$\sigma = \frac{M_z}{Z_x} \pm \frac{P}{A}, \text{ Pa} \tag{7-78}$$

where

σ = combined stress, Pa
M_z = moment along z-axis, N·m
Z_x = section modulus about x-axis given by I_x/c, with c as distance of extreme fiber from x-axis, m^3
P = axial force, N
A = cross-sectional area, m^2.

If the axial force P is tensile, it must be added to the tensile bending stress and subtracted from compressive bending stress, i.e., the appropriate algebraic sign in Eq. 7-78 should be used. The effect of shearing stresses is neglected. If shearing stresses are included in the analysis, an effective stress σ_e (von Mises' failure condition) must be calculated as follows (Ref. 2):

$$\sigma_e = \sqrt{\sigma^2 + 3\tau^2}, \text{ Pa.} \tag{7-79}$$

This stress σ_e must be checked against the yield stress for the material for strength requirements. The criteria (Eq. 7-79) are based von Mises' failure condition. (The maximum shear stress failure criterion is used in preliminary design.) Stresses are calculated only for a selected number of cross sections, as shown in Fig. 7-26(B) (Ref. 4), i.e., where M_{ci} and P_i denote the bending moment of the cradle and the axial force, respectively, at Section i. These cross sections are selected at some critical locations where either cross-sectional properties change or forces are transmitted.

At Section 1 ($x = 0.396$ m):

$$M_{c1} = \eta_R T_V, \text{ N·m}$$
$$P_1 = T_H, \text{ N.} \tag{7-80}$$

At Section 2 ($x = 0.645$ m):

$$M_{c2} = M_{c1} - \alpha_1 f_1, \text{ N·m}$$
$$P_2 = T_H - f_1, \text{ N.} \tag{7-81}$$

THIS DOCUMENT PROVIDED BY THE ABBOTT AEROSPACE
TECHNICAL LIBRARY
ABBOTTAEROSPACE.COM

At Section 3 ($x = 1.295$ m):

$$M_{c3} = \eta_{EQ}T_V - (\eta_{EQ} - \eta_R)S_1 - \alpha_1 f_1, \text{ N·m}$$
$$P_3 = T_H - f_1, \text{ N.} \tag{7-82}$$

At Section 4 ($x = 1.448$ m):

$$M_{c4} = M_{c3} - \zeta_{EQ}F_E\cos\lambda, \text{ N·m}$$
$$P_4 = P_3 - F_E\cos\lambda, \text{ N.}$$

At Section 5 ($x = 1.715$ m):

$$M_{c5} = \eta_{EL}T_V - (\eta_{EL} - \eta_R)S_1 + (\eta_{EL} - \eta_{EQ})F_E\sin\lambda - \zeta_{EQ}F_E\cos\lambda - \alpha_1 f_1, \text{ N·m}$$
$$P_5 = P_4, \text{ N.} \tag{7-83}$$

At Section 6 ($x = 1.905$ m):

$$M_{c6} = M_{c5} - \zeta_{EL}F_s\cos\tau, \text{ N·m}$$
$$P_6 = P_5 - F_s\cos\tau, \text{ N.} \tag{7-84}$$

At Section 7 ($x = 2.419$ m):

$$M_{c7} = \eta_F T_V - (\eta_F - \eta_R)S_1 + (\eta_F - \eta_{EQ})F_E\sin\lambda$$
$$- (\eta_F - \eta_{EL})F_s\sin\tau - \alpha_1 f_1 - \zeta_{EQ}F_E\cos\lambda - \zeta_{EL}F_s\cos\tau, \text{ N·m} \tag{7-85}$$
$$P_7 = P_6, \text{ N.}$$

(Negative values of λ correspond to F_E above the barrel axis and vice versa. Negative values of τ correspond to F_s above the barrel axis and vice versa.)

Note that the moment diagram will not close, i.e., $M_{c7} \neq 0$, since in predicting the forces,

1. Weight was neglected.
2. Accelerations were neglected.
3. Frictional forces were estimated crudely.

These equations, however, do provide a realistic model to the cradle body and establish a more reasonable basis for structural design than has been available in the past. A conservative design procedure is to consider the maximum bending moment and the maximum axial force at a particular cross section to be acting simultaneously. This is done even if the moment and force are occurring at different times or angles of elevation. This philosophy is applied in the design calculations that follow. Five cases, i.e., five different values for $(\gamma + \theta)$, will be considered.

Case 1. $\gamma + \theta = 0$ deg. (Calculated values for M_{ci} and P_i—using Eqs. 7-80 through 7-85 and the data from Tables 7-5 and 7-6—are listed in Table 7-7.)

Distances:

$\eta_R = 0.564$ m
$\eta_{EL} = 1.772$ m
$\eta_{EQ} = 1.403$ m
$\eta_F = 2.883$ m

THIS DOCUMENT PROVIDED BY THE ABBOTT AEROSPACE
TECHNICAL LIBRARY
ABBOTTAEROSPACE.COM

TABLE 7-7
VALUES OF M_{cl} AND P_t FOR CASE 1

Section	Moment M_{cl}, N·m	Axial Force P_t, N
1	14,980	224,200
2	14,835	222,310
3	29,195	222,310
4	12,700	140,980
5	13,200	140,980
6	−8,130	642
7	−46,700	642

$\alpha_1 = 0.076$ m
$\zeta_{EQ} = 0.203$ m
$\zeta_{EL} = 0.152$ m
$\alpha_2 = 0.1302$ m.

Forces:

$T_V = 26{,}580$ N
$T_H = 224{,}200$ N
$S_1 = 9475$ N
$f_1 = 1890$ N
$F_E = 82{,}850$ N
$F_s = 144{,}890$ N.

Angles:

$\lambda = -10.97$ deg
$\tau = 14.4$ deg.

Case 2. $\gamma + \theta = 35$ deg. (Calculated values for M_{cl} and P_t—using Eqs. 7-80 through 7-85 and the data from Tables 7-5 and 7-6—are listed in Table 7-8.)
Distances: Same as Case 1.

Forces:

$T_V = 21{,}430$ N
$T_H = 206{,}205$ N
$S_1 = 140$ N
$f_1 = 28$ N
$F_E = 63{,}725$ N
$F_s = 143{,}600$ N.

Angles:

$\lambda = 11.39$ deg
$\tau = 2.97$ deg.

Case 3. $\gamma + \theta = 45$ deg. (Calculated values for M_{cl} and P_t—using Eqs. 7-80 through 7-85 and the data from Tables 7-5 and 7-6—are listed in Table 7-9.)
Distances: Same as Case 1.

Forces:

$T_V = 24{,}450$ N
$T_H = 209{,}675$ N
$S_1 = 9245$ N

THIS DOCUMENT PROVIDED BY THE ABBOTT AEROSPACE
TECHNICAL LIBRARY
ABBOTTAEROSPACE.COM

TABLE 7-8
VALUES OF M_{ai} AND P_i FOR CASE 2

Section	Moment M_{ai}, N·m	Axial Force P_i, N
1	12,080	206,205
2	12,077	206,000
3	29,960	206,000
4	17,265	144,000
5	29,800	144,000
6	7,970	300
7	37,300	300

TABLE 7-9
VALUES OF M_{ai} AND P_i FOR CASE 3

Section	Moment M_{ai}, N·m	Axial Force P_i, N
1	13,780	209,675
2	13,600	207,800
3	26,400	207,800
4	14,400	149,000
5	23,800	149,000
6	1,670	1,150
7	30,500	1,150

$f_1 = 1850$ N
$F_E = 59{,}990$ N
$F_s = 147{,}575$ N.

Angles:
$\lambda = 9.85$ deg
$\tau = -0.30$ deg.

Case 4. $\gamma + \theta = 50$ deg. (Calculated values for M_{ai} and P_i—using Eqs. 7-80 through 7-85 and the data from Tables 7-5 and 7-6—are listed in Table 7-10.)
Distances: Same as Case 1.

Forces:
$T_V = 37{,}565$ N
$T_H = 277{,}120$ N
$S_1 = 25{,}230$ N
$f_1 = 5049$ N
$F_E = 58{,}270$ N
$F_s = 212{,}450$ N.

Angles:
$\lambda = 8.65$ deg
$\tau = -1.93$ deg.

Case 5. $\gamma + \theta = 75$ deg. (Calculated values for M_{ai} and P_i—using Eqs. 7-80 through 7-85 and the data from Tables 7-5 and 7-6—are listed in Table 7-11.)
Distances: Same as Case 1.

Forces:
$T_V = 31{,}875$ N
$T_H = 275{,}770$ N
$S_1 = 38{,}260$ N
$f_1 = 7650$ N
$F_E = 53{,}165$ N
$F_s = 212{,}020$ N.

Angles:
$\lambda = -0.57$ deg
$\tau = -9.8$ deg.

THIS DOCUMENT PROVIDED BY THE ABBOTT AEROSPACE
TECHNICAL LIBRARY
ABBOTTAEROSPACE.COM

TABLE 7-10
VALUES OF M_{ci} AND P_i FOR CASE 4

Section	Moment M_{ci}, N·m	Axial Force P_i, N
1	21,170	277,120
2	20,800	272,100
3	31,200	272,100
4	22,400	215,500
5	39,300	215,500
6	−9,831	2,164
7	26,400	2,164

TABLE 7-11
VALUES OF M_{ci} AND P_i FOR CASE 5

Section	Moment M_{ci}, N·m	Axial Force P_i, N
1	17,960	275,770
2	17,380	268,100
3	12,020	268,100
4	1,230	215,000
5	−1,319	215,000
6	−33,080	6,033
7	−664	6,033

The maximum bending moments M_{max} and maximum axial forces P_{max} at each section are determined by examining Tables 7-7 through 7-11. These maximum values are listed in Table 7-12.

TABLE 7-12
MAXIMUM BENDING MOMENTS AND MAXIMUM AXIAL FORCES

Section	Maximum Bending Moment M_{max}, N·m		Maximum Axial Force P_{max}, N	
	M_{max}	Case and Elevation	P_{max}	Case and Elevation
1	21,170	Case 4, 50 deg	277,120	Case 4, 50 deg
2	20,800	Case 4, 50 deg	272,100	Case 4, 50 deg
3	31,200	Case 4, 50 deg	272,100	Case 4, 50 deg
4	22,400	Case 4, 50 deg	215,500	Case 4, 50 deg
5	39,300 −1,319	Case 4, 50 deg Case 5, 75 deg	215,500	Case 4, 50 deg
6	−33,080 7,970	Case 5, 75 deg Case 2, 35 deg	6,033	Case 5, 75 deg
7	−46,700 37,700	Case 1, 0 deg Case 2, 35 deg	6,033	Case 5, 75 deg

7-5.2.1 Stress Calculations for Section 1

At Section 1 the maximum bending moment and maximum axial stress both occur at 50 deg, Case 4. Therefore,

$$S_c = \frac{P_{max}}{A} = \frac{277{,}120}{0.0121} = 22.9 \text{ MPa}$$

$$S_b = \frac{M_{max}}{Z_1} = \frac{21{,}170}{0.00088} = 24.1 \text{ MPa}$$

$$\sigma = S_c + S_b = 47 \text{ MPa}$$

THIS DOCUMENT PROVIDED BY THE ABBOTT AEROSPACE
TECHNICAL LIBRARY
ABBOTTAEROSPACE.COM

where

S_c = tensile stress in cradle section due to axial force, Pa
S_b = tensile stress in cradle section due to bending moment, Pa
P_{max} = maximum axial force (See Table 7-12.), N
A = cross-sectional area (See Table 7-14.), m^2
M_{max} = maximum bending moment (See Table 7-12.), N·m
Z_1 = section modulus on lower side of cradle (See Table 7-4.), m^3
σ = bending stress, Pa.

7-5.2.2 Stress Calculations for Section 2

At Section 2 the maximum bending moment and maximum axial stress both occur at 50 deg, Case 4. Therefore,

$$S_c = \frac{P_{max}}{A} = \frac{272{,}100}{0.0121} = 22.5 \text{ MPa}$$

$$S_b = \frac{M_{max}}{Z_1} = \frac{20{,}800}{0.00088} = 23.6 \text{ MPa}$$

$$\sigma = S_c + S_b = 46.1 \text{ MPa}.$$

7-5.2.3 Stress Calculations for Section 3

At Section 3 the maximum bending moment and maximum axial stress occur at 50 deg, Case 4. Therefore,

$$S_c = \frac{P_{max}}{A} = \frac{272{,}100}{0.0187} = 14.6 \text{ MPa}$$

$$S_b = \frac{M_{max}}{Z_1} = \frac{31{,}200}{0.00066} = 47.3 \text{ MPa}$$

$$\sigma = S_c + S_b = 61.9 \text{ MPa}.$$

7-5.2.4 Stress Calculations for Section 4

At Section 4 the maximum bending moment and maximum axial stress both occur at 50 deg, Case 4. Therefore,

$$S_c = \frac{P_{max}}{A} = \frac{215{,}500}{0.0187} = 11.5 \text{ MPa}$$

$$S_b = \frac{M_{max}}{Z_1} = \frac{22{,}400}{0.00066} = 33.9 \text{ MPa}$$

$$\sigma = S_c + S_b = 45.4 \text{ MPa}.$$

7-5.2.5 Stress Calculations for Section 5

At Section 5 the maximum bending moment and the maximum axial force occur at 50 deg, Case 4. Therefore,

THIS DOCUMENT PROVIDED BY THE ABBOTT AEROSPACE
TECHNICAL LIBRARY
ABBOTTAEROSPACE.COM

$$S_c = \frac{P_{max}}{A} = \frac{215{,}500}{0.0219} = 9.8 \text{ MPa}$$

$$S_b = \frac{M_{max}}{Z_1} = \frac{39{,}300}{0.00080} = 49.1 \text{ MPa}$$

$$\sigma = S_c + S_b = 58.9 \text{ MPa}.$$

The resultant stress value is obviously lower for $M = -1319$ N·m for the 75-deg elevation, Case 5.

7-5.2.6 Stress Calculations for Section 6

At Section 6 the maximum bending moment and the maximum axial load occur at 75 deg, Case 5. Therefore,

$$S_c = \frac{P_{max}}{A} = \frac{6033}{0.0219} = 0.28 \text{ MPa}$$

$$S_b = \frac{M_{max}}{Z_1} = \frac{33{,}080}{0.00080} = 41.4 \text{ MPa}$$

$$\sigma = S_c + S_b = 41.7 \text{ MPa}.$$

The stress value is lower when $M = 7970$ N·m is considered.

7-5.2.7 Stress Calculations for Section 7

At Section 7 the maximum bending moment occurs at 0 deg, Case 1, and the maximum axial force occurs at 75 deg, Case 5. Therefore,

$$S_c = \frac{P_{max}}{A} = \frac{6033}{0.0097} = 0.62 \text{ MPa}$$

$$S_b = \frac{M_{max}}{Z_1} = \frac{46{,}700}{0.00058} = 80.5 \text{ MPa}$$

$$\sigma = S_c + S_b = 81.1 \text{ MPa}.$$

The stress value is lower when $M = 37{,}700$ N·m is considered.

7-6 DESIGN FOR RIFLING TORQUE

The design data show that at 0.005196 s the cradle arms are subjected to the maximum torque produced by the rifling torque reaction on the guide assemblies shown in Fig. 7-27. The resulting torsional shear stress is maximum on the outside of the center fiber of each cradle arm. At this point the bending stresses are zero. The octahedral shear stress theory or von Mises' yield condition (Ref. 2) is used to combine the torsional shear stress with the uniform compressive stress produced by the axial component of the trunnion reaction. That is, Eq. 7-79 is used to calculate the effective stress, which should be less than the material yield stress for a safe design.

THIS DOCUMENT PROVIDED BY THE ABBOTT AEROSPACE
TECHNICAL LIBRARY
ABBOTTAEROSPACE.COM

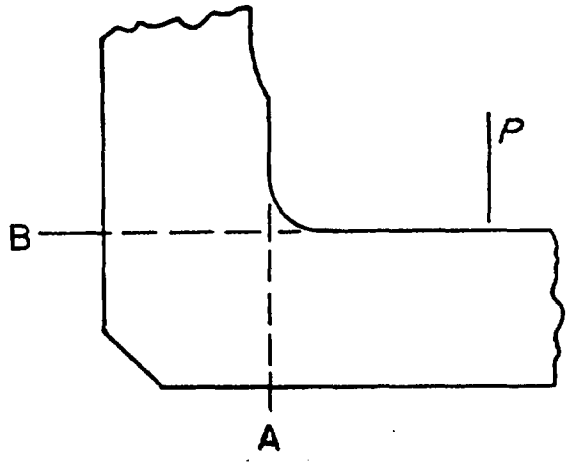

Figure 7-27. Torque Reaction on Guide Assembly

Note that beyond Section 3, the axial force (See Table 7-12.) producing uniform compressive stress is reduced by the elevating mechanism and the equilibrator reactions. Hence we shall consider the sections 0.127 m, 0.254 m, and 1.016 m as representative of the stress conditions. (The values given indicate distances from the trunnion.)

Design data are

Axial force $P = 146$ kN
Twist of rifling $N_r = 20$ cal/turn
Propellant gas force $F_g = 728$ kN
Bore radius $R_b = 0.077$ m
Distance between reactions on rails $d_r = 0.603$ m.

The rifling torque T_r is given by Eq. 7-11 as

$$T_r = \frac{0.6\pi^2 R_b^3 F_g}{N_r}, \text{ N·m.}$$

Therefore, based on the given data, $T_r = 983.5$ N·m. The force F_r' on the guides due to the rifling torque is

$$F_r' = \frac{T_r}{d_r}, \text{ N} \tag{7-86}$$

$$F_r' = \frac{983.5}{0.603} = 1631 \text{ N.}$$

The torque T on the cradle arm is

$$T = D_b F_r' \text{ , N·m} \tag{7-87}$$

where

D_b = bore diameter, m
$T = 2\,(0.077)(1631) = 252$ N·m.

THIS DOCUMENT PROVIDED BY THE ABBOTT AEROSPACE
TECHNICAL LIBRARY
ABBOTTAEROSPACE.COM

7-6.1 STRESSES AT SECTION 0.127 m

Design data are

Cross section width $b = 0.203$ m
Cross section height $h = 0.076$ m
Axial force $P = 146$ kN
Torque $T = 252$ N·m.

The shear stress τ is given by

$$\tau = \frac{T}{\alpha b h^2}, \text{ Pa} \tag{7-88}$$

where

$\alpha = f(b/h)$ for rectangular cross sections, dimensionless
$= f(0.203/0.076) = f(2.67) = 0.26$ (from Ref. 3).

Therefore, by Eq. 7-88

$$\tau = \frac{252}{(0.26)(0.203)(0.076)^2} = 0.83 \text{ MPa.}$$

The tensile stress σ is

$$\sigma = \frac{P}{A} = \frac{146 \times 10^3}{(0.203)(0.076)} = 9.5 \text{ MPa.}$$

Therefore, by Eq. 7-81 the effective stress σ_e is

$$\sigma_e = \sqrt{\sigma^2 + 3\tau^2} = [(9.5)^2 + 3(0.83)^2]^{1/2}$$

$$= 9.61 \text{ MPa.}$$

7-6.2 STRESSES AT SECTION 0.254 m

Design data are

$b = 0.203$ m
$h = 0.073$ m
$P = 146$ kN
$T = 252$ N·m.

Therefore, by Eq. 7-88

$$\tau = \frac{252}{(0.267)(0.203)(0.073)^2} = 0.87 \text{ MPa}$$

where

$\alpha = f(0.203/0.073) = f(2.78) = 0.267.$

The tensile stress σ is

$$\sigma = \frac{P}{A} = \frac{146 \times 10^3}{(0.203)(0.073)} = 9.9 \text{ MPa.}$$

THIS DOCUMENT PROVIDED BY THE ABBOTT AEROSPACE
TECHNICAL LIBRARY
ABBOTTAEROSPACE.COM

Therefore, by Eq. 7-79 the effective stress σ_e is

$$\sigma_e = \sqrt{\sigma^2 + 3\tau^2} = [(9.9)^2 + 3(0.87)^2]^{1/2} = 10 \text{ MPa.}$$

7-6.3 STRESSES AT SECTION 1.016 m

Design data are

$b = 0.203$ m
$h = 0.203$ m
$t = 0.0127$ m
$P = 146$ kN
$T = 252$ N·m.

Since a thin-walled section is now being considered, the shear stress τ is given by

$$\tau = \frac{T}{2bht}, \text{ Pa} \tag{7-89}$$

where

t = section thickness, m.

Therefore, by Eq. 7-89

$$\tau = \frac{252}{2(0.203)(0.203)(0.0127)} = 0.24 \text{ MPa.}$$

The tensile stress σ is

$$\sigma = \frac{P}{A} = \frac{146 \times 10^3}{(0.203)(0.203)} = 3.5 \text{ MPa.}$$

Therefore, the effective stress σ_e is by Eq. 7-79

$$\sigma_e = \sqrt{\sigma^2 + 3\tau^2} = [(3.5)^2 + 3(0.24)^2]^{1/2}$$

$$= 3.6 \text{ MPa.}$$

All stresses calculated are in the acceptable range, i.e., below the allowable stress of the material.

7-7 ADVANCED DESIGN TECHNIQUES

Although the methods of analysis and design discussed in previous paragraphs have been adequate in the past, they are inadequate for more realistic design of complex structures. The given methods provide a good tool for analysis and design by hand calculations during the preliminary design stage because simplified determinate structural models are adequate at the preliminary design stage. However, for many complex structures—such as the cradle—geometry, loading, and boundary conditions are quite complex and determinate models are inadequate. Therefore, refined structural models and analysis methods must be used for the final design. In this paragraph advanced design techniques for cradle structures are presented.

"Advanced design techniques" means that a refined model for the cradle structure is used to represent its geometry accurately. Also the boundary and loading conditions are specified so that they closely match the actual environment. This can be done using available stress analysis methods and computer software. A very

THIS DOCUMENT PROVIDED BY THE ABBOTT AEROSPACE
TECHNICAL LIBRARY
ABBOTTAEROSPACE.COM

powerful stress analysis technique, the finite element method, has been developed and tested over the last two decades, and many computer programs for stress analysis based on this method are available commercially. These programs are being widely used in the industry for the design of practical structural systems and should be used for the design of towed artillery systems. Discussion of use of the method for analysis and design of top and bottom carriage structures is presented in Chapters 8 and 9.

An introduction to the finite element method is given in Appendix B. Various terminologies used in the method, modeling concepts, and procedures are presented there. A designer who is not familiar with these ideas must review material given in Appendix B. Also an introduction to a commercially available computer program, NASTRAN, for stress analysis is given in Appendix B. This introduction should give the user an overview of the capabilities of the program and the type of data needed to use it.

7-7.1 FINITE ELEMENT MODEL

As noted in Appendix C, development of a finite element model for the structural system requires great care and understanding of the basic behavior of the structure. The designer should spend time and effort in modeling the system, i.e., he should investigate the possibility of using different finite elements to model the structure. A discussion of these aspects for the cradle structure of M198 towed Howitzer is presented in this paragraph.

The cradle is a three-dimensional structure with two planes of symmetry. The cradle arms are hollow, rectangular sections fabricated by welding plates. Several finite element models for the structure are possible. The simplest model is presented first and is followed by more complex models. The clip reactions are the only external forces acting on the cradle. The equilibrators and elevating struts provide the support points as do the trunnion bearings. Although the trunnion support can be well-approximated by a pin support, the equilibrator and elevating struts are more difficult to model. When the designs of equilibrators and elevating struts are known, they can be treated as elastic elements in the model.

The cradle is a long structural member subjected to bending and shear loads in two planes and torque about its longitudinal axis. This information suggests a possible use of general three-dimensional beam element to model the cradle. A simple beam finite element model for the cradle is shown in Fig. 7-28. This model is similar to the one used in par. 7-5 for stress analysis by hand calculations. As shown in Fig. 7-28, the model consists of 17 grid points and 13 beam finite elements. Since the cradle structure is symmetric and is loaded symmetrically, only one arm of the cradle need be analyzed. If the loading is unsymmetric, however, then the entire cradle structure should be included in the model. Since the curved portion of the structure constitutes a small fraction of the entire length, this portion is neglected in the model. Fig. 7-28 is essentially a two-dimensional model for the cradle. Grid point 1 corresponds to the trunnion support, and grid points 13 and 17 correspond to the points of attachment of the cradle to the equilibrator and elevating strut, respectively. At grid points 3 and 12 the clip reactions and the corresponding frictional forces and moments act. Note that the support points for the equilibrator and elevating strut are offset from the centerline of the cradle. Elements 14 and 15, which provide the points of support, are treated as rigid elements. This treatment ensures that the reaction forces are transmitted entirely to the centerline of the cradle. The equilibrator and elevating strut provide flexible support and hence can be modeled as spring elements, and their properties can be determined analytically if their constructional features are known or can be evaluated by using the test data. Since this is a two-dimensional model, each grid point has only three degrees of freedom—i.e., displacements in the x- and z-directions and rotation about the y-axis. Grid point 1 has one degree of freedom, and grid points 15 and 16 are totally restrained since they represent the other end of the equilibrator and elevating strut, respectively. Since the cross-sectional properties change rapidly along the length of the cradle, more finite elements may be introduced to obtain better results.

Model 2 is an improvement on the previous model and is shown in Fig. 7-29. The curved segment of the cradle is likely to cause some amount of torsional stresses in the structure. Grid point 12 is not a free joint but corresponds to the plane of symmetry. The curved segment between grid points 10 and 12 can be approximated by a series of straight three-dimensional beam elements. Grid point 12 has only one restrained degree of freedom along the y-axis. For this model each grid point has all six degrees of freedom. Grid point 1 has no displacement degree of freedom in the x-, y-, and z-directions. Grid points 15 and 16 are totally restrained. Since bending can now take place in two planes, more cross-sectional properties are required for this model—i.e., I_{xx}, I_{yy}, and I_{xy}—together with torsional and shear constraints.

The beam is a line-finite element with uniform cross-sectional properties. It is, therefore, incapable of modeling complex cross-sectional shapes and abrupt changes in the geometry. Also loads on the structure

THIS DOCUMENT PROVIDED BY THE ABBOTT AEROSPACE
TECHNICAL LIBRARY
ABBOTTAEROSPACE.COM

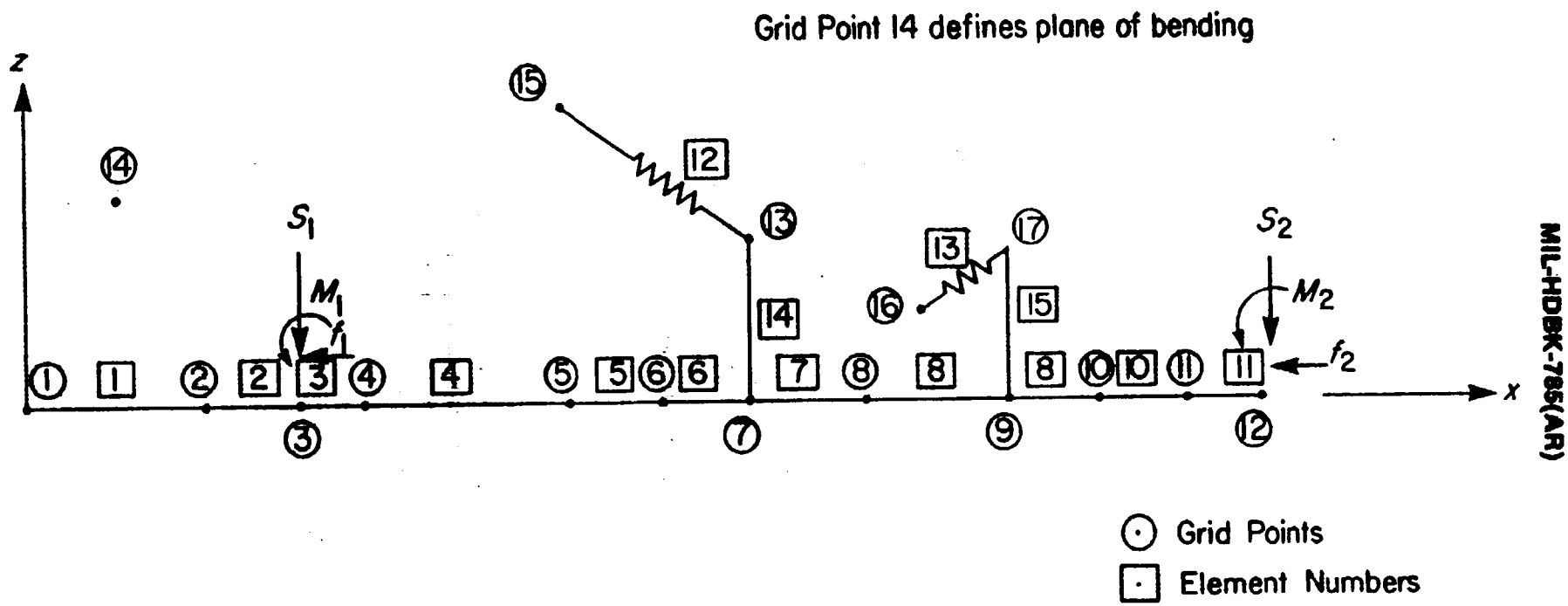

Figure 7-28. NASTRAN Model 1 for Cradle of M198

THIS DOCUMENT PROVIDED BY THE ABBOTT AEROSPACE
TECHNICAL LIBRARY
ABBOTTAEROSPACE.COM

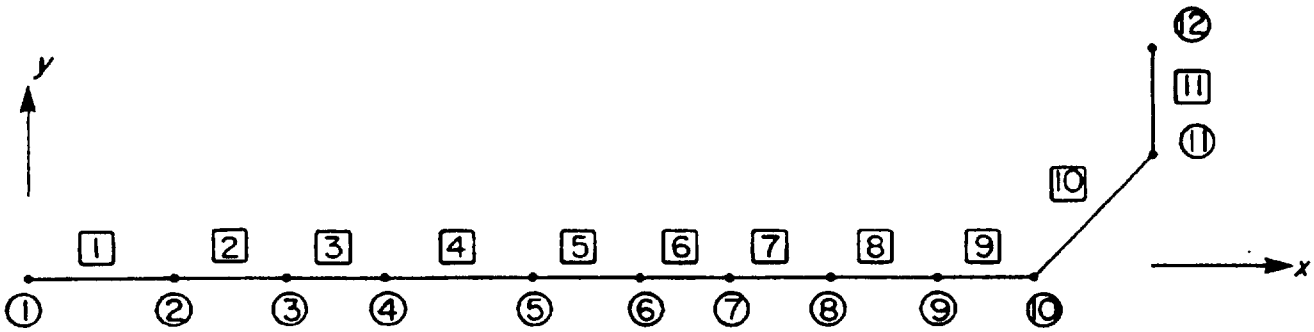

(A) Top View

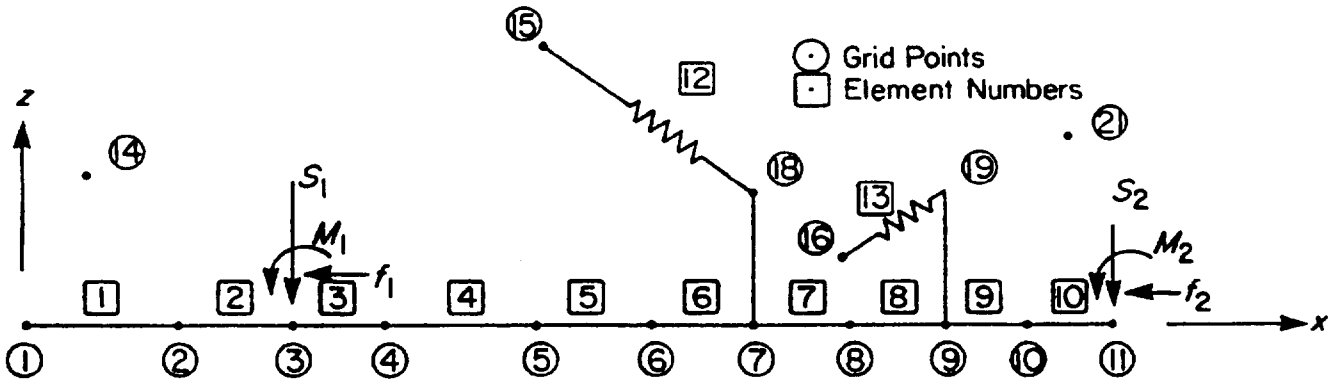

(B) Front View

Figure 7-29. NASTRAN Model 2 for Cradle of M198

cannot be represented very accurately. Model 3, shown in Fig. 7-30, is an improvement containing these features because the cradle structure is modeled by using flat plate-finite elements. The boundary conditions are the same as in the previous model, but they now correspond to different grid points. Also note that attachments of the equilibrators and elevating strut are no longer confined to one grid point lying in one plane. These connections can be made to represent the physical situation as closely as is possible.

There are certain advantages and disadvantages to the beam- and plate-finite element models for the cradle. In the beam-type finite element model, the number of grid points and finite elements is relatively small. However, for each finite element, the amount of data to be calculated by hand is quite large. For the plate-like finite element model, the number of grid points and finite elements is quite large, but the amount of data to be calculated by hand is quite small. Both models can yield satisfactory results. The plate-type finite element model, however, requires more computation effort, and it offers more flexibility with regard to subsequent changes in geometry of the structure or thickness of plate elements. For the beam-type model, any changes in geometry or addition of elements require calculations for new sectional properties.

The top carriage structure for the M198 towed Howitzer has construction that is similar to the cradle structure. Finite element models for the top carriage structure are discussed in par. 8-6. The finite element modeling discussion presented in par. 8-6 applies also to the cradle structure.

It should be noted that when the number of finite elements and grid points is increased for a model, better prediction of stresses is obtained. With more grid points and finite elements, however, the computational cost is increased. Thus this tradeoff between the size of the finite element model and the computational cost should be kept in mind.

THIS DOCUMENT PROVIDED BY THE ABBOTT AEROSPACE
TECHNICAL LIBRARY
ABBOTTAEROSPACE.COM

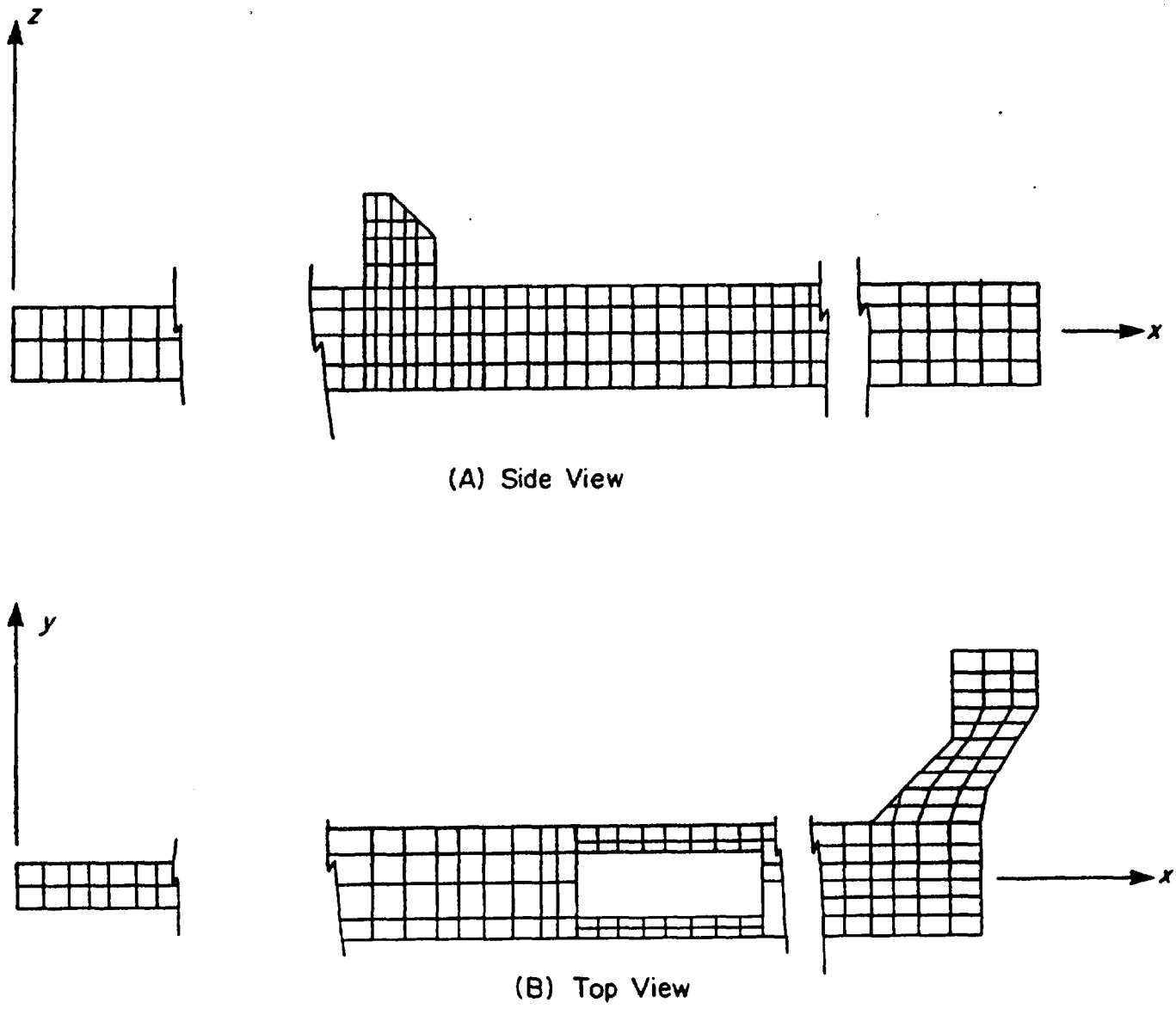

Figure 7-30. NASTRAN Model 3

7-7.2 NASTRAN STRESS ANALYSIS

Stress analysis for the finite element model shown in Fig. 7-28 (Model 1) was carried out using the NASTRAN computer code. (Refer to Appendix B for an introduction to NASTRAN.) The equilibrator and elevating strut were treated as elastic spring elements. NASTRAN analysis results were quite close to the results obtained using the hand calculations in par. 7-5.2. This closeness is quite reasonable because similar assumptions are used in both procedures.

The plate-type finite element model for the cradle is not subjected to NASTRAN stress analysis; however, this model is similar to the plate-type finite element model for the top carriage structure. The plate-finite element model for the top carriage structure was analyzed using NASTRAN. The result obtained for the top carriage structure is presented in par. 8-6. The discussion presented in par. 8-6 also applies to the plate-type model for the cradle structure.

THIS DOCUMENT PROVIDED BY THE ABBOTT AEROSPACE
TECHNICAL LIBRARY
ABBOTTAEROSPACE.COM

REFERENCES

1. DOD-HDBK-778(AR), *Recoil Systems*, July 1988.
2. A. C. Ugural and S. K. Fenster, *Advanced Strength of Materials and Applied Elasticity*, American Elsevier, New York, NY, 1975.
3. R. J. Roark, *Formulas for Stress and Strain*, McGraw-Hill Book Co., New York, NY, 1975.
4. J. W. Frantz and M. C. Nerdahl, *Mathematical Models for Engineering Analysis and Design of Howitzers, Medium, Towed, 155-mm, XM198*, RE-TR-70-186 and its supplement, Artillery Systems Laboratory, US Army Weapons Command, Rock Island, IL, October 1970.
5. C. M. Robinder and D. E. Hebdon, Jr., *Stress Analysis of 155-mm Towed Howitzer, XM198, Serial Numbers 3 through 10—Cradle*, SWERR-R-TN-1-73, US Army Weapons Command, Rock Island, IL, January 1973.

THIS DOCUMENT PROVIDED BY THE ABBOTT AEROSPACE
TECHNICAL LIBRARY
ABBOTTAEROSPACE.COM

CHAPTER 8
TOP CARRIAGE DESIGN

This chapter presents design procedures for the top carriage structure of towed artillery systems. Functions of the top carriage structure and the equipment associated with it are described. For preliminary design of the structure, simplified and statically determinate models are used. Usually, the mechanics of the deformable bodies approach can be used at the preliminary design stage, and this approach is illustrated. For final design of the structure, more realistic models that are usually statically indeterminate are used. Here the finite element method coupled with computer simulations can be used as a fast and reliable design tool. Stress analysis for the structure is performed using a computer program, and results of computer simulations are presented and discussed.

8-0 LIST OF SYMBOLS

A = area of cross section, m^2
A' = area of section above point q (hatched area in Fig. 8-8), m^2
a = moment arm from section to point of lifting force along y-axis, m
b = moment arm from section to point of lifting force along x-axis, m
= width of section measured through q, m
c = moment arm from section to point of equilibrator force along y-axis, m
d = moment arm from section to point of equilibrator force along x-axis, m
= depth of section, m
e = moment arm from section to point of trunnion force along y-axis, m
F = lifting force, N
F = force vector, N
F_A = trunnion reaction parallel to bore centerline (CL), N
F_E = equilibrator force, N
F_{E_x} = component of equilibrator force parallel to x-axis, N
F_{E_y} = component of equilibrator force parallel to y-axis, N
F_F = sum of equilibrator and trunnion forces along the y-axis, N
F_G = force, N
F_N = trunnion reaction perpendicular to bore centerline (CL), N
F_T = trunnion force, N
F_z = force in elevating strut, N
F_X = component of trunnion force along x-axis, N
F_Y = component of trunnion force along y-axis, N
F_x = component of lifting force along x-axis (forward), N
F_y = component of lifting force along y-axis (up), N
F_z = component of lifting force along z-axis (sideways), N
F_1, F_2, F_3 = components of lifting force for Segment 1, Sections 1 and 2 along the x-, z-, and y-coordinate axes, respectively, N
F_4, F_5, F_6 = components of lifting force for Segment 2, Sections 3 through 9 along x-, z-, and y-coordinate axes, respectively, N
F_7, F_8, F_9 = components of lifting force for Segment 3, Sections 10 through 20 along the x-, z-, and y-coordinate axes, respectively, N
F_{1A}-F_{9A} = F_1 through F_9 under Condition A, N
F_{1B}-F_{9B} = F_1 through F_9 under Condition B, N

THIS DOCUMENT PROVIDED BY THE ABBOTT AEROSPACE
TECHNICAL LIBRARY
ABBOTTAEROSPACE.COM

f = moment arm from section to point of trunnion force along x-axis, m
I_z = moment of inertia of cross section about z-axis, m^4
i,j,k = unit vectors along x-, y-, and z-axes, respectively, m
M = moment vector, N·m
M_B = moment transmitted through traverse bearing to bottom carriage, N·m
M_E = moment due to equilibrator force, N·m
M_G = moment, N·m
M_T = moment due to trunnion forces, N·m
M_x = moment about x-axis due to lifting force, N·m
M_y = moment about y-axis due to lifting force, N·m
M_z = moment about z-axis due to lifting force, N·m
r = vector from point of application of force to point about which moment is taken, m
r = moment arm, m
S_1,S_2,S_3,S_4 = stresses at points 1, 2, 3, and 4, respectively, for a section, Pa
$S_{1E},S_{2E},S_{3E},S_{4E}$ = stresses at points 1, 2, 3, and 4, respectively, for a section due to equilibrator forces only, Pa
$S_{1L},S_{2L},S_{3L},S_{4L}$ = stresses at points 1, 2, 3, and 4, respectively, for a section due to lifting force only, Pa
$S_{1ET},S_{2ET},S_{3ET},S_{4ET}$ = stresses at points 1, 2, 3, and 4, respectively, for a section due to equilibrator and trunnion forces combined, Pa
$S_{1LE},S_{2LE},S_{3LE},S_{4LE}$ = stresses at points 1, 2, 3, and 4, respectively, for a section due to lifting force and equilibrator force combined, Pa
T_{cy} = vertical reaction from traverse bearing, N
T_{cx} = horizontal reaction from traverse bearing, N
t_1 = wall thickness at P, m
t_2 = wall thickness at Q, m
V_x = vertical shear force along x-direction at section containing point q, N
w = width of section, m
$\bar{x}$ = distance from neutral axis to centroid of A', m
Z_{1x} = section modulus about x-axis at point 1, m^3
Z_{2x} = section modulus about x-axis at point 2, m^3
Z_{1z} = section modulus about z-axis at point 1, m^3
Z_{2z} = section modulus about z-axis at point 2, m^3
α = lifting angle in xz-plane, deg
β = lifting angle in xy-plane, deg
$\gamma + \theta$ = angle between bore centerline and horizontal, deg
$\gamma + \theta - \lambda$ = angle between equilibrator and horizontal, deg
$\gamma + \theta - \lambda - \phi_i$ = angle between equilibrator force and any x-axis, deg
$\gamma + \theta - \phi_3$ = angle between bore centerline and Segment 3 x-axis, deg
θ = angle between gun cradle and horizontal, deg
τ = shear stress, Pa
τ_P = torsional shearing stress at point P, Pa
τ_Q = torsional shearing stress at point Q, Pa
ϕ_i = angle between plane of any Section i and horizontal, deg
ϕ_1 = angle between plane of Sections 1 and 2 and horizontal, deg
ϕ_2 = angle between plane of Sections 3-9 and horizontal, deg
ϕ_3 = angle between plane of Sections 10-20 and horizontal, deg

THIS DOCUMENT PROVIDED BY THE ABBOTT AEROSPACE
TECHNICAL LIBRARY
ABBOTTAEROSPACE.COM

8-1 INTRODUCTION

The top carriage is a primary supporting structure of the weapon. It supports the tipping parts through trunnion bearings, transmits all firing loads from the cradle to the bottom carriage or other supporting structures, anchors the equilibrators, and houses the elevating and the traversing mechanisms and the power units needed for these mechanisms. In traverse the top carriage moves with the cradle.

As indicated in Chapter 2, design of the top carriage structure is an iterative process. An estimate of the weight and size of the top carriage structure is the starting point. Once preliminary sizes of other components have been determined, system dynamic models are used to determine maximum loads transmitted to the top carriage. (Refer to par. 3-1 for system dynamic models and load determination.) Once the loads carried by the top carriage structure are known, detailed stress analysis of the structure can be carried out. The designer then decides whether further changes in various parts of the structure are warranted. If no changes are necessary, a final design has been achieved; otherwise, necessary changes are made, and the design process is repeated. Usually a few iterations will be required to reach a final design. This design process is discussed in this chapter. As an example of top carriage design, the M198 towed Howitzer is considered. Stress analysis for the structure is initially performed by using a traditional mechanics of materials approach. Since most of the calculations are carried out using desk calculators, simplifying assumptions are made regarding the geometry and support conditions for the structure. Usually, determinate structural models are used to carry out the stress analysis by hand; more recently, however, finite element techniques have been used for stress analysis of complex structural systems. These techniques allow a designer to model accurately complex geometries and support conditions for the structure, and the techniques permit stresses in the structure to be predicted more precisely. A general description of the finite element technique is given in Appendix C, and use of the finite element technique for top carriage structures also is illustrated in this chapter.

Par. 8-2 describes various equipment—such as the equilibrator, the traversing and elevating mechanisms, the trunnion bearings, and the traverse bearing—associated with the top carriage. The top carriage and its functions are described in par. 8-3. A detailed description of the stress analysis for the trunnion arms of the top carriage that is performed by using a basic mechanics of materials approach is presented in pars. 8-4 and 8-5. The finite element approach, performed by using the NASTRAN computer program, is presented in par. 8-6.

8-2 EQUIPMENT ASSOCIATED WITH TOP CARRIAGE

8-2.1 EQUILIBRATORS

An equilibrator is a force-producing mechanism of a weapon that counterbalances the weight of the tipping parts about the weapon trunnions. The equilibrators are more directly associated with the cradle, but the terminals of the equilibrators on the top carriage are considered to be parts of the top carriage. The terminals are fixed structures bolted or welded to the side frames, and each holds the pin or bearing about which the equilibrator pivots. Design of equilibrators is presented in Chapter 5.

8-2.2 ELEVATING MECHANISMS

The long range of projectiles and missiles requires precise aiming to assure a reasonable degree of accuracy. Handwheel or power-operated mechanisms are provided to enable gunners to attain precise position in elevation and azimuth and to hold these positions during firing. Two types of elevating mechanisms are described in Chapter 4—the ball-screw type and the pinion-and-arc type. In the case of the pinion-and-arc arrangement, the top carriage houses all components of the elevating mechanism except for the elevating arc, which is attached to the cradle. These components include the pinion, the rest of the elevating gear train, the handwheel, and a power unit if it is necessary. In recent weapon developments two struts have been used in the elevating mechanism. In this arrangement the base of the strut is attached to the top carriage, and the top of the strut is attached to the side of the cradle. Other arrangements of struts are possible as shown in Figs. 2-15 and 2-16. Design of elevating mechanisms is presented in Chapter 4.

8-2.3 TRAVERSING MECHANISMS

The traversing mechanism rotates the traversing parts, which generally consist of cannon and other tipping parts, and the top carriage. Like the elevating mechanism, it consists essentially of gear trains or linkages with one terminal at the power source and the other on the traversing part. Manual and power operated form the two general types of traversing mechanisms. Design of the traversing mechanism is presented in Chapter 4.

THIS DOCUMENT PROVIDED BY THE ABBOTT AEROSPACE
TECHNICAL LIBRARY
ABBOTTAEROSPACE.COM

8-2.4 TRUNNION BEARINGS

The trunnion bearings provide low-friction rotating elements that are essential during elevation. They also transmit firing loads from the cradle to the top carriage. The design of trunnion bearings is presented in Chapter 6.

8-2.5 TRAVERSE BEARINGS

The traverse bearing provides a low-friction means for rotating the traversing parts. The traverse bearing incorporates both radial and thrust features. The radial component supports the weapon laterally through its pintle or stanchion, whereas the axial component supports the weapon weight. Firing loads are transmitted through the bearing to the bottom carriage. The radial unit transmits the horizontal components of the loads, and the axial unit transmits the vertical components of the loads. The design of traverse bearings is presented in Chapter 6.

8-3 DESCRIPTION OF TOP CARRIAGE

The top carriage is the primary supporting structure of the weapon. Just as a rigid cradle is a requisite, a rigid top carriage also is needed to extend the base required for firm control. The functions of the top carriage are to

1. Support the tipping parts through the trunnion bearings
2. Transmit all firing loads from the cradle to the bottom carriage or other supporting structures
3. Anchor the equilibrators
4. House the elevating and traversing mechanisms and the power units, if needed, for these mechanisms.

In this paragraph top carriage structures for towed weapon systems are described, and materials for their fabrication are discussed.

8-3.1 TYPES OF TOP CARRIAGES

There are two types of top carriages: single recoil and double recoil. Double recoil top carriages are not used in modern weapons; consequently, they are not discussed in this handbook.

The top carriage structure for a single-recoil weapon can vary. Fig. 8-1 shows the top carriage structure for some older weapons; Fig. 8-2 shows the top carriage structure for a modern M198 towed Howitzer. The top carriage is a simple structure, consisting basically of two side frames supported by a base structure, and is generally supported by a bottom carriage or equivalent structure. It has no motion other than traversing. Whatever complexity the structure ultimately acquires is due primarily to the provision of convenient and adequate attachments for the mechanisms that it supports.

The top carriage structure for M198 is a hollow box construction fabricated by welding thin plates. Various holes and attachments are introduced for the purpose of anchoring the equilibrators, the elevating mechanism, and the trunnion bearings. Trunnion bearings, equilibrators, and parts of the elevating and traversing mechanisms are assembled to the side frames. For the sake of symmetry, a unit of two components such as trunnion bearings or twin equilibrators is used—each unit is attached to each side of the frame. If large loads are involved and a unit of one component is desired, it should be centrally located. This applies to a single equilibrator and to the elevating pinion, and each is attached to the top carriage by a shaft spanning the side frames. However, if a worm and worm gear segment replace the pinion and elevating gear, the worm is usually mounted on the base structure. The side frames provide a similar arrangement for the traversing mechanism.

The base structure, aside from supporting the side frames, supports the traverse bearing, which turns about the pintle. The pintle fits in the bearing and transmits the horizontal force of the top carriage to the bottom carriage. The base structure also transmits the thrust, or vertical load, from the top carriage to the bottom carriage. The lower surface of the base structure has a flat ring or racer that provides the required smooth bearing surface. This bearing surface may be machined directly on the top carriage or it may be a separate piece bolted to the base.

8-3.2 CONSTRUCTION AND MANUFACTURING PROCEDURES

Top carriages are usually made of steel or an aluminum alloy, but other materials should not be excluded if they have the required physical properties. Castings may be used if weight is not a critical factor. Top carriages can have large fillets and thus eliminate harmful stress concentrations at sharp corners. Forgings should be used if high strength-to-weight ratios are needed, but weldments make reliable structures and are probably the least expensive. The built-up (welded) unit is relatively simple and light, and the joints are permanent and more

THIS DOCUMENT PROVIDED BY THE ABBOTT AEROSPACE
TECHNICAL LIBRARY
ABBOTTAEROSPACE.COM

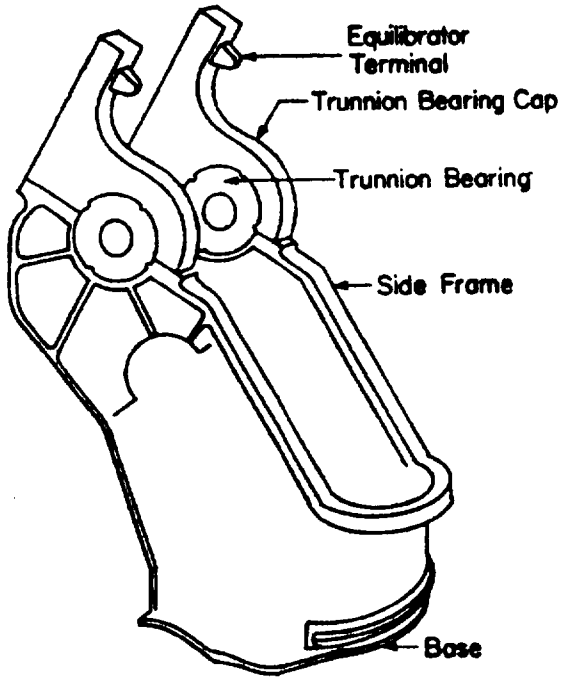

Figure 8-1. Typical Top Carriage Structure

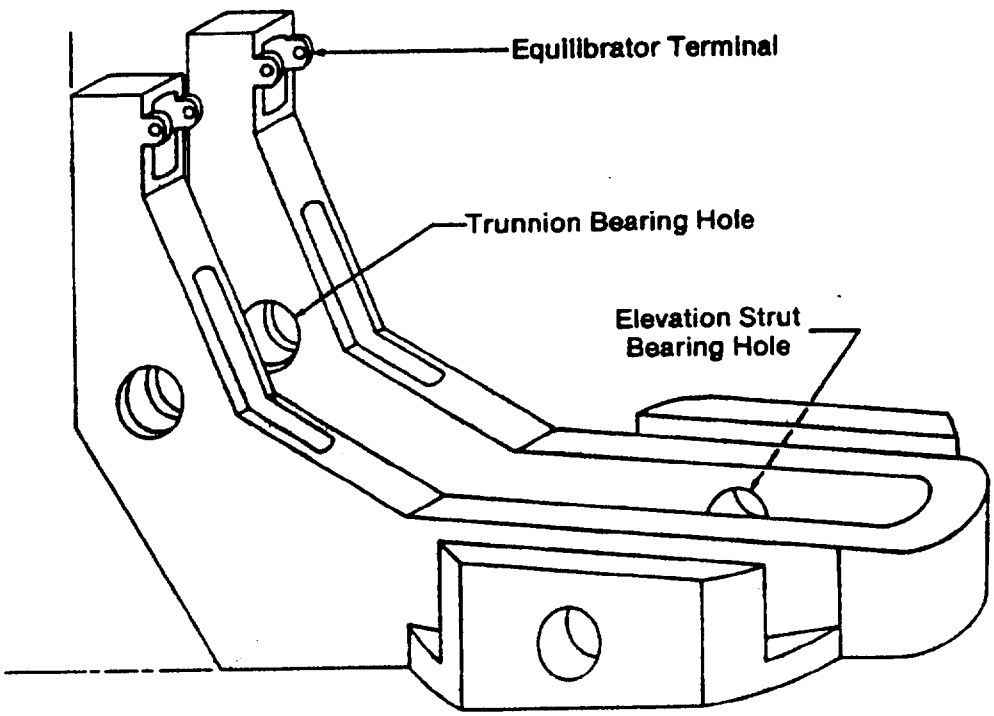

Figure 8-2. Top Carriage Structure for M198 Towed Howitzer

THIS DOCUMENT PROVIDED BY THE ABBOTT AEROSPACE
TECHNICAL LIBRARY
ABBOTTAEROSPACE.COM

rigid than if they were bolted or riveted. Weldments can be made from available stock, and construction takes only a short time; these are reasons for the low cost. Combined castings and mill stock also can be used to make weldments. Although forgings and castings are not as susceptible to warpage as weldments, all should be stress relieved by heat treatment to insure dimensional stability.

Fittings and brackets for attaching equipment should be located near flanges and stiffeners. Local reinforcements at these fittings will carry and distribute the loads to the rigid structural members. For strength and efficiency, welded joints are recommended between fitting and carriage if disassembly is not essential. Additional reinforcements should be made where necessary to provide the torsional strength that is needed to support unsymmetrical loads during transport.

Regardless of the method of construction, the side frames of the top carriage are rigidly attached to the base structure. The base structure supports the traverse bearing. The racer of the bearing may be either integral with the base structure or, as a separate part, may be bolted to it. In some top carriages the base structure is replaced by a pintle housing that extends to the side frames. All sliding surfaces usually have a surface finish of 32 microinch, root mean square (rms). The top carriage for the M198 towed Howitzer is an aluminum alloy weldment. The cross section at any point is essentially a hollow, rectangular box.

Attachment fittings may be a part of the general structure or fastened to it by some mechanical means. For example, the top of the side frames may be machined into the trunnion bearing housing, or they may be made into seats for the housing. Trunnion caps are bolted and keyed to the housings. Some structures have elongated caps to provide attachment lugs on the inner side of each side frame.

Although special equipment may be required, top carriages are manufactured by standard shop practices. Special equipment, such as heat treating and machining equipment capable of handling bulky and irregular structures, might be required. Such special equipment is necessary for structures that may warp during fabrication. The stress relieving of a properly restrained and supported structure, however, will eliminate warpage to a large degree. Furthermore, if a structural member must have a finished surface, the practice of making it oversize is recommended. Then, those minor irregularities present after heat treatment can be removed when the member is being machined to size.

8-3.3 MATERIALS FOR TOP CARRIAGES

The structures of the top carriage have four requisites pertaining to physical properties, namely, strength, rigidity, weldability, and light weight. No material that meets these requirements should be excluded, but steel and aluminum are obvious candidates because each has advantages. Steel has a high modulus of elasticity and can have very high strength, but steels of moderate strength are apt to be more appropriate because the resulting bulk is needed for rigidity. Because steel is sufficiently hard to impede scoring and is compatible with bronze to impede galling, it makes a good sliding surface. Aluminum alloys, having all the essential requirements, also are excellent structural materials. The strengths of aluminium alloys match those of moderate strength steels, and the aluminum alloys weigh only one-third as much. Their modulus of elasticity is also lower; consequently, aluminum alloys have one-third the rigidity of similar steel structures. Added bulk increases the rigidity of the aluminum alloy but at the expense of increased weight, although the weight may still be less than a comparable steel structure. Aluminum is a notoriously poor sliding material, but this deficiency can be overcome by covering its sliding surfaces with good bearing materials, such as steel or hard bearing bronze. The designer must weigh the relative merits of all suitable materials and select the one that will result in the most efficient design.

8-4 PRELIMINARY DESIGN OF TOP CARRIAGE

As noted in Chapter 2, design of components of a weapon system is an iterative process requiring interaction among various weapon design teams. At the preliminary design stage, the designer needs to estimate the weight of the top carriage. This is needed in the system dynamic analysis for load determination and for estimating the weight of the weapon system. Current state of the art requires that the weight of the top carriage be estimated based on historical data for existing weapon systems and the designer's experience. Better mathematical models, however, must be developed in the future to predict accurately the weight of the top carriage structure.

This paragraph describes considerations in the design of the top carriage together with load analysis. Methods for calculating stresses, based on fundamental concepts of mechanics of deformable bodies, are presented. These methods are used in later paragraphs to illustrate their use in actual design.

Functional requirements, rigidity, and strength are three predominant design criteria for any component.

THIS DOCUMENT PROVIDED BY THE ABBOTT AEROSPACE
TECHNICAL LIBRARY
ABBOTTAEROSPACE.COM

Rigidity is needed to insure good weapon accuracy, particularly if fire control equipment is mounted on the side frames. Although strength and rigidity usually go hand in hand, the structure may be too flexible, and a means must be devised for providing the necessary stiffness. For strength, the top carriage must carry the applied forces of recoil and transport. The functional requirements involve little more than deciding on the type of top carriage and selecting the best suited locations for the equipment and secondary structures.

There are four interdependent design factors—recoil force, forces during transportation, length of recoil, and trunnion height. Any of these may be used as a starting point. For example, assume that the maximum height is given for a weapon in the horizontal firing position. This establishes the trunnion height, which, together with the maximum angle of elevation, determines the recoil stroke. If longer recoil distances are desired, a pit must be dug for the necessary ground clearance. In present mobile mount design, however, this practice is discouraged. In another approach, the recoil distance may be selected, and the recoil force and trunnion height determined.

The structure should be designed for simplicity, symmetry, and compactness, and these qualities depend somewhat on each other. A simple structure is easy to fabricate and is usually a light and efficient one. A symmetrical structure also tends to maintain simplicity because (1) the load will be distributed more uniformly and (2) eccentric loads that lead to heavy reinforcements are avoided. A compact structure is likely to reduce weight. In other words, every effort should be made to find favorable locations for all structural members and equipment.

The top carriage should be compact and yet have room for various structural units and operating equipment. Clearance is the major criterion, although ease of maintenance also should be considered when locating this equipment. Ground clearance determines the trunnion height, and the required clearance for the recoiling parts determines the space between the side frames. The problem now is to fit the operating units where they can function most effectively and where clearances will be ample either in this space or on the outer sides of the top carriage. These operating units include the equilibrator, the elevating unit, the traversing unit, and loading devices. One favorable feature of the equilibrator is that if its geometry is maintained, it can occupy any position on the carriage without losing its effectiveness provided no interference exists between it and other units of the structure. On the other hand, the elevating and traversing units, if possible, should be located between the side frames near the elevating arc and traversing gear. Handwheels are located near each other where they are readily accessible and easily operated, and power units should be located near their respective gears. Loading devices are attached to the rear of the side frames within easy access of the breech. Additional human factors that should be considered in the design are described in Chapter 11.

The designer should be aware that the weapon he is creating can be manufactured in a relatively short time, but its activity in the field can extend through many years. While in use the weapon will be serviced and repaired often, many times under the stress of time and weather. It must be capable of ready, partial disassembly in the field to remove malfunctioning controls, gear boxes, or shafts with a minimum of time and effort. Any necessity for removing serviceable items to reach the source of trouble not only wastes time and effort but also imposes additional problems of weather protection and realignment of these items. Assembly during manufacture is relatively easy due to sequential bench operations and readily available handling equipment. While the weapon system is in the design stage, consideration must be given to both the orderly shop assembly program as well as to the field operation where only the damaged subassembly need be removed from the top carriage. Design for maintainability is considered further in Chapter 10.

8-4.1 LOAD ANALYSIS

Before a detailed stress analysis of the top carriage structure can be performed, it is necessary to determine the loads applied to the structure at various points. The loads to be determined for the top carriage are the firing loads, ground and air transportation loads, airdrop loads, equilibrator load, and elevating gear or elevating strut loads. Equilibrator loads are determined from the design of equilibrators as explained in Chapter 5. The load from the elevating mechanism attachment is determined from the design of the elevating mechanism as explained in Chapter 4.

To determine loads transmitted to the top carriage structure due to firing, transportation, and airdrop, one needs a dynamic model for the weapons system. A dynamic model for the system cannot be developed, however, unless the designer has estimated weights and sizes of various components. This is referred to as the preliminary design phase. During this phase historical data and the designer's past experience become extremely important in estimating preliminary sizes of various components. Preliminary design of a towed weapon is discussed in Chapter 2. Once a preliminary model for the system has been developed, dynamic

THIS DOCUMENT PROVIDED BY THE ABBOTT AEROSPACE
TECHNICAL LIBRARY
ABBOTTAEROSPACE.COM

analysis of the system is performed for various previously mentioned loading conditions. From the result of a dynamic analysis, reactions at various joints of the structure can be determined. Maximum joint forces then become design loads for the relevant components. This process of dynamic analysis and determination of loads for various components is presented in detail in Chapter 3.

The number of loading conditions for which the top carriage and other components have to be designed can be quite large. For example, there are as many firing conditions as there are angles of elevation. The ground transportation conditions include normal travel, braking, and the 30% side slope. Air transportation conditions may include airlift by helicopters or transportation by large cargo planes. The loads imposed during counterrecoil must also be considered. If stress and other design calculations are to be done using desk calculators, the problem of analyzing each and every load can be a very tedious and time-consuming task. Thus the designer has to select a few critical loading conditions judiciously and analyze the design for only those conditions. For example, firing loads are generally considered for maximum, minimum, and some intermediate angle of elevation. Also, since 30% side slope conditions involve only low transport speeds, this loading condition may not be critical.

Generally, the loads determined from the preceding analysis are multiplied by load factors because the load factor is the desired factor of safety. Load factors of 1.5 to 5 have been used in design.

8-4.2 STRESS ANALYSIS

After all external loads have been determined, it is necessary to determine stresses at various points of the structure for specific loading cases. Due to complex geometry and support conditions of the top carriage, accurate stress analysis can be quite difficult. In the past simplified models for the top carriage have been used to calculate stresses at various points. More sophisticated computer programs, however, are now available and can be used to account for complex geometry and support conditions to provide a more accurate stress analysis. These computer programs are based on modern finite element methods. The finite element method of stress analysis is described in Appendix C, and an introduction to a well developed and widely used computer code for stress analysis is presented in Appendix B. These computer-based methods for stress analysis have considerable potential to aid the weapon designer and may be used even at the preliminary design stage. The finite element method for the top carriage is described in par. 8-6.

In this paragraph stress analysis of the top carriage structure that uses the basic mechanics of materials approach is described. This type of analysis has been used in the past for the design of weapons and is intended primarily for hand calculations using desk or small calculators. The basic idea of this approach is to use statically determinate models since equations of equilibrium are adequate to determine all the unknown forces. A free-body diagram for the component is developed, and moments, shearing forces, and torques acting at various sections are determined. By the use of these forces and moments, stresses can be calculated.

The designer needs to develop a free-body diagram for the top carriage before he can calculate stresses at various points of the structure. To develop this free-body diagram, the designer needs to know points of application and direction of various forces, support conditions, and geometry of the top carriage. The geometry of the top carriage is determined through the preliminary design procedures. The weight of the top carriage, center of gravity, and cross-sectional properties are then calculated. Equilibrator attachment points and the type of traversing and elevating mechanisms also are known from the preliminary design data. Knowing this information, the designer can develop a free-body diagram for the top carriage of the system. Since a statically determinate model has been assumed, equations of equilibrium are sufficient to solve for the unknown reactions or other forces.

Once various forces and moments at a section are known, a basic mechanics of materials approach is used to calculate bending stresses, torsional shear stresses, shear stresses due to lateral loads, and direct stresses due to axial loads (Ref. 1). These stresses are then appropriately combined to check for the failure of the section. Details of this procedure are presented in par. 8-5.

8-5 SAMPLE TOP CARRIAGE DESIGN PROBLEM

In this paragraph stress analysis for the top carriage structure of the M198 towed Howitzer is presented. The top carriage structure for the weapon is an aluminum weldment, and the overall geometry of the structure is shown in Fig. 8-2. The cross section of each side frame of the top carriage is primarily a hollow, rectangular box. This example is taken from Ref. 2, in which a basic mechanics of materials approach has been used to carry out stress calculations primarily in longhand.

A free-body diagram of the top carriage structure for the M198 towed Howitzer is given in Fig. 8-3. All of the

THIS DOCUMENT PROVIDED BY THE ABBOTT AEROSPACE
TECHNICAL LIBRARY
ABBOTTAEROSPACE.COM

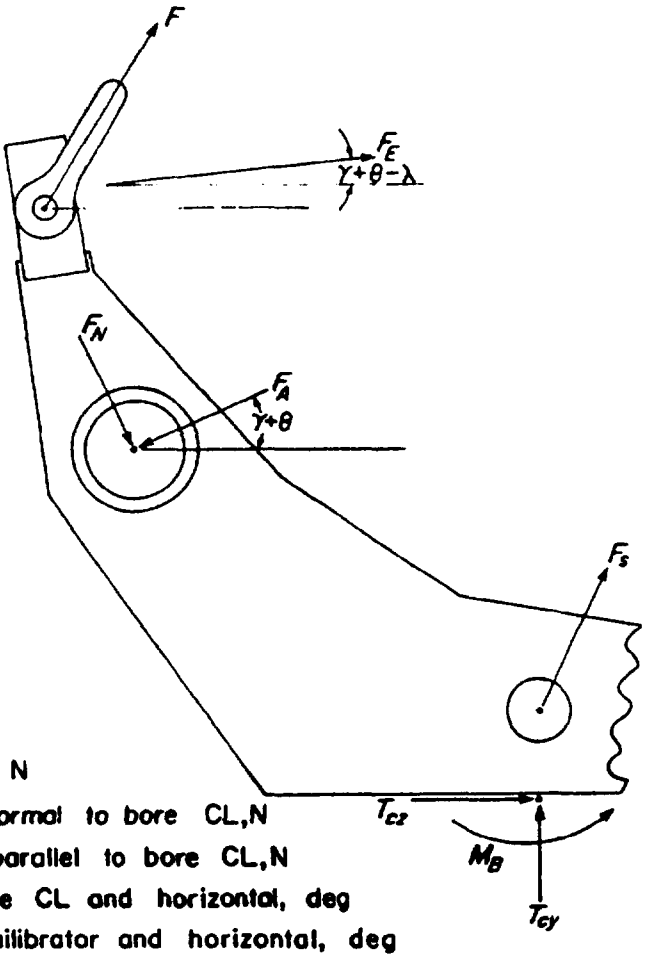

F = lifting force, N
F_E = equilibrator force, N
F_N = trunnion reaction normal to bore CL, N
F_A = trunnion reaction parallel to bore CL, N
$\gamma+\theta$ = angle between bore CL and horizontal, deg
$\gamma+\theta-\lambda$ = angle between equilibrator and horizontal, deg
F_s = force in elevating strut, N
T_{cz} = horizontal reaction from traverse bearing, N
T_{cy} = vertical reaction from traverse bearing, N
M_B = moment transmitted through traverse bearing to bottom carriage, N·m

Figure 8-3. Free-Body Diagram of Top Carriage (Ref. 2)

forces in Fig. 8-3 act in one plane, the firing plane of the weapon, except for the lifting force F. The top carriage is subjected to a force F during airlift of the weapon. Direction of this force depends on lifting conditions, and in general, this force is not in the same plane as the other forces. The lifting force is constant, whereas the other forces vary with the angle of elevation and time. Time, however, is generally not taken as a variable in the design of the system. The time history of the various forces is calculated using the dynamic model for the system. (Refer to par. 3-3.) Despite the fact that the maximum values of all the forces do not occur at the same time, maximum values are used in design because this is the most conservative approach.

For the purpose of calculating stresses, the top carriage structure is divided into three segments, i.e.,

1. The top segment, or head, where the equilibrator is attached, and lugs for airlift are provided
2. The structure between the top head and the trunnion bearing
3. The structure between the trunnion bearing and the base.

Stresses are calculated at several sections in each segment. In order to perform stress calculations, each side of the top carriage structure is treated as a cantilever beam subjected to general loads, and to facilitate analysis of this beam, a separate coordinate system is used for each of the three segments of the structure. Sections for stress calculation and the coordinate systems are shown in Fig. 8-4. In all, there are 20 sections for which stresses are checked. The distance for various sections is measured independently for each segment and measured along the centroidal axis for the segment. Moment arms are shown in Fig. 8-5.

THIS DOCUMENT PROVIDED BY THE ABBOTT AEROSPACE
TECHNICAL LIBRARY
ABBOTTAEROSPACE.COM

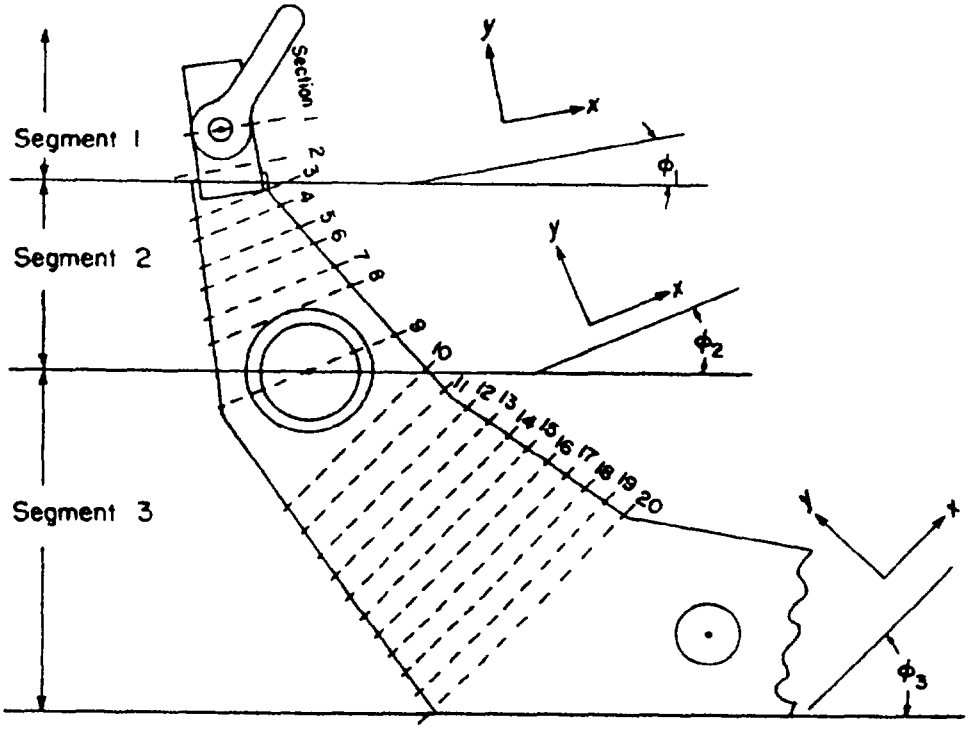

ϕ_1 = angle between plane of Sections 1 and 2 and horizontal, deg
ϕ_2 = angle between plane of Sections 3–9 and horizontal, deg
ϕ_3 = angle between plane of Sections 10–20 and horizontal, deg

Figure 8-4. Segments and Sections for Load Analysis (Ref. 2)

All loads are not applied simultaneously to the top carriage. There are four loading cases for the top carriage of the M198 for which stress analysis is carried out (Ref. 2). The designer should examine all possible load combinations for a weapon system and carry out stress calculations for the most critical few cases. The four cases for the present example are

1. *Case 1. Lifting Force Only.* The force due to airlifting of the weapon is known. Moments, shearing forces, and axial forces due to this lift force are calculated at any section of the top carriage structure. Bending, shearing, and axial stresses are then calculated at any point of a section.
2. *Case 2. Equilibrator Force Only.* Since the equilibrator force F_E is a planar force, there is only one moment component in the firing plane due to this force.
3. *Case 3. Lifting and Equilibrator Forces Combined.* This loading case occurs during airlift of the weapon. Stresses for this case are obtained by combining stresses for Cases 1 and 2.
4. *Case 4. Equilibrator and Trunnion Forces Combined.* The trunnion forces also cause a moment about the z-axis since these forces lie in the xy-plane. This loading case occurs during firing of the weapon at various angles of elevation, during airdrop, and during ground transportation. For the present example, however, stress calculations are presented only for firing conditions. Five firing elevation angles — 0 deg, 35 deg, 45 deg, 50 deg, and 75 deg—are considered. Stress calculations for other cases are carried out in a similar fashion.

There are other loading conditions that the designer should analyze. These are loads during elevation of the weapon, loads during traversing of the weapon, and loads during various transportation conditions. Stress analysis for these loading conditions is carried out in a manner similar to the one presented here.

THIS DOCUMENT PROVIDED BY THE ABBOTT AEROSPACE
TECHNICAL LIBRARY
ABBOTTAEROSPACE.COM

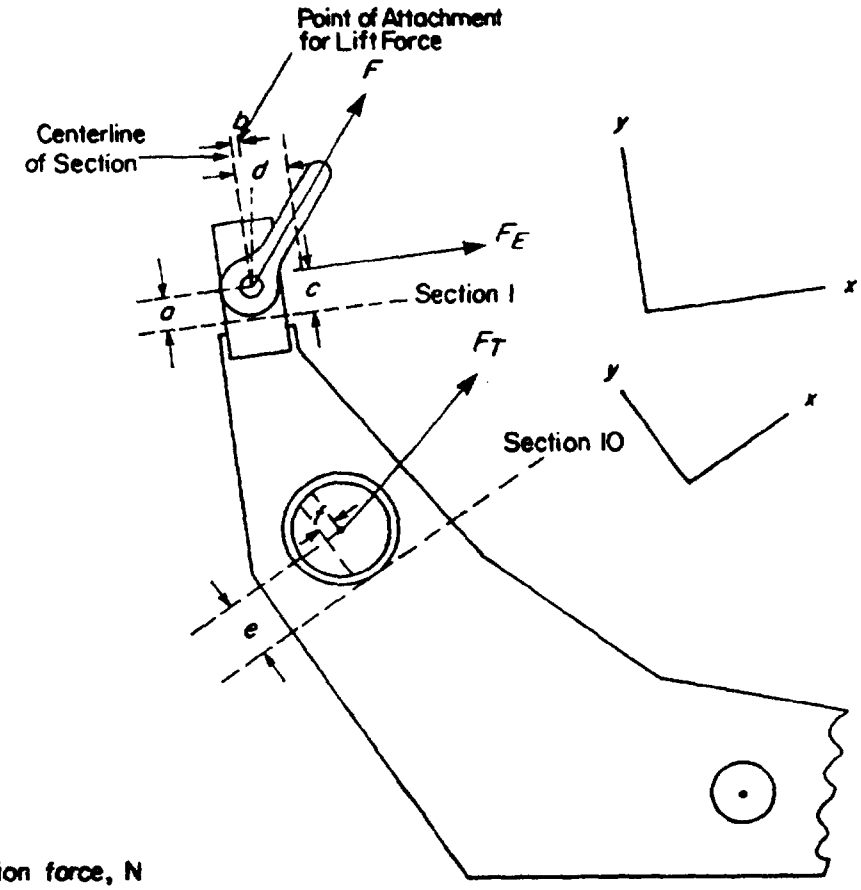

F_T = trunnion force, N
a = moment arm from section to point of lifting force along y-axis, m
b = moment arm from section to point of lifting force along x-axis, m
c = moment arm from section to point of equilibrator force along y-axis, m
d = moment arm from section to point of equilibrator force along x-axis, m
e = moment arm from section to point of trunnion force along y-axis, m
f = moment arm from section to point of trunnion force along x-axis, m

Figure 8-5. Moment Arms (Ref. 2)

8-5.1 LOAD ANALYSIS

In this paragraph loads that are used in stress analysis of the top carriage for the M198 are summarized. These loads are taken from Ref. 2.

8-5.1.1 Lifting Load

The lifting lug is made of round steel stock bent in the shape of an upside-down U. It straddles the top of the trunnion and is pinned to it.

The force on the top carriage during airlift of the weapon is calculated as

1. Estimated total weight of the weapon	66,720 N
2. Add 40% for airlift	93,408 N
3. Use a factor of safety of 5	467,040 N
4. Divide the load evenly among 4 lugs	116,760 N.

The load during airlift of the weapon for one side of the top carriage structure is then taken as 116,760 N.

The lifting force must be resolved into components along x-, y-, and z-directions. There are two severe conditions of airlift, and both must be analyzed. These two conditions of airlift differ in lifting angles in the xz- and xy-planes as described later. Fig. 8-6 shows the lifting force and its components along the x-, y-, and z-coordinate directions.

THIS DOCUMENT PROVIDED BY THE ABBOTT AEROSPACE
TECHNICAL LIBRARY
ABBOTTAEROSPACE.COM

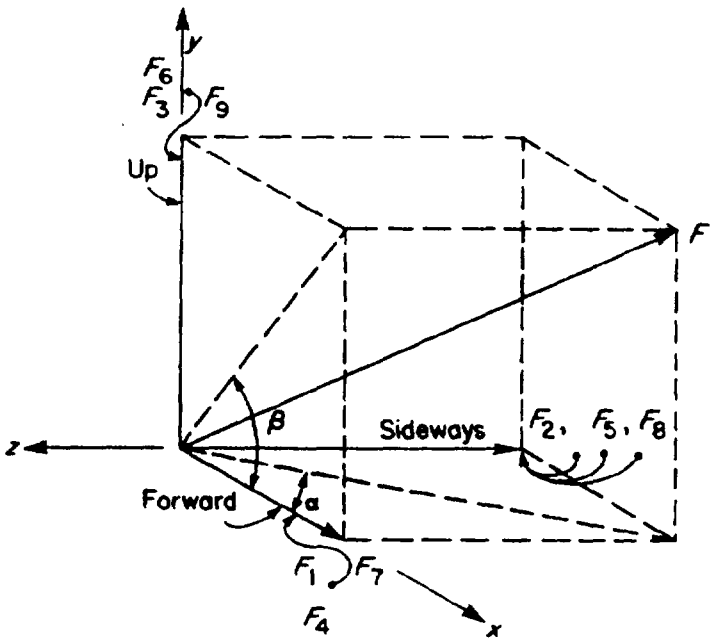

α = lifting angle in xz-plane, deg
β = lifting angle in xy-plane, deg
F_1, F_2, F_3 = components of lifting force for Segment 1, Sections 1 and 2, along x-, z-, and y-coordinates, respectively, N
F_4, F_5, F_6 = components of lifting force for Segment 2, Sections 3 through 9, along x-, z-, and y-coordinates, respectively, N
F_7, F_8, F_9 = components of lifting force for Segment 3, Sections 10 through 20, along x-, z-, and y- coordinates, respectively, N

Figure 8-6. Components of Lifting Force F in Lifting Lug Parallel and Perpendicular to Sections

The lifting force components for various segments of the top carriage are calculated by

$$F_x = \sqrt{\frac{F^2}{1 + \tan^2\alpha + \tan^2\beta}}, \text{ N} \tag{8-1}$$

$$F_y = F_x \tan\beta, \text{ N} \tag{8-2}$$

$$F_z = F_x \tan\alpha, \text{ N} \tag{8-3}$$

where

F_x = component of lifting force along x-axis (forward), N
F_y = component of lifting force along y-axis (up), N
F_z = component of lifting force along z-axis (sideways), N
F = lifting force, N.

Calculations for each segment are shown in the paragraphs that follow. Subscripts A and B on forces F_1 to F_9 indicate loading conditions A and B, respectively.

THIS DOCUMENT PROVIDED BY THE ABBOTT AEROSPACE
TECHNICAL LIBRARY
ABBOTTAEROSPACE.COM

1. *Segment 1, Sections 1 and 2:*

Given:

$F = 116{,}760$ N

Condition *A*:

$\alpha = 6$ deg, $\beta = 71.75$ deg

Condition *B*:

$\alpha = 8$ deg, $\beta = 69.75$ deg.

Substitution in Eqs. 8-1, 8-2, 8-3 gives

$$F_{1A} = \sqrt{\frac{(116{,}760)^2}{1 + \tan^2 6° + \tan^2 71.75°}}$$

$$= 36{,}545 \text{ N}$$

$$F_{2A} = F_{1A}\tan\alpha$$

$$= 36{,}545\tan 6°$$

$$= 3841 \text{ N}$$

$$F_{3A} = F_{1A}\tan\beta$$

$$= 36{,}545\tan 71.75°$$

$$= 110{,}826 \text{ N}.$$

Similarly,

$$F_{1B} = 40{,}365 \text{ N}$$

$$F_{2B} = 5673 \text{ N}$$

$$F_{3B} = 109{,}414 \text{ N}.$$

2. *Segment 2, Sections 3 through 9:*

Given:

$F = 116{,}760$ N

Condition *A*:

$\alpha = 6$ deg, $\beta = 58.80$ deg

Condition *B*:

$\alpha = 8$ deg, $\beta = 56.80$ deg.

THIS DOCUMENT PROVIDED BY THE ABBOTT AEROSPACE
TECHNICAL LIBRARY
ABBOTTAEROSPACE.COM

Substitution in Eqs. 8-1, 8-2, 8-3 gives

$$F_{4A} = 60{,}395 \text{ N}$$

$$F_{5A} = 6348 \text{ N}$$

$$F_{6A} = 99{,}725 \text{ N}$$

$$F_{4B} = 63{,}745 \text{ N}$$

$$F_{5B} = 8959 \text{ N}$$

$$F_{6B} = 97{,}412 \text{ N.}$$

3. *Segment 3, Sections 10 through 20:*

Given:
$F = 116{,}760$ N

Condition *A*:
$\alpha = 6$ deg, $\beta = 31$ deg

Condition *B*:
$\alpha = 8$ deg, $\beta = 29$ deg.

Substitution in Eqs. 8-1, 8-2, 8-3 gives

$$F_{7A} = 99{,}679 \text{ N}$$

$$F_{8A} = 10{,}477 \text{ N}$$

$$F_{9A} = 59{,}893 \text{ N}$$

$$F_{7B} = 101{,}358 \text{ N}$$

$$F_{8B} = 14{,}245 \text{ N}$$

$$F_{9B} = 56{,}184 \text{ N.}$$

8-5.1.2 Equilibrator Load

The equilibrator load, like the lifting load, must be resolved into components along the x- and y-axes of each section. These components are calculated by

$$F_{E_x} = F_E \cos(\gamma + \theta - \lambda - \phi_i), \text{ N} \tag{8-4}$$

$$F_{E_y} = F_E \sin(\gamma + \theta - \lambda - \phi_i), \text{ N} \tag{8-5}$$

where

F_{E_x} = component of equilibrator force parallel to x-axis, N
F_{E_y} = component of equilibrator force parallel to y-axis, N
$\gamma + \theta - \lambda - \phi_i$ = angle between equilibrator force and any x-axis, deg.

THIS DOCUMENT PROVIDED BY THE ABBOTT AEROSPACE
TECHNICAL LIBRARY
ABBOTTAEROSPACE.COM

Components of the equilibrator force for all sections are given in Table 8-1. Sample calculations for Segment 1, Sections 1 and 2, at minimum elevation are provided.

From Table 8-1

1. $\phi_1 = 8.25$ deg
2. $\gamma + \theta - \lambda - \phi_1 = -8.25$ deg
3. $F_E = 73{,}395$ N.

Substitution in Eqs. 8-4 and 8-5 gives

$$F_{E_x} = 73{,}395\cos(-8.25°)$$

$$= 72{,}635 \text{ N}$$

$$F_{E_y} = 73{,}395\sin(-8.25°)$$

$$= -10{,}532 \text{ N}$$

as shown in Table 8-1.

8-5.1.3 Trunnion Load

The trunnion loads must also be resolved into components along the x- and y-axes of each section. The trunnion loads act only on Segment 3, Sections 10 through 20. These components are calculated by

$$F_X = F_A\cos(\gamma + \theta - \phi_3) + F_N\sin(\gamma + \theta - \phi_3) \tag{8-6}$$

$$F_Y = F_A\sin(\gamma + \theta - \phi_3) - F_N\cos(\gamma + \theta - \phi_3) \tag{8-7}$$

where

F_X = component of trunnion force along x-axis, N
F_Y = component of trunnion force along y-axis, N
$\gamma + \theta - \phi_3$ = angle between bore centerline and Segment 3 x-axis, deg.

TABLE 8-1
ANALYSIS OF EQUILIBRATOR AND TRUNNION LOADS FOR SELECTED FIRING ANGLES (Ref. 2)

Section	$\gamma+\theta$, deg	$\gamma+\theta-\lambda$, deg	ϕ_n, deg	$\gamma+\theta-\phi_n$, deg	$\gamma+\theta-\lambda-\phi_n$, deg	F_E, N	F_{E_x}, N	F_{E_y}, N	F_N, N	F_A, N	F_X, N	F_Y, N
	–	0	8.25	−8.25	−8.25	73.395	72.635	−10.532				
1	0	10.97	8.25	−8.25	2.72	82.848	82.754	3.932				
	35	23.61	8.25	26.75	15.36	63.725	61.447	16.881				
and	45	35.15	8.25	36.75	26.90	59.993	53.503	27.143				
	50	41.35	8.25	41.75	33.10	58.271	48.815	31.822				
2	75	75.57	8.25	66.75	67.32	53.165	20.497	49.055				
	–	0	21.2	−21.2	−21.2	71.838	68.427	−26.542				
3	0	10.97	21.2	−21.2	−10.23	82.848	81.531	−14.715				
	35	23.61	21.2	13.8	2.41	63.725	63.667	2.678				
to	45	35.15	21.2	23.8	13.95	59.993	58.222	14.461				
	50	41.35	21.2	28.8	20.15	58.271	54.704	20.075				
9	75	75.57	21.2	53.8	54.37	53.165	30.973	43.214				
	–	0	49.3	−49.3	−49.3	71.838	47.863	−55.643				
10	0	10.97	49.3	−49.3	−38.33	82.848	64.988	−51.381	26.578	−224.203	−166.354	152.644
	35	23.61	49.3	−14.3	−25.69	63.725	57.426	−27.623	21.431	−206.205	−205.111	30.163
to	45	35.15	49.3	−4.3	−14.15	59.993	58.174	−14.666	24.452	−209.675	−210.916	−8.661
	50	41.35	49.3	0.7	−7.95	58.271	57.711	−8.060	37.565	−277.118	−276.638	−40.946
20	75	75.57	49.3	25.7	26.27	53.165	47.676	23.531	31.920	−275.770	−234.648	−148.353

THIS DOCUMENT PROVIDED BY THE ABBOTT AEROSPACE
TECHNICAL LIBRARY
ABBOTTAEROSPACE.COM

Values of F_X and F_Y for all sections, 10 through 20, are given in Table 8-1. Sample calculations for Segment 3, Sections 10 through 20, at 75-deg elevation are provided.

From Table 8-1

1. $\gamma + \theta = 75$ deg
2. $\phi_3 = 49.3$ deg
3. $\gamma + \theta - \phi_3 = 25.7$ deg
4. $F_A = -275{,}770$ N
5. $F_N = 31{,}920$ N.

Substitution in Eqs. 8-6 and 8-7 gives

$$F_X = (-275{,}770)\cos 25.7° + 31{,}920\sin 25.7° = -234{,}648 \text{ N}$$

$$F_Y = (-275{,}770)\sin 25.7° - 31{,}920\cos 25.7° = -148{,}353 \text{ N}$$

as shown in Table 8-1.

8-5.2 STRESS ANALYSIS

To calculate stresses at various sections, it is necessary to calculate moments and forces at these sections. Moments M_G are calculated by the general equation

$$M_G = F_G r, \text{ N·m} \tag{8-8}$$

where

F_G = force, N
r = moment arm, m.

Values for moment arms are given in Table 8-2.

8-5.2.1 Case 1. Lifting Force Only

Moments and force components for all sections due to the lifting force for Conditions *A* and *B* are given in Table 8-3. Sample calculations for Section 1, Condition *A*, are provided in this paragraph.

From par. 8-5.1.1

$F_{1A} = 36{,}545$ N
$F_{2A} = 3841$ N
$F_{3A} = 110{,}823$ N.

From Table 8-2 the values of moment arms a and b are

$a = 0.01905$ m
$b = 0.00767$ m.

The moment M_x about the x-axis due to the lifting force F is

$$\begin{aligned} M_x &= F_{2A}a \\ &= 3841 \times 0.01905 \\ &= 73.2 \text{ N·m.} \end{aligned}$$

The moment M_y about the y-axis due to the lifting force F is

$$\begin{aligned} M_y &= -F_{2A}b \\ &= -3841 \times 0.00767 \\ &= -29.5 \text{ N·m.} \end{aligned}$$

THIS DOCUMENT PROVIDED BY THE ABBOTT AEROSPACE
TECHNICAL LIBRARY
ABBOTTAEROSPACE.COM

TABLE 8-2
MOMENT ARMS* TO ALL SECTIONS (Ref. 2)

Section	a, m	b, m	c, m	d, m	e, m	f, m
1	0.01905	0.00767	0.06782	0.1491		
2	0.0993	0.0339	0.1481	0.1753		
3	0.1265	0.0501	0.1422	0.1996		
4	0.1984	0.03937	0.2141	0.1890		
5	0.2238	0.03937	0.2395	0.1890		
6	0.2631	0.02362	0.2789	0.1732		
7	0.3150	0.03937	0.3307	0.1890		
8	0.4084	0.03937	0.4242	0.1890		
9	0.5105	0.01207	0.5263	0.1618		
10	0.5649	0.2710	0.5080	0.4112	0.1016	0.05486
11	0.6157	0.2725	0.5588	0.4128	0.1524	0.05639
12	0.6665	0.3231	0.6096	0.4633	0.2032	0.1069
13	0.7173	0.3239	0.6604	0.4641	0.2540	0.1077
14	0.7681	0.3292	0.7112	0.4694	0.3048	0.1130
15	0.8189	0.2949	0.7620	0.4351	0.3556	0.07874
16	0.8697	0.3099	0.8128	0.4501	0.4064	0.09373
17	0.9205	0.3132	0.8636	0.4534	0.4572	0.09703
18	0.9713	0.3167	0.9144	0.4569	0.5080	0.1006
19	1.0221	0.3769	0.9652	0.5171	0.5588	0.1608
20	1.0516	0.3640	0.9947	0.5042	0.5883	0.1478

*a and b are moment arms—along y- and x-axes, respectively—due to lifting force.
c and d are moment arms—along y- and x-axes, respectively—due to equilibrator force.
e and f are moment arms—along y- and x-axes, respectively—due to firing force on trunnions.

The moment M_z about the z-axis due to the lifting force F is

$$M_z = F_{1A}a - F_{3A}b$$
$$= 36{,}545 \times 0.01905 - 110{,}830 \times 0.00767$$
$$= -154 \text{ N·m.}$$

It is sometimes convenient to use the vector cross product approach and write the moment vector M at a point as

$$M = r \times F, \text{ N·m}$$

where

r = vector from the point of application of force to point about which moment is being taken, m
F = force vector, N.

As an example, the moment vector and force vector for Section 1, Condition A, are defined as follows:

$$r = -bi - aj = -0.00767i - 0.01905j, \text{ m}$$

THIS DOCUMENT PROVIDED BY THE ABBOTT AEROSPACE
TECHNICAL LIBRARY
ABBOTTAEROSPACE.COM

TABLE 8-3
MOMENTS AND NORMAL FORCES CREATED ON ALL SECTIONS BY LIFTING FORCE *F* FOR LOADING CONDITIONS *A* AND *B* (Ref. 2)

Segment	Section	Load Condition *A*			Load Condition *B*		
		M_x, N·m	M_z, N·m	F_y, N	M_x, N·m	M_z, N·m	F_y, N
	1	73.2	−154	110,830	108	−70	109,416
1	2	382	−123	110,830	563	304	109,416
	3	803	2,641	99,853	1,134	3,183	97,625
	4	1,259	8,051	99,853	1,779	8,814	97,625
	5	1,421	9,585	99,853	2,007	10,435	97,625
2	6	1,671	13,536	99,853	2,360	14,485	97,625
	7	1,999	15,093	99,853	2,825	16,254	97,625
	8	2,593	20,739	99,853	3,663	22,218	97,625
	9	3,241	29,633	99,853	4,579	31,400	97,625
	10	5,941	40,221	60,101	8,099	42,300	56,539
	11	6,475	45,212	60,101	8,828	47,396	56,539
	12	7,009	47,256	60,101	9,556	49,720	56,539
	13	7,543	52,292	60,101	10,285	54,859	56,539
	14	8,078	57,053	60,101	11,013	59,740	56,539
3	15	8,612	64,196	60,101	11,741	66,861	56,539
	16	9,146	68,378	60,101	12,470	71,196	56,539
	17	9,680	73,261	60,101	13,198	76,191	56,539
	18	10,215	78,129	60,101	13,926	81,172	56,539
	19	10,749	79,593	60,101	14,655	82,951	56,539
	20	11,059	83,319	60,101	15,077	86,689	56,539

$$F = F_{1A}i + F_{3A}j + F_{2A}k = 36{,}545i + 110{,}823j - 3841k, \text{ N}.$$

Therefore, the moments M_x, M_y, and M_z for Section 1 are calculated from these definitions by use of the matrix form of the cross product as

$$M = \begin{bmatrix} i & j & k \\ -0.00767 & -0.01905 & 0 \\ 36{,}545 & 110{,}823 & -3841 \end{bmatrix}$$

$$= +73.2i - 29.5j - 154k, \quad \text{N·m}.$$

Thus the x-, y-, and z-components of the moment vector are 73.2 N·m, −29.5 N·m, and −154 N·m, respectively, as previously calculated.

Fig. 8-7 shows a typical cross section of the frame for the top carriage of the M198. It is possible to calculate the stresses at various points of the cross section by using the data given in Table 8-3. Stresses are calculated at

THIS DOCUMENT PROVIDED BY THE ABBOTT AEROSPACE
TECHNICAL LIBRARY
ABBOTTAEROSPACE.COM

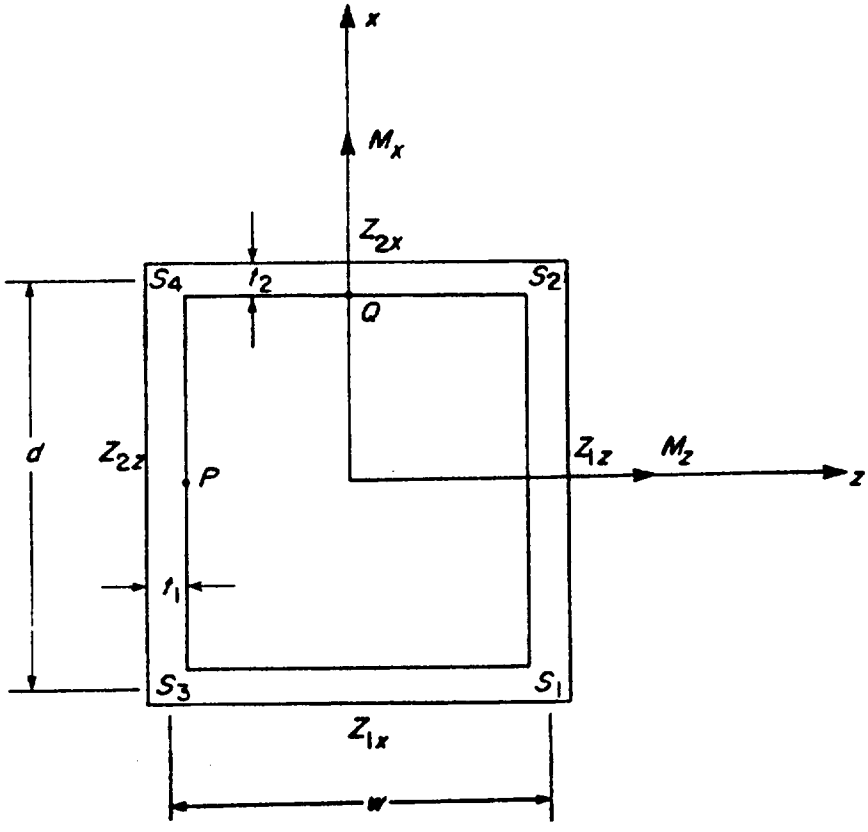

M_x = moment about x-axis due to lifting force, N·m
M_z = moment about z-axis due to lifting force, N·m
Z_{1x} = section modulus about x-axis at point 1, m^3
Z_{2x} = section modulus about x-axis at point 2, m^3
Z_{1z} = section modulus about z-axis at point 1, m^3
Z_{2z} = section modulus about z-axis at point 2, m^3

Figure 8-7. Cross Section of Side Frame of Top Carriage for M198

the four corners due to bending in two planes and the direct force in the y-direction. Expressions for these stress calculations are

$$S_{1L} = \frac{M_z}{Z_{1x}} + \frac{M_x}{Z_{1z}} + \frac{F_y}{A}, \text{ Pa} \tag{8-9}$$

$$S_{2L} = -\frac{M_z}{Z_{2x}} + \frac{M_x}{Z_{1z}} + \frac{F_y}{A}, \text{ Pa} \tag{8-10}$$

$$S_{3L} = \frac{M_z}{Z_{1x}} - \frac{M_x}{Z_{2z}} + \frac{F_y}{A}, \text{ Pa} \tag{8-11}$$

$$S_{4L} = -\frac{M_z}{Z_{2x}} - \frac{M_x}{Z_{2z}} + \frac{F_y}{A}, \text{ Pa} \tag{8-12}$$

THIS DOCUMENT PROVIDED BY THE ABBOTT AEROSPACE
TECHNICAL LIBRARY
ABBOTTAEROSPACE.COM

where

$S_{1L}, S_{2L},$
S_{3L}, S_{4L} = stresses at points 1, 2, 3, and 4, respectively, for a section due to lifting force only, Pa
Z_{1x} = section modulus about x-axis at point 1, m^3
Z_{2x} = section modulus about x-axis at point 2, m^3
Z_{1z} = section modulus about z-axis at point 1, m^3
Z_{2z} = section modulus about z-axis at point 2, m^3
A = area of cross section, m^2.

Stresses for lifting conditions *A* and *B* are given in Table 8-4. Sample calculations for Section 1 follow.
From Table 8-3

$M_x = 73.2$ N·m
$M_z = -154$ N·m
$F_y = 110{,}830$ N.

From Ref. 2

$Z_{1x} = 6.84 \times 10^{-4}$ m^3
$Z_{2x} = 7.26 \times 10^{-4}$ m^3
$Z_{1z} = 9.07 \times 10^{-4}$ m^3

TABLE 8-4
MAXIMUM TENSILE (+) AND COMPRESSIVE (−) STRESSES IN ALL SECTIONS OF TRUNNION ARMS CREATED BY LIFTING FORCE ALONE (Ref. 2)

Section	Load Condition *A*				Load Condition *B*			
	S_{1L}, MPa	S_{2L}, MPa	S_{3L}, MPa	S_{4L}, MPa	S_{1L}, MPa	S_{2L}, MPa	S_{3L}, MPa	S_{4L}, MPa
1	7.55	7.99	7.41	7.85	7.60	7.80	7.36	7.56
2	10.36	10.81	9.32	9.76	11.10	10.0	9.55	8.45
3	13.66	4.42	11.51	2.28	14.77	3.64	11.74	0.612
4	31.85	1.88	26.48	−3.48	34.06	1.25	26.48	−6.32
5	33.56	−0.06	27.72	−5.90	35.95	−0.654	27.69	−8.912
6	48.91	−17.76	43.05	−23.61	52.47	−18.87	44.20	−27.15
7	36.49	−10.60	30.24	−16.86	39.38	−11.34	30.54	−20.18
8	38.24	−13.47	31.01	−20.70	41.38	−14.02	31.17	−24.24
9	37.55	−9.354	29.48	−17.42	40.73	−8.970	29.33	−20.37
10	40.78	−14.54	31.83	−23.49	44.00	−14.18	31.79	−26.39
11	48.75	−15.98	36.44	−28.29	52.68	−15.17	35.90	−31.95
12	62.78	−38.51	41.66	−59.63	68.72	−37.85	39.92	−66.65
13	64.36	−38.86	40.82	−62.39	70.38	−37.90	38.29	−69.99
14	64.31	−40.99	41.37	−63.93	70.36	−39.89	39.09	−71.16
15	59.56	−22.92	37.89	−44.58	65.06	−20.84	35.52	−50.38
16	58.90	−32.52	39.28	−52.14	64.14	−31.05	37.39	−57.80
17	55.91	−30.42	35.77	−50.56	61.06	−28.72	33.60	−56.18
18	51.52	−26.62	30.87	−47.27	56.54	−24.64	28.39	−52.79
19	27.95	−18.84	10.78	−36.01	31.65	−17.12	8.245	−40.53
20	33.28	−21.42	14.13	−40.57	37.46	−19.46	11.35	−45.56

THIS DOCUMENT PROVIDED BY THE ABBOTT AEROSPACE
TECHNICAL LIBRARY
ABBOTTAEROSPACE.COM

$Z_{2x} = 12.0\times10^{-4}$ m^3
$A = 1.44\times10^{-2}$ m^2.

Substitution in Eqs. 8-9 through 8-12 gives

$$S_{1L} = \frac{-154}{6.84\times10^{-4}} + \frac{73.2}{9.07\times10^{-4}} + \frac{110{,}830}{1.44\times10^{-2}} = 7.55 \text{ MPa}$$

$$S_{2L} = -\frac{-154}{7.26\times10^{-4}} + \frac{73.2}{9.07\times10^{-4}} + \frac{110{,}830}{1.44\times10^{-2}} = 7.99 \text{ MPa}$$

$$S_{3L} = \frac{-154}{6.84\times10^{-4}} - \frac{73.2}{12.0\times10^{-4}} + \frac{110{,}830}{1.44\times10^{-2}} = 7.41 \text{ MPa}$$

$$S_{4L} = -\frac{-154}{7.26\times10^{-4}} - \frac{73.2}{12.0\times10^{-4}} + \frac{110{,}830}{1.44\times10^{-2}} = 7.85 \text{ MPa.}$$

The twisting moment M_y produces shearing stress in a section. This shearing stress is calculated using the theory of torsion of thin-walled sections (Ref. 1). Accordingly, torsional shearing stresses at points P and Q of Fig. 8-7 are given as

$$\tau_P = \frac{M_y}{2dwt_1}, \text{ Pa} \qquad (8\text{-}13)$$

$$\tau_Q = \frac{M_y}{2dwt_2}, \text{ Pa} \qquad (8\text{-}14)$$

where

τ_P = torsional shearing stress at point P, Pa
τ_Q = torsional shearing stress at point Q, Pa
d = depth of section, m
w = width of section, m
t_1 = wall thickness at P, m
t_2 = wall thickness at Q, m.

Note that in Eqs. 8-13 and 8-14 dw represents the rectangular area using centerline-to-centerline dimensions for the cross section as shown in Fig. 8-7. Torsional shearing stresses for a few sections are given in Table 8-5. Note that these stresses are small compared to stresses due to M_x, M_z, and F_y. Therefore, all sections are assumed to be safe against torsional shear stress failure.

TABLE 8-5
TORSIONAL SHEARING STRESSES FOR SECTIONS 1, 2, 4, AND 10

Section	M_y, N·m	t_1, m	t_2, m	τ_P, MPa	τ_Q, MPa
1	43.5	0.0175	0.0175	0.0276	0.0276
2	192.1	0.0175	0.0175	0.1172	0.1172
4	223.3	0.00787	0.00787	0.269	0.269
10	1,672.5	0.00787	0.00787	1.296	1.296

THIS DOCUMENT PROVIDED BY THE ABBOTT AEROSPACE
TECHNICAL LIBRARY
ABBOTTAEROSPACE.COM

8-5.2.2 Case 2. Equilibrator Force Only

The equilibrator force F_E acts in the xy-plane only and produces a moment about the z-axis. This force has been calculated for various angles of elevation, and values are found in Table 8-1. Moment arms c and d for equilibrator forces are given in Table 8-2. The moment M_E induced by the equilibrator force is

$$M_E = F_{E_y}d - F_{E_x}c, \text{ N·m} \tag{8-15}$$

where

F_{E_y} = component of equilibrator force parallel to y-axis, N
F_{E_x} = component of equilibrator force parallel to x-axis, N.

Moments due to the equilibrator force for all sections at selected elevations are given in Table 8-6. Sample calculations for Section 1 at minimum elevation follow.

From Table 8-1

$F_{E_x} = 72{,}635$ N
$F_{E_y} = -10{,}533$ N.

From Table 8-2

$c = 0.0678$ m
$d = 0.149$ m.

Substitution in Eq. 8-15 gives

$$M_E = -10{,}533 \times 0.149 - 72{,}635 \times 0.0678$$
$$= -6494 \text{ N·m.}$$

Stresses due to the moment M_E and equilibrator force F_{E_y} are calculated by

$$S_{1E} = S_{3E} = -\frac{M_E}{Z_{1x}} + \frac{F_{E_y}}{A}, \text{ Pa} \tag{8-16}$$

$$S_{2E} = S_{4E} = \frac{M_E}{Z_{2x}} + \frac{F_{E_y}}{A}, \text{ Pa} \tag{8-17}$$

where

$S_{1E}, S_{2E}, S_{3E}, S_{4E}$ = stresses at points 1, 2, 3, and 4, respectively, for a section due to equilibrator forces only, Pa.

Maximum tensile (+) and compressive (−) stresses in all sections due to the equilibrator force are given in Table 8-7. Sample calculations for Section 1 follow.

From Ref. 2

$Z_{1x} = 6.84 \times 10^{-4}$ m^3
$Z_{2x} = 7.26 \times 10^{-4}$ m^3
$A = 1.44 \times 10^{-2}$ m^2.

From Table 8-1

$F_{E_y} = -10{,}533$ N.

From Table 8-6

$M_E = -6494$ N·m.

THIS DOCUMENT PROVIDED BY THE ABBOTT AEROSPACE
TECHNICAL LIBRARY
ABBOTTAEROSPACE.COM

TABLE 8-6
MOMENTS CREATED BY EQUILIBRATOR FORCE ON ALL SECTIONS FOR SELECTED ANGLES OF ELEVATION (Ref. 2)

Section	Elevation $\gamma + \theta$, deg	M_E, N·m	Section	Elevation $\gamma + \theta$, deg	M_E, N·m	Section	Elevation $\gamma + \theta$, deg	M_E, N·m
1	—	−6,490	8	—	−34,041	15	—	−60,676
	0	−5,067		0	−37,364		0	−71,876
	35	−1,650		35	−26,500		35	−55,777
	45	418.5		45	−21,964		45	−50,709
	50	1,434		50	−19,410		50	−47,482
	75	5,924		75	−4,972		75	−26,090
2	—	−12,602	9	—	−40,306	16	—	−63,946
	0	−11,565		0	−45,289		0	−75,948
	35	−6,141		35	−33,074		35	−59,108
	45	−3,166		45	−28,302		45	−53,834
	50	−1,651		50	−25,542		50	−50,535
	75	5,562		75	−9,309		75	−28,160
3	—	−15,032	10	—	−47,196	17	—	−66,561
	0	−14,535		0	−54,143		0	−79,419
	35	−8,521		35	−40,532		35	−62,117
	45	−5,395		45	−35,583		45	−56,887
	50	−3,773		50	−32,631		50	−53,493
	75	4,222		75	−14,543		75	−30,504
4	—	−19,667	11	—	−49,712	18	—	−69,191
	0	−20,238		0	−57,523		0	−82,903
	35	−13,126		35	−43,491		35	−65,132
	45	−9,734		45	−38,560		45	−59,895
	50	−7,919		50	−35,575		50	−56,453
	75	−1,535		75	−16,929		75	−32,842
5	—	−21,405	12	—	−54,956	19	—	−74,972
	0	−22,309		0	−63,421		0	−89,297
	35	−14,744		35	−47,804		35	−69,713
	45	−11,213		45	−42,257		45	−63,733
	50	−9,309		50	−38,915		50	−59,870
	75	747.8		75	−18,161		75	−33,848
6	—	−23,681	13	—	−57,429	20	—	−75,661
	0	−25,287		0	−66,762		0	−90,547
	35	−17,292		35	−50,743		35	−71,047
	45	−13,733		45	−45,223		45	−65,257
	50	−11,779		50	−41,852		50	−61,466
	75	−1,150		75	−20,565		75	−35,557
7	—	−27,645	14	—	−60,158			
	0	−29,743		0	−70,337			
	35	−20,549		35	−53,807			
	45	−16,522		45	−48,257			
	50	−14,297		50	−44,827			
	75	−2,079		75	−22,862			

THIS DOCUMENT PROVIDED BY THE ABBOTT AEROSPACE
TECHNICAL LIBRARY
ABBOTTAEROSPACE.COM

TABLE 8-7
MAXIMUM TENSILE (+) AND COMPRESSIVE (−) STRESSES IN ALL SECTIONS CREATED BY EQUILIBRATOR FORCE ALONE (Ref. 2)

Sections	S_{1E} and S_{3E}, MPa	S_{2E} and S_{4E}, MPa
1	8.76	11.6
2	17.10	−28.4
3	21.6	−31.0
4	35.6	−39.8
5	37.1	−41.2
6	66.9	−57.7
7	45.0	−47.9
8	45.3	−47.9
9	39.9	−31.8
10	43.1	−31.3
11	47.1	−35.3
12	57.8	−78.2
13	55.8	−76.0
14	53.4	−76.4
15	45.6	−46.8
16	47.7	−53.8
17	43.1	−50.6
18	37.3	−45.6
19	17.1	−35.4
20	20.7	−38.7

Substitution in Eq. 8-16 gives

$$S_{1E} = S_{3E} = -\frac{-6494}{6.84\times10^{-4}} + \frac{-10{,}533}{1.44\times10^{-2}}$$

$$= 8.76 \text{ MPa.}$$

Similarly, S_{1E} and S_{3E} are calculated for other angles of elevation and are given in Table 8-8.

TABLE 8-8. SAMPLE TENSILE STRESS CALCULATIONS

Elevation, deg	S_{1E} and S_{3E}, MPa
minimum	8.76
0	7.68
35	3.58
45	1.27
50	0.11
75	−5.26.

The maximum tensile stress S_{1E} and S_{3E} in Table 8-8 is 8.76 MPa and is therefore the value for Section 1 in Table 8-7. In a similar manner Eq. 8-17 is used to calculate the maximum stress S_{2E} and S_{4E} shown in Table 8-7.

THIS DOCUMENT PROVIDED BY THE ABBOTT AEROSPACE
TECHNICAL LIBRARY
ABBOTTAEROSPACE.COM

8-5.2.3 Case 3. Lifting and Equilibrator Forces Combined

The stresses induced by lifting forces only and by equilibrator forces only can be algebraically combined to obtain the stress induced by combining these forces. These values are given in Table 8-9 and can be calculated by combining the values of the lifting forces in Table 8-4 and the equilibrator forces given in Table 8-7. A sample calculation for S_{1LE}, Section 1, is provided.

From Table 8-4, Section 1, $S_{1L} = 7.55$ MPa.

From Table 8-7, Section 1, $S_{1E} = 8.76$ MPa.

Total stress, S_{1LE}, Section 1, for lifting and equilibrator forces combined is

$$S_{1LE} = 7.60 + 8.76 = 16.36 \text{ MPa}$$

as shown in Table 8-9 for S_{1LE}, Section 1.

8-5.2.4 Case 4. Equilibrator and Trunnion Forces Combined

Stresses due to equilibrator forces were discussed in par. 8-5.2.2. Stresses due to trunnion forces will be discussed, calculated, and then combined with the stresses due to equilibrator forces.

TABLE 8-9
MAXIMUM TENSILE (+) AND COMPRESSIVE (−) STRESSES IN ALL SECTIONS CREATED BY LIFTING AND EQUILIBRATOR FORCE COMBINED (Ref. 2)

Section	S_{1LE}, MPa	S_{2LE}, MPa	S_{3LE}, MPa	S_{4LE}, MPa
1	16.36	19.59	16.17	19.45
2	28.20			−19.95
3	36.37	−27.36	33.34	−30.39
4	69.66			−46.12
5	73.05			−50.11
6	119.37			−84.85
7	84.38			−68.08
8	86.68			−72.14
9	80.63			−52.17
10	87.10			−57.69
11	99.78			−67.25
12	126.52			−144.85
13	126.18			−145.99
14	123.76			−147.56
15	110.66			−97.18
16	111.84			−111.60
17	104.16			−106.78
18	93.84			−98.39
19	48.75			−75.93
20	58.16			−84.26

Note: The stress values that are significantly less than the maximum tensile or compressive stresses are not shown in the table. To arrive at the values in this table, take the values—either plus or minus—from Table 8-4 and add them to the values of Table 8-7, which will result in the maximum value for tensile (+) stress and compressive (−) stress.

THIS DOCUMENT PROVIDED BY THE ABBOTT AEROSPACE
TECHNICAL LIBRARY
ABBOTTAEROSPACE.COM

Trunnion forces act only on Sections 10 through 20 and, like equilibrator forces, act only in the xy-plane. Moments produced by these forces are moments about the z-axis. Trunnion forces F_N and F_A have components F_X and F_Y that are parallel and perpendicular to a section, respectively.

Moments M_T due to trunnion forces are given by

$$M_T = F_Y f - F_X e, \text{ N·m} \tag{8-18}$$

where

e = moment arm from section to point of trunnion force along y-axis, m
f = moment arm from section to point of trunnion force along x-axis, m.

Moments due to trunnion forces at selected angles of elevation are given in Table 8-10. Sample calculations for Section 10 at 0 deg elevation are provided.

From Table 8-1

$F_X = -166{,}354$ N
$F_Y = 152{,}644$ N.

From Table 8-2

$e = 0.1016$ m
$f = 0.05486$ m.

Substitution in Eq. 8-18 gives

$$M_T = 152{,}644 \times 0.05486 - (-166{,}354) \times 0.1016 = 25{,}276 \text{ N·m}$$

as shown in Table 8-10 for Section 10 at 0 deg.

TABLE 8-10
MOMENTS CREATED BY TRUNNION FORCES ON SECTIONS 10-20 FOR SELECTED ANGLES OF ELEVATION (Ref. 2)

Section	Elevation $\gamma + \theta$, deg	M_T, N·m	Section	Elevation $\gamma + \theta$, deg	M_T, N·m	Section	Elevation $\gamma + \theta$, deg	M_T, N·m
10	0	25,276	14	0	67,957	18	0	99,860
	35	22,494		35	65,927		35	107,229
	45	20,954		45	63,308		45	106,273
	50	25,860		50	79,691		50	136,412
	75	15,705		75	54,763		75	104,293
11	0	33,959	15	0	71,174	19	0	117,500
	35	32,959		35	75,312		35	119,465
	45	31,655		45	74,319		45	116,466
	50	39,850		50	95,148		50	148,001
	75	27,400		75	71,770		75	107,286
12	0	50,126	16	0	81,912	20	0	120,424
	35	44,904		35	86,183		35	125,117
	45	41,932		45	84,904		45	122,793
	50	51,834		50	108,587		50	156,682
	75	31,825		75	81,468		75	116,122
13	0	58,693	17	0	90,867			
	35	55,346		35	96,703			
	45	52,639		45	95,590			
	50	65,856		50	122,505			
	75	43,633		75	92,900			

THIS DOCUMENT PROVIDED BY THE ABBOTT AEROSPACE
TECHNICAL LIBRARY
ABBOTTAEROSPACE.COM

Maximum tensile (+) and compressive (−) stresses S_{1ET}, S_{2ET}, S_{3ET}, and S_{4ET}, Sections 10 through 20, created by equilibrator and trunnion forces at points, 1, 2, 3, and 4, respectively, are given by

$$S_{1ET} = S_{3ET} = -\frac{M_E + M_T}{Z_{1x}} + \frac{F_F}{A}, \text{ Pa} \tag{8-19}$$

$$S_{2ET} = S_{4ET} = \frac{M_E + M_T}{Z_{2x}} + \frac{F_F}{A}, \text{ Pa} \tag{8-20}$$

where

$F_F = F_{E_y} + F_Y =$ sum of equilibrator and trunnion forces along the y-axis, N.

The sums of moments $M_E + M_T$ about the z-axis are given in Table 8-11. Stresses for Sections 10 through 20 due to moments about the z-axis are given in Table 8-12. Sample calculations for Section 10 at 0 deg elevation follow.

From Ref. 2

$Z_{1x} = 1.193 \times 10^{-3}$ m^3

$Z_{2x} = 1.86 \times 10^{-3}$ m^3

$A = 2.31 \times 10^{-2}$ m^2.

From Table 8-11

$$M_E + M_T = -28{,}867 \text{ N·m.}$$

TABLE 8-11
SUM OF MOMENTS M_E AND M_T FROM EQUILIBRATOR AND TRUNNION FORCES ON SECTIONS 10-20 FOR SELECTED ANGLES OF ELEVATION (Ref. 2)

Section	Elevation $\gamma + \theta$, deg	$M_E + M_T$, N·m	Section	Elevation $\gamma + \theta$, deg	$M_E + M_T$, N·m	Section	Elevation $\gamma + \theta$, deg	$M_E + M_T$, N·m
10	0	−28,867	14	0	−2,379	18	0	16,958
	35	−18,038		35	12,119		35	42,097
	45	−14,629		45	15,051		45	46,378
	50	−6,772		50	34,863		50	79,959
	75	1,163		75	31,901		75	71,451
11	0	−23,563	15	0	−702	19	0	28,203
	35	−10,532		35	19,535		35	49,752
	45	−6,905		45	23,610		45	52,733
	50	4,275		50	47,665		50	88,130
	75	10,472		75	45,679		75	73,439
12	0	−13,295	16	0	5,964	20	0	29,878
	35	−2,901		35	27,075		35	54,071
	45	−325		45	31,020		45	57,536
	50	12,931		50	58,052		50	95,216
	75	13,664		75	53,309		75	80,565
13	0	−8,069	17	0	11,448			
	35	4,603		35	34,586			
	45	7,416		45	38,702			
	50	24,004		50	69,012			
	75	23,068		75	62,396			

THIS DOCUMENT PROVIDED BY THE ABBOTT AEROSPACE
TECHNICAL LIBRARY
ABBOTTAEROSPACE.COM

From Table 8-1
$F_{E_y} = -51{,}381$ N.
$F_Y = 152{,}644$ N.

Substitution in Eq. 8-19 gives

$$S_{1ET} = S_{3ET} = -\frac{-28{,}867}{1.193\times10^{-3}} + \frac{-51{,}381 + 152{,}644}{2.31\times10^{-2}}$$

$$= 28.6 \text{ MPa}$$

as shown in Table 8-12 for Section 10, 0 deg.
Maximum tensile and compressive stresses for Sections 10 through 20 are given in Table 8-13.

8-5.2.5 Transverse Shear Stress Calculations

In all the previous calculations shear stresses due to transverse loads at any section are not calculated because all sections are assumed to be safe in shear (Ref. 2). This is reasonable because the sections are deep and shearing forces are small. In par. 8-6, where finite element stress analysis of the top carriage structure is presented, this assumption is verified by analyzing the computer results. It is indeed observed from the computer solution that the shearing stresses due to transverse shearing loads are quite small.

TABLE 8-12
MAXIMUM TENSILE (+) AND COMPRESSIVE (−) STRESSES IN TRUNNION ARMS CREATED BY EQUILIBRATOR AND TRUNNION FORCES AT SELECTED ANGLES OF ELEVATION (Ref. 2)

Section		Stress, MPa				
		Elevation				
		0 deg	35 deg	45 deg	50 deg	75 deg
10	S_{1ET}, S_{3ET}	28.6	15.231	11.252	3.558	−6.371
	S_{2ET}, S_{4ET}	−11.142	−9.584	−8.774	−5.757	4.771
11	S_{1ET}, S_{3ET}	26.097	9.287	4.695	−6.440	−16.037
	S_{2ET}, S_{4ET}	−7.646	−5.799	−5.192	−0.317	−1.048
12	S_{1ET}, S_{3ET}	22.553	3.096	−1.855	−17.327	−25.104
	S_{2ET}, S_{4ET}	5.950	−3.116	−2.551	10.397	4.185
13	S_{1ET}, S_{3ET}	17.003	−5.144	−9.032	−26.497	−32.881
	S_{2ET}, S_{4ET}	1.076	3.944	5.674	20.891	12.659
14	S_{1ET}, S_{3ET}	11.445	−12.576	−14.638	−33.440	−38.080
	S_{2ET}, S_{4ET}	7.053	9.791	13.141	30.909	20.802
15	S_{1ET}, S_{3ET}	8.129	−13.259	−18.016	−36.515	−40.865
	S_{2ET}, S_{4ET}	7.226	11.845	12.321	24.739	17.830
16	S_{1ET}, S_{3ET}	1.862	−17.920	−22.043	−41.569	−42.775
	S_{2ET}, S_{4ET}	9.846	18.285	19.436	36.060	28.510
17	S_{1ET}, S_{3ET}	−0.883	−19.891	−23.739	−42.755	−43.224
	S_{2ET}, S_{4ET}	12.604	20.871	21.870	38.583	30.316
18	S_{1ET}, S_{3ET}	−2.565	−20.250	−23.766	−41.472	−41.576
	S_{2ET}, S_{4ET}	14.396	21.863	22.629	38.514	29.903
19	S_{1ET}, S_{3ET}	−2.110	−10.556	−12.197	−20.707	−20.567
	S_{2ET}, S_{4ET}	14.479	18.706	18.816	31.061	22.622
20	S_{1ET}, S_{3ET}	−3.185	−13.590	−15.589	−25.242	−25.814
	S_{2ET}, S_{4ET}	16.437	21.919	22.194	36.280	27.090

THIS DOCUMENT PROVIDED BY THE ABBOTT AEROSPACE
TECHNICAL LIBRARY
ABBOTTAEROSPACE.COM

TABLE 8-13
MAXIMUM TENSILE (+) AND COMPRESSIVE (−) STRESSES IN SECTIONS 10-20 OF TRUNNION ARMS CREATED BY EQUILIBRATOR AND TRUNNION FORCES COMBINED (Ref. 2)

Sections	S_{1ET} and S_{3ET}, MPa	S_{2ET} and S_{4ET}, MPa
10	28.6	11.2
11	26.1	3.8
12	−25.1	5.96
13	−32.9	20.9
14	−38.1	30.9
15	−40.9	24.7
16	−42.8	36.1
17	−43.2	38.6
18	−41.6	38.5
19	−20.8	31.1
20	−26.2	36.3

The shearing stresses can be calculated, however, by using the standard mechanics of materials approach (Ref. 4). For this calculation consider a cross section of the beam shown in Fig. 8-8(A). The shear stress τ at any point q is given as

$$\tau = \frac{V_x A' \bar{x}}{I_z b}, \text{ Pa} \qquad (8\text{-}21)$$

where

V_x = vertical shear force along x-direction at section containing point q, N
A' = area of section above q (hatched area in Fig. 8-2), m^2
$\bar{x}$ = distance from neutral axis to centroid of A', m
b = width of section measured through q, m
I_z = moment of inertia of cross section about z-axis, m^4.

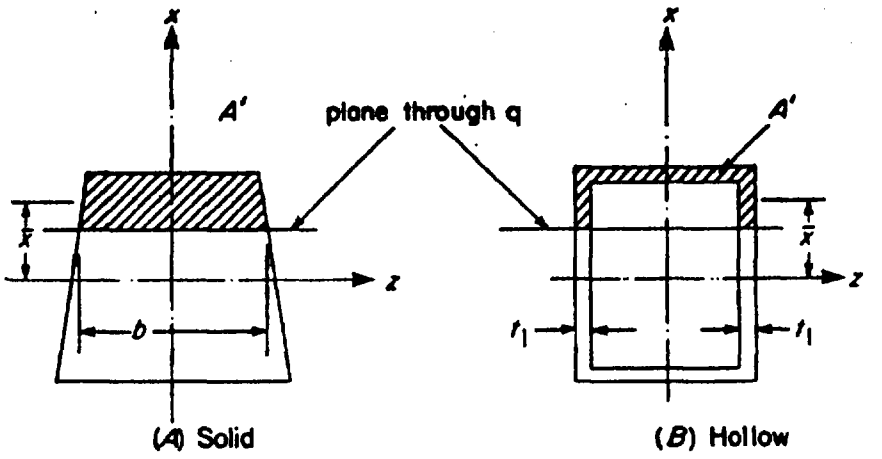

Figure 8-8. Beam Cross Sections

THIS DOCUMENT PROVIDED BY THE ABBOTT AEROSPACE
TECHNICAL LIBRARY
ABBOTTAEROSPACE.COM

If there is shearing force along the z-axis, an equation similar to Eq. 8-21 can be used to calculate transverse shear stress in the z-direction.

For the hollow rectangular section shown in Fig. 8-8(B), $b = 2t_1$ for use in Eq. 8-21 and A' is the hatched area shown. It should be noted that maximum transverse shearing stress for rectangular, hollow rectangular, and circular sections occurs at the neutral axis of the cross section.

The aluminum plates (alloys 5083-0 or 5086, Ref. 5) used for the top carriage have a yield point of 123.2 MPa with a maximum allowable design stress of 103.4 MPa. No stresses in Table 8-13 exceed the maximum allowable design stress, so the selected design is adequate. If, however, the stresses did exceed the allowable stress at any point, the section would have to be strengthened. Accordingly, the stress analysis would have to be repeated until a safe structure was obtained.

8-6 ADVANCED DESIGN TECHNIQUES FOR TOP CARRIAGE STRUCTURES

Advanced techniques for the design of top carriages imply the use of more refined and indeterminate models in analysis and design of the structure. Refined models for the top carriage signify that the model accounts for changes in geometry of the structure so that a more accurate response can be determined. Realistic boundary conditions and loading systems are used in refined models. The finite element method is a natural method for estimating stresses and deflection for such refined models. Thus the finite element method with the aid of a computer is used to analyze and design the top carriage.

Fundamental concepts of the finite element method are presented in Appendix C. General modeling ideas discussed there are also applicable to the top carriage structure. The designer should review the material given in Appendix C to familiarize himself with the finite element method.

This paragraph presents finite element modeling concepts for the top carriage structure. Several finite element models are described. Stresses for these models are obtained by using the NASTRAN computer program.

8-6.1 FINITE ELEMENT MODEL

As noted in Appendix C, development of a finite element model for the structural system requires great care, intuition, experience, and understanding of the basic behavior of the structure. Designers should spend time and effort in modeling the system and should study possibilities of using different finite elements to model the structure. Some discussion with regard to these points is presented for the top carriage structure of M198 in the paragraphs that follow.

The top carriage structure of M198 is fabricated by welding plates of various thicknesses. The basic cross section of one side of the structure is a hollow rectangular box; the geometry of the structure, however, is quite complex. The cross section of the frame changes at several locations, and there are various openings and attachments to accommodate other equipment. Therefore, a precise finite element model of the system is quite complex and requires several hundred nodal points and finite elements. Two possible finite element models for the top carriage structure are described, and their relative advantages and disadvantages are discussed. These models should be used as a guide to model the top carriage and other components of a new system.

As noted in par. 8-5, the side frame of top carriage structure behaves as a cantilever beam subjected to general loads. This suggests the use of beam-type finite elements in modeling the top carriage structure. A 43-beam finite element model (These are called CBAR elements in NASTRAN.) of the top carriage structure is shown in Fig. 8-9. The model has 45 nodal points, which are also referred to as grid points. Grid point 1 is considered to be completely fixed. Grid point 43 is not connected to any finite element but is used to define the xy-plane, grid points 44 and 45 define points of application of the lifting and equilibrator forces, respectively, and the trunnion force is applied at grid point 23. Forces used in the finite element model are the same as those used in par. 8-5.

To complete the beam-type finite element model of the top carriage, the designer needs to provide cross-sectional properties of various beam finite elements. These properties include various moments of inertia, section moduli, location of the neutral axis, fiber locations for bending stress calculations, shear stress recovery factors, and material properties. Depending on the geometry of the system, this can represent a substantial amount of data to be calculated by the designer. For the top carriage of M198 these data are calculated in Ref. 2 and are used for the present finite element model. To obtain a better estimate of stresses at various points, a finer finite element model having 82 beam elements is used in actual calculations presented in the next paragraph.

THIS DOCUMENT PROVIDED BY THE ABBOTT AEROSPACE
TECHNICAL LIBRARY
ABBOTTAEROSPACE.COM

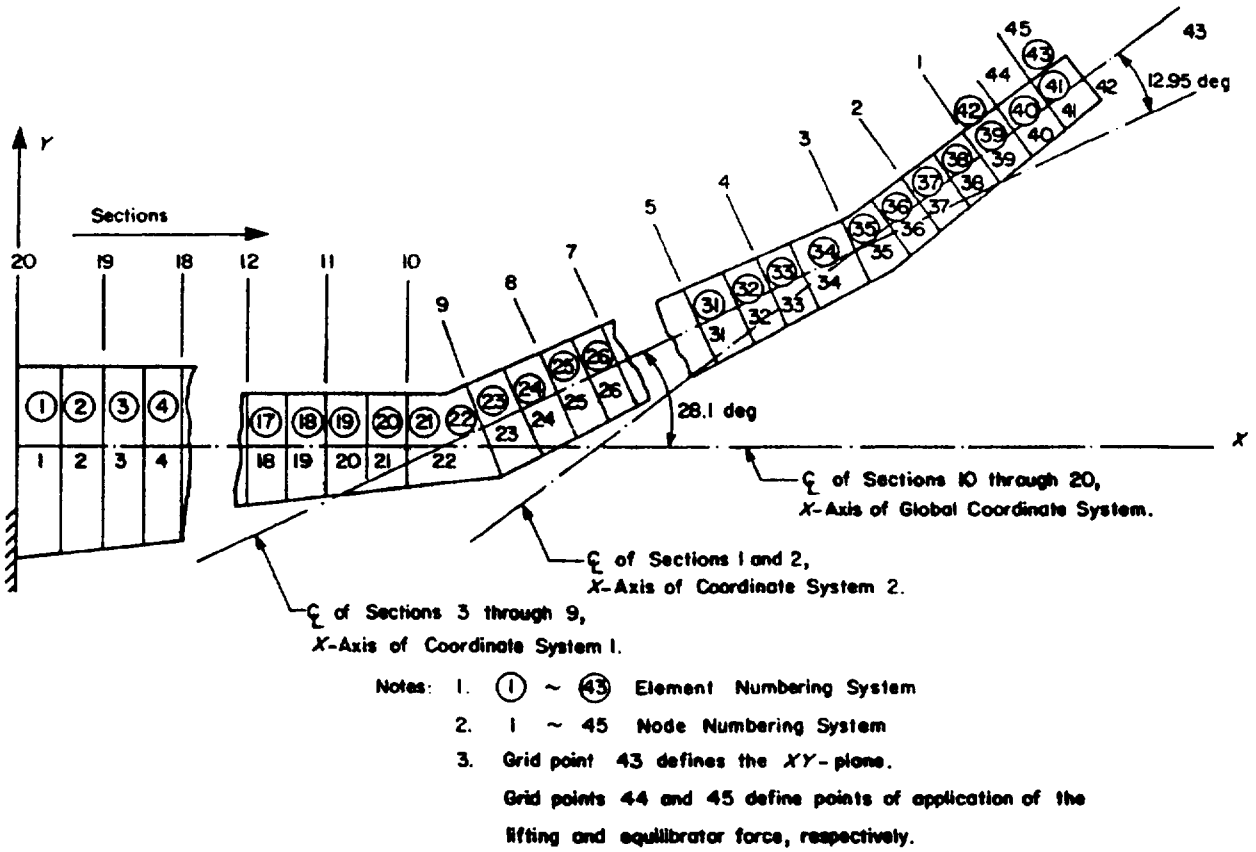

Figure 8-9. Finite Element Model for Beam Elements

Another finite element model for the top carriage structure can be developed by using plate-type elements. This finite element model, developed by using general triangular and quadrilateral finite elements, is shown in Fig. 8-10. The model consists of 232 grid points, 46 general triangular plate elements, and 238 general quadrilateral elements. Various forces are applied at the grid points as in the case of the beam-type finite element model. To complete the finite element modeling of the structure, the designer must specify thickness, moments of inertia, and material properties of all finite elements. These properties are taken from Ref. 2. This model for the top carriage should not be viewed as the final model; instead, it should be used as a guide for developing the final refined model.

There are certain advantages and disadvantages of the two finite element models described. In the beam-type finite element model, the number of grid points and finite elements is relatively small. For each finite element, however, the amount of data to be calculated by hand is quite large. The data to be calculated include the cross-sectional area, location of neutral axis, sectional moments of inertia, and fiber locations for stress calculations. For the plate-type finite element model, the number of grid points and finite elements can be quite large; therefore, the designer has to spend time preparing data cards. This problem can be alleviated if proper hardware and software are available to prepare the geometry data automatically. Data to be calculated by hand for this finite element model are the moments of inertia of the plate about the centroidal axis. Another advantage of the plate-type finite element model is that stress concentration at notches, holes, and abrupt changes in geometry can be readily obtained.

Another point of comparison between the finite element models is the cost of computer runs. For example, on an IBM 370-158, the beam finite element model with 82 beam elements requires 17 s of computing time; the 282-plate finite element model requires 158 s of computing time. (Note that the computing times can vary for a different installation and local environment of the same computers.) Consequently, the computational costs can be substantially different for different finite element models.

In par. 8-6.2 the results of stress analysis using the finite element models are compared with the results obtained by the hand calculations in par. 8-5.

THIS DOCUMENT PROVIDED BY THE ABBOTT AEROSPACE
TECHNICAL LIBRARY
ABBOTTAEROSPACE.COM

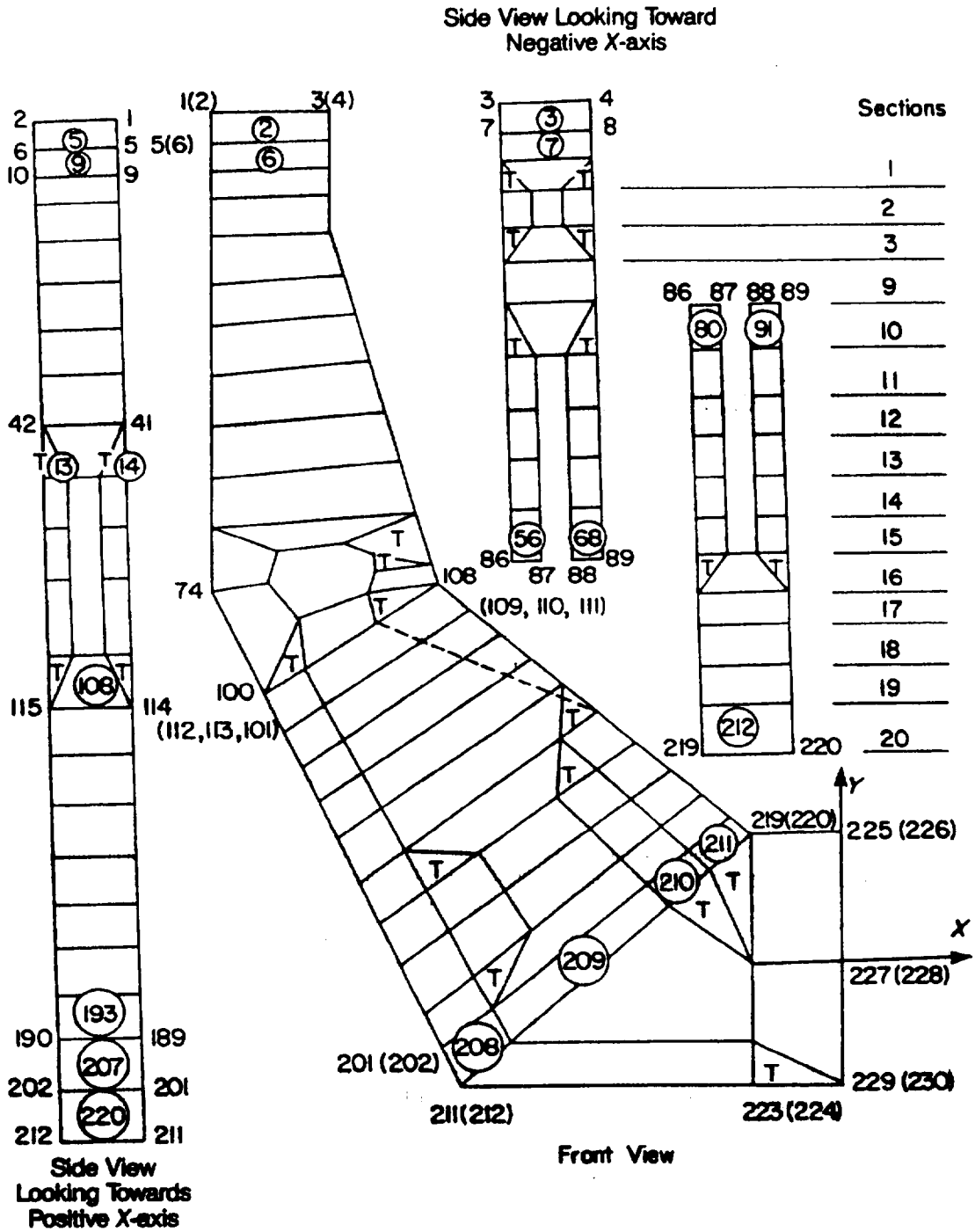

Notes: 1. 1 – 232 Node numbering (hidden nodes are in parenthesis).

2. ① – (238) Quadrilateral elements numbering (hidden elements do not appear).

3. T ① – T (46) Triangular elements numbering (hidden elements do not appear).

4. All nodes and finite elements are not shown.

Figure 8-10. Finite Element Model for Plate Elements

THIS DOCUMENT PROVIDED BY THE ABBOTT AEROSPACE
TECHNICAL LIBRARY
ABBOTTAEROSPACE.COM

8-6.2 NASTRAN STRESS ANALYSIS

The two finite element models presented in par. 8-6.1 are analyzed using the NASTRAN computer program. For the beam-type finite element model, the sectional properties are known at the 20 cross sections defined in par. 8-5. Interpolation is used to calculate sectional properties at other locations. The offset vector capability of NASTRAN is used to define the neutral axis of a section in which the centroidal and the neutral axes do not coincide. Stress analysis is carried out for 43- as well as 82-beam element models. Stresses are obtained for the following six cases:

1. Case 1. Lifting force only (Condition A)
2. Case 2. Lifting force only (Condition B)
3. Case 3. Equilibrator force only
4. Case 4. Lifting force (A) and equilibrator force combined
5. Case 5. Lifting force (B) and equilibrator force combined
6. Case 6. Equilibrator force and trunnion force due to firing combined.

All six cases can be solved with just one run of the computer program. Cases 1 and 2 are really not necessary because they do not occur independently. They are analyzed, however, to compare computer solutions with the hand solutions.

In the computer solution the equilibrator force and the trunnion forces for 0 deg elevation angle are used. Coordinate systems are shown in Fig. 8-9. Stress analysis for other firing elevation angles can be carried in the same computer run.

Results with 43- and 82-beam finite element models for all cases indicate that the two solutions are quite close to each other. A comparison of the computer and hand results also shows close agreement between the two solutions. Tables 8-14, 8-15, and 8-16 summarize comparison of two solutions for Cases 3, 4, and 6. These are Cases 2, 3, and 4, respectively, of par. 8-5.

The NASTRAN program is also used to analyze the plate finite element model of the top carriage structure. Stresses obtained with this model did not agree with those obtained using the beam-type finite element model and were generally lower than those obtained using the beam-type model. The plate finite element model for the top carriage structure appears to be quite crude. A more refined model with fine grid mesh should be used to obtain a more accurate stress analysis.

THIS DOCUMENT PROVIDED BY THE ABBOTT AEROSPACE
TECHNICAL LIBRARY
ABBOTTAEROSPACE.COM

TABLE 8-14
COMPARISON OF FINITE ELEMENT AND HAND CALCULATIONS OF STRESSES CREATED BY THE EQUILIBRATOR FORCE ALONE

Section	S_{1E} and S_{3E}, MPa		S_{2E} and S_{4E}, MPa	
	Analytic	82 Bar Elements	Analytic	82 Bar Elements
1	8.76	11.79	−11.56	−14.82
2	17.05	20.90	−28.41	−38.16
3	21.57	25.32	−31.01	−38.84
4	35.58	36.33	−39.69	−48.93
5	37.10	37.16	−41.18	−49.44
6	66.91	68.04	−57.67	−62.21
7	44.97	43.13	−47.86	−51.84
8	45.31	42.24	−47.89	−49.89
9	39.86	35.85	−31.84	−32.73
10	43.17	41.24	−31.33	−31.56
11	47.08	43.80	−35.29	−35.07
12	57.79	53.28	−78.17	−77.07
13	55.77	50.32	−76.03	−73.94
14	53.41	47.41	−76.43	−73.09
15	45.60	39.32	−46.75	−44.23
16	47.71	41.02	−53.85	−50.30
17	43.09	36.74	−50.52	−46.35
18	37.29	31.25	−45.64	−41.60
19	17.13	15.47	−35.39	−32.24
20	20.71	26.95	−38.75	−52.61

THIS DOCUMENT PROVIDED BY THE ABBOTT AEROSPACE
TECHNICAL LIBRARY
ABBOTTAEROSPACE.COM

TABLE 8-15
COMPARISON OF FINITE ELEMENT AND HAND CALCULATIONS OF STRESSES CREATED BY LIFTING AND EQUILIBRATOR FORCES COMBINED

Section	S_{1LE}, MPa		S_{4LE}, MPa	
	Analytic	82 Bar Elements	Analytic	82 Bar Elements
1	16.3	19.38	−16.15	−7.26
2	28.15	31.23	−19.96	−28.41
3	35.80	37.97	−33.72	−35.49
4	68.25	68.11	−44.70	−50.66
5	71.54	70.74	−48.57	−53.53
6	117.9	117.87	−83.30	−83.14
7	82.73	79.74	−66.42	−66.41
8	84.82	80.64	−70.25	−71.13
9	78.41	72.84	−50.21	−50.46
10	82.86	74.46	−54.04	−49.20
11	94.82	83.69	−62.17	−56.45
12	117.8	103.64	−134.26	−124.38
13	117.01	102.53	−135.77	−123.04
14	114.32	99.88	−138.14	−125.53
15	101.74	88.23	−88.21	−79.17
16	103.77	89.98	−103.57	−93.70
17	90.27	83.46	−98.40	−88.14
18	85.34	73.93	−89.92	−80.40
19	41.71	38.56	−68.84	−61.92
20	50.28	64.23	−76.43	−102.14

THIS DOCUMENT PROVIDED BY THE ABBOTT AEROSPACE
TECHNICAL LIBRARY
ABBOTTAEROSPACE.COM

TABLE 8-16
COMPARISON OF FINITE ELEMENT AND HAND CALCULATIONS OF STRESSES CREATED BY EQUILIBRATOR AND TRUNNION FORCES COMBINED

Section	S_{1ET}, MPa		S_{4ET}, MPa	
	Analytic	82 Bar Elements	Analytic	82 Bar Elements
10	28.6	26.68	−11.14	−11.38
11	26.10	22.86	−7.65	−7.43
12	22.55	18.09	−5.95	−4.89
13	17.0	11.56	1.08	3.08
14	11.45	5.48	7.05	10.10
15	8.13	1.88	7.23	9.74
16	1.86	−4.47	9.85	13.99
17	−0.88	−7.18	12.60	16.75
18	−2.56	−8.55	14.40	18.40
19	−2.11	−5.54	14.48	17.09
20	−3.19	−12.27	16.44	28.59

REFERENCES

1. A. P. Boresi and O. M. Sidebottom, *Advanced Mechanics of Materials*, 4th Edition, John Wiley and Sons, Inc., New York, NY 1985.
2. B. L. Hofgaard and W. L. Renaud, *Stress Analysis of 155-mm Towed Howitzer M198 Numbers 3 through 10*, Top Carriage, Report No. SWERR-R-TN-2-73, Rock Island Arsenal, Rock Island, IL, January 1973.
3. A. C. Ugural and S. K. Fenster, *Advanced Strength and Applied Elasticity*, American Elsevier, New York, NY, 1975.
4. R. J. Roark, *Formulas for Stress and Strain*, McGraw-Hill Book Co., New York, NY, 1975.
5. *Aluminum Standards and Data*, The Aluminum Association, Inc., New York, NY, 1976.

THIS DOCUMENT PROVIDED BY THE ABBOTT AEROSPACE
TECHNICAL LIBRARY
ABBOTTAEROSPACE.COM

CHAPTER 9
BOTTOM CARRIAGE DESIGN

This chapter describes the design of bottom carriage structures for towed artillery systems. The material follows essentially the same outline as the ones for Chapters 7 and 8. After introductory information, types of bottom carriage structures and "on-carriage traverse" and "off-carriage traverse" configurations for bottom carriages are discussed. The preliminary design of bottom carriages is followed by a discussion of loading and stress analyses together with firing, towing, and transportation loads (airdrop, helicopter sling, and rail transportation). Basic mechanics of deformable bodies concepts are used to develop general procedures for stress analysis of the bottom carriage. The general procedures are illustrated by describing detailed design of the bottom carriage for the M198 towed Howitzer. The use of finite element method for the design of bottom carriage structures is presented. General finite element modeling concepts also are presented. A finite element model for the M198 bottom carriage is developed. The NASTRAN program is used to analyze the finite element model of the bottom carriage structure. Stresses obtained using the finite element method are compared to stresses obtained using the mechanics of deformable bodies. Finally the difficult problem of bottom carriage-soil structure interaction is discussed.

9-0 LIST OF SYMBOLS

A = flange thickness, m
A_{cs} = area of cross section, m^2
A_c, A_c^* = constants shown in bending moment equations, dimensionless
B = total depth of trail cross section, m
= section property shown in Fig. 9-13, m
b = maximum spacing of ribs, m
B_c, B_c^* = constants shown in bending moment equations, dimensionless
B_{RM} = bearing moment acting on bottom carriage, N·m
B_{RR} = in-plane (plane of traverse bearing) component of bearing reaction on bottom carriage, N
B_{RT} = normal component (normal to plane of traverse bearing) of bearing reaction on bottom carriage, N
B'_{RR} = proportion of load due to B_{RR}, N
B'_{RT} = proportion of load due to B_{RT}, N
C = section property shown in Fig. 9-13, m
C_c, C_c^* = constants shown in bending moment equations, dimensionless
D = section property shown in Fig. 9-13, m
D_c, D_c^* = constants shown in bending moment equations, dimensionless
d = yield ratio, dimensionless
d_1 = distance between R_T and R_B, m
d_2 = distance between R_T and F_T, or R_B and F_B, m
E = Young's modulus of elasticity, MPa
E_c, E_c^* = constants shown in bending moment equations, dimensionless
F = area of angle section, m^2
F_B = force at bottom lug of bottom carriage, N
F_c, F_c^* = constants shown in bending moment equations, dimensionless
F_E = equilibrator force, N
F_g = elevating gear force, N
F_j = jack reaction, N
F_L = force transmitted by trail lugs to bottom carriage lugs, N

THIS DOCUMENT PROVIDED BY THE ABBOTT AEROSPACE
TECHNICAL LIBRARY
ABBOTTAEROSPACE.COM

F_T = trunnion force, N
F_{top} = force at top lug of bottom carriage, N
F_V = total vertical load due to B_{RM} and B_{RT}, N
F' = equivalent force due to B_{RM}, N
G = distance of centroid of angle section from its short flange, m
G_c, G_c^* = constants shown in bending moment equations, dimensionless
H = vertical depth of spade, m
= section property shown in Fig. 9-13, m
H_c, H_c^* = constants shown in bending moment equations, dimensionless
h = height of plate, m
I = area moment of inertia, m^4
I_c, I_c^* = constants shown in bending moment equations, dimensionless
I_{yy} = area moment of inertia about yy-axis, m^4
J_c, J_c^* = constants shown in bending moment equations, dimensionless
K = area moment of inertia of angle section about its centroidal axis, m^4
K_c = constant defined in Eq. 9-24, dimensionless
K_{ep} = coefficient of earth pressure, dimensionless
K' = constant of proportionality, N/m^2
L_{arc} = representative arc length, m
L_{ma} = length of moment arm, m
ℓ_i = circumferential distance of ith segment, m
M = fixed end moment at A or B, N·m
M_b = bending moment about point P, N·m
$(M_b)_{max}$ = maximum bending moment, N·m
$(M_b)_{total}$ = total bending moment, N·m
M_1 = moment at right-trail hinge pin due to R_1 and R_2, N·m
M_2 = moment at left-trail hinge pin due to R_3 and R_4, N·m
$(M_2)_{component}$ = component of M_2, N·m
M' = moment contribution of an equivalent force, N·m.
N_X = nodal force in X-direction, N
N_Y = nodal force in Y-direction, N
N_Z = nodal force in Z-direction, N
P = rolling loads, N
p = linear pressure (force/unit length) as a function of distance from bearing center due to B_{RM}, N/m
p_{max} = linear pressure when $x = r$, N/m
p' = maximum linear pressure at grid points, N/m
R = resultant of loads, N
R_B = trail force acting at bottom on trail pin, N
R_b = centerline radius of bottom lug, m
R_f = float reaction, N
R_i = inner radius of lower lug, m
R_o = outer radius of lower lug, m
R_s = spade reaction, N
R_T = trail force acting at top on trail pin, N
R_1 = right-trail float reaction, N
R_2 = right-trail spade reaction, N

THIS DOCUMENT PROVIDED BY THE ABBOTT AEROSPACE
TECHNICAL LIBRARY
ABBOTTAEROSPACE.COM

R_3 = left-trail float reaction, N
R_4 = left-trail spade reaction, N
R_5 = front-float reaction, N
r = bearing radius, m
S_a = maximum axial stress, MPa
S_b = maximum bending stress, MPa
S_T = total maximum stress, MPa
ds = differential arc length as shown in Fig. 9-16, m
T_c = constant shown in bending moment equations, dimensionless
t = thickness of plate, m
x = distance of XX from trail-float reaction, m
= distance of section from trail-float reaction, m
= length as shown in Fig. 9-16, m
Δx = distance between two consecutive divisions, m
x' = distance from A along AB for any section on AB (See Fig. 9-11.), m
X, Y, Z = coordinate system for finite element model, m
Y = horizontal displacement of spade, m
$\bar{Y}_H$ = horizontal distance of centroid of cross section from right edge, m
$\bar{Y}_V$ = vertical distance of centroid of cross section from bottom edge, m
y = distance of a fiber from centerline of lug, m
= distance of section from trail-spade reaction, m
= distance of centroid of XX from trail spade reaction, m
Z = section modulus of cross section, m^3
Z_b = section modulus for bottom fiber, m^3
Z_t = section modulus for top fiber, m^3
Z_1, Z_2 = section moduli, m^3
z = curved beam factor, dimensionless
β = contact angle, deg
θ = angle between grid points (See Fig. 9-36.), deg
$d\theta$ = differential angle as shown in Fig. 9-16, rad
θ_i = angle between two radii defining ith segment, rad
θ' = angle between line OA and radial line identified by arrow in Fig. 9-37, deg
ν = Poisson's ratio, dimensionless
σ = combined bending and tensile stress, Pa
σ_1 = bottom bending stress, MPa
σ_2 = top bending stress, MPa
σ_{cr} = critical buckling stress, MPa

9-1 INTRODUCTION

This chapter presents information on the fundamental operating principles and design of bottom carriages; it discusses the types of bottom carriages, their components, and functions; and it provides design data and procedures for analysis and design of the bottom carriage. Also considered are the requirements that each component must meet.

The bottom carriage is the part of a towed artillery system that supports the top carriage and provides the pivot for the traversing parts. The bottom carriage and its components—including wheels, trails, and outriggers—provide the structural foundation for the weapon. When emplaced and during firing, the bottom carriage transmits carriage loads to the ground. During transit, it may become the chassis. Bottom carriage may be a general term for all types of ground supporting structures, or it may be a specific term such as the

THIS DOCUMENT PROVIDED BY THE ABBOTT AEROSPACE
TECHNICAL LIBRARY
ABBOTTAEROSPACE.COM

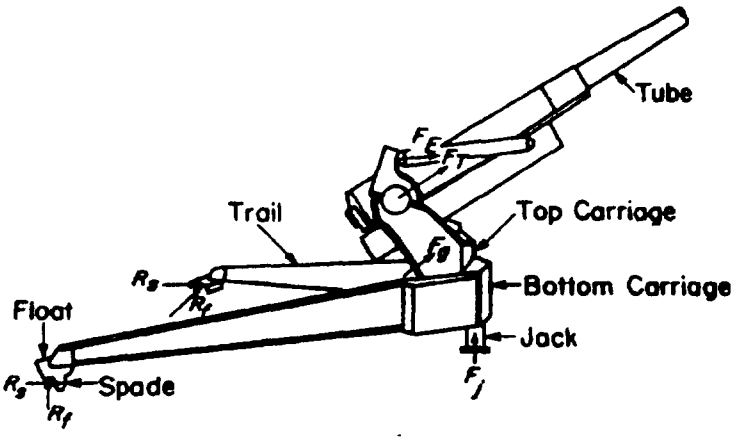

F_E = equilibrator force, N
F_g = elevating gear force, N
F_T = trunnion force, N
F_j = jack reaction, N
R_f = float reaction, N
R_s = spade reaction, N

Figure 9-1. Split Trail Gun Showing Primary Loads

bottom carriage for a single recoil weapon. In the conventional single recoil weapon, the bottom carriage links the top carriage to the trails and forward supports during firing. It also links the top carriage to the trails and wheels during transport. No translation occurs, however, between top and bottom carriages. Except for weapons equipped for unlimited traverse, the split trails, jacks, or floats at the forward end usually carry the recoil forces to the ground. Fig. 9-1 shows a split trail gun and primary loads. Only limited fine traverse is available for this weapon after emplacement. Therefore, it is necessary at emplacement to orient the gun in the proper general direction.

Loads are transmitted from the top carriage to the bottom carriage through the traverse bearing. Generally, radial bearings carry the horizontal components, and thrust bearings carry the vertical components of the firing loads. An angular contact-type bearing—a four-point contact ball bearing—of large diameter and many rolling elements has proved satisfactory as a traverse bearing. In addition to being capable of carrying axial and radial loads, the bearing also is capable of transmitting bending moments such as the overturning moment during recoil. Fig. 9-2 shows details of the rolling elements and the loading diagram. The distance between the points of contact of the load P is called the rolling diameter. The inner and outer path diameters are clearly shown for the four-point ball bearing in Fig. 9-2. The separators distribute torque more uniformly during traverse and provide for uniform support. Other advantages derived from the bearing are its ability to carry all firing loads whether or not uniformly distributed, its adaptability to either single or double recoil gun structures, and its low frictional properties.

The bottom carriage for a soft recoil system differs from that for a conventional recoil system mainly because of the smaller recoil forces obtained in the soft recoil system, i.e., smaller recoil forces require a lighter and smaller bottom carriage to transmit loads to the ground during firing. Usually a single baseplate pivoted to the top carriage serves the purpose. Fig. 9-3, Ref. 1, shows a schematic representation of the soft recoil XM204 towed Howitzer. It should be noted that the carriage has a long box trail with rollers at the end. The rollers rest on the ground during firing and roll when the gun orientation (traverse) is changed. Contrary to conventional recoil systems, the trail in soft recoil systems is in the forward direction. Analysis and design of the bottom carriage, i.e., baseplate, in this case can be performed using conventional methods.

THIS DOCUMENT PROVIDED BY THE ABBOTT AEROSPACE
TECHNICAL LIBRARY
ABBOTTAEROSPACE.COM

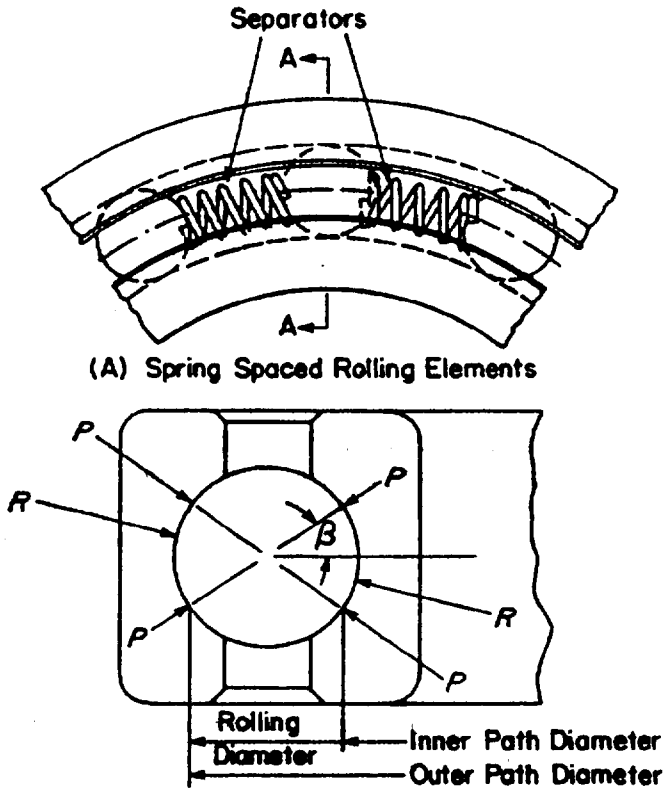

P = rolling loads, N
R = resultant of loads, N
β = contact angle, deg

Figure 9-2. Four-Point Contact Ball Bearing

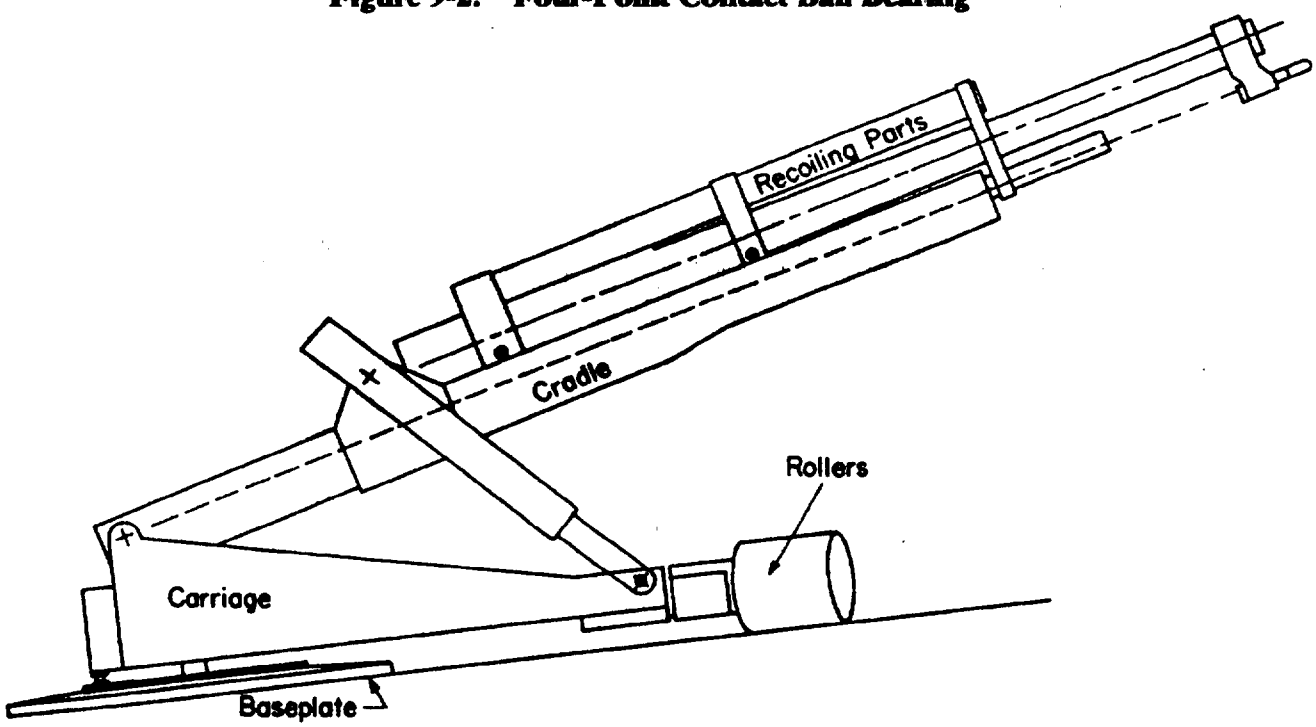

Figure 9-3. Schematic Representation of Soft Recoil XM204 Towed Howitzer (Ref. 1)

THIS DOCUMENT PROVIDED BY THE ABBOTT AEROSPACE
TECHNICAL LIBRARY
ABBOTTAEROSPACE.COM

9-2 TYPES OF BOTTOM CARRIAGES

9-2.1 STRUCTURES FOR BOTTOM CARRIAGES

Although the definition of bottom carriage is specific enough, the immediate structure supporting the top carriage is not always identified as the bottom carriage. Such terms as platform and pedestal apply equally well. The lines of demarcation grouping the various structures according to their respective categories are nebulous and cannot be sharply defined. Since their functions are similar, however, all are included in the general class of bottom carriages. Not only the basic structure but all components, such as trails, outriggers, spades, and floats, are also considered. These components also include the limber frames and bogie. Bottom carriages can be grouped into two categories according to whether or not they allow off-carriage traverse. Bottom carriages for weapons that have off-carriage traverse differ from those that have only on-carriage traverse. Each of these two categories of bottom carriages is described. Although some of the bottom carriage structures are not used in modern towed weapons, they are included for historical purposes.

9-2.1.1 Bottom Carriage for On-Carriage Traverse Weapons

Here the term "on-carriage traverse" implies that, during traverse, the top carriage moves relative to the bottom carriage through a traverse bearing and a traverse mechanism. Bottom carriages included in this category range from very simple to quite complex structures. In some light artillery mounts the forward part of the trails also serves as the bottom carriage. Some mounts employ simple attachments that are little more than brackets attached to the axle, whereas others have structures that serve as both chassis and bottom carriage. The more complex units—which include firing platforms, pedestals, and bottom carriages—serve as the supporting structure for the general range of weapons from light through heavy weapons. A description of some supporting structures follows:

1. *Supporting Bracket.* The supporting bracket is a compact structure that serves as the bottom carriage of some light field pieces. It supports the top carriage and transmits the load to the ground via trails and axle supports. Fig. 9-4 shows this type of installation. Brackets on the axle provide attachments for trails, top carriage, wheels, and firing supports.

2. *Equalizing Support.* The equalizing support is a beam, usually tubular, with brackets for attaching the top carriage, axle, and trails (Fig. 9-5). The central bracket serves a two-fold purpose by providing the pintle housing for the top carriage and the horizontal spindle about which the axle rotates to compensate for uneven terrain. The spindle transmits most of the vertical component of the firing load to the ground through the axle and wheels or firing support. The remainder of the vertical component and the entire horizontal component

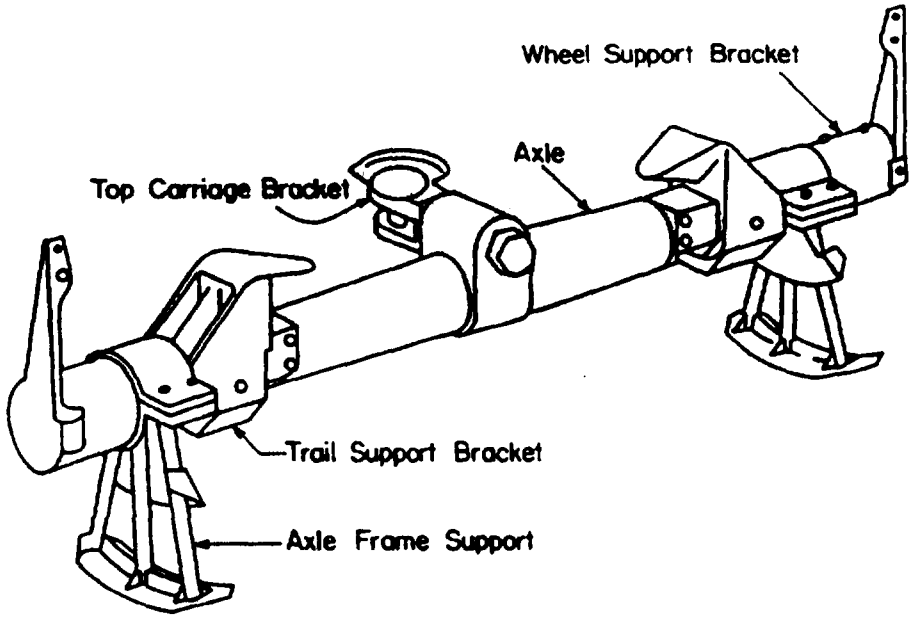

Figure 9-4. Supporting Bracket Installation

THIS DOCUMENT PROVIDED BY THE ABBOTT AEROSPACE
TECHNICAL LIBRARY
ABBOTTAEROSPACE.COM

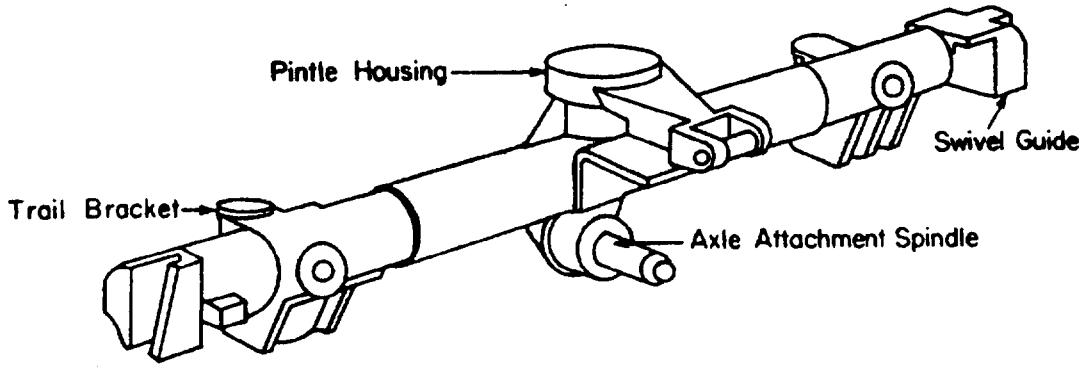

Figure 9-5. Equalizing Support

are transmitted by the trails that are attached to brackets located near the ends of the support. In addition to the three main brackets, two others outside the trail brackets provide vertical retaining grooves for confining axle rotation to one plane.

3. *Firing Platform (240-mm Howitzer M1918M1 Type)*:

The firing platform (Fig. 9-6), as the name implies, is a flat structure that supports the weapon during firing and transmits firing loads to the ground. Two of its components, the pintle and rear sector, transmit top carriage loads to the platform. The pintle functions as the pivot for the traversing parts and, as a structural member, supports horizontal and vertical loads. The sector has two functions: to support vertical loads and to provide the bearing surface for the rolling elements of the top carriage during traverse.

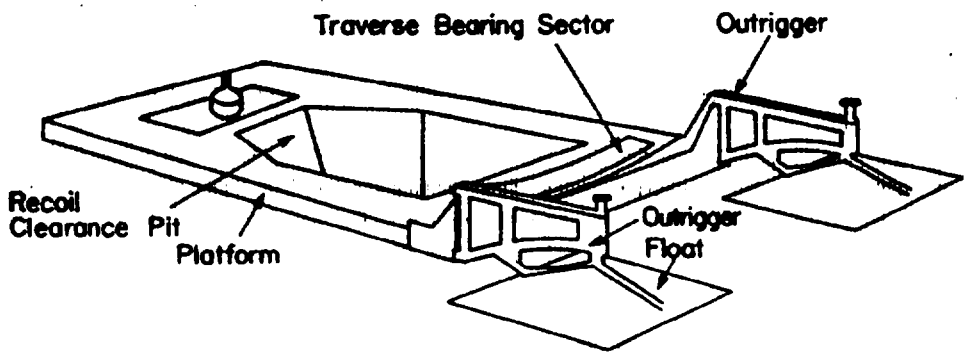

Figure 9-6. Firing Platform

The main structure with three other components, namely, the trunk that fits into the emplacement pit and two outriggers with floats, is responsible for directing the firing loads to the ground; the trunk is for the horizontal loads and the others are for the vertical loads. The outriggers and floats, by effectively increasing the length of the base, lend stability to the weapon. The platform has a large recess immediately to the rear of the pintle that is formed by the hollow structure of the trunk and provides clearance for the recoiling parts. An emplacement of this type is limited to small adjustments in elevation and traverse.

4. *Bottom Carriage for the M198, 155-mm Howitzer.* Fig. 9-7 shows the bottom carriage for the 155-mm M198 Howitzer (Ref. 2). The top carriage is linked to the bottom carriage through a traverse bearing that transmits loads to the bottom carriage during firing. The part immediately supporting the traverse bearing is similar to a cylindrical box with interior, vertical stiffening plates and is connected to towing wheels on one side and to two split trails on the other. Each trail is again box shaped and has a spade and a float at the end. Spades are driven into the ground at the firing site, whereas the floats rest on ground. Trails give stability to the weapon during firing and act as a link between the prime mover and the weapon during transportation. Also

THIS DOCUMENT PROVIDED BY THE ABBOTT AEROSPACE
TECHNICAL LIBRARY
ABBOTTAEROSPACE.COM

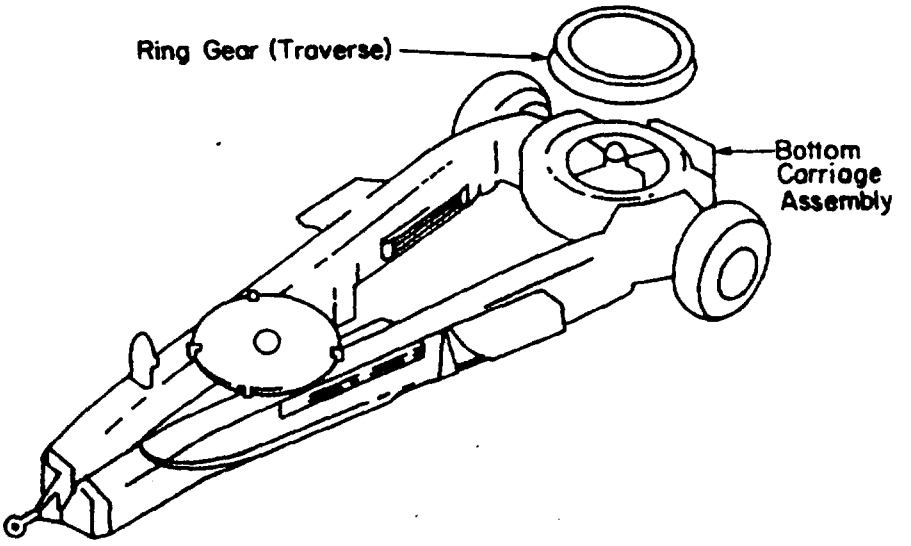

Figure 9-7. M198 Towed Howitzer Bottom Carriage

trails are usually designed to have an angle of 70 deg between them at the time of firing. This configuration allows a limited on-carriage traverse of approximately 45 deg (Ref. 3).

5. *Pedestal*:

The pedestal, shown in Fig. 9-8, is the firing base and also serves as the chassis during transport. This design is usually reserved for antiaircraft use because it is particularly suited for high angles of elevation in all directions. The structure is composed of three units, i.e., the leveling socket assembly (shown in Fig. 9-9), the pedestal, and the four outriggers. The leveling socket is the immediate support of the top carriage and, in turn, is supported by the pedestal. Two retractable hydraulic jacks, fitted into outriggers, lower and raise the mount on and off the leveling socket.

The leveling socket is a circular structure and has the traversing gear, roller bearing, and clip ring assembled to its upper side. All are associated with the traversing parts. The gear is the fixed member of the traversing gear train, the bearing is the low friction element, and the clip ring is the retainer that precludes tipping of the traversing parts. A hemispherical bearing, which fits over its male counterpart on the pedestal and permits only tipping motion for leveling purposes, is attached to the lower side of the leveling socket. Leveling is accomplished by four leveling screws supported on special pads of the pedestal; the screws bear against the leveling socket and restore it to the horizontal plane (Fig. 9-10). The angular displacements are small, on the order of 5 deg, and can compensate for only minor irregularities of the terrain.

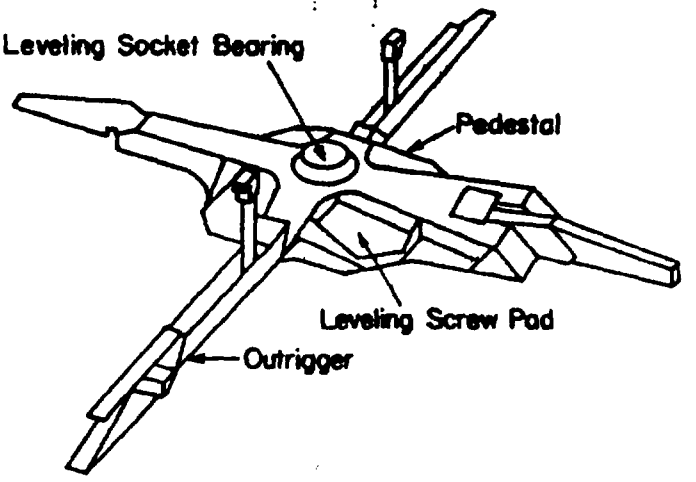

Figure 9-8. Pedestal

THIS DOCUMENT PROVIDED BY THE ABBOTT AEROSPACE
TECHNICAL LIBRARY
ABBOTTAEROSPACE.COM

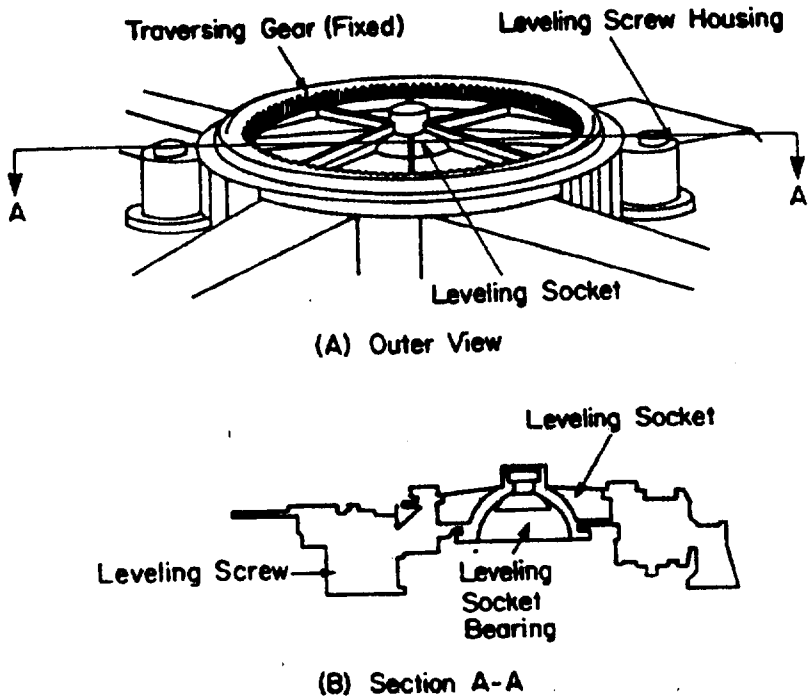

Figure 9-9. Leveling Socket Assembly

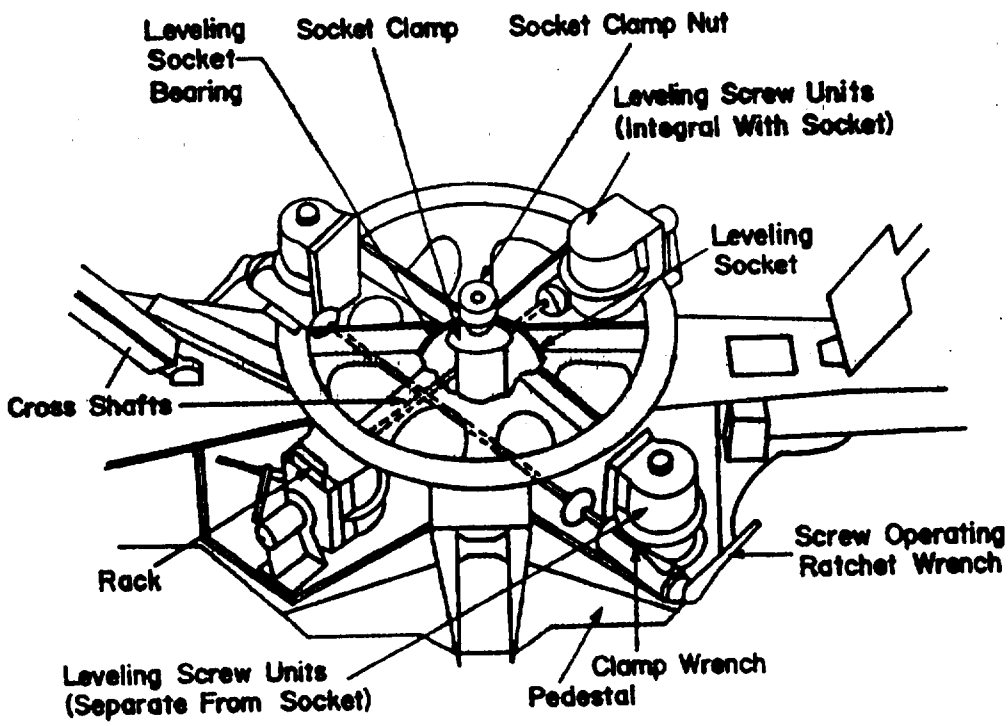

Figure 9-10. Leveling Mechanism

THIS DOCUMENT PROVIDED BY THE ABBOTT AEROSPACE
TECHNICAL LIBRARY
ABBOTTAEROSPACE.COM

The pedestal conducts all forces to the ground—either directly or through its four outriggers—and becomes the chassis of the weapon during transport. The outriggers, hinged to it, are used primarily during firing. Pins make the hinged joint rigid, but during transport they are withdrawn, and the outriggers retract by folding upright against the main structure. One outrigger becomes the prop for the gun tube while in this retracted position.

9-2.1.2 Bottom Carriage for Off-Carriage Traverse Weapons

The term "off-carriage traverse" implies that the traversing of the weapon takes place *off* the bottom carriage, such as near the end of the trails. The bottom carriage for such weapons can be significantly different from those for the "on-carriage traverse" weapons. Two bottom carriages having off-carriage traverse are described in the following paragraphs:

1. *Bottom Carriage for XM204, 105-mm, Light Towed Howitzer.* Fig. 9-3 is a schematic representation of a soft recoil XM204 towed Howitzer (Ref. 1). This weapon, with its unique trails-forward configuration, is the first towed artillery system to employ the soft recoil cycle. The XM204 Howitzer features improved firing stability (due to lower recoil reactions), reduced weight and package size, increased rate of fire (because of reduced cycle time), reduced overpressure (due to smaller charges and reduced forces) in crew area, 6400-mil off-carriage traverse, a simplified recoil system, and a greater range than its predecessors. There is usually no distinction made between top and bottom carriage for XM204 and M102 Howitzers; the top and bottom carriages are jointly termed "a carriage". The XM204 carriage is composed of a welded box-section undercarriage, a traversing beam assembly, a cradle and buffer assembly, a ball-screw-type elevating mechanism, a retractable suspension system, and a firing base. The carriage has a 6400-mil off-carriage traverse capability and has an elevating range from −87 to +1323 mils. Elevating and traversing handwheels are provided on both sides of the carriage.

2. *Bottom Carriage for the M102, 105-mm Light Towed Howitzer.* Fig. 1-13 shows the M102 Howitzer consisting of an M137E1 cannon and an M37 recoil mechanism mounted on an M31 carriage. The weapon is traversed and elevated by handwheels located on the sides of the carriage. A 6400-mil traverse capability is provided because the carriage pivots around the center of a circular base by means of a roller located at the rear of the "wishbone"-shaped box-trail assembly. The elevation mechanism employs a pair of ball-screw assemblies to elevate the tipping parts through an elevation range of −5 to +75 deg. Under normal conditions and average terrain, this weapon can be returned to proper deflection within one-half turn of the handwheel after firing a maximum charge at low quadrant angles of elevation. The weapon is staked in firing position. Holes are incorporated in the firing base for the stakes, which are provided as standard equipment.

9-2.2 MATERIALS

Bottom carriages are subjected to high stress levels during firing because of impulsive and repetitive loadings. It is necessary, therefore, that tough, high-strength material be used for bottom carriages. Structural steel possesses the desired properties and has been used extensively in the past for bottom carriages; however, the transportation of weapons demands light weight. A high-strength aluminum alloy, KO-1—containing silver, manganese, magnesium, titanium, and copper (Ref. 4)—satisfies these requirements; however, the bottom carriage for the 155-mm M198 Howitzer is not made of aluminum alloy. The alloy is as strong as steel but is much lighter. The specific gravity of the KO-1 alloy is 30% less than that of steel, yet the yield points of the two materials are nearly equal. Another important property of a material to be used for bottom carriages is the modulus of elasticity. The higher the modulus of elasticity, the greater the stiffness. Also the stiffer the carriage, the smaller the deflections. Tests conducted on steel and aluminum alloy bottom carriages indicate that aluminum alloy has a vertical spring rate about 87% lower at the hinge pins than steel does (Ref. 2). In other words, for the same loading the aluminum alloy bottom carriage will have about 8% greater vertical deflection at the pins than the steel bottom carriage will. The alloy, however, exhibits a better elastic range than the steel. In shock loading, a high-strength and less-stiff material is preferable over a stiff material. The total permanent vertical set at the hinge pins for the alloy is 1.867 mm, whereas for the steel it is 3.264 mm. These observations indicate the suitability of both materials against deformations. In general, for the parts of the bottom carriage for which high stress levels are anticipated, a high-strength, lightweight material should be selected. However, those parts that are inherently large in size but are subjected to low stress levels may be made of low-strength, lightweight material. Regardless of the choice, care must be exercised in selecting a material that is readily available.

THIS DOCUMENT PROVIDED BY THE ABBOTT AEROSPACE
TECHNICAL LIBRARY
ABBOTTAEROSPACE.COM

9-2.3 MANUFACTURING ASPECTS

The type of construction of the individual parts—whether forgings, castings, or mill stock—should be left to the discretion of the designer. He should be guided, however, by the relative suitability of each type for each application. Many times, forging or casting is a matter of economics rather than other considerations. Forgings demonstrate their greatest advantage in applications requiring high strength-to-weight ratios. The high cost of forgings is the chief disadvantage. Castings may be used if weight is not critical. Large fillets moderate the stress concentration at reentrant angles. After machining operations are completed, castings are usually ready for installation. It is assumed that they have been stress relieved before machining to insure dimensional stability.

Because of bulkiness and a lengthy manufacturing process, mill stock generally is used for built-up structures. Availability and low cost are its greatest assets. Weldments are preferred because they are relatively simple and light. Construction requires only a short time, and although weldments are prone to warp, this tendency is overcome by stress relieving through heat treatment. Regardless of the type of construction, the method of construction and material selected must show compatibility with low cost, light weight, ease of manufacturing, and availability of material.

9-3 PRELIMINARY DESIGN OF BOTTOM CARRIAGE

As for all structures, the bottom carriage design should be directed toward simplicity, symmetry, and compactness. These criteria are usually compatible; the realization of one stimulates the incorporation of the other two. All tend to reduce the weight. A compact bottom carriage also helps to provide a low silhouette for the weapon. Symmetry means uniformly applied loads and ultimately a stronger, lighter unit because eccentric loads require heavy local reinforcements. If both the applied and structural loads are symmetrical, deflections will be symmetrical with fewer adverse effects upon the accuracy of the weapon than would occur if symmetry did not prevail. Simplicity is always a major factor. A simple structure means ease of manufacture, ease of assembly, and ease of maintenance—all of which are conducive to low costs.

Another problem confronting the designer relates to the selection of material. Lightweight structures are preferred for transportability, and highly stressed components should be made of material with high strength-to-weight ratios. If applied loads are relatively small and the sizes of the components are inherently large, lightweight, low-strength materials should be given preference. Regardless of the choice, however, care must be exercised in selecting a material that is readily available. If a shortage of the original choice is anticipated, it may be prudent to design a structure based on one material so that it can be easily modified to conform to the physical properties of another. This practice, however, can be dangerous if, in trying to include too many variables, the net result is an inferior structure.

A prime asset of any weapon is a short emplacement time. Emplacement includes two general operations: the preparation of the terrain and the positioning of the weapon. Other than the selection of a suitable location that includes a favorable ground condition, little can be done to speed emplacement. Assume that the terrain is favorable; then any disturbance to it in order to position and secure the bottom carriage and its components will add to the emplacement time. This time includes digging clearance holes for the recoiling parts and holes for trail spades. Arrangement of the bottom carriage components in a firing position occasionally requires considerable time, particularly for heavy structures, and thus creates the need for power-operated equipment. Power from the prime mover is readily available, or auxiliary units, either detached from or assembled to the weapon, may be used. If power units are assembled to the weapon, emplacement time will be reduced further—at least by the duration of the hookup period. Not only does the power-operated handling equipment decrease emplacement time, but it also reduces to a minimum the size of the operating crew required.

The bottom carriage of a conventional recoil weapon is one compact structure, usually a casting or a weldment. The simpler types, namely, the supporting bracket and equalizing support, may be added to this group. Provision must be made for the attachments of the top carriage and its associated parts and for the various ground supports and attachments required during firing and transport. The bottom carriage includes the pintle or its equivalent, some components of the traverse bearing, and either traversing gear or mechanism. The ground supports and attachments may include trails or outriggers, tow bar unit, jacks, and the transport units such as bogie and limber.

The pintle is the stanchion about which the top carriage rotates. Paired with the traverse bearing, it links the top and bottom carriages and is capable of transmitting both horizontal and vertical loads. Pintles are simple structures, little more than cylindrical pins, and are readily machined of forged steel.

THIS DOCUMENT PROVIDED BY THE ABBOTT AEROSPACE
TECHNICAL LIBRARY
ABBOTTAEROSPACE.COM

Some weapons, particularly antiaircraft weapons that are mounted on pedestals, substitute the more elaborate leveling socket for the pintle. The body of the socket (shown in Fig. 9-9) is a large, circular, concave steel casting whose center is formed into a hemispherical socket. Its counterpart on the pedestal is also a steel casting (Fig. 9-8). The two bearing surfaces are held snug by a steel clamp that extends through the mating hemisphere and is drawn tight by a nut that bears against the outer surface of the upper member.

Several types of construction are suitable for ground supports of bottom carriages. Trails and outriggers are built-up box beams. Either the complete structure may be made of mill stock or the hinge at one end and the spade and float at the other may be forged or cast. Weldments are used in preference to riveted structures. Tow bar and steering units are usually of welded tubular construction. The moving parts of jacks are forgings or are machined from mill stock, whereas jack housings and axle firing supports are steel castings. The structures of bogies and limbers are well suited to be fabricated as weldments.

9-3.1 LOAD ANALYSIS

This paragraph presents a general discussion of the external loads that the bottom carriage supports under different situations, e.g., firing, towing, and airlift.

As explained in Chapter 3, the bottom carriage is subjected to ground reactions transmitted through spades and floats in addition to reactions transmitted by the top carriage through the traverse bearing and inertial loads, if any. Evaluation of these loads for different dynamic modeling is also explained in Chapter 3. A general procedure for evaluating ground and top carriage reactions is to assume the sizes of all components of the weapon assembly so that the location of their mass centers is known. Then a suitable dynamic model is chosen to obtain the desired accuracy in evaluation of loads. Equations of motion are then formulated for the specified external loading input. Solutions of these equations yield the desired ground and top carriage reactions.

Of all the loading conditions, the loads experienced during firing are usually the most severe. All firing conditions should be investigated during recoil and counterrecoil and for selected angles of elevation and traverse. Usually the maximum, minimum, and some intermediate angles with top zone charge provide the critical design loads. Transport conditions include normal travel, braking, and 30% side slope. The critical load is found by multiplying the actual load by the load factor: 1.5 for firing, 3.0 for sprung transport loads, and 5.0 for unsprung transport loads. The side slope condition is not prevalent because the speed is slow; therefore, a load factor of 1.0 is adequate. Axiomatically, when stresses are computed for the actual applied loads, the load factor becomes the factor of safety. Transport conditions seldom yield critical design loads for the bottom carriage, but they are the sole basis of design for the associated structures of bogie, limber, and towing unit.

9-3.2 STRESS ANALYSIS

The objective of stress analysis in preliminary design is to estimate the stress levels attained in a component under different loading conditions. It should also locate specific areas of high stress levels so that the designer may strengthen those areas by suitable measures. A detailed stress analysis demands state of stress (stress tensor) at each point of the component that is analyzed. There are several methods to obtain detailed stress analysis—the finite element method or the theory of elasticity approach may be used. Each method has its advantages and disadvantages and the selection of a method depends on the type of problem. Usually, these methods call for expertise in stress analysis and accessibility to modern, high-speed, high-storage computers. To estimate stress levels in preliminary design, however, the procedures presented in Chapters 7 and 8 can be used. Thus highly simplified models may be used for the component under consideration. The stress analyst searches for dominant internal actions—such as flexure, shear, in-plane or axial loading, and twisting—in different parts of each component. Then the geometry—i.e., relative dimensions such as ratios of length/width, length/depth, or area/thickness—of these parts and their boundary conditions are given consideration to determine whether they could be approximated as ideal elements for which standard stress analysis theories exist and whether equations are available to evaluate stresses. Sometimes when the boundary conditions or the configurations of these parts make them statically indeterminate, proper assumptions are made to render them determinate. The assumptions to be made usually require ingenuity and experience on the part of the analyst. Usually, assumptions are made to maintain dominant actions and to ignore relatively small actions in the parts that are to be rendered statically determinate. After modeling parts of a component, free-body diagrams of these parts under a given external loading are drawn. It is then possible to determine

THIS DOCUMENT PROVIDED BY THE ABBOTT AEROSPACE
TECHNICAL LIBRARY
ABBOTTAEROSPACE.COM

reactions on the boundaries of various parts by judiciously employing equations of equilibrium. Once the boundary actions are known, each part can be analyzed separately. Each part is then sectioned to expose internal loading at places of interest. Standard equations are then used to determine the stresses at the points of interest. When stresses at points of interest in a component for the given loading have been obtained, the procedure is repeated for other external loadings and the stresses are superimposed if two or more loading conditions act simultaneously. The size of the component is then adjusted to satisfy failure stress constraints. The procedure outlined in this paragraph is illustrated in par. 9-4.

9-4 SAMPLE BOTTOM CARRIAGE DESIGN PROBLEM

Sample design calculations for the bottom carriage of the M198 towed Howitzer are presented in this paragraph. These calculations are based on the substance of par. 9-3. Note that the sample design procedure presented herein is not the only way to design a bottom carriage. Several variations are possible depending on designers' experience, desired accuracy, and the assumptions made in the process. Usually, beam-type modeling is used for stress analysis.

9-4.1 LOAD ANALYSIS

For the purpose of this paragraph it is assumed that the preliminary design of the bottom carriage is available—i.e., materials, shapes, and sizes of all the components of the bottom carriage are known. Further, as noted earlier, all loading conditions should be investigated to obtain the worst combination of loads that results in maximum stress and/or deflection levels. As for the bottom carriage, the loading conditions to be considered are firing, towing or transportation on ground, airdrop, helicopter sling, and rail transportation. Firing loads usually are critical, and consequently, these loads are used to illustrate stress analysis and the design of bottom carriages. Other loads can be treated similarly.

As explained in Chapter 3, the designer must first develop a dynamic model for the system, and equations of motion for the model are written. Then for the given input, such as the firing loads, the equations of motion are integrated to obtain generalized coordinates, velocities, and accelerations as functions of time. Since accelerations are known at any instant, inertial loads for any component can be determined by using d'Alembert's principle. These and other loads are used to determine reactions at various interfaces; these reactions then become design loads for components. Some dynamic analysis programs, such as the Dynamic Analysis and Design System (DADS), automatically give forces of constraint that can be used for the design of components.

By considering the free-body diagram of the top carriage, it is possible to obtain reactions at the traverse bearing. These reactions are in the form of two concentrated forces—one perpendicular to the plane of the bearing and the other in the plane—through the center of the bearing and a moment vector in the plane of the bearing. When these reactions have been obtained, a free-body diagram for the bottom carriage is drawn, and here the term bottom carriage includes trails, spades, floats, and the main body under the traverse bearing. Fig. 9-11 shows the free-body diagram for the main body of the bottom carriage, whereas Fig. 9-12 shows the free-body diagram for the right trail. Since the designer is interested in the maximum values of functions such as bending moment, shear force, and axial force (internal forces) at all critical sections—particularly those where the geometry, external loading, or material properties change abruptly—these functions must be evaluated at various sections for different loading conditions. For the M198 towed Howitzer, several elevation angles in the range of −5 to 75 deg and various traverse angles in the range of 0 to 22.5 deg (on either the left or right side) can be considered. Usually, discrete values of elevation and traverse angles are chosen that are likely to give maximum values for various internal forces in the carriage. Table 9-1 shows the external reactions for the chosen elevations of 35 deg, 55 deg, and 75 deg; traverse angle of 22.5 deg; and time instances of 0.1390, 0.092, 0.141, and 0.149 s in short recoil. Two time instances are used for the angle of elevation of 35 deg because these time instances are likely to give maximum values for various internal forces.

9-4.2 STRESS ANALYSIS

The designer is interested in the maximum values of stresses caused by maximum internal forces such as shear force, bending or twisting moment, and axial and/or in-plane forces because once the maximum stresses are known, the problem is treated as a static one. To obtain a good estimate of maximum internal forces, the designer must analyze the structure for each chosen external loading. The maximum value of internal forces acting at each section is then selected from among the values obtained for different external loads. The maximum internal force envelope can then be drawn, and maximum stresses evaluated for all the sections.

THIS DOCUMENT PROVIDED BY THE ABBOTT AEROSPACE
TECHNICAL LIBRARY
ABBOTTAEROSPACE.COM

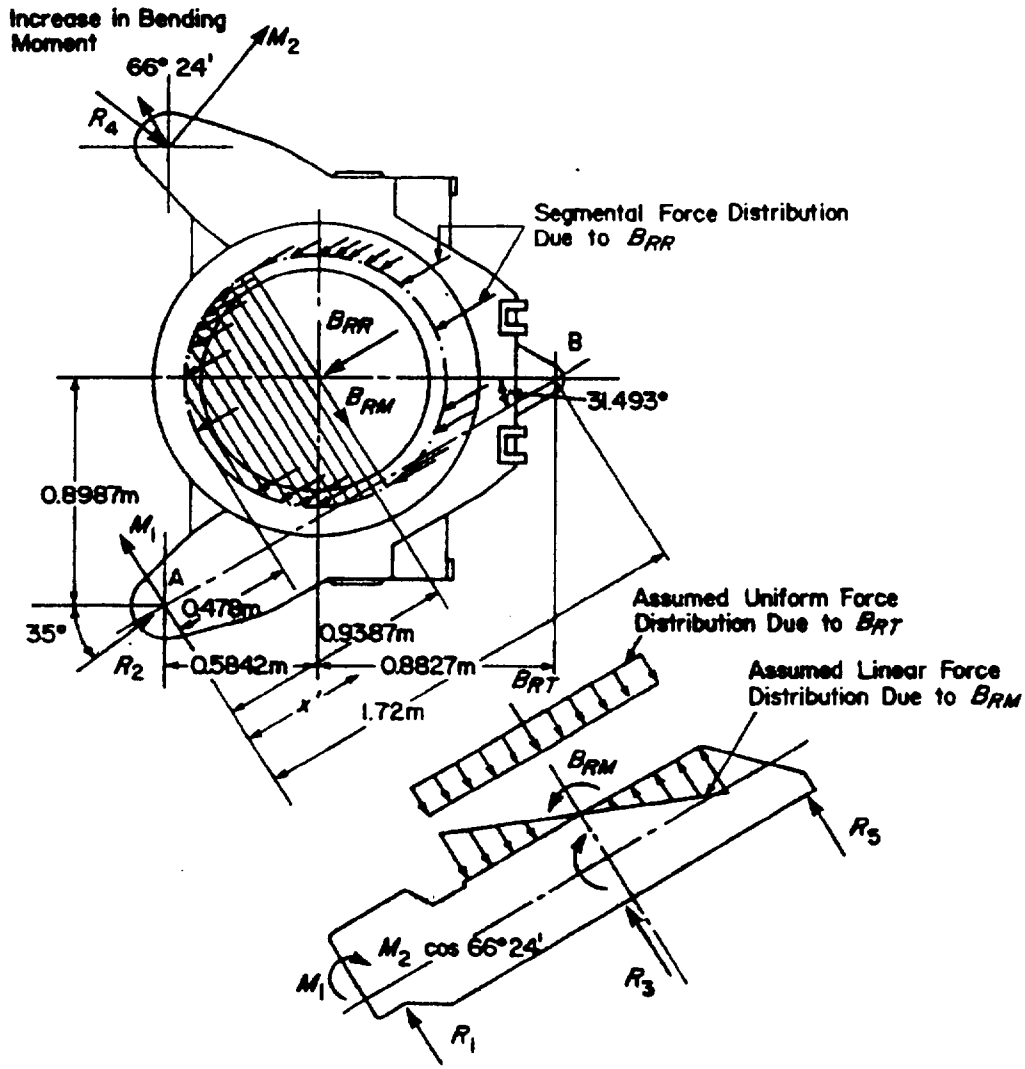

A = right-trail-hinge pin point
B = front-float point
x' = distance from A along AB for any section on AB, m
R_1 = right-trail float reaction, N
R_2 = right-trail spade reaction, N
R_3 = left-trail float reaction, N
R_4 = left-trail spade reaction, N
R_5 = front-float reaction, N
M_1 = moment at right-trail hinge pin due to R_1 and R_2, N·m
M_2 = moment at left-trail hinge pin due to R_3 and R_4, N·m
B_{RR} = in-plane (plane of traverse bearing) component of bearing reaction on bottom carriage, N
B_{RT} = normal component (normal to plane of traverse bearing) of bearing reaction on bottom carriage, N
B_{RM} = bearing moment acting on bottom carriage, N·m

Figure 9-11. Bottom Carriage (Main Body) Free-Body Diagram 22.5 deg Traverse (Ref. 6)

THIS DOCUMENT PROVIDED BY THE ABBOTT AEROSPACE
TECHNICAL LIBRARY
ABBOTTAEROSPACE.COM

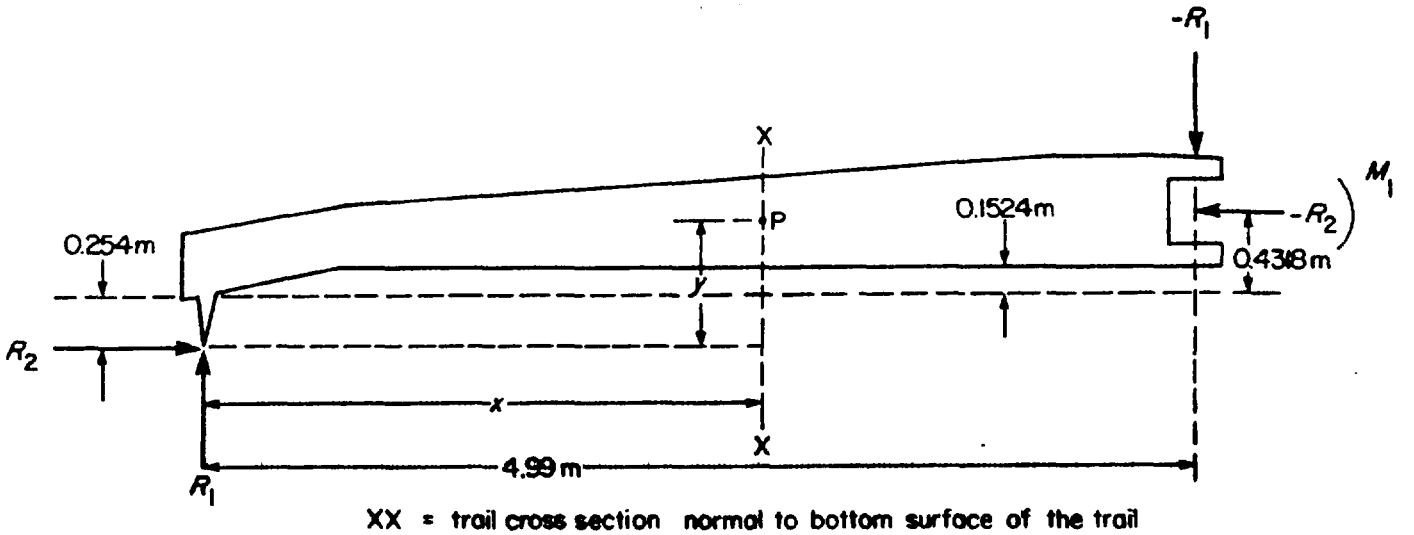

XX = trail cross section normal to bottom surface of the trail

x = distance of XX from trail float reaction, m

y = distance of centroid of XX from trail spade reaction, m

Figure 9-12. Free-Body Diagram for Right Trail (Ref. 6)

TABLE 9-1
FORCES ON BOTTOM CARRIAGE FOR FOUR LOADING CONDITIONS (Ref. 6)
(From dynamic force analysis (traverse = 22.5 deg))

Condition	A	B	C	D
Elevation, deg	35	35	55	75
Short or long recoil	short	short	short	short
Time, s	0.1390	0.092	0.141	0.149
Right-trail float reaction R_1, N	93,773	80,766	93,457	77,973
Right-trail spade reaction R_2, N	192,190	192,572	134,523	49,202
Left-trail float reaction R_3, N	33,233	33,006	38,397	38,161
Left-trail spade reaction R_4, N	61,532	61,701	43,103	15,764
Front-float reaction R, N	18,607	80,063	—	—
Bearing radial force B_{RR}, N	224,999	—	157,489	57,604
Bearing thrust force B_{RT}, N	123,709	—	210,613	268,569
Bearing moment B_{RM}, N·m	418,578	—	417,660	346,105

9-4.2.1 Trails

Trails are basically beam columns. At low angles of elevation axial loads are relatively large; however, for higher angles of elevation, bending moments and shear forces are dominant. A sample calculation for Section 28 is provided.

As shown on Fig. 9-12, the centroid of Section 28 is point P, and the bending moment M_b about point P is

$$M_b = R_1 x - R_2 y, \text{ N·m} \tag{9-1}$$

where

R_1 = right-trail float reaction, N
R_2 = right-trail spade reaction, N
x = distance of section from trail-float reaction, m
y = distance of section centroid from trail-spade reaction, m.

THIS DOCUMENT PROVIDED BY THE ABBOTT AEROSPACE
TECHNICAL LIBRARY
ABBOTTAEROSPACE.COM

From Table 9-1, Condition A,
$R_1 = 93{,}773$ N
$R_2 = 192{,}190$ N.

From Table 9-2
$x = 4.7752$ m
$y = 0.6855$ m.

TABLE 9-2
TRAIL SECTION PROPERTIES (Ref. 6)

Section	x, m	y, m	A, m	B, m	I, m^4	Z, m^3	A_{sh}, m^2
1	0.000	0.5715	0.00635	0.3302	6.730 E-4	4.077 E-3	5.18 E-2
2	0.0318	0.5716	0.00639	0.3305	1.634 E-4	9.886 E-4	9.63 E-3
3	0.1270	0.5720	0.00651	0.3314	1.659 E-4	1.001 E-3	9.70 E-3
4	0.2540	0.5726	0.00667	0.3326	1.692 E-4	1.017 E-3	9.79 E-3
5	0.3810	0.5732	0.00684	0.3339	1.725 E-4	1.034 E-3	9.89 E-3
6	0.5080	0.5738	0.00700	0.3351	1.759 E-4	1.050 E-3	9.98 E-3
7	0.6350	0.5744	0.00716	0.3363	1.794 E-4	1.067 E-3	1.01 E-2
8	0.7620	0.5750	0.00732	0.3375	1.828 E-4	1.083 E-3	1.01 E-2
9	1.0160	0.5833	0.00764	0.3541	2.087 E-4	1.179 E-3	1.05 E-2
10	1.2700	0.5916	0.00797	0.3705	2.368 E-4	1.278 E-3	1.09 E-2
11	1.5240	0.5999	0.00829	0.3871	2.674 E-4	1.382 E-3	1.13 E-2
12	1.7780	0.6082	0.00861	0.4036	3.595 E-4	1.781 E-3	1.38 E-2
13	2.0320	0.6164	0.00894	0.4201	4.007 E-4	1.908 E-3	1.41 E-2
14	2.2860	0.6247	0.00926	0.4366	4.445 E-4	2.038 E-3	1.45 E-2
15	2.5400	0.6329	0.00958	0.4531	4.920 E-4	2.172 E-3	1.49 E-2
16	2.7940	0.6412	0.00990	0.4696	5.419 E-4	2.308 E-3	1.52 E-2
17	3.0480	0.6494	0.01023	0.4861	5.956 E-4	2.450 E-3	1.56 E-2
18	3.3020	0.6577	0.01055	0.5026	6.522 E-4	2.595 E-3	1.60 E-2
19	3.5560	0.6760	0.01087	0.5192	7.122 E-4	2.743 E-3	1.63 E-2
20	3.8100	0.6742	0.01120	0.5357	7.754 E-4	2.895 E-3	1.67 E-2
21	4.0640	0.6825	0.01152	0.5522	8.425 E-4	3.051 E-3	1.71 E-2
22	4.1656	0.6847	0.01165	0.5567	8.624 E-4	3.098 E-3	1.72 E-2
23	4.3180	0.6849	0.01184	0.5571	8.703 E-4	3.125 E-3	1.73 E-2
24	4.4704	0.6854	0.01204	0.5575	8.778 E-4	3.149 E-3	1.74 E-2
25	4.5466	0.6852	0.01213	0.5577	10.364 E-4	3.717 E-3	1.97 E-2
26	4.6228	0.6853	0.01223	0.5579	12.645 E-4	4.533 E-3	2.28 E-2
27	4.6990	0.6854	0.01233	0.5581	13.669 E-4	4.899 E-3	2.62 E-2
28	4.7752	0.6855	0.01243	0.5582	19.084 E-4	6.830 E-3	3.88 E-2
29	4.9911	0.6858	0.01270	0.5588	12.911 E-4	4.621 E-3	2.73 E-2

NOTE: This table uses the expression E followed by a number to indicate the power of 10. For example, 6.730 E-4 = 6.730×10^{-4}.

Substitution in Eq. 9-1 gives

$$M_b = (93{,}773)\,(4.775) - (192{,}190)\,(0.6855)$$
$$= 316{,}019 \text{ N·m.}$$

Similarly, values for M_b for the other conditions are

Condition B	Condition C	Condition D
253,666 N·m	354,060 N·m	338,609 N·m

Thus the maximum bending moment M_b at Section 28 is 354,060 N·m as shown in Table 9-3 (Ref. 5).

THIS DOCUMENT PROVIDED BY THE ABBOTT AEROSPACE
TECHNICAL LIBRARY
ABBOTTAEROSPACE.COM

TABLE 9-3
MAXIMUM STRESSES IN TRAIL (Ref. 6)

Section	x, m	Axial Stress S_a, MPa	Bending Moment M_b, kN·m	Bending Stress S_b, MPa	Total Stress S_T, MPa
1	0	3.32	91.71	22.49	25.80
2	0.0318	19.99	90.68	91.77	111.76
3	0.1270	19.85	87.59	87.48	107.33
4	0.2540	19.66	83.47	82.02	101.69
5	0.3810	19.48	79.35	76.74	96.22
6	0.5080	19.30	75.23	71.62	90.91
7	0.6350	19.12	71.11	66.66	85.78
8	0.7620	19.18	67.87	62.66	81.84
9	1.0160	18.28	63.16	53.52	71.81
10	1.2700	17.66	72.86	57.00	74.67
11	1.5240	17.10	92.86	67.22	84.32
12	1.7780	13.98	112.85	63.36	77.34
13	2.0320	13.62	132.84	69.64	83.27
14	2.2860	13.27	152.84	75.04	88.31
15	2.5400	12.95	172.83	79.60	92.55
16	2.7940	12.64	192.83	83.51	96.15
17	3.0480	12.34	212.82	86.87	99.21
18	3.3020	12.06	232.81	89.75	101.81
19	3.5560	11.79	252.81	92.16	103.95
20	3.8100	11.53	272.80	94.21	105.75
21	4.0640	11.29	292.80	95.96	107.25
22	4.1656	—	—	—	—
23	4.3180	11.14	312.79	100.09	111.23
24	4.4704	9.78	325.53	103.36	113.14
25	4.5466	9.78	332.66	95.75	105.53
26	4.6228	8.45	339.78	75.13	83.58
27	4.6990	7.66	346.90	71.04	78.69
28	4.7752	4.96	354.06	51.84	57.27
29	4.9911	7.05	374.20	81.26	88.32

The maximum axial stress S_a is calculated by using the maximum axial force R_2 experienced under any of the stated conditions and is expressed as

$$S_a = \frac{R_2}{A_{cs}}, \text{ MPa} \qquad (9\text{-}2)$$

where

A_{cs} = area of cross section, m^2. (Figs. 9-13 and 9-14 provide dimensions for cross sections.)

From Table 9-1
$R_2 = 192{,}572$ N.

From Table 9-2 at Section 28
$A_{cs} = 3.88\times10^{-2}$ m^2.

Substitution in Eq. 9-2 gives

$$S_a = \frac{192{,}572}{3.88\times10^{-2}}$$

$$= 4.96 \text{ MPa}$$

THIS DOCUMENT PROVIDED BY THE ABBOTT AEROSPACE
TECHNICAL LIBRARY
ABBOTTAEROSPACE.COM

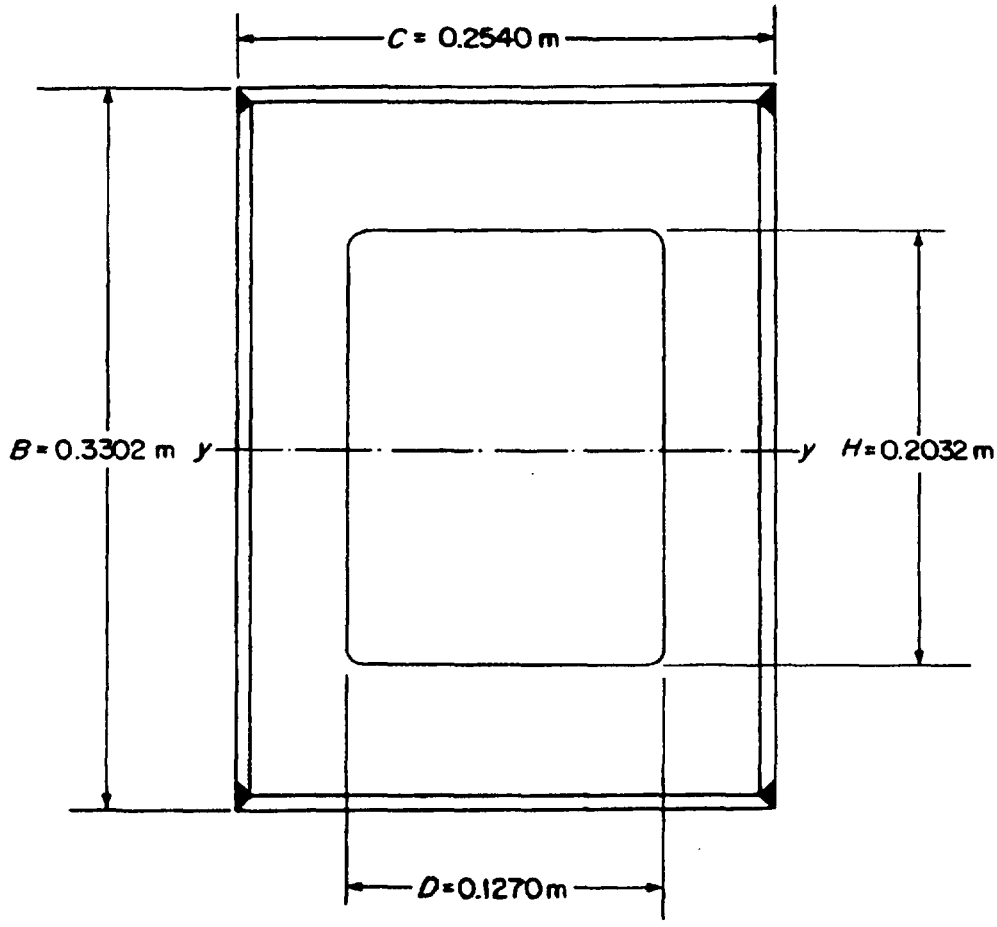

B, C, D, and *H* are cross sectional dimensions for section I as shown in the above figure.

Figure 9-13. Section Properties (Trail) at Section 1 (Ref. 6)

as shown in Table 9-3.

The maximum bending stress S_b at Section 28 is calculated by using the maximum bending moment M_b experienced under any of the stated conditions and is expressed as

$$S_b = \frac{M_b}{Z}, \text{ MPa} \tag{9-3}$$

where

Z = section modulus of cross section, m^3.

From Table 9-3

M_b = 354,061 N·m.

From Table 9-2

$Z = 6.83 \times 10^{-3}$ m^3.

THIS DOCUMENT PROVIDED BY THE ABBOTT AEROSPACE
TECHNICAL LIBRARY
ABBOTTAEROSPACE.COM

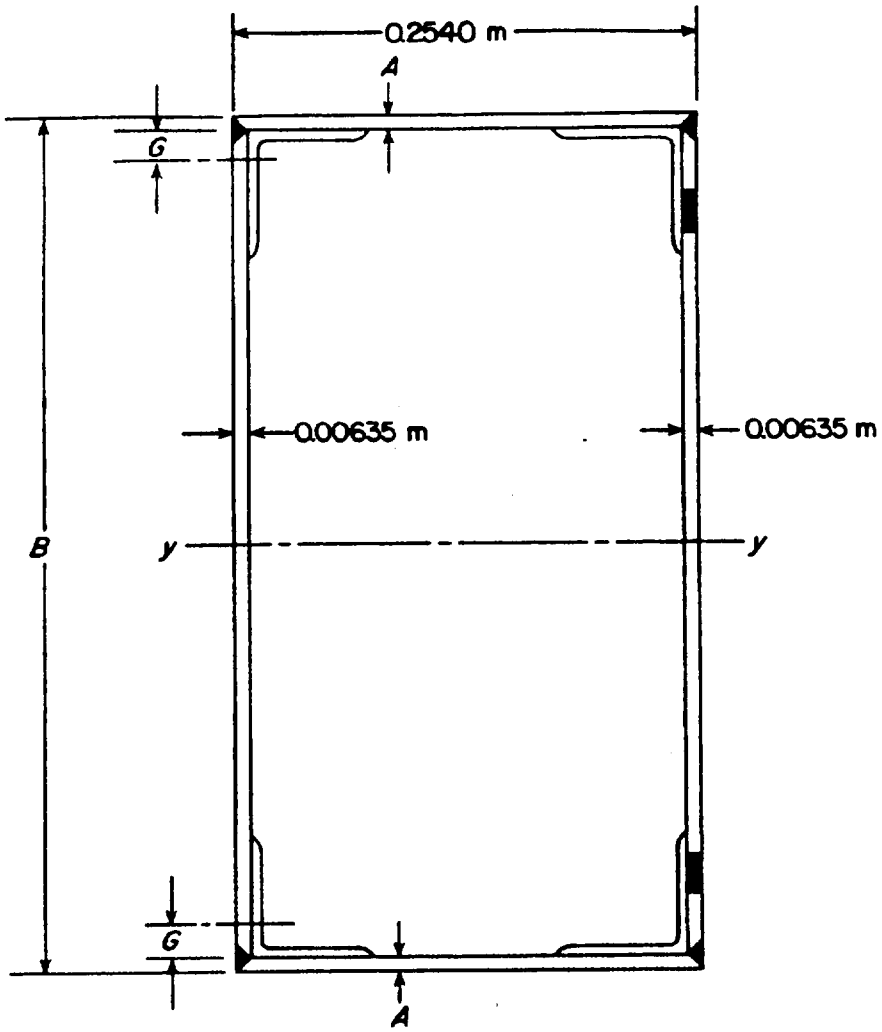

A = flange thickness, m

B = total depth of trail cross section, m

F = area of angle section, m^2

G = distance of centroid of angle section from its short flange, m

Figure 9-14. Section Properties (Trail) at Sections 2 Through 24 (Ref. 6)

Substitution in Eq. 9-3 gives

$$S_b = \frac{354{,}061}{6.83 \times 10^{-3}}$$

$$= 51.84 \text{ MPa}$$

as shown in Table 9-3.

The total maximum stress S_T is calculated by adding the maximum axial stress and maximum bending stress. For Section 28—using the R_2 values from Table 9-1 and the previously calculated M_b values—the values of S_a and S_b under the stipulated conditions are

THIS DOCUMENT PROVIDED BY THE ABBOTT AEROSPACE
TECHNICAL LIBRARY
ABBOTTAEROSPACE.COM

	S_a, MPa	S_b, MPa
Condition A	4.95	46.27
Condition B	4.96	38.60
Condition C	3.47	51.84
Condition D	1.27	49.58.

Using the maximum values of S_a and S_b. the total maximum stress S_T is

$$S_T = 4.96 + 51.84 = 56.80 \text{ MPa.}$$

9-4.2.2 Bottom Carriage Main Body

The forces and moments transmitted from the top carriage to the bottom carriage are transmitted through the traverse bearing. The moments occur during firing and are the products of rifling torque and the applied loads of the top carriage. The contact between the traverse bearing and the bottom carriage is through the circumference of the bearing. It is, therefore, necessary to find an equivalent distribution of these concentrated forces and moments along the circumference of the bearing. The reactive force normal to the plane of the bearing, referred to as the bearing-thrust force B_{RT} in Table 9-1, may be assumed to be uniformly distributed along the circumference. Also, for the sake of simplicity in the analysis, it may similarly be assumed that the in-plane-bearing reactive force, referred to as the bearing-radial force B_{RR} in Table 9-1, is equally distributed along the circumference. These assumptions simplify the stress analysis. Load distribution due to the bearing moment B_{RM} (Table 9-1) may be assumed to vary linearly, as shown in Fig. 9-11. It is easier to deal with a number of concentrated forces along the circumference of the traverse bearing instead of with distributed forces. Let the radius r of the bearing be divided into 10 equal lengths, as shown in Fig. 9-15. Then,

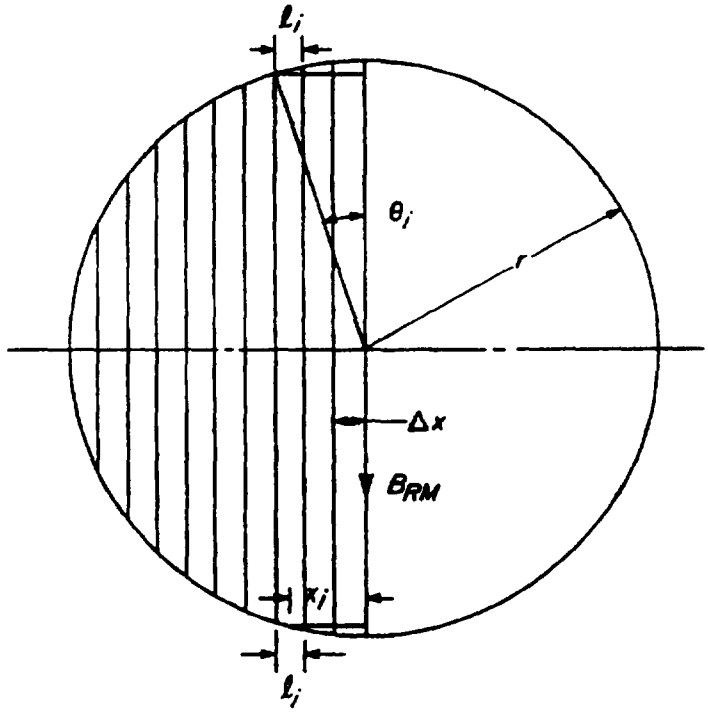

Δx = distance between two consecutive divisions, m

ℓ_i = circumferential distance of ith segment, m

θ_i = angle between two radii defining ith segment, rad.

r = radius of bearing, m

Figure 9-15. Division of Bearing Radius Into 10 Equal Parts (Ref. 6)

THIS DOCUMENT PROVIDED BY THE ABBOTT AEROSPACE
TECHNICAL LIBRARY
ABBOTTAEROSPACE.COM

$$\left.\begin{aligned} \ell_i &= r(\theta_i - \theta_{i-1}),\ \text{m} \\ \text{and} \\ \sin\theta_i &= \frac{(ir/10)}{r} = \frac{i}{10} \text{ or } \theta_i = \text{Sin}^{-1}\left(\frac{i}{10}\right) \end{aligned}\right\} \quad (9\text{-}4)$$

where

ℓ_i = circumferential distance of the ith segment, m
θ_i = angle between two radii defining ith segment, rad
r = radius of bearing, m.

Let the bearing thrust force B_{RT} be divided into a number of smaller concentrated forces along the circumference of the bearing. Then

$$\text{force/unit length} = B_{RT}/(2\pi r),\ \text{N/m} \quad (9\text{-}5)$$

$$\text{force/segment (both arcs)} = 2\ell_i\left(\frac{B_{RT}}{2\pi r}\right) = \ell_i\left(\frac{B_{RT}}{\pi r}\right),\ \text{N.} \quad (9\text{-}6)$$

The substitution of the expression for ℓ_i from Eq. 9-4 into Eq. 9-6 gives

$$[\text{force/segment (both arcs)}]_{RT} = \frac{(\theta_i - \theta_{i-1})B_{RT}}{\pi},\ \text{N.} \quad (9\text{-}7)$$

Table 9-4 gives the multiplying factors $(\theta_i - \theta_{i-1})/\pi$ for B_{RT} as a function of both arc lengths, i.e., $2\ell_i, i = 1, 2, \ldots, 10$ (Ref. 6). Note that the force/segment is assumed to act at the center of the length ℓ_i. Similarly, for the in-plane bearing force B_{RR},

$$[\text{force/segment (both arcs)}]_{RR} = \frac{(\theta_i - \theta_{i-1})B_{RR}}{\pi},\ \text{N.} \quad (9\text{-}8)$$

Table 9-4 can be used to obtain the multiplying factors for B_{RR}.

TABLE 9-4
PORTION OF B_{RR} OR B_{RT} TRANSMITTED TO EACH SEGMENT (Ref. 6)

Segment i	$\frac{\theta_i - \theta_{i-1}}{\pi}$
1	0.0319
2	0.0320
3	0.0331
4	0.0340
5	0.0357
6	0.0381
7	0.0420
8	0.0484
9	0.0612
10	0.1436

THIS DOCUMENT PROVIDED BY THE ABBOTT AEROSPACE
TECHNICAL LIBRARY
ABBOTTAEROSPACE.COM

Now consider the force distribution due to the bearing moment B_{RM}. The linear pressure p, force per unit length, as a function of the distance x from the bearing center is

$$p = K'x, \text{ N/m} \tag{9-9}$$

where

K' = constant of proportionality (to be determined later), N/m^2.
x = length as shown in Fig. 9-16, m.

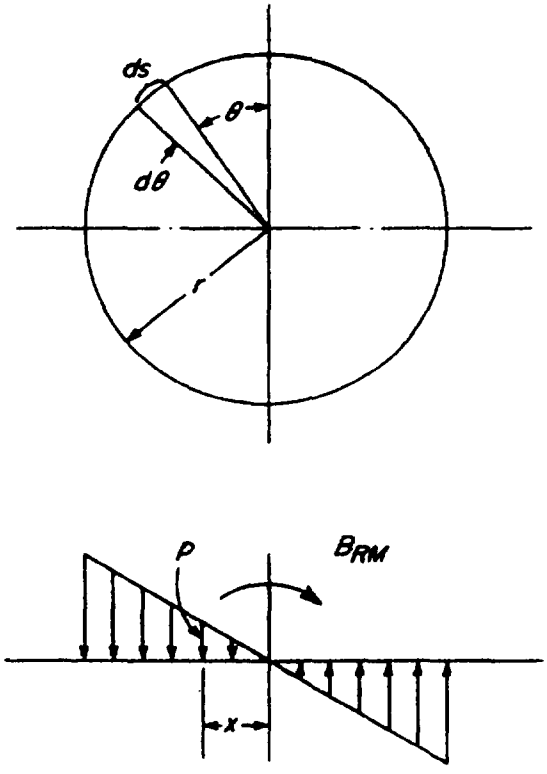

The moment is reacted by a force along the bearing. This force is proportional to the distance x from the center of rotation.

Figure 9-16. Bearing Reaction, Moment (Ref. 6)

The length x, from Fig. 9-16, is

$$x = r\sin\theta, \text{ m} \tag{9-10}$$

and, therefore,

$$B_{RM} = 2\int_0^{\pi r} xp\,ds, \text{ N} \tag{9-11}$$

where

ds = differential arc length, m.

Therefore, by substitution of the expressions for p and x from Eqs. 9-9 and 9-10, respectively, into Eq. 9-11, the result is

THIS DOCUMENT PROVIDED BY THE ABBOTT AEROSPACE
TECHNICAL LIBRARY
ABBOTTAEROSPACE.COM

$$B_{RM} = 2\int_0^{\pi}(r\sin\theta)(K'r\sin\theta)(rd\theta)$$
$$= 2K'r^3\int_0^{\pi}\sin^2\theta d\theta \qquad (9\text{-}12)$$
$$= K'r^3\pi, \text{ N·m}$$

or

$$K' = \frac{B_{RM}}{\pi r^3}, \text{ N/m}^2. \qquad (9\text{-}13)$$

Therefore, from Eq. 9-9,

$$p = \frac{B_{RM}x}{\pi r^3}, \text{ N/m} \qquad (9\text{-}14)$$

and p_{max}, the pressure when $x = r$, is

$$p_{max} = \frac{B_{RM}}{\pi r^2}, \text{ N/m}. \qquad (9\text{-}15)$$

Refer to Fig. 9-15,

$$\text{force/segment (both arcs)} = 2K'\left(\frac{x_i + x_{i-1}}{2}\right)\ell_i$$
$$= 2K'\ell_i\left(\frac{r\sin\theta_i + r\sin\theta_{i-1}}{2}\right). \qquad (9\text{-}16)$$

However, from Fig. 9-15,

$$\sin\theta_i = \frac{i}{10}. \qquad (9\text{-}17)$$

Therefore, the substitution of the expression for $\sin\theta_i$ from Eq. 9-17 into Eq. 9-16 gives

$$\text{force/segment (both arcs)} = \frac{2K'r\ell_i}{2}\left(\frac{i}{10} + \frac{i-1}{10}\right), \text{ N} \qquad (9\text{-}18)$$
$$= \frac{2K'\ell_i r}{20}(2i - 1), \text{ N}$$

which, upon substitution of the expression for ℓ_i from Eq. 9-4, yields

$$= 2K'r(\theta_i - \theta_{i-1})\ \frac{r}{20}(2i - 1), \text{ N}$$

THIS DOCUMENT PROVIDED BY THE ABBOTT AEROSPACE
TECHNICAL LIBRARY
ABBOTTAEROSPACE.COM

$$= \frac{2B_{RM}}{\pi r^2}(\theta_i - \theta_{i-1})\ \frac{r}{20}\ (2i-1),\ \text{N}$$

since $K'r = B_{RM}/(\pi r^2)$ from Eq. 9-13. The distance x of the segmental force from the center of the bearing (Fig. 9-15) is

$$x = \frac{r}{20}\ (2i-1),\ \text{m}. \tag{9-19}$$

Therefore, for $r = 0.508$ m (Ref. 7),

$$\text{force/segment (both arcs)} = \frac{B_{RM}}{5.08\pi}(\theta_i - \theta_{i-1})(2i-1),\ \text{N}. \tag{9-20}$$

The location of the force due to B_{RM} is given by $x = 0.0254(2i-1)$ m. Table 9-5—calculated by using the data from Table 9-4 and applying Eq. 9-20—shows segmental forces and their locations for all the segments. Force locations for the last two segments have been adjusted to compensate for the force locations not being at the exact center of each segment.

TABLE 9-5
NORMAL FORCE DISTRIBUTION DUE TO B_{RM} (Ref. 6)

i	Force/Segment (both arcs), N	Location of Force (distance from center of bearing), m
1	$0.000160B_{RM}$	0.0254
2	$0.000480B_{RM}$	0.0762
3	$0.000828B_{RM}$	0.1270
4	$0.001190B_{RM}$	0.1778
5	$0.001607B_{RM}$	0.2286
6	$0.002096B_{RM}$	0.2794
7	$0.002730B_{RM}$	0.3302
8	$0.003630B_{RM}$	0.3810
9	$0.005263B_{RM}$	0.4369
10	$0.003857B_{RM}$	0.4902

It is now possible to obtain bending moments at several sections a distance x' from the trail hinge pin A, as shown in Fig. 9-11. Although free-body diagrams for the main body and trail are drawn separately in Figs. 9-11 and 9-12, bending moment equations are derived by considering trails and the main body as one free body. Note the following facts relative to the forces, as a function of x', that contribute to the bending moment:

1. For $0 \le x' < 0.478$ m. The bending moment is due to R_1 and R_2.
2. For $0.478\ \text{m} < x' < 0.9787$ m. The bending moment is due to R_1, R_2, and the segmental forces due to B_{RR}, B_{RT}, and B_{RM}.
3. For $0.9787\ \text{m} < x' \le 1.72$ m. The bending moment is due to R_1 and R_2, segmental forces due to B_{RR}, B_{RT}, and B_{RM}, and the components of M_1 normal to AB (Fig. 9-11).

For values of x' greater than 0.9387 m, there is an increase in the bending moment over the amount shown in the bending moment equations of Table 9-6. This increase in the bending moment (M_2 component) is due to the moment applied at the left hinge pin given as

$$(M_2)_{component} = M_2 \cos 66°24' \text{ (from Fig. 9-11)}.$$

THIS DOCUMENT PROVIDED BY THE ABBOTT AEROSPACE
TECHNICAL LIBRARY
ABBOTTAEROSPACE.COM

TABLE 9-6
EQUATIONS FOR BENDING MOMENT (Ref. 6)

x', m	Equation, N·m
0	$4.9911R_1 - 0.6858R_2$
0.3429	$(4.9911 + x')R_1 - 0.5779R_2$
<0.4780	$(4.9911 + x')R_1 - 0.5779R_2$
>0.4780	$(4.9911 + x')R_1 - 0.5779R_2 - 0.1436T_c$
0.5314	$(4.9911 + x')R_1 - 0.5779R_2 - (x' - 0.4780)A_c - 0.2050T_c$
0.5872	$(4.9911 + x')R_1 - 0.5779R_2 - (x' - 0.4780)A_c - (x' - 0.5314)B_c - 0.2531T_c$
0.6379	$(4.9911 + x')R_1 - 0.5779R_2 - (x' - 0.4780)A_c - (x' - 0.5314)B_c - (x' - 0.5872)C_c - 0.2958T_c$
0.6887	$(4.9911 + x')R_1 - 0.5779R_2 - (x' - 0.4780)A_c - (x' - 0.5314)B_c - (x' - 0.5872)C_c - (x' - 0.6379)D_c - 0.3337T_c$
0.7394	$(4.9911 + x')R_1 - 0.5779R_2 - (x' - 0.4780)A_c - (x' - 0.5314)B_c - (x' - 0.5872)C_c - (x' - 0.6379)D_c - (x' - 0.6887)E_c - 0.3693T_c$
0.7901	$(4.9911 + x')R_1 - 0.5779R_2 - (x' - 0.4780)A_c - (x' - 0.5314)B_c - (x' - 0.5872)C_c - (x' - 0.6379)D_c - (x' - 0.6887)E_c - (x' - 0.7394)F_c - 0.4034T_c$
0.8408	$(4.9911 + x')R_1 - 0.5779R_2 - (x' - 0.4780)A_c - (x' - 0.5314)B_c - (x' - 0.5872)C_c - (x' - 0.6379)D_c - (x' - 0.6887)E_c - (x' - 0.7394)F_c - (x' - 0.7901)G_c - 0.4359T_c$
0.8915	$(4.9911 + x')R_1 - 0.5779R_2 - (x' - 0.4780)A_c - (x' - 0.5314)B_c - (x' - 0.5872)C_c - (x' - 0.6379)D_c - (x' - 0.6887)E_c - (x' - 0.7394)F_c - (x' - 0.7901)G_c - (x' - 0.8408)H_c - 0.4680T_c$
0.9387	$(4.9911 + x')R_1 - 0.5779R_2 - (x' - 0.4780)A_c - (x' - 0.5314)B_c - (x' - 0.5872)C_c - (x' - 0.6379)D_c - (x' - 0.6887)E_c - (x' - 0.7394)F_c - (x' - 0.7901)G_c - (x' - 0.8408)H_c - (x' - 0.8915)I_c - 0.4680T_c$
0.9422	$(4.9911 + x')R_1 - 0.5779R_2 - (x' - 0.4780)A_c - (x' - 0.5314)B_c - (x' - 0.5872)C_c - (x' - 0.6379)D_c - (x' - 0.6887)E_c - (x' - 0.7394)F_c - (x' - 0.7901)G_c - (x' - 0.8408)H_c - (x' - 0.8915)I_c - 0.5000T_c + (x' - 0.9387)R_3$
0.9929	$(4.9911 + x')R_1 - 0.5779R_2 - (x' - 0.4780)A_c - (x' - 0.5314)B_c - (x' - 0.5872)C_c - (x' - 0.6379)D_c - (x' - 0.6887)E_c - (x' - 0.7394)F_c - (x' - 0.7901)G_c - (x' - 0.8408)H_c - (x' - 0.8915)I_c - (x' - 0.9422)J_c - 0.5321T_c + (x' - 0.9387)R_3$
1.0436	$(4.9911 + x')R_1 - 0.5779R_2 - (x' - 0.4780)A_c - (x' - 0.5314)B_c - (x' - 0.5872)C_c - (x' - 0.6379)D_c - (x' - 0.6887)E_c - (x' - 0.7394)F_c - (x' - 0.7901)G_c - (x' - 0.8408)H_c - (x' - 0.8915)I_c - (x' - 0.9422)J_c - 0.5642\ T_c + (x' - 0.9387)R_3 - (x' - 0.9929)J_c^*$
1.0943	$(4.9911 + x')R_1 - 0.5779R_2 - (x' - 0.4780)A_c - (x' - 0.5314)B_c - (x' - 0.5872)C_c - (x' - 0.6379)D_c - (x' - 0.6887)E_c - (x' - 0.7394)F_c - (x' - 0.7901)G_c - (x' - 0.8408)H_c - (x' - 0.8915)I_c - (x' - 0.9422)J_c - 0.5967T_c + (x' - 0.9387)R_3 - (x' - 0.9929)J_c^* - (x' - 1.0436)I_c^*$
1.1450	$(4.9911 + x')R_1 - 0.5779R_2 - (x' - 0.4780)A_c - (x' - 0.5314)B_c - (x' - 0.5872)C_c - (x' - 0.6379)D_c - (x' - 0.6887)E_c - (x' - 0.7394)F_c - (x' - 0.7901)G_c - (x' - 0.8408)H_c - (x' - 0.8915)I_c - (x' - 0.9422)J_c - 0.6308T_c + (x' - 0.9387)R_3 - (x' - 0.9929)J_c^* - (x' - 1.0436)I_c^* - (x' - 1.0943)H_c^*$

(cont'd on next page)

THIS DOCUMENT PROVIDED BY THE ABBOTT AEROSPACE
TECHNICAL LIBRARY
ABBOTTAEROSPACE.COM

TABLE 9-6 (cont'd)

1.1957	$(4.9911 + x')R_1 - 0.5779R_2 - (x' - 0.4780)A_c - (x' - 0.5314)B_c$ $\cdots - (x' - 0.9422)J_c - 0.6664T_c + (x' - 0.9387)R_3$ $- (x' - 0.9929)J_c^* - (x' - 1.0436)I_c^* - (x' - 1.0943)H_c^*$ $- (x' - 1.1450)G_c^*$
1.2464	$(4.9911 + x')R_1 - 0.5779R_2 - (x' - 0.4780)A_c - (x' - 0.5314)B_c$ $\cdots - (x' - 0.9422)J_c - 0.7043T_c + (x' - 0.9387)R_3$ $- (x' - 0.9929)J_c^* - (x' - 1.0436)I_c^* - (x' - 1.0943)H_c^*$ $- (x' - 1.1450)G_c^* - (x' - 1.1957)F_c^*$
1.2971	$(4.9911 + x')R_1 - 0.5779R_2 - (x' - 0.4780)A_c - (x' - 0.5314)B_c$ $\cdots - (x' - 0.9422)J_c - 0.7470T_c + (x' - 0.9387)R_3$ $- (x' - 0.9929)J_c^* - (x' - 1.0436)I_c^* - (x' - 1.0943)H_c^*$ $- (x' - 1.1450)G_c^* - (x' - 1.1957)F_c^* - (x' - 1.2464)E_c^*$
1.3478	$(4.9911 + x')R_1 - 0.5779R_2 - (x' - 0.4780)A_c - (x' - 0.5314)B_c$ $\cdots - (x' - 0.9422)J_c - 0.7951T_c + (x' - 0.9387)R_3$ $- (x' - 0.9929)J_c^* - (x' - 1.0436)I_c^* - (x' - 1.0943)H_c^*$ $- (x' - 1.1450)G_c^* - (x' - 1.1957)F_c^* - (x' - 1.2464)E_c^*$ $- (x' - 1.2971)D_c^*$
1.4036	$(4.9911 + x')R_1 - 0.5779R_2 - (x' - 0.4780)A_c - (x' - 0.5314)B_c$ $\cdots - (x' - 0.9422)J_c - 0.8565T_c + (x' - 0.9387)R_3$ $- (x' - 0.9929)J_c^* - (x' - 1.0436)I_c^* - (x' - 1.0943)H_c^*$ $- (x' - 1.1450)G_c^* - (x' - 1.1957)F_c^* - (x' - 1.2464)E_c^*$ $- (x' - 1.2971)D_c^* - (x' - 1.3478)C_c^*$
1.4571	$(4.9911 + x')R_1 - 0.5779R_2 - (x' - 0.4780)A_c - (x' - 0.5314)B_c$ $\cdots - (x' - 0.9422)J_c - 1.000T_c + (x' - 0.9387)R_3$ $- (x' - 0.9929)J_c^* - (x' - 1.0436)I_c^* - (x' - 1.0943)H_c^*$ $- (x' - 1.1450)G_c^* - (x' - 1.1957)F_c^* - (x' - 1.2464)E_c^*$ $- (x' - 1.2971)D_c^* - (x' - 1.3478)C_c^* - (x' - 1.4036)B_c^*$
1.7202	$(4.9911 + x')R_1 - 0.5779R_2 - (x' - 0.4780)A_c - (x' - 0.5314)B_c$ $\cdots - (x' - 0.9422)J_c - 1.000T_c + (x' - 0.9387)R_3$ $- (x' - 0.9929)J_c^* - (x' - 1.0436)I_c^* - (x' - 1.0943)H_c^*$ $- (x' - 1.1450)G_c^* - (x' - 1.1957)F_c^* - (x' - 1.2464)E_c^*$ $- (x' - 1.2971)D_c^* - (x' - 1.3478)C_c^* - (x' - 1.4036)B_c^*$ $- (x' - 1.4571)A_c^*$

Note: These equations were converted to SI units from Ref. 6 and could be programmed to obtain the bending moments. The cross sections selected in the table are the critical sections where the loads contributing to the bending moment equation change. The bending moment equations are written based on the discussion of par. 9-4.2.2.

Here the moment is

$$M_2 = 4.9911R_3 - 0.5779R_4, \text{ N·m}$$

since the lever arms for reactions R_3 and R_4 are 4.9911 and 0.5779 m, respectively, from the left hinge pin.

To illustrate the calculations for bending moment, consider a section at $x' = 0.9422$ m and an elevation angle of 75 deg. Table 9-1 provides the following data:

$R_1 = 77{,}973$ N
$R_2 = 49{,}202$ N
$R_3 = 38{,}161$ N
$R_4 = 15{,}764$ N
$B_{RR} = 57{,}604$ N
$B_{RT} = 268{,}569$ N
$B_{RM} = 346{,}105$ N·m.

THIS DOCUMENT PROVIDED BY THE ABBOTT AEROSPACE
TECHNICAL LIBRARY
ABBOTTAEROSPACE.COM

Because the section under consideration ($x' = 0.9422$ m) is greater than 0.9387 m, there is an increase in the bending moment given as

$$(M_2)_{component} = (4.9911 \times 38{,}161 - 0.5779 \times 15{,}764)\cos 66°24' \text{ N·m}$$
$$= 181{,}355 \cos 66°24' = 72{,}605 \text{ N·m.}$$

By use of the equations given in Table 9-7 for the bending moment at $x' = 0.9422$ m, the values of the various constants are

$$A_c = 0.5457 \times 346{,}105 + 0.1436 \times 268{,}569 = 227{,}435 \text{ N}$$
$$B_c = 0.208 \times 346{,}105 + 0.0614 \times 268{,}569 = 88{,}480 \text{ N}$$
$$C_c = 0.1419 \times 346{,}105 + 0.0481 \times 268{,}569 = 62{,}030 \text{ N}$$
$$D_c = 0.1091 \times 346{,}105 + 0.0427 \times 268{,}569 = 49{,}228 \text{ N}$$
$$E_c = 0.082 \times 346{,}105 + 0.0379 \times 268{,}569 = 38{,}559 \text{ N}$$
$$F_c = 0.06315 \times 346{,}105 + 0.0356 \times 268{,}569 = 31{,}418 \text{ N}$$
$$G_c = 0.04693 \times 346{,}105 + 0.0341 \times 268{,}569 = 25{,}401 \text{ N}$$
$$H_c = 0.03197 \times 346{,}105 + 0.0325 \times 268{,}569 = 19{,}793 \text{ N}$$
$$I_c = 0.01898 \times 346{,}105 + 0.0321 \times 268{,}569 = 15{,}190 \text{ N}$$
$$T_c = 0.1778 \times 57{,}604 = 10{,}242 \text{ N·m.}$$

For this particular cross section it is not necessary to calculate the constants A_c^*, B_c^* etc., given in Table 9-7 because they are not required to determine the moment at $x' = 0.9422$ m. Therefore, the bending moment M_b at $x' = 0.9422$ m—from the equations in Table 9-6—is

$$M_b = (4.99 + 0.9422)77{,}973 - 0.5779(49{,}202) - (0.9422 - 0.478)227{,}435$$
$$- (0.9422 - 0.5314)88{,}480 - (0.9422 - 0.5873)62{,}030$$
$$- (0.9422 - 0.638)49{,}228 - (0.9422 - 0.6887)38{,}559 - (0.9422 - 0.7394)31{,}418$$
$$- (0.9422 - 0.7901)25{,}401 - (0.9422 - 0.8408)19{,}793$$
$$- (0.9422 - 0.8915)15{,}190 - 0.5(10{,}242) + (0.9422 - 0.9387)38{,}161 = 227{,}517 \text{ N·m.}$$

Therefore, the total bending moment $(M_b)_{total}$ at this section is

$$(M_b)_{total} = M_b + (M_2)_{component}$$
$$= 227{,}519 + 72{,}605 = 300{,}122 \text{ N·m.}$$

Similarly, if the firing loads at elevation angles of 35 deg and 55 deg are considered, the total bending moments at the section ($x' = 0.9422$ m) are 264,099 N·m and 272,277 N·m, respectively. Thus the maximum total bending moment at the section $x' = 0.9422$ is 300,122 N·m. Fig. 9-17 shows the maximum total bending moments at all the sections. Table 9-8 gives the values of the bending moments based on the equations in Table 9-6; Table 9-9 gives the total bending moments inclusive of the increase in bending moment due to the $(M_2)_{component}$ for the sections between $0.9387 \leq x' < 1.7202$ m. It is observed from Fig. 9-17 that the bending moments are high in the region $0 \leq x' \leq 0.5588$ m. Further, for sections beyond $x' = 0.5588$ m, the section modulus Z remains nearly the same as it is for the section $x' = 0.5588$ m while the bending moment decreases

THIS DOCUMENT PROVIDED BY THE ABBOTT AEROSPACE
TECHNICAL LIBRARY
ABBOTTAEROSPACE.COM

TABLE 9-7
VALUES OF CONSTANTS SHOWN IN BENDING MOMENT EQUATIONS (Ref. 6)

$$
\begin{aligned}
A_c &= 0.5457B_{RM} + 0.1436B_{RT} \\
A_c^* &= -0.5457B_{RM} + 0.1436B_{RT} \\
B_c &= 0.208B_{RM} + 0.0614B_{RT} \\
B_c^* &= -0.208B_{RM} + 0.0614B_{RT} \\
C_c &= 0.1419B_{RM} + 0.0481B_{RT} \\
C_c^* &= -0.1419B_{RM} + 0.0481B_{RT} \\
D_c &= 0.1091B_{RM} + 0.0427B_{RT} \\
D_c^* &= -0.1091B_{RM} + 0.0427B_{RT} \\
E_c &= 0.082B_{RM} + 0.0379B_{RT} \\
E_c^* &= -0.082B_{RM} + 0.0379B_{RT} \\
F_c &= 0.06315B_{RM} + 0.0356B_{RT} \\
F_c^* &= -0.06315B_{RM} + 0.0356B_{RT} \\
G_c &= 0.04693B_{RM} + 0.0341B_{RT} \\
G_c^* &= -0.04693B_{RM} + 0.0341B_{RT} \\
H_c &= 0.03197B_{RM} + 0.0325B_{RT} \\
H_c^* &= -0.03197B_{RM} + 0.0325B_{RT} \\
I_c &= 0.01898B_{RM} + 0.0321B_{RT} \\
I_c^* &= -0.01898B_{RM} + 0.0321B_{RT} \\
J_c &= 0.006338B_{RM} + 0.0321B_{RT} \\
J_c^* &= -0.006338B_{RM} + 0.0321B_{RT} \\
T_c &= 0.1778B_{RR}
\end{aligned}
$$

Notation: B_{RM} = bearing moment acting on bottom carriage, N·m
B_{RR} = in-plane component of bearing reaction on bottom carriage, N
B_{RT} = normal component of bearing reaction on bottom carriage, N

rapidly. Therefore, the bending stresses will be much less for the sections between $0.5588 \leq x' \leq 1.72$ m. Figs. 9-18 to 9-21 show four typical cross sections between $0 \leq x' \leq 0.0762$ m. Section properties of various cross sections are tabulated in Table 9-10. Note that the bending moments are all sagging (convex curvature) and thus produce compressive stresses at the top and tensile stresses at the bottom.

Table 9-11 gives bending stresses for various sections. To illustrate the stress calculations, consider the section $x' = 0.0762$ m. From Fig. 9-17 observe that the maximum total bending moment $(M_b)_{total}$ at the section is 386,408 N·m, and Table 9-10 shows the section moduli as

$$Z_t = 2.196\times10^{-3}\ \text{m}^3 \text{ and } Z_b = 1.898\times10^{-3}\ \text{m}^3.$$

Therefore, the bottom bending stress σ_1 and top bending stress σ_2 are, respectively,

$$\sigma_1 = \frac{\max(M_b)_{total}}{Z_b} \tag{9-21}$$

$$= \frac{386{,}408}{1.898\times10^{-3}} = 203.587\ \text{MPa}$$

THIS DOCUMENT PROVIDED BY THE ABBOTT AEROSPACE
TECHNICAL LIBRARY
ABBOTTAEROSPACE.COM

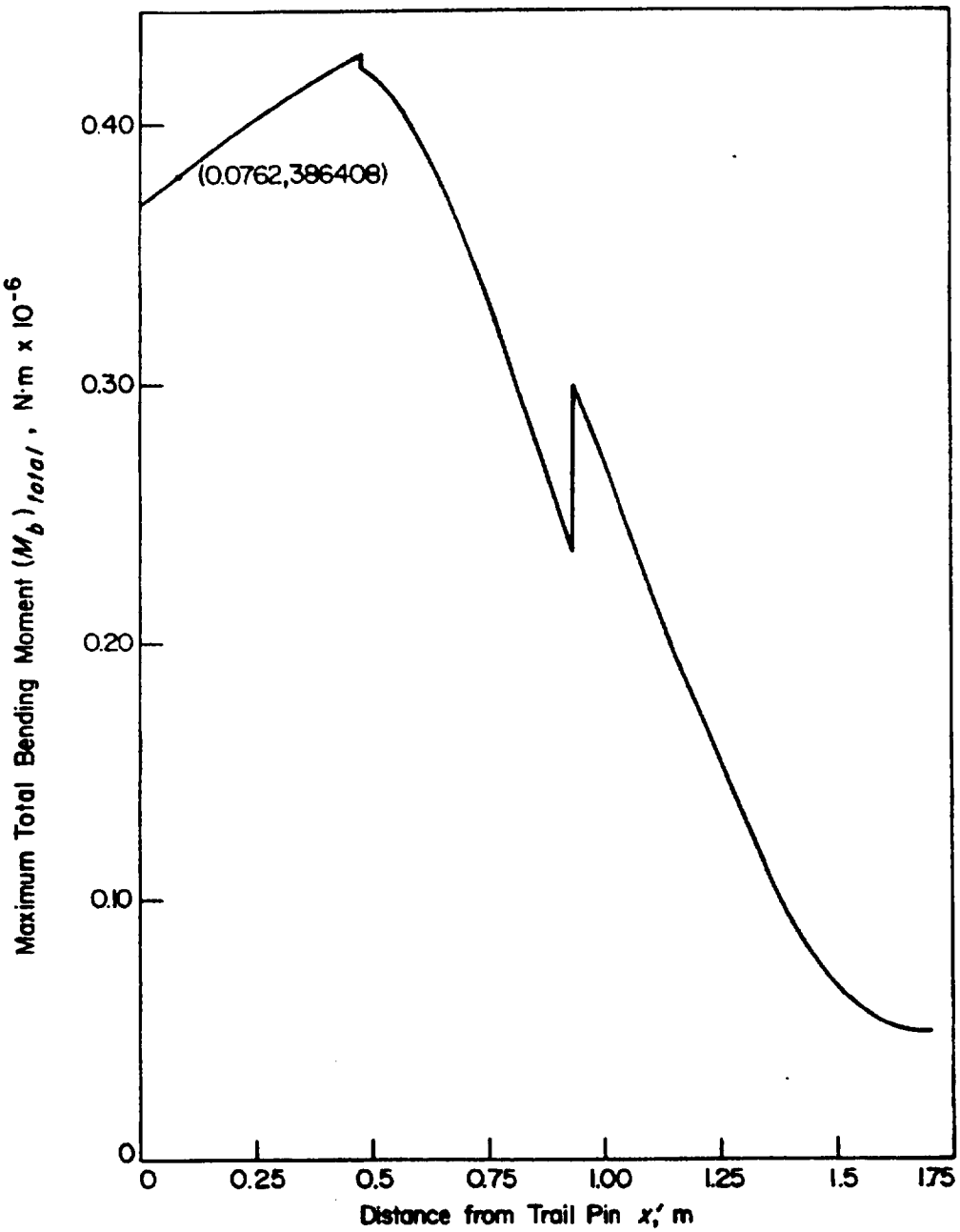

Figure 9-17. Bottom Carriage Maximum Bending Moments (Axis Through One Trail Pin and Firing Pedestal) (Ref. 6)

$$\sigma_2 = \frac{\max(M_b)_{total}}{Z_t} \tag{9-22}$$

$$= \frac{386{,}408}{2.196 \times 10^{-3}} = 175.96 \text{ MPa.}$$

Note that the compressive stresses due to R_2 and R_4 are neglected because they are small compared with the bending stresses.

THIS DOCUMENT PROVIDED BY THE ABBOTT AEROSPACE
TECHNICAL LIBRARY
ABBOTTAEROSPACE.COM

TABLE 9-8
BENDING MOMENTS M_b IN MAIN BODY OF BOTTOM CARRIAGE (Ref. 6)

Bending Moment M_b (Computer Output), N·m			
x', m	Elevation, 35 deg	Elevation, 55 deg	Elevation, 75 deg
0	336,226	374,198	355,428
0.3429	389,126	420,766	387,476
<0.4780	401,799	433,395	398,012
>0.4780	396,055	429,536	396,541
0.5314	385,469	419,101	387,941
0.5872	369,742	403,032	374,155
0.6379	352,202	385,096	358,515
0.6887	332,130	364,514	340,386
0.7394	310,449	341,866	320,405
0.7901	287,135	317,544	298,815
0.8408	262,677	291,908	275,955
0.8915	237,342	265,248	252,086
0.9387	214,405	240,556	229,468
0.9422	211,537	237,996	227,594
0.9929	186,962	212,077	204,355
1.0436	162,320	185,948	180,789
1.0943	137,849	159,853	157,102
1.1450	113,799	134,057	133,527
1.1957	90,469	108,848	110,295
1.2464	68,161	84,530	87,660
1.2971	47,151	61,403	65,886
1.3478	27,981	39,994	45,399
1.4036	9,529	19,096	24,788
1.4571	−7,304	732	7,122
1.7202	−6,444	−18,612	−32,993

TABLE 9-9
TOTAL BENDING MOMENTS (M_b) IN MAIN BODY OF BOTTOM CARRIAGE FOR SECTIONS BEYOND $x' = 0.9387$ m (Ref. 6)

Bending Moment $(M_b)_{total}$ (Computer Output), N·m			
x', m	Elevation, 35 deg	Elevation, 55 deg	Elevation, 75 deg
0.9387	266,562	307,307	302,073
0.9422	263,695	304,748	300,122
0.9929	239,120	278,828	276,960
1.0436	214,477	252,699	253,394
1.0943	190,007	226,605	229,707
1.1450	165,956	200,808	206,132
1.1957	142,627	175,599	182,900
1.2464	120,319	151,283	160,265
1.2971	99,309	128,155	138,491
1.3478	80,140	106,746	118,005
1.4036	61,687	85,848	97,394
1.4571	44,854	67,485	79,728
1.7202	45,715	48,140	39,613

THIS DOCUMENT PROVIDED BY THE ABBOTT AEROSPACE
TECHNICAL LIBRARY
ABBOTTAEROSPACE.COM

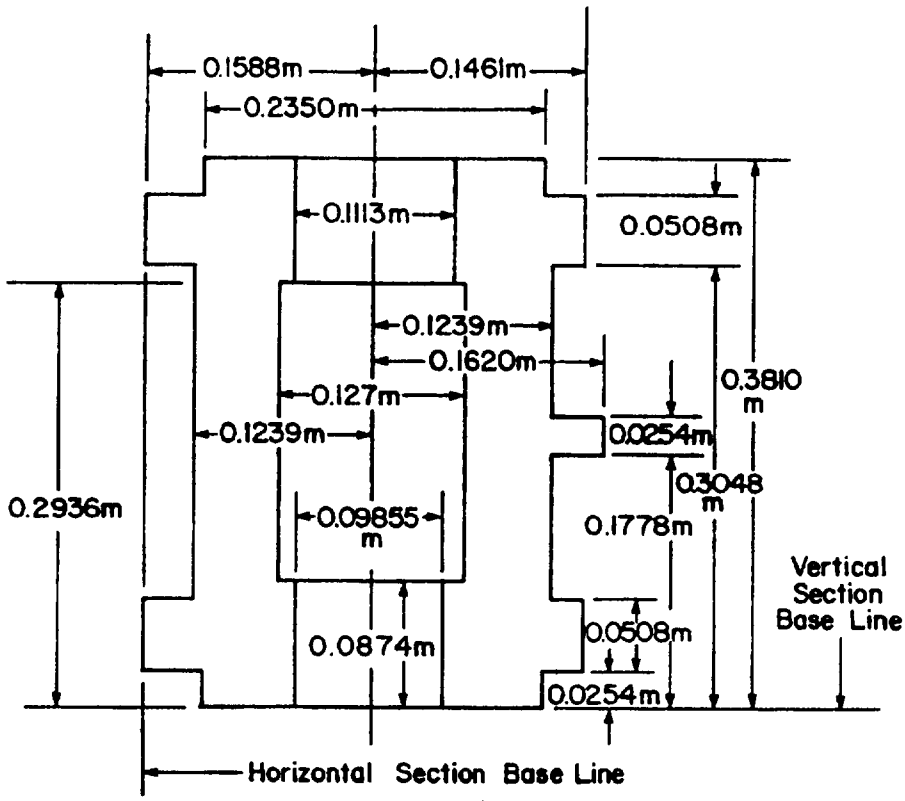

Figure 9-18. Bottom Carriage Section Properties at Section 1 (Ref. 6)

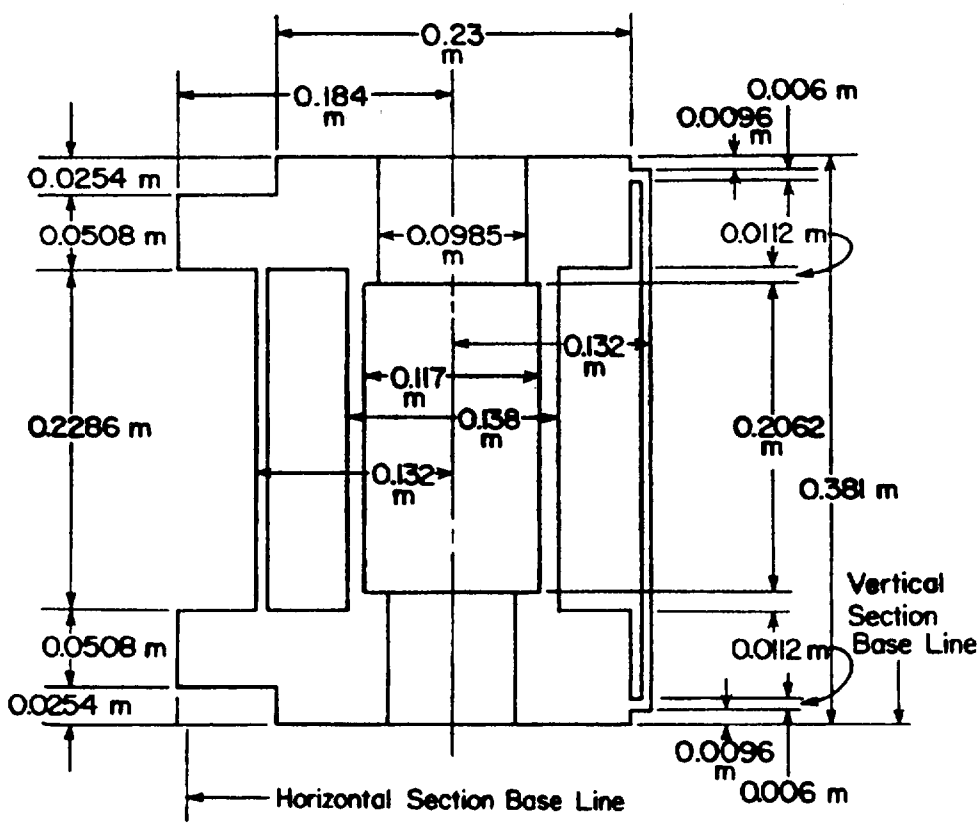

Figure 9-19. Bottom Carriage Section Properties at Section 2 (Ref. 6)

THIS DOCUMENT PROVIDED BY THE ABBOTT AEROSPACE
TECHNICAL LIBRARY
ABBOTTAEROSPACE.COM

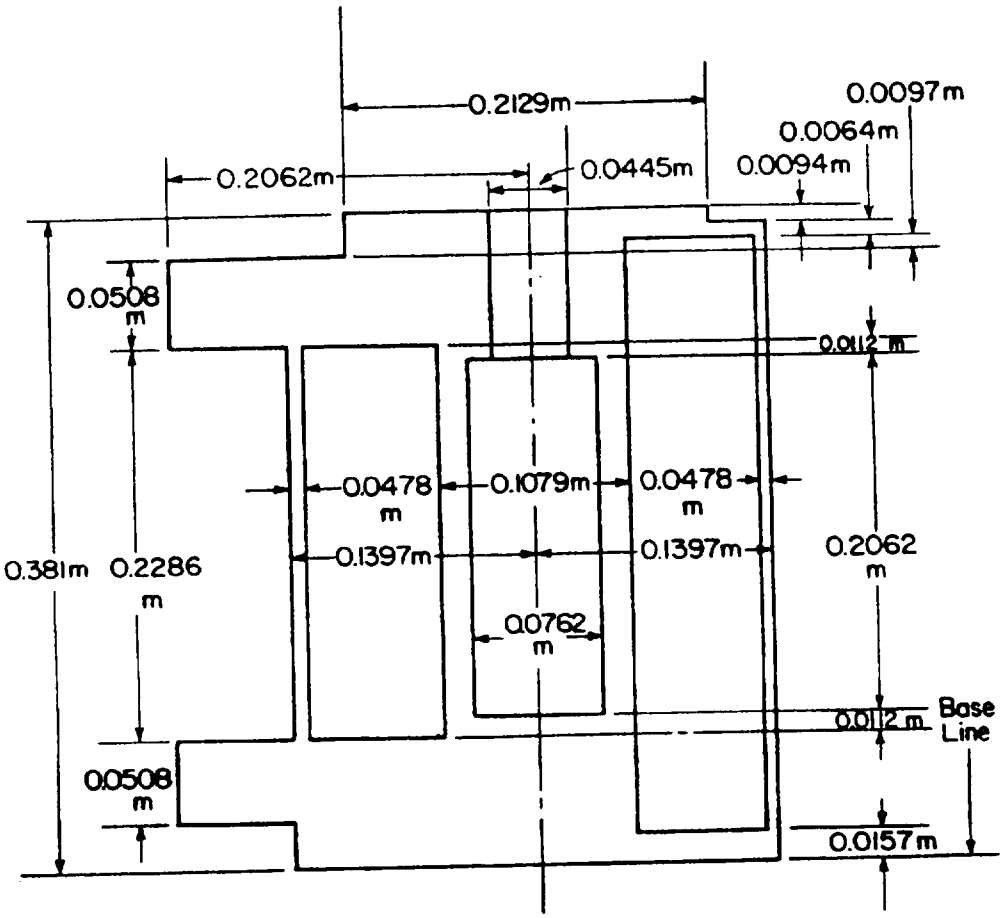

Figure 9-20. Bottom Carriage Section Properties at Section 3 (Ref. 6)

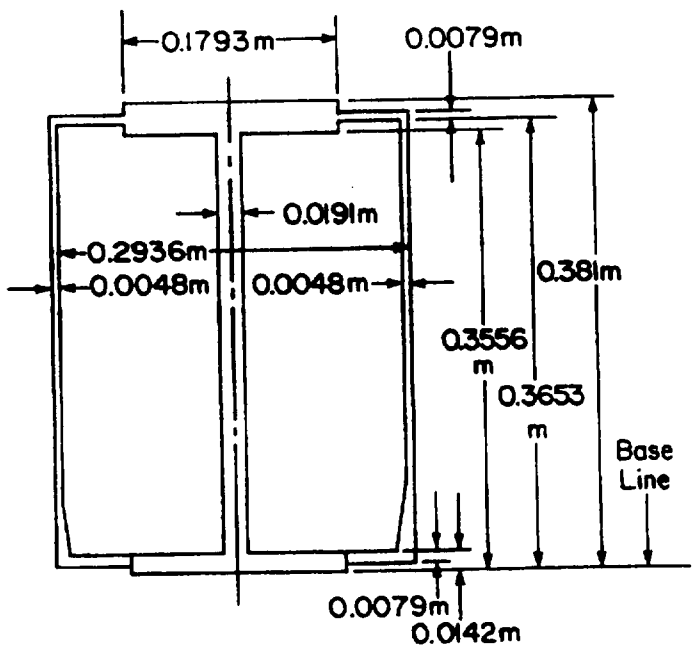

Figure 9-21. Bottom Carriage Section Properties at Section 4 (Ref. 6)

THIS DOCUMENT PROVIDED BY THE ABBOTT AEROSPACE
TECHNICAL LIBRARY
ABBOTTAEROSPACE.COM

TABLE 9-10
SECTION PROPERTIES FOR MAIN BODY OF BOTTOM CARRIAGE (Ref. 6)

Section	x', m	Area A_{cs}, m^2	Moment of Inertia I, m^4	Section Modulus Z_b, m^3*	Section Modulus Z_t, m^3*
1	0.0000	5.4864 E-2	7.118 E-4	3.736 E-3	3.736 E-3
2	0.0254	3.7006 E-2	7.101 E-4	3.728 E-3	3.728 E-3
3	0.0508	4.5271 E-2	8.512 E-4	4.921 E-3	4.097 E-3
4	0.0762	1.8994 E-2	3.878 E-4	1.898 E-3	2.196 E-3
5	0.1016	1.6168 E-2	3.366 E-4	1.685 E-3	1.858 E-3
6	0.1270	1.1445 E-2	2.283 E-4	1.316 E-3	1.191 E-3
7	0.1524	1.0690 E-2	2.343 E-4	1.293 E-3	1.249 E-3
8	0.1778	1.1258 E-2	2.773 E-4	1.442 E-3	1.395 E-3
9	0.2032	1.1581 E-2	2.992 E-4	1.558 E-3	1.409 E-3
10	0.2286	1.2226 E-2	3.754 E-4	1.794 E-3	1.576 E-3
11	0.2540	1.2342 E-2	3.900 E-4	1.848 E-3	1.585 E-3
12	0.2794	1.4297 E-2	4.079 E-4	1.975 E-3	1.608 E-3
13	0.3048	1.9245 E-2	4.867 E-4	2.406 E-3	1.888 E-3
14	0.3556	2.0516 E-2	5.897 E-4	2.797 E-3	2.363 E-3
15	0.4064	2.2194 E-2	6.229 E-4	3.027 E-3	2.448 E-3
16	0.4572	2.3484 E-2	6.304 E-4	3.092 E-3	2.460 E-3
17	0.5080	2.8387 E-2	6.692 E-4	3.232 E-3	2.897 E-3
18	0.5588	2.2516 E-2	5.698 E-4	3.102 E-3	2.488 E-3

*Section modulus Z_b is for the lower side of the bottom carriage; section modulus Z_t is for the upper side.

Note: This table uses the expression E followed by a number to indicte the power of 10. For example, 5.4864 E-4 = 5.4864×10^{-4}.

TABLE 9-11
STRESSES IN MAIN BODY OF BOTTOM CARRIAGE (Ref. 6)

x', m	Maximum Total Bending Moment $(M_b)_{total}$, kN·m	Bottom Bending Stress σ_1, MPa	Top Bending Stress σ_2, MPa
0.0000	375.110	100.40	100.40
0.0254	378.499	101.53	101.53
0.0508	383.018	77.83	93.49
0.0762	386.408	203.59	175.96
0.1016	388.668	230.66	209.19
0.1270	393.187	298.77	332.98
0.1524	396.577	306.71	317.52
0.1778	399.966	277.37	286.71
0.2032	403.356	258.89	286.27
0.2286	406.745	226.73	258.09
0.2540	410.135	221.93	258.76
0.2794	413.524	209.38	257.17
0.3048	415.784	172.81	220.22
0.3556	422.563	151.08	178.82
0.4064	427.083	141.09	174.46
0.4572	431.602	139.59	175.45
0.5080	422.563	130.74	145.86
0.5588	410.135	132.22	164.85

Note: 1. The maximum total bending moment given in the table is read from the graph of maximum bending moment versus distance from trail pin given in Fig. 9-17.
2. Bending stresses will be much less for the sections between $0.5588 \leq x' \leq 1.72$ m and are not given in the table.

THIS DOCUMENT PROVIDED BY THE ABBOTT AEROSPACE
TECHNICAL LIBRARY
ABBOTTAEROSPACE.COM

9-4.2.3 Buckling of Vertical Plates

Another important consideration in the design of the main body is to check for local buckling of the vertical plates. The traverse bearing transmits a vertical load to the cylindrical vertical plates of the main body. These cylindrical plates should be supported at some interval (ribbed) to avoid failure by buckling. Dynamic analysis of the bottom carriage (par. 9-4) and the analysis of bearing reactions show that a maximum force of 289,134 N is transmitted through the arc AB of the bearing, as shown in Fig. 9-22. The length of the arc may be approximated by the length of the chords as

$$z^2 = y^2 - x^2$$
$$b^2 = z^2 + a^2 = y^2 - x^2 + a^2$$
$$b = \sqrt{y^2 - x^2 + a^2}. \qquad (9\text{-}23)$$

where

$a = y - x = 0.0508$ m
$x = 0.4572$ m
$y = 0.508$ m.

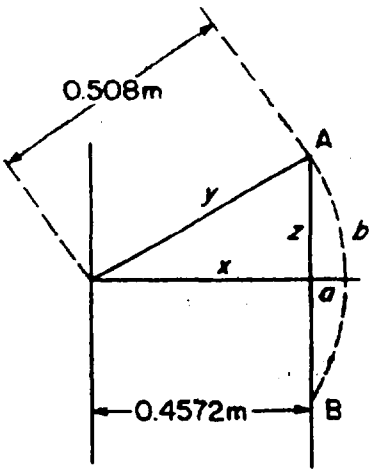

Figure 9-22. Bearing Arc Length AB

Therefore, the total cord length AB is

$$AB = 2\sqrt{(0.508)^2 - (0.4572)^2 + (0.0508)^2}$$
$$= 0.454 \text{ m.}$$

The vertical plate has a thickness of 0.003048 m and a height of 0.3586 m (Ref. 7). Therefore, compressive stress σ in the plate is

$$\sigma = 289{,}134/(0.454 \times 0.003048)$$
$$= 209.943 \text{ MPa.}$$

The required spacing of the ribs can now be determined so that the critical buckling stress is limited to the calculated stress value. The critical buckling stress equation given in Ref. 8 is

THIS DOCUMENT PROVIDED BY THE ABBOTT AEROSPACE
TECHNICAL LIBRARY
ABBOTTAEROSPACE.COM

$$\sigma_{cr} = \frac{K_c \pi^2 E}{12(1-\nu^2)} \left(\frac{t}{b}\right)^2 \text{, MPa} \tag{9-24}$$

where

σ_{cr} = critical buckling stress, MPa
t = thickness of plate = 0.003048 m
b = maximum spacing of ribs, m
h = height of plate = 0.3586 m
ν = Poisson's ratio = 0.3, dimensionless
E = Young's modulus of elasticity = 206,843 MPa
K_c = 4 for $h/b > 1.3$, dimensionless.

From Eq. 9-24

$$b = \left(\frac{K_c \pi^2 E}{12(1-\nu^2)\sigma_{cr}}\right)^{1/2} t, \text{ m.} \tag{9-25}$$

Therefore, substitution of $\sigma_{cr} = \sigma = 209.943$ MPa from the results of previous calculation in $b = 0.1819$ m. Therefore, the support ribs should be closer than 0.1819 m.

9-4.2.4 Bottom Carriage Trail Lugs

Another region in which stress could be severe is the contact surface between the trail pin and the trail lugs. The reactions on the trail pin are resolved into forces along and normal to the pin axis, as shown in Fig. 9-23. The notation used in Fig. 9-23 is

R_T = trail force acting at top on trail pin, N
R_B = trail force acting at bottom on trail pin, N
F_{top} = force at top lug of bottom carriage, N
F_B = force at bottom lug of bottom carriage, N
F_L = force transmitted by trail lugs to bottom carriage lugs, N
d_1 = distance between R_T and R_B, m
d_2 = distance between R_T and F_{top} or R_B and F_B, m.

The right-trail float reaction R_1 pulls the trail off the lower lug of the bottom carriage and thereby applies all the force to the upper lug. Refer to Fig. 9-23

$$R_T = \frac{M_1}{d_1} + \frac{R_2}{2}, \text{ N} \tag{9-26}$$

$$R_B = \frac{M_1}{d_1} - \frac{R_2}{2}, \text{ N} \tag{9-27}$$

$$F_{top} = \frac{M_1}{d_1 + 2d_2} + \frac{R_2}{2}, \text{ N} \tag{9-28}$$

$$F_B = \frac{M_1}{d_1 + 2d_2} - \frac{R_2}{2}, \text{ N} \tag{9-29}$$

$$F_L = R_1, \text{ N} \tag{9-30}$$

THIS DOCUMENT PROVIDED BY THE ABBOTT AEROSPACE
TECHNICAL LIBRARY
ABBOTTAEROSPACE.COM

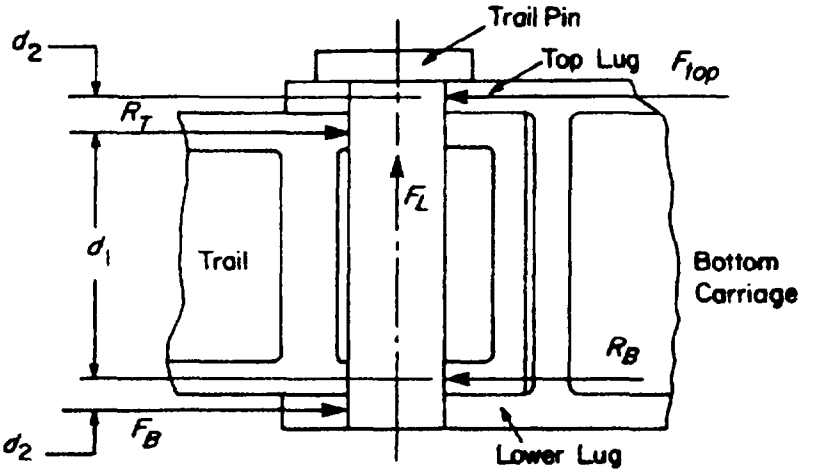

R_T = trail force acting at top on trail pin, N
R_B = trail force acting at bottom on trail pin, N
F_{top} = force at top lug of bottom carriage, N
F_B = force at bottom lug of bottom carriage, N
F_L = force transmitted by trail lugs to bottom carriage lugs, N
d_1 = distance between R_T and R_B, m
d_2 = distance between R_T and F_{top} or R_B and F_B, m

Figure 9-23. Trail Lugs

where
M_1 = moment at right-trail hinge pin due to R_1 and R_2, N·m.

Figs. 9-24 and 9-25 show cross sections and their properties for lower and upper lugs, respectively. It may be noted from Fig. 9-26 that the force F_{top} on the upper lug acts against the main body of the bottom carriage and thus produces compressive contact stresses. Force F_B, however, acting away from the main body, is more critical because it produces bending and axial stresses in the lower lug. The lower lug may be considered a semicircular beam fixed at the ends A and B, as shown in Fig. 9-27. The force F_B may be assumed to be uniformly distributed along the semicircular arc. The maximum bending moment $(M_b)_{max}$ is at either the end of A or B and is given by (Ref. 10)

$$(M_b)_{max} = -\frac{R_b F_B}{8}, \text{ N·m} \tag{9-31}$$

and the combined bending and tensile stress σ is (Ref. 10)

$$\sigma = \frac{F_B}{2A} + \frac{M}{AR_b}\left[1 + \frac{1}{z}\left(\frac{y}{R_b + y}\right)\right], \text{ Pa}$$

and by substituting the expression for M_b from Eq. 9-31,

$$= \frac{F_B}{2A}\left\{1 - \frac{1}{4}\left[1 + \frac{1}{z}\left(\frac{y}{R_b + y}\right)\right]\right\}, \text{ Pa} \tag{9-32}$$

THIS DOCUMENT PROVIDED BY THE ABBOTT AEROSPACE
TECHNICAL LIBRARY
ABBOTTAEROSPACE.COM

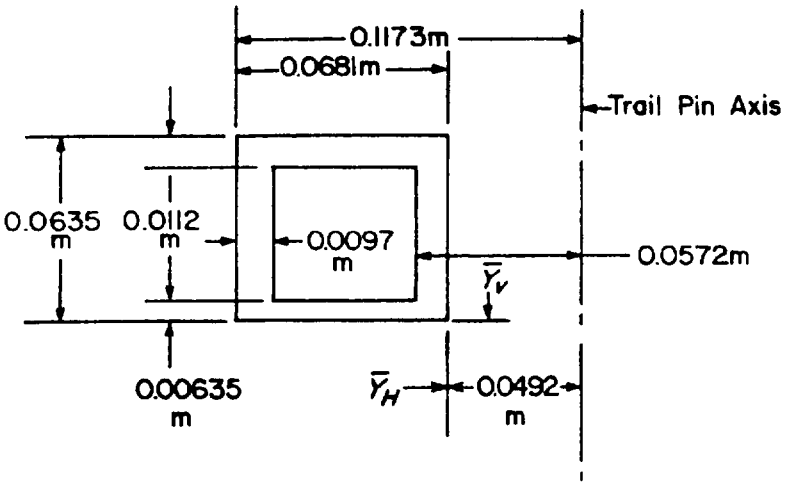

Vertical		Horizontal	
A_{CS}	= 0.002 m^2	A_{CS}	= 0.002 m^2
$\bar{Y}_V$	= 0.0345 m	$\bar{Y}_H$	= 0.0351 m
I	= 1.04E-6 m^4	I	= 1.18E-6 m^4
Z_1	= $\frac{I}{\bar{Y}_V}$ = 30.1 E-6 m^3	Z_1	= $\frac{I}{\bar{Y}_H}$ = 33.6E-6 m^3
Z_2	= $\frac{I}{0.0635 - \bar{Y}_V}$ = 35.6E-6 m^3	Z_2	= $\frac{I}{0.0681 - \bar{Y}_H}$ = 35.6E-6 m^3

where

$\bar{Y}_H$ = horizontal distance of centroid of cross section from right edge, m
$\bar{Y}_V$ = vertical distance of centroid of cross section from bottom edge, m
A_{CS} = area of cross section, m^2
I = area moment of inertia, m^4
Z_1 and Z_2 = section moduli, m^3

Figure 9-24. Lower Lug

where

F_B = force at bottom lug of bottom carriage, N
R_b = centerline radius of the bottom lug, m
M = fixed-end bending moment at A or B, N·m
y = distance of a fiber from centerline of lug, m.

Table 9-I indicates the following firing loads R_1 and R_2 at an elevation angle of 55 deg:

$$R_1 = 93{,}457 \text{ N}, \quad R_2 = 134{,}523 \text{ N}.$$

Therefore, moment M_1, from Fig. 9-12, is given as

$$M_1 = 4.99R_1 - (0.254 + 0.4318)R_2 = 374{,}095 \text{ N·m}.$$

THIS DOCUMENT PROVIDED BY THE ABBOTT AEROSPACE
TECHNICAL LIBRARY
ABBOTTAEROSPACE.COM

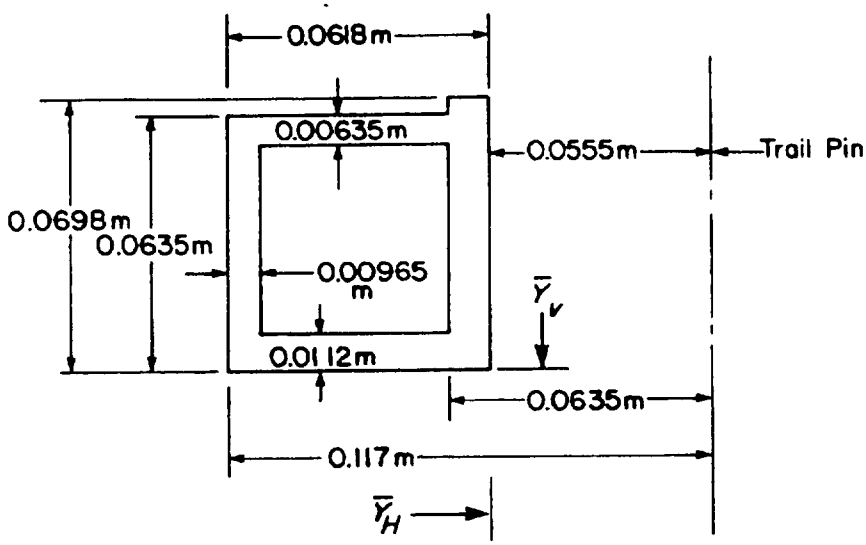

Vertical		Horizontal	
A_{CS}	= 1.94E-3 m^2	A_{CS}	= 1.94E-3 m^2
$\bar{Y}_v$	= 0.0301 m	$\bar{Y}_H$	= 0.0310 m
I	= 1.01E-6 m^4	I	= 0.95E-6 m^4
Z_1	$= \frac{I}{\bar{Y}_v}$ = 33.5E-6 m^3	Z_1	$= \frac{I}{\bar{Y}_H}$ = 30.7E-6 m^3
Z_2	$= \frac{I}{0.0698-\bar{Y}_v}$ = 25.4E-6 m^3	Z_2	$= \frac{I}{0.0618-\bar{Y}_H}$ = 30.9E-6 m^3

Distance between center of gravity of the lugs = 0.4401 m

where

$\bar{Y}_H$ = horizontal distance of centroid of cross section from right edge, m

$\bar{Y}_v$ = vertical distance of centroid of cross section from bottom edge, m

A_{CS} = area of cross section, m^2

I = area moment of inertia, m^4

Z_1 and Z_2 = section moduli, m^3

Figure 9-25. Upper Lug

Reference to Figs. 9-23 and 9-26 indicates that

$$d_1 + 2d_2 = 0.44132 \text{ m}.$$

This value for $(d_1 + 2d_2)$ substituted into Eq. 9-27 yields

$$F_B = \frac{374{,}095}{0.44132} - \frac{134{,}523}{2} = 780{,}411 \text{ N}.$$

THIS DOCUMENT PROVIDED BY THE ABBOTT AEROSPACE
TECHNICAL LIBRARY
ABBOTTAEROSPACE.COM

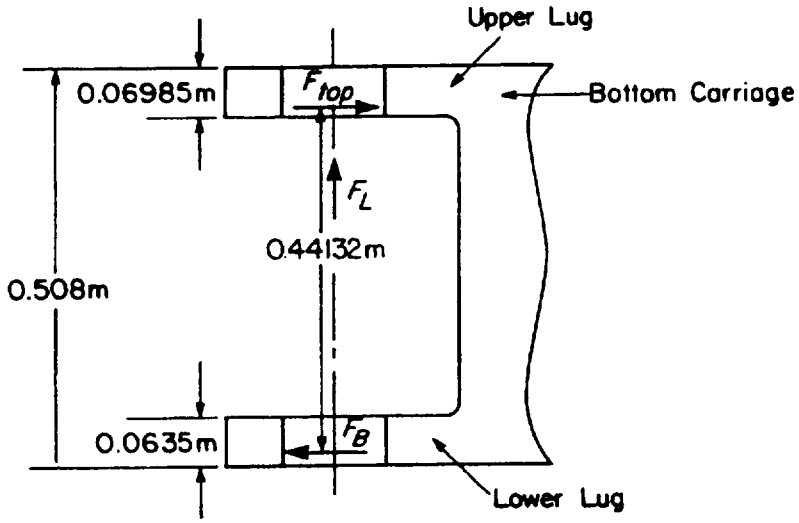

Figure 9-26. Bottom Carriage Trail Lugs

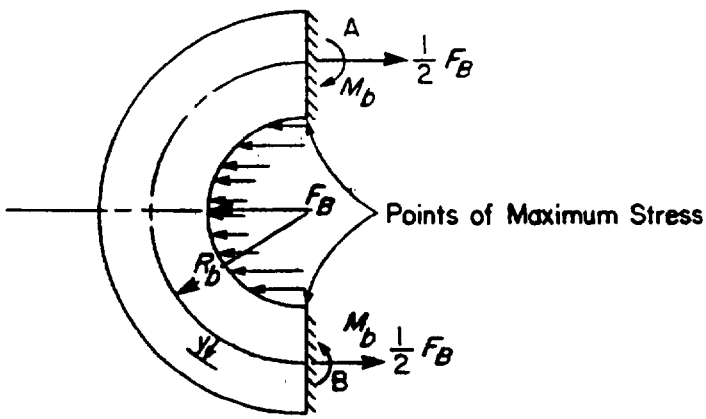

F_B = force at bottom lug of bottom carriage, N
R_b = centerline radius of bottom lug, m
M = fixed-end bending moment at A or B, N·m
y = distance of a fiber from centerline of lug, m.

Figure 9-27. Lower Lug as a Curved Beam Fixed at A and B

For the lower lug (Refer to Figs. 9-24 and 9-27.) assume the following data to demonstrate the calculation of the combined and bending stress σ:

$A = 0.002$ m^2 (area of cross section)
$y = -0.035$ m (for fiber in contact with pin, i.e., from centerline of lug)
$R_b = 0.08425$ m (centerline radius of bottom lug).

To calculate the combined and bending stress σ from eq. 9-32, it is necessary to know the curved beam factor z given by (Refs. 7 and 10)

$$z = \sum_{j=1}^{n} [t_j(\ln R_{oj} - \ln R_{ij})] \frac{R_b}{A} - 1, \text{ dimensionless} \qquad (9\text{-}33)$$

THIS DOCUMENT PROVIDED BY THE ABBOTT AEROSPACE
TECHNICAL LIBRARY
ABBOTTAEROSPACE.COM

where

Σ = sum over all cross sections
t = thickness of cross section plate, m
R_o = outer radius of lower lug, m
R_i = inner radius of lower lug, m

and lower lug is treated as a curved beam, as shown in Figs. 9-24 and 9-27.

$$z = [(0.0112 + 0.00635)(\ln 0.1174 - \ln 0.0572) + 0.0635(\ln 0.0572 - \ln 0.0492)$$

$$+ (0.0635 - 0.0112 - 0.00635)(\ln 0.1173 - \ln 0.1076)]\ 0.08425/0.002 - 1$$

$$= 0.10166 \text{ dimensionless.}$$

Therefore, by Eq. 9-32 and the substitution of $z = 0.10166$ for the cross section of Fig. 9-24, the combined bending and tensile stress σ is

$$\sigma = \frac{776{,}539}{2 \times 0.002}\left\{1 - \frac{1}{4}\left[1 + \frac{1}{0.10166}\left(\frac{-0.035}{0.08425 - 0.035}\right)\right]\right\}$$

$$= 484.88 \text{ MPa.}$$

9-5 ADVANCED DESIGN FOR BOTTOM CARRIAGE STRUCTURES

A conventional technique for the design of bottom carriages is illustrated in par. 9-4 for the structure of the M198 towed Howitzer. The design philosophy is first to assume material and sectional properties (design variables) for the structure. Considerable simplifying assumptions are then made to compute stresses and deflections. If computed stresses and deflections are less than or equal to the corresponding predetermined allowable values, the design is considered acceptable. Otherwise, properties of the overstressed sections are changed, and the procedure is repeated until an acceptable design is obtained. Although this conventional design philosophy is not changed in the discussion that follows, the advanced design techniques use more accurate methods of analysis and employ greater logic in selecting the new design variables at each step. Usually, the objective of any design is to obtain a structure that satisfies all the performance requirements and is of minimum cost. This is an optimization problem, and several techniques are available to solve such a problem.

The purpose of par. 9-5, therefore, is to discuss the use of the finite element method (FEM) of analysis for bottom carriage structures. The bottom carriage for the M198 towed Howitzer is used as an example, and the results obtained by using this advanced method are compared with those obtained in par. 9-4.

9-5.1 FINITE ELEMENT MODEL

9-5.1.1 General

The main body of the M198 bottom carriage has a shape in the form of a box with vertical plate stiffeners between the top and bottom surfaces, as shown in Fig. 9-11. The actual geometry of the main body is quite complicated due to the fact that it has matching geometry for attachment of trails, traverse gear, speed shift mechanism, and front float. For the purpose of demonstration of the FEM, however, a simplified geometry representing a load-carrying configuration is considered. Several considerations in developing an FEM are presented in the following paragraphs:

1. *Coordinate Systems.* A rectangular cartesian coordinate system is the basic system used to define grid point locations and loads. This system is represented by X-, Y-, and Z-axes, as shown in Fig. 9-28. Besides the basic coordinate system, there are element coordinate systems to represent shape, size, and orientation of each element. Element coordinate systems for the bar, quadrilateral plate, and triangular plate elements that are used to model the bottom carriage are shown in Figs. 9-29, 9-30 and 9-31, respectively. Table 9-12 shows the X-, Y-, and Z-coordinates of the grid points in the basic coordinate system.

THIS DOCUMENT PROVIDED BY THE ABBOTT AEROSPACE
TECHNICAL LIBRARY
ABBOTTAEROSPACE.COM

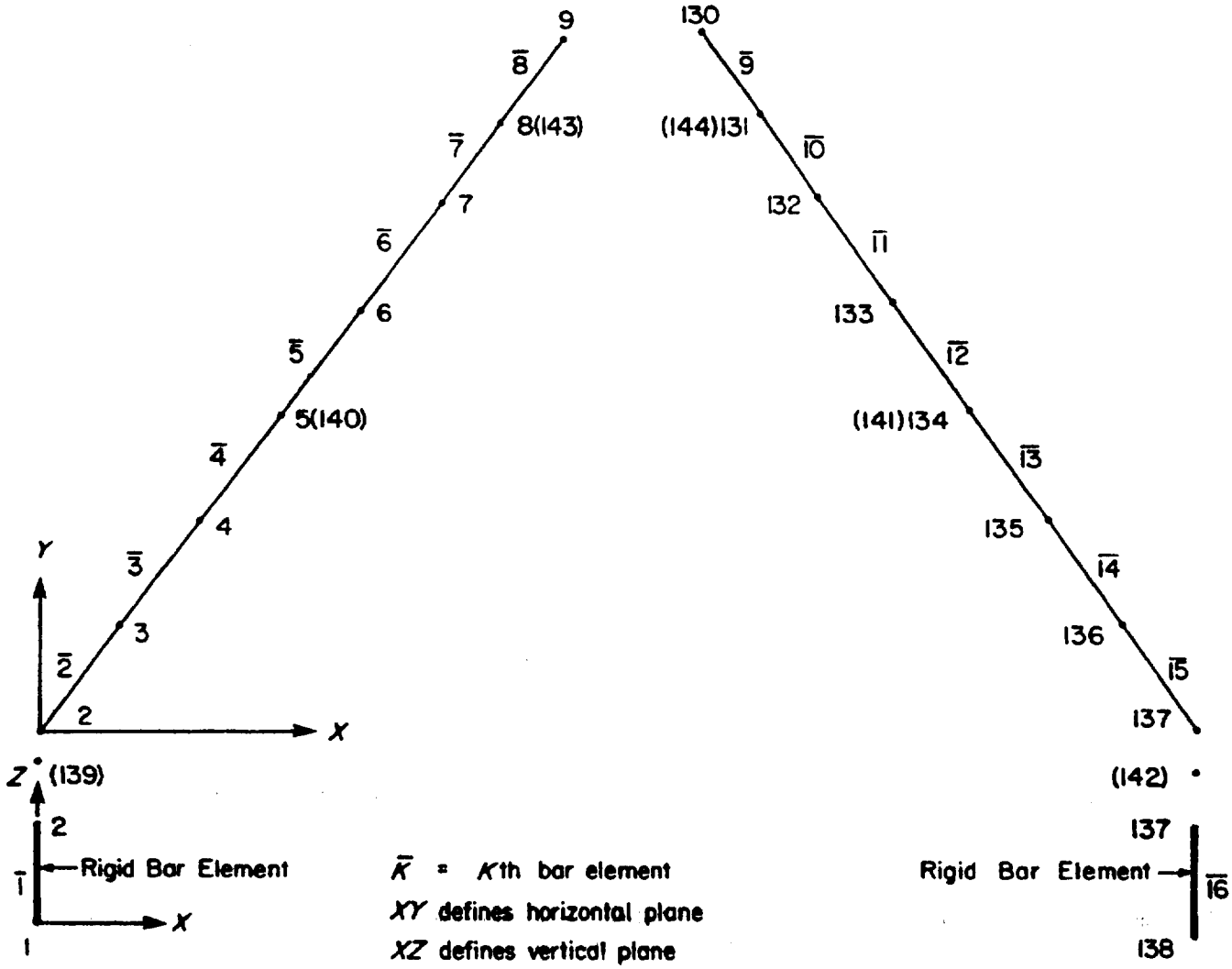

Figure 9-28. Finite Element Model of Trails (Nodes and Elements)

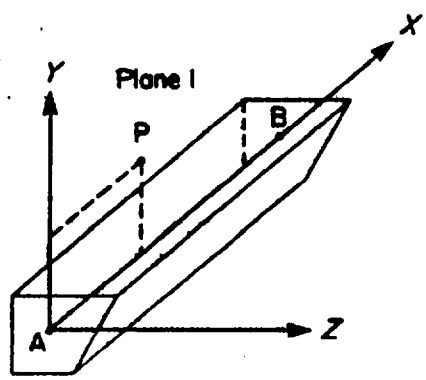

Note: Point P shown in this figure defines the *XY*-plane which helps to define the plane of bending for a general purpose finite element program.

Figure 9-29. Element Coordinate System for Bar Element

THIS DOCUMENT PROVIDED BY THE ABBOTT AEROSPACE
TECHNICAL LIBRARY
ABBOTTAEROSPACE.COM

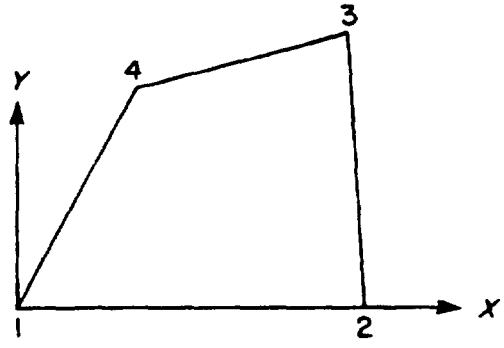

Figure 9-30. Element Coordinate System for QUAD2 Element (Quadrilateral Plate Element)

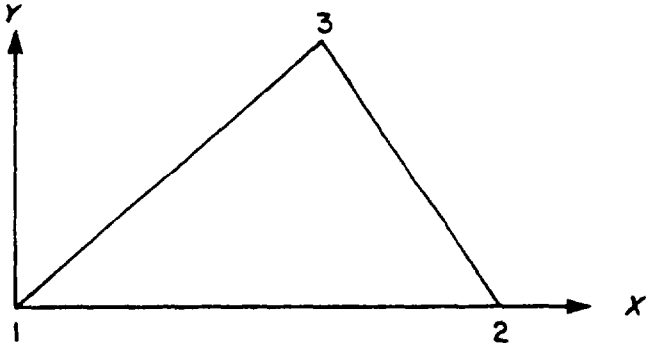

Figure 9-31. Element Coordinate System for TRIA2 Element (Triangular Plate Element)

2. *Node Selection:*

The degree of desired accuracy of the analysis usually determines the number of nodes, i.e., the more nodes, the better the representation of deformed surfaces, and the greater the accuracy of analysis. Locations, where large undulations of the deformed surface are envisaged, are represented with higher node density, which results in a greater number of finite elements at these locations. Nodes should be provided at physical intersections or meetings of members or plates and at each point of application of a concentrated load. Sufficient nodes should be used to represent boundaries of the structure. The location and number of nodes also depend on the type of elements needed to represent the behavior of the structure. For more discussion on finite element modeling, Chapters 7 and 8 and Appendix C should be consulted.

Figs. 9-32 to 9-35 show the nodes used to make discrete, as well as to define, the element orientations for the M198 bottom carriage structure that is composed of a main body and two trails. The loads transmitted from the traverse bearing to the bottom carriage are through nodes 59, 47, 37, 30, 34, 42, 53, 65, 71, 91, 107, 112, 101, 95, 85, and 77. (See Fig. 9-32.) All these nodes lie on the circumference of 0.4572 m, i.e., the radius of the traverse bearing. However, the actual radius of the bearing is 0.508 m, and the sample calculations in par. 9-4 use the actual radius of 0.508 m for load transmission. This change is made to reduce the number of nodes and elements in the model. There is a cylindrical (0.4572 m radius), vertical stiffening plate between the top and bottom plates of the main body, and all of the previously mentioned nodes are on the physical intersection of the top and the vertical stiffening plates. These nodes are used out of necessity to define the structural configuration of the main body. Indeed, it is possible to provide additional nodes at the actual points of load transmission; however, this would increase the number of nodes and finite elements. Loads transmitted at the traverse bearing must be transformed to equivalent loads at the nodal points. These calculations are shown later in this paragraph.

3. *Node Numbering.* Node numbering is another important consideration in modeling because it determines the computing efficiency for the analysis. The major portion of the computing time is usually spent on the decomposition of the system stiffness matrix. Decomposition time for the stiffness matrix depends on

THIS DOCUMENT PROVIDED BY THE ABBOTT AEROSPACE
TECHNICAL LIBRARY
ABBOTTAEROSPACE.COM

TABLE 9-12
GRID POINT COORDINATES IN BASIC COORDINATE SYSTEM

Grid Point Number	X, m	Y, m	Z, m	Grid Point Number	X, m	Y, m	Z, m	Grid Point Number	X, m	Y, m	Z, m
1	0.0	0.0	0.0	50	3.398	4.941	0.457	99	3.893	4.697	0.457
2	0.0	0.0	0.419	51	3.275	5.032	0.457	100	3.893	4.653	0.813
3	0.437	0.624	0.575	52	3.514	4.129	0.915	101	4.236	4.653	0.813
4	0.874	1.248	0.599	53	3.578	4.252	0.813	102	4.524	4.653	0.915
5	1.311	1.872	0.625	54	3.744	4.554	0.813	103	4.524	4.653	0.457
6	1.748	2.497	0.649	55	3.744	4.554	0.457	104	4.236	4.653	0.457
7	2.185	3.121	0.674	56	3.578	4.252	0.457	105	3.893	4.653	0.457
8	2.564	3.662	0.685	57	3.514	4.129	0.457	106	3.855	4.610	0.813
9	2.862	4.088	0.686	58	3.385	5.371	0.559	107	4.139	4.389	0.813
10	2.760	4.138	0.915	59	3.744	5.135	0.813	108	4.350	4.226	0.915
11	2.925	4.179	0.915	60	3.744	4.792	0.813	109	4.350	4.226	0.457
12	2.925	4.179	0.457	61	3.744	4.792	0.457	110	4.139	4.389	0.457
13	2.760	4.138	0.457	62	3.744	5.135	0.457	111	3.855	4.610	0.457
14	2.964	4.039	0.915	63	3.385	5.371	0.457	112	4.206	4.520	0.813
15	2.964	4.039	0.457	64	3.744	4.077	0.915	113	4.454	4.408	0.915
16	2.964	4.231	0.915	65	3.744	4.212	0.813	114	4.454	4.408	0.457
17	3.047	4.343	0.915	66	3.744	4.212	0.457	115	4.206	4.520	0.457
18	3.096	4.408	0.915	67	3.744	4.077	0.457	116	4.503	4.343	0.915
19	3.096	4.408	0.457	68	3.744	5.546	0.559	117	4.586	4.231	0.915
20	3.047	4.343	0.457	69	3.806	5.546	0.457	118	4.625	4.179	0.915
21	2.964	4.231	0.457	70	3.806	4.077	0.915	119	4.625	4.179	0.457
22	3.200	4.226	0.915	71	3.806	4.212	0.813	120	4.586	4.231	0.457
23	3.200	4.226	0.457	72	3.806	4.554	0.813	121	4.503	4.343	0.457
24	2.833	4.308	0.915	73	3.806	4.554	0.457	122	4.662	4.433	0.915
25	2.888	4.433	0.915	74	3.806	4.212	0.457	123	4.717	4.308	0.915
26	3.026	4.653	0.915	75	3.806	4.077	0.457	124	4.790	4.138	0.915
27	3.026	4.653	0.457	76	3.806	5.546	0.559	125	4.662	4.433	0.457
28	2.888	4.433	0.457	77	3.806	5.135	0.813	126	4.717	4.308	0.457
29	2.833	4.308	0.457	78	3.806	4.792	0.813	127	4.790	4.138	0.457
30	3.314	4.653	0.813	79	3.806	4.792	0.457	128	4.586	4.039	0.915
31	3.657	4.653	0.813	80	3.806	5.135	0.457	129	4.586	4.039	0.457
32	3.657	4.653	0.457	81	4.165	5.546	0.457	130	4.688	4.088	0.686
33	3.314	4.653	0.457	82	4.165	5.371	0.559	131	4.987	3.662	0.685
34	3.344	4.520	0.813	83	4.275	5.371	0.457	132	5.366	3.121	0.674
35	3.344	4.520	0.457	84	4.152	5.032	0.813	133	5.803	2.497	0.649
36	3.057	4.697	0.915	85	3.855	4.941	0.813	134	6.240	1.872	0.625
37	3.314	4.697	0.813	86	3.855	4.739	0.813	135	6.677	1.248	0.599
38	3.657	4.697	0.813	87	4.152	4.739	0.457	136	7.114	0.624	0.575
39	3.657	4.697	0.457	88	4.275	4.941	0.457	137	7.551	0.0	0.419
40	3.314	4.697	0.457	89	4.036	5.032	0.457	138	7.551	0.0	0.0
41	3.057	4.697	0.457	90	3.972	4.129	0.915	139	0.0	−0.3	0.2
42	3.411	4.389	0.813	91	4.036	4.252	0.813	140	1.311	1.872	2.000
43	3.695	4.610	0.813	92	3.972	4.129	0.457	141	6.240	1.872	2.000
44	3.695	4.610	0.457	93	3.893	4.252	0.457	142	7.551	−0.3	0.2
45	3.411	4.389	0.457	94	4.236	4.697	0.813	143	2.564	3.662	0.685
46	3.275	5.032	0.813	95	4.493	4.697	0.813	144	4.987	3.662	0.685
47	3.398	4.941	0.813	96	4.493	4.697	0.915				
48	3.695	4.739	0.813	97	4.236	4.697	0.457				
49	3.695	4.739	0.457	98	3.893	4.697	0.457				

THIS DOCUMENT PROVIDED BY THE ABBOTT AEROSPACE
TECHNICAL LIBRARY
ABBOTTAEROSPACE.COM

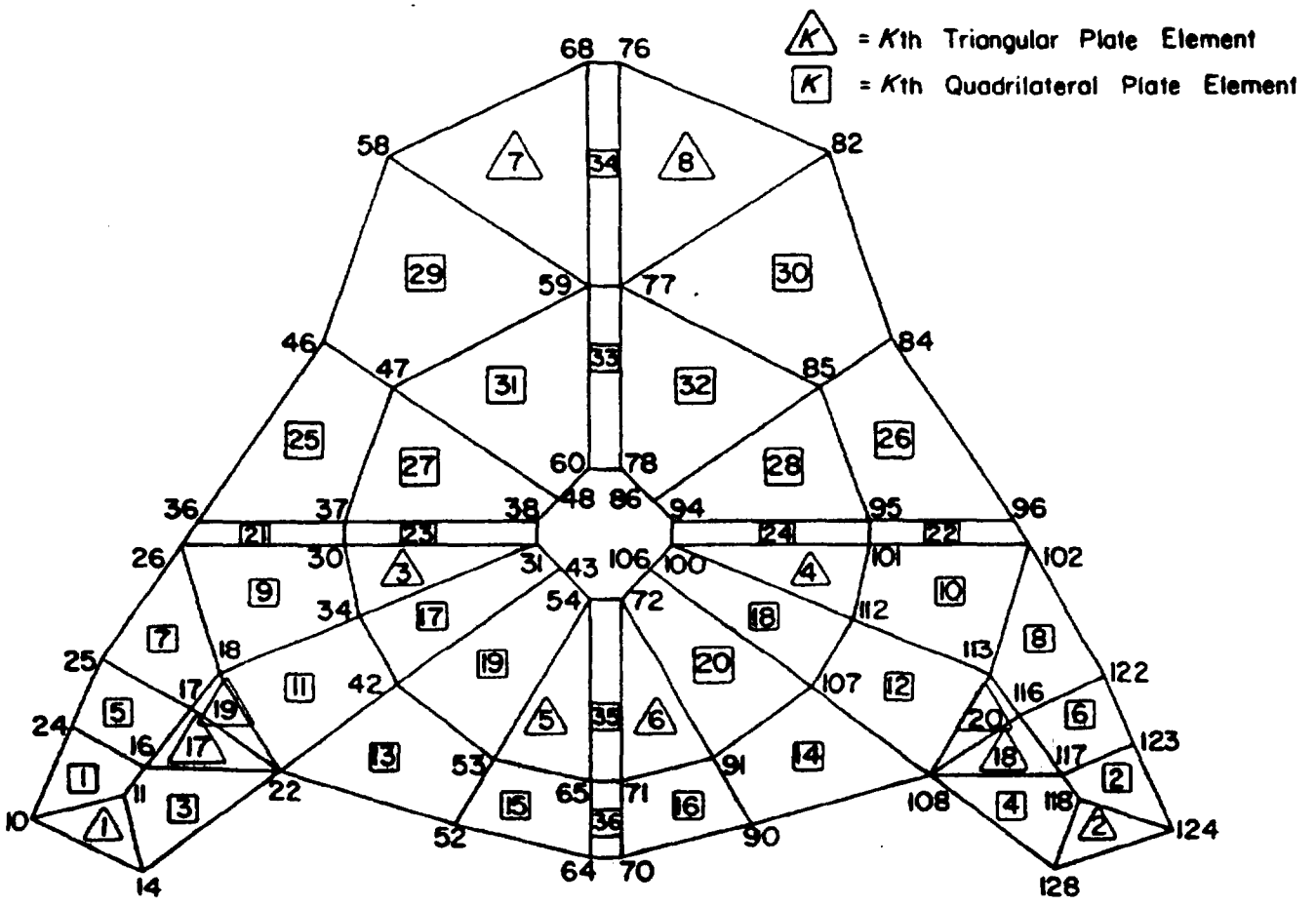

Figure 9-32. Top View of Main Body—Finite Element Model (Nodes and Elements)

the band width and the number of active columns in the matrix. The band width and the number of active columns in turn depend on the node numbering. Note here that the proper renumbering of the nodes for the bottom carriage model reduced the estimated computation time from 956 s to 1.07 s. To obtain a relatively small band width that results in less computation time, the nodes are numbered such that the maximum difference between the numbers of the nodes that are connected directly by interelement boundaries is a minimum. Observing the geometry of nodes and elements, the analyst develops a proper strategy of numbering the nodes. Usually, it requires a few trials to decide the best numbering strategy for a complicated structure like the bottom carriage structure. Modern software is also available that automatically numbers nodes for maximum efficiency.

4. *Selection of Types of Elements.* Most commercial computer programs for finite element analysis have an extensive finite element library. NASTRAN, for example, has various one-, two-, and three-dimensional finite elements. (Refer to Appendix B.) The selection of types of elements for various regions of a structure depends on the structural behavior and geometry. The main body of the bottom carriage is formed out of steel plates welded together, and the loading is such that it produces bending as well as in-plane straining of these plates. Quadrilateral and triangular plate elements having bending and in-plane stiffness, therefore, are chosen to model the main body. Trails—modeled by bar (beam) elements—are long, box-shaped members subjected to bending and axial loads. The trails, however, could have been made discrete as plate elements—a procedure that requires greater effort to prepare data and results in an increased number of nodes and finite elements.

5. *Boundary Conditions and Nodal Degrees of Freedom.* During firing the M198 bottom carriage rests on the floats and spades at the rear end of the trails and the front float. Spades are embedded in the ground, and reactions R_1 and R_2 act as shown in Fig. 9-12. Note that R_2 (similarly R_4) acts at a point that is a distance y

THIS DOCUMENT PROVIDED BY THE ABBOTT AEROSPACE
TECHNICAL LIBRARY
ABBOTTAEROSPACE.COM

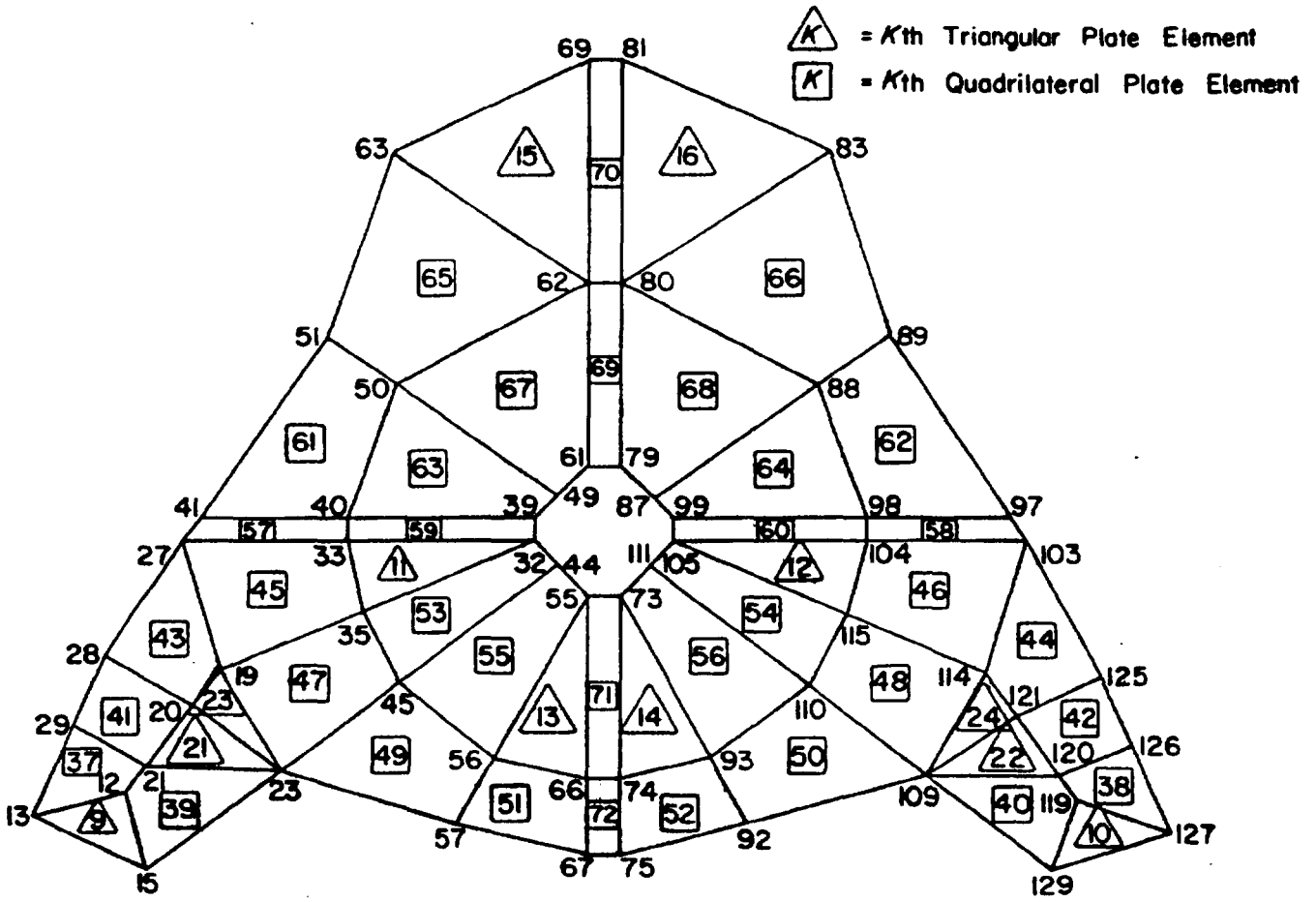

Figure 9-33. Bottom View of Main Body—Finite Element Model (Nodes and Elements)

below the centroid of the cross section. To represent the locations of R_1 and R_2 (and similarly R_3 and R_4) properly on the model, a rigid bar element joining the centroid of the trail end to a point vertically below it (centroid) in the ground at a distance y is provided. The rigid bar element is used to transmit the reactions R_1 and R_2 to the trail end. (A rigid bar element is like an ordinary bar element except for the very high values of modulus of elasticity and area moments of inertia, which make it stiff enough to be considered rigid.) The point where R_1 and R_2 intersect (Refer to Fig. 9-12.) offers no resistance to rotation, and there are no moments acting at this point. Therefore, this point is best modeled as a ball and socket joint that offers translational resistance and not rotational resistance. Therefore, the translations along the X-, Y-, and Z-axes—represented by numbers 1, 2, and 3, respectively, in NASTRAN—need to be restrained completely at this point. Similarly, there is a point corresponding to the intersection of reactions R_3 and R_4 where these translations are restrained. The connection between the main body and a trail is a pin connection that permits rotation along the vertical axis and restrains other rotations and translations. During firing, however, even the rotation about the vertical axis is restrained by a latch. This connection, therefore, is modeled by providing four rigid bar elements between the front-end node of a trail (e.g., 9) and the four nodes—10, 14, 13, and 15—on the main body that are connected to the trail. These connections are shown in Fig. 9-35. The reaction R_5 is assumed to be acting at nodes 69 and 81. (See Fig. 9-34.) Because the front float offers resistance to vertical translation only, nodes 69 and 81 are restrained translationally in the vertical direction.

9-5.1.2 Computation of Equivalent Loads

The loads—namely B_{RR}, B_{RT}, and B_{RM}, as shown in Table 9-1—are assumed to be transmitted through the grid points 59, 47, 37, 30, 34, 42, 53, 65, 71, 91, 107, 112, 101, 95, 85, and 77, as shown in Fig. 9-34. For the computation of equivalent loads at these grid points, the same assumptions discussed in par. 9-4 are made.

THIS DOCUMENT PROVIDED BY THE ABBOTT AEROSPACE
TECHNICAL LIBRARY
ABBOTTAEROSPACE.COM

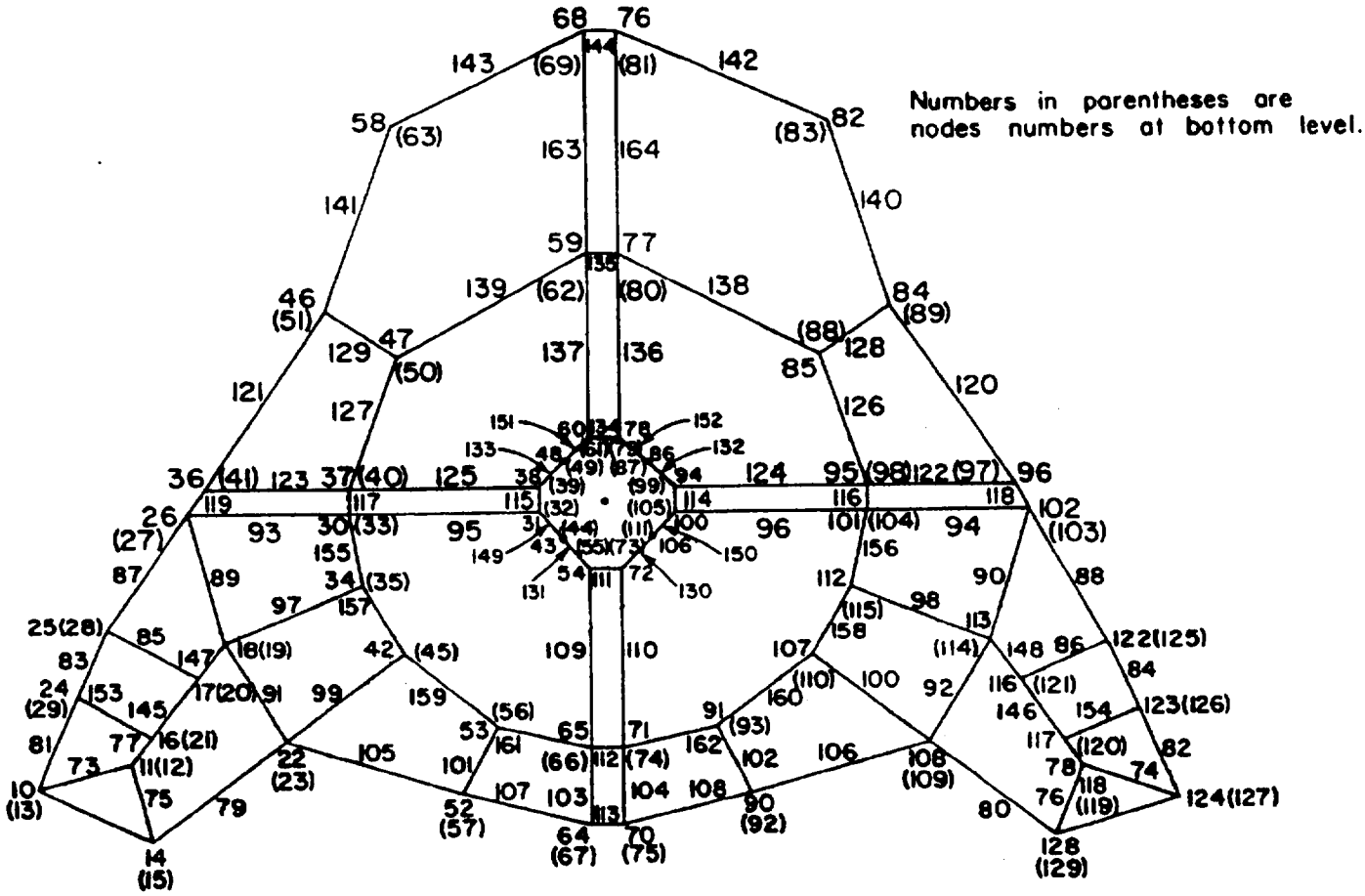

Figure 9-34. Top View of Main Body—Finite Element Model (Vertical Plate Elements)

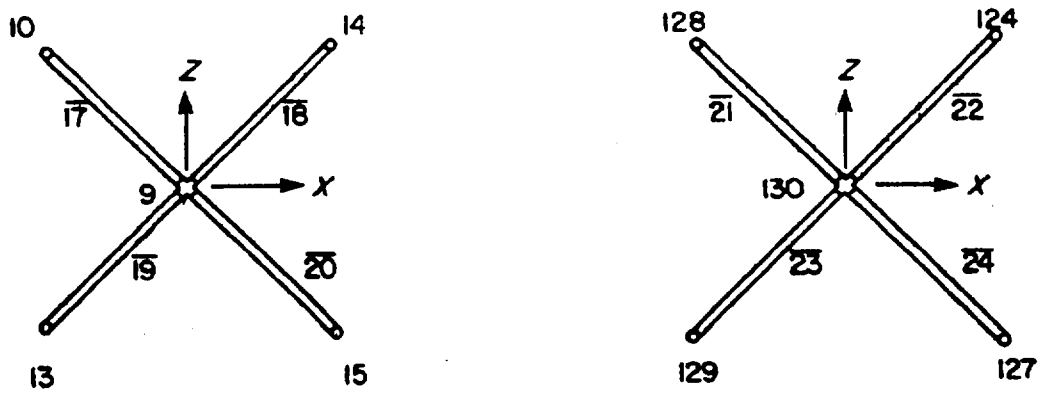

Figure 9-35. Modeling of Connection Between Trails and Main Body

THIS DOCUMENT PROVIDED BY THE ABBOTT AEROSPACE
TECHNICAL LIBRARY
ABBOTTAEROSPACE.COM

Briefly, these assumptions are (1) the in-plane force B_{RR} and normal force B_{RT} are uniformly distributed along the circumference of the traverse bearing and (2) the moment B_{RM} produces a linear pressure p (force/unit length) distribution. Calculations based on these two assumptions follow:

1. *Equivalent Loads Due to B_{RR} and B_{RT}.* It is relatively easy to evaluate the equivalent loads due to B_{RR} and B_{RT}. The angles, which decide the proportions of B_{RR} and B_{RT} at the grid points, are shown in Fig. 9-36. The proportion of the load is given by

$$B'_{RR} = \left(\frac{\theta}{360} \right) B_{RR}, \text{ N} \tag{9-34}$$

and

$$B'_{RT} = \left(\frac{\theta}{360} \right) B_{RT}, \text{ N} \tag{9-35}$$

where

B'_{RR} = proportion of load due to B_{RR}, N
B'_{RT} = proportion of load due to B_{RT}, N
θ = angle between grid points (See Fig. 9-36.), deg.

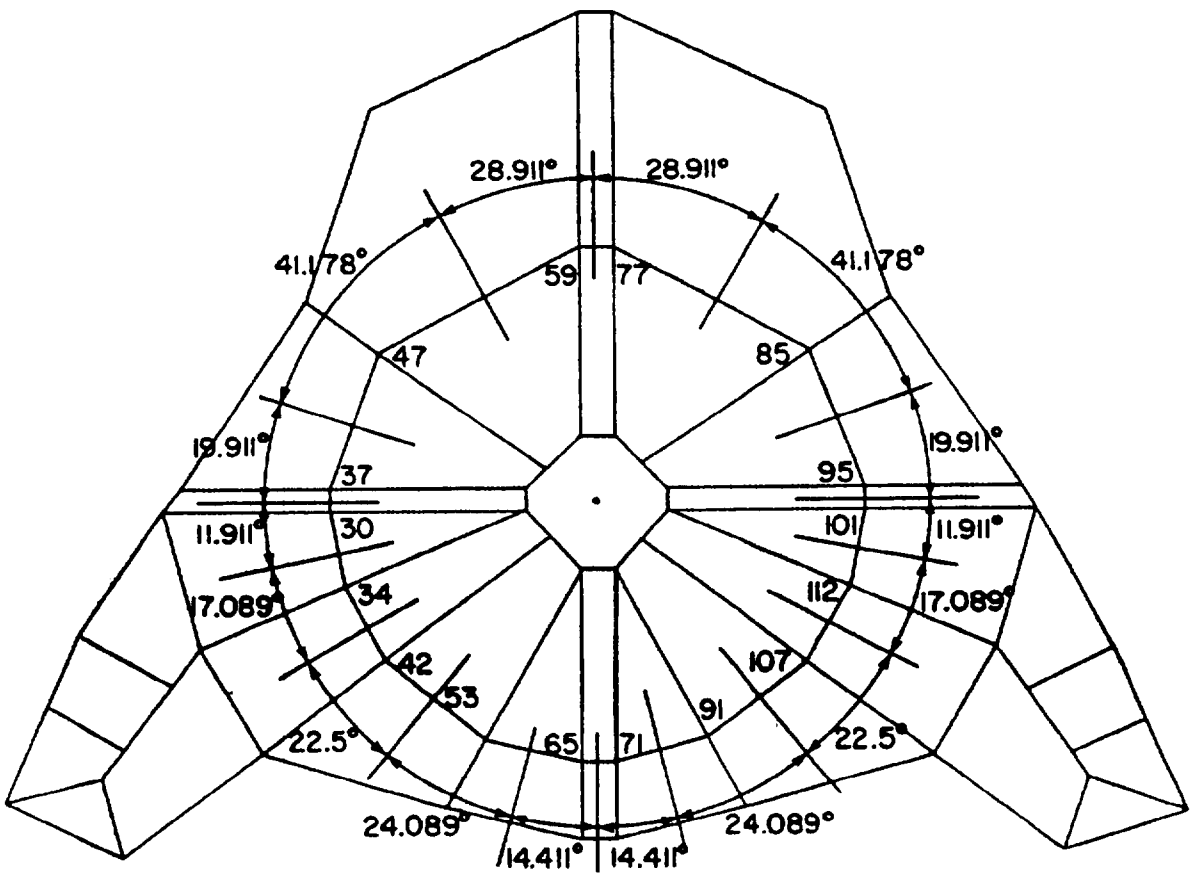

Figure 9-36. Representative Angles Associated With Load-Carrying Grid Points

THIS DOCUMENT PROVIDED BY THE ABBOTT AEROSPACE
TECHNICAL LIBRARY
ABBOTTAEROSPACE.COM

For example, by Eq. 9-34, at grid point 59

$$B'_{RR} = \left(\frac{28.91}{360} \right) 224{,}998 = 18{,}069 \text{ N}.$$

The distributed loads B'_{RR} and B'_{RT} at the various grid points—calculated by Eq. 9-34 or Eq. 9-35—are given in Tables 9-13 and 9-14, respectively. The loads B_{RR} and B_{RT} are taken from Table 9-1.

2. *Linear Pressure p.* Let p be the maximum linear pressure, i.e., force per unit length, due to the moment B_{RM}. This pressure p is experienced at points C and D, shown in Fig. 9-37. Note that the points C and D are the centers of gravity of the linear pressure due to the moment B_{RM}. Pressures p' at the grid points are proportional to the projections of the radii corresponding to those grid points, i.e.,

$$p' = p\cos\theta', \text{ N/m} \tag{9-36}$$

where

θ' = angle between line OA and radial line identified by an arrow in Fig. 9-37, deg.

For example, by Eq. 9-36 and the angle θ' indicated in Fig. 9-37, the pressure p' at point 59 is

$$p' = p\,|\cos 152.329°|, \text{ N/m}.$$

Linear pressures at the other grid points are calculated similarly and are shown in Table 9-15.

A further approximation assumption is now made, i.e., that the linear pressures p' evaluated at the grid points are uniform for the corresponding representative arc lengths. Thus

$$L_{arc} = (2\pi r)\left(\frac{\theta}{360} \right), \text{ m}$$

$$= \frac{\pi r \theta}{180}, \text{ m} \tag{9-37}$$

TABLE 9-13
EQUIVALENT DISTRIBUTION OF B_{RR} AT GRID POINTS

Grid Point	B'_{RR} at 35 deg, N	B'_{RR} at 55 deg, N	B'_{RR} at 75 deg, N
59	18,069	12,648	4,626
47	25,736	18,014	6,589
37	12,444	8,711	3,186
30	7,444	5,211	1,906
34	10,681	7,476	2,734
42	14,062	9,843	3,600
53	15,056	10,538	3,855
65	9,007	6,304	2,306
71	9,007	6,304	2,306
91	15,056	10,538	3,855
107	14,062	9,843	3,600
112	10,681	7,476	2,734
101	7,444	5,211	1,906
95	12,444	8,711	3,186
85	25,736	18,014	6,589
77	18,069	12,648	4,626
Total	224,998	157,490	57,604

THIS DOCUMENT PROVIDED BY THE ABBOTT AEROSPACE
TECHNICAL LIBRARY
ABBOTTAEROSPACE.COM

TABLE 9-14
EQUIVALENT VERTICAL LOAD DISTRIBUTION OF B_{RT} AT LOAD-CARRYING GRID POINTS

Grid Point	B_{RT} at 35 deg, N	B_{RT} at 55 deg, N	B_{RT} at 75 deg, N
59	9,935	16,914	21,568
47	14,150	24,091	30,720
37	6,842	11,649	14,854
30	4,093	6,968	8,886
34	5,872	9,998	12,749
42	7,732	13,163	16,786
53	8,278	14,093	17,971
65	4,952	8,431	10,751
71	4,952	8,431	10,751
91	8,278	14,093	17,971
107	7,732	13,163	16,786
112	5,872	9,998	12,749
101	4,093	6,968	8,886
95	6,842	11,649	14,854
85	14,150	24,091	30,720
77	9,935	16,914	21,568
Total	123,708	210,614	268,570

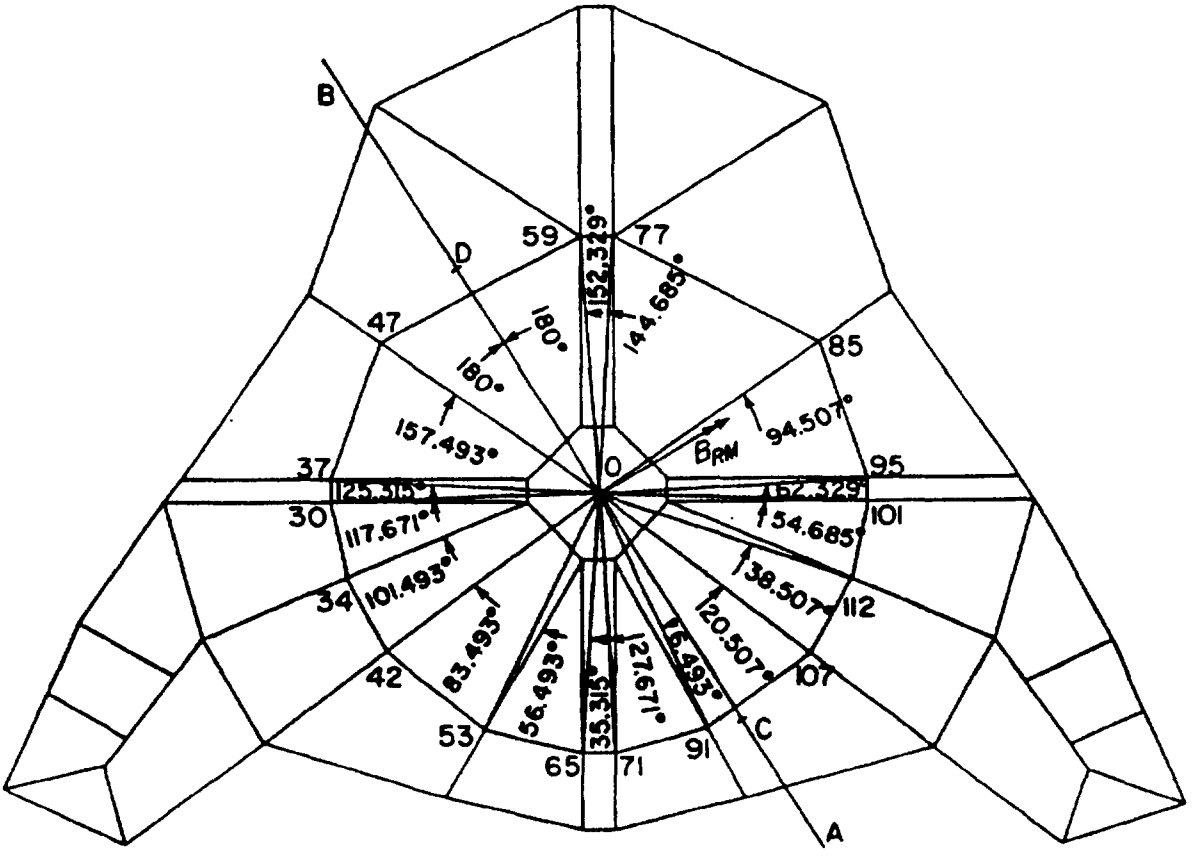

Figure 9-37. Angles for Calculation of Projected Radii on OA

THIS DOCUMENT PROVIDED BY THE ABBOTT AEROSPACE
TECHNICAL LIBRARY
ABBOTTAEROSPACE.COM

TABLE 9-15
PROPORTION p' OF p AT GRID POINTS
(Refer to Fig. 9-37)

Grid Point	Proportion p' of p
59	cos 152.329° = |−0.8856|
47	cos 157.493° = |−0.9238|
37	cos 125.315° = |−0.5781|
30	cos 117.671° = |−0.4644|
34	cos 101.493° = |−0.1992|
42	cos 83.493° = 0.1133
53	cos 56.493° = 0.5520
65	cos 35.315° = 0.8160
71	cos 27.671° = 0.8856
91	cos 6.493° = 0.9936
107	cos 20.507° = 0.9366
112	cos 38.507° = 0.7825
101	cos 54.685° = 0.5781
95	cos 62.329° = 0.4644
85	cos 94.507° = |−0.07858|
77	cos 144.685° = |−0.8160|

Note: The notation $|-x|$ is interpreted as the absolute value of x.

where

L_{arc} = representative arc length, m
r = bearing radius, m
θ = angle between grid points (See Fig. 9-36.), deg.

For example, the L_{arc} for grid point 59 is

$$L_{arc} = 0.4572 \left(\frac{\pi}{180} \right) (28.911) = 0.2307 \text{ m}$$

where 0.4572 m represents the traverse bearing radius, and 28.911 deg is the representative angle for grid point 59, as shown in Fig. 9-36.

Thus the moment contribution M' of an equivalent force at grid point 59 is given by distribution

$$M' = p' L_{arc} L_{ma}, \text{ N·m} \tag{9-38}$$

where

L_{ma} = length of moment arm, m.

For example, the moment contribution M' at grid point 59 is

$$M' = |-0.8865p|(0.2307)(0.4049)$$

$$= 0.08281p, \text{ N·m}$$

where

$-0.8865p$ = expression for p' from Table 9-15, N·m
0.2307 = representative arc length L_{arc} from Table 9-16, m
0.4099 = length of moment arm L_{ma} from Table 9-17, m.

THIS DOCUMENT PROVIDED BY THE ABBOTT AEROSPACE
TECHNICAL LIBRARY
ABBOTTAEROSPACE.COM

TABLE 9-16
REPRESENTATIVE ARC LENGTHS
FOR LOAD-CARRYING GRID POINTS
(Refer to Fig. 9-36)

Grid Point	Representative Arc Length L_{arc}, m
59	0.2307
47	0.3286
37	0.1589
30	0.0950
34	0.1364
42	0.1795
53	0.1922
65	0.1150
71	0.1150
91	0.1922
107	0.1795
112	0.1364
101	0.0951
95	0.1589
85	0.3286
77	0.2307

TABLE 9-17
MOMENT CONTRIBUTIONS M' DUE TO EQUIVALENT LOADS AT GRID POINTS

Grid Point	Equivalent Force F', N	Moment Arm L_{arm}, m	Moment Contribution M', N·m
59	$\|-0.8856p \times 0.2307\|$	0.4049	$(8.2724\text{ E-}2)p$
47	$\|-0.9238p \times 0.3286\|$	0.4224	$(1.2822\text{ E-}1)p$
37	$\|-0.5781p \times 0.1589\|$	0.2643	$(2.4279\text{ E-}2)p$
30	$\|-0.4644p \times 0.0950\|$	0.2123	$(9.3663\text{ E-}3)p$
34	$\|-0.1992p \times 0.1364\|$	0.0911	$(2.4753\text{ E-}3)p$
42	$0.1133p \times 0.1795$	0.0518	$(1.0535\text{ E-}3)p$
53	$0.5520p \times 0.1922$	0.2524	$(2.6778\text{ E-}2)p$
65	$0.8160p \times 0.1150$	0.3731	$(3.5012\text{ E-}2)p$
71	$0.8856p \times 0.1150$	0.4049	$(4.1237\text{ E-}2)p$
91	$0.9936p \times 0.1922$	0.4543	$(8.6758\text{ E-}2)p$
107	$0.9366p \times 0.1795$	0.4232	$(7.1148\text{ E-}2)p$
112	$0.7825p \times 0.1364$	0.3577	$(3.8178\text{ E-}2)p$
101	$0.5781p \times 0.0951$	0.2643	$(1.4515\text{ E-}2)p$
95	$0.4644p \times 0.1589$	0.2123	$(1.5666\text{ E-}2)p$
85	$\|-0.0786p \times 0.3286\|$	0.0359	$(9.2722\text{ E-}4)p$
77	$\|-0.8160p \times 0.2307\|$	0.3731	$(7.0237\text{ E-}2)p$
	Total bending moment B_{RM} =		$0.6486p$

Note: The distances under the column "Moment Arm" are obtained from the detailed drawings of the bottom carriage. This table uses the expression E followed by a number to indicate the power of 10. For example, $8.2724 \times E\text{-}2 = 8.2724 \times 10^{-2}$.

Moment contributions for all grid points are shown in Table 9-17. The sum of all these grid point moment distributions should equal the total bearing moment B_{RM}, i.e.,

$$B_{RM} = \Sigma M_i', \text{ N·m} \tag{9-39}$$

from which the value of the maximum linear pressure p resulting from B_{RM} can be calculated. Since from Table 9-17

THIS DOCUMENT PROVIDED BY THE ABBOTT AEROSPACE
TECHNICAL LIBRARY
ABBOTTAEROSPACE.COM

$$B_{RM} = 0.6486p$$

or

$$p = \frac{B_{RM}}{0.6486}\ , \text{N·m}, \qquad (9\text{-}40)$$

p can be determined if B_{RM} is known. The values for p at the three elevations shown in Table 9-18 were arrived at by substituting the values for B_{RM} from Table 9-1 into Eq. 9-40, i.e.,

$$p_{35} = \frac{(B_{RM})_{35}}{0.6486} = \frac{418{,}578}{0.6486} = 645{,}356 \text{ N/m}$$

$$p_{55} = \frac{(B_{RM})_{55}}{0.6486} = \frac{417{,}660}{0.6486} = 643{,}941 \text{ N/m}$$

$$p_{75} = \frac{(B_{RM})_{75}}{0.6486} = \frac{346{,}105}{0.6486} = 533{,}619 \text{ N/m}.$$

TABLE 9-18
EQUIVALENT GRID POINT FORCES F' DUE TO B_{RM}

Grid Point	Equivalent Forces, N			
	Elevation →	At 35 deg	At 55 deg	At 75 deg
	max. force/length p →	645,356 N/m	643,941 N/m	533,619 N/m
59	0.2043p	−131,851	−131,562	−109,022
47	0.3036p	−195,905	−195,475	−161,986
37	0.09186p	−59,282	−59,152	−49,018
30	0.04412p	−28,472	−28,409	−23,542
34	0.02717p	−17,535	−17,496	−14,499
42	0.02034p	13,125	13,096	10,852
53	0.1061p	68,469	68,319	56,614
65	0.09384p	60,560	60,427	50,075
71	0.1018p	65,726	65,581	54,346
91	0.1910p	123,244	122,973	101,905
107	0.1681p	108,497	108,259	89,712
112	0.1067p	68,881	68,729	56,954
101	0.05492p	35,443	35,365	29,306
95	0.07379p	47,623	47,518	39,377
85	0.02583p	−16,668	−16,632	−13,782
77	0.1883p	−121,489	−121,222	−100,454

Negative force is upward.
Positive force is downward.

Table 9-18 shows the equivalent forces F' due to B_{RM}. Table 9-19 shows the algebraic additions of the equivalent vertical loads F_V due to both B_{RT} and B_{RM}. The entries in Table 9-19 were obtained by adding the corresponding elements—$(R_{RT})_{ij}$ from Table 9-14 plus $(R_{BM})_{ij}$ from Table 9-18. For example, for grid point 59 at 30 deg elevation

$$F_V = 9935 + (-131{,}851) = -121{,}916 \text{ N}.$$

THIS DOCUMENT PROVIDED BY THE ABBOTT AEROSPACE
TECHNICAL LIBRARY
ABBOTTAEROSPACE.COM

TABLE 9-19
TOTAL VERTICAL LOAD F_V DUE TO B_{RM} AND B_{RT}

Grid Point	Total Vertical Load F_V, N		
	At 35 deg	At 55 deg	At 75 deg
59	−121,916	−114,648	−87,454
47	−181,755	−171,384	−131,266
37	−52,440	−47,503	−34,164
30	−24,379	−21,441	−14,656
34	−11,663	−7,498	−1,750
42	20,857	26,259	27,638
53	76,747	82,412	74,585
65	65,512	68,658	60,826
71	70,678	74,012	65,097
91	131,522	137,066	119,876
107	116,229	121,422	106,498
112	74,753	78,727	69,703
101	39,536	42,333	38,192
95	54,465	59,167	52,231
85	−2,518	−7,459	−16,938
77	−111,554	−104,308	−78,886

Negative load is upward.
Positive load is downward.

Note that the vertical loads—designated N_z in Tables 9-20, 9-21, and 9-22—are along the Z-axis or are the Z-components of the equivalent concentrated loads. By resolving the equivalent forces B'_{RR} (Table 9-13) due to B_{RR} into their X- and Y-components, the equivalent loads—N_X, N_Y, and N_Z—become known for all grid points. The three load components are shown in Tables 9-20, 9-21, and 9-22 for elevation angles of 35 deg, 55 deg, and 75 deg, respectively.

9-5.2 NASTRAN STRESS ANALYSIS

Preparation of the bulk data deck is the major effort in obtaining stress analysis of a finite element model using the NASTRAN program. The data in the bulk data deck contain all the details—such as, geometric properties, material properties, elements, constraints, and applied loads—of the structural model and various

TABLE 9-20
NODAL FORCES FOR ELEVATION OF 35 DEG

Node	N_X, N	N_Y, N	N_Z, N
59	9,439	−15,408	121,916
47	13,444	−21,945	181,755
37	6,501	−10,611	52,440
30	3,889	−6,348	24,379
34	5,580	−9,108	11,663
42	7,646	−11,991	−20,857
53	7,865	−12,838	−76,747
65	4,705	−7,680	−65,512
71	4,705	−7,680	−70,678
91	7,865	−12,838	−131,522
107	7,646	−11,991	−116,229
112	5,580	−9,108	−74,753
101	3,889	−6,348	−39,536
95	6,501	−10,611	−54,465
85	13,444	−21,945	2,518
77	9,439	−15,408	111,584

THIS DOCUMENT PROVIDED BY THE ABBOTT AEROSPACE
TECHNICAL LIBRARY
ABBOTTAEROSPACE.COM

TABLE 9-21
NODAL FORCES FOR ELEVATION OF 55 DEG

Node	N_X, N	N_Y, N	N_Z, N
59	6,607	−10,785	114,648
47	9,410	−15,361	171,384
37	4,551	−7,428	−47,503
30	2,722	−4,443	−21,441
34	3,905	−6,375	−7,498
42	5,142	−8,393	−26,259
53	5,505	−8,986	−82,412
65	3,293	−5,375	−68,858
71	3,293	−5,375	−74,012
91	5,505	−8,986	−137,066
107	5,142	−8,393	−121,422
112	3,905	−6,375	−78,727
101	2,722	−4,443	−42,333
95	4,551	−7,428	−59,167
85	9,410	−15,361	−7,459
77	6,607	−10,785	104,308

TABLE 9-22
NODAL FORCES FOR ELEVATION OF 75 DEG

Node	N_X, N	N_Y, N	N_Z, N
59	2,417	−3,945	87,454
47	3,442	−5,618	131,266
37	1,664	−2,717	34,164
30	996	−1,625	14,656
34	1,428	−2,331	1,750
42	1,881	−3,070	−27,638
53	2,014	−3,287	−74,585
65	1,207	−1,966	−60,826
71	1,207	−1,966	−65,097
91	2,014	−3,287	−119,876
107	1,881	−3,070	−106,498
112	1,428	−2,331	−69,703
101	996	−1,625	−38,192
95	1,664	−2,717	−54,231
85	3,442	−5,618	−16,938
77	2,417	−3,945	78,886

conditions for the solution. Several bulk data lines are thoroughly explained in Section 2.4 of the NASTRAN User's Manual. A general introduction to the NASTRAN computer program is given in Appendix B. A computer output using three load sets—namely, those corresponding to elevation angles of 75 deg, 55 deg, and 35 deg—is obtained. The output gives

1. Six components of displacement at each grid point in the basic coordinate system
2. Forces in the elements—namely, triangular, quadrilateral plates, and bar elements—in the element coordinate system
3. Stresses in the elements in the element coordinate system.

The results obtained from NASTRAN are compared with those obtained by using the simple mechanics of deformable bodies approach (conventional) as discussed in par. 9-4. Table 9-23 shows the comparison of results, i.e., shows that the vertical reactions R_i and the maximum bending moment in the trails obtained by the two methods agree fairly well. The maximum stress in the main body obtained by the FEM approach,

THIS DOCUMENT PROVIDED BY THE ABBOTT AEROSPACE
TECHNICAL LIBRARY
ABBOTTAEROSPACE.COM

TABLE 9-23
COMPARISON OF THE RESULTS FROM FEM (FINITE ELEMENT METHOD) AND CONVENTIONAL STRESS ANALYSIS

Function	Elevation			Max. for Three Elevations
	75 deg	55 deg	35 deg	
1. Max. vertical deflection, mm	9.726	8.83	7.04	9.726
	†	†	†	†
2. Vertical reaction (right) R_1, kN	79.421	97.378	98.773	98.773
	(77.973)	(93.457)	(93.773)	(93.773)
3. Horizontal reaction (right) R_2, kN	57.34	155.64	143.36	155.64
	(49.20)	(134.50)	(192.20)	(192.20)
4. Vertical reaction (left) R_3, kN	26.1	22.9	16.3	26.1
	(38.2)	(38.4)	(33.2)	(38.4)
5. Horizontal reaction (left) R_4, kN	12.28	(36.86)	4.1	36.86
	(15.80)	(43.10)	(61.17)	(61.6)
6. Max. bending moment in trails, kN·m	358.61	384.3	347.9	384.3
	*	*	*	(374.2)
7. Max. stress in main body, MPa	157.72	182.8	177.5	182.8
	*	*	*	(332.98)

Note: Figures in parentheses are for the conventional stress analysis; those without parentheses are for the FEM. The quantities marked as † cannot be calculated by conventional analysis methods. The quantities marked as * are not significant enough to be calculated for all angles of elevation since only the maximum of these quantities are of interest.

however, is about 45% less than that obtained by the conventional method. This difference is due to the fact that the conventional method considered the main body a simple beam. This assumption is unrealistic and results in the neglect of lateral stiffness and gives rise to higher values of stresses. Locations of the maximum bending moment in the trails and the maximum stress in the main body are identical for both methods.

9-6 BOTTOM CARRIAGE-SOIL INTERACTION

The bottom carriage is the main weapon component that transmits firing loads to the ground. In doing so it plays an important role of providing stable and steady support to the weapon system. The importance of these two aspects, namely, stability and steadiness, cannot be overemphasized as far as the accuracy of firing is concerned. Stability during firing is governed by the geometry, size, and support locations for the bottom carriage main body and trails. A large-spanned bottom carriage provides a large contact area. Thus there is a good possibility that the firing loads would fall in the contact area and thereby preclude the hopping of the carriage. The steadiness of the weapon, on the other hand, depends on how firmly the ground grips the bottom carriage supports. The soil-structure interaction plays a major role in this aspect. A thorough understanding of this interaction is an important consideration in making a dynamic model of the weapon system. Conversely, a lack of understanding in this regard leads to the modeling of the structure with improper boundary conditions, and as a consequence, this error may result in formulation of a problem that is drastically different from the intended one. To be able to ascertain soil behavior under firing loads, several properties—such as the type of the soil, its density, moisture content, internal friction, cohesion, shear strength, and load-deflection characteristics—should be known. These and other related properties of soil are known for certain types of soils but only under laboratory conditions. Besides soil properties, soil history regarding its formation, consolidation, and precompression should also be known to estimate prestress in the soil mass. Because it is often very difficult to obtain all relevant data for the soil, the designer must make assumptions to predict its behavior.

As presented in Chapter 2, the M198 bottom carriage has two rear supports, each in the form of a float (resting on ground) and a spade (driven into ground). The front support is in the form of a large float (or firing base) that either simply rests on the ground or is spiked into the ground. The paragraphs that follow present considerations and basic principles regarding the interaction of the ground with the spades and floats.

THIS DOCUMENT PROVIDED BY THE ABBOTT AEROSPACE
TECHNICAL LIBRARY
ABBOTTAEROSPACE.COM

9-6.1 TRAIL SPADE/GROUND INTERACTION

Trail spades act as anchors in granular and/or cohesive soils during firing. In a recoil cycle the spades are pushed against the soil mass with a varying force. The pushing causes the soil mass to exert passive earth pressure on one side of the spade and an active earth pressure on the other side. The magnitude and distribution of these pressures depend on the internal friction, cohesion, density, and water content of the soil. Active and passive pressures are also functions of the yield ratio. The yield ratio d for the spade is defined as the ratio of the horizontal displacement Y to the vertical depth H of the spade. Fig. 9-38 is divided into two regions, i.e., an active earth pressure on the right and a passive earth pressure on the left. Fig. 9-38 illustrates that for relatively small yield ratios d, the active earth pressure attains its minimum value but remains fairly constant even for higher values of the yield ratio. The passive earth pressure, however, continues to build up with increasing (negative) yield ratios. Spade movement of sufficient magnitude causes mobilization of the shear strength of the soil, and there are several theories to ascertain lateral pressures on the spade. Rankine's theory is widely used for the purpose. When the spade movement is very small, the soil mass may be considered at rest; again, there are several factors that determine the lateral pressure on the spade. One of the important factors, which is usually unknown, is the prestress condition of the soil, which depends on the history of loading and unloading of the soil mass. The prediction of lateral earth pressure on the spades is further complicated by the fact that the loads transmitted by the spades to the ground are dynamic in nature, and the soil behavior under such loading is not yet well understood.

9-6.2 FIRING BASE (WITH AND WITHOUT STAKES)—GROUND INTERACTION

A firing base without stakes acts primarily as a footing subjected to vertical and lateral loads. An important consideration in the design of a firing base is, therefore, the bearing capacity of the ground. The larger the bearing capacity of the ground, the lesser is the area requirement of the firing base in transmitting vertical loads to the ground. The bearing capacity of the ground depends on several factors such as the consolidation and compaction history of the soil mass at the site, cohesion, internal friction, ground water level, and type of soil.

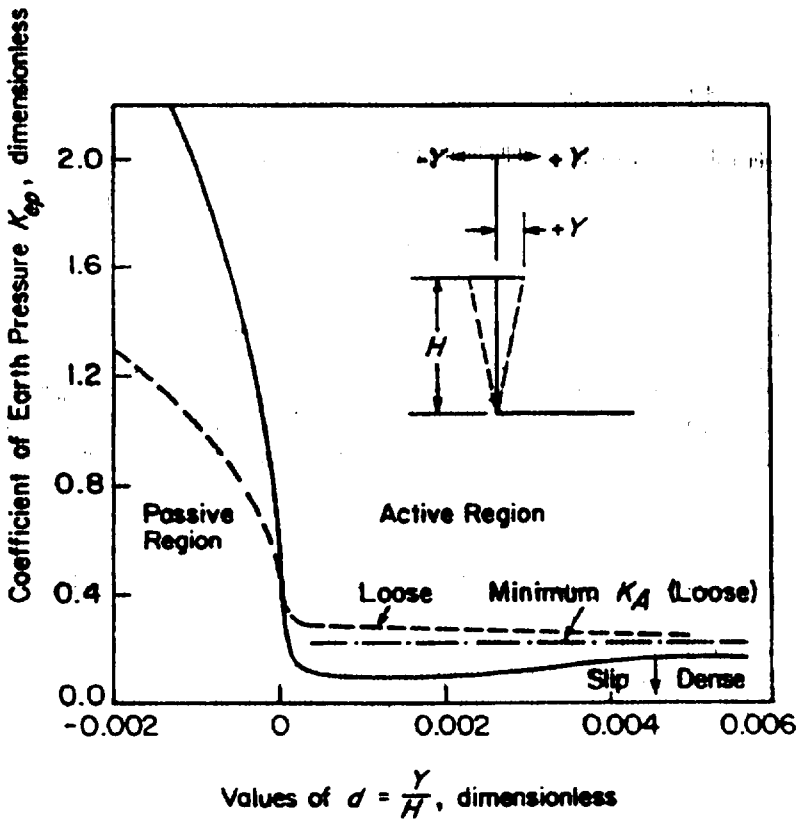

Figure 9-38. Influence of Relative Density of Sand and Effective Yield Y on Coefficient of Earth Pressure K_{φ}

THIS DOCUMENT PROVIDED BY THE ABBOTT AEROSPACE
TECHNICAL LIBRARY
ABBOTTAEROSPACE.COM

There are field tests such as standard penetration tests and plate load tests to determine the safe bearing capacity of the soil. Details for these tests are given in Ref. 9. A firing base with spikes acts like a group of piles with a pile head. A pile is simply a column-like structural member that is driven into the ground to anchor the firing base firmly. A pile head is the uppermost part of a pile. Skin friction of the spikes contributes to the bearing capacity of the firing base.

9-6.3 EFFECTS OF SOIL VARIABILITY

Naturally occurring soils have great variations in their compositions and engineering properties. The design of the bottom carriage has to account for the variability of the soils that may occur at different sites. There are several soil classifications; the one widely used in engineering is the "unified soil classification system". Soils in this system are divided into 15 groups, each of which has distinct engineering properties. The criteria for classification are

1. Percentage of gravel, sand, and fines—in accordance with the grain sizes
2. Shape of grain—size curve—for coarse-grained soils
3. Plasticity and compressibility characteristics—for fine-grained soils and organic soils.

The important properties and relative desirability for various uses of each soil category can be found in many textbooks on soil engineering. Bottom carriage design should consider the complete range of soil properties. For some clayey soils the bearing capacity may be as low as 50,000 Pa, whereas for some silty sands it may be as high as 300,000 Pa. It may be worthwhile to design floats, spades, and firing bases for different ranges of bearing capacity, internal friction, and cohesion, and then to select the proper one for the site under consideration. Even though it may not be practical to issue artillery pieces with detachable spades at the present time, selecting the proper parts and assembling them on site should be kept in mind for the future design practice.

REFERENCES

1. M. C. Nerdahl and J. W. Frantz, *Mathematical Models for Engineering Analysis and Design—Howitzer, Light, Towed: 105-mm, Soft Recoil XM 204*, Technical Report R-RRA-S-3-28-73, Artillery Weapon Systems Directorate, Weapons Laboratory, US Army Weapons Command, Rock Island, IL, May 1973.
2. C. Shaffer, *Initial Testing of a High-Strength, Cast Aluminum Bottom Carriage for the 155-mm Howitzer, XM198 (AD)*, Technical Report, SWERR-TR-72-82, Artillery Weapon Systems Directorate, Weapons Laboratory, US Army Weapons Command, Rock Island, IL, November 1972.
3. M. C. Nerdahl and H. O. Sand, *Design Data for Towed Artillery Weapon Systems*, Technical Notes, N-RRA-N-3-10-73, Artillery Weapon Systems Directorate, Weapons Laboratory, US Army Weapons Command, Rock Island, IL, February 1973.
4. *Monolithic High-Strength Aluminum Bottom Carriage Structure for 155-mm Howitzer, XM198*, Final Report R-CR-74-028, Northern Ordnance Division, FMC Corporation, Minneapolis, MN, May 1974.
5. C. M. Robinder, *Stress Analysis of 155-mm Towed Howitzer, XM198, Serial Numbers 1 and 2*, Technical Report, SWERR-TR-72-16, Research Directorate, Weapons Laboratory, US Army Weapons Command, Rock Island, IL, March 1972.
6. C. M. Robinder, *155-mm Howitzer XM198—Design Calculations*, Technical Note, SWERR-R4-72, Research Directorate, Weapons Laboratory, US Army Weapons Command, Rock Island, IL, March 1972.
7. C. M. Robinder, *Stress Analysis of 155-mm Towed Howitzer XM198, Serial Numbers 3 through 10—Bottom Carriage*, N-RR-T-3-13-73, Research Directorate, Weapons Laboratory, US Army Weapons Command, Rock Island, IL, February 1973.
8. A. P. Boresi, O. M. Sidebottom, F. B. Seely, and J. O. Smith, *Advanced Mechanics of Materials*, Third Edition, John Wiley and Sons, Inc., New York, NY, 1978.
9. K. Terzaghi, *Theoretical Soil Mechanics*, John Wiley and Sons, Inc., New York, NY, 1954.
10. R. J. Roark and W. C. Young, *Formulas for Stress and Strain*, McGraw-Hill Book Co., New York, NY, 1975.

THIS DOCUMENT PROVIDED BY THE ABBOTT AEROSPACE
TECHNICAL LIBRARY
ABBOTTAEROSPACE.COM

CHAPTER 10
DESIGN FOR MAINTAINABILITY

The design of equipment for maintainability can have a substantial impact on system performance. No matter how reliable the system is, it will eventually fail, and when it does, it must be repaired. The speed and ease of repair will determine the availability and cost of the system during its lifetime. This chapter presents the general considerations for maintainability—such as accessibility, simplification, standardization, lubrication, interchangeability, and other factors. The designer should be aware of the maintenance and rebuild aspects of fielded weapons during design of the system.

10-1 INTRODUCTION

Equipment design has been found consistently to have a greater effect on maintenance efficiency than such personnel variables as aptitude or training. Maintainability is a quality of the combined features and characteristics of equipment design, job aids, and job supports. Good maintainability features facilitate the rapidity, economy, ease, and accuracy with which maintenance operations can be performed. Thus the system can be kept in or readily returned to an operating condition by average personnel under the environmental conditions in which the system will be maintained. The lack of satisfactory reliability and maintainability in military equipment has three serious effects:

1. The success of vital military missions may be jeopardized.
2. Support costs may be heavy and impose a strain on production, supply, and storage.
3. Many skilled maintenance personnel may be needed, which would impose a heavy logistical burden on the armed services.

To overcome these shortcomings and improve materiel availability, designers must give greater emphasis to those factors that make equipment more reliable and maintainable in the field.

Maintainability is a measure of the ease and rapidity with which a system or equipment can be restored to operational status following a failure. It is characteristic of equipment design and installation, personnel availability in the required skill levels, adequacy of maintenance procedures and test equipment, and the physical environment under which maintenance is performed. One expression of maintainability is the probability that an item will be retained in or restored to a specified condition within a given period of time when the maintenance is performed in accordance with prescribed procedures and resources.

This chapter presents an introduction to general considerations for maintainability—such as accessibility, simplification, standardization, lubrication, and interchangeability. DOD-HDBK-791 (AM) (Ref. 1) provides detailed information on these, and other, aspects of maintainability. Additional information on the subject may be found in Refs. 2, 3, 4, and 5.

10-2 CATEGORIES OF MAINTENANCE

To maintain combat readiness, designs must be planned for support as well as for performance. Military maintenance is usually stratified into several levels that generally correspond both to the skill of the personnel and to the degree of difficulty of the maintenance task. Stratification by level of maintenance is made essential by the demands for tactical deployment of the equipment. It is also a solution to the problem of efficiently using maintenance personnel of varying skills. The Department of the Army has grouped all maintenance into four categories, i.e., unit, direct support, general support, and depot. Equipment design must adequately take into account the skills available at each maintenance level.

10-2.1 UNIT MAINTENANCE

Unit maintenance is that maintenance normally authorized for, performed by, and the responsibility of a using organization and operator on equipment in its possession. Maintenance performed by the equipment operator usually consists only of inspecting, cleaning, servicing, preserving, and adjusting the equipment. Maintenance performed by the repairmen of the unit consists of making minor repairs and replacements. The removed components, if repairable, usually are forwarded to the next higher level for reworking.

THIS DOCUMENT PROVIDED BY THE ABBOTT AEROSPACE
TECHNICAL LIBRARY
ABBOTTAEROSPACE.COM

10-2.2 DIRECT SUPPORT MAINTENANCE

Direct support maintenance is that maintenance normally authorized for and performed by designated maintenance activities in direct support of using organizations. This category of maintenance is limited to the repair of end-items or unserviceable assemblies in support of the using organization on a return-to-user basis. Direct support units are designed to provide close support for combat troops and to facilitate tactical operations. This mobility requirement limits the equipment and supplies and, therefore, the repair jobs that can be undertaken. At this level failed components and equipment are repaired by replacement of parts and subassemblies.

10-2.3 GENERAL SUPPORT MAINTENANCE

General support maintenance is that maintenance authorized and performed by designated organizations in support of the Army supply system. The primary mission of a general maintenance unit is to repair items that cannot be repaired by direct support units. Normally, general support maintenance organizations will repair or overhaul material to required maintenance standards, i.e., to a ready-to-issue condition, based upon the Army's area supply requirements. The units exist to serve the lower levels of maintenance within a given geographical area. A general support organization will also assist in repairs that overflow from direct support units; however, they rarely deal directly with the equipment user. Companies and detachments specializing in general supply, ammunition supply, maintenance by commodities, and other services comprise the general support units.

10-2.4 DEPOT MAINTENANCE

Depot maintenance is that maintenance which, through overhaul of economically repairable material, augments the procurement program in satisfying overall Army requirements and, if required, provides for repair of materiel beyond the capability of general support organizations. This level of maintenance provides the major supply base for end-items and for the parts and supplies required to maintain and repair the end-items. Facilities are available for completely overhauling and rebuilding equipment. Assembly line methods are used whenever practical, and normal supply support is accomplished on an overhaul-and-return-to-stock basis. Depot maintenance functions also include repair and reclamation services that are beyond the capabilities of general support maintenance.

10-3 ACCESSIBILITY

Accessibility is a design feature that affects the ease of admission to an area for the performance of visual or manipulative maintenance. A component is accessible if a few, simple steps are required to gain access to it.

Controls, checkpoints, inspection windows, lubrication, and pneumatic and hydraulic replenishing points are built into the equipment so that it can be kept operating at peak performance. If these service points are inaccessible, routine maintenance becomes difficult or is neglected. Access is made more difficult when there is little space for hands and tools. In such cases there are also risks of injury to personnel as well as of damage to material. Access must be provided to all points, items, units, and components that require or may require testing, servicing, adjusting, removal, replacement, or repair.

The type, size, shape, and location of access should be based upon a thorough understanding of

1. Operational location, setting (establishment), and environment of the unit
2. Frequency with which the access must be entered
3. Maintenance actions to be performed through the access
4. Time required for the performance of these actions
5. Types of tools and accessories required by these actions
6. Work clearances required for performance of these actions
7. Type of clothing likely to be worn by the technician
8. Distance to which the technician must reach within the access
9. Visual requirements of the technician in performing the task
10. Packaging of the items and elements behind the access
11. Mounting of items, units, and elements behind the access
12. Hazards involved in or related to use of the access
13. Size, shape, weight, and clearance requirements of logical combinations of human appendages, tools, and units that must enter the access.

THIS DOCUMENT PROVIDED BY THE ABBOTT AEROSPACE
TECHNICAL LIBRARY
ABBOTTAEROSPACE.COM

10-4 IDENTIFICATION AND LABELING

Identification and labeling are inherent elements of maintainability. The maintenance technician's task will be more difficult, take longer, and consequently, will increase the risk of error if he cannot readily identify components, parts, controls, and test points for maintenance operations.

Identification and labeling can be defined as the adequate marking of parts, components, controls, and test points to facilitate repair and replacement during maintenance operations.

Proper identification is present if the component is readily identified for repair, replacement, or service with minimum effort by the technician. Equipment should be marked for identification in accordance with MIL-STD-130 (Ref. 6) by stamping, engraving, permanent labeling, or other permanent methods. Equipment identification should include permanent data with regard to its function, capacity, capabilities, limits, ranges, frequency, and current requirement.

The following rules should be used in marking parts:

1. Make markings accurate and sufficient to identify the referenced part.
2. Locate markings on or immediately adjacent to the referenced part in a consistent manner that will eliminate any possibility of confusion.
3. Make marking permanent enough to last the life of the equipment.
4. Place markings so that they are visible without removing other parts.
5. Orient markings so that they can be read with the unit in the normal installed position.
6. Mark stacked parts and modules so that they can be individually recognized.
7. Identify individually enclosed or shielded parts on the outside of the enclosure.
8. Mark identically the fixed and removable parts of a plug-in subassembly.
9. Identify clearly individual sections of dual parts.

10-5 INTERCHANGEABILITY

Interchangeability is a condition in which two or more parts are physically and functionally interchangeable in all possible applications—i.e., both parts are capable of full, mutual substitution in all directions. Standardization is the process by which interchangeability is realized. Two types of interchangeability can be present:

1. Functional interchangeability exists when a part or unit, regardless of its physical specifications, can perform the specific functions of another part or unit.
2. Physical interchangeability exists when any two or more parts or units made to the same specification can be mounted, connected, and used effectively in the same position in an assembly or system. Where physical interchangeability exists, however, functional interchangeability is highly desirable.

There are two broad classifications of interchangeable parts:

1. Universally interchangeable parts that are required to be interchangeable in the field even though manufactured by different facilities
2. Locally interchangeable parts that are interchangeable with other like components made in the same facility. These parts, however, are not necessarily interchangeable with those made in other facilities.

Interchangeability requirements should be determined from consideration of field conditions as well as from consideration of economy of manufacture and inspection. Liberal tolerances are essential for interchangeability. Tolerances should be assigned to component features for position, concentricity, symmetry, alignment, squareness, and parallelism when the control of these factors is important for correct functioning or correct assembly.

10-6 STANDARDIZATION

Standardization is the use of common items, parts, materials, and practices throughout the life cycle of systems and equipment. It denotes any effort to select, design, or manufacture parts, components, assemblies, equipment, associated tools, service materials, or procedures so they are either identical to or physically or functionally interchangeable with other parts—the so-called "form, fit, and function" criteria.

Standardization significantly reduces both the acquisition and the support costs of a system over its life cycle and results in increased maintainability and reliability. The primary goals of standardization are to

1. Reduce the number of different models and makes of equipment in use.
2. Maximize the use of common parts in different equipment.
3. Minimize the number of different types of parts, assemblies, etc.
4. Use only a few basic types and varieties of parts.

THIS DOCUMENT PROVIDED BY THE ABBOTT AEROSPACE
TECHNICAL LIBRARY
ABBOTTAEROSPACE.COM

5. Control, simplify, and reduce part coding, numbering practices, and storage problems.
6. Maximize the use of standard off-the-shelf items and components.
7. Maximize the use of interchangeable parts.

To facilitate the supply of replacement parts that are of standard, rather than of special, manufacture use American National Standards Institute (ANSI) or Military Standard (MIL-STD) parts wherever they are suitable for the purpose and identify them on the drawing by their part number.

Common hardware parts—such as screws, bolts, nuts, and cotter pins—should be ANSI or MIL-STD parts without alteration. In applications for which no suitable corresponding ANSI or MIL-STD part is available, commercial parts may be used if they conform to the other requirements.

10-7 SAFETY

The design of any equipment must embody features for the protection of personnel and equipment from electrical and mechanical hazards and from dangers that might arise from fire, elevated operating temperatures, and toxic fumes. To minimize the possibility of physical injury, all component edges and corners should be rounded to maximum radii. Thin edges should be avoided, and construction should be such that the unit can be carried without danger of cutting the hands on the edges.

To prevent hazardous protrusions from surfaces, flathead screws should be used wherever sufficient thickness is available; otherwise, panhead screws should be used. All exposed surfaces should be machined smooth, covered, or coated to prevent the possibility of skin abrasion.

Shields and guards should be made part of the equipment to prevent personnel from accidently coming in contact with rotating or oscillating parts such as gears, couplings, levers, cams, latches, or heavy solenoid equipment. Moving parts should be enclosed or shielded by guards; where such protection is impossible, adequate warning signs should be provided. Additional information on this topic may be found in Ref. 7.

10-8 SERVICING AND LUBRICATION

Ease of servicing is one of the most important elements of maintainability that affects preventive maintenance routines. The purpose of preventive maintenance is to avoid or detect incipient mechanical failures in equipment and to insure that appropriate action is taken before expensive and time-consuming repairs or replacements are required. The capability for rapid lubrication should be built into the equipment and should be of equal design importance with the proper functional design of the equipment.

Working surfaces subject to wear or deterioration should be provided with appropriate means of lubrication. Commercial grade lubricants should be used whenever possible; the use of special lubricants should be avoided. Equipment should be designed to use only one type of oil and one type of grease and to have a minimum number of lubrication fittings. When this is not practical, the types and grades should be kept to a minimum.

Lubrication, besides reducing friction and wear between moving parts, can serve as a seal to exclude undesirable substances from the area being lubricated and can act as a carrier for rust preventives, antifriction agents, and extreme additives.

10-9 SIMPLIFICATION

Simplification should be the constant goal of every design engineer. Equipment design should represent the simplest configuration possible consistent with function requirements, expected service, and performance conditions. The designer, by implementing the principles outlined herein, should make the user believe that complex equipment is really simple.

There are two jobs associated with any equipment—operating it and maintaining it. The more human factor engineering is considered in the design of new equipment, the better these two jobs can be done. In designing equipment, effort should be directed toward simplifying the operator's and maintenance person's jobs. Chapter 11 is devoted to human factors.

THIS DOCUMENT PROVIDED BY THE ABBOTT AEROSPACE
TECHNICAL LIBRARY
ABBOTTAEROSPACE.COM

REFERENCES

1. DOD-HDBK-791 (AM), *Maintainability Design Techniques*, 17 March 1988.
2. H. P. Van Cott and R. G. Kinkade, *Human Engineering Guide to Equipment Design*, McGraw-Hill Book Co., Inc., New York, NY, 1972.
3. DARCOM-P 706-132, Engineering Design Handbook, *Maintenance Engineering Techniques*, June 1975.
4. DARCOM-P 706-133, Engineering Design Handbook, *Maintainability Engineering Theory and Practice*, January 1976.
5. AR 750-1, *Army Materiel Maintenance Concepts and Policies*, 15 March 1983.
6. MIL-STD-130 , *Identification Marking of US Military Property*, 2 July 1984.
7. MIL-HDBK-764 (MI), *System Safety Engineering Design Guide for Army Materiel*, October 1989.

THIS DOCUMENT PROVIDED BY THE ABBOTT AEROSPACE
TECHNICAL LIBRARY
ABBOTTAEROSPACE.COM

THIS DOCUMENT PROVIDED BY THE ABBOTT AEROSPACE
TECHNICAL LIBRARY
ABBOTTAEROSPACE.COM

CHAPTER 11
HUMAN FACTORS

This chapter presents important human factors that must be considered in the design of any equipment. In the design of equipment, a human being must be considered a component of the system. Therefore, human body measurements must be considered during design to accommodate persons of various sizes; also forces required to be generated by various body parts to operate the system must be considered in the design process. Accordingly, applicable data are presented. Selection of the best controls from the wide variety currently available is critical to design for effective human-machine performance. Because of their importance, general principles for the design of controls are presented. The design of good displays for the system is also included.

11-1 INTRODUCTION

During the design and development of a system, the human factors engineer not only considers the interests of the user but also provides information about the human being as a system component. Human factors relate a person's size, strength, and other capabilities to perform the necessary task.

This chapter presents basic human factors that should be considered in the design of weapon systems. The anthropometry, humans as a system component, design of controls, and design of displays are discussed. For more details on these topics see Refs. 1, 2, and 3.

11-2 HUMAN BODY MEASUREMENTS (ANTHROPOMETRY)

One important consideration in system design is information on body measurements that is required to insure that equipment will accommodate operators and maintenance personnel of various anthropometric profiles.

The designer has two basic sources of information on body measurements: (1) anthropometric surveys in which measurements of a sample of the population are made and (2) experiments under circumstances that stimulate conditions for which the system is being designed. Which of these sources or what combination is used depends on the availability of adequate anthropometric surveys and on the cost of experiments in both time and money. The designer must design equipment so that a majority of the population for which it is designed can operate and maintain it. However, a small percentage of the population, i.e., those individuals having extreme measurements, may have to contend with a less efficient or less comfortable design.

If a group of potential users for whom machines are to be designed were identical, it would be a relatively simple matter to provide the designer with a necessary set of human capability criteria. This cannot be done, however, because the working population is highly variable. As an example, employment of women in the work force is constantly increasing. Thus, in the design of any equipment, this segment of the population must be considered.

A major difference between the capabilities of a man and a woman arises when lifting or lowering an object is considered. A randomly selected group of women may average between 43 to 85% of the strength of a similarly selected group of men; therefore, the between-sex variance is dependent upon the type of activity and training of those involved. Tables 11-1 (Ref. 4) and 11-2 (Ref. 4) show how much mass groups of people will voluntarily lift or lower on an infrequent basis. These values are for a relatively compact load that is easily held with both hands in front of the body.

One property of the load that directly affects the load-carrying capability is the horizontally measured distance of the load center of gravity from the torso, in particular, from the lower back region. The size of the load often dictates this property. Fig. 11-1 (Ref. 4) shows this effect for a load being lifted with both hands when it is at about hip height. The authors recommend that objects to be manually handled should be designed in order to (1) locate the load center of gravity as close to the person's torso as possible and (2) provide lifting handles or designated grasp points at the appropriate places.

There is considerable difference between the capabilities of men and women with regard to grasping activities. Fig. 11-2 (Ref. 4) shows the results of the linear grip capabilities of 50 men and 50 women

THIS DOCUMENT PROVIDED BY THE ABBOTT AEROSPACE
TECHNICAL LIBRARY
ABBOTTAEROSPACE.COM

TABLE 11-1
MAXIMUM MASSES ACCEPTABLE TO VARIOUS PERCENTAGES OF MALE AND FEMALE POPULATIONS WHILE LIFTING A 0.48 × 0.34× 0.14 m TOTE BOX (Ref. 4)

Operation	Lift by Industrial Men, kg	Capability, %	Lift by Industrial Women, kg
Shoulder	13.2	90	10.9
Height	17.7	75	11.8
to	22.2	50	13.2
Arm	26.8	25	14.5
Reach	30.8	10	15.9
Knuckle	15.4	90	11.3
Height	19.5	75	13.2
to	24.0	50	15.4
Shoulder	28.1	25	17.2
Height	32.2	10	19.1
Floor	16.8	90	12.7
Level	20.4	75	15.0
to	24.5	50	16.8
Knuckle	28.6	25	19.1
Height	31.8	10	21.3

S. H. Snook and V. M. Ciriello, "Maximum Weights and Work Loads Acceptable to Female Workers", *JOM*, 16(8):527, 1974. ● by American College of Occupational Medicine.

TABLE 11-2
MAXIMUM MASSES ACCEPTABLE TO VARIOUS PERCENTAGES OF MALE AND FEMALE POPULATIONS WHILE LOWERING A 0.48 × 0.34× 0.14 m TOTE BOX (Ref. 4)

Operation	Lift by Industrial Men, kg	Capability, %	Lift by Industrial Women, kg
Arm	13.2	90	10.9
Reach	16.3	75	12.3
to	20.0	50	13.6
Shoulder	24.0	25	15.0
Height	27.2	10	16.3
Shoulder	17.7	90	11.8
Height	20.9	75	14.1
to	25.0	50	15.9
Knuckle	28.6	25	17.7
Height	31.8	10	20.0
Knuckle	16.3	90	13.6
Height	21.8	75	15.4
to	28.1	50	17.2
Floor	34.0	25	19.5
Level	39.9	10	20.9

S. H. Snook and V. M. Ciriello, "Maximum Weights and Work Loads Acceptable to Female Workers", *JOM*, 16(8):527, 1974. ● by American College of Occupational Medicine.

THIS DOCUMENT PROVIDED BY THE ABBOTT AEROSPACE
TECHNICAL LIBRARY
ABBOTTAEROSPACE.COM

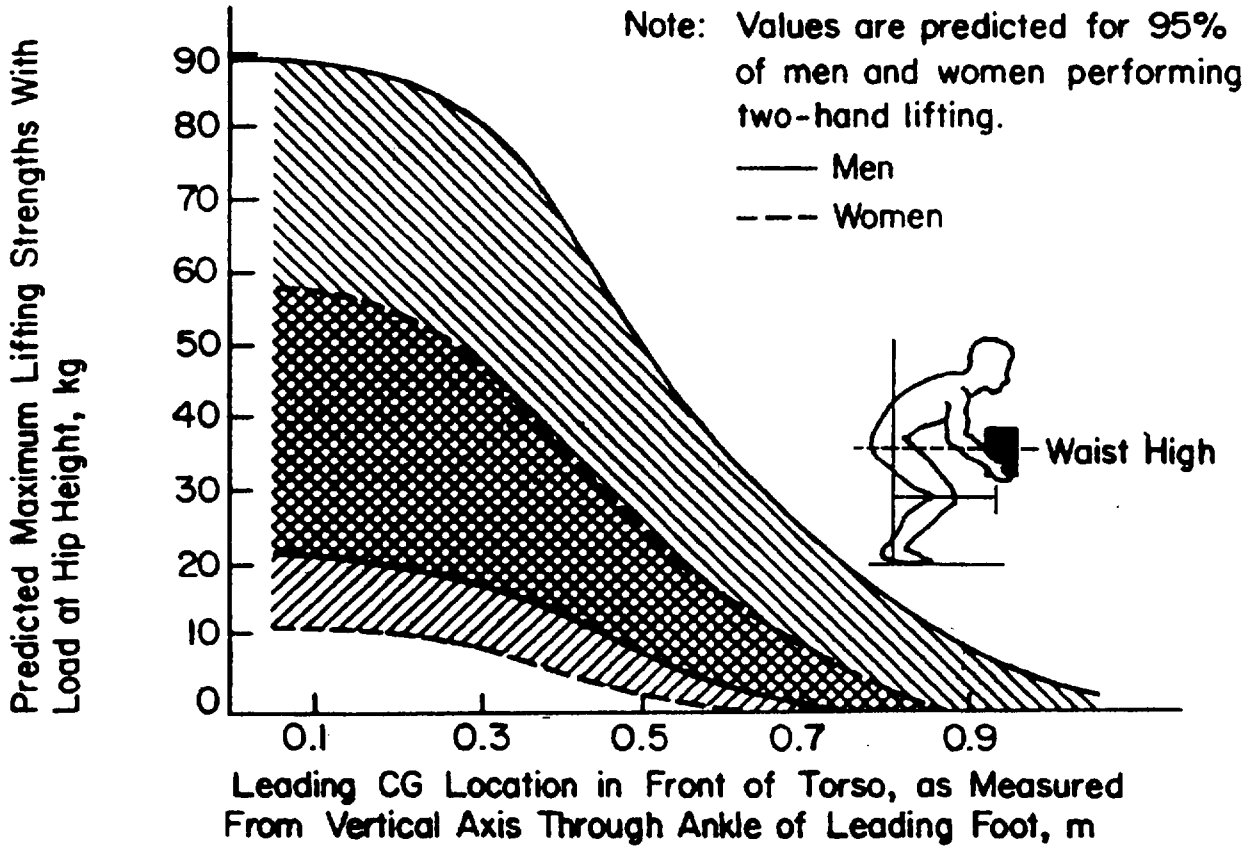

Reprinted from *AIIE Transactions*, March 1972. Copyright Institute of Industrial Engineers, 25 Technology Park/Atlanta, Norcross, GA 30092.

Figure 11-1. Maximum Lifting Strengths for Varying Load Locations of Center of Gravity (CG) (Ref. 4)

employed in a large electronics component manufacturing plant. If a significant gripping force is required, a reduction in size below that needed simply to grasp the object is necessary.

Anthropometric data for various attitudes and activities for both males and females are shown in detail in Ref. 3. These data should be considered in equipment design. Associated with body dimensions is the force that must also be considered in the design process. The following conclusions on application of the force and strength of body components should be of value to designers (Ref. 1):

1. The amount of force that can be exerted is determined by the positions of the body and members applying the force, the direction of application, and the object to which it is applied.
2. The greatest force is developed in pulling toward the body. Pull is greater from a sitting than from a standing position. A momentary pull can be as great as 1112 N, whereas the maximum steady pull is approximately 290 N.
3. Maximum exertable force increases with the use of the entire arm and shoulder. However, using only fingers requires the least energy per given amount of force applied.
4. Push is greater than pull for side-to-side motion; approximately 400 N is the maximum.
5. The maximum handgrip for a 25-yr-old man is approximately 556 N. Usually, the stronger hand can exert an average of 45 N greater than the other hand.
6. The mass lifting capacity is shown in Fig. 11-3 (Ref. 5). The curve is based on data obtained with men whose average age was 21.6 yr. They lifted objects of convenient size and shape and had unlimited room to do it.

THIS DOCUMENT PROVIDED BY THE ABBOTT AEROSPACE
TECHNICAL LIBRARY
ABBOTTAEROSPACE.COM

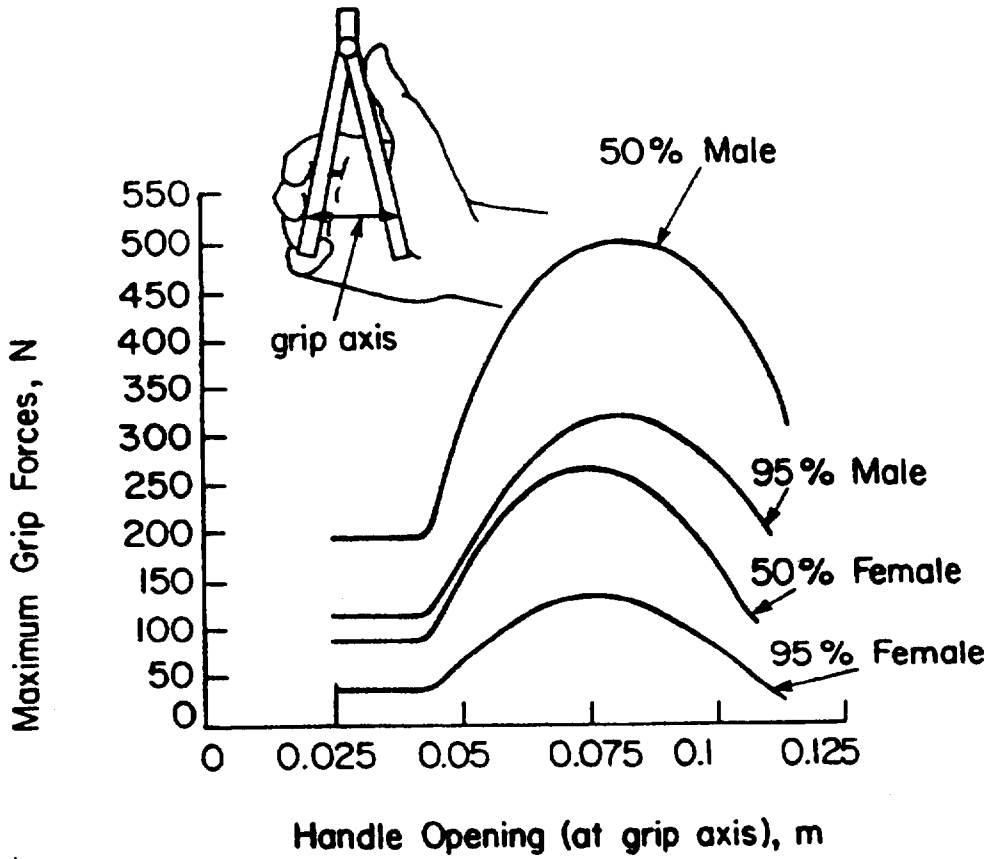

Reprinted with permission. Copyright © 1977 by Pendell Printing Inc.

Figure 11-2. Maximum Linear Grip Strengths for Various Handle Openings (Ref. 4)

THIS DOCUMENT PROVIDED BY THE ABBOTT AEROSPACE
TECHNICAL LIBRARY
ABBOTTAEROSPACE.COM

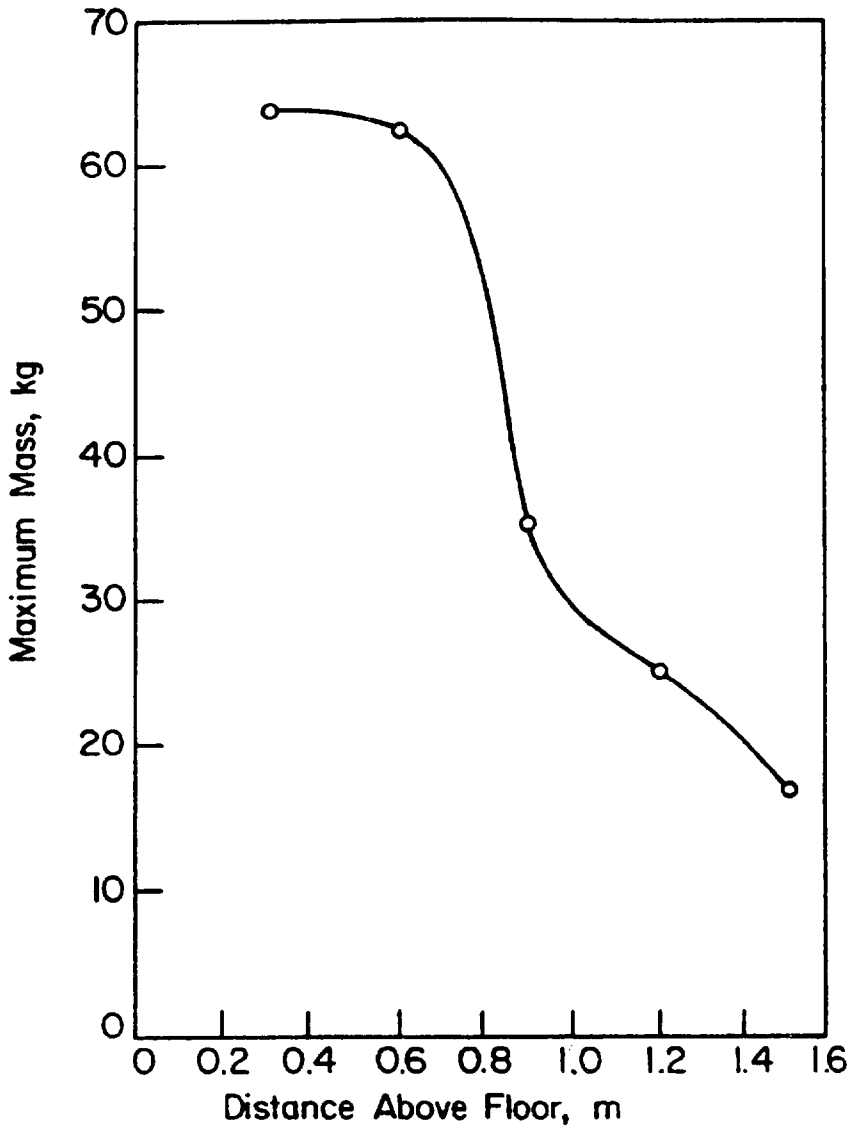

Figure 11-3. Maximum Mass Lifting Capacity (Ref. 5)

11-3 THE HUMAN BEING AS A SYSTEM COMPONENT

A person is viewed as an information processing component of the entire weapon system. By using information processing as a model, four human subsystems can be identified: sensing, information processing, memory or storage, and response. Interrelationships among these functional subsystems are shown in Fig. 11-4 (Ref. 1—Fig. 11-4 appears in Ref. 1 with credit to Refs. 6, 7, and 8.).

The human sensing subsystem detects and encodes energies from noise, recognizes information patterns, makes decisions, and selects appropriate responses from among available options. The memory subsystem provides long-term and short-term storage of encoded information. The response subsystem transduces processed information into action.

It is important for designers to have a better understanding of the sensory capacities of the maintenance person. A human's sensing system consists of receptors responsive to specific types and ranges of physical energy. Table 11-3 (Ref. 1) shows the human sense organs, the types of energy that stimulate them, their corresponding sensations, and the origin of stimulation.

THIS DOCUMENT PROVIDED BY THE ABBOTT AEROSPACE
TECHNICAL LIBRARY
ABBOTTAEROSPACE.COM

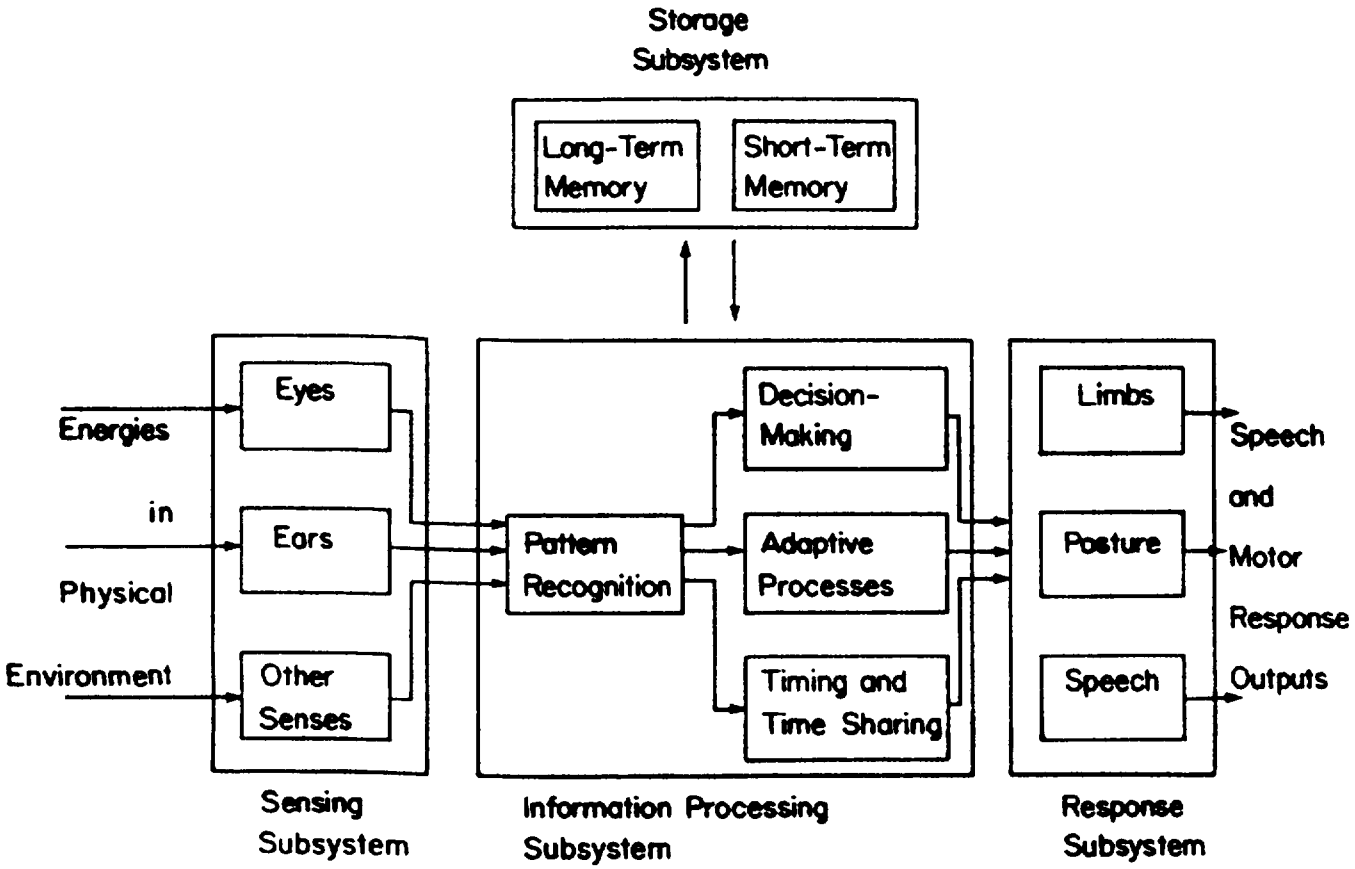

Used with permission.

Figure 11-4. The Human Information Processing System (Ref. 1 with credit to Refs. 6, 7 and 8)

11-3.1 VISUAL PRESENTATION OF INFORMATION

Humans can perceive all colors while looking straight ahead. Color perception begins to decrease, however, as the viewing angle increases. As the angle of viewing increases, the color-differentiation ability varies between green to white. This is well illustrated in Fig. 11-5. As shown in Fig. 11-5(A) the viewer can discern the color green 20 deg above and 20 deg below the normal to the eye. The available number of colors for coding depends on whether colored lights or reflected colors are used. In general, more saturated colors can be obtained with lights than with surface pigments or reflected colors. More coding steps, however, are available with surface pigments under certain conditions, but surface pigments may lead to serious distortion if used under certain kinds of illumination. For example, color coding on maps and charts might be completely lost if they are used in rooms lighted with red light.

Color-weak people (So few people are absolutely color blind that they can be ignored.) will not see colors the way "normal" people do, and any color coding will be useless for them. Colors should, therefore, be selected that do not confuse color-weak people, e.g., distinct contrasts, such as yellow and blue, or color coding augmented with shape coding should be used.

11-3.2 SKIN SENSES

Skin senses include touch sense, temperature, and pain. Of these, the tactual, or touch, sense provides the most information for task performance; the others are primarily sources of information used for body protection.

As equipment becomes more complex, it is necessary that maintenance personnel use all their senses most efficiently. A person's ability to interpret visual and auditory stimuli is closely associated with the sense of touch. The sensory cues received by the skin and muscles can be used to some degree to convey messages to the

THIS DOCUMENT PROVIDED BY THE ABBOTT AEROSPACE
TECHNICAL LIBRARY
ABBOTTAEROSPACE.COM

TABLE 11-3
HUMAN SENSES AND ENERGIES THAT STIMULATE THEM (Ref. 1)

Sensation	Sense Organ	Stimulation	Origin
Sight	Eye	Some electromagnetic waves	External
Hearing	Ear	Some amplitude and frequency variations of pressure in surrounding media	External
Rotation	Semicircular canals	Change of fluid pressures in inner ear	Internal
Falling and Rectilinear Movement	Otoliths	Position changes of small, bony bodies in inner ear	Internal
Taste	Specialized cells in tongue and mouth	Chemical substances	External on contact
Smell	Specialized cells in mucous membrane at top of nasal cavity	Vaporized chemical substances	External
Touch	Skin	Surface deformation	On contact
Pressure	Skin and underlying tissue	Surface deformation	On contact
Temperature	Skin and underlying tissue	Temperature changes of surrounding media or objects, friction, and some chemicals	External on contact
Pain	Unknown, but thought to be free nerve endings	Intense pressure, heat, cold, shock, and some chemicals	External on contact
Position and Movement (kinesthesis)	Muscle nerve endings	Muscle stretching	Internal
Mechanical Vibration	No specific organ	Amplitude and frequency variations of pressure	External on contact

Reprinted with permission from *Selected Papers on Human Factors in the Design and Use of Control Systems*, edited by H. W. Sinaiko. Copyright © by Dover Publications, Inc., New York, NY, 1961.

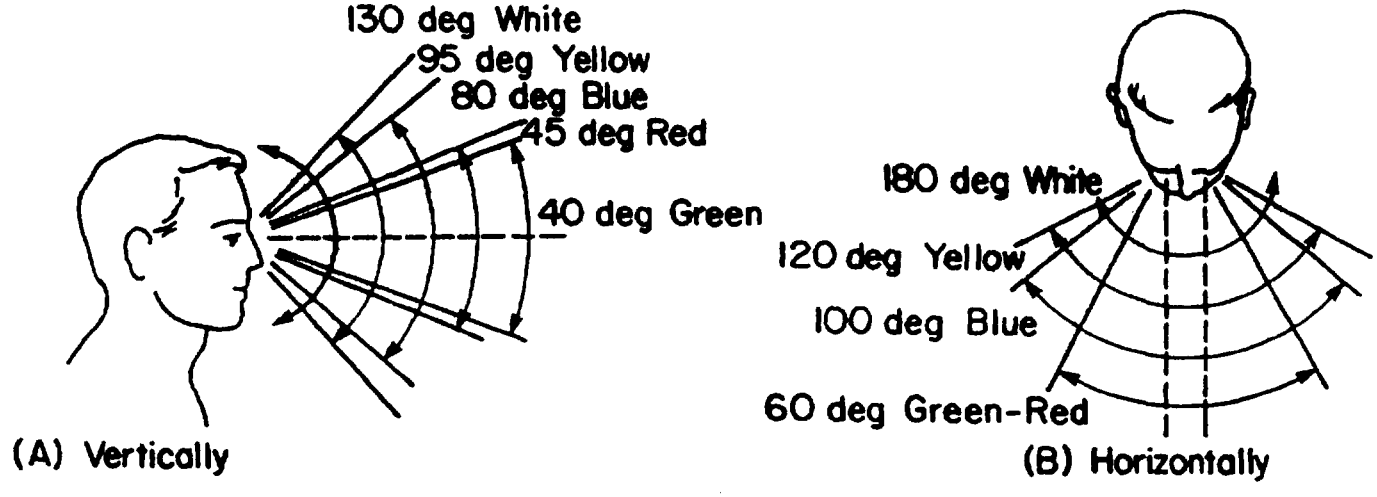

Figure 11-5. Approximate Limits of Normal Color Differentiation

THIS DOCUMENT PROVIDED BY THE ABBOTT AEROSPACE
TECHNICAL LIBRARY
ABBOTTAEROSPACE.COM

brain that relieve the eyes and ears of part of the task they would otherwise perform. For example, the control knob shapes illustrated in Fig. 11-6 (Ref. 3) can be easily recognized by touch alone, and many of these knob shapes could be adapted for use when the user must rely completely on his sense of touch, for instance, when a knob must be put in an out-of-the-way place.

11-3.3 NOISE

The effects of noise and blast upon humans are complex and varied. A soldier's reaction to noise extends beyond the auditory system; it can contribute to such feelings as well-being, boredom, irritability, fatigue, or loss of combat effectiveness. The reaction is not due to noise intensity alone; frequency is also a contributing factor. Excessive noise also can make oral communication ineffectual or impossible and can damage hearing. Refs. 9, 10, and 11 provide guidance on noise limitations and hearing protection. The following recommendations should be considered to reduce the effects of noise:

1. In designing equipment that necessitates maintenance activities in the presence of extreme noise, reduce the amount of noise produced where possible by proper acoustical design, mufflers, soundproofing, and other devices.
2. Keep sound levels in maintenance areas that require the presence of the maintenance technician below 80 dB.
3. Provide warnings to prevent unprotected maintenance personnel from entering areas—even for short periods—with noise levels above 108 dB.

Table 11-4 shows the intensity levels of some common sounds and their effect on personnel. A howitzer firing a maximum charge will produce a blast intensity of approximately 200 dB; obviously, ear protection for the crew is required. Detailed information on noise, i.e., its characteristics and effects on military personnel, is contained in Appendix B, Ref. 3.

11-4 DESIGN OF CONTROLS

Selecting the best control from the wide variety currently available is critical to design for effective human-machine performance. Control selection should be dictated by suitability for a particular task because the best control for one task may be inadequate for another.

The following general principles apply to the design of all types of controls, whatever their purpose or mode of operation:

1. The maximum force, speed, accuracy, or range of body movement required to operate a control should not exceed the limits of the least capable operator, and normal requirements for control operation should be considerably less than the maximum capabilities of most operators.
2. The number of controls should be kept to a minimum, and the control movements should be as simple and as easy to perform as possible.
3. Control movements that seem "natural" for the operator are more efficient and less fatiguing than those that seem awkward or difficult.
4. Control movements should be as small as possible, consistent with the requirements of accuracy and "feel".

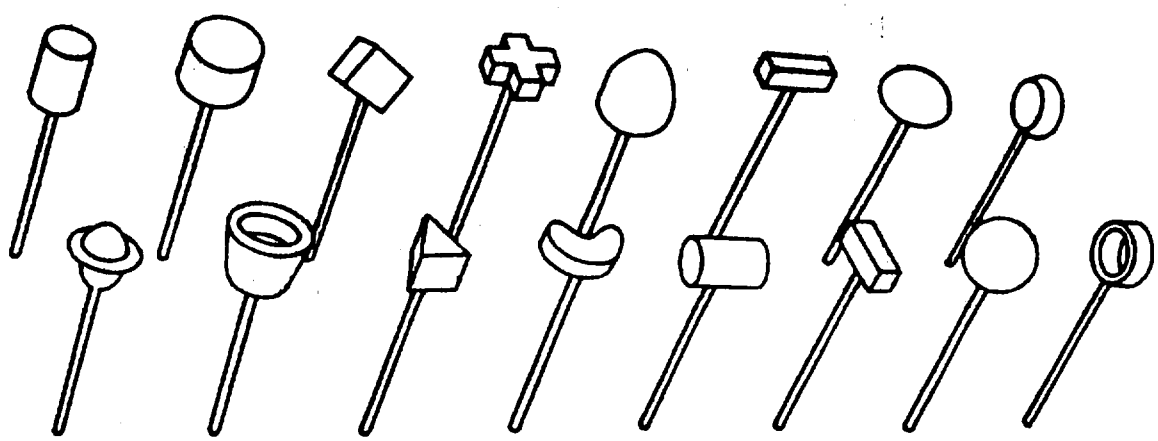

Figure 11-6. Easily Recognizable Knob Shapes (Ref. 3)

THIS DOCUMENT PROVIDED BY THE ABBOTT AEROSPACE
TECHNICAL LIBRARY
ABBOTTAEROSPACE.COM

TABLE 11-4
SOUND INTENSITY LEVELS

Effect on Personnel	Intensity Level, dB	Remarks
Levels unacceptable as dangerous to personnel	150	Maximum permissible (regardless of the amount of reduction in the ear canal)
	130	Approximate threshold of pain
	120	Loud thunder
	100	
Reduction in efficiency may occur above this point	90	City bus
Acceptable noise level	80	
	70	Heavy traffic
	60	Normal conversation
	50	
	40	Quiet residential area
	30	
	20	Voice whisper
	10	Motion picture sound studio
	0	Approximate threshold of hearing

5. Controls should have sufficient resistance so as to reduce the possibility of inadvertent activation by the weight of a hand or foot. For controls requiring a single application of force, a reasonable maximum resistance is half of the operator's greatest strength. For controls operated continuously or for long periods, resistances should be much lower.

6. When an operator cannot apply enough unaided force to operate the controls and power-boosted or fully powered control systems are necessary, artificial resistance cues should be provided.

7. Controls should be designed to stand abuse, for example, emergency or panic responses frequently impose large forces on controls.

8. Controls should provide a positive indication of activation so that malfunction will be obvious to the operator.

9. Control actions should result in a positive indication to the operator that there has been a system response.

10. Control surfaces should be designed to prevent the activating agent—hand, finger, or foot—from slipping.

The function and direction of conventional control movements, shown in Table 11-5 (Ref. 3), should be consistent with that of the controlled object or display. General situations in which linear (or nonlinear) and rotary control should be used are shown in Fig. 11-7 (Ref. 1). When force and range settings are the primary considerations, controls recommended in Table 11-6 (Ref. 3) should be used. The general design guidelines—application criteria, dimensions, displacement, and separation—for controls are discussed in Ref. 3.

THIS DOCUMENT PROVIDED BY THE ABBOTT AEROSPACE
TECHNICAL LIBRARY
ABBOTTAEROSPACE.COM

TABLE 11-5
CONVENTIONAL CONTROL MOVEMENTS (Ref. 3)

Direction of Movement	Function
Up, right, forward, clockwise, pull (push-pull-type switch)	On
Down, left, rearward, counterclockwise, push	Off
Clockwise, right	Right
Counterclockwise, left	Left
Up, back	Raise
Down, forward	Lower
Up, rearward, pull	Retract
Down, forward, push	Extend
Forward, up, right, clockwise	Increase
Rearward, down, left, counterclockwise	Decrease
Counterclockwise	Open Valve
Clockwise	Close Valve

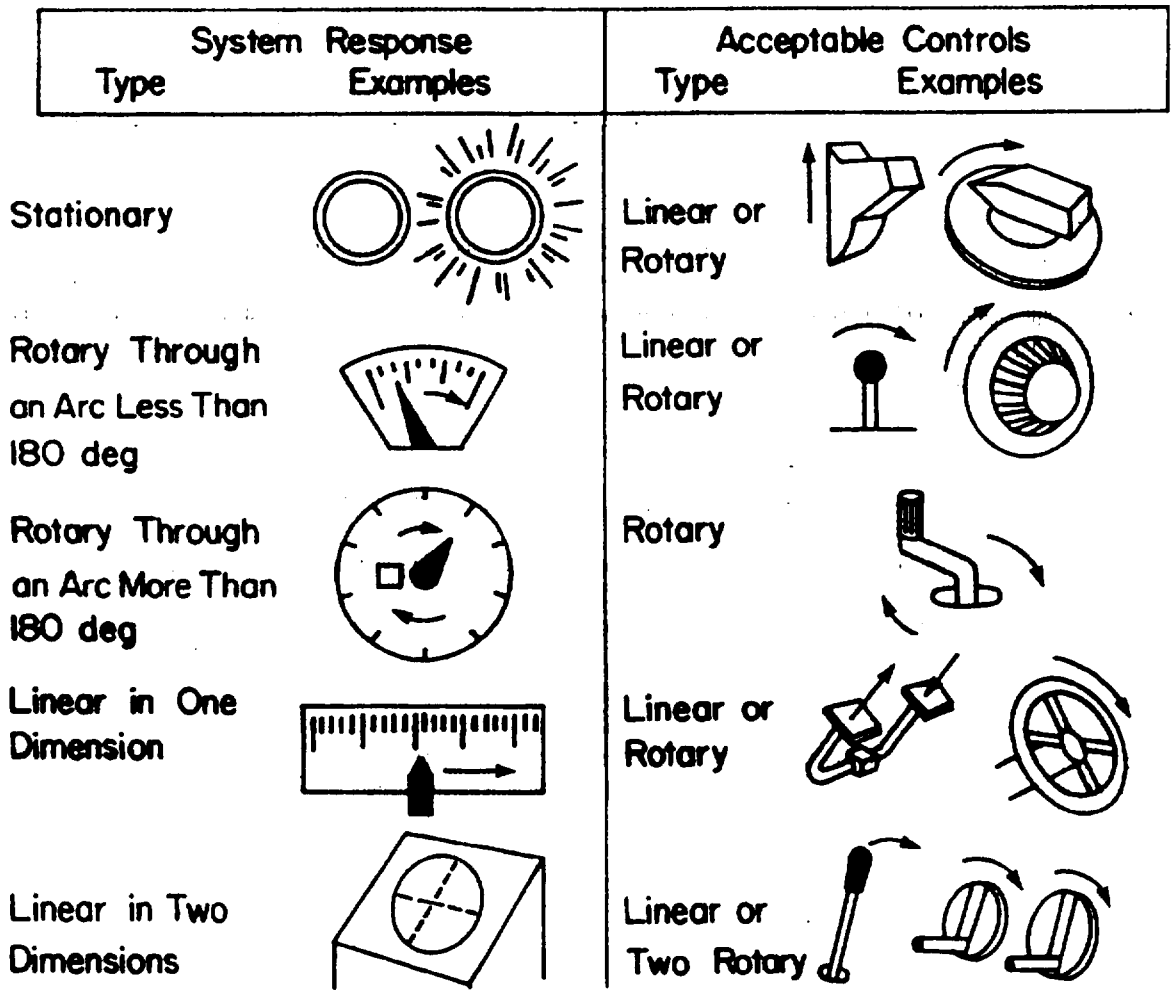

Reprinted with permission. *Human Engineering Guide to Equipment Design* by C.T. Morgan, J. S. Cook, III, A. Chapanis, and M. W. Lund. Copyright © 1963 McGraw-Hill Book Company, Inc.

Figure 11-7. Acceptable Controls for Various Types of System Responses (Ref. 1)

THIS DOCUMENT PROVIDED BY THE ABBOTT AEROSPACE
TECHNICAL LIBRARY
ABBOTTAEROSPACE.COM

TABLE 11-6
RECOMMENDED MANUAL CONTROLS WHERE FORCE AND RANGE SETTINGS ARE IMPORTANT (Ref. 3)

Control Function	Control Type
Small Actuation Force Controls and . . .	
2 Discrete Positions	Key Lock Push Button Toggle Switch Legend Switch Slide Switch
3 Discrete Positions	Rotary Selector Switch Toggle Switch Push Button
4 to 24 Discrete Positions	Rotary Selector Switch
Continuous Setting (linear and less than 360 deg)	Continuous Rotary Knob Joystick or Lever
Continuous Slewing and Fine Adjustment	Crank Continuous Rotary Knob
Large Actuation Force Controls and . . .	
2 Discrete Positions	Foot Push Button Hand Push Button Detent Lever
3 to 24 Discrete Positions	Detent Lever Rotary Selector Switch
Continuous Setting (linear and less than 360 deg)	Handwheel Joystick or Lever Crank Two-Axis Grip Handle
Continuous Setting (more than 360 deg)	Crank Handwheel Valve Two-Axis Grip Handle

11-5 DESIGN OF DISPLAYS

The function of a display is to provide the operator with information on which he can act. This information is usually presented by dials and scales, counters, scopes, warning lights, buzzers, and printed materials. The ultimate goal in selecting displays is to choose those that provide the operator with the exact amount of information required to carry out the functions of the system. The display, however, should not present the operator with more information than is necessary. Guidance for displays follows:

1. Use dials, scales, gages, or meters for the following conditions:
   a. To indicate direction of movement or orientation in space
   b. To distinguish an increasing or decreasing trend of the values measured by the instrument
   c. When only an approximate reading is important
   d. For check reading rather than continuous monitoring.
2. Use direct-reading counters for the following:
   a. For accurate and rapid reading of stationary or slowly changing quantitative information
   b. As an indication of revolutions in multirevolution indicators
   c. When economy of panel space is important.

THIS DOCUMENT PROVIDED BY THE ABBOTT AEROSPACE
TECHNICAL LIBRARY
ABBOTTAEROSPACE.COM

3. Use scopes in the following situations:
   a. To provide continuous monitoring activity
   b. To monitor direction of movement of another vehicle
   c. To monitor or check-read frequency or amplitude waves.
4. Use lights in the following situations:

a. For qualitative go/ no-go indicators, on-off indicators, malfunction indicators, emergency warning lights, inoperative equipment indicators, caution indicators, and indicators for operability of separate components

   b. For critical information when there is sufficient space on the panel
   c. As warm-up indicators.
5. Use auditory displays for the following situations:
   a. To notify the operator of the end or that he is approaching the end of an operating cycle
   b. As an emergency or warning device
   c. When the immediate reaction of the operator is important.

REFERENCES

1. H. P. Van Cott and R. G. Kinkade, *Human Engineering Guide to Equipment Design*, McGraw-Hill Book Co., Inc., New York, NY, 1973.
2. A. Damon, H. W. Stoudt, and R. A. McFarland, *The Human Body in Equipment Design*, Harvard University Press, Cambridge, MA, 1966.
3. MIL-HDBK-759 , *Human Factors Engineering Design for Army Materiel*, 1 July 1987.
4. L. Greenberg and D. B. Chaffin, *Workers and Their Tools: A Guide to the Ergonomic Design of Hand Tools and Small Presses*, Pendell Publishing Company, Midland, MI, 1977.
5. J. W. Altman *et. al.*, *Guide to Design of Electronic Equipment for Maintainability*, WADC-TR-56-218, Wright Air Development Center, Wright-Patterson AFB, OH, 1956.
6. A. T. Welford, "The Measurement of Sensory-Motor Performance: Survey and Appraisal of Twelve Years' Progress", Ergonomics 3, 189-230 (1960).
7. R. E. Pew, "Human Information Processing Concepts for System Engineers". In R. E. Machol, Ed., *System Engineering Handbook*, McGraw-Hill Book Company, Inc., New York, NY, 1965.
8. E. J. McCormick, *Human Factors Engineering*, McGraw-Hill Book Company, Inc. New York, NY, 1964.
9. MIL-STD-1474 (MI), *Noise Limits for Army Materiel*, 18 June 1979.
10. AR 40-5, *Health and Environment*, 1 July 1985.
11. TB MED 501, *Noise and Conservation of Hearing*, 7 March 1972.

THIS DOCUMENT PROVIDED BY THE ABBOTT AEROSPACE
TECHNICAL LIBRARY
ABBOTTAEROSPACE.COM

APPENDIX A
PRINCIPLES OF DYNAMICS

This appendix defines and illustrates basic principles of dynamics. Newton's three laws of motion are stated. Conservation laws for momentum and energy are summarized. D'Alembert's principle for defining "inertia forces" is stated. Vector methods for determining position, velocity, and acceleration of points in moving coordinate systems—relative to a fixed coordinate system—are discussed and illustrated. Calculations for kinetic and potential energy are presented and illustrated with an example. Concepts of generalized coordinates and generalized forces for use in Lagrange's equations of motion are discussed and illustrated. An application of Lagrange's equations is given for a 2-degree-of-freedom artillery model.

A-0 LIST OF SYMBOLS

$\boldsymbol{a}$ = acceleration vector, m/s^2
$\boldsymbol{a}_A$ = acceleration vector in inertial reference frame of point A, m/s^2
a_x = x-component of $\boldsymbol{a}_A$ in inertial reference frame, m/s^2
a_y = y-component of $\boldsymbol{a}_A$ in inertial reference frame, m/s^2
$B(t)$ = breech force, N
d = distance between points O and O'
dm = differential mass, kg
$\boldsymbol{F}_i$ = ith force vector acting on body, N
$f(q_1,...,q_s)$ = vector function of s-generalized coordinates for system
g = acceleration due to gravity, m/s^2
$\boldsymbol{H}$ = angular momentum vector, $kg \cdot m^2/s$
$\boldsymbol{H}_A$ = angular momentum vector about A, $kg \cdot m^2/s$
h = height of mass measured from some suitable datum, m
I_A = moment of inertia of nonrecoiling mass, i.e., mass A, $kg \cdot m^2$
I_B = moment of inertia of recoiling mass, i.e., mass B, $kg \cdot m^2$
I_O = moment of inertia of body about its center of mass O, $kg \cdot m^2$
$I_{O'}$ = moment of inertia of body about point O', $kg \cdot m^2$
$\boldsymbol{i}$ = unit vector along inertial x-axis, dimensionless
$\boldsymbol{i}'$ = unit vector along x'-axis, dimensionless
$\boldsymbol{i}_1'$ = unit vector along x_1'-axis, dimensionless
$\boldsymbol{i}_2'$ = unit vector along x_2'-axis, dimensionless
$\boldsymbol{j}$ = unit vector along inertial y-axis, dimensionless
$\boldsymbol{j}'$ = unit vector along y'-axis, dimensionless
$\boldsymbol{j}_1'$ = unit vector along y_1'-axis, dimensionless
$\boldsymbol{j}_2'$ = unit vector along y_2'-axis, dimensionless
K_L = linear spring constant, N/m
K_T = torsional spring constant, $N \cdot m/rad$
$K(t)$ = recoil force, N
$\boldsymbol{k}$ = unit vector perpendicular to the xy-plane, dimensionless
ℓ = elongation of spring from its free length, m
$\boldsymbol{M}_A$ = moment vector of total force about A, $N \cdot m$
m = mass of body, kg
m_A = mass of nonrecoiling parts, kg
m_B = mass of recoiling parts, kg

THIS DOCUMENT PROVIDED BY THE ABBOTT AEROSPACE
TECHNICAL LIBRARY
ABBOTTAEROSPACE.COM

n = total number of forces acting on body, dimensionless
p = linear momentum vector, kg·m/s
Q_i = generalized force (or torque) corresponding to the generalized coordinate q_i, N or N·m
q_i = ith generalized coordinate, m or rad
$\dot{q}_i$ = generalized velocity corresponding to generalized coordinate q_i, m/s or rad/s
r = position vector of O' in inertial reference frame, m
r = distance of dm from O, m
r_A = position vector of nonrecoiling mass A, m
= position vector in the inertial reference frame of point A, m
r_B = position vector of center of recoiling mass B, m
δr_i = virtual displacement of ith F_i, m
s = total number of generalized coordinates, dimensionless
T = kinetic energy of system, J
V = potential energy, J
V_A = potential energy of force at point A, J
V_B = potential energy of force at point B, J
V_L = potential energy of force of linear spring, J
V_T = potential energy due to force of torsional spring, J
v = velocity vector of body, m/s
v_A = velocity vector in inertial reference frame of point A, m/s
$|v_A|$ = magnitude of v_A, m/s
v_{A_x} = x-component of v_A, m
v_B = velocity vector in inertial reference frame of point B, m/s
$|v_B|$ = magnitude of v_B, m/s
v_{A_y} = y-component of v_A, m
W_{AB} = work done by force in moving particle from point A to point B, J
δW = virtual work, J
$x_{O'}$ = x-component of r in inertial reference frame, m
x'_{1A} = coordinate of A along x'_1-axis, m
x'_{1O_2} = coordinate of O_2 along x'_1-axis in $x'_1y'_1$-reference frame, m
$y_{O'}$ = y-component of r in inertial reference frame, m
y'_{1A} = coordinate of A along y'_1-axis, m
y'_{1O_2} = coordinate of O_2 along y'_1-axis in $x'_1y'_1$-reference frame, m
η = y'-component of vector ρ_A, m
= coordinate of B along y'_2-axis in $x'_2y'_2$-reference frame, m
θ = angle between positive x'-axis and positive x-axis, rad
θ_1 = pitch angle of weapon, rad
θ_2 = angle of elevation of cradle relative to bottom carriage, rad
ξ = x' coordinate of vector ρ'_A, m
= coordinate of B along x'_2-axis in $x'_2y'_2$-reference frame, m
ρ'_A = position vector of point A in local $x'y'$-coordinate system, m
ϕ = change in angle of spring from free angle, rad
ω = angular velocity of body, rad/s
ω_A = angular velocity of nonrecoiling mass A, rad/s
ω_B = angular velocity of recoiling mass B, rad/s

THIS DOCUMENT PROVIDED BY THE ABBOTT AEROSPACE
TECHNICAL LIBRARY
ABBOTTAEROSPACE.COM

A-1 NEWTON'S EQUATIONS OF MOTION AND D'ALEMBERT'S PRINCIPLE

Newtonian mechanics is based on three laws. These laws are stated relative to fixed reference frames in which they are valid. These reference frames, called inertial systems of reference, represent a class of reference frames that are at rest or moving with uniform velocity with respect to one another. For practical purposes in artillery design, it is possible to assume an inertial system that is fixed in the earth.

Newton's three laws of motion (Ref. 1) may be stated as

1. First Law. If there are no forces acting upon a particle, the particle will move in a straight line with constant velocity.

2. Second Law. A particle acted upon by a force moves so that the force vector is equal to the time rate of change of the linear momentum vector.

3. Third Law. When two particles exert forces upon one another, the forces are equal in magnitude and opposite in direction.

Newton's second law is of major consequence here. For a rigid body, it can be expressed as

$$\sum_{i=1}^{n} F_i = \frac{dp}{dt}, \text{ N} \tag{A-1}$$

with linear momentum defined as

$$p = mv, \text{ kg·m/s} \tag{A-2}$$

where

F_i = ith force vector acting on body, N
n = total number of forces acting on body, dimensionless
p = linear momentum vector, kg·m/s
m = mass of body, kg
v = velocity vector of body, m/s.

Since the mass of the body is constant, the right-hand side of Eq. A-1 can be written as

$$\sum_{i=1}^{n} F_i = ma, \text{ N} \tag{A-3}$$

where

$a = dv/dt$ = acceleration vector, m/s^2.

In Newtonian and Lagrangian mechanics angular momentum is frequently involved. Angular momentum H for the planar case can be written as (Ref. 1)

$$H = I_O \omega k, \text{ kg·m}^2/\text{s} \tag{A-4}$$

where

H = angular momentum vector, kg·m^2/s
I_O = moment of inertia of body about its center of mass O, kg·m^2
ω = angular velocity of body, rad/s
k = unit vector perpendicular to the xy-plane, dimensionless.

The moment of inertia I_O is defined as

$$I_O = \int_m r^2 dm, \text{ kg·m}^2 \tag{A-5}$$

where, as shown in Fig. A-1,

dm = differential mass, kg
r = distance of dm from O, m.

THIS DOCUMENT PROVIDED BY THE ABBOTT AEROSPACE
TECHNICAL LIBRARY
ABBOTTAEROSPACE.COM

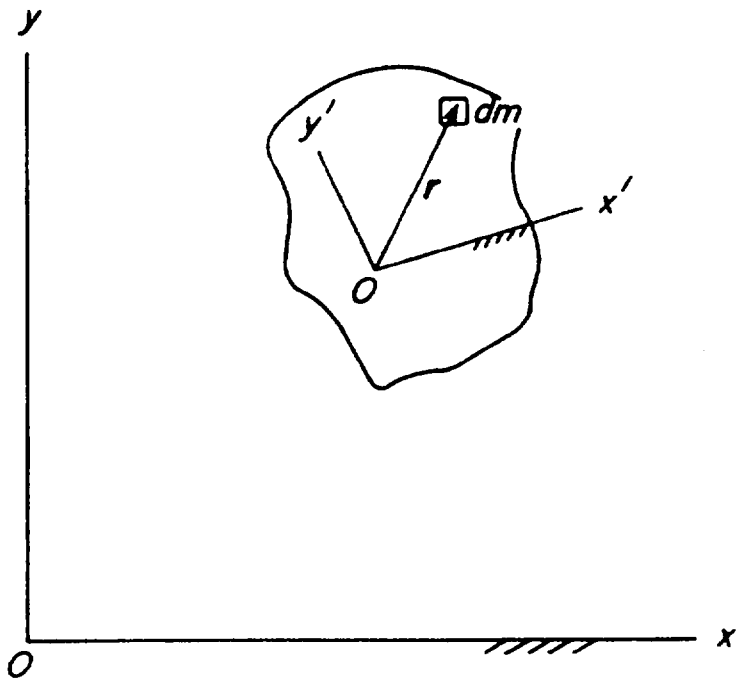

Figure A-1. Position Vector of Mass Element

For the planar case considered here, it is evident that the moment of inertia depends upon the point about which this quantity is computed. The moment of inertia about the center of mass of the body having been determined, it is possible to determine the moment of inertia about any other point by using the parallel axis theorem. According to this theorem (Ref. 1), the moment of inertia $I_{O'}$, about point O' can be written as

$$I_{O'} = I_O + md^2, \text{ kg·m}^2 \tag{A-6}$$

where

I_O = moment of inertia about point O, kg·m^2
m = mass of body, kg
d = distance between points O and O', m.

The principle of conservation of angular momentum is an extension of Newton's equations of motion and states (Ref. 1) that the moment about a fixed point A in the inertial reference frame of the total external force applied to a particle is equal to the time rate of change of the angular momentum of the particle about the same fixed point, or

$$\boldsymbol{M}_A = \dot{\boldsymbol{H}}_A, \text{ N·m} \tag{A-7}$$

where

$\boldsymbol{M}_A$ = moment vector of external force about A, N·m
$\dot{\boldsymbol{H}}_A$ = time rate of change of angular momentum vector about A, kg·m^2/s.

From Eq. A-7 it is evident that if $\boldsymbol{M}_A$ is zero, $\boldsymbol{H}_A$ must be constant in magnitude and direction and thus is conserved.

Another conservation principle of significant consequence is the principle of conservation of energy. This principle states that the sum of the kinetic and potential energy is constant for a conservative system. A conservative system could be defined as one acted upon by forces that are not dissipative in nature and that any process taking place under the influence of these forces is reversible (Ref. 1).

THIS DOCUMENT PROVIDED BY THE ABBOTT AEROSPACE
TECHNICAL LIBRARY
ABBOTTAEROSPACE.COM

Newton's second law of motion, Eq. A-3, can be rewritten as

$$\sum_{i=1}^{n} F_i - ma = 0. \tag{A-8}$$

If the $-ma$ term is interpreted as representing another force, known as an inertial force, then Eq. A-8 states that the vector sum of all forces, external or inertial, is zero. But this is just the form of the force summation equation of statics, and the methods of analysis for static problems apply. Thus, in a sense, the dynamics problem has been reduced to a statics problem. D'Alembert's principle can now be stated as "The laws of static equilibrium apply to a dynamical system if the inertial forces, as well as the actual external forces, are considered as applied forces acting on the system.".

A-2 CALCULATION OF VELOCITY AND ACCELERATION

The study of motion of single particles and rigid bodies is called kinematics, which is purely mathematical in nature and does not involve any physical laws, such as Newton's law. Computation of velocity and acceleration is, however, an important step in developing equations of motion for the system.

In discussing the motion of a point or rigid body, a frame of reference must be specified. Unlike Newton's laws of motion that only apply in an inertial reference frame, there are no preferred frames of reference in the derivation of the kinematical equations. Since the kinematical equations will be further required for use in dynamic equations of motion, however, it is desirable to write the kinematical equations in an inertial reference frame.

Consider Fig. A-2, with point A moving in a local $x'y'$-reference frame, which is translating and rotating in the xy-inertial reference frame. The choice of the local reference frame is essentially arbitrary. However, this reference frame should be chosen so that is it convenient to describe (1) the motion of a typical point A in it and (2) the motion of this local reference frame in the inertial reference frame.

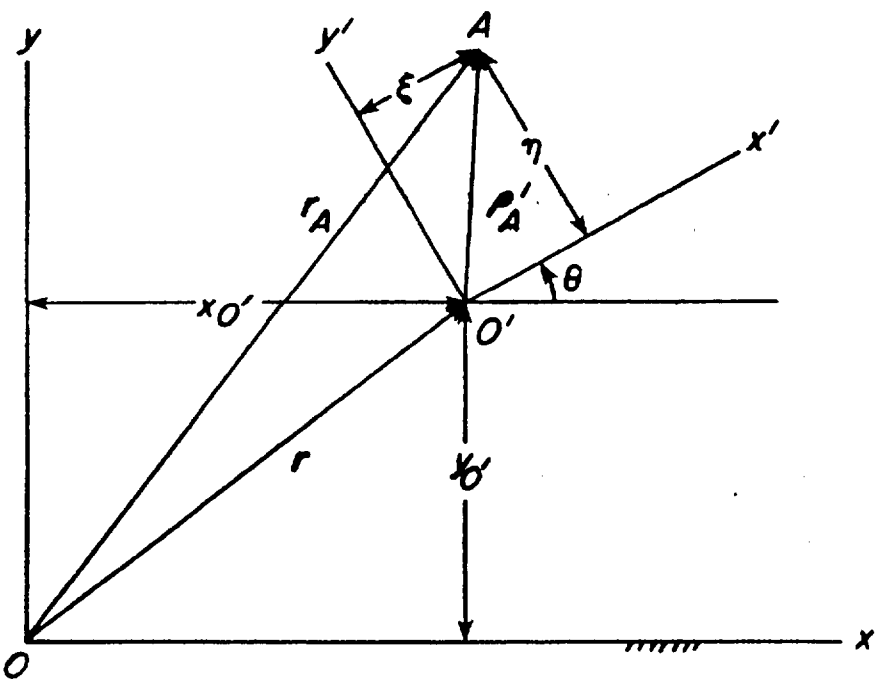

Figure A-2. Location of Point A in Global System

Point A is located in the local reference frame by the position vector ρ_A', i.e.,

$$\rho_A' = \xi i' + \eta j', \text{ m} \tag{A-9}$$

THIS DOCUMENT PROVIDED BY THE ABBOTT AEROSPACE
TECHNICAL LIBRARY
ABBOTTAEROSPACE.COM

where

ρ_A' = position vector of point A in the local $x'y'$-coordinate system, m
ξ = x'-component of vector ρ_A', m
η = y'-component of vector ρ_A', m
i' = unit vector along x'-axis, dimensionless
j' = unit vector along y'-axis, dimensionless.

The origin O' of the $x'y'$-reference frame can, in turn, be located in the xy-inertial reference frame by the position vector r, i.e.,

$$r = x_{O'}i + y_{O'}j, \text{ m} \tag{A-10}$$

where

r = position vector of O' in inertial reference frame, m
$x_{O'}$ = x-component of r in inertial reference frame, m
$y_{O'}$ = y-component of r in inertial reference frame, m
i = unit vector along inertial x-axis, dimensionless.
j = unit vector along inertial y-axis, dimensionless.

Point A can now be located in the inertial reference frame by the position vector r_A. (See Fig. A-2.) By use of the vector identity for summation of vectors,

$$r_A = r + \rho', \text{ m} \tag{A-11}$$

where

r_A = position vector in the inertial reference frame of point A, m.

Substitution for r and ρ' from Eqs. A-9 and A-10, respectively, into Eq. A-11 gives

$$r_A = x_{O'}i + y_{O'}j + \xi i' + \eta j', \text{ m.} \tag{A-12}$$

The unit vectors i' and j' in the moving frame can be expressed in terms of the unit vectors in the inertial reference frame (Ref. 2) by the transformation matrix

$$[i'] = \begin{bmatrix} \cos\theta & \sin\theta \\ -\sin\theta & \cos\theta \end{bmatrix} \quad [i] \tag{A-13}$$

and similarly for j', where

θ = angle between positive x'-axis and positive x-axis, rad.

Substitution of i' and j' from Eq. A-13 into Eq. A-12 gives

$$r_A = (x_{O'} + \xi\cos\theta - \eta\sin\theta)i + (y_{O'} + \xi\sin\theta + \eta\cos\theta)j, \text{ m.} \tag{A-14}$$

From Eq. A-14 it should be noted that $(x_{O'} + \xi\cos\theta - \eta\sin\theta)$ is the x-component of the vector r_A and $(y_{O'} + \xi\sin\theta + \eta\cos\theta)$ is the y-component of vector r_A.

To obtain the expression for the velocity of point A, differentiate r_A (Eq. A-14) with respect to time, i.e.,

$$\frac{dr_A}{dt} = \dot{r}_A = \frac{d}{dt}[(x_{O'} + \xi\cos\theta - \eta\sin\theta)i] + \frac{d}{dt}[(y_{O'} + \xi\sin\theta + \eta\cos\theta)j], \text{ m/s.} \tag{A-15}$$

THIS DOCUMENT PROVIDED BY THE ABBOTT AEROSPACE
TECHNICAL LIBRARY
ABBOTTAEROSPACE.COM

Since i and j are unit vectors in the inertial reference frame, they do not change with time. Thus Eq. A-15 can be written as

$$\dot{r}_A = [\dot{x}_{O'} + \dot{\xi}\cos\theta - \dot{\eta}\sin\theta - \dot{\theta}(\xi\sin\theta + \eta\cos\theta)]i$$

$$+ [\dot{y}_{O'} + \dot{\xi}\sin\theta + \dot{\eta}\cos\theta + \dot{\theta}(\xi\cos\theta - \eta\sin\theta)]j, \text{ m/s.} \quad \text{(A-16)}$$

Denote the velocity of point A as v_A. Then in the inertial reference frame,

$$\dot{r}_A = v_A = v_{A_x}i + v_{A_y}j, \text{ m/s} \quad \text{(A-17)}$$

where

v_A = velocity vector in inertial reference frame of point A, m/s
v_{A_x} = x-component of v_A, m/s
v_{A_y} = y-component of v_A, m/s.

By comparing Eqs. A-17 and A-16, the velocity components of point A can be identified as

$$v_{A_x} = \dot{x}_{O'} + \dot{\xi}\cos\theta - \dot{\eta}\sin\theta - \dot{\theta}(\xi\sin\theta + \eta\cos\theta), \text{ m/s} \quad \text{(A-18)}$$

$$v_{A_y} = \dot{y}_{O'} + \dot{\xi}\sin\theta + \dot{\eta}\cos\theta + \dot{\theta}(\xi\cos\theta - \eta\sin\theta), \text{ m/s.} \quad \text{(A-19)}$$

The velocity components of v_A are thus expressed in terms of the motion of point A in the local reference frame and the motion of the local reference frame in the inertial reference frame. Thus a judicious choice of the local reference frame can make computation of the velocity components from Eqs. A-18 and A-19 a simple matter.

To obtain the acceleration of point A in the inertial reference frame, differentiate Eq. A-16 once again with respect to time to obtain

$$a_A = \ddot{r}_A = [\ddot{x}_{O'} + \ddot{\xi}\cos\theta - \ddot{\eta}\sin\theta - \ddot{\theta}(\xi\sin\theta + \eta\cos\theta)$$

$$-2\dot{\theta}(\dot{\xi}\sin\theta + \dot{\eta}\cos\theta) - \dot{\theta}^2(\xi\cos\theta - \eta\sin\theta)]i$$

$$+ [\ddot{y}_{O'} + \ddot{\xi}\sin\theta + \ddot{\eta}\cos\theta + \ddot{\theta}(\xi\cos\theta - \eta\sin\theta)$$

$$+ 2\dot{\theta}(\dot{\xi}\cos\theta - \dot{\eta}\sin\theta) - \dot{\theta}^2(\xi\sin\theta + \eta\cos\theta)]j, \text{ m/s}^2 \quad \text{(A-20)}$$

where

a_A = acceleration vector in inertial reference frame of point A, m/s^2
$\ddot{}$ = second derivative with respect to time, i.e., acceleration.

From Eq. A-20, the x- and y-components of acceleration of point A in the inertial reference frame can be written as

$$a_x = \ddot{x}_{O'} + \ddot{\xi}\cos\theta - \ddot{\eta}\sin\theta - \ddot{\theta}(\xi\sin\theta + \eta\cos\theta)$$

$$-2\dot{\theta}(\dot{\xi}\sin\theta + \dot{\eta}\cos\theta) - \dot{\theta}^2(\xi\cos\theta - \eta\sin\theta), \text{ m/s}^2 \quad \text{(A-21)}$$

$$a_y = \ddot{y}_{O'} + \ddot{\xi}\sin\theta + \ddot{\eta}\cos\theta + \ddot{\theta}(\xi\cos\theta - \eta\sin\theta)$$

$$+2\dot{\theta}(\dot{\xi}\cos\theta - \dot{\eta}\sin\theta) - \dot{\theta}^2(\xi\sin\theta + \eta\cos\theta), \text{ m/s}^2 \quad \text{(A-22)}$$

THIS DOCUMENT PROVIDED BY THE ABBOTT AEROSPACE
TECHNICAL LIBRARY
ABBOTTAEROSPACE.COM

where

a_x = x-component of a_A in inertial reference frame, m/s^2
a_y = y-component of a_A in inertial reference frame, m/s^2.

The procedure just described can be generalized to points moving in reference frames, which are moving in other reference frames, which are moving in an inertial reference frame. First, however, it is essential to choose proper reference frames to locate the points of interest. The position vectors of these points can then be written first in terms of the local reference systems and then in terms of the inertial reference system. The position vectors can then be differentiated once with respect to time to arrive at velocities. Differentiation of the position vectors twice gives the acceleration of the point of interest.

A-3 GENERALIZED COORDINATES, KINETIC ENERGY, GENERALIZED FORCES, AND POTENTIAL ENERGY

Consider a 2-degree-of-freedom model of an artillery system shown in Fig. A-3. The degrees of freedom are the recoiling motion of the recoiling parts and the pitching of the entire system about an axis through the spades. The recoiling parts translate in the $x_2'y_2'$-local reference frame attached to the cradle. The $x_1'y_1'$-local coordinate system rotates in the global xy-coordinate system about point O. This rotation represents pitching of the weapon. Specified coordinates x_{1A}' and y_{1A}' fix the location of point A, the center of mass of nonrecoiling parts, in the $x_1'y_1'$-reference frame. Coordinates x_{1O_2}' and y_{1O_2}' fix the location of origin O_2 of the $x_2'y_2'$-reference

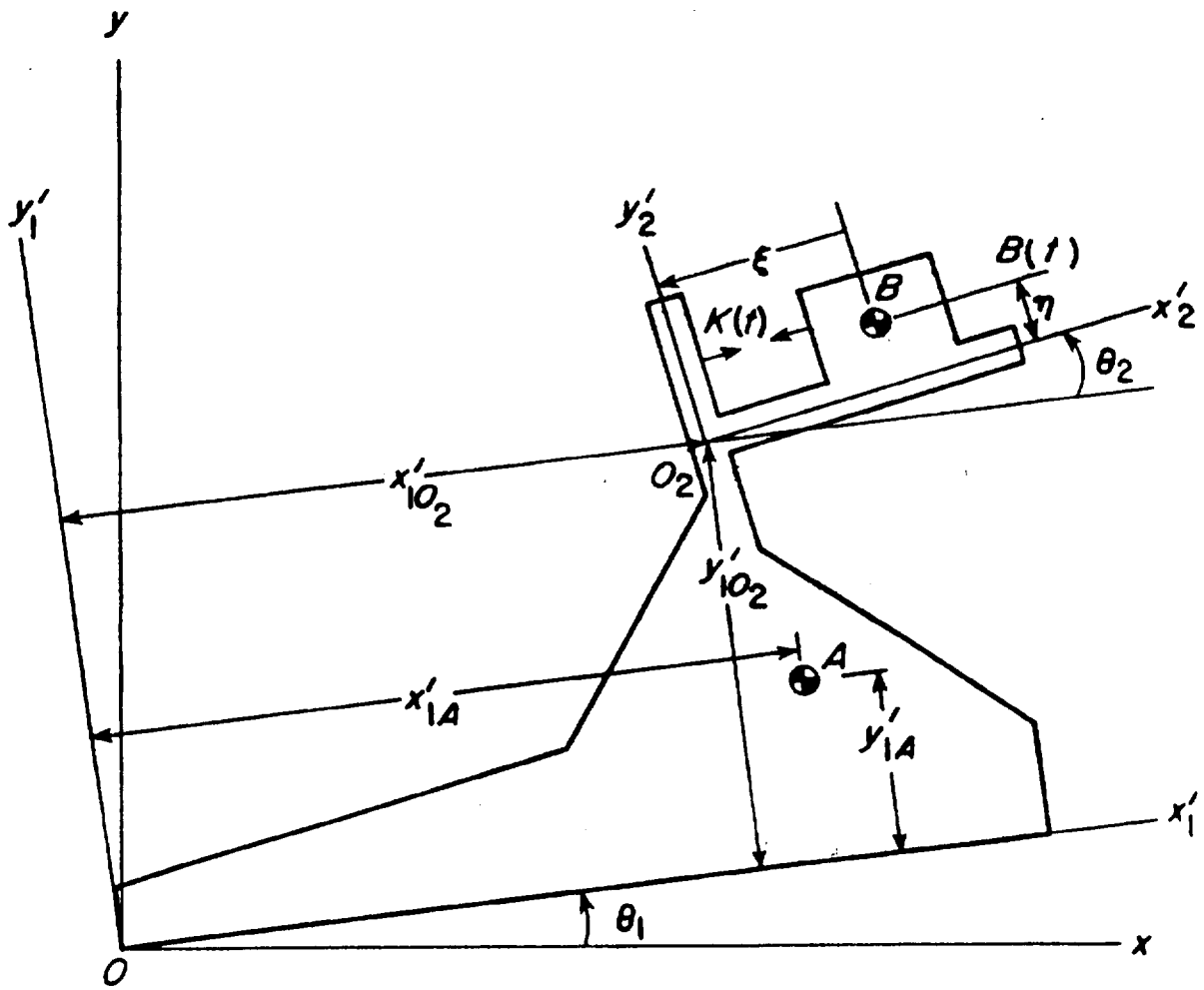

Figure A-3. Simplified 2-Degree-of-Freedom Artillery Model

THIS DOCUMENT PROVIDED BY THE ABBOTT AEROSPACE
TECHNICAL LIBRARY
ABBOTTAEROSPACE.COM

frame in the $x_1'y_1'$-reference frame. To specify the location of all parts of the system completely, the pitch angle θ_1 and distance ξ must be specified. These quantities are the generalized coordinates for the model.

It is now required to write the position, velocity, and acceleration of all parts of the system in terms of specified data and the generalized coordinates. The location of point A is given by the position vector r_A as

$$r_A = x_{1A}'i_1' + y_{1A}'j_1', \text{ m} \tag{A-23}$$

where

r_A = position vector of point A in the $x_1'y_1'$-reference frame, m
x_{1A}' = coordinate of A along x_1'-axis, m
y_{1A}' = coordinate of A along y_1'-axis, m
i_1' = unit vector along x_1'-axis, dimensionless
j_1' = unit vector along y_1'-axis, dimensionless.

Write i_1' and j_1' in terms of i and j, as in Eq. A-13, to give

$$r_A = (x_{1A}'\cos\theta_1 - y_{1A}'\sin\theta_1)i + (x_{1A}'\sin\theta_1 + y_{1A}'\cos\theta_1)j, \text{ m} \tag{A-24}$$

where

θ_1 = pitch angle of weapon, rad.

The position vector for the recoiling mass B can be written as

$$r_B = x_{1O_2}'i_1' + y_{1O_2}'j_1' + \xi i_2' + \eta j_2', \text{ m} \tag{A-25}$$

where

r_B = position vector of center of recoiling mass B, m
x_{1O_2}' = coordinate of O_2 along x_1'-axis in $x_1'y_1'$-reference frame, m
y_{1O_2}' = coordinate of O_2 along y_1'-axis in $x_1'y_1'$-reference frame, m
ξ = coordinate of B along x_2'-axis in $x_2'y_2'$-reference frame, m
η = coordinate of B along y_2'-axis in $x_2'y_2'$-reference frame, m
i_2' = unit vector along x_2'-axis, dimensionless
j_2' = unit vector along y_2'-axis, dimensionless.

Writing unit vectors in the $x_2'y_2'$-reference frame in terms of those in $x_1'y_1'$-reference frame gives

$$i_2' = \cos\theta_2 i_1' + \sin\theta_2 j_1' \tag{A-26}$$

$$j_2' = -\sin\theta_2 i_1' + \cos\theta_2 j_1' \tag{A-27}$$

where

θ_2 = angle of elevation of cradle relative to bottom carriage, rad.

Substitution of i_2' and j_2' from Eqs. A-26 and A-27 into Eq. A-25 gives

$$r_B = (x_{1O_2}' + \xi\cos\theta_2 - \eta\sin\theta_2)i_1' + (y_{1O_2}' + \xi\sin\theta_2 + \eta\cos\theta_2)j_1', \text{ m.} \tag{A-28}$$

From Eq. A-13 the vectors i_1' and j_1' can be written in terms of unit vectors i and j. This allows Eq. A-28 to be written in the form

$$r_B = [(x_{1O_2}' + \xi\cos\theta_2 - \eta\sin\theta_2)\cos\theta_1 - (y_{1O_2}' + \xi\sin\theta_2 + \eta\cos\theta_2)\sin\theta_1]i$$
$$+ [(x_{1O_2}' + \xi\cos\theta_2 - \eta\sin\theta_2)\sin\theta_1 + (y_{1O_2}' + \xi\sin\theta_2 + \eta\cos\theta_2)\cos\theta_1]j, \text{ m.} \tag{A-29}$$

THIS DOCUMENT PROVIDED BY THE ABBOTT AEROSPACE
TECHNICAL LIBRARY
ABBOTTAEROSPACE.COM

Expand Eq. A-29 and use the following trigonometric identities

$$\sin(\alpha + \beta) = \sin\alpha \cos\beta + \cos\alpha \sin\beta \tag{A-30}$$

$$\cos(\alpha + \beta) = \cos\alpha \cos\beta - \sin\alpha \sin\beta \tag{A-31}$$

to give

$$\begin{aligned} r_B = {} & [x'_{1O_2}\cos\theta_1 - y'_{1O_2}\sin\theta_1 + \xi\cos(\theta_1 + \theta_2) - \eta\sin(\theta_1 + \theta_2)]i \\ & + [x'_{1O_2}\sin\theta_1 + y'_{1O_2}\cos\theta_1 + \xi\sin(\theta_1 + \theta_2) + \eta\cos(\theta_1 + \theta_2)]j, \text{ m.} \end{aligned} \tag{A-32}$$

As pointed out at the beginning of this paragraph, θ_1 and ξ have been designated as the generalized coordinates. Usually, generalized coordinates are identified by variables q_i. The following definition can now be made:

$$\theta_1 \equiv q_1, \text{ rad} \tag{A-33}$$

$$\xi \equiv q_2, \text{ m.} \tag{A-34}$$

Eqs. A-24 and A-32 for the position vectors of points A and B, respectively, in terms of the generalized coordinates, can be written as

$$r_A = (x'_{1A}\cos q_1 - y'_{1A}\sin q_1)i + (x'_{1A}\sin q_1 + y'_{1A}\cos q_1)j, \text{ m} \tag{A-35}$$

$$\begin{aligned} r_B = {} & [x'_{1O_2}\cos q_1 - y'_{1O_2}\sin q_1 + q_2\cos(q_1 + \theta_2) - \eta\sin(q_1 + \theta_2)]i \\ & + [x'_{1O_2}\sin q_1 + y'_{1O_2}\cos q_1 + q_2\sin(q_1 + \theta_2) + \eta\cos(q_1 + \theta_2)]j, \text{ m.} \end{aligned} \tag{A-36}$$

The velocity of point A in the inertial reference frame can now be determined by differentiating Eq. A-35 with respect to time, i.e.,

$$\dot{r}_A = v_A = -(x'_{1A}\sin q_1 + y'_{1A}\cos q_1)\dot{q}_1 i + (x'_{1A}\cos q_1 - y'_{1A}\sin q_1)\dot{q}_1 j, \text{ m/s} \tag{A-37}$$

where

v_A = velocity vector in inertial reference frame of point A, m/s
$\dot{q}_i$ = generalized velocity corresponding to generalized coordinate q_i, m/s.

Similarly, the velocity v_B of point B in the inertial reference frame can be determined by differentiating Eq. A-36 with respect to time, i.e.,

$$\begin{aligned} \dot{r}_B = v_B = {} & \{[-x'_{1O_2}\sin q_1 - y'_{1O_2}\cos q_1 - q_2\sin(q_1 + \theta_2) \\ & - \eta\cos(q_1 + \theta_2)]\dot{q}_1 + \cos(q_1 + \theta_2)\dot{q}_2\}i \\ & + \{[x'_{1O_2}\cos q_1 - y'_{1O_2}\sin q_1 + q_2\cos(q_1 + \theta_2) \\ & - \eta\sin(q_1 + \theta_2)]\dot{q}_1 + \sin(q_1 + \theta_2)\dot{q}_2\}j, \text{ m/s.} \end{aligned} \tag{A-38}$$

The kinetic energy T for the entire system can be computed by summing the kinetic energies—translational and rotational—of the two masses, i.e.,

THIS DOCUMENT PROVIDED BY THE ABBOTT AEROSPACE
TECHNICAL LIBRARY
ABBOTTAEROSPACE.COM

$$T = \frac{m_A|v_A|^2}{2} + \frac{m_B|v_B|^2}{2} + \frac{I_A\omega_A^2}{2} + \frac{I_B\omega_B^2}{2}, \text{ J} \tag{A-39}$$

where

T = kinetic energy of system, J
m_A = mass of nonrecoiling parts, kg
m_B = mass of recoiling parts, kg
$|v_A|$ = magnitude of v_A, m/s
$|v_B|$ = magnitude of v_B, m/s
I_A = moment of inertia of nonrecoiling parts, i.e., mass A, kg·m^2
I_B = moment of inertia of recoiling parts, i.e., mass B, kg·m^2
ω_A = angular velocity of nonrecoiling mass A, rad/s
ω_B = angular velocity of recoiling mass B, rad/s.

From Eq. A-37, the square of the magnitude of the velocity v_A is

$$|v_A|^2 = [(x'_{1A}\sin q_1 + y'_{1A}\cos q_1)^2 + (x'_{1A}\cos q_1 - y'_{1A}\sin q_1)^2]\dot{q}_1^2, \text{ m}^2/\text{s}^2. \tag{A-40}$$

Expanding Eq. A-40 and using the trigonometric identity

$$\sin^2\alpha + \cos^2\alpha = 1, \tag{A-41}$$

Eq. A-40 can be simplified to

$$|v_A|^2 = [(x'_{1A})^2 + (y'_{1A})^2]\dot{q}_1^2, \text{ m}^2/\text{s}^2. \tag{A-42}$$

From Eq. A-38, the square of the magnitude of the velocity v_B is

$$\begin{aligned}|v_B|^2 = \{&[-x'_{1O_2}\sin q_1 - y'_{1O_2}\cos q_1 - q_2\sin(q_1 + \theta_2) - \eta\cos(q_1 + \theta_2)]\dot{q}_1 \\ &+ \dot{q}_2\cos(q_1 + \theta_2)\}^2 + \{[x'_{1O_2}\cos q_1 - y'_{1O_2}\sin q_1 + q_2\cos(q_1 + \theta_2) \\ &- \eta\sin(q_1 + \theta_2)]\dot{q}_1 + \dot{q}_2\sin(q_1 + \theta_2)\}^2, \text{ m}^2/\text{s}^2.\end{aligned} \tag{A-43}$$

Expand Eq. A-43 and simplify by the substitution of trigonometric identities to give

$$\begin{aligned}|v_B|^2 = &[(x'_{1O_2})^2 + (y'_{1O_2})^2 + q_2^2 + \eta^2 + 2x'_{1O_2}q_2\cos\theta_2 - x'_{1O_2}\eta\sin\theta_2 \\ &+ 2y'_{1O_2}\eta\cos\theta_2]\dot{q}_1 + 2(x'_{1O_2}\sin\theta_2 - y'_{1O_2}\cos\theta_2 - \eta)\dot{q}_1\dot{q}_2 \\ &+ \dot{q}_2^2, \text{ m}^2/\text{s}^2.\end{aligned} \tag{A-44}$$

Since mass A is free to rotate about O, $\omega_A = \dot{q}_1$, rad/s. Also since the recoiling parts rotate with the cradle, $\omega_B = \dot{q}_1$, rad/s.

The kinetic energy of Eq. A-39 is thus

THIS DOCUMENT PROVIDED BY THE ABBOTT AEROSPACE
TECHNICAL LIBRARY
ABBOTTAEROSPACE.COM

$$T = \frac{m_A}{2}\left[(x'_{1A})^2 + (y'_{1A})^2\right]\dot{q}_1^2 + \frac{m_B}{2}\left\{\left[(x'_{1O_2})^2 + (y'_{1O_2})^2 + q_2^2 + \eta^2 + 2x'_{1O_2}q_2\cos\theta_2 - 2x'_{1O_2}\eta\sin\theta_2 + 2y'_{1O_2}q_2\sin\theta_2 + 2y'_{1O_2}\eta\cos\theta_2\right]\dot{q}_1^2 + \dot{q}_2^2 + 2(x'_{1O_2}\sin\theta_2 - y'_{1O_2}\cos\theta_2 - \eta)\dot{q}_1\dot{q}_2\right\} + \frac{I_A\dot{q}_1^2}{2} + \frac{I_B\dot{q}_1^2}{2}, \text{ J.} \quad \text{(A-45)}$$

Consider a system being acted upon by a system of forces. The system is now given a virtual displacement. A virtual displacement is defined as a small displacement given to the system without the passage of time. The applied forces are also assumed to remain constant during this interval. The work done by the forces on the system due to this virtual displacement is called virtual work. The virtual work done on the system can be written as

$$\delta W = \sum_{i=1}^{n} \boldsymbol{F}_i \cdot \delta \boldsymbol{r}_i, \text{ J} \quad \text{(A-46)}$$

where

δW = virtual work, J
$\boldsymbol{F}_i$ = ith force acting on system, N
$\delta \boldsymbol{r}_i$ = virtual displacement of ith $\boldsymbol{F}_i$, m
n = total number of forces acting on the system, dimensionless.

The principle of virtual work states that the condition for equilibrium of a system is that the virtual work of the applied forces must vanish (Ref. 1)

$$\sum_{i=1}^{n} \boldsymbol{F}_i \cdot \delta \boldsymbol{r}_i = 0. \quad \text{(A-47)}$$

Eq. A-47 is written in terms of virtual physical displacements. These displacements may or may not be independent. As noted earlier, all physical displacements of the system can be written as a function of the generalized coordinates, i.e.,

$$\boldsymbol{r}_i = \boldsymbol{f}(q_1,\ldots,q_s), \text{ m} \quad \text{(A-48)}$$

where

$\boldsymbol{f}(q_1,\ldots,q_s)$ = vector function of s-generalized coordinates for the system.

The virtual displacement can thus be written in terms of variations in generalized coordinates as (Ref. 1)

$$\delta \boldsymbol{r}_i = \sum_{j=1}^{s} \left(\frac{\partial \boldsymbol{r}_i}{\partial q_j}\right) \delta q_j, \text{ m.} \quad \text{(A-49)}$$

Therefore, the virtual work expression can be written as

$$\delta W = \sum_{i=1}^{n} \boldsymbol{F}_i \cdot \left(\sum_{j=1}^{s} \frac{\partial \boldsymbol{r}_i}{\partial q_j}\right) \delta q_j = \sum_{j=1}^{s} \left(\sum_{i=1}^{n} \boldsymbol{F}_i \cdot \frac{\partial \boldsymbol{r}_i}{\partial q_j}\right) \delta q_j, \text{ J.} \quad \text{(A-50)}$$

The quantities within parentheses can be looked upon as a force system that undergoes a virtual displacement of the generalized coordinates and does the same amount of virtual work as the externally applied force system. These forces are defined to be the generalized forces

THIS DOCUMENT PROVIDED BY THE ABBOTT AEROSPACE
TECHNICAL LIBRARY
ABBOTTAEROSPACE.COM

$$Q_i = \sum_{j=1}^{n} \boldsymbol{F}_j \cdot \frac{\partial \boldsymbol{r}_j}{\partial q_i}, \text{ N or N·m (torque)} \tag{A-51}$$

where

Q_i = generalized force (or torque) corresponding to the generalized coordinate q_i, N or N·m.

The dimensions of torque associated with Q_i will occur when one of the q_i is an angle.

Externally applied forces can be classified as either conservative or nonconservative. A conservative force is defined as a force that is not dissipative, i.e., any mechanical process taking place under its influence is reversible (Ref. 1). Nonconservative forces, on the other hand, are dissipative in nature, and the mechanical process taking place under their influence is nonreversible. For conservative forces it is possible to define a quantity called potential energy V, such that the work done by the force on the particle to which it is applied in moving from point A to point B is equal to the decrease in potential energy. This can be stated as

$$W_{AB} = V_A - V_B, \text{ J} \tag{A-52}$$

where

W_{AB} = work done by force in moving particle from point A to point B, J
V_A = potential energy of force at point A, J
V_B = potential energy of force at point B, J.

The potential energy of gravitational force acting on a mass m can be written as

$$V = mgh, \text{ J} \tag{A-53}$$

where

g = acceleration due to gravity, m/s^2
h = height of particle measured from some suitable datum, m.

The potential energy V_L of the force of a linear spring is given as (Ref. 1)

$$V_L = \frac{K_L \ell^2}{2}, \text{ J} \tag{A-54}$$

where

K_L = linear spring constant, N/m
ℓ = elongation of spring from its free length, m.

The potential energy V_T due to a torsional spring can similarly be expressed as

$$V_T = \frac{K_T \phi^2}{2}, \text{ J} \tag{A-55}$$

where

K_T = torsional spring constant, N·m/rad
ϕ = change in angle of spring from free angle, rad.

A useful relation between potential energy and generalized force is (Ref. 1)

$$Q_i = -\frac{dV}{\partial q_i}, \; i = 1, \ldots, s, \text{ N or N·m (torque).} \tag{A-56}$$

THIS DOCUMENT PROVIDED BY THE ABBOTT AEROSPACE
TECHNICAL LIBRARY
ABBOTTAEROSPACE.COM

Thus, if certain internal and external forces are conservative, their potential energy can be easily written in terms of generalized coordinates and Eq. A-56 can be used to calculate their generalized forces.

A-4 LAGRANGE'S EQUATIONS OF MOTION

A systematic and generally applicable method of constructing the equations of motion for a system, in terms of independent generalized coordinates, is the use of Lagrange's equations of motion. Regardless of whether forces acting on a system are conservative, generalized forces Q_i, $i = 1, ..., s$ are defined. In terms of these generalized forces and kinetic energy $T = T(q_1,..., q_s, \dot{q}_1,..., \dot{q}_s)$, Lagrange's equations of motion are (See Ref. 1 for a derivation.)

$$\frac{d}{dt}\left(\frac{\partial T}{\partial \dot{q}_i}\right) - \frac{\partial T}{\partial q_i} = Q_i,\ i = 1, ..., s,\ \text{N.} \tag{A-57}$$

It is important that the q_i be independent, i.e., not be related by constraints; otherwise, Eq. A-57 is not valid.

A valuable aspect of Lagrange's equations of motion is that internal forces that do no work may be ignored. For example, reaction forces in frictionless forces between bodies do no work, so they have no influence on the equations of motion.

Consider the 2-degree-of-freedom model in Fig. A-3. The forces acting on this system are (1) the weight of mass A, (2) weight of recoiling mass B, (3) breech force $B(t)$ acting on the recoiling parts, and (4) recoil force $K(t)$ acting between the recoiling and nonrecoiling parts. Before the equations of motion for this model can be written, the generalized forces on the system have to be computed, i.e.,

$$F_1 = -M_A g j,\ \text{N} \tag{A-58}$$

$$F_2 = -M_t g j,\ \text{N} \tag{A-59}$$

$$F_3 = -B(t) i_2',\ \text{N} \tag{A-60}$$

$$F_4 = \pm K(t) i_2',\ \text{N} \tag{A-61}$$

where

$B(t)$ = breech force, N
$K(t)$ = recoil force, N.

Transform i_2' in terms of the unit vectors i and j in the inertial frame to give

$$F_3 = -B(t)[\cos(\theta_1 + \theta_2) i + \sin(\theta_1 + \theta_2) j],\ \text{N.}$$

Substitute q_1 for θ_1 from Eq. A-33 to give

$$F_3 = -B(t)[\cos(q_1 + \theta_2) i + \sin(q_1 + \theta_2) j],\ \text{N·m.} \tag{A-62}$$

From Eq. A-35

$$r_A = (x_{1A}' \cos q_1 - y_{1A}' \sin q_1) i + (x_{1A}' \sin q_1 + y_{1A}' \cos q_1) j,\ \text{m.} \tag{A-63}$$

From Eq. A-36

THIS DOCUMENT PROVIDED BY THE ABBOTT AEROSPACE
TECHNICAL LIBRARY
ABBOTTAEROSPACE.COM

$$r_B = [x'_{1O_2}\cos q_1 - y'_{1O_2}\sin q_1 + q_2\cos(q_1 + \theta_2) - \eta\sin(q_1 + \theta_2)]i + [x'_{1O_2}\sin q_1 + y'_{1O_2}\cos q_1 + q_2\sin(q_1 + \theta_2) + \eta\cos(q_1 + \theta_2)]j, \text{ m.} \quad \text{(A-64)}$$

From Eq. A-51 the generalized forces Q_i can be computed as

$$Q_1 = -m_A g[x'_{1A}\cos q_1 - y'_{1A}\sin q_1] - m_B g[x'_{1O_2}\cos q_1 - y'_{1O_2}\sin q_1 + q_2\cos(q_1 + \theta_2) - \eta\sin(q_1 + \theta_2)] - B(t)\{\cos(q_1 + \theta_2) \times [-x'_{1O_2}\sin q_1 - y'_{1O_2}\cos q_1 - q_2\sin(q_1 + \theta_2) - \eta\cos(q_1 + \theta_2)] + \sin(q_1 + \theta_2)[x'_{1O_2}\cos q_1 - y'_{1O_2}\sin q_1 + q_2\cos(q_1 + \theta_2) - \eta\sin(q_1 + \theta_2)]\}, \text{ N·m (since } q_1 = \theta). \quad \text{(A-65)}$$

$$Q_2 = -m_B g\sin(q_1 + \theta_2) - B(t)[\sin^2(q_1 + \theta_2) + \cos^2(q_1 + \theta_2)] + K(t), \text{ N}$$

which simplifies to

$$Q_2 = -m_B g\sin(q_1 + \theta_2) - B(t) + K(t), \text{ N.} \quad \text{(A-66)}$$

Since two generalized coordinates were used to represent this model, two Lagrange equations are required. By use of Eq. A-57, the Lagrange equations can be written as

$$\frac{d}{dt}\left(\frac{\partial T}{\partial \dot{q}_1}\right) - \frac{\partial T}{\partial q_1} = Q_1, \text{ N·m} \quad \text{(A-67)}$$

$$\frac{d}{dt}\left(\frac{\partial T}{\partial \dot{q}_2}\right) - \frac{\partial T}{\partial q_2} = Q_2, \text{ N.} \quad \text{(A-68)}$$

Take the derivatives of the kinetic energy expression given by Eq. A-45

$$\frac{d}{dt}\left(\frac{\partial T}{\partial \dot{q}_1}\right) = \ddot{q}_1\{m_A(x_A^2 + y_A^2) + I_A + I_B + m_B[(x'_{1O_2})^2 + (y'_{1O_2})^2 + q_2^2 + \eta^2 + 2x'_{1O_2}q_2\cos\theta_2 - 2x'_{1O_2}\eta\sin\theta_2 + 2y'_{1O_2}q_2\sin\theta_2 + 2y'_{1O_2}\eta\cos\theta_2]\} - 2m_B\ddot{q}_2(x'_{1O_2}\sin\theta_2 + y'_{1O_2}\cos\theta_2 + \eta) + 2\dot{q}_1\dot{q}_2 m_B(q_2 + x'_{1O_2}\cos\theta_2 + y'_{1O_2}\sin\theta_2), \text{ N·m} \quad \text{(A-69)}$$

$$\frac{\partial T}{\partial q_1} = 0 \quad \text{(A-70)}$$

THIS DOCUMENT PROVIDED BY THE ABBOTT AEROSPACE
TECHNICAL LIBRARY
ABBOTTAEROSPACE.COM

$$\frac{d}{dt}\left(\frac{\partial T}{\partial \dot{q}_2}\right) = m_B[\ddot{q}_2 + \ddot{q}_1(x'_{1O_2}\sin\theta_2 - y'_{1O_2}\cos\theta_2 - \eta)], \text{ N} \tag{A-71}$$

$$\frac{\partial T}{\partial q_2} = -\dot{q}_1^2 m_B(q_2 + x'_{1O_2}\cos\theta_2 + y'_{1O_2}\sin\theta_2), \text{ N.} \tag{A-72}$$

The equations of motion of the 2-degree-of-freedom model can be written—substituting into Eq. A-67 and A-68—as

$$\begin{aligned}
&\ddot{q}_1\{m_A[(x'_{1A})^2 + (y'_{1A})^2] + I_A + I_B + m_B[(x'_{1O_2})^2 + (y'_{1O_2})^2 + q_2^2 + \eta^2 + 2x'_{1O_2}q_2\cos\theta_2 \\
&\quad - 2x'_{1O_2}\eta\sin\theta_2 + 2y'_{1O_2}q_2\sin\theta_2 + 2y'_{1O_2}\eta\cos\theta_2]\} \\
&\quad - 2m_B\ddot{q}_2(-x'_{1O_2}\sin\theta_2 + y'_{1O_2}\cos\theta_2 + \eta) \\
&\quad + 2\dot{q}_1\dot{q}_2 m_B(q_2 + x'_{1O_2}\cos\theta_2 + y'_{1O_2}\sin\theta_2) \\
&\quad = -m_A g(x'_{1A}\cos q_1 + y'_{1A}\sin q_1) - m_B g[x'_{1O_2}\cos q_1 - y'_{1O_2}\sin q_1 \\
&\quad + q_2\cos(q_1 + \theta_2) - \eta\sin(q_1 + \theta_2)] - B(t)[\cos(q_1 + \theta_2) \\
&\quad \times [-x'_{1O_2}\sin q_1 - y'_{1O_2}\cos q_1 - q_2\sin(q_1 + \theta_2) \\
&\quad - \eta\cos(q_1 + \theta_2)] + \sin(q_1 + \theta_2)[x'_{1O_2}\cos q_1 - y'_{1O_2}\sin q_1 \\
&\quad + q_2\cos(q_1 + \theta_2) - \eta\sin(q_1 + \theta_2)]\}, \text{ N·m}
\end{aligned} \tag{A-73}$$

and

$$\begin{aligned}
&\ddot{q}_2 m_B + \ddot{q}_1 m_B(x'_{1O_2}\sin\theta_2 - y'_{1O_2}\cos\theta_2 - \eta) - \dot{q}_1^2 m_B(q_2 + x'_{1O_2}\cos\theta_2 + y'_{1O_2}\sin\theta_2) \\
&\quad = -m_B g\sin(q_1 + \theta_2) - B(t) + K(t), \text{ N.}
\end{aligned} \tag{A-74}$$

Eqs. A-73 and A-74 are the Lagrangian equations of motion for this 2-degree-of-freedom model. Clearly, these nonlinear equations cannot be solved in closed form. The most practical means of solving them is to employ numerical integration methods on a digital computer. (See Ref. 2.)

REFERENCES

1. D. T. Greenwood, *Principles of Dynamics*, Prentice-Hall, Inc., Englewood Cliffs, NJ, 1965.
2. E. J. Haug, *Computer-Aided Kinematics and Dynamics of Mechanical Systems*, Allyn & Bacon, Boston, MA, 1987.

THIS DOCUMENT PROVIDED BY THE ABBOTT AEROSPACE
TECHNICAL LIBRARY
ABBOTTAEROSPACE.COM

APPENDIX B
INTRODUCTION TO NASTRAN

Software for stress analysis of complex structural systems that use the finite element method is available. This appendix presents an introduction to a widely used software system called NASTRAN. The main purpose of the appendix is to introduce a designer to the finite element modeling concepts and to the types of data that are required to use the program for stress analysis. Modeling of the system program and the system capabilities are discussed in detail. This discussion includes the finite element library, options for solution methods, and material properties and load specification options that are available in the program. Many other computer programs are available that have similar capabilities; however, these computer programs require similar data.

B-1 INTRODUCTION

The purpose of this appendix is to provide the designer with a brief overview of the NASA STRUCTURAL ANALYSIS (NASTRAN) (Level 17.5*) computer program. The program has been extended beyond Level 17.5. Some commercial vendors have made extensive modifications to the program. The basic structure of the program, however, remains unchanged as described here. Note that although NASTRAN capabilities are described, similar explanations are applicable to other computer programs as well. The input data structure and capabilities of various programs may differ somewhat. Most computer programs, however, are based on the same fundamental theory of the finite element method as described in Appendix C.

Before NASTRAN or other computer programs may be used, the designer must familiarize himself with at least those portions of the User's Manual (Ref. 1) that concern the problem. Also, reference to the Programmer's Manual (Ref. 2) or the Theoretical Manual (Ref. 3) is necessary because error messages or difficulties may be encountered while using a program.

The NASTRAN computer program can also be used to analyze nonstructural problems, but only the stress analysis of large complex structural systems is covered here.

B-2 SUMMARY OF NASTRAN CAPABILITY

The entire data deck for NASTRAN is divided into three segments—the Executive Control Deck, the Case Control Deck, and the Bulk Data Deck. Details of these data decks are given in par. B-6. In this paragraph the structural analysis capability of the NASTRAN computer program is described. There are two basic options in the program: the rigid format option and the direct matrix abstraction program (DMAP) option. Each is described in the paragraphs that follow.

B-2.1 RIGID FORMAT OPTION

There are standard options, called the rigid form options, for structural analysis available in the NASTRAN. The analyst can select an option that is most suitable for his problem; each option has a designated number that must be specified in the Executive Control Deck. For more details regarding rigid format options, consult Sections 3.2 and 9.1 of the Theoretical Manual (Ref. 3) and Section 3 of the User's Manual (Ref. 1).

B-2.1.1 Static Analyses

There are four static analysis options available:

1. *Basic Static Analysis Option.* This option solves for the response of complex structures to static loads. It yields grid point displacements, constraint forces, and member stresses, as well as structural weight, information about dynamic balancing, and plots of deformation (optional).
2. *Static Analysis With Inertia Relief Option.* This option solves for responses to static loads and to inertia loads resulting from steady accelerations. This option also generates plots of all static load deformations and yields weight and dynamic balancing information (optional).

*Level 17.5 means the NASTRAN program has gone through 17 major revisions since it was released for use.

THIS DOCUMENT PROVIDED BY THE ABBOTT AEROSPACE
TECHNICAL LIBRARY
ABBOTTAEROSPACE.COM

3. *Static Analysis With Differential Stiffness Option.* This option solves for the response to a single loading condition and then determines the differential stiffness effect caused by large nonlinear motion. The term differential stiffness applies to linear terms in the equations of motion of an elastic body that arise from a simultaneous consideration of large nonlinear motions and the applied loads. It is a first-order approximation to large deformation effects. Differential stiffness is directly proportional to the level of applied loads. This option yields the usual static analysis results for a single loading and then yields displacement, force, and stress information for each increment of the differential stiffness factor. It also yields weight and dynamic balance information and generates tables or plots of combined linear and differential stiffness responses (optional).

4. *Piecewise Linear Analysis of Nonlinear Static Response Option.* This option solves for the response of complex nonlinear elastic or plastic structures with nonlinear stress-dependent material properties. The stiffness matrix is modified incrementally as the loads reach piecewise linear threshold values. The load level is increased to its full value by small increments so that the stiffness properties can be assumed to be constant over each increment. It yields accumulated displacements, forces, and stresses at the end of each increment. It also gives weight and dynamic balance information and generates tables or plots of deformations accumulated after each linear increment (optional).

B-2.1.2 Elastic Stability Analysis

The Buckling Analysis option performs a differential stiffness analysis of a complex structure. It then performs an eigenvalue analysis on the pair of matrices consisting of the linear stiffness matrix and the differential stiffness matrix to determine the value of the load that would cause buckling of the structure; it also gives the buckling mode. This option is equipped to handle only first-order buckling and not postbuckling displacements, i.e., postbuckling analysis is not performed. It yields displacement, force, and stress information at the threshold load for buckling and also gives weight and dynamic balance information and generates tables or plots of buckling modes (optional).

B-2.1.3 Dynamic Analysis

There are seven dynamic analysis options available:

1. *Normal Mode Analysis Option.* This option solves for natural frequencies and mode shapes of complex structures. It yields normalized modal displacements, grid point displacements, constraint forces, normalized modal element forces, and stresses. This option also gives weight and dynamic balance information and generates tables or plots of normalized mode shapes (optional).

2. *Transient Response, Modal Method Option.* This option solves for the response of complex structures to time-varying loads in which damping can be either viscous or structural. A real eigenvalue analysis operates on structural mass and stiffness matrices to define generalized modal coordinates. The differential equations are reformulated in terms of modal coordinates as an uncoupled set. Integration is performed by finite differences on the uncoupled modal differential equations. This option yields the time-varying displacements, velocities, accelerations, constraint forces at grid points, and the time-varying forces and stresses in elements. It also yields weight and dynamic balance information and generates tables or plots of any output quantity against either time or frequency (optional). It also generates plots of structural deformation at specified instants of time (optional).

3. *Transient Response, Direct Integration Method Option.* This option solves and yields the same information as described under the Transient Response, Modal Method. The only difference is that integration is performed by finite differences on the coupled differential equations as formulated directly in terms of grid point degrees of freedom.

4. *Frequency and Random Response, Modal Method Option.* This option solves the two problems in frequency space by performing real eigenvalue analysis on the matrices with grid point degrees of freedom to set up small matrices in modal coordinates before doing the following two analyses:

a. It solves the response of a complex structure having either viscous and/or structural damping to a spectrum of steady sinusoidal forcing. It yields the real and imaginary parts of displacements, velocities, accelerations, and constraint forces at grid points. It also gives the real and imaginary parts of forces and stress in elements. These output quantities can be normalized to a unit forcing amplitude to form a transfer function. It plots output quantities against frequency (optional).

b. It solves the response of a complex structure, characterized by the previous transfer functions, to stationary random forcing functions applied in the form of a cross-spectral density. It yields the autospectral

THIS DOCUMENT PROVIDED BY THE ABBOTT AEROSPACE
TECHNICAL LIBRARY
ABBOTTAEROSPACE.COM

density in that quantity used in the transfer functions. It also transforms autospectra to autocorrelation functions and plots density functions against frequency and correlation functions against time. This format also gives weight and dynamic balance information and generates various tables and plots (optional).

5. *Frequency and Random Response, Direct Integration Method Option.* This option operates on the matrices as formulated directly in terms of grid point degrees of freedom.

6. *Complex Eigenvalue Analysis, Modal Method Option.* This option solves for frequencies and eigenvectors of the complex vibration modes of complicated structures in which the damping can be either viscous or structural. A real eigenvalue analysis operates on matrices with grid point degrees of freedom to set up smaller matrices in modal coordinates before extracting complex eigenvalues. It yields normalized complex eigenvectors of grid point displacement, constraint forces, and complex element forces and stresses. Weight and dynamic balance information are also given.

7. *Complex Eigenvalue Analysis, Direct Integration Method Option.* This option operates on the matrices as formulated directly from the grid point degrees of freedom.

B-2.2 DIRECT MATRIX ABSTRACTION PROGRAM (DMAP) OPTION

If an analyst wants to initiate a case not provided for in the rigid formats, he can organize his own problem steps by using a language called DMAP. The executive control, the input file processor, and the output file processor are made to operate automatically with the analyst's DMAP program, so he need not concern himself with core assignments and secondary storage assignments. The user needs only to specify the sequence of matrix operations and the module selections that are needed to solve the mathematical formulation of the particular case. Consult Section 5 of the User's Manual (Ref. 1) for more details.

B-3 MODELING OF THE STRUCTURE

This paragraph describes general modeling aspects—such as coordinate systems, grid points, constraints, structural elements, and applied loads—for the structures.

B-3.1 GEOMETRIC PROPERTIES

The organization of the structure to be analyzed is established by the selection of a reference system. The reference system can be chosen as a geometric coordinate frame or a collection of scalar connections. Section 2.4 of the User's Manual (Ref. 1) should be consulted for more details.

B-3.1.1 Coordinate System

A rectangular cartesian coordinate system is the basic system used to define grid point locations and loads. The basic cartesian coordinates can be transformed to the following coordinate systems: (1) basic cylindrical, (2) basic spherical, (3) local cartesian, (4) local cylindrical, and (5) local spherical. The CORDIC, CORDIR, and CORDIS cards are used to define cylindrical, rectangular, and spherical local coordinate systems, respectively, in terms of three geometric grid points that have been previously defined. CORD2C, CORD2R, and CORD2S cards are in terms of the coordinates of three points in a previously defined coordinate system.

B-3.1.2 Grid, Scalar, and Extra Points

A discussion of these point terms follows:

1. *Grid Point.* This point has six degrees of freedom—three translations and three rotations—unless constrained. The grid points are defined on GRID bulk data decks by specifying their coordinates in either the basic or local coordinate system. The local coordinate system used to define directions of motion may be different from the local coordinate system used to locate the grid points. Both the location coordinate system and the displacement coordinate system are specified on the GRID card for each grid point. The grid point constraints specified on the GRID card usually are restricted to those degrees of freedom that will not be elastically constrained and hence must be removed from the model to avoid singularities in the structural stiffness matrix.

2. *Scalar Point.* This point has only one degree of freedom that may or may not have vector connotation, depending on the problem. Scalar points are defined either on an SPOINT card or by reference on a connection card for scalar element.

3. *Extra Points.* These points are nongeometric points used in connection with transfer functions and other forms of direct matrix input used in dynamic analysis and are defined on EPOINT cards.

THIS DOCUMENT PROVIDED BY THE ABBOTT AEROSPACE
TECHNICAL LIBRARY
ABBOTTAEROSPACE.COM

B-3.2 CONSTRAINTS

Structural matrices are assembled in terms of all structural grid points. (They may include the scalar points or extra points.) Various constraints are applied to these matrices to remove undesired singularities, provide boundary conditions, define rigid elements, and provide other desired characteristics for the structural model. The two basic kinds of constraints are discussed in the paragraphs that follow.

B-3.2.1 Single-Point Constraints

The elements connected to a grid point may not provide resistance to motion in certain directions and thus cause the stiffness matrix to be singular. Single-point constraints are used to specify this kind of boundary condition by removing these degrees of freedom from the stiffness matrix and are defined on SPC, SPC1, SPCADD, SPCAX cards, or on the GRID cards.

B-3.2.2 Multipoint Constraints

Multipoint constraints are used to constrain a degree of freedom to be equal to a linear combination of the values of other degrees of freedom. Multipoint constraints are defined on MPC, MPCADD, and MPCAX cards.

B-3.3 STRUCTURAL ELEMENTS

Structural elements are defined on connection cards that identify the grid points to which the element is connected. The mnemonics for all such cards have a prefix of the letter "C" followed by an indication of the type of elements. The geometric properties such as thickness, cross-sectional areas, and moment of inertia of these elements are defined on the property definition cards that have a prefix of the letter "P" followed by the indication of the type of element. Consult Section 2.4 of the User's Manual (Ref. 1) for more details.

The elastic element contains one-, two-, and three-dimensional elements, which are discussed in the paragraphs that follow.

B-3.3.1 One-Dimensional Elements

These elements consist of bar, rod, tube, and scalar types. Each is defined in the following paragraphs:

1. *Bar Element*. The element is defined on the CBAR card, and its properties are defined on the PBAR card. It includes extension, torsion, bending in two perpendicular planes, and the associated transverse shear loads that produce only couples resulting in longitudinal stresses.
2. *Rod Element*. The element is defined on the CROD card, and its properties are defined on the PROD card. (Both the connection and property information can be simply defined on the CONROD card.) The rod element includes extensional and torsional properties only.
3. *Tube Element*. The element is defined on the CTUBE card, and its properties are defined on the PTUBE card. It is assumed to have a circular cross section and is a special form of rod element.
4. *Scalar Elements*. These elements are connected between pairs of degrees of freedom (at either scalar or geometric grid points) or between one degree of freedom and ground. Scalar elements are available as springs, masses, and viscous dampers. Scalar spring elements are useful for representing elastic properties that cannot be conveniently modeled with the usual metric structural elements. Scalar masses are useful for selective representation of inertia properties such as those that occur when a concentrated mass is effectively isolated for motion in one direction only. The scalar damper is used to provide viscous damping between two selected degrees of freedom or between one degree of freedom and ground. Refer to Sections 5.5 and 5.6 of the Theoretical Manual (Ref. 3) and Section 1.3.8 of the User's Manual (Ref. 1) for more details.

B-3.3.2 Two-Dimensional Elements

These elements consist of shear panel, twist panel, and triangular plate types. Each is defined in the following paragraphs:

1. *Shear Panel Element*. This element is defined on the CSHEAR card, and its properties are defined on the PSHEAR card. It can resist the action of tangential forces applied to its edges but cannot resist the action of normal forces.
2. *Twist Panel Element*. This element is defined on the CTWIST card, and its properties are defined on the PTWIST card. It supports only moments about in-plane axes directed out of the sides.
3. *Triangular Plate Element*. This element includes two different stress systems (membrane and bending).

THIS DOCUMENT PROVIDED BY THE ABBOTT AEROSPACE
TECHNICAL LIBRARY
ABBOTTAEROSPACE.COM

There are five different forms that are defined by connection cards, i.e.,

a. CTRMEM. Triangular element with finite in-plane stiffness, i.e., only membrane effects are considered, and zero bending stiffness. Its properties are defined on the PTRMEM card.

b. CTRBSC. Basic triangular element from which the bending properties of the other plate elements are formed. Its properties are defined on the PTRBSC card.

c. CTRPLT. Triangular element with zero in-plane stiffness and finite bending stiffness. Its properties are defined on the PTRPLT card.

d. CTRIA1. Triangular element with both in-plane and bending stiffness. It is designed for nonhomogeneous cross sections, and its properties are defined on the PTRIA1 card.

e. CTRIA2. Triangular element with both in-plane and bending stiffness. It is designed for homogeneous cross sections, and its properties are defined on the PTRIA2 card.

4. *Quadrilateral Plate Element.* This element also includes membrane and bending stress systems. There are six different forms defined by connection cards, i.e.,

a. CQDMEM. Quadrilateral element consisting of four overlapping CTRMEM elements. Its properties are defined on the PQDMEM card.

b. CQDMEM1. An isoparametric quadrilateral membrane element. Its properties are defined on the PQDMEM1 card.

c. CQDMEM2. A quadrilateral membrane element consisting of four nonoverlapping CTRMEM elements. Its properties are defined on the PQDMEM2 card.

d. CQDPLT. Quadrilateral element with zero in-plane stiffness, i.e., no membrane effects, and finite bending stiffness. Its properties are defined on the PQDPLT card.

e. CQUAD1. Quadrilateral element with both in-plane and bending stiffness. It is designed for nonhomogeneous cross sections, and its properties are defined on the PQUAD1 card.

f. CQUAD2. Quadrilateral element with both in-plane and bending stiffness. It is designed for homogeneous cross sections, and its properties are defined on the PQUAD2 card.

B-3.3.3 Three-Dimensional Element

These elements consist of conical shell, axisymmetric shell, and solid polyhedron types. Each is defined in the following paragraphs:

1. *Conical Shell Element.* This element is made up of straight-line generators but covers the range from cylinders to cones and discs. The properties of the conical shell element are assumed to be symmetrical with respect to the axis of the shell. Loads and deflections, however, need not be axisymmetric because they are expanded in a Fourier series with respect to the azimuthal coordinate. Differential stiffness options are available with this element. The element can be used to support membrane, bending, and transverse shear loads.

2. *Axisymmetric Shell Elements.* Two types of elements are provided that have an axisymmetric geometric configuration and that are restricted to axisymmetric applied loading. The first type is the ring element, which may have a triangular or trapezoidal cross section, and, in the limiting case, becomes a solid core element. (Refer to Section 5.11 of the NASTRAN Theoretical Manual (Ref. 3).) These elements are used for the modeling of axisymmetric, thick-walled structures of arbitrary profile. The second type is the toroidal ring element which, in the limiting case, becomes a cap element. (Refer to Section 5.10 of the Theoretical Manual (Ref. 3).) The element supports membrane and bending loads. These elements are used for the analysis of axisymmetric solids with axisymmetric loads.

3. *Solid Polyhedron Elements.* These elements are used to model three-dimensional elastic regions that do not have axial symmetry. The geometry of the polyhedron elements is defined by grid points at the vertices. Three types of solid polyhedron elements—a tetrahedron, a wedge, and a hexahedron—are provided for general solid structures. (Refer to Section 5.12 of the Theoretical Manual (Ref. 3) and Section 1.3.10 of the User's Manual (Ref. 1).) The tetrahedron is a triangular pyramid that can be constructed among any four noncoplanar vertices. It is the basic building block that is used to build up the other elements. The wedge is a truncated triangular pyramid defined by six vertices; it has two triangular and three quadrilateral faces. The hexahedron is a generalized cube having six quadrilateral faces.

B-4 MATERIAL PROPERTIES

The material properties are represented in as general a form as possible and are listed in Table B-1. Definitions of material properties of Table B-1 follow:

THIS DOCUMENT PROVIDED BY THE ABBOTT AEROSPACE
TECHNICAL LIBRARY
ABBOTTAEROSPACE.COM

TABLE B-1
GENERAL MATERIAL PROPERTIES

Elastic Modulus	Mass
Isotropic	Structural density
Orthotropic	Nonstructural mass
Anisotropic	Lumped properties
Temperature-dependent	Coupled properties
Stress-dependent	Weight
	Center of gravity

1. *Elastic Moduli.* These can be as simple as the usual Young's modulus, Poisson's ratio, or shear modulus; or the analyst can employ orthotropic constants or a complete anisotropic set of 21 moduli. Moduli can be made to be temperature-dependent or stress-dependent.

2. *Mass.* This is considered to be associated with grid points. Mass is subdivided into two categories: (1) structural mass determined from the density of the load-carrying members and (2) nonstructural mass determined from a distribution factor to represent such items as ablative coatings or acoustic blankets. In problems of dynamics, the forces at one point due to the influence of mass at other points are referred to as coupled mass. Weight can be determined from whatever gravitational acceleration is supplied.

Materials properties are defined on MATi, MATTi, or MAST1 cards. Consult Section 2.4 of the User's Manual (Ref. 1) for more details.

B-5 APPLIED LOADS

There are three types of applied loads, namely,

1. *Static Loads:*

Static loads are applied to geometric and scalar grid points in a variety of ways, including

a. Surface loads	Point force on grid points
	Surface pressure
b. Body force	Gravity loads
	Centrifugal steady rotational forces
	Steady accelerations
c. Induced scalar forces	Electric
	Hydraulic
d. Enforced forces	Thermal
	Element deformation
	Grid point displacements.

The LOAD card defines a static loading condition that is a linear combination of load sets and is requested in the Case Control Deck.

The different static loads are defined on FORCE, MOMENT, PLOAD2, GRAV, RFORCE, TEMPPi, and DEFORM cards.

2. *Frequency-Dependent Loads.* The DLOAD card is used to define linear combinations of frequency-dependent loads that are defined on RLOAD1 or RLOAD2 cards.

3. *Time-Dependent Loads.* The PLOAD card is used to define linear combinations of time-dependent loads that are defined on TLOAD1 or TLOAD2 cards.

B-6 NASTRAN DATA ORGANIZATION

The input deck begins with the required resident operating system control cards. The type and number of these cards will vary with the installation. The operating system control cards are followed by the NASTRAN Data Deck, which consists of three sections: (1) Executive Control Deck, (2) Case Control Deck, and (3) Bulk Data Deck. Each deck is described in the paragraphs that follow.

THIS DOCUMENT PROVIDED BY THE ABBOTT AEROSPACE
TECHNICAL LIBRARY
ABBOTTAEROSPACE.COM

B-6.1 EXECUTIVE CONTROL DECK

The Executive Control Deck identifies the job and the type of solution to be performed. It also declares the general conditions—such as maximum time allowed, type of system diagnostics desired, restart conditions, and whether or not the job is to be checkpointed—under which the job is to be executed. If the job is to be executed with a rigid format, the number of the rigid format is declared along with any alterations to the rigid format that may be desired.

The format of the Executive Control cards is free field. The name of the operation begins in column 1 and is separated from the operand by one or two blanks. Consult Section 2.2 of the User's Manual (Ref. 1) for more details. The individual Executive Control cards are

1. ID A1, A2 (Required) A1, A2. These are any legal alphanumeric fields chosen by the user for problem identification.
2. RESTART A1, A2, K1/K2/K3 (Required for Restart) A1, A2. These are fields taken from the ID card of the previously checkpointed problem. (Refer to Section 2.2 of the User's Manual (Ref. 1).) K1/K2/K3 indicates the month/day/year, respectively, that the problem tape was generated.
3. UMF K1, K2 (Required when using User's Master File). The symbol definitions are
   a. K1. User-specified tape identification number
   b. K2. Problem identification number.
4. CHKPNT A1 (Optional). The entry for the symbol A1 is "Yes, if problem is to be checkpointed; No, if problem is not to be checkpointed.".
5. APP A (Required). The entry for the symbol A indicates the approach—DISPLACEMENT, HEAT, or DMAP—to be used.
6. SOL K1 (Required when using a rigid format). The entry for the symbol K1 indicates the solution number of Rigid Format.
7. ALTER K1, K2 (Optional). The entries for the symbols K1 and K2 are the first and last DMAP instructions, respectively, of the series to be deleted and replaced with any following DMAP instructions.
8. TIME K (Required). The symbol K indicates the maximum allowable executive time in minutes.
9. ENDALTER (Required when using ALTER).
10. BEGIN (Required when using DMAP approach). This designation indicates the beginning of a DMAP sequence.
11. END (Required when using a DMAP approach). This designation indicates the end of a DMAP sequence.
12. CEND (Required). This indicates the end of Executive Control cards.

B-6.2 CASE CONTROL DECK

The Case Control Deck has several functions, namely,

1. The deck defines the subcase structure for the problem, such as
   a. SUBCASE. Defines the beginning of a subcase that is terminated by the next subcase delimiters encountered.
   b. SUBCOM. Defines a combination of two or more immediately preceding subcases in statistics problems.
   c. SUBSEQ. Gives the coefficients for making the linear combination of SUBCOM.
   d. MODES. Repeats the subcase in which it appears MODES times for eigenvalue problems.
2. The deck makes selections from the Bulk Data Deck, such as
   a. DEFORM. Selects element deformation set.
   b. LOAD. Selects static loading condition.
   c. SPC. Selects set of single-point constraints.
   d. K2PP. Selects direct-input stiffness matrices.
   e. TFL. Selects transfer functions.
   f. METHOD. Selects the conditions for real eigenvalue analysis.
   g. TEMPERATURE. Selects the thermal field for determining both the equivalent static loads and material properties.
3. The deck makes output requests for printing, punching, and plotting, such as
   a. TITLE. Defines a text to be printed on the first line of each page of output.
   b. LABEL. Defines a text to be printed on the third line of each page of output.

THIS DOCUMENT PROVIDED BY THE ABBOTT AEROSPACE
TECHNICAL LIBRARY
ABBOTTAEROSPACE.COM

c. ECHO. Selects echo options for Bulk Data Deck.
d. SET. Defines the lists of point numbers, element numbers, or frequencies for use in output requests.
e. SACCELERATION. Requests the acceleration of the independent components for a selected set of points of modal coordinates for problems in dynamics.
f. ELFORCE. Requests the forces in a set of structural elements.
g. STRESS. Requests the stresses in a set of structural elements.
h. SPCFORCE. Requests the single-point forces of constraint at a set of points.
i. DISPLACEMENT. Requests the displacements for a selected set of physical points.

B-6.3 BULK DATA DECK

The primary NASTRAN input medium is the Bulk Data Deck. These cards contain all the details—such as geometric properties, material properties, elements, constraints, and applied loads—of the structural model and various conditions for the solution. The bulk data card format is variable to the extent that any quantity except the mnemonic can be punched anywhere within a specified 8- or 16-column field.

For large problems the Bulk Data Deck may consist of several thousand cards. The detailed descriptions of the bulk data cards are contained in the NASTRAN User's Manual (Ref. 1), Section 2.4.

B-7 SUMMARY OF NASTRAN STRESS ANALYSIS PROCEDURE

The entire procedure for analysis of a structure may be summarized as

1. Step 1. The first step in analysis of a structure by NASTRAN is to develop a finite element idealization for the structure. In this step, choose a global coordinate system and introduce a finite element grid for the structure.
2. Step 2. Depending on the type of structure and externally applied loads, select a set of structural elements that models the structure as accurately as possible. Modeling of the structure is discussed in par. B-3.
3. Step 3. Number the elements and grid points.
4. Step 4. Compute coordinates of every grid point corresponding to the global coordinate system.
5. Step 5. Identify boundary conditions for the structure.
6. Step 6. Identify loading systems acting on the structure.
7. Step 7. Depending on the type of problem, select a Rigid Format for structural analysis.
8. Step 8. Prepare the Bulk Data Deck for the problem.
9. Step 9. Prepare proper Executive Control and Case Control Decks.

REFERENCES

1. NASTRAN User's Manual, SP 222 (Available from: COSMIC, 112 Barrow Hall, University of Georgia, Athens, GA).
2. NASTRAN Programmer's Manual, SP 223 (Available from: COSMIC, 112 Barrow Hall, University of Georgia, Athens, GA).
3. NASTRAN Theoretical Manual, SP 221 (Available from: COSMIC, 112 Barrow Hall, University of Georgia, Athens, GA).

THIS DOCUMENT PROVIDED BY THE ABBOTT AEROSPACE
TECHNICAL LIBRARY
ABBOTTAEROSPACE.COM

APPENDIX C
STRESS ANALYSIS BY FINITE ELEMENTS

This appendix presents an introduction to the finite element method of stress analysis. Stress analysis of structural components that are subjected to quasi-static loads is discussed first. Then dynamic stress analysis of structural components is presented followed by the finite element modeling of structural systems. A procedure for developing elemental stiffness and mass matrices for various elements is described. Synthesis of stiffness and mass matrices for the entire finite element model of the system is also discussed.

C-0 LIST OF SYMBOLS

A = cross-sectional area, m^2
$[A]$ = Boolean transformation matrix, dimensionless
$[A^i]$ = Boolean transformation matrix for ith finite element, dimensionless
$[B]$ = matrix obtained by differentiating matrix $[N]$, m^{-1} or dimensionless
$[C]$ = generalized damping matrix, N·s/m, N·s/rad, N·s, or N·m·s/rad
C_c = critical damping, N·s/m
$[\bar{C}]$ = matrix defined by Eq. C-54
c = damping coefficient, N·s/m
$[D]$ = matrix of elastic constants, Pa
E = Young's modulus, Pa
F = vector function of loads applied inside finite element, N or N·m
$F(t)$ = applied forcing function, N or N·m
f = displacement function as defined in Eq. C-1, m
= 2×1 vector function for a plane body and 3×1 for a three-dimensional body representing displacement field, m
$\dot{f}$ = velocity function, m/s
I = moment of inertia, m^4
$[I_3]$ = 3×3 identity matrix, dimensionless
$[K]$ = structural stiffness matrix synthesized from element stiffness matrices, N, N/m, N/rad, or N·m/rad
$[\bar{K}]$ = matrix defined in Eq. C-46 or Eq. C-50, N·m
k = spring constant, N/m
$[k]$ = element stiffness matrix in global coordinate system, N, N/m, N/rad, or N·m/rad
$[k']$ = element stiffness matrix in local coordinate system, N/m
$[k^i]$ = stiffness matrix for ith element in global coordinate system, N, N/m, N/rad, or N·m/rad
$[\bar{k}]$ = composite stiffness matrix whose each diagonal element is a submatrix representing stiffness matrix for a finite element, N, N/m, N/rad, or N·m/rad
k_i = ith spring constant, N/m
L = length of member or element, m
M = oscillator mass, kg
$[M]$ = generalized mass matrix for system, kg, kg·m, or $kg·m^2$
$[\bar{M}]$ = matrix defined in Eq. C-46 or C-50, $kg·m^2$
m = element of generalized mass matrix in the global coordinate system, kg, kg·m, $kg·m^2$

THIS DOCUMENT PROVIDED BY THE ABBOTT AEROSPACE
TECHNICAL LIBRARY
ABBOTTAEROSPACE.COM

$[m^i]$ = generalized mass matrix for ith finite element in global coordinate system, kg, kg·m, or kg·m^2
$[m']$ = element of generalized mass matrix in local coordinate system, kg, kg·m, or kg·m^2
$[m'(1)]$ = generalized mass matrix defined in Eq. C-37, kg, kg·m, or kg·m^2
$[m'(2)]$ = generalized mass matrix defined in Eq. C-38, kg, kg·m, or kg·m^2
m_i = ith mass, kg, kg·m, or kg·m^2
$[N]$ = matrix of known functions, dimensionless
NE = total number of finite elements, dimensionless
p = vector of element nodal forces, N or N·m
p' = equivalent nodal forces, N or N·m
p' = vector of generalized nodal forces corresponding to nodal displacements r', N or N·m
p'_ℓ = ℓth generalized nodal force, N or N·m
$\bar{p}$ = composite vector of element nodal forces, N or N·m
r = vector of element generalized nodal displacements in global coordinate system, m or rad
r' = vector of generalized nodal displacements for an element in a local coordinate system, m or rad
r'_ℓ = ℓth generalized nodal displacement in local coordinate system, m or rad
$\bar{r}$ = composite vector of element nodal displacements in global coordinate system, m or rad
S = vector of generalized nodal forces or loads, N or N·m
= equivalent load vector, n
$S(t)$ = vector of generalized nodal forces, N or N·m
$\bar{S}$ = vector defined by Eq. C-55
s_i = ith force, N
T = kinetic energy of an element, J
t = thickness, m
= time, s
u = x-displacement, m
V = volume, m^3
= volume of element, m^3
= potential energy, J
v = y-displacement, m
v_0 = vector of initial generalized velocities, m/s or rad/s
v_0 = initial velocity, m/s
w = z-displacement, m
$[X^{(0)}]$ = $n \times q$, matrix each column of which is assumed eigenvectors, m or rad
x', y', z' = local coordinate system, m
$[Y^{(0)}]$ = matrix defined in Eq. C-48
y = eigenvector or mode shape, rad or m
y^i = ith eigenvector, rad or m
z = vector of independent generalized nodal displacements for finite element model, m or rad
z = displacement in basic oscillator model, m
z_i = ith generalized displacement degree of freedom, m
z_0 = vector of initial generalized displacements, m or rad
z_0 = initial displacement, m
ϵ = strain vector, dimensionless

THIS DOCUMENT PROVIDED BY THE ABBOTT AEROSPACE
TECHNICAL LIBRARY
ABBOTTAEROSPACE.COM

ζ = damping ratio, dimensionless
= eigenvalue, s^{-2}
= damping coefficient, dimensionless
= eigenvalue, $(rad/s)^2$
ζ_i = ith eigenvalue, $(rad/s)^2$
$\eta = y'/L$, dimensionless
$\eta(t)$ = vector of normal coordinates, dimensionless
η_0 = vector of initial coordinates, m or rad
θ = phase angle, rad
$[\lambda]$ = transformation matrix constructed from direction cosines of local coordinate system relative to global coordinate system, dimensionless
$\xi = x'/L$, dimensionless
ρ = mass density, kg/m^3
σ = vector of stresses, Pa
τ = variable of integration, s
$[\Phi]$ = matrix each column of which is a mode shape (modal matrix), m or rad
$[\bar{\Phi}]$ = $q \times q$ matrix each column of which is the unknown multipliers (eigenvectors) of the transformation, dimensionless
ω = system natural frequency, rad/s
ω_D = damped natural frequency, rad/s
$[\Omega^2]$ = diagonal matrix in which each diagonal term is the square of the frequency, s^{-2}

C-1 INTRODUCTION

The finite element technique was developed in the 1950s by structural engineers for the analysis of structural systems. The excellent performance of the method led to research that put it on a firm mathematical foundation in the mid-1960s when a variational formulation of the method was developed. The latter formulation is quite general and allows the use of the finite element method in other engineering fields such as fluid mechanics, heat transfer, and in general problems of mathematical physics. In this appendix the finite element method is presented as an analysis technique for complex structural systems.

The finite element technique has not been used very extensively for stress analysis of artillery systems. Some applications, however, of the method to advanced problems in artillery systems appeared as early as 1970 (Ref. 1). In 1974 the NASTRAN computer program was used to analyze the elevating bracket for the M109 Self-Propelled Howitzer (Ref. 2). Application of the finite element stress analysis method to weapon design problems is expected to increase significantly.

Several commercially available general-purpose computer programs based on the finite element method have been developed for stress analysis. The conclusion that this method has been well accepted by the industrial community is based on the fact that most design offices have either their own or have access to several standard computer programs for stress analysis. Many of these programs are interactive and allow the designer to observe various outputs almost instantaneously. While sitting at a terminal, a designer can change the design of a system and obtain its response immediately. This is referred to as computer-aided design.

The basic procedure of finite element stress analysis is first to develop a finite element model of the desired structural system. This includes definition of the geometry of the structure, material properties, sizes of various parts, support conditions for the structure, types of finite elements to be used to represent the structure, finite element mesh, and loading conditions. Development of the finite element model requires time, effort, and knowledge of the general behavior of the structure. To facilitate development of the geometric model, computer programs are available that automatically assign nodal coordinates and finite elements. Many of these programs are interactive and can give plots of the finite element model on a graphics terminal. By using this capability, designers can quickly verify the model. Once the basic model has been developed, designers can

THIS DOCUMENT PROVIDED BY THE ABBOTT AEROSPACE
TECHNICAL LIBRARY
ABBOTTAEROSPACE.COM

use it to advantage in analyzing the system for various loading and support conditions. The designer can readily change the basic geometry of the structure or its parts—thickness, depth, width, etc.—and study the effects of the changes on the response of the system. Designers can also change the support conditions and study different loading cases in a relatively short time. In other words, once the finite element model has been developed, the designer has a tool with which to perform different analyses in a short time and to develop an acceptable design of the system.

This appendix presents an introduction to the theory of the finite element method. Development of the method for dynamic response problems is also presented. For a more detailed presentation of the theory of the method, excellent textbooks are available (Refs. 3, 4, and 5). For more advanced topics on the finite element methods, Refs. 6 and 7 should be consulted. It is emphasized that finite element analysis is *not* for use by beginners. The prerequisites for the use of finite element analysis are

1. A good, reliable computer program
2. A designer experienced in the field or with a thorough theoretical knowledge of the method
3. A designer astute enough and experienced enough to verify the analysis with testing; the computer results should not be regarded as infallible truth.

To set the stage for a discussion of finite element stress analysis, consider an elastic solid of arbitrary shape that is rigidly supported and subjected to externally applied loads as shown in Fig. C-1. To analyze the deformation of the solid, the designer might attempt to integrate the equilibrium equations of elasticity subject to an appropriate set of boundary conditions. In general this problem is quite difficult, if not impossible, to solve. This approach has been followed for solids with regular shapes, simple boundary conditions, and regular loads. For irregular solids with complex boundary conditions subjected to irregular loads, the theory of elasticity approach is quite difficult to use. For such problems a numerical method for stress analysis is needed, and the finite element method is such a method. The method is very powerful and useful because it can treat irregular shapes, complex boundary conditions, and complex loading cases.

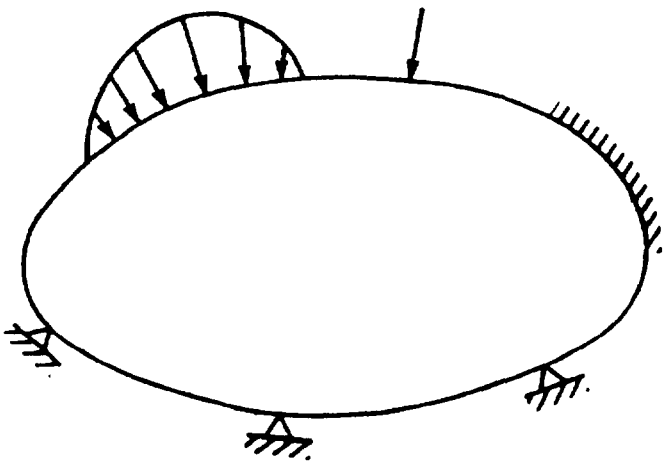

Figure C-1. Elastic Solid of Arbitrary Shape

The finite element method is based on a firm mathematical foundation (variational principles), which can be quite sophisticated and complex. In this appendix, however, a more physical approach for the method is adopted. The basic idea of the finite element method based on this approach is to divide the structure, or the structural component, whose stress analysis is desired into a number of finite elements, i.e., a number of smaller pieces. The structure may have an irregular shape and complex boundary conditions, but each of the finite elements has well-defined, regular boundaries and specific points of load application. These finite elements are assumed to be connected only at the end points, and all loads are assumed to be applied at the end points. These assumpions imply that all the loads applied inside the finite element must be transferred to the nodal points, and the equivalent load concept is used to accomplish this objective. Equilibrium equations for a finite element can be obtained in a matrix form that involves forces and displacements at the end points and also the element material and geometric properties. This is explained later in the appendix. Equilibrium

THIS DOCUMENT PROVIDED BY THE ABBOTT AEROSPACE
TECHNICAL LIBRARY
ABBOTTAEROSPACE.COM

equations for all finite elements are then combined to obtain an equilibrium equation for the entire system, and this equation is solved for the unknown displacements at the grid points. From these displacements stresses are calculated. The mathematics of this procedure is developed in the appendix.

C-2 STRESS ANALYSIS FOR QUASI-STATIC LOADING

In this paragraph the finite element procedures for stress analysis of structures and structural components subjected to quasi-static loads is described. Loads such as uniform pressures, concentrated loads, gravity loads, thermal loads, initial strains, and loads due to other body forces are discussed. The basic ideas of finite element modeling are also discussed, and equilibrium equations for a finite element are derived. The idea of transforming elemental equilibrium equations from a local to a global coordinate system is presented. Finally, a procedure for generating equilibrium equations for the entire finite element model of the structure is described.

It should be noted that there are three finite element methods that have been developed during the past two decades, i.e.,

1. Stiffness, or displacement, method, in which displacements at various points of the structure are the primary solution variables. By the use of these displacements, stresses are calculated at any point on the structure
2. Flexibility or force method, in which internal forces or stresses are the primary solution variables
3. Hybrid method, in which both displacements and stresses at certain points are the primary solution variables. The displacement method is the most versatile and widely used method of stress analysis, and most computer programs for stress analysis are based on this method. Therefore, only this method is described in this appendix.

C-2.1 FINITE ELEMENT MODELING

Development of a finite element model for the structure or the structural component is quite crucial for proper stress analysis. Accordingly, designers should take time to develop a proper finite element model for the system.

Development of a finite element model for a system involves the definition of a network of grid points for the structure, selection of proper finite elements to represent behavior of the structure, definition of geometric properties (cross-sectional area, thickness, moment of inertia, and other such data), specification of material properties, definition of proper boundary conditions, specification of loads for various loading cases, and the assumption of a proper displacement field for each finite element. Thus development of a proper finite element model can be a time-consuming and costly step. Proper software and hardware can greatly facilitate this task for the designer.

Several finite elements are usually incorporated into commercially available computer programs. Here only a few of the basic finite elements are described to introduce the concept of nodal displacements of finite elements. Fig. C-2 shows four typical finite elements. In this figure the following notation is used:

r'_ℓ = ℓth generalized nodal displacement in local coordinate system, m or rad
p'_ℓ = ℓth generalized nodal force, N or N·m
x', y', z' = local coordinate system, m
L = length of element, m
E = Young's modulus, Pa
A = cross-sectional area, m^2
I = moment of inertia, m^4
t = thickness, m.

The spatial truss element of Fig. C-2(A) has six nodal degrees of freedom. These are displacements in the x'-, y'-, z'-directions of nodes 1 and 2 designated as r'_1 to r'_6. This element is capable of resisting only axial forces just as members of a truss structure. Thus the element can be used to model axial force members such as springs, axial compression, and tension members.

The planar beam element of Fig. C-2(B) also has six nodal degrees of freedom. These are displacements in the x'- and y'-directions of nodes 1 and 2, and rotation about the z'-axis of ends 1 and 2. These generalized displacements are designated as r'_1 to r'_6. The element is capable of carrying loads in the $x'y'$-plane and moments

THIS DOCUMENT PROVIDED BY THE ABBOTT AEROSPACE
TECHNICAL LIBRARY
ABBOTTAEROSPACE.COM

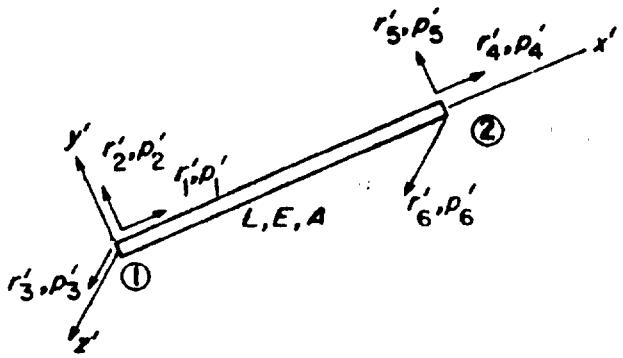

(A) Typical Truss Element With Nodal Displacements and Forces in a Local Reference Frame

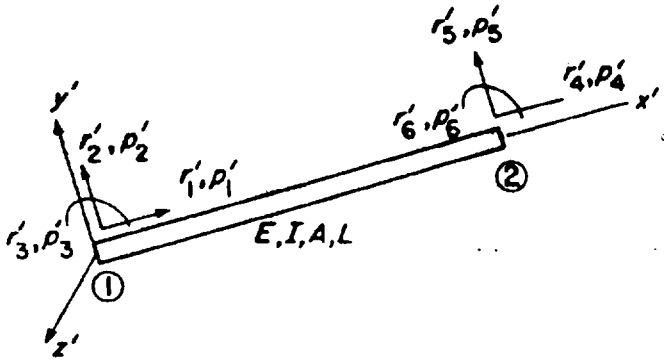

(B) A Typical Planar Beam Element With Nodal Displacements and Forces in a Local Reference Frame

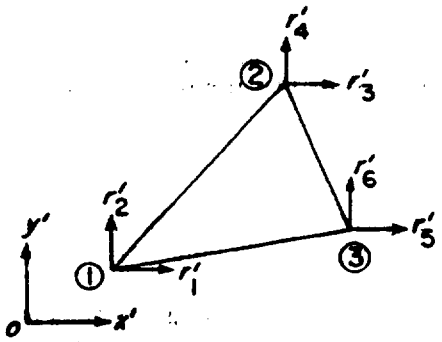

(C) Triangular Plate Element (inplane forces)

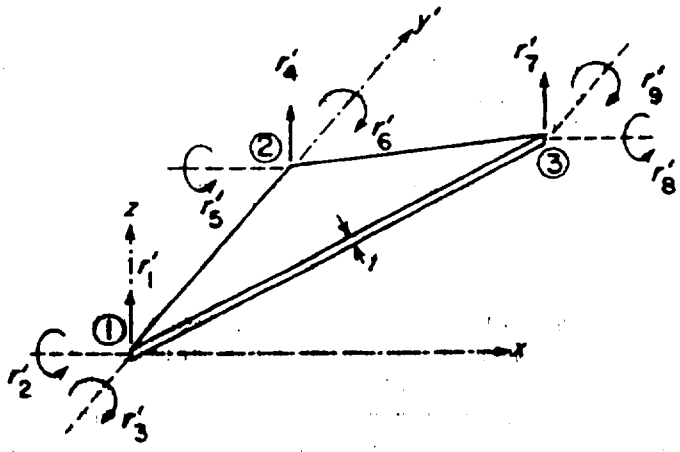

(D) Triangular Plate Element in Bending

Figure C-2. Some Finite Elements

about the z'-axis. Long, slender members of a structural system can be modeled by using this finite element. A spatial beam element having 12 degrees of freedom can be used to model three-dimensional structural systems. The truss and beam finite elements are called the line elements.

Fig. C-2(C) shows a triangular plate element capable of carrying in-plane forces. This element can be used to model plane elasticity problems, i.e., plane stress or plane strain problems. The element has six nodal degrees of freedom. These are x'- and y'-displacements of the three nodal points.

Fig. C-2(D) shows a triangular plate bending element. This element is capable of carrying loads normal to the $x'y'$-plane and should be used to model thin, flat members that are subjected to normal loads causing bending of the member. The element has nine degrees of freedom. Displacement in the z'-direction and rotation about the x'- and y'-axes are the three generalized displacement variables at each node of the element. Many other plate-bending elements have been developed.

There are many other finite elements that may be used to model a structural system. These include tetrahedron and hexahedron elements to model three-dimensional solids, quadrilateral plate elements, axisymmetrical elements, shell elements, and other higher order elements. The designer should consult the

THIS DOCUMENT PROVIDED BY THE ABBOTT AEROSPACE
TECHNICAL LIBRARY
ABBOTTAEROSPACE.COM

software user's manual to become familiar with the finite element library available in the computer program. Most of these finite elements can be combined to model complex structural systems.

As an example of modeling of a structural system, consider a hollow rectangular cantilever beam shown in Fig. C-3. For stress analysis several finite element models for the beam can be developed. The simplest of these is a line element model that uses a general beam element. A beam finite element model of the cantilever beam is shown in Fig. C-4(A). The model may consist of several nodal points. Depending upon the type of loads the

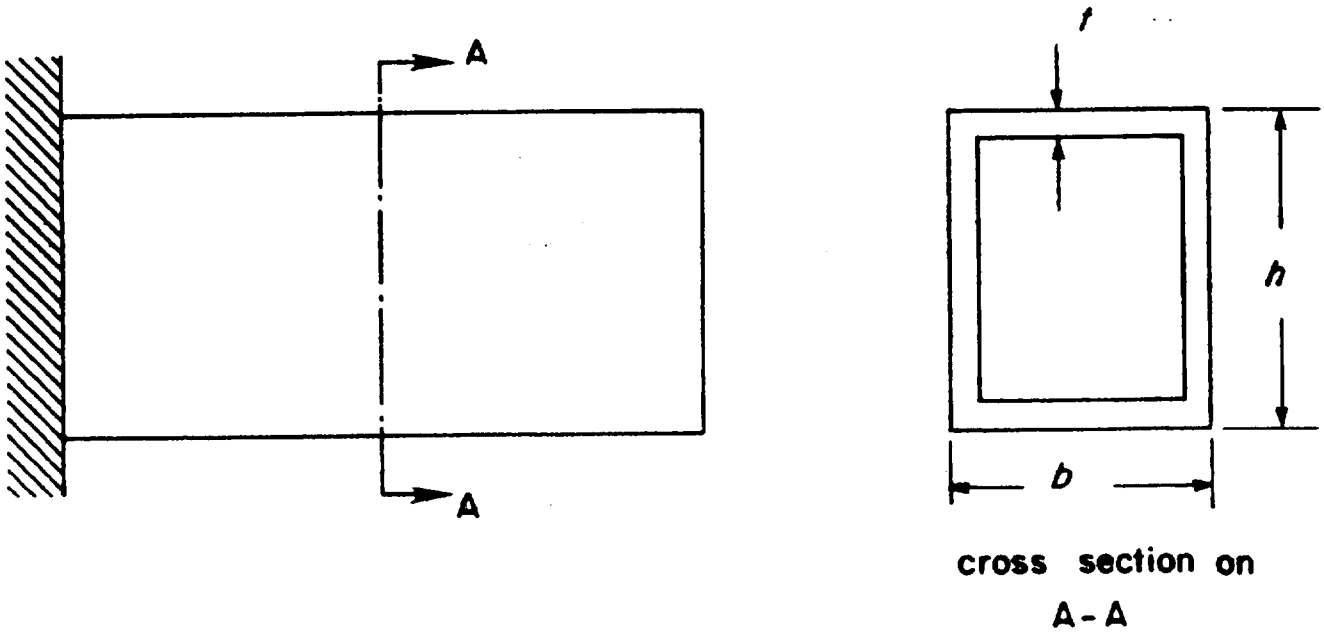

Figure C-3. Hollow Rectangular Cantilever Beam

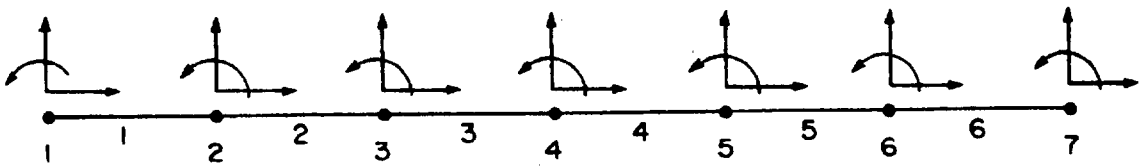

(A) A Planar Beam Finite Element Model

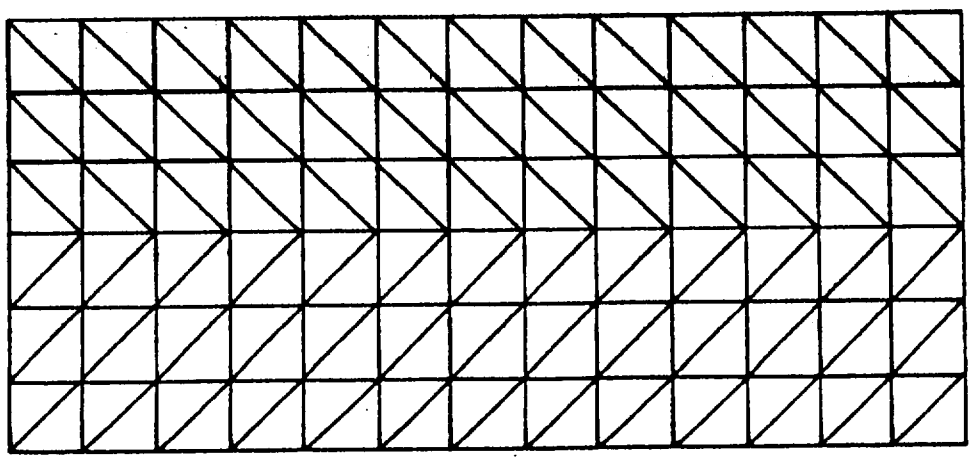

(B) Plate Finite Element for One Surface

Figure C-4. Finite Element Models for Hollow Rectangular Beam

THIS DOCUMENT PROVIDED BY THE ABBOTT AEROSPACE
TECHNICAL LIBRARY
ABBOTTAEROSPACE.COM

member supports, planar or three-dimensional beam elements can be used. For the planar beam finite element model, each node has three degrees of freedom, as shown in Fig. C-4(A); for the general three-dimensional beam finite element model, each node has six degrees of freedom. To complete the beam-type finite element model of the cantilever beam, the designer needs to calculate various cross-sectional properties for all finite elements. Properties such as moments of inertia, section moduli, shear stress factors, torsional constant, and cross-sectional area must be specified. Also the boundary condition that node 1 is completely fixed (zero degrees of freedom) must be specified.

The cantilever beam can also be modeled using triangular or quadrilateral plate finite elements. For this model, each of the four sides of the beam has a network of grid points, as shown in Fig. C-4(B). Each of the nodal points can have three or six degrees of freedom, depending on the type of finite elements used. The total number of degrees of freedom for the model depends on the total number of nodes used. Cross-sectional properties needed to complete the plate finite element model for the beam are thickness of the plate and its moment of inertia about the middle surface.

Both models can be used for stress analysis of the beam. The plate model generally requires a large number of nodes for reasonably accurate stress analysis. Plate elements, however, can be used to great advantage in modeling irregular shapes, holes, and abrupt changes in the geometry. The beam model requires a considerably smaller number of nodes. However, a lot more data for each finite element must be calculated by hand to complete the model. For long, slender members having reasonably smooth geometry, the beam-type finite element model is quite reasonable and is the most economical way of predicting stresses. For short, thick members for which geometry changes are abrupt, the plate-type finite element should be used.

C-2.2 ELEMENT STIFFNESS PROPERTIES

For stress analysis of elastic structural and mechanical systems, displacements of all the nodal points of the system are the primary unknowns. Once these displacements are known, strains and stresses are readily calculated. The basic idea of the finite element technique is to express the displacement field inside a body in terms of known functions (usually polynominals) and displacements at predetermined points on the body. These points are selected as a systematic network of grid points (the finite element grid) called "nodal points", and their displacements are called "nodal displacements". Therefore, in the finite element technique, the displacements at all points of the system are known once the nodal displacements have been determined. The nodal displacements are calculated by solving a system of algebraic equilibrium equations for the entire body. The advantage of the finite element technique of stress analysis is that the equilibrium equations for the entire body can be constructed from equilibrium equations for individual finite elements. The equilibrium equations for many standard elements are available in the literature (Refs. 3 through 7). This subparagraph presents a way of developing the finite element equilibrium equations in terms of the nodal displacements.

A note about units of various quantities used in finite element analysis is in order. The units for generalized displacements are meters or radians, and the units for generalized forces are newtons or newton · meters. The units for other quantities should be derived from the preceding definitions. For example, the units of a stiffness coefficient may be newtons, newtons per meter, newtons per radian, or newton·meters per radian. For some matrices, units are not shown because each coefficient can have different units.

Once a finite element grid has been defined on a body, it is assumed that the finite elements are only connected at nodal points. Let the displacement field for a finite element be represented as

$$f = [N]r', \text{ m} \qquad \text{(C-1)}$$

where

f = 2×1 vector function for a plane body and 3×1 for a three-dimensional body representing the displacement field, m

$[N]$ = matrix of known functions, dimensionless for translations and meters for rotations

r' = vector of generalized nodal displacements for an element, m or rad.

Dimensions of the matrix $[N]$ and the vector r' depend on the number of degrees of freedom of the element. The matrix $[N]$ is also referred to as the "shape function".

THIS DOCUMENT PROVIDED BY THE ABBOTT AEROSPACE
TECHNICAL LIBRARY
ABBOTTAEROSPACE.COM

As examples of shape functions, consider the spatial truss and planar beam elements shown in Figs. C-2(A) and C-2(B), respectively. In these figures, end displacements and forces are shown in a local coordinate system. For the truss element of Fig. C-2(A), displacement components inside the element are functions of only the coordinate x'. The displacement function of Eq. C-1 in this simple case is given as

$$\begin{bmatrix} u \\ v \\ w \end{bmatrix} = \begin{bmatrix} (1-\xi) & 0 & 0 & \xi & 0 & 0 \\ 0 & (1-\xi) & 0 & 0 & \xi & 0 \\ 0 & 0 & (1-\xi) & 0 & 0 & \xi \end{bmatrix} \begin{bmatrix} r_1' \\ r_2' \\ r_3' \\ r_4' \\ r_5' \\ r_6' \end{bmatrix} \quad \text{(C-2)}$$

where

$\xi = x'/L$, dimensionless
u,v,w = x-, y-, and z-displacements, respectively, m.

From Eq. C-2 the shape function $[N(x')]$ can be readily identified. Similarly, for the beam element of Fig. C-2(B), the displacement function of f equals $[u(x',y')\ v(x',y')]^T$. The shape function $[N(x',y')]$ is obtained by solving the elementary beam differential equation. If shear deformation effects are neglected, the shape function is given as

$$[N] = \begin{bmatrix} (1-\xi) & 6(\xi-\xi^2)\eta & -(1-4\xi+3\xi^2)\eta L & \xi \\ 0 & (1-3\xi^2+2\xi^3) & \xi(1-2\xi+\xi^2)L & 0 \\ -6(\xi-\xi^2)\eta & (2\xi-3\xi^2)\eta L & & \\ \xi^2(3-2\xi) & \xi^2(-1+\xi)L & & \end{bmatrix}, \text{ dimensionless or m} \quad \text{(C-3)}$$

where

$\xi = x'/L$, dimensionless
$\eta = y'/L$, dimensionless.

It is noted here that, in general, the shape functions are selected to satisfy proper smoothness properties (continuity and differentiability). This is done to obtain a displacement field that satisfies certain smoothness properties as we go from one finite element to an adjoining finite element. This requirement for the shape functions is based on the desire to obtain a reasonable approximation of the solution by using the finite element method. Also these requirements guarantee improvement of the finite element solution as the finite element mesh is further refined.

The displacement field of Eq. C-1 is now used to obtain the strains

$$\epsilon = [B]r', \text{ dimensionless} \quad \text{(C-4)}$$

where

ϵ = strain vector, dimensionless
$[B]$ = matrix obtained by differentiating terms in the matrix $[N]$, m^{-1} or dimensionless.

Thus Eq. C-4 expresses the strain field for the finite element in terms of the generalized nodal displacements r'. For the truss element of Fig. C-2(A), there is only axial strain ($\epsilon_x = \partial u/\partial x'$) and the matrix $[B]$ of Eq. C-4 is just

$$[B] = \frac{1}{L}[-1 \quad 0 \quad 0 \quad 1 \quad 0 \quad 0], \ m^{-1}. \quad \text{(C-5)}$$

THIS DOCUMENT PROVIDED BY THE ABBOTT AEROSPACE
TECHNICAL LIBRARY
ABBOTTAEROSPACE.COM

For the beam element of Fig. C-2(B), there is only axial strain ($\epsilon_x = \partial u/\partial x'$) due to the elementary beam theory, and the matrix $[B]$—obtained by differentiating the first row of matrix $[N]$ in Eq. C-3 by ξ—is

$$[B] = \frac{1}{L}[-1 \quad 6(1-2\xi)\eta \quad 2(2-3\xi)\eta L \quad 1 \quad 6(2\xi-1)\eta \quad 2(1-3\xi)\eta L],$$
$$m^{-1} \text{ or dimensionless.} \tag{C-6}$$

The equilibrium equations for an element can now be obtained from the principle of virtual work, or stationary potential energy. By writing the virtual work of all the forces and equating it to zero, the result is

$$\int_V \delta\epsilon \cdot \sigma dV - \delta r' \cdot p' = 0 \tag{C-7}$$

where

σ = vector of stresses, Pa
p' = vector of generalized nodal forces that correspond to nodal displacements r', N or N·m
V = volume of element, m^3.

Note that in Eq. C-7 the integration over the volume of the element is denoted symbolically as $\int_V$. To express Eq. C-7 in a more usable form, a stress-strain law is required. The generalized Hooke's Law is used, which, in matrix notation, is

$$\sigma = [D]\epsilon, \text{ Pa} \tag{C-8}$$

where

$[D]$ = matrix of elastic constants, Pa.

By substituting Eqs. C-4 and C-8 into Eq. C-7, the principle of virtual work is expressed as

$$\delta r' \cdot [(\int_V [B]^T[D][B]dV r') - p'] = 0. \tag{C-9}$$

Since all components of $\delta r'$ are arbitrary, Eq. C-9 is satisfied only when the term in square brackets is zero, or

$$p' = [k']r', \text{ N or N·m} \tag{C-10}$$

where the matrix $[k']$ is given as

$$[k'] = \int_v ([B]^T[D][B])dV, \text{ N, N/m, N/rad, or N·m/rad.} \tag{C-11}$$

The symmetric matrix $[k']$ is called the element stiffness matrix in a local coordinate system. The term k'_{ij} in the matrix $[k']$ can be interpreted as the nodal force in the ith direction due to a unit displacement in the jth direction. Note that elements of the matrix $[k']$ can be derived directly by the use of this physical interpretation of the terms k'_{ij}.

For the truss and beam elements of Figs. C-2(A) and C-2(B), the matrix $[D]$ is simply the scalar $D = E$. By substituting approximate matrices $[B]$ and $[D]$ into Eq. C-11 and carrying out the indicated integration, the element stiffness matrix for the truss element is

$$[k'] = \frac{AE}{L}\begin{bmatrix} 1 & 0 & 0 & -1 & 0 & 0 \\ & 0 & 0 & 0 & 0 & 0 \\ & & 0 & 0 & 0 & 0 \\ & & & 1 & 0 & 0 \\ \text{Symmetric} & & & & 0 & 0 \\ & & & & & 0 \end{bmatrix}, \text{ N/m} \tag{C-12}$$

THIS DOCUMENT PROVIDED BY THE ABBOTT AEROSPACE
TECHNICAL LIBRARY
ABBOTTAEROSPACE.COM

and for the beam element is

$$[k'] = \frac{EI}{L^3}\begin{bmatrix} \frac{AL^2}{I} & 0 & 0 & -\frac{AL^2}{I} & 0 & 0 \\ & 12 & 6L & 0 & -12 & 6L \\ & & 4L^2 & 0 & -6L & 2L^2 \\ & & & \frac{AL^2}{I} & 0 & 0 \\ & \text{Symmetric} & & & 12 & -6L \\ & & & & & 4L^2 \end{bmatrix}, \text{N, N/m, N/rad, or N·m/rad} \quad \text{(C-13)}$$

where

I = moment of inertia, m^4.

Before a stiffness matrix for the entire structure can be constructed, element stiffness matrices must be transformed into the global coordinate system. The element force-displacement relationship in the global coordinate system is written as

$$p = [k]r, \text{ N} \quad \text{(C-14)}$$

where

p = vector of element nodal forces, N or N·m
r = vector of nodal displacement, m or rad
$[k]$ = element stiffness matrix in global coordinate system, N, N/m, N/rad, or N·m /rad.

Let the transformation from a local to the global system be defined as

$$r' = [\lambda]r, \text{ m or rad} \quad \text{(C-15)}$$

where

$[\lambda]$ = transformation matrix constructed from direction cosines of local coordinate system relative to global coordinate system, dimensionless.

From equivalence of the virtual work of forces p and p', the equation for p becomes

$$p = [\lambda]^T p', \text{ N or N/m.} \quad \text{(C-16)}$$

By substituting Eqs. C-10 and C-15 into Eq. C-16 and comparing the result with Eq. C-14, the element stiffness matrix $[k]$ is identified as

$$[k] = [\lambda]^T[k'][\lambda], \text{ N, N/m, N/rad, or N·m/rad.} \quad \text{(C-17)}$$

C-2.3 EQUILIBRIUM EQUATIONS FOR FINITE ELEMENT MODEL

Let z be a vector of independent generalized displacements and S be a corresponding vector of equivalent nodal forces for the entire finite element model of the structural system. Then the equilibrium equation in terms of displacements for the entire system is given as (Refs. 3 to 7)

$$[K]z = S, \text{ N or N·m} \quad \text{(C-18)}$$

THIS DOCUMENT PROVIDED BY THE ABBOTT AEROSPACE
TECHNICAL LIBRARY
ABBOTTAEROSPACE.COM

where

$[K]$ = structural stiffness matrix synthesized from element stiffness matrices, N, N/m, N/rad, or N·m/rad.

Let

$\bar{p}$ = composite vector of element nodal forces, N or N·m
$\bar{r}$ = composite vector of element nodal displacements, m or rad
$[\bar{k}]$ = composite stiffness matrix whose end diagonal element is a submatrix representing stiffness matrix for a finite element, N, N/m, N/rad, or N·m/rad,

then the equilibrium equation for all the finite elements is compactly written in matrix form as

$$\bar{p} = [\bar{k}]\bar{r}, \text{ N or N·m.} \tag{C-19}$$

Now a compatibility relationship between $\bar{r}$ and z is expressed as

$$\bar{r} = [A]z, \text{ m} \tag{C-20}$$

where

$[A]$ = Boolean matrix each row of which has a unit element in only one position that relates a component of $\bar{r}$ to a component of z, dimensionless.

The equilibrium equation between S and $\bar{p}$ is obtained by using the principle of virtual work as

$$S = [A]^T\bar{p}, \text{ N or N/m.} \tag{C-21}$$

By substituting Eqs. C-19 and C-20 into Eq. C-21 and comparing the result with Eq. C-18, the equation for $[K]$ becomes

$$[K] = [A]^T[\bar{k}][A], \text{ N, N/m, N/rad, or N·m/rad} \tag{C-22}$$

which is a general equation for synthesizing the structural stiffness matrix. Eq. C-22 may be written as the summation

$$[K] = \sum_{i=1}^{NE}[A^i]^T[k^i][A^i], \text{ N/m} \tag{C-23}$$

where the superscript i refers to the ith finite element and

NE = total number of finite elements, dimensionless
$[A^i]$ = Boolean matrix for ith finite element, dimensionless.

Before Eq. C-18 can be solved for nodal displacements of the finite element model, the equivalent load vector S must be determined. Let

F = vector function of loads applied inside finite element, N or N·m
p' = vector of equivalent generalized nodal forces, N or N·m.

From the equivalence of virtual work of the forces F and p',

$$p' = \int_V [N]^T F dV, \text{ N or N/m.} \tag{C-24}$$

By using Eq. C-24, the forces that are applied inside the element are transformed to equivalent nodal forces. These forces, when combined with the other externally applied loads at the nodal points, then give the force vector S that is used in Eq. C-18.

THIS DOCUMENT PROVIDED BY THE ABBOTT AEROSPACE
TECHNICAL LIBRARY
ABBOTTAEROSPACE.COM

C-2.4 SUMMARY OF PROCEDURE

The entire procedure for the calculation of nodal displacements, stresses, and strains at various points of a structure is summarized in the following steps:

1. Step 1. Make the continuum discrete by introducing the finite element grid, numbering the nodes, and numbering the elements. Select proper finite elements for the model. Identify boundary conditions.
2. Step 2. Select interpolation functions for the finite elements as in Eq. C-1.
3. Step 3. Compute element stiffness matrices by using Eq. C-11. Note that boundary conditions are imposed after assembling the structural stiffness matrix $[K]$.
4. Step 4. Solve matrix Eq. C-18.
5. Step 5. Calculate stresses by using Eqs. C-20, C-15, C-4, and C-3.
6. Step 6. Calculate additional displacements, if necessary, by using Eq. C-1.

Since this procedure is programmed in several commercially available computer programs, the designer has only to develop a finite element model mentioned in Step 1 according to the requirements for the input data for the available computer program. All other steps are carried out automatically by the program.

C-3 INTRODUCTION TO DYNAMIC STRESS ANALYSIS

In this paragraph, a method for stress analysis of structures and structural elements subjected to dynamic loads is presented. It is clear that the components of the towed artillery system are subjected to transient dynamic loads during firing and transportation. In the past, the quasi-static methods of stress analysis and design presented in this handbook were adequate in developing new systems. These methods may be quite conservative, however, because the maximum value of various forces acting over the entire time interval is used in design. Since these maximum values for various forces do not occur simultaneously, this approach results in a conservative design for the system.

The main solution variables for dynamic stress analysis of a system, as in the case of static analysis, are the displacements at various points of the system. The difference is that the displacements in the dynamic case are time dependent, whereas in the static case they are not. Once displacements are known, stresses are calculated at any time by using Eqs. C-4 and C-8.

Several methods for calculating displacements of a system subjected to dynamic loads are available. The first step in dynamic analysis of an elastic system is to write the equations of motion. The Lagrangian approach described in Appendix A can be used to define the equations of motion for an elastic system. These equations of motion are in terms of displacements, and several methods are available for integrating them. These include direct integration methods using finite difference techniques, transfer function method, modal superposition method, and frequency domain response method. Most computer programs for stress analysis have options for using any of these methods to integrate the equations of motion and obtain a dynamic response. In this paragraph the modal superposition method, or normal modes method, which is most commonly used for small displacement analysis, is described and illustrated. Several textbooks are available in the literature for more detailed discussions of various methods.

C-3.1 FINITE ELEMENT MODELS

A dynamic stress analysis of a complex structural system starts with the development of a finite element model for the system. This involves the definition of a network of grid points for the system; selection of type of finite elements to be used and their connectivities; selection of a global coordinate system, materials, and geometric properties; and loading conditions for the system. Stiffness, damping, and mass properties are calculated based on the type of finite elements selected. Elemental properties are then combined to obtain system properties, as in the case of static analysis. These system properties are then used to define the equations of motion for the system.

General aspects for development of finite element models for complex structures for dynamic response analysis are the same as those discussed in par. C-2.1. Most computer programs generally accept the same data for static as well as dynamic stress analysis. Additional data needed for a dynamic analysis are mass density of the material, nonstructural masses, if any, dynamic loading for the system, and initial conditions for the solution. These additional data are needed in the computer program for developing equations of motion and their integration.

THIS DOCUMENT PROVIDED BY THE ABBOTT AEROSPACE
TECHNICAL LIBRARY
ABBOTTAEROSPACE.COM

C-3.2 DYNAMIC STRESS ANALYSIS

The most commonly used method for linear structural dynamics is the modal synthesis technique. This is also known in the literature as the normal modes method and is described later in this appendix. In this method several natural frequencies and mode shapes for the finite element model of the system are calculated. These data are used to uncouple equations of motion for the finite element model of the system. The uncoupled equations of motion are in terms of normal coordinates and can be solved one at a time. Thus, in terms of the normal coordinates, a number of equations of motion must be solved to compute the response of the entire system. In terms of normal coordinates, each equation of motion is the same as for any single-degree-of-freedom system; therefore, it is important to study these particular systems. The single-degree-of-freedom system is discussed in the following paragraph.

C-3.2.1 Single-Degree-of-Freedom Systems

A simple system consisting of a mass restrained by an elastic element and a viscous element is considered. Any structure with a single dynamic degree of freedom is reducible to such a system. The system shown in Fig. C-5 is frequently referred to as the "basic oscillator". It consists of a mass M (kg) restrained by a spring of stiffness k (N/m) and a viscous damper, which offers a resisting force $-c\dot{z}$ (N) proportional to the magnitude of velocity $\dot{z}$ (m/s) but opposite to its direction of motion; c (N·s/m) is the damping coefficient. The displacement z (m) due to an applied force $F(t)$ (N) is measured from a position in which the spring is unstretched.

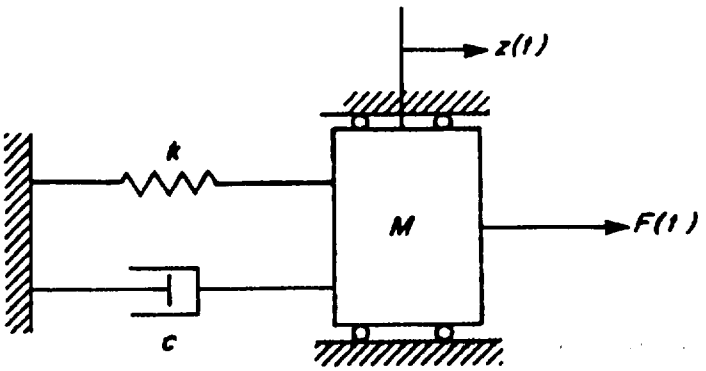

Figure C-5. One-Degree-of-Freedom System (Basic Oscillator)

The equation of motion for the basic oscillator can be obtained by using Newton's laws or the Lagrangian approach discussed in Appendix A. By using either approach the equation of motion is

$$M\ddot{z} + c\dot{z} + kz = F(t) \tag{C-25}$$

with initial conditions

$$z(0) = z_0, \text{ m}$$
$$\dot{z}(0) = v_0, \text{ m/s} \tag{C-26}$$

where

z_0 = initial displacement, m
v_0 = initial velocity, m/s.

By dividing throughout by M, Eq. C-25 becomes

$$\ddot{z} + 2\omega\zeta\dot{z} + \omega^2 z = F(t)/M \tag{C-27}$$

THIS DOCUMENT PROVIDED BY THE ABBOTT AEROSPACE
TECHNICAL LIBRARY
ABBOTTAEROSPACE.COM

where

$\omega = \sqrt{k/M}$ = natural frequency of system, rad/s
$\zeta = -c/C_c$ = damping ratio, dimensionless
$C_c = 2\sqrt{kM}$ = critical damping, N·s/m
c = system damping, N·s/m.

Eq. C-27 can be solved readily for a given $F(t)$ and the initial conditions; however, a general solution of Eq. C-27 is also available. This solution for underdamped systems, which is usually the case, is given by the following expression known as the Duhamel's integral (Ref. 8):

$$z(t) = e^{-\zeta\omega t}\left[\frac{v_0 + z_0\zeta\omega}{\omega_D}\sin(\omega_D t) + z_0\cos(\omega_D t)\right] + \frac{1}{M\omega_D}\int_0^t F(\tau)e^{-\zeta\omega(t-\tau)}\sin[\omega_D(t-\tau)]d\tau, \text{ m} \qquad \text{(C-28)}$$

where

$\omega_D = \omega\sqrt{1-\zeta^2}$ = damped natural frequency, Hz
τ = variable of integration, s
t = time, s.

The first part of the solution in Eq. C-28 is due to nonhomogeneous initial conditions, and the second part is due to the applied forcing function $F(t)$. Eq. C-28 can be used to solve for displacement $z(t)$ of the mass M, as shown in Fig. C-5, subjected to any forcing function $F(t)$ and the initial conditions. The forcing function $F(t)$ may be given as an analytic expression or in the form of a table of force values at various points in time. If the analytic expression for the forcing function is simple, then the integral in Eq. C-28 can be evaluated in a closed form. For complex forms of the forcing function, numerical integration methods are used to evaluate the displacement response $z(t)$. For many standard forcing functions, the integral in Eq. C-28 has been evaluated in a closed form. Equations for closed-form integrals are available in the literature (Ref. 3).

It is shown in the next paragraph that Eq. C-28 also can be used to obtain a dynamic response for multidegree-of-freedom systems.

C-3.2.2 Multidegree-of-Freedom Systems

Most vibrational systems encountered in physical situations have distributed properties, such as mass and stiffness. Most components of an artillery system fall into this class. Systems of this type are said to possess an infinite number of degrees of freedom because the system is fully described only when the motion is known at every one of its points. In many cases the mass and stiffness distributions are highly nonuniform, and for such systems, it may be more feasible to construct discrete mathematical models that need only a finite number of parameters to describe the mass and stiffness properties. In this manner a system with an infinite number of degrees of freedom is reduced to a system with only a finite number of degrees of freedom. Therefore, the finite element method provides a natural vehicle for reducing a system with infinite degrees of freedom to the one that has only a finite number of degrees of freedom.

The motion of multidegree-of-freedom systems is generally described by a finite set of simultaneous second-order ordinary differential equations. Several methods are available for integration of these equations. For linear systems with small displacement approximation, a very effective method is based on the transformation of solution variables to a new set of variables. The linear transformation of variables is defined so that the resulting differential equations are uncoupled in new variables and can be solved one by one. The transformation matrix that has this property of uncoupling the system equations of motion is formed from mode shapes for the undamped free vibration problem for the system. This transformation matrix is known as modal matrix, and the method of computing dynamic response is called the mode superposition method or the normal modes method.

A first step in dynamic analysis of a multidegree-of-freedom system is to develop the equation of motion.

THIS DOCUMENT PROVIDED BY THE ABBOTT AEROSPACE
TECHNICAL LIBRARY
ABBOTTAEROSPACE.COM

The Lagrangian approach of Appendix A can be used to write the equation of motion for the system. In general, the equation of motion for any multidegree-of-freedom system is given as

$$[M]\ddot{z} + [C]\dot{z} + [K]z = S(t) \tag{C-29}$$

where

$[K]$ = stiffness matrix, N, N/m, N/rad, or N·m/rad
$[M]$ = generalized mass matrix for system, kg, kg·m, or kg·m^2
$[C]$ = generalized damping matrix, N·s/m, N·s, or N·m·s/rad
z = vector of generalized displacements for finite element model, m or rad
$S(t)$ = vector of generalized nodal forces, N or N·m.

The stiffness matrix $[K]$ is the same as that described earlier. The mass matrix $[M]$ for the system can be calculated from mass matrices for individual finite elements by using a procedure that is identical to the one used for the stiffness matrix. The shape function of Eq. C-1 is used to develop the mass matrix for a finite element.

The mass matrix for an element can be computed by writing the kinetic energy as a quadratic form in generalized velocities. The kinetic energy T of an element is given as (Ref. 8)

$$T = \frac{1}{2}\int_V \dot{f} \cdot \dot{f}\, \rho\, dV, \text{ J} \tag{C-30}$$

where

ρ = mass density, kg/m^3
V = volume of element, m^3
f = velocity function, m/s.

Substituting for f from Eq. C-1 in terms of the shape function N gives

$$T = \frac{1}{2}\{\ddot{r}'\}[m']\{\ddot{r}'\}, \text{ J} \tag{C-31}$$

where $[m']$ is the element generalized mass matrix in the local coordinate system, which is given as

$$[m'] = \int_V \rho [N]^T [N] dV, \text{ kg, kg·m, or kg·m}^2. \tag{C-32}$$

By introducing the coordinate transformation of Eq. C-15, the kinetic energy may be expressed in terms of the global generalized nodal velocities of the element, and the element mass matrix $[m]$ in the global coordinate system may be identified as

$$[m] = [\lambda]^T [m'] [\lambda], \text{ kg, kg·m, or kg·m}^2. \tag{C-33}$$

The kinetic energy of the entire structure is obtained by summing up the kinetic energies of each of the NE individual elements. When the compatibility Eq. C-20 is introduced in the resulting expression, the mass matrix $[M]$ for the structure is given as

$$[M] = \sum_{i=1}^{NE} [A^i]^T [m^i] [A^i], \text{ kg, kg·m, or kg·m}^2 \tag{C-34}$$

where

$[A^i]$ = Boolean transformation matrix for ith finite element, dimensionless
$[m^i]$ = generalized mass matrix for ith finite element in global coordinate system, kg, kg·m, or kg·m^2.

THIS DOCUMENT PROVIDED BY THE ABBOTT AEROSPACE
TECHNICAL LIBRARY
ABBOTTAEROSPACE.COM

By using Eq. C-32 and the shape functions from Eqs. C-2 and C-3, the mass matrix $[m']$ for the truss element previously described is

$$[m'] = \frac{\rho AL}{6}\begin{bmatrix} 2[I_3] & [I_3] \\ [I_3] & 2[I_3] \end{bmatrix}, \text{ kg} \tag{C-35}$$

where

A = cross-sectional area, m^2

and for the beam element previously described the mass matrix $[m']$ is the summation of two matrices given as follows:

$$[m'] = [m'(1)] + [m'(2)] \tag{C-36}$$

where

$$[m'(1)] = \frac{\rho AL}{420}\begin{bmatrix} 140 & 0 & 0 & 70 & 0 & 0 \\ & 156 & 22L & 0 & 54 & -13L \\ & & 4L^2 & 0 & 13L & -3L^2 \\ & & & 140 & 0 & 0 \\ \text{Symmetric} & & & & 156 & -22L \\ & & & & & 4L^2 \end{bmatrix}, \text{ kg, kg·m, or kg·m}^2 \tag{C-37}$$

$$[m'(2)] = \frac{\rho I}{30L}\begin{bmatrix} 0 & 0 & 0 & 70 & 0 & 0 \\ & 36 & 3L & 0 & -36 & 3L \\ & & 4L^2 & 0 & -3L & L^2 \\ & & & 0 & 0 & 0 \\ \text{Symmetric} & & & & 36 & -3L \\ & & & & & 4L^2 \end{bmatrix}, \text{ kg, kg·m, or kg·m}^2 \tag{C-38}$$

and $[I_3]$ is the 3X3 identity matrix. The mass matrix of Eq. C-37 represents translational inertia of the beam, whereas the mass matrix of Eq. C-38 represents the rotary inertia.

The damping matrix for the system can be calculated in a similar manner by using material damping for each finite element (Ref. 8). In practice, however, this calculation is rarely done because material damping is usually quite small and is neglected in practical analysis. This omission is quite reasonable since it gives a conservative estimate for stresses and displacements.

The next step in dynamic stress analysis is to consider the undamped free vibration problem for the system and to define an eigenvalue problem for the determination of eigenvalues (square of frequencies) and eigenvectors (mode shapes). The equation of motion, Eq. C-29, is then reduced to

$$[M]\ddot{z} + [K]z = 0 \tag{C-39}$$

with homogeneous initial conditions.

Free harmonic motion of the system is assumed as

$$z = y\sin(\omega t + \theta), \text{ m or rad} \tag{C-40}$$

where

y = eigenvector or mode shape, m or rad
ω = natural frequency of system, rad/s
θ = phase angle, rad.

THIS DOCUMENT PROVIDED BY THE ABBOTT AEROSPACE
TECHNICAL LIBRARY
ABBOTTAEROSPACE.COM

Substituting Eq. C-40 into Eq. C-39 and defining $\zeta = \omega^2$ give—with the order of vector multiplication as shown—

$$[K]y = \zeta[M]y. \tag{C-41}$$

Eq. C-41 is the generalized eigenvalue problem that must be solved for natural frequencies and the corresponding mode shapes (the eigenvectors).

Several numerical methods are available (Ref. 9) for calculation of natural frequencies and the corresponding mode shapes for the system of Eqs. C-41. Most commercially available computer programs have options of using these methods for eigenvalue analysis. Here a method, referred to as the subspace iteration technique (Ref. 9), that is quite effective and efficient is described. Since several frequencies and mode shapes are needed, Eq. C-41 is rewritten for the ith eigenvalue and eigenvector as

$$[K]y^i = \zeta_i[M]y^i \tag{C-42}$$

where

$\zeta_i = i$th eigenvalue
$y^i = i$th eigenvector.

By writing Eq. C-42 for q eigenvalues and eigenvectors, the result is

$$[K] = [M][\Phi][\Omega^2] \tag{C-43}$$

where

$[\Phi] = n \times q$ matrix whose ith column is the ith mode shape y^i, m or rad
$[\Omega^2] = q \times q$ diagonal matrix in which each diagonal term is the square of frequency, s^{-2}
$[K]$ = structural stiffness matrix synthesized from stiffness element matrices, N, N/m, N/rad, or N·m/rad.

The basic idea of the subspace iteration method is quite similar to the general Rayleigh-Ritz method. The starting point for this method is a set of p linearly independent vectors. These vectors form a basis for the p-dimensional vector space. The mode shapes for the system are expressed as linear combinations of the assumed basis vectors. The multipliers of the linear combination are obtained by solving a reduced eigenvalue problem. An iterative process is then used to improve the assumed basis vectors until convergence is obtained.

It is suggested (Ref. 9) that when p-mode shapes are required, one should start with $q = \min\{2p, (p + 8), n\}$—i.e., a minimum of $2p$, $(p + 8)$, or n—linearly independent vectors. This improves the accuracy of the first p-eigenvectors and the corresponding eigenvalues. Define a linear transformation:

$$[\Phi^{(0)}]^\dagger = [X^{(0)}][\Phi], \text{ m or rad} \tag{C-44}$$

where

$[X^{(0)}] = n \times q$ matrix, each column of which is the assumed eigenvectors, m or rad
$[\bar{\Phi}] = q \times q$ matrix, each element of which is the unknown multipliers (eigenvectors) of the transformation, dimensionless.

Substituting Eq. C-44 into Eq. C-43 and premultiplying by $[X^{(0)}]^T$ give

$$[\bar{K}][\bar{\Phi}] = [\bar{M}][\bar{\Phi}][\Omega^2] \tag{C-45}$$

†The superscript indicates the iteration number.

THIS DOCUMENT PROVIDED BY THE ABBOTT AEROSPACE
TECHNICAL LIBRARY
ABBOTTAEROSPACE.COM

where

$$[\bar{K}] = [X^{(0)}]^T [K] [X^{(0)}]$$
$$[\bar{M}] = [X^{(0)}]^T [M] [X^{(0)}]. \quad \text{(C-46)}$$

Eq. C-45 is a reduced eigenproblem of dimension q that is solved for $[\bar{\Phi}] [\Omega^2]$. Eq. C-43 is then used to obtain approximate system mode shapes. An improved set of eigenvectors in the matrix $[X^{(1)}]$ is now determined from the equation

$$[K] [X^{(1)}] = [Y^{(0)}] \quad \text{(C-47)}$$

where

$$[Y^{(0)}] = [M][\Phi^{(0)}]. \quad \text{(C-48)}$$

The matrix $[X^{(0)}]$ in Eq. C-44 is now replaced by the matrix $[X^{(1)}]$, and the iterative process is continued until the eigenvalues determined from Eq. C-45 converge to within a prescribed tolerance.

The subspace iteration algorithm for calculation of eigenvalues and eigenvectors is summarized as follows:

1. Step 1. Start with an $n \times q$ matrix $[X^{(0)}]$, each column of which is an estimate of q eigenvectors.
2. Step 2. Compute $[Y^{(0)}]$ from Eq. C-48 by using the finite element operations of Eq. C-35.
3. Step 3. Solve Eq. C-47 and let the solution be denoted as $[\bar{X}^{(1)}]$.
4. Step 4. Compute

$$[Y^{(1)}] = [M] [\bar{X}^{(1)}] \quad \text{(C-49)}$$

by using finite element operations of Eq. C-35.

Step 5. Calculate the following $q \times q$ matrices:

$$[\bar{K}] = [\bar{X}^{(1)}]^T [Y^{(0)}] \text{ and } [\bar{M}] = [X^{(1)}]^T [\bar{Y}^{(1)}]. \quad \text{(C-50)}$$

Step 6. Solve for all eigenvalues and eigenvectors of the projected eigenvalue problem of Eq. C-45. Note that the generalized Jacobi iteration or any other method of solving an eigenvalue problem may be used in this step (Ref. 9).

Step 7. Compute

$$[X^{(1)}] = [\bar{X}^{(1)}] [\Phi] \text{ and } [Y^{(1)}] = [\bar{Y}^{(1)}] [\Phi]. \quad \text{(C-51)}$$

Step 8. Check for convergence of eigenvalues. If all the ratios

$$|\omega_i^{2(1)} - \omega_i^{2(0)}| / \omega_i^{2(1)} \quad \text{(C-52)}$$

are within a specified tolerance, stop the iterative process. Otherwise, return to Step 3 with $[Y^{(0)}] = [Y^{(1)}]$. After convergence, the first p-columns of $[X^{(1)}]$ are the required eigenvectors, and the first p-elements in $[\Omega^2]$ are the corresponding eigenvalues.

Once the eigenvectors have been determined, they may be orthonormalized with respect to the mass matrix such that $[\Phi]^T [M] [\Phi] = [I]$ where $[I]$ is the identity matrix. In that case, $[\Phi]^T [K] [\Phi]$ is a diagonal matrix containing eigenvalues as its diagonal elements.

THIS DOCUMENT PROVIDED BY THE ABBOTT AEROSPACE
TECHNICAL LIBRARY
ABBOTTAEROSPACE.COM

After eigenvalues and eigenvectors for Eq. C-42 have been determined, the transformation of the dependent variable $z(t)$ mentioned previously can be defined. Let $\eta(t)$ represent a vector of new variables called the normal coordinates. A linear transformation from $z(t)$to $\eta(t)$ coordinates is defined as

$$z(t) = [\Phi]\eta(t), \text{ m or rad} \tag{C-53}$$

where

$[\Phi]$ = modal matrix, m or rad.

The number of components in $\eta(t)$ is equal to the number of columns in the matrix $[\Phi]$. If all eigenvectors are included in the matrix $[\Phi]$, dimensions of z and η are the same. For most practical design problems, however, higher modes contribute very little to the dynamic response; accordingly, they are not included in the matrix $[\Phi]$. If n is the dimension of z, generally less than $n/2$ modes are sufficient to calculate the dynamic response. Let p be the number of columns in the matrix $[\Phi]$.

Substituting the transformation of Eq. C-53 into the equation of motion C-29 and multiplying it by $[\Phi]^T$ give

$$[\bar{M}]\ddot{\eta} + [\bar{C}]\dot{\eta} + [\bar{K}]\eta = \bar{S} \tag{C-54}$$

where $[\bar{M}]$ and $[\bar{K}]$ are defined in Eq. C-46 and

$$\left.\begin{aligned} [\bar{C}] &= [\Phi]^T[C][\Phi] \\ \bar{S} &= [\Phi]^T S. \end{aligned}\right\} \tag{C-55}$$

Since $[\Phi]$ is a matrix of eigenvectors for the eigenvalue problem of Eq. C-43, $[\bar{M}]$ and $[\bar{K}]$ are diagonal matrices (due to orthogonality of eigenvectors with respect to $[K]$ and $[M]$). In general neither $[C]$ nor $[\bar{C}]$ is a diagonal matrix, so Eqs. C-54 remain coupled. In practice, however, $[\bar{C}]$ is treated as a diagonal matrix since material damping is fairly small. A procedure that has been followed in practice is to assume the diagonal elements of $[C]$ to be 2 to 10% of the critical modal damping; thus Eqs. C-54 are uncoupled and can be solved one at a time. When the matrix $[C]$ cannot be assumed to be diagonal, the normal modes method of dynamic analysis is not appropriate. In such case, direct integration of Eqs. C-29 or some other procedure should be used.

When Eqs. C-54 are uncoupled, they can be written in the form

$$[\bar{M}_i]\ddot{\eta}_i + [\bar{C}_i]\dot{\eta}_i + [\bar{K}_i]\eta_i = \bar{S}_i, \; i = 1, 2, \ldots, p. \tag{C-56}$$

By comparing Eq. C-56 with Eq. C-25, it can be seen that the two equations have identical form. Therefore, Duhamel's integral given in Eq. C-28 can be used to solve for normal coordinates $\eta_i(t)$. However, before η_i's may be solved using Eq. C-28, the initial conditions for Eq. C-29 must be transformed to normal coordinates η_i's. Let the initial conditions for Eq. C-29 be given as

$$z(0) = z_0 \tag{C-57}$$

$$\dot{z}(0) = v_0 \tag{C-58}$$

where

z_0 = vector of initial generalized displacments, m or rad
v_0 = vector of initial generalized velocities, m/s or rad/s.

THIS DOCUMENT PROVIDED BY THE ABBOTT AEROSPACE
TECHNICAL LIBRARY
ABBOTTAEROSPACE.COM

Substituting Eq. C-57 into the transformation Eq. C-53 gives

$$z_0 = [\Phi]\eta_0 \tag{C-59}$$

where

$\eta_0 = \eta(0)$, a vector of initial conditions for the normal coordinates η.

Eq. C-59 cannot be solved directly for η_0 unless all eigenvectors are included in $[\Phi]$. (Otherwise $[\Phi]$ is not even a square matrix.) A procedure that has been used in the past is to premultiply both sides of Eq. C-59 by $[\Phi]^T[M]$. The result is

$$[\Phi]^T[M]z_0 = [\Phi]^T[M][\Phi]\eta_0 = [\bar{M}]\eta_0 \tag{C-60}$$

where

$[\bar{M}] = [\Phi]^T[M][\Phi]$.

Therefore, η_0 is given as

$$\eta_0 = [\bar{M}]^{-1}[\Phi]^T[M]z_0. \tag{C-61}$$

Similarly the initial velocity vector $\dot{\eta}_0$ for normal coordinates is given as

$$\dot{\eta}_0 = [\bar{M}]^{-1}[\Phi]^T[M]v_0. \tag{C-62}$$

Thus the normal modes procedure of dynamic stress analysis is to solve first for the normal coordinates η_i's from Eq. C-56. Transformation Eq. C-53 is then used to calculate physical displacement z_i's. Once all displacements are known, a standard stress recovery procedure—using Eqs. C-20, C-15, C-4, and C-3—is used to calculate stresses at any point in the structure at any time.

C-3.3 SAMPLE CALCULATIONS

In this paragraph a simple two-degree-of-freedom system shown in Fig. C-6 is considered to illustrate the procedure of dynamic response analysis given in the previous paragraph. For this system two masses m_1 and m_2 are connected by three springs with spring constants k_1, k_2, and k_3. The system has two generalized displacement degrees of freedom z_1 and z_2 and is subjected to two forces s_1 and s_2. The problem is to determine the dynamic response of the system by using the normal modes method of analysis.

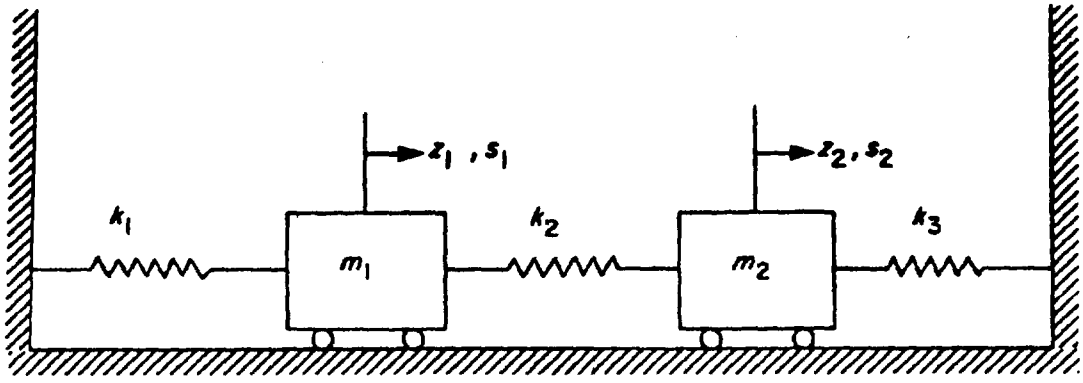

Figure C-6. Two-Degree-of-Freedom Model

THIS DOCUMENT PROVIDED BY THE ABBOTT AEROSPACE
TECHNICAL LIBRARY
ABBOTTAEROSPACE.COM

A first step in dynamic analysis is to write equations of motion for the system. The Lagrangian approach of Appendix A will be used. Therefore, expressions for the kinetic and potential energies are required. The kinetic energy T of the system is given as

$$T = \frac{m_1 \dot{z}_1^2}{2} + \frac{m_2 \dot{z}_2^2}{2}$$

$$= \frac{1}{2}\{\dot{z}\cdot[M]\dot{z}\}, \text{ J} \qquad \text{(C-63)}$$

where $[M]$ is the mass matrix given as

$$[M] = \begin{bmatrix} m_1 & 0 \\ 0 & m_2 \end{bmatrix}, \text{ kg.} \qquad \text{(C-64)}$$

The potential energy V stored in elastic springs is

$$V = \frac{k_1 z_1^2}{2} + \frac{k_3 z_2^2}{2} + \frac{k_2 (z_1 - z_2)^2}{2}$$

$$= \frac{1}{2}\{z\cdot[K]z\}, \text{ J} \qquad \text{(C-65)}$$

where (K) is the stiffness matrix given as

$$[K] = \begin{bmatrix} k_1 + k_2 & -k_2 \\ -k_2 & k_2 + k_3 \end{bmatrix}, \text{ N/m.} \qquad \text{(C-66)}$$

Therefore, the equations of motion for the system are

$$\begin{bmatrix} m_1 & 0 \\ 0 & m_2 \end{bmatrix} \begin{bmatrix} \ddot{z}_1 \\ \ddot{z}_2 \end{bmatrix} + \begin{bmatrix} k_1 + k_2 & -k_2 \\ -k_2 & k_2 + k_3 \end{bmatrix} \begin{bmatrix} z_1 \\ z_2 \end{bmatrix} = \begin{bmatrix} S_1 \\ S_2 \end{bmatrix} \qquad \text{(C-67)}$$

where the vector S is determined by Eq. C-55.
To determine z_1 and z_2 from Eq. C-67, it is necessary to solve for the eigenvalues and eigenvectors of the problem

$$\begin{bmatrix} k_1 + k_2 & -k_2 \\ -k_2 & k_2 + k_3 \end{bmatrix} \begin{bmatrix} y_1 \\ y_2 \end{bmatrix} = \zeta \begin{bmatrix} m_1 & 0 \\ 0 & m_2 \end{bmatrix} \begin{bmatrix} y_1 \\ y_2 \end{bmatrix} \qquad \text{(C-68)}$$

where ζ is an eigenvalue and

$$y = \begin{bmatrix} y_1 \\ y_2 \end{bmatrix}, \text{ m}$$

THIS DOCUMENT PROVIDED BY THE ABBOTT AEROSPACE
TECHNICAL LIBRARY
ABBOTTAEROSPACE.COM

is an eigenvector. For the purpose of numerical calculation, let $m_1 = m_2 = 14.594$ kg, and $k_1 = k_2 = k_3 = 145.94$ kN/m. Therefore, Eq. C-68 becomes

$$14.594(10^4)\begin{bmatrix} 2 & -1 \\ -1 & 2 \end{bmatrix}\begin{bmatrix} y_1 \\ y_2 \end{bmatrix} = \zeta(14.594)\begin{bmatrix} 1 & 0 \\ 0 & 1 \end{bmatrix}. \tag{C-69}$$

Solving Eqs. C-69 for the two eigenvalues gives

$$\begin{aligned} \zeta_1 &= 10^4\ (\text{rad/s})^2 \\ \zeta_2 &= 3\times10^4\ (\text{rad/s})^2. \end{aligned} \tag{C-70}$$

The corresponding natural frequencies are

$$\begin{aligned} \omega_1 &= 100.0\ \text{rad/s} \\ \omega_2 &= 173.2\ \text{rad/s}. \end{aligned} \tag{C-71}$$

Eigenvectors y^1 and y^2 corresponding to the two eigenvalues are obtained from Eq. C-69 and are given as

$$\left.\begin{aligned} y^1 &= \frac{1}{\sqrt{2}}\begin{bmatrix} 1 \\ 1 \end{bmatrix}, \text{m} \\ y^2 &= \frac{1}{\sqrt{2}}\begin{bmatrix} 1 \\ -1 \end{bmatrix}, \text{m}. \end{aligned}\right\} \tag{C-72}$$

Thus the modal matrix $[\Phi]$ of Eq. C-53 is given as

$$[\Phi] = \frac{1}{\sqrt{2}}\begin{bmatrix} 1 & 1 \\ 1 & -1 \end{bmatrix}, \text{m}. \tag{C-73}$$

By substituting various quantities in Eq. C-46, the matrices $[\bar{M}]$ and $[\bar{K}]$ are

$$\begin{aligned} [\bar{M}] &= 14.594\begin{bmatrix} 1 & 0 \\ 0 & 1 \end{bmatrix}, \text{kg·m}^2 \\ [\bar{K}] &= 14.594\ (10^4)\begin{bmatrix} 1 & 0 \\ 0 & 3 \end{bmatrix}, \text{N·m}. \end{aligned} \tag{C-74}$$

Also the vector $\bar{S}$ of Eq. C-55 is

$$\bar{S} = \frac{1}{\sqrt{2}}\begin{bmatrix} s_1 + s_2 \\ s_1 - s_2 \end{bmatrix}, \text{N·m}. \tag{C-75}$$

THIS DOCUMENT PROVIDED BY THE ABBOTT AEROSPACE
TECHNICAL LIBRARY
ABBOTTAEROSPACE.COM

Therefore, uncoupled equations of motion given in Eq. C-54 are

$$14.594\begin{bmatrix} 1 & 0 \\ 0 & 1 \end{bmatrix}\begin{bmatrix} \ddot{\eta}_1 \\ \ddot{\eta}_2 \end{bmatrix} + 14.594(10^4)\begin{bmatrix} 1 & 0 \\ 0 & 3 \end{bmatrix}\begin{bmatrix} \eta_1 \\ \eta_2 \end{bmatrix} = \begin{bmatrix} \bar{s}_1 \\ \bar{s}_2 \end{bmatrix}. \qquad \text{(C-76)}$$

Thus, once the forces $s_1(t)$ and $s_2(t)$ are specified, Eqs. C-76 can be readily solved for η_1 and η_2. Eq. C-53 then gives the physical displacement for the system.

The procedure for dynamic stress analysis presented here can be used to analyze components of the towed artillery system such as cradle, top carriage, and bottom carriage. Finite element models for such systems have a large number of degrees of freedom; therefore, hand calculations are not possible. Most computer programs such as NASTRAN, however, have dynamic stress analysis capability. Therefore, once a finite element model has been developed, static as well as dynamic analyses can be performed routinely by using these programs. For towed artillery components dynamic stress analysis can be performed once dynamic load histories are specified. Dynamic stress analysis for the top carriage structure (finite element model of Fig. 8-9) was performed using NASTRAN. Arbitrary sinusoidal forces were input to the model. Tables of dynamic displacements and stresses were obtained.

REFERENCES

1. S. G. Sawyer, *Application of Finite Element Method of Stress Analysis to Ordnance Problems*, BRL Report No. 1497, Ballistic Research Laboratory, Aberdeen Proving Ground, MD, September 1980.
2. J. O. Nazario, *NASTRAN: Basic Theory and Application to the M109A1 Elevating Bracket*, Technical Note R-TN-74-015, Rodman Laboratory, Rock Island Arsenal, Rock Island, IL, June 1974.
3. J.S. Przemieniecki, *Theory of Matrix Structural Analysis*, McGraw-Hill Book Company, Inc., New York, NY, 1968.
4. R. D. Cook, *Concepts and Applications of Finite Element Analysis*, John Wiley & Sons, New York, NY, 1974.
5. O. C. Zienkiewicz, *The Finite Element Method*, McGraw-Hill Book Company, Inc., New York, NY, 1978.
6. J. T. Oden, *Finite Elements of Nonlinear Continua*, McGraw-Hill Book Company, Inc., New York, NY, 1972.
7. K. H. Huebner, *The Finite Element Method for Engineers*, John Wiley & Sons, Inc., New York, NY, 1975.
8. R. W. Clough and J. Penzien, *Dynamics of Structures*, McGraw-Hill Book Company, Inc., New York, NY, 1975.
9. K. J. Bathe and E. L. Wilson, *Numerical Methods in Finite Element Analysis*, Prentice-Hall, Inc., Englewood Cliffs, NJ, 1976.

THIS DOCUMENT PROVIDED BY THE ABBOTT AEROSPACE
TECHNICAL LIBRARY
ABBOTTAEROSPACE.COM

GLOSSARY

A

Aim. To point or direct a weapon so that its projectile is expected to strike the target.

Angle of Elevation. The vertical angle between the axis of the bore and the line of sight. Thus the angle of elevation is the vertical angle above the line of sight through which the axis of the bore must be raised so that the projectile will carry to the target.

Antibacklash Device. A mechanism that applies static torque in two directions in a gear train, to provide positive tooth contact, regardless of which direction the gears are to be turned.

Azimuth. The direction of fire expressed as a horizontal angle.

B

Base Plate. The bottom structure of a carriage that rests on ground.

Bogie. The rear transporting unit of a gun carriage.

Bottom Carriage. The lower supporting structure of a gun that supports the top carriage and provides for traversing the weapon.

Breech Force. The force due to the propellant gases that drives the gun rearward in recoil.

Breech Ring. A breechblock housing that is screwed or shrunk on the rear of a cannon.

Breechblock. The part of a cannon that closes the breech.

Buffer. The shock absorber for the counterrecoiling parts.

Buffing Force. The resistance provided by the buffer to the counterrecoiling parts.

C

Cannon. The component of a gun or howitzer that consists of the complete assembly of gun tube, breech mechanism, firing mechanism, and muzzle brake.

Carriage. The supporting structure of a weapon.

Clip. The component of a discontinuous guide used for alignment of recoiling parts.

Coarse Elevation. Placement of a cannon in the approximate elevation required.

Concentric Recoil Mechanism. A recoil mechanism that is concentric with the gun tube.

Control Rod. A rod in the recoil cylinder with grooves to form orifices for fluid flow.

Counterrecoil. Forward movement of a gun returning to firing position (battery) after recoil.

Cradle. The nonrecoiling structure of a weapon that houses the recoiling parts and rotates about the trunnions to elevate the cannon.

Cradle, O-type. A cradle that supports the gun tube within a cylindrical housing.

Cradle, U-type. A cradle that supports the gun tube on longitudinal guides.

D

Depress. To decrease the angle of elevation.

Double Recoil Gun. A weapon in which the gun recoils on the top carriage and the top carriage recoils on the bottom carriage.

THIS DOCUMENT PROVIDED BY THE ABBOTT AEROSPACE
TECHNICAL LIBRARY
ABBOTTAEROSPACE.COM

E

Effective Orifice Area. Orifice area multiplied by the discharge coefficient.

Elevating Arc. An upright, geared arc attached to a weapon or carriage by which the weapon is elevated or depressed.

Elevating Cylinder. The cylinder that actuates a hydraulic elevating mechanism.

Elevating Mechanism. The mechanism on a gun carriage that elevates or depresses the weapon.

Elevating Mechanism, Hydraulic. An elevating mechanism operated by hydraulic pressure. It normally employs a cylinder, piston, and rod assembly that acts as a strut between the carriage and cradle.

Elevating Mechanism, Screw and Nut Type. An elevating mechanism that is activated by turning a screw or nut.

Elevating Strut. A strut whose variation in length controls elevation of the weapon.

Elevating System. All components involved in elevating or depressing a weapon.

Elevation. The vertical angular position of a weapon with reference to the horizontal.

Emplacement. Act of fixing a gun in a prepared position from which it may be fired.

Equilibrator. The force-producing mechanism that provides a moment about the trunnions of a gun cradle and opposes that caused by the unbalanced weight of the tipping parts.

Equilibrator Force. The force generated by the equilibrator.

Equilibrator Moment. The moment about the trunnions that is produced by the equilibrator.

Equivalent Orifice. Combined effect of all orifices active in parallel or series.

F

Factor of Safety. The ratio of material strength to allowable stress.

Fine Elevation. Precise positioning of a weapon in elevation.

Finite Element Model. A discrete model of a continuous structure for stress analysis. Usually a computer program is used for numerical computation of stresses with a finite element model.

Fire Control. Control over direction, volume, and time of fire of weapons.

Firing Conditions. The various loads imposed on the weapon during all phases of firing.

Firing Couple, Elevation. The couple about the trunnion axis generated by the resultant firing forces and the trunnion reaction.

Firing Couple, Traverse. The couple about the traversing axis generated by the firing forces.

Firing Cycle. The sequence of operation of a weapon from loading through firing.

Firing Jack. An adjustable device that levels and supports a weapon during firing.

Firing Platform. The structure that rests on the ground and provides a means to rotate a weapon for general positioning purposes.

Float. A horizontal structure attached to the trail or bottom carriage to distribute the vertical forces to the ground.

Floating Piston. A piston that separates hydraulic fluid from gas in the recuperator.

G

Gear Ratio. The ratio of input speed to output speed in a gear train; the mechanical advantage of gears or gear trains.

Gear Train. A group of meshing gears that operate in sequence to transmit motion or power.

THIS DOCUMENT PROVIDED BY THE ABBOTT AEROSPACE
TECHNICAL LIBRARY
ABBOTTAEROSPACE.COM

Ground Clearance. The space between the breech and ground at the end of recoil at the highest angle of elevation. The undercarriage clearance during transport.

Guide. Channel-shaped structure of the cradle, which provides sliding surface and support to the recoiling parts during the recoil cycle.

Guide, Continuous. A guide that is made of one continuous member.

Guide, Discontinuous. A guide that is made of several short lengths spaced at regular intervals. *See* clip.

Gun Mount. The structure that supports a gun.

H

Handwheel. A wheel designed for readily applying manual effort to operate a gear train.

Hydraulic Strut. A structural member—consisting of a cylinder, piston, and piston rod—whose length can be varied by hydraulic pressure.

I

In-Battery. The position of the recoiling parts in the extreme forward position in the cradle.

J

Jack. Adjustable lifting mechanism used to support and stabilize a gun carriage.

L

Laying. The act of directing or adjusting the aim of a weapon.

Load Factor. The ratio of design load to actual load.

Loading Device. Equipment used for transferring ammunition into the firing chamber of a weapon.

Loading Trough. A structure with side retainers used to carry ammunition as it is rammed into the breech.

Locking Device. A fastening device that prevents inadvertent motion.

Lug, Gun. An appendage of the breech ring for attaching the recoil mechanism.

M

Modal Matrix. A matrix whose columns are mode shapes for the structure.

Modal Synthesis (normal modes method; mode superposition method). A method of dynamic analysis in which unknown displacements are expressed in terms of mode shapes and normal coordinates.

Mode Shapes (normal modes). A normalized deformed shape of a structure in free vibration.

Mount. The supporting structure of a weapon, which transmits firing loads to the ground or to another structure.

Muzzle Preponderance. Unbalance of the tipping parts of a weapon when the weight of the muzzle end exerts a greater moment about the trunnions than does the weight of the breech end.

N

No-Bak Device. A device that delivers power at one end of a gear train that turns in either direction but which will prevent a reverse torque at the other end from entering the original power source.

Nonstructural Mass. External masses that are attached to a structure. These are usually nonload-bearing parts of the structure.

Normal Coordinates. Generalized coordinates (function of time) that are introduced as unknowns in modal expansion of the displacement vector, in the mode superposition method. Linear equations of motion are usually uncoupled in terms of normal coordinates.

THIS DOCUMENT PROVIDED BY THE ABBOTT AEROSPACE
TECHNICAL LIBRARY
ABBOTTAEROSPACE.COM

O

Orifice. Opening through which fluid flows during recoil or counterrecoil. Area of orifice determines the fluid flow, pressure, velocity, and resisting force.

Outriggers. Supporting and stabilizing structures that extend outward from and are attached to the bottom carriage.

P

Pedestal. Base or support of a mount. It may serve as either top or bottom carriage, depending on details of construction.

Pintle. A vertical pin about which a weapon traverses.

Platform Firing. A structure for mobile weapons that serves as a bottom support to distribute firing forces to the ground and to give stability.

Projectile. Missile fired from a gun.

Propellant Gas. Gas generated by burning propellant.

Propellant Gas Force. The force exerted on the base of a projectile by the propellant gases.

Propellant Gas Period. The duration of propellant gas activity.

R

Racer. The flat circular annulus that forms the contact surface of rolling elements of a bearing.

Rail. A supporting member of the recoiling parts that slides in a guide.

Rail, Continuous. A rail that is made of one member.

Rail, Discontinuous. A rail that is made of several short lengths spaced at regular intervals.

Recoil. The movement of the gun tube and attached parts in the direction opposite to projectile travel.

Recoil Cycle. The complete sequence of recoil activity.

Recoil Cylinder. The cylinder that houses the recoil brake.

Recoil Force. The total resistance to movement of the recoiling parts.

Recoil Mechanism. The unit that absorbs the energy of recoil and stores some for returning the recoiling parts to battery.

Recoil Stroke. The distance traveled by the recoiling parts during recoil.

Recoiling Parts. The components of a weapon that move in recoil.

Recuperator. Equipment that stores some of the energy of recoil for counterrecoil.

Running Loads. The applied loads on bearings while in motion.

S

Self-Propelled Weapon. A weapon that incorporates its own prime mover.

Side Frames. The side structure of the top carriage, i.e., the immediate supports of the trunnions.

Single-Recoil Gun. A gun having only one complete recoiling unit.

Sleigh. The housing of a gun tube that slides in a U-type cradle during the recoil cycle.

Slide. See rail.

Slip Clutch. A clutch designed to transmit a predetermined torque and to slip at a greater torque.

Spade. A vertical or inclined structure attached to a trail or bottom carriage that penetrates into soil.

THIS DOCUMENT PROVIDED BY THE ABBOTT AEROSPACE
TECHNICAL LIBRARY
ABBOTTAEROSPACE.COM

T

Tipping Moment. The couple created by firing forces and the inertia of the tipping parts.

Tipping Parts. The assembled structure of a weapon rotates about the cradle trunnions.

Top Carriage. The upper structure of a gun carriage that supports the tipping parts and moves with the cradle in traverse.

Torque, Rifling. The reaction on the gun tube of the angular accelerating forces on the projectile.

Trail. A rearward thrust member of a weapon that stabilizes the weapon during firing and serves as a connecting link between weapon and prime mover during transport.

Transport Conditions. The various loads imposed on the weapon during all phases of transport; the relative position of parts when the weapon is prepared for transport.

Traverse. The horizontal angular displacement of a weapon.

Traverse Bearing. The combined radial and thrust bearing on which the top carriage traverses.

Traverse, Coarse. General positioning of a weapon in azimuth.

Traverse, Fine. Precise positioning of a weapon in azimuth.

Traverse, Limited. The training of a weapon in azimuth through an arc that is limited by the structure.

Traverse, Unlimited. The training of a weapon in azimuth, in either direction, without limit.

Traversing Bearing. The bearing on which the traversing parts rotate.

Traversing Gear. The large gear or gear segment that is the final member of the traversing gear train.

Traversing Mechanism. The mechanism that turns the weapon in the horizontal plane.

Traversing Parts. The unit that consists of all components of a weapon that move in traverse.

Trunnion. The cylindrical structural component of the cradle that serves as the pivot for the tipping parts and transmits recoil forces.

Trunnion Bearings. The bearings in which the trunnions rotate.

Trunnion Cap. The removable portion of the trunnion bearing housing.

Trunnion Force. The force supported by the trunnions during any weapon activity.

Trunnion Height. The distance measured from ground to the center of the trunnions when the weapon rests on a horizontal plane.

Tube, Gun. A hollow cylinder, usually of steel, in which a round of ammunition is fired and directed.

Tube Whip. The flexing of a gun tube due to accelerating forces normal to the tube axis.

U

Upsetting Moment. The couple created by firing forces and the inertia of the recoiling parts.

W

Weight Moment. The moment about the trunnion axis caused by the weight of the tipping parts.

Weight Moment. The moment about the cradle trunnions produced by the weight of the tipping parts.

THIS DOCUMENT PROVIDED BY THE ABBOTT AEROSPACE
TECHNICAL LIBRARY
ABBOTTAEROSPACE.COM

THIS DOCUMENT PROVIDED BY THE ABBOTT AEROSPACE
TECHNICAL LIBRARY
ABBOTTAEROSPACE.COM

INDEX

A

One-degree-of-freedom model, 3-18
Two-degree-of-freedom model, 3-22, C-21
Three-degree-of-freedom model, 3-28

Abrasive wear, 6-1
Accessibility, 10-2
Accumulator, 5-6
Active coils, 5-29
Actuator force, 3-45
Adams-Bashforth equations, 3-39
Adams-Moulton equations, 3-39
Adiabatic compression, 5-34
Advanced design techniques, 7-61
  for bottom carriage structures, 9-40
  for top carriage structures, 8-30
Airdrop requirements, 2-7
Ammunition, 1-3
Angle of approach, 2-29
  departure, 2-29
  elevation, 1-16
  internal shearing resistance, 2-28
Angular momentum, A-3
Antibacklash device, 4-22
  gearing, 4-22
Antifriction bearing, 6-4
Applied load, B-6
Approximate balance equilibrator, 5-20, 5-26, 5-32
Average shearing stress, 7-30
Axisymmetric shell element, B-5

B

Backlash, 4-22, 4-23
Ball bearing, 6-4
  bushing, 6-2
  joint and follower bearing, 6-13
  screw-elevating mechanism, 4-2
Ballistic modeling, 2-8
Bar element, B-4
Base ring and race traverse, 4-15
Basic oscillator, C-14
Beam element, 7-62, C-5, C-11, C-17
Bearing capacity, 6-10
  capacity of soil, 2-26
  characteristic number, 6-7, 6-9
  forces, 9-15
  friction, 6-3
  functions, 6-1
  lubrication, 6-6, 6-11
  seal, 6-11
  shield, 6-11
Bending moment, 9-15
  stress, 9-18
Blast overpressure, 2-7, 2-13
Body-fixed coordinate system, 3-41, 3-43
Bottom carriage. 1-8, 9-3, C-24
  main body, 9-20
  soil interaction, 9-55
  trails, 9-6, 9-7, 9-11, 9-13, 9-15, 9-16
  trail lugs, 9-35
  types, 9-6
Boyle's law of isothermal expansion, 5-33
Braking requirements, 2-30
Breech force, 1-15, 2-8, 3-18
  weight, 2-10
Buckling analysis, B-2
  stress, 9-34
Bulk data deck, B-8

C

Cam mechanism, 4-27
Captive nut, 4-2
Case control deck, B-7
Categories of maintenance, 10-1
Center of mass, A-4
Chain-type equilibrator, 5-6
Clip reactions, 3-6
Clips, 7-25
Clutch, 4-7, 4-8
Coarse traverse, 4-15
Coil diameter, 5-29
Color perception, 11-6
Compatibility relationship, C-12
Computer-aided design, C-3
Concentric springs, 5-25
Concept definition, 2-4
Conical shell element, B-5
Conservation of angular momentum, A-4
  energy, A-4
Conservative force, A-13
Consistent with constraints, 3-43
Constraints, 3-42
Construction and manufacturing procedures
  for bottom carriage, 9-11
  for cradle, 7-10
  for equilibrator components, 5-28, 5-40
  for top carriage, 8-4
Contact pressure, 6-3
  stresses, 6-9
Conventional recoil system, 3-20, 9-4
Cradle, 1-17, 7-1, C-24,
Curvature correction factor, 5-29

THIS DOCUMENT PROVIDED BY THE ABBOTT AEROSPACE
TECHNICAL LIBRARY
ABBOTTAEROSPACE.COM

INDEX cont'd

D

D'Alembert's principle, 1-20, 3-5, 3-29, A-3, A-5
Damped natural frequency, C-15
Damping coefficient, 3-45
Damping matrix, C-16, C-17
Demand curve, 3-13
Depot maintenance, 10-2
Design of cradle body, 7-28
  for rifling torque, 7-58
  of controls, 11-8
  of displays, 11-11
  of equilibrator components, 5-28, 5-40
  sensitivity analysis, 3-33
Direct support maintenance, 10-2
Displacement method, C-5
Double recoil mechanism, 1-14
Double-row bearings, 6-5
Duhamel's integral, C-15
Dynamic analysis, B-2, 9-13
  loads, 2-5, 3-5
  modeling, 2-5
  reaction forces, 3-29
  stability, 2-32
  stress analysis, C-13, C-14

E

Effect of friction on sliding surfaces, 7-9
  soil variability, 9-57
  temperature variation, 7-9
Effective full-charge, 2-7
  spring rate, 5-25
  stress, 7-52
Eigenvectors, B-3, C-18
Elastic stability analysis, B-2
Element nodal forces, C-11
  stiffness matrix, C-10
  stiffness properties, C-8
Elevating arc, 7-15
  gear arc, 7-40
  mechanism, 1-9, 4-2, 7-7, 8-3
  screw, 4-2
End assemblies, 2-18
Energy requirement, 5-19
Equalizing support, 9-6
Equation manipulation languages, 3-39
  method, 3-40
Equilibrating force, 5-9
Equilibrator, 1-9, 5-1, 7-7, 8-3
  component design and
    manufacturing processes, 5-28, 5-40
  components, 5-28, 5-40
    adjustment devises, 5-45
    cylinder, 5-41
    packing assembly, 5-43
    piston rod, 5-42
    spring, 5-28
    terminals, 5-42
  force, 5-12, 8-10, 8-22
  imbalance minimization, 5-48
  load, 7-37, 8-14
  moment, 4-4, 5-15
  moment arm, 5-13, 5-24
  optimization, 5-48
Equilibrium equation, C-11
Equipment associated with top carriage, 8-3
  associated with cradles, 7-6
Equivalent load, 6-11, 9-45
  load vector, C-12
Executive control deck, B-7
Explicit methods, 3-39

F

Fine traverse, 4-15
Finite element method, 7-62, 8-8, C-3
  model, 7-62, 8-30, 9-40, C-3, C-5, C-11, C-13
Fire control, 1-10
Firing base, 1-13, 4-25, 9-56
  couple, 4-5, 4-21, 4-22
  loads, 7-11, 9-13
  platform, 9-7
  stability, 9-10
  torque, 4-6, 4-22
First-order differential equation, 3-34
Float, 2-26, 9-6, 9-13
Force method, C-5
Free-body diagram, 3-6
Free recoil velocity, 1-16
Frequency-dependent loads, B-6
Friction clutch, 4-8
  effects on equilibration, 5-22
  free, 3-42
Frictional torques, 5-22

G

G-loading, 3-5
Galvanic corrosion, 4-9
Gas ejection period, 2-10, 2-11, 2-12
Gas strut equilibrator, 5-6
Gear ratio, 4-3, 4-4, 4-19
  train, 4-3, 4-4, 4-13, 4-19, 4-24
General support maintenance, 10-2
Generalized eigenvalue problem, C-18
  force, 3-20, 3-26, A-13
Geneva mechanism, 4-27
Geometric properties, B-3
Global coordinate system, 3-41
Gradient projection method, 5-51
Grid point, 9-40, B-3

THIS DOCUMENT PROVIDED BY THE ABBOTT AEROSPACE
TECHNICAL LIBRARY
ABBOTTAEROSPACE.COM

INDEX cont'd

H

Handwheel, 4-2, 4-9, 4-13, 4-24
  effort, 4-4, 4-9, 6-3
  force, 4-9, 4-18
Harmonic drive, 4-22
Helical compression spring, 5-28
Hop, 3-33
  stability, 2-37
Human body measurements, 11-1
  factors, 2-7, 11-1
  sensing subsystem, 11-5
Hybrid method, C-5
Hydraulic system, 4-25
Hydropneumatic equilibrator, 5-6
  recoil mechanism, 1-6

I

Identification, 10-3
Implicit method, 3-39
Importance factor, 2-37
Impulse of breech force, 1-15
In-battery firing, 3-20
  sustaining factor, 2-18
Independent generalized coordinates, A-14
Inertial force, A-5
  loads, 3-5
  reference frame, A-5
Initial conditions, 3-34
Initial-value problem, 1-19
Interchangeability, 10-3
Interior ballistics, 1-14
Internal forces, 3-44
Irreversible worm, 4-23
Isothermal gas law, 3-8

J

Jacks, 9-11
Joints, 3-42
Journal bearing, 6-6

K

Kinematic model, 3-13, A-5,
Kinematics of perfect equilibration, 5-18
Kinetic energy, 3-20, A-8, C-16
Kinetostatic approach, 3-29

L

Lagrange multipliers, 3-46
Lagrange's equations of motion, 3-18, 3-27, A-14
Large diameter bearings, 6-13
LeDuc equation, 2-8
  parameter, 2-8
Leakage factor, 5-11, 5-45
Least square method, 5-48
Length of recoil, 1-16
Lifting and equilibrator forces combined, 8-25
Lifting force, 8-10, 8-11, 8-16
Lifting load analysis, 7-31, 8-11
Limit stop, 4-3
Linear momentum, 3-5, A-3
Load analysis, 7-30, 7-34, 8-11, 9-12, 9-13
  for cradle, 7-11
  for top carriage, 8-7
Local buckling, 9-34
Locking clutch, 4-2, 4-23
Lubrication of bearings, 6-6, 6-11
Lugs, 8-6

M

Maintainability, 2-8, 10-1
Mass matrix, C-16
Material properties, B-5
Materials
  for bottom carriage, 9-10
  for cradle, 7-10
  for top carriage, 8-4, 8-6
Manufacturing procedures
  for bottom carriage, 9-11
  for cradle, 7-10
  for equilibrator, 5-28, 5-40
  for top carriage, 8-4
Maximum chamber pressure, 2-9
  shear stress theory, 7-20
  spring deflection, 5-30
Mechanical brake, 4-2
Modal matrix, C-15, C-20
  synthesis, C-14
Mode shape, C-14, C-18
  superposition method, C-15
Model validation, 3-33
Modeling of a structure, B-3
Mohr's circle, 2-29
Mohr-Coulomb law, 2-28
Moment of inertia, A-3
Momentum of projectile and gas, 2-11
Multidegree-of-freedom system, C-15
Multipoint constraints, B-4
Multistep methods, 3-37, 3-38
  numerical integration algorithm, 3-38
Muzzle brake, 1-5, 2-7, 2-12
  brake factor, 2-10
  preponderance, 5-5, 5-9

N

NASTRAN, 7-65, 8-33, 9-44, B-1, C-3, C-24
  capability, B-1
  stress analysis, 9-53

THIS DOCUMENT PROVIDED BY THE ABBOTT AEROSPACE
TECHNICAL LIBRARY
ABBOTTAEROSPACE.COM

INDEX cont'd

Natural frequencies, C-14
Needle bearings, 6-5
Newton's equations of motion, 1-16, 3-20, A-3
  laws of motion, A-3
Newton-Raphson method, 3-39
No-back device, 4-2, 4-7, 4-23
Nodal displacement, C-8
  point, C-8
Noise, 11-8
Nonstructural mass, C-13
Nonconservative force, A-13
Nonlinear programming methods, 5-50
Normal coordinates, C-20
  mode, C-14
  modes method, C-15
Numerical integration, 3-34
  algorithm, 3-36

O

O-type cradle, 7-8, 7-9
Octahedral shear stress theory, 7-58
Off-carriage traverse, 1-10, 4-12, 4-18, 6-13, 9-6, 9-10
On-carriage traverse, 4-12, 9-6
Operational constraints, 2-6
Out-of-battery, 3-20
Outrigger, 9-6, 9-11

P

Packing, 5-11, 5-43
  friction, 5-11
  friction force, 5-11
  ring, 5-11
Parallel axis theorem, A-4
Parameter variations, 2-37
Pedestal, 9-8
Perfect balance, 5-12
  balance equilibrator, 5-25
  equilibration, 5-12, 5-15, 5-18
Performance rating, 2-37
Permanent deformation, 6-2
Pinion, 4-3
  and arc elevation mechanisms, 4-3
Pintle, 8-4, 9-11
  bearing, 6-12
  traverse, 4-13
Pitching degree of freedom, 3-22
Planar mechanical system, 3-42
Plate bending element, C-6
  finite elements, 7-64
Pneumatic equilibrator, 5-6, 5-32
  tires, 4-25
Potential energy, 3-26, A-13
Precision bearings, 6-6
Predictor-corrector algorithm, 3-39
Preliminary design calculations, 7-34 to 7-49
  of bottom carriage, 9-11
  of cradle, 7-10
  of top carriage, 8-6
Preliminary sizing, 2-23
Pressure factor, 5-11
Principle of virtual work, 3-45, A-12
Pull-type equilibrator, 5-5
Push-type equilibrator, 5-5
Puteaux recoil mechanism, 2-15

Q

Quadrilateral plate element, B-5
Quasistatic loads, 3-5
  model, 1-20

R

Racer, 8-4
Radial expansion of cylinder, 2-17
  load, 6-2, 6-11
Rails, 7-7
  and slides, 7-35
Rated load, 6-3
Rayleigh-Ritz method, C-18
Reaction force, 3-29, 3-46
  time, 2-8
Recoil attachment to cradle, 7-12
  cylinder, 2-15
  cylinder design pressure, 2-15
  equation, 3-18
  force, 1-16, 3-18
  linkage, 4-27
  mechanism, 1-6, 7-6
  piston, 2-15
  rod, 2-15
  system, 1-6
Recoiling parts, 1-15, 3-18
Recuperator forces, 2-18
Reduced overpressure, 9-10
Refined design calculations, 7-49 to 7-58
Reliability, 2-8
Residual imbalance, 4-7
Rifling torque, 7-43, 7-45
Rigid format option, B-1
Rod element, B-4
Roll stability, 2-32
Roller bearing, 6-5, 6-6, 6-10
Rolling element, 6-2
Rotational joint, 3-42, 3-43
Runge-Kutta method, 3-37

S

Safety, 10-4

THIS DOCUMENT PROVIDED BY THE ABBOTT AEROSPACE
TECHNICAL LIBRARY
ABBOTTAEROSPACE.COM

INDEX cont'd

Sample bottom carriage design problem, 9-13
cradle design problem, 7-33
top carriage design problem, 8-8
Scalar element, B-4
Screw-nut, 4-15
Seal, 6-11
Second-order differential equation, 3-34
Self-aligning bearing, 6-5, 6-11
Self-locking worm, 4-24
Semifixed ammunition, 1-5
Separate loading ammunition, 1-4
Separator, 6-4
Servicing lubrication, 10-4
Shape function, C-9
Shear panel element, B-4
Shearing stress, 7-30, 7-52
Shield, 6-5, 6-11
Side frame, 8-4
Simplification, 10-4
Single-degree-of-freedom systems, C-14
Single-point constraint, B-4
Single-row bearing, 6-5
Single-step method, 3-37
Skin senses, 11-6
Slenderness ratio, 5-25
Sliding surface, 7-9
Slip clutch, 4-8, 4-24
Small angle approximation, 3-24
Smith no-back device, 4-8
Soft recoil, 1-13, 3-20, 9-10
system, 9-4
Solid polyhedron element, B-5
Sommerfeld number, 6-9
Spade, 2-26, 9-6, 9-7, 9-13
Specific dynamic capacity, 6-10, 6-11
Speed shift, 2-7, 4-13
jack, 4-25
Spherical roller thrust bearing, 6-5
Spring coefficient, 3-45
deflection, 5-29
design, 5-28
energy, 5-19
equilibrator, 5-6, 5-25
rate, 5-29
strut equilibrator, 5-6
wire, 5-29
Spring-damper-actuator, 3-43
force, 3-44
Spurt rate of fire, 2-7
Square jaw clutch, 4-8
Stability index, 2-37
Standardization, 10-3
Static analysis, B-1
frictional torque, 4-4, 4-21
load, 3-5
load rating, 6-2
Straight roller bearings, 6-5
Strength requirements of the cradle structure, 7-20
Stress analysis, 8-8, 8-16, 9-12, 9-13, C-3
for quasi-static loading, C-5
Stress and deflection, 7-45
Stress calculations, 7-30
Structural elements, B-4
stiffness matrix, C-12
Structures for bottom carriage, 9-6
Stuffing box, 2-18
Subshape iteration algorithm, C-18, C-19
Supporting bracket, 9-6
Surface endurance limit, 6-3
Suspension system, 4-25
Sustained rate of fire, 2-7
Symbolic manipulation, 3-39
System design procedure, 2-4
requirements, 2-6

T

Tapered roller bearing, 6-5
Thick-walled cylinder, 2-9
Thrust, 6-12
load, 6-1, 6-11
Time-dependent loads, B-6
grid, 3-36
step, 3-36
Tires, 2-30
Top carriage, 1-7, 8-1, C-24
Torsion bar equilibrator, 5-6
Torsional spring, 3-33
Towed artillery weapon system, 1-1
Towing considerations, 2-29
Tradeoffs, 2-5, 2-37
Trails, 9-6, 9-7, 9-11, 9-13, 9-15, 9-16
spade/ground interaction, 9-56
Transformation matrix, 3-16
Translational bearing, 6-1, 6-2
Transverse shear stress, 8-28
Trapezoidal method, 3-38
Travel gear, 1-10
load, 3-6
lock, 4-9, 4-24
Traverse bearing, 6-1, 6-12, 6-13, 8-4, 9-11, 9-13, 9-20
Traversing mechanism, 1-10, 4-12, 8-3
parts, 4-13
Triangular plate element, B-4, C-6
Truncation error, 3-37
Trunnion, 1-7, 7-6
and equilibrator forces combined, 8-25
bearing, 6-1, 6-6, 7-43, 8-4
design, 7-20
force, 8-10
height, 8-7
load, 7-42, 8-15
location, 7-20
Truss element, C-5, C-10, C-17

THIS DOCUMENT PROVIDED BY THE ABBOTT AEROSPACE
TECHNICAL LIBRARY
ABBOTTAEROSPACE.COM

INDEX cont'd

Tube and breech assembly, 1-4
element, B-4
wall thickness, 2-9
weight, 2-10
Turning radius, 5-12
Twist panel element, B-4
Types of bottom carriage, 9-6
of cradle, 7-7
of top carriages, 8-4

U

U-type cradle, 7-7, 7-8
Unbalanced equlibrator moment, 4-4
Uncoupled equations of motion, C-14
Undamped free vibration, C-17
Underdamped systems, C-15
Unit maintenance, 10-1

V

Variability in ignition delay, 3-20
Variable recoil linkage, 4-27
Variational form of Lagrange's equations, 3-45
Variations in generalized coordinates, A-12
Velocity relation, 3-43
Virtual displacement, 3-43, A-12
Virtual work, 3-45, A-12
Visual presentation of information, 11-6
von Mise's failure condition, 7-52
yield criterion, 2-17, 7-58
Vulnerability considerations, 5-12

W

Wave generator, 4-22
Weapon hop, 3-33
stability, 2-30, 3-33
Wearing in, 6-2
Weight moment, 5-5, 5-12, 5-20, 5-23, 5-36
of tipping parts, 5-9, 5-15
Wire diameter, 5-29
Wishbone boxtrail, 1-13
Workless, 3-42
Worm gear, 4-3
gear drive, 4-22

THIS DOCUMENT PROVIDED BY THE ABBOTT AEROSPACE
TECHNICAL LIBRARY
ABBOTTAEROSPACE.COM

Subject term (keyword) listing

Angle of Elevation
Azimuth
Base Plate
Breech
Buffer
Carriage
Cradle
Equilibrator
Fire Control
Firing Couple
Gear Ratio
Gun Mount
Hydraulic Strut
Loading Device
Locking Device
Moment
Mount
Nonstructural Mass
Orifice
Pedestal
Propellant
Racer
Rail
Recoil
Recuperator
Self Propelled
Sleigh
Torque
Traverse
Trunnion
Tube
Upsetting Moment
Weight Moment

Concluding material

Custodian:
Army-AR

Preparing activity:
Army-AR

(Project 10GP-A008)

THIS DOCUMENT PROVIDED BY THE ABBOTT AEROSPACE
TECHNICAL LIBRARY
ABBOTTAEROSPACE.COM

THIS DOCUMENT PROVIDED BY THE ABBOTT AEROSPACE
TECHNICAL LIBRARY
ABBOTTAEROSPACE.COM

INSTRUCTIONS: In a continuing effort to make our standardization documents better, the DoD provides this form for use in submitting comments and suggestions for improvements. All users of military standardization documents are invited to provide suggestions. This form may be detached, folded along the lines indicated, taped along the loose edge *(DO NOT STAPLE)*, and mailed. In block 5, be as specific as possible about particular problem areas such as wording which required interpretation, was too rigid, restrictive, loose, ambiguous, or was incompatible, and give proposed wording changes which would alleviate the problems. Enter in block 6 any remarks not related to a specific paragraph of the document. If block 7 is filled out, an acknowledgement will be mailed to you within 30 days to let you know that your comments were received and are being considered.

NOTE. This form may not be used to request copies of documents, nor to request waivers, deviations, or clarification of specification requirements on current contracts. Comments submitted on this form do not constitute or imply authorization to waive any portion of the referenced document(s) or to amend contractual requirements.

(Fold along this line)

(Fold along this line)

DEPARTMENT OF THE ARMY

NO POSTAGE NECESSARY IF MAILED IN THE UNITED STATES

OFFICIAL BUSINESS
PENALTY FOR PRIVATE USE $300

BUSINESS REPLY MAIL
FIRST CLASS PERMIT NO 12062 WASHINGTON D C

POSTAGE WILL BE PAID BY THE DEPARTMENT OF THE ARMY

Commander
US Army Armament Research, Development, and Engineering Center
ATTN: SMCAR-BAC-S
Picatinny Arsenal, NJ 07806-5001

THIS DOCUMENT PROVIDED BY THE ABBOTT AEROSPACE
TECHNICAL LIBRARY
ABBOTTAEROSPACE.COM

STANDARDIZATION DOCUMENT IMPROVEMENT PROPOSAL

(See Instructions - Reverse Side)

1. DOCUMENT NUMBER	2. DOCUMENT TITLE
MIL-HDBK-785(AR)	Design of Towed Artillery Weapon Systems

3a. NAME OF SUBMITTING ORGANIZATION	4. TYPE OF ORGANIZATION *(Mark one)*
	☐ VENDOR
b. ADDRESS *(Street, City, State, ZIP Code)*	☐ USER
	☐ MANUFACTURER
	☐ OTHER *(Specify)*: _____

5. PROBLEM AREAS

a. Paragraph Number and Wording:

b. Recommended Wording:

c. Reason/Rationale for Recommendation:

6. REMARKS

7a. NAME OF SUBMITTER *(Last, First, MI)* – Optional	b. WORK TELEPHONE NUMBER *(Include Area Code)* – Optional
c. MAILING ADDRESS *(Street, City, State, ZIP Code)* – Optional	8. DATE OF SUBMISSION *(YYMMDD)*

DD FORM 82 MAR 1426 PREVIOUS EDITION IS OBSOLETE.